JAEA-Review
2007-060

JAEA-Review

JAEA Takasaki Annual Report 2006

(Ed.) Shigeru TANAKA

Takasaki Advanced Radiation Research Institute

March 2008

Japan Atomic Energy Agency

日本原子力研究開発機構

本レポートは日本原子力研究開発機構が不定期に発行する成果報告書です。
本レポートの入手並びに著作権利用に関するお問い合わせは、下記あてにお問い合わせ下さい。
なお、本レポートの全文は日本原子力研究開発機構ホームページ（http://www.jaea.go.jp/index.shtml）より発信されています。このほか財団法人原子力弘済会資料センター*では実費による複写頒布を行っております。

〒319-1195　茨城県那珂郡東海村白方白根 2 番地 4
日本原子力研究開発機構　研究技術情報部　研究技術情報課
電話 029-282-6387, Fax 029-282-5920

*〒319-1195　茨城県那珂郡東海村白方白根 2 番地 4　日本原子力研究開発機構内

This report is issued irregularly by Japan Atomic Energy Agency
Inquiries about availability and/or copyright of this report should be addressed to
Intellectual Resources Section, Intellectual Resources Department,
Japan Atomic Energy Agency
2-4 Shirakata Shirane, Tokai-mura, Naka-gun, Ibaraki-ken 319-1195 Japan
Tel +81-29-282-6387, Fax　+81-29-282-5920

JAEA-Review 2007-060

JAEA Takasaki Annual Report 2006

(Ed.) Shigeru TANAKA

Takasaki Advanced Radiation Research Institute

Japan Atomic Energy Agency

Watanuki-machi, Takasaki-shi, Gunma-ken

(Received December 27, 2007)

JAEA Takasaki annual report 2006 describes research and development activities performed from April 1, 2006 to March 31, 2007 with Takasaki Ion Accelerators for Advanced Radiation Application (TIARA, four ion accelerators), and electron/gamma-ray irradiation facilities (an electron accelerator and three ^{60}Co gamma-ray irradiation facilities) at Takasaki Advanced Radiation Research Institute, Japan Atomic Energy Agency (JAEA Takasaki). These activities are classified into four research fields: 1) space, nuclear and energy engineering, 2) environmental conservation and resource security, 3) biotechnology and medical application, and 4) advanced materials, analysis and novel technology. This annual report contains 186 reports consisting of 178 research papers and 8 status reports on operation/maintenance of the irradiation facilities described above, and a list of publications, related press-releases, TV programs, patents, and the type of research collaborations as Appendices.

Keywords: TIARA, Ion Accelerators, Electron Accelerator, Gamma-ray Facilities, Nuclear and Energy Engineering, Environment Conservation, Resource Security, Biotechnology, Medical Application, Advanced Materials, Analysis, Novel Technology, Materials for Space, Semiconductors, Inorganic Materials, Organic Materials, Functional Materials, Radiation Chemistry, Radiation Biology, Radioisotope Production, Nuclear Chemistry, Material Analyses, Solid State Physics, Microbeam Technology, Accelerator Technology, Accelerator Operation, Safety Control

---

高崎量子応用研究所研究年報 2006

日本原子力研究開発機構 高崎量子応用研究所
（編） 田中 茂

（２００７年１２月２７日受理）

高崎量子応用研究所研究年報 2006 は、同研究所にある TIARA 施設（イオン加速器 4 基）及び電子･ガンマ線照射施設（電子加速器 1 基、^{60}Co ガンマ線照射施設 3 棟）を利用して 2006 年 4 月 1 日から 2007 年 3 月 31 日までの間に行われた研究・技術開発成果をまとめたものである。この研究年報には、１）宇宙・原子力・エネルギー、２）環境・資源、３）バイオ技術・医学応用、４）先端材料・計測・基盤技術の 4 分野に分類した 178 編の論文及び 8 編の施設の運転･管理状況報告からなる合計 186 編を収録する。また、論文リスト、新聞発表、テレビ放映、出願特許、及び研究実施形態・利用施設の一覧表を付録として含む。

高崎量子応用研究所：〒370-1292 群馬県高崎市綿貫町 1233
編集委員：（著者代表）田中 茂、伊藤 久義、田中 淳、神谷 富裕、
鳴海 一雅、小嶋 拓治、河田 靖、中村 義輝、橘 宏行

PREFACE

This report covers research and development activities in Takasaki Advanced Radiation Research Institute, JAEA, during the period from April 2006 to March 2007, conducted with TIARA (Takasaki Ion Accelerators for Advanced Radiation Application), electron beam and Co-60 gamma-ray irradiation facilities.

One hundred eighty seven papers are appeared in this annual report in the fields of

1) Space, Nuclear and Energy Engineering,
2) Environmental Conservation and Resource Security,
3) Biotechnology and Medical Application,
4) Advanced Materials, Analysis and Novel Technology,
5) Status of Irradiation Facilities.

In the field of Space, Nuclear and Energy Engineering, the radiation resistance of solar cells and integrated circuits newly developed for space application has been evaluated using high-energy electrons, protons and heavy ions. Experimental and theoretical investigations of transient currents induced in typical device structures such as SOI (silicon on insulator) by energetic ions have been performed for clarifying mechanisms behind single event phenomena in order to develop prediction methods of the reliability of semiconductor devices, which will be used in radiation environment. Radiation resistant devices have also been developed using wide band-gap semiconductors like SiC and GaN. Radiation degradation of organic materials, e.g., insulating materials in superconducting coils of ITER, coaxial cables for J-PARC, and grease for the equipments of nuclear-cycle reprocessing have been examined for aiming at their practical usage. Radiation effects involving irradiation assisted stress corrosion cracking (IASCC) in structural materials of fusion, fast breeder and light water reactors have been intensively investigated using TIARA for securing reactor safety. In addition, high quality polymer electrolyte membranes have been fabricated using ion beams, electron beams and gamma-rays for their application to fuel cells.

In the field of Environmental Conservation and Resource Security, metal ion adsorbents have been developed with radiation grafting technique for removing toxic elements such as Cd, Pb and B in industrial waste water. R&D of graft adsorbents based on plant-derived polymers like polylactic acid (PLA) and carboxymethylcellulose (CMC) has been started. Radiation grafting technique has also been applied to improve the properties of materials for industrial use; low power-loss millimeter-wave planar antennas and high quality rubber wipers for automobiles have been successfully developed. Biodegradable hydro-gels and polymers from CMC and PLA have been investigated using radiation cross-linking, leading to the success in fabricating novel elastic CMC gels and elastic PLA materials with high heat resistance. Concerning environmental purification using electron beams and gamma-rays, new process technologies have been developed for the decomposition and removal of trace amount of pollutants such as formaldehyde in sterilization gas, dioxin wastes and endocrine disrupting chemicals.

In the field of Biotechnology and Medical Application, the ion beam breeding technique has been applied for many varieties of plants and microorganisms such as flower, crop, vegetable, yeast, alga and fungus. Functional analyses of radiation-response proteins of the radioresistant bacterium and the elucidation of characteristics of ion beam-induced damage and mutation have been progressed. Molecular mechanisms in radiation-induced bystander

effects were investigated in normal and cancer cells using heavy-ion microbeams in the aspects of initiators/mediators and the role of gap junction. The effect of ionizing radiation on the food-NaCl associative learning behavior in *Caenorhabditis elegance* was also investigated. Compartment model was applied to the positron imaging of a tobacco leaf and succeeded in obtaining parametric imaging of two photosynthetic processes, photoassimilation and sucrose-export. A new radionuclide for medical application, Br-76, was produced by using AVF cyclotron and examined for the diagnosis of cancer by positron emission tomography, PET. Clarification of the dynamics of anticancer drug was studied by analyzing trace elements in tumor cells using the in-air micro-PIXE system.

In the field of Advanced Materials, Analysis and Novel Technology, development of hydrogen gas sensor using tungsten trioxide (WO_3) has been conducted; it was founded that ion irradiation to WO_3 films improved their gasochromic coloration by introducing oxygen vacancies. In order to measure the three-dimensional distribution of elements in biological samples, such as carbon, hydrogen, and oxygen using the in-air micro PIXE system, STIM (Scanning Transmission Ion Microscopy) / CT (computed tomography) method was developed and introduced to the system; three-dimensional reconstruction of an insect's head was successfully obtained using all tomograms with the system. All-permanent-magnet type ECR ion source (LECR) has been developed since 2003, and beam current of O^{7+} was increased from 0.6 to 1.8 μA by the modification of the LECR in 2006. Negative Ge cluster ions were generated by a Cs sputter ion source, and Ge clusters up to Ge_4 at the beam current of nano ampere order was extracted from the source. Three-dimensional micro structures were fabricated with the Proton Beam Writing (PBW) technique using protons at two different beam energies of 1.2-and 3.0-MeV impinging on a layer of negative resist material. In the development of monitor and dosimeter for radiation, measurement technique of two dimensional dose distribution was developed by using B3 film dosimeters and a PC-scanner.

All the accelerators in TIARA, namely the AVF cyclotron, the 3-MV tandem accelerator, the 3MV single-ended accelerator and the 400-kV ion implanter, have been operated steadily as well as an electron accelerator and irradiation systems in Co-60 gamma-ray irradiation facilities. Especially, the cyclotron has been operated in this fiscal year providing ion-beams to all users perfectly without any cancellation of machine time, although there occurred 324 machine troubles. The total operation time of the cyclotron from the first-beam provision reached 50,000 h in April 2007, as the result of such continuous back-up efforts.

Hideki Namba,
Director General
Takasaki Advanced Radiation Research Institute
Japan Atomic Energy Agency

Contents

This is a blank page.

1 Space, Nuclear and Energy Engineering

This is a blank page.

1-01 Effect of Base-layer Carrier Concentration on Radiation Resistance of AlInGaP Solar Cell

C. Morioka [a)], M. Imaizumi [a)], T. Takamoto [b)], T. Ohshima [c)], S. Sato [c)], H. Miyamoto [c)] and K. Kibe [a)]

[a)]Institute of Aerospace Technology, JAXA, [b)]Solar System Division, Sharp Corporation, [c)]Environment and Industrial Materials Research Division, QuBS, JAEA

Optimum epitaxial layer structure of an AlInGaP solar cell as a top subcell in a triple-junction (3J) space solar cell has been studied. In 2006, the base-layer carrier concentration in AlInGaP single-junction (1J) solar cells was varied in order to clarify the suitable carrier concentration for radiation resistance of the cell.

AlInGaP 1J solar cell epitaxial wafers were grown by metal-organic vapor phase epitaxy (MOVPE). The carrier concentration in base-layer was varied for 1×10^{16} cm^{-3}, 3×10^{16} cm^{-3} and 3×10^{17} cm^{-3}. Solar cells were fabricated from the wafers. However, anti-reflection coating was not formed on the surface of the cells to avoid the effect of difference in reflectance. The cell size is 1cm×1cm. The cells were irradiated with 1MeV electrons (nitrogen ambient) and 3MeV protons (in vacuum) at room temperature.[1)]

Figures 1 and 2 depict the radiation degradation of the short-circuit current (Isc) and the open-circuit voltage (Voc) of the AlInGaP 1J solar cells due to 1MeV-electron and 3MeV-proton irradiations, respectively. In the case of degradation of Isc, there seems to be no significant dependency on the carrier concentration, while the cell with the concentration of 3×10^{17} cm^{-3} degrades greater than those with the concentration of the order of 10^{16} cm^{-3}.

These results indicate that the minority-carrier diffusion length in the p-AlInGaP base layer and its radiation degradation are not affected by the base-layer carrier concentration between 1×10^{16} cm^{-3} and 3×10^{17} cm^{-3}. On the other hand, the carrier removal effect due to the irradiation, which results in the decrease in built-in potential at the AlInGaP n/p junctions, is greater when the base-layer carrier concentration becomes in the order of 10^{17} cm^{-3}.

Reference

1) C. Morioka et al., Proc. of 4th World Conference on Photovoltaic Ener. Conv., Waikoloa, 2006, pp.1846-1849.

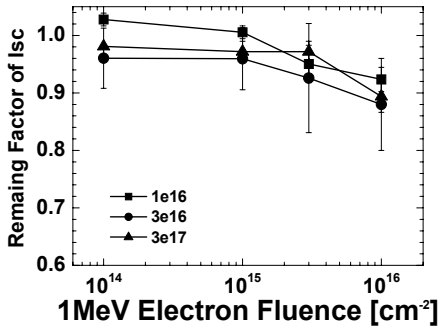

(a) Short-circuit current (Isc)

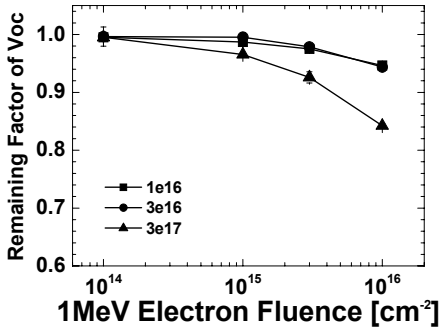

(b) Open-circuit voltage (Voc)

Fig.1 Degradation of short-circuit current and open-circuit voltage of AlInGaP solar cells with different base-layer carrier concentration due to 1MeV electrons.

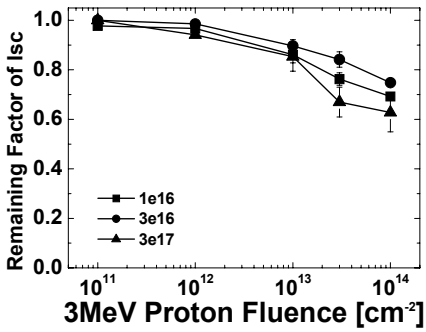

(a) Short-circuit current (Isc)

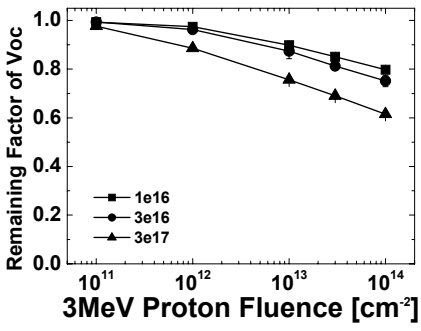

(b) Open-circuit voltage (Voc)

Fig.2 Degradation of short-circuit current and open-circuit voltage of AlInGaP solar cells with different base-layer carrier concentration due to 3MeV protons.

1-02 Evaluation of Radiation Hardened Logic Circuits Utilizing 0.15μm SOI Technology for Space Application

H. Shindou [a)], M. Midorikawa [a)], Y. Satoh [a)], S. Kuboyama [a)], T. Hirao [b)] and T. Ohshima [b)]

[a)]Institute of Aerospace Technology, Japan Aerospace Exploration Agency (JAXA),
[b)]Environment and Industrial Materials Research Division, QuBS, JAEA

Semiconductor devices with Silicon On Insulator (SOI) technology are utilized for high-performance and low-power electronics such as computer servers for high-end commercial markets. SOI is a layered structure consisting of a thin layer of silicon mounted on an insulating substrate. The typical cross section image is shown in Fig.1. SOI technology is also very attractive as semiconductor devices for space application. SOI devices are expected to have an advantage over equivalent bulk technology devices for Single-Event Effects (SEEs) caused by heavy ions and high-energy protons because the sensitive volume for SEEs is much smaller than that of bulk Si devices. In JAXA, now we continuously perform the design and evaluation of radiation hardened logic circuits utilizing 0.15μm fully depleted SOI process technology[1)]. This study is indispensable in order to develop next generation semiconductor devices for space application such as high-speed Microprocessors (MPUs) and Field Programmable Gate Arrays (FPGAs).

This year, several kinds of radiation hardened logic circuits such as latch and flip flop were designed and evaluated. In this report we describe the evaluation results of latch circuit as a representative case. Two types of radiation hardened latch circuit (Basic type and Optimized type) were designed and installed in the test chips. In general, Single Event Transient (SET) pulse is generated when an ion particle hit on the p-n junction of transistors.

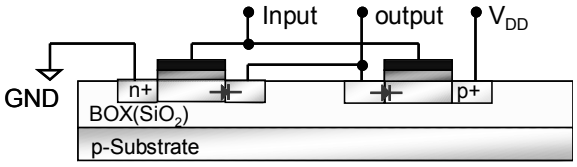

Fig. 1 Cross section image of SOI device

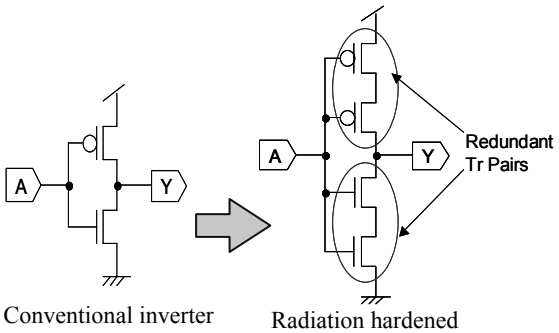

Fig. 2 Concept of the radiation hardened inverter logic circuits with redundant transistors

The propagation of this pulse noise leads to the malfunction of logic circuit (i.e. SEE). For SOI technologies, it is possible to eliminate the SET pulse generation on the output terminal by using circuit techniques [1)]. Figure 2 shows the concept of the radiation hardened inverter logic circuits with redundant transistors. By using this, various types of radiation hardened logic circuit can be constructed. For the basic type latch circuit, SET-free inverter circuit is fully applied on the data input logic and the inverter loop. However the area, power consumption, speed penalties are too large compared to the conventional latch circuits. For the optimized type, some redundant p-type transistors are removed in order to minimize the penalty mentioned above. Test chips were fabricated with a 0.15 μm fully depleted SOI commercial process at OKI (Tokyo, Japan). Figure 3 shows the pictures of test device. In this chip, each kind of latch circuit composes the 4kbit memory array.

Kr and Xe ion irradiation test results are shown in Table 1. Some amount of SEU was observed only when Xe ion irradiated. It was confirmed that both types of latch circuits have a very good radiation tolerance. We plan to continue this study in order to construct the radiation hardened logic cell library for space SOI.

Reference

1) A. Makihara et al., IEEE Trans. Nucl. Sci., Vol. 52, 2524 (2005).

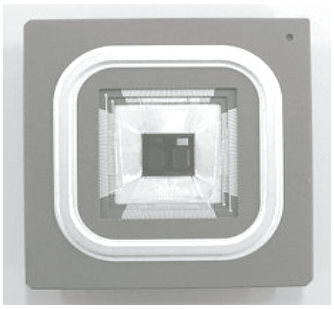

Fig. 3 Outline of the test

Table 1 Heavy ion irradiation test result

Ion	Fluence [particles/cm²]	# of Errors	
		Basic type	Optimized type
Kr	1.33E+8	0	0
Xe	1.50E+8	3*	49

*These errors may be attributable to considerable degradation caused by local total ionizing dose effect.

1-03 Transportation of Charge Induced in MOS Capacitor by Heavy-ion Irradiation

T. Hirao [a)], S. Onoda [a)], Y. Takahashi [b)], K. Ohnishi [b)] and T. Ohshima [a)]

[a)]Enviroment and Industrial Materials Research Division, QuBS, JAEA,
[b)]College of Science and Technology, Nihon University

One of the most detrimental effects on semiconductor devices in radiation environments is single-event effects (SEEs). When a high-energy heavy ion strikes the device, electron-hole (e-h) pairs are generated along the ion-track and they lead to transient currents at the terminal of devices.

Musseau et al. proposed that the silicon-on-insulator (SOI) is one of the most promising structures to achieve higher SEE tolerant devices, because the charge collection can be suppressed by the existence of a buried oxide layer [1)]. However, the anomalous charge collection in the SOI device was reported recently [2)]. This fact suggests that dense charges generated under a buried oxide contribute to the charge collection. Therefore it is important to make clear the charge collection mechanisms through an insulation (oxide) layer due to heavy ion irradiation. In a previous study, we have measured transient currents induced through an oxide layer by ion incidence using metal oxide semiconductor (MOS) capacitors to understand the charge collection mechanisms in SOI devices. As a result, the transient current induced in MOS capacitors can be qualitatively interpreted in terms of displacement current [3)]. However, the quantitative analysis has not yet done.

In this report, we perform numerical simulations on transient currents induced in MOS capacitors using an optimized physical model, and compare calculated results to experimental results.

The MOS capacitors used in this study are fabricated on p-type Si substrates. The concentration of boron acceptors in the substrate is 4.63×10^{15} /cm^3. The oxide layer at a thickness of 31 nm was formed using dry oxidation at 1050 ^{o}C for 30 min. Aluminum was applied as the gate metal. Heavy ion irradiation experiments were carried out using the 3MV tandem accelerator at TIARA. The transient currents induced in the MOS capacitors by 15 MeV-oxygen ion incidence were collected by transient ion beam induced current (TIBIC) measurement system with single ion hit (SIH) system.

The transient currents were simulated by using the Technology Computer Aided Design (TCAD) version 10 provided by Synopsys. The DESS package in TCAD was used to simultaneously solve the Poisson and e-h continuity equations under the cylindrical symmetry (quasi-three dimensional) conditions. The following models were assumed in all simulations: (1) Fermi–Dirac statistics, (2) bandgap narrowing, (3) mobility model dependent on doping concentration, and carrier density, (4) high field saturation, and (5) incomplete ionization. In addition, since the ion initial track structure strongly affects the transient current, the distributions of e-h pairs are calculated by considering the δ-electron production with MeV ion penetration and keV δ-electron transmission theory, instead of the cylindrical track structure generally accepted in TCAD simulations.

Figure 1 shows the comparison of the experimental results with the simulated results. The total collected charges do not show strong bias dependence and slightly decrease with increasing bias. On the other hand, as for the peak currents, the values increase with increasing bias. As a result, the peak currents and the total collected charges obtained by time integration of transient currents agree well with the measured values, errors being less than 10%.

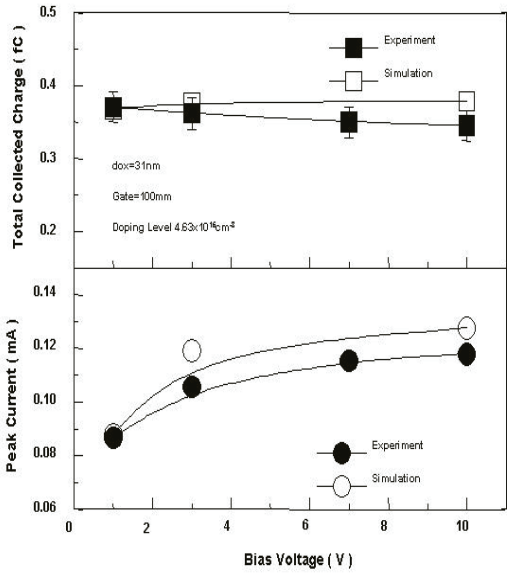

Fig.1 Comparison of the experimental results with simulated results. Bias dependence Peak Current and Total Collected Charge.

References

1) O. Musseau et al., IEEE Trans. Nucl. Sci., Vol. NS-43, No.2, p. 603 (1996)
2) P.E. Dodd et al., IEEE Trans. Nucl. Sci., Vol. NS-48, No.6, p. 1893 (2001)
3) Y. Takahashi et al., The IEICE Trans. Electron. Vol. J89-C, No.3, p. 104 (2006).

1-04 Heavy-ion Induced Current in Silicon-on-insulator Based Devices

K. Ohnishi [a)], Y. Takahashi [a)], Y. Nakajima [a)], T. Nagasawa [a)], M. Fugane [a)], R. Imagawa [a)], K. Nomoto [a)], T. Hirao [b)], S. Onoda [b)] and K. Mishima [a)]

[a)]Nihon University, [b)]Environment and Industrial Materials Research Division, QuBS, JAEA

In order to clarify the charge collection mechanism through a buried oxide layer in SOI structure, the single heavy-ion induced transient gate current in MOSFET has been investigated. The transient gate current with both positive and negative peaks is observed by hitting an ion to gate area, and the amount of collected charge converges on zero within 100ns after irradiation. The transient current in n-MOSFET is larger and also shorter than p-MOSFET because of mobility difference between electrons and holes. It is also confirmed that the current peak increases with applied drain voltage during irradiation.

宇宙環境下で半導体デバイスを使用する場合、重イオンなど高速荷電粒子の照射により誘起される電流に起因した、シングルイベント現象が問題となる。能動領域の薄膜化が可能なSOI (Silicon on Insulator) デバイスは、埋め込み酸化膜の存在により能動領域が限定されているために高い耐放射線性が予想されているものの、予想を大きく上回る電荷収集が観測されるとの報告[1)]もあり、酸化膜を有する構造における重イオン誘起電流の発生メカニズム解明が非常に重要である。本研究では、MOS構造の重イオン照射誘起電流の評価により、酸化膜を介した電荷収集機構について検討を行ってきた[2)]。今回はpチャネルおよびnチャネルMOSFETに対する照射実験を行い、電流発生機構について検討を行った。

Alゲートp-MOSFETおよびn-MOSFET（ゲート酸化膜厚 d_{ox}=40 nm，ゲート長 L=100 μm，ゲート幅 W=300μm）を作製し、日本原子力研究開発機構の重イオンマイクロビームシステムを使用して酸素イオン（15MeV）の照射を行った。なお、照射による損傷を軽減し、かつ単一イオンの入射に起因した誘起電流を正確に測定するため、Single Ion Hitシステムを用いて単一イオン照射を実施し、高速オシロスコープにより照射誘起過渡電流を測定した。

図1に、ソース・ドレイン電極を接地した状態で、MOSFETゲート領域に重イオンを照射した際の、ゲート電極における照射誘起電流および収集電荷量（電流積分値）を示す。なお照射中のゲート印加電圧は、p-, n-MOSFETそれぞれ-10および+10 Vであり、ゲートから電源方向へ流れ出す電流を正方向として表示した。結果より、照射後1ー2 ns程度に酸化膜印加電界方向の鋭い電流ピークが、その後、反対方向の小さな電流がそれぞれ観測されること、また、収集電荷量は照射後数10nsで0に収束することがわかった。以上の結果より、酸化膜を介した重イオン照射誘起電流は、変位電流によるものが支配的であることを確認し。p-MOSFETの場合、照射により基板内で発生した正孔の酸化膜界面での蓄積による酸化膜電界の急速な変化により大きな正方向電流が流れ、これら過剰正孔のドレイン・ソースによる収集により初期状態に戻る際に、逆方向電流が発生したものと考えられる。また、 n-MOSFETの方が短時間・大振幅の電流ピークとなった。これは、正孔に比べて電子の移動度が高いことに起因する。

また、照射誘起ゲート電流のドレイン電圧依存性の評価を行った。その結果、pチャネル，nチャネル形共に、電流ピーク値は照射中に印加したドレイン電圧（絶対値）と共に、大きくなることがわかった。ドレイン電圧印加時には、ドレイン近傍のゲート酸化膜電界はソース近傍に比べて小さくなる（表面電位が大きくなる）。ただし、重イオンが入射されると、照射により発生した高密度の正孔が内部電界により基板表面に引き寄せられ、チャネル部分全体に蓄積されるため、表面電位は場所によらずほぼ同電位になることが予想される。すなわち、ドレイン近傍の酸化膜電界の変化速度は、ドレイン電圧と共に大きくなるものと考えられる。以上のメカニズムにより、重イオン照射誘起ゲート電流のドレイン電圧依存性を説明できることがわかった。

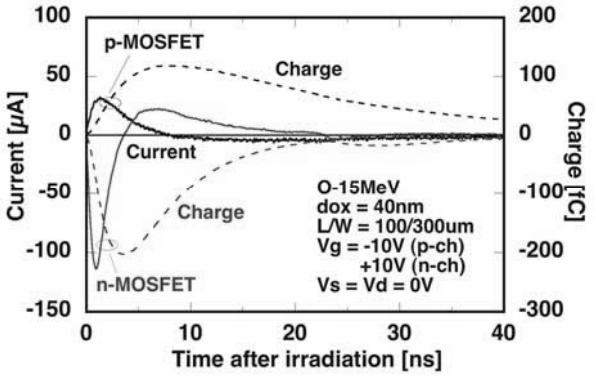

Fig.1 Heavy-ion induced gate currents (solid lines) and collected charges (dashed line) in p- and n-MOSFET.

References

1) T. Hirao et. al.:“Study of single-event current pulses induced in SOI diodes by collimated swift heavy-ions micro-beams,” Nuclear Instruments and Methods in Physics Research B 206（2003）457-461.

2) 高橋芳浩 他:“MOS構造における重イオン照射誘起電流”, 電子情報通信学会論文誌, Vol.J89-C, No.3（2006）pp.104-112.

1-05 Bias Dependence of the Single Event Transient Currents due to Nuclear Products in Semiconductors II

S. Onoda [a)], T. Hirao [a)], T. Ohshima [a)], H. Kaneko [b)] and T. Sanami [c)]

[a)]Environment and Industrial Materials Research Division, QuBS, JAEA,
[b)]Department of Advanced Radiation Technology, TARRI, JAEA,
[c)]Radiation Science Center, KEK

High energy neutrons and protons can trigger Bit Error Rate (BER) degradation in optical data links used in radiation environments[1,2]. It is known that the photodetectors, which are the principle component of optical receivers, are more prone to BER degradation than external encoding electronics. Although the direct ionization results in BER degradation in the photodetectors operated under low optical power level, it is also possible for the secondaries generated by nuclear reactions to induce BER degradation. In silicon based materials, the inelastic as well as elastic reactions generate high-energy secondaries such as He, C, N, O, F, Ne, Na, Mg, Al, Si, P, and recoiling Si atoms with energies up to several tens of MeV. The ionizing energy loss of these secondaries induces a current on the terminal of the photodetector resulting in a Single Event Transient (SET) current that contributes to BER degradation.

In order to clarify the carrier dynamics resulting in the SET currents in Si pin photodiodes due to neutrons, we have measured the SET current induced by energetic heavy ions (C, O, and Si ions) assuming secandaries. Then we have evaluated the bias dependence of the SET characteristics such as collected charge, peak current, fall time and rise time, respectively.

The device examined in this work was a commercial 1.5 GHz (at -3 dB) Si pin photodiode with a diameter of 450 μm. The p-layer width was about 0.2 μm, the depletion width was about 15 μm at -10 V as estimated by the capacitance-Voltage (C-V) and cross-sectional Transient Ion Beam Induced Current (TIBIC) methods. All proton induced SET currents were measured at various biases from -5 to -30 V.

Figure 1 (a, b, c) show the bias dependence of the collected charge, the peak current, the fall time, and the rise time due to C, O, and Si ions with energy up to 15 MeV, respectively. As shown, the charge increases in proportion to ion energy for all ions and does not depend on ion energy. The peak current increases with increasing applied bias although fall time and rise time decrease. These facts show that the higher bias leads to the faster drift velocity of carriers, which results in the higher peak current and shorter fall and rise time. On the other hand, the peak current decreases with increasing atomic number. The most probable reason is that the charge screening effect is influenced considerably when the atomic number incresaes[3].

References

1) E. Petersen, IEEE NSREC Short Course, section III (1997)
2) S. Onoda et al., JAEA Takasaki annual report 2006 (2007) 9
3) S. Onoda et. al, IEEE Trans. Nucl. Sci., vol. 53, no. 6 (2006) 373

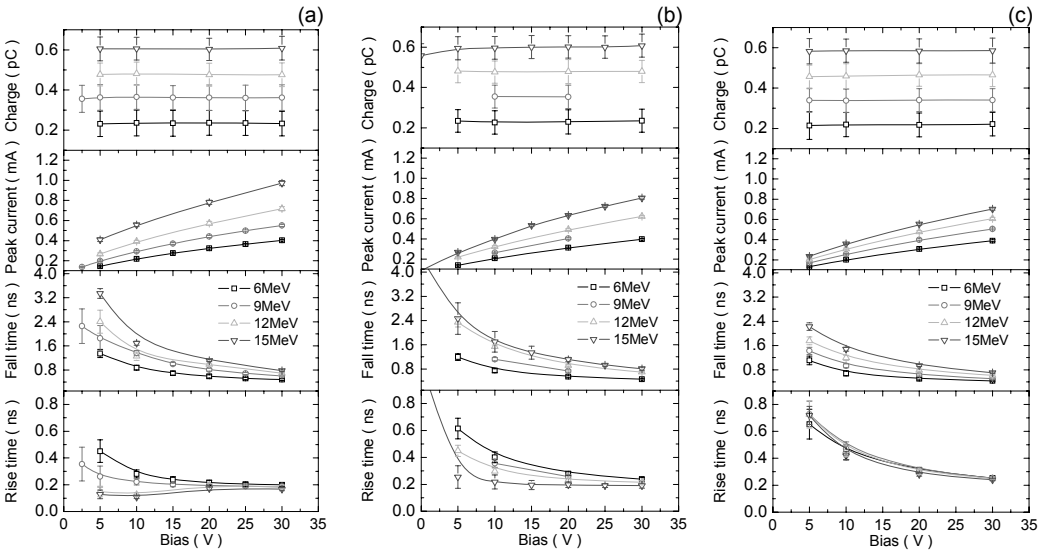

Fig.1 Bias dependence of the SET current characteristics such as the collected charge, the peak current, the fall time, and the rise time induced by (a) C, (b) O, and (c) Si ions with energy up to 15 MeV.

1-06 Study of Charge Induced in 6H-SiC n^+p Diodes by Gold Ion Incidence

T. Ohshima [a)], S. Onoda [a)], S. Hishiki [a)], N. Iwamoto [a,b)], A. Sakamoto [c)], I. Nakano [c)], G. Wagner [d)] and K. Kawano [b)]

[a)]Environment and Industrial Materials Research Division, QuBS, JAEA, [b)]The University of Electro-Communications, [c)]Faculty of Science, Okayama University, [d)] Institute of Crystal Growth

Silicon carbide (SiC) is expected to be applied to particle detectors used in radiation environments since SiC has superior radiation tolerance[1)]. For this purpose, it is important to clarify the behavior of charge generated in SiC by ion incidence. In a previous study [2)], it was reported that the Charge Collection Efficiency (CCE) obtained from 4H-SiC diodes irradiated with alpha particles was 100 %. The CCE of 100 % was also reported for 6H-SiC diodes irradiated with oxygen (O) ions [3)]. These results suggest that SiC is suitable for particle detectors. For the development of particle detectors, the CCE of SiC diodes should be evaluated using a wide variety of ions. In this study, we evaluate charge generated in 6H-SiC diodes by 12MeV-gold (Au) ions.

The samples used in this study were 6H-SiC n^+p diodes fabricated on 30 μm thick p-type epitaxial layer with an aluminum (Al) concentration of $8x10^{14}$ - $1x10^{15}$ /cm^3. The epitaxial layer was grown on a p-type substrate (3.5^o off, Si-face) by chemical vapor deposition. The 100nm thick n^+ region was formed using phosphorus (P) ion implantation (a mean P concentration of $5x10^{19}$ /cm^3) at 800 ^{o}C followed by annealing at 1650 ^{o}C for 5 min in argon (Ar). Al electrodes were formed using a liftoff technique. The diodes were irradiated with 12 MeV-Au microbeams under applied reverse biases, and transient current generated by irradiation of Au ions was measured using the Transient Ion Beam Induced Current (TIBIC) system [4)].

Figure 1 shows the value of collected charge as a function of applied reverse bias. The estimated value of charge generated in the depletion layer (ideal value) is also represented as a broken line. In the estimation, ionizing energies deposited from 12 MeV Au ions into SiC were calculated by Monte Carlo simulation code SRIM2003 [5)]. The energy for the generation of an e-h pair ($E_{e\text{-}h}$) in 6H-SiC is assumed to be 7.8 eV (= $2.8E_g$) on the analogy of $E_{e\text{-}h}$ in Si since the value of the energy for 6H-SiC has not yet been determined. The collected charge of 0.1 pC is obtained and the value does not depend on the applied biases. On the other hand, the ideal value is estimated to be 0.195 pC. Since the depletion layer is estimated to be 5 μm at an applied bias of 20V and the range of 12 MeV-Au is 1.9μm, the obtained result indicates that approximately half of charge generated in the depletion layer is not collected despite under the reverse biases.

The CCEs for 6H-SiC diodes irradiated with 12 MeV-O, silicon (Si), nickel (Ni) ions were also investigated. In the case of O and Si ions, the CCE obtained for this diode showed more than 95 %. On the other hand, the values of the CCE for Ni- and Au-irradiated diodes are 86 and 53 %, respectively. The distributions of e-h pairs were calculated using the method developed by Kobetch and Katz (KK) [6,7)]. As the result, the estimated result indicates that the density of e-h pairs in Au-irradiated SiC is 100 times higher than that in O-irradiated SiC. Therefore, the decrease in the CCE by Au irradiation obtained in this study can be interpreted in terms of the recombination of carriers generated in depletion layer because the recombination of generated carriers might occur in such high dense plasma.

This study was partially supported by the Ministry and Education, Science, Sports and Culture, Grant-in-Aid for Scientific Research (B), 2006, 18360458.

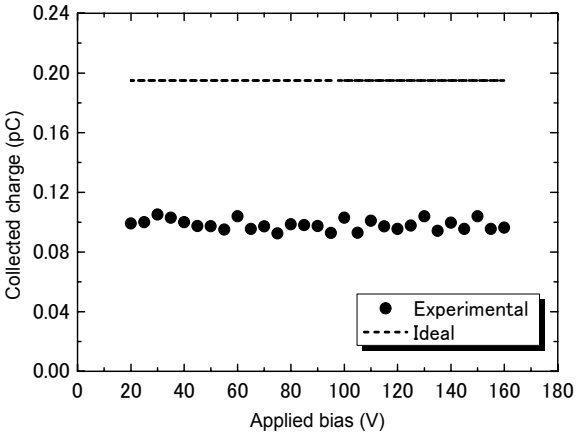

Fig. 1 Value of collected charge obtained for a 6H-SiC diode by 12 MeV-Au irradiation as a function of applied reverse bias.

References

1) T. Ohshima et al.: J. Appl. Phys. 96 (2001) 3038.
2) F. Nava et al.: Nucl. Instr. Meth. A 505 (2003) 645.
3) T. Ohshima et al.: Nucl. Instr. Meth. A 541 (2005) 236.
4) J. S. Laird et al.: Nucl. Instr. and Meth. B 181 (2001) 87.
5) J. F. Ziegler, Handbook of Ion Implantation Technology, Elssevier Science Publishers B.V., The Netherland (1992) pp.1-68.
6) R. Katz et al.: Rad. Eff.and Def. Sol. 114 (1990) 15.
7) E. J. Kobetich, R. Katz: Phy. Rev. 170 (1968) 391

1-07 EPR Identification of Intrinsic Defects in 4H-SiC: Positively-charged Carbon Antisite-vacancy Pairs

T. Umeda [a)], N. Mizuochi [a)], J. Isoya [a)], S. Hishiki [b)], N. Morishita [b)] and T. Ohshima [b)]

[a)]Graduate School of Library, Information and Media Studies, University of Tsukuba,
[b)]Environment and Industrial Materials Research Division, QuBS, JAEA

To improve the radiation hardness of SiC devices, identification of radiation-induced defects are required. We use electron paramagnetic resonance (EPR) technique for microscopic structural identification of intrinsic defects in 4*H*-SiC. To track the angular dependence of the ^{29}Si/^{13}C hyperfine (HF) lines which does lead to decisive structure determination, it is desirable to produce the intrinsic defect of interest selectively at sufficient concentration. We took a sort of defect engineering approach by using various combinations of the temperature and the dose of 2 MeV electron irradiation (1×10^{17}–1×10^{19} e/cm^2), the temperature (400–1200 °C) of heat-treatment after irradiation, and 4*H*-SiC samples (3×10×1.5 mm) of both *n*- and *p*-type of different dopant concentrations.

Carbon antisite-vacancy pair $C_{Si}V_C$, which is one of nearest neighbor carbon atoms moving into the vacant silicon site with a carbon vacancy left, corresponds to a bistable counterpart of silicon vacancy (Fig.1). The negative charge state $[C_{Si}V_C]^-$ which was identified in irradiated *n*-type 4*H*-SiC (2×10^{18} e/cm^2, 800 °C) gives the SI5 EPR spectrum which had been originally observed in HPSI (high-purity semi-insulating) substrates. Thus, $C_{Si}V_C$ is a dominant carrier-compensating, intrinsic defect producing the SI properties. Theoretical studies predicted that the positive charge state $[C_{Si}V_C]^+$ should be much more stable than silicon vacancy in p-type while $[C_{Si}V_C]^-$ should be metastable in *n*-type[2,3)].

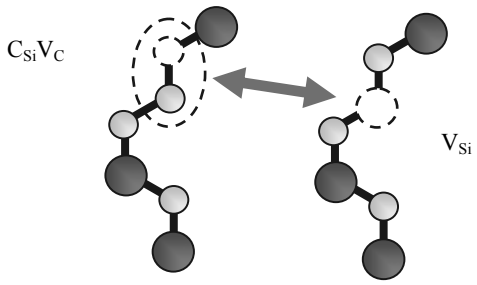

.Fig.1 Bistability of $C_{Si}V_C$ and silicon vacancy (V_{Si})

In the present work, the positive charge state $[C_{Si}V_C]^+$ (S=1/2) has been identified in electron-irradiated *p*-type (B-doped) 4*H*-SiC ($2–10\times10^{18}$ e/cm^2, 800 °C, RT carrier concentration before irradiation ~10^{15} cm^{-3})[4)]. The EPR spectra labeled *HEI*9a/b and *HEI*10a/b (Fig.2) were recorded at 295K on a Bruker E500 X-band spectrometer.

In 4*H*-SiC, both silicon and carbon atoms have two inequivalent lattice sites, hexagonal (*h*) and quasi-cubic (*k*) sites. For each of four spectra, *HEI*9a/b (C_{3v}) and *HEI*10a/b (C_{1h}), the ^{13}C (I=1/2, natural abundance 1.1 %) HF tensor has been determined from the fitting of the angular dependence of the HF lines (See Fig.2 for **B**//*c*). The ^{13}C HF tensors obtained are useful to assign each of four spectra to one of (*hh*, *kk*, *hk*, *kh*) configurations by comparing with the HF tensors of four configurations estimated by *ab initio* supercell calculations. Here, *hh* represents the configuration that both carbon-antisite and carbon-vacancy are *h* sites. The unpaired electron strongly localizes on each C_{Si} atom (55-58 %) with a dominant *p*-character. The angle θ between the *p*-orbital direction and the *c*-axis is 0° for *HEI*9a/b and 109° for *HEI*10a/b. The observed ^{29}Si HF splittings agree with those obtained by *ab initio* supercell calculations[4)].

Observation of four sets of spectra, which all exhibit similar dose dependence and thermal behavior (Fig.3) and are assignable to four configurations (*hh*, *kk*, *hk*, *kh*), respectively, is a strong basis that *HEI*9/10 is arising from $[C_{Si}V_C]^+$.

We apply photo-EPR technique which measures the EPR signal intensity as a function of the wavelength of illuminating light, to determine the defect level in the band gap. It has been determined that the electronic level of $C_{Si}V_C^+$ is located at around E_V+1.4eV.

References

1) T. Umeda *et al*., Phys. Rev. Lett., 96, 145501 (2006)
2) M. Bockstedte *et al*., Phys. Rev. B, 68, 205201 (2003)
3) E. Rauls *et al*., Phys. Rev. B, 68, 155208 (2003)
4) T. Umeda *et al*., Phys. Rev. B, 75, 245202 (2007)

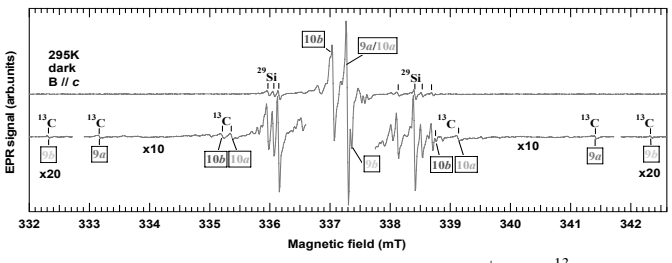

Fig.2 EPR spectra (labeled *HEI*9/10) of $[C_{Si}V_C]^+$. The ^{13}C and ^{29}Si HF lines of *HEI*9a/b and *HEI*10a/b are indicated.

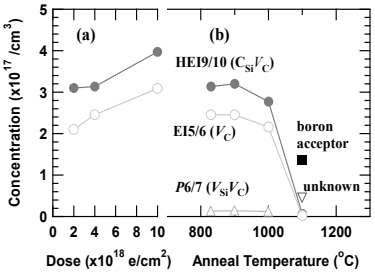

Fig. 3 Dose dependence and anneal-temperature dependence of the concentrations.

1-08 Mechanisms of Decrease in Hole Concentration in Al-doped 4H-SiC by Irradiation of 200 keV Electrons

H. Matsuura [a)], S. Hishiki [b)], T. Ohshima [b)] and H. Itoh [b)]

[a)]Department of Electronic Engineering and Computer Science, Osaka Electro-Communication University, [b)]Environment and Industrial Materials Research Division, QuBS, JAEA

From the temperature dependence of the hole concentration p(T) in Al-doped 4H-SiC epilayers irradiated with 4.6 MeV electrons, we reported that the density (N_{Al}) of a shallow acceptor with Ev + 0.2 eV, which is an Al atom at a Si sublattice site, was significantly reduced, while the density (N_{Defect}) of a deep acceptor with Ev + 0.35 eV was slightly decreased,[1)] as shown by triangles of Fig. 1. Here, Ev is the valence band maximum. In unirradiated epilayers,[2)] on the other hand, $N_{Defect} = 0.6\ N_{Al}$ in a range of N_{Al} between $8x10^{14}$ and $5x10^{16}$ cm^{-3}, as shown by open symbols of Fig. 1.

Since electrons with <0.3 MeV can displace only carbon (C) atoms in SiC whereas electrons with >0.5 MeV displace all the atoms (i.e., C, Al and Si) in SiC,[3)] we investigate the changes of N_{Al} and N_{Defect} in a 10 μm-thick Al-doped 4H-SiC epilayer by irradiation of 200 keV electrons. After the Hall-effect measurement was carried out in the epilayer irradiated with $1x10^{16}$ cm^{-2} fluence, the epilayer was irradiated with $2x10^{16}$ cm^{-2} fluence. Figure 2 shows p(T) denoted by open circles (unirradiated), solid circles (fluence: $1x10^{16}$ cm^{-2}) and solid diamonds (total fluence: $3x10^{16}$ cm^{-2}). At low temperatures, p(T) decreases with increasing fluence, whereas p(T) seems unchanged at high temperatures, indicating that by irradiation of 200 keV electrons the N_{Al} is decreased while the sum of N_{Al} and N_{Defect} is unchanged.

From the analysis of p(T), the values of N_{Al} and N_{Defect} were determined, and are shown as an open circle (unirradiated), a solid circle (fluence: $1x10^{16}$ cm^{-2}) and a solid diamond (total fluence: $3x10^{16}$ cm^{-2}) of Fig. 1. Different from the changes of N_{Al} and N_{Defect} by irradiation of 4.6 MeV electrons, N_{Al} decreases with increasing fluence of 200 keV electrons, while N_{Defect} increases. Moreover, the decrement of N_{Al} is nearly equal to the increment of N_{Defect}. Therefore, the displacement of only C atoms by irradiation of 200 keV electrons is considered to change the Al acceptor into the deep acceptor.

The changes of N_{Al} and N_{Defect} by irradiation at more fluences ($5x10^{16}$ and $7x10^{16}$ cm^{-2}) of 200 keV electrons are now investigated.

References

1) H. Matsuura *et al.*: Appl. Phys. Lett. 83 (2003) 4981.
2) H. Matsuura *et al.*: J. Appl. Phys. 96 (2004) 2708.
3) H. Matsuura *et al.*: Physica B 376-377 (2006) 342.

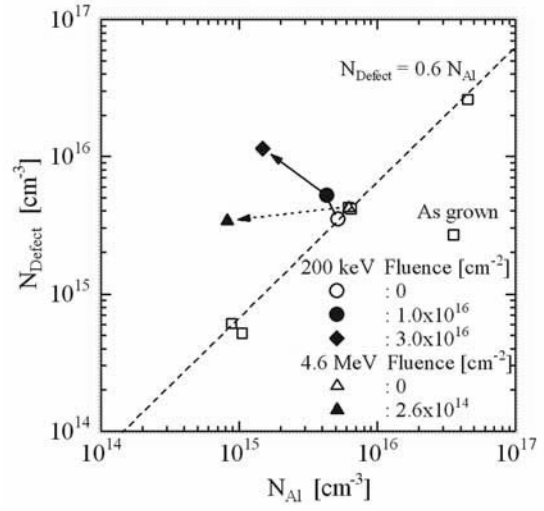

Fig.1 Relationship between N_{Al} and N_{Deep}. The open symbols of squares, circle and triangle are the relationship before irradiation. The solid circle and diamond represent the relationships after irradiation of $1x10^{16}$ and $3x10^{16}$ cm^{-2} with 200 keV electrons, respectively. The solid triangle represents the relationship after irradiation of $2.6x10^{14}$ cm^{-2} with 4.6 MeV electrons.

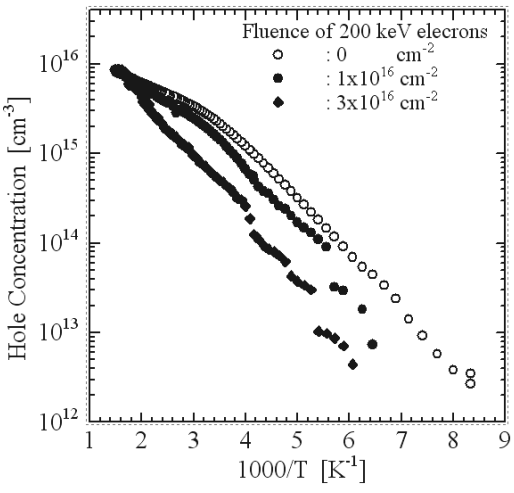

Fig.2 Temperature dependence of hole concentration. The open circles represent p(T) before irradiation, and the solid circles and diamonds represent p(T) after irradiation of $1x10^{16}$ and $3x10^{16}$ cm^{-2} with 200 keV electrons, respectively.

1-09 First-principles Molecular Dynamics Simulation of SiO_2/SiC Interface of Silicon Carbide Devices

A. Miyashita [a)], T. Ohnuma [b)], M. Iwasawa [b)], H. Tsuchida [b)] and M. Yoshikawa [a)]

[a)]Environment and Industrial Materials Research Division, QuBS, JAEA, [b)]Materials Science Research Laboratory, CRIEPI

Silicon carbide (SiC) semiconductor devices are expected to be used in severe environments such as outer space and nuclear power plants. The performance of the SiC MOSFET device is below theoretically expected levels because the defect in SiO_2/SiC interface degrades the electrical performance of the device. The relation among atomic structures, interface defects and electrical characteristics is not clear at present. In this study, we tried to solve these problems by the computer simulation of electronic structure of the SiO_2/SiC interface. It is important to construct an amorphous SiO_2 (*a*-SiO_2) structure on SiC to emulate the real device interface structure by the computer simulation because the oxide layer of the real device is an amorphous structure. We aimed to generate *a*-SiO_2/SiC structure with large-scale (1000 atoms scale model) calculation to which the amorphous structure was able to be constructed.

Amorphous SiO_2/SiC interface structure is made by applying the heating and quenching calculation that uses the first-principles molecular dynamics code VASP[1)] (Vienna ab-initio Simulation Program) to the atomic interface structure model that consists of SiC crystal substrate and crystalline SiO_2 thin layers. The heating and quenching calculation of 444 atoms of SiO_2/SiC interface structure that had been done last year used the condition of 3.0 ps heating by 4000 K and the cooling speed of -1000 K/ps. It was confirmed that the SiO_2 layers of the interface structure were almost amorphous structure.[2-3)]. The atomic density of the interface structure was obtained in the direction of the perpendicular of the interface. (Fig.1) In the SiO_2 layers near the interface, a periodic change of the density that reflects the crystalline structure was not seen; therefore, these layers are good amorphous structures. However, the density of the SiO_2 layers near the surface shows a periodic density change. It is guessed that the recrystallization occurred from the surface in the quenching process because the crystalline structure remained near the SiO_2 surface. It was suggested that the continuance annealing is necessary.

The generation of *a*-SiO_2/SiC interface structure was tried by using the large scale model that consisted of 1017 atoms.

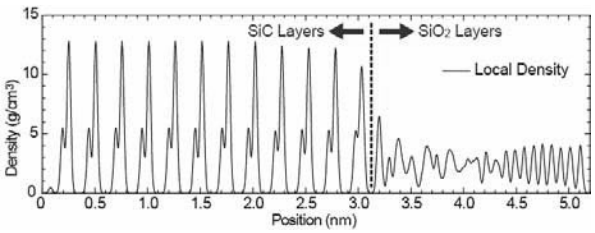

Fig.1 The atomic density of the 444 atoms of SiO_2/SiC interface structure at room temperature.

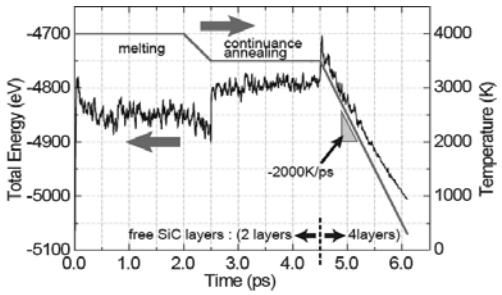

Fig.2 The temperature condition of the heating and quenching process and the total energy of the interface structure model.

In the large scale model, the following conditions were used to improve the amorphous structure near the surface. Figure 2 shows the temperature condition of the heating and quenching process and the total energy of the interface structure model. The SiO_2 layer has melted being heated by 2 ps at the temperature of 4000K on the condition of fixing SiC layers except 2 interfacial layers, surface Si of SiO_2 layers and H that terminate surface Si. The interface structure has been cooled down to the temperature of 3500K. After the removal of H and release of surface Si, the interface structure was continuously annealed for 2 ps. Then the interface structure was quenched to the room temperature. It was confirmed that the recrystallization had not occurred in the quenching process because the periodic change of density had not been observed after the interface structure had been quenched to the room temperature. As a result of the radial pair distribution function (RDF) analysis of the SiO_2 layers, the bond length and the bond angle of Si and O have been obtained. The Si-O bond length, the Si-O-Si bond angle, and the O-Si-O bond angle of the SiO_2 layers are 0.165 nm, 135 deg, and 109 deg, respectively. There is a small peak about 0.23 nm in partial RDF of Si and Si. This means the Si-Si bonding actually exists in SiO_2 layers as a defect structure. The short range order of the bond length and the bond angle obtained from the result of the analysis of these partial RDF has suited the condition of *a*-SiO_2. Therefore, it was confirmed that an excellent *a*-SiO_2/SiC interface structure was generated by heating and quenching calculation.

References

1) G.Kresse et al., Phys. Rev. B54, (1996) 11169.
2) A.Miyashita et al., Annual Report of the Earth Simulator Center Apr.2005-Mar.2006, (2006) 287.
3) A.Miyashita et al., Materials Science Forum 556-557, (2007) 521.

1-10 Development of Optoelectronic Devices for Radiation Environments - Optical Gain of Eu Implanted AlGaN -

A. Wakahara [a)], H. Okada [a)], F. Oikawa [a)], H. Kawai [a)], T. Shimojyo [a)], T. Ohshima [b)] and S. Sato [b)]

[a)]Department of Electrical and Electronic Engineering, Toyohashi University of Technology,
[b)]Environment and Industrial Materials Research Division, QuBS, JAEA

Temperature dependent luminescence and the optical gain of AlGaN doped with Eu ions are investigated for demonstrating the capability of rare-earth doped light emitting devices for radiation and/or hard environments. The Eu related photoemission, caused by 4f inner shell transitions, shows excellent thermal stability and even at 400K the luminescence intensity is more than 50% for low temperature (10K) case. Optical gain and loss measurements are carried out using variable stripe length and shifting excitation spot methods, respectively. The estimated optical gain is as high as 100 cm^{-1}, which is comparable to that reported molecular-beam-epitaxy grown GaN:Eu sample.

現在のSi系集積回路技術は、微細加工技術・集積化技術により高度な機能と高速動作を実現してきた。放射線環境下に対しても、SOI技術の導入により問題解決が進められつつある。信号伝達の観点からは、宇宙空間に於いても光通信が有望とされているが、光源として用いられている少数キャリアの再結合による発光デバイスは放射線損傷の影響を強く受けるため、その寿命、信頼性など解決すべき問題が多い。本プロジェクトでは、耐熱性・対放射線に優れ、環境温度の変化により発光波長、発光効率が影響を受けにくい希土類イオンを発光中心として導入したIII族窒化物半導体を用いて、多数キャリアベースの発光デバイス実現の可能性を検討した。

AlGaN発光層への希土類添加は、原子力機構・高崎研のイオン注入装置を用いて、加速電圧100～350 keV、ドーズ量1×10^{13} cm^{-2}～8×10^{15} cm^{-2}とし、室温にてEuを注入した。イオン注入後、窒素抜けを防ぐためNH_3を含むN_2雰囲気中にて、1100 ℃、2minのアニールを行い注入損傷の回復を図った[1)]。

Rutherford Back-Scattering(RBS)測定より推定したEuイオンの結晶中での位置は、Euからの散乱はチャネリング条件に於いてもランダム配置の7割程度の散乱強度があり、格子間位置を占めるEuが多数有ることを示している。一方、Extended X-ray Absorption Fine Spectra(EXAFS)の解析結果からは、EuはGaサイトを占めるとの結果が得られており[2)]、両者が共存していると思われる。

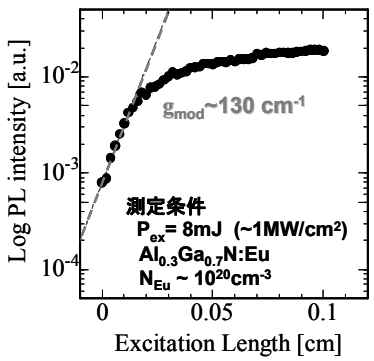

Fig.1 Optical gain measurement for $Al_{0.3}Ga_{0.7}N$:Eu at 300K. The Eu dose was 1×10^{15} cm^{-2}. The excitation power density was ~1 MW/cm^2.

発光特性の耐温度特性評価は、ArFエキシマレーザ(193 nm、100 J/cm^2・pulse)を励起光光源として用いたホトルミネセンス法により10Kから400Kの範囲で行った。発光強度の測定温度依存性は極めて小さく、Al組成がx>0.3の試料では、400Kに於いても10Kでの発光強度の50%以上の強度を維持しており、チップ温度が大きく変化する環境下での光デバイスの発光層として十分な安定性を有している。

次に、Eu添加AlGaNの発光デバイスとしての可能性を検証するため、光増幅率および伝搬損失の評価を行った。光増幅率は、Variable Stripe Length(VSL)法[3)]を用いて求めた。伝搬損失は、Shifting Excitation Spot (SES)法により求めた。Fig.1に測定結果を示す。イオン注入法を用いて、活性層厚が50nm程度と非常に薄いにも係わらず100 cm^{-1}を越える大きな光増幅率を示し、伝搬損失も10 cm^{-1}以下と十分小さく光増幅器およびレーザへの応用が十分可能な特性が得られている。ここで得られた結果は、分子線エピタキシャル成長法により作製された高品質なGaN:Euで報告されている値[4)]と同程度以上の特性が得られており、イオン注入法を用いた新しい半導体発光デバイスプロセスへの展開が期待される。

References

1) A. Wakahara, Optical Materials, 28 (2006) 731
2) H. Ofuchi et al., Physica B, 376-377 (2006) 496
3) K. L. Shaklee et al., J. Lumin. 7 (1973) 284
4) J. H. Park et al., Appl. Phys. Lett., 85 (2004) 4588

1-11 Gamma Radiation Effects on GaN Based Electron Devices

H. Kameoka [a)], M. Okada [a)], J. P. Ao [a)], Y. Ohno [a)] and T. Hirao [b)]

[a)]Institute of Technology and Science, The University of Tokushima,
[b)]Environment and Industrial Materials Research Division, QuBS, JAEA

GaN electronic devices, especially AlGaN/GaN Heterostrure Field Effect Transistor (HFETs), are expected for high-frequency and high-power applications due to wide-bandgap and III-V semiconductor characteristics [1, 2]. Since the application includes power module and microwave power transmission for space solar power system, the employment of GaN-based devices in artificial satellite in space is being considered. The purpose of this research is to investigate the tolerance of these devices under γ-ray irradiation in space and other harsh environment [3-5].

The sample AlGaN/GaN HFETs were fabricated on (0001) sapphire substrate. It consisted of a buffer layer, a 3 μm undoped GaN layer, a 6 nm undoped AlGaN barrier, a 12 nm Si-doped AlGaN layer with doping concentration of 4×10^{18} cm^{-3}, and a 6 nm undoped AlGaN barrier layer (Fig. 1). The Al mole fraction of all the AlGaN layers was 25 %. Ohmic contact was formed using lift-off technique with electron-beam-evaporated Ti/Al/Ni/Au (50/200/40/30 nm). They were annealed at 850 ºC for 1 minute in N_2.

The samples were irradiated with Co sources at JAEA Takasaki. The total dose of γ-ray was 8.9 Mrad and 86.7 Mrad at the dose rate of $1x10^6$ rad/h. The channel length and width of the measured transistor was 4 μm and 50 μm, respectively.

If the FETs are damaged, variations will appear in the gate leakage current, threshold voltage or carrier drift mobility. As shown in Fig. 2, each sample has inherently different gate leakage currents, but they did not change after the irradiation. Also, the threshold voltages did not change. Only the difference was the increase of drain current (I_D).

Converting drain voltage (V_D) versus drain current characteristics into drain voltage versus drain conductance (G_D) characteristics, it was found that the variation was only in low drain voltages and a constant resistance variation regardless of the gate bias. From these facts, the variation is attributable to improvement in the ohmic contact by γ-ray irradiation. The annealing in the fabrication process may have been insufficient. [6]

Radiation experiments under a DC bias condition were done on different Metal-Insulator-Semiconductor (MIS) HFET. The FET has 10nm SiN on AlGaN layer deposited by sputtering. DC bias of -9V was applied to the gate electrode while the drain terminal was kept open.

After irradiation of γ-ray at 1 Mrad, no particular variation was observed except for small ohmic contact improvement similar to the previous experiment (Fig. 3).

Although material and process technologies for AlGaN/GaN HFETs have not yet been well controlled and the performance variations exist even without radiation, no particular degradation was observed even under extremely high dose irradiation of 87 Mrad.

References

1) Y. F. Wu, et al., IEEE Trans Electron Dev., 48, 586 (2001).
2) J. P. Ao, et al., IEEE Electron Dev. Lett., 24, 500 (2003).
3) C. W. Wang, et al., J. Appl. Phys., 88, 6355 (2000).
4) B. Luo, et al., Appl. Phys. Lett., 80, 604 (2002).
5) O. Aktas, et al., Solid-State Electronics, 48, 471 (2004).
6) J.P. Ao, et al., SSDM 2005, pp.478-479, Kobe(2005).

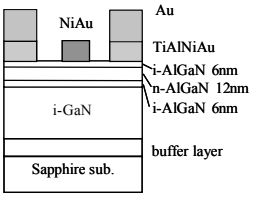

Fig. 1 Schematic cross section of sample AlGaN/GaN HFET.

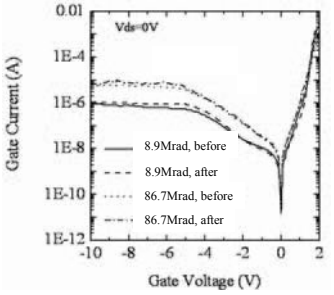

Fig. 2 Gate leakage current before and after irradiation of γ-rays at 86.7 Mrad and 8.9 Mrad. No bias was applied. Drain to source voltage(Vds) was zero.

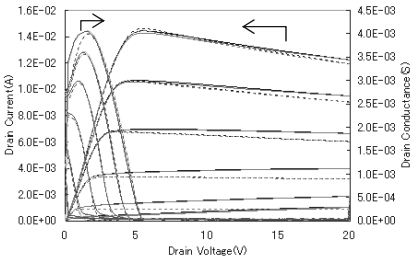

Fig.3 I_D-V_D and G_D-V_D characteristics of the MISHFET, before and after 1 Mrad irradiation under the gate bias of –9V.

1-12 Study of the Radiation Damages of Practical Used Semiconductor Devices

H. Ohyama [a)], S. Kuboyama [b)] and T. Hirao [c)]

[a)]Kumamoto National College of Technology
[b)]Institute of Aerospace Technology, Japan Aerospace Exploration Agency(JAXA)
[c)]Environment and Industrial Materials Research Division, QuBS, JAEA

In this report, the impact of radiation damage on the device performance of 4H-SiC Metal Semiconductor Field Effect Transistors (MESFETs) and GaAlAs Light Emitting Diodes (LEDs) are investigated under different fluence and fluence rate conditions.

4H-SiC MESFETs were fabricated on 4H-SiC semi-insulating wafers with an epitaxital layer produced by CREE. The length and width of the gate were 0.5 and 100 μm, respectively. GaAlAs-double hetero junction-LEDs (Sharp GL3UR44) with light wavelength 660 nm were also used in this study.

Electron irradiations into the samples were done at room temperature using the 2-MV electron accelerator at JAEA, Takasaki. The used electron fluence ranged from 1 x 10^{13} to 1 x 10^{17} e/cm^2. Before and after irradiation, the input drain-source current/Gate-souce voltage characteristics (I_{DS}-V_{GS}) of the SiC-MESFETs and I/V characteristics of the GaAlAs LEDs were measured with a parameter analyzer (HP-4156).

To investigate the recovery behavior due to annealing of radiation damage, isochronal thermal annealing was carried out for 15 min at temperatures between 100 and 300 ^{o}C under nitrogen flow without bias.

Figure 1 shows the annealing rate of I_{DS} as a function of annealing temperature for thy MESFETs irradiated with electrons at 5x10^{16} e/cm^2. Assuming that the recovery process is a first order reaction, the activation energy of the recovery is estimated from Fig.1 to be 0.27 eV.

Figure 2 shows the typical results of I/V characteristics for different electron fluence rates (4.68 x 10^{11} and 4.68 x 10^{12} e/cm^{2}sec). Total fluence was selected for 1 x 10^{15} e/cm^2. From this figure, it is noted that the remarkable degradation is observed for low dose rate condition than for high rate irradiation. This fluence rate dependence of degradation can be explained in terms of the heat impact in bulk crystal during irradiation.

References

1) C. Claeys and E. Simoen,, Springer Verlag, New York (2002).
2) H. Ohyama et. al., Physica B, **376-377**, 382 (2006).
3) H. Ohyama et. al., to be published in Journal of Materials Science.

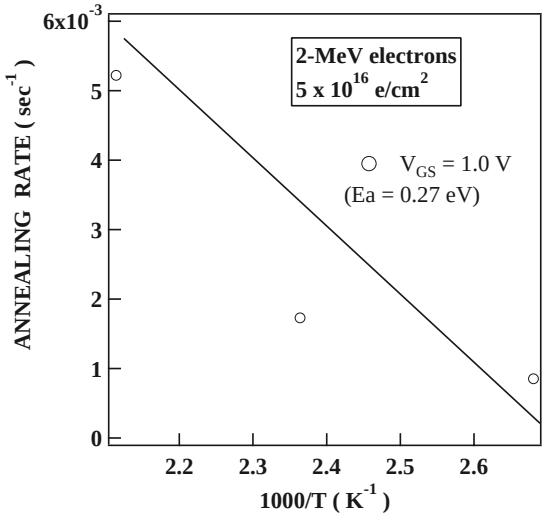

Fig.1 Annealing rate of I_{DS} as a function of annealing temperature for SiC-MESFETs.

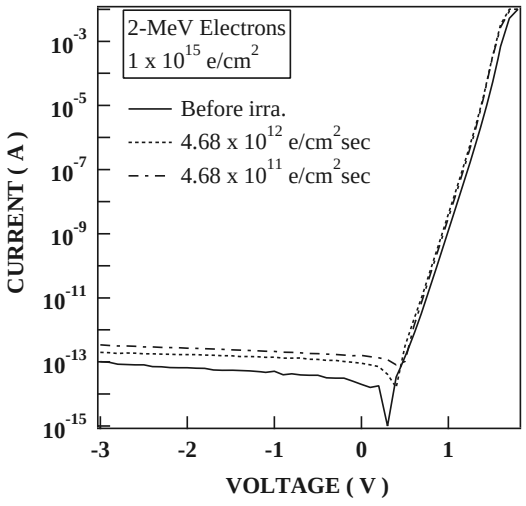

Fig.2 I/V characteristics of electron-irradiated GaAlAs LEDs at different fluence rates.

.

1-13 Radiation Resistance of Insulating Material for ITER Superconducting Coil -Gas Evolution-

A. Idesaki [a)], N. Koizumi [b)], M. Gokan [a)], N. Morishita [a)], M. Sugimoto [b)], T. Ohshima [a)] and K. Okuno [b)]

[a)]Environment and Industrial Materials Research Division, QuBS, JAEA
[b)]ITER Project Unit, FRDD, JAEA

A laminated material composed of glass cloth / polyimide film / epoxy resin will be used as an electrical insulating material in the superconducting coil of the International Thermonuclear Experimental Reactor (ITER). This material is fabricated by impregnation of epoxy resin into a glass cloth / polyimide film prepreg and subsequent curing. Therefore, the viscosity and pot-life (time to cure the resin) of the epoxy raw material are very important for the fabrication of the insulating material. In addition, sufficient mechanical and electrical properties are required. Moreover, the insulating material must show high radiation resistance and thermal resistance, because it will be exposed to severe environments such as high radiation field and low temperature of 4K.

In this work, the gas evolution from laminated materials by gamma ray irradiation at 77K was investigated, and the difference of gas evolution behavior due to difference of components in the epoxy resin was discussed.

Two kinds of the laminated materials with different components of epoxy resin were investigated (Table 1). Each sample was put into a glass tube, and the glass tube was evacuated and sealed. The samples were irradiated by gamma rays up to dose of 30 MGy as maximum at a dose rate of 37.5 kGy/h at 77K, and then the gas analysis was conducted by a gas chromatograph at room temperature after storage of the samples at room temperature for 16 hours.

Figure 1 shows the evolved gases from the laminated materials by the irradiation of gamma rays at 77K. The total amount of evolved gas increased almost linearly with increasing in the dose. Main components of the evolved gases were hydrogen (H_2), carbon monoxide (CO) and carbon dioxide (CO_2). Hydrocarbon gases such as methane (CH_4) were evolved as minor components with an order of 10^{-8}-10^{-7} mol/g. We have investigated the gas evolution from a polyimide film by the irradiation of gamma rays at 77K[1)]. It was found that the total amount of evolved gases was in an order of 10^{-9}mol/g. Therefore, the gas evolution from the laminated materials shown in the Fig. 1 is attributed by decomposition of the epoxy resin. Comparing the sample A with the sample B, the amount of the evolved gases from the sample A containing cyanate ester was about 60 % less than that from sample B containing TGDDM. This suggests that the insulating material for the superconducting coil with low gas evolution can be obtained by using the cyanate ester as a raw material for epoxy resin.

Table 1 The components of epoxy resin used in this work.

Sample	Components of epoxy resin
A	DGEBF + Cyanate Ester
B	DGEBF + TGDDM

DGEBF : Diglycidyl ether of bispehnol F

TGDDM :N,N,N',N'-tetraglycidyl-4,4'-diaminophenylmethane

Reference

1) A. Idesaki, et al., *Advances in Cryogenic Engineering*, Vol. 52(2006)pp.330-334.

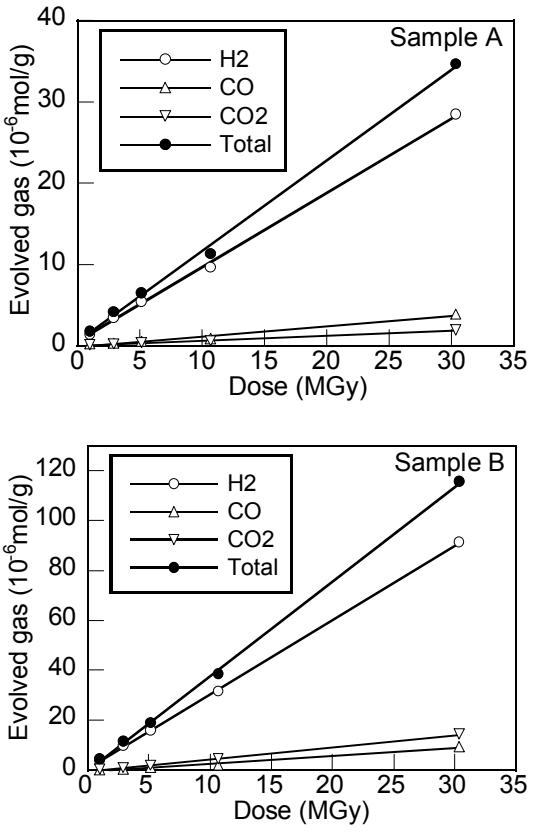

Fig.1 The evolved gases from the laminated materials by the irradiation of gamma rays at 77K. The measurements were conducted at room temperature after storage at room temperature for 16 hours.

1-14 Gamma-ray Irradiation Test of Instrumentation and Operational Amplifier for Remote Maintenance System of ITER

N. Takeda [a)], S. Kakudate [a)], N. Oyake [a)], M. Nakahira [a)], K. Shibanuma [a)], A. Idesaki [b)], M. Gokan [b)], N. Morishita [b)], S. Baba [c)], H. Okamoto [c)] and T. Hirose [c)]

[a)]ITER Project Unit, FRDD, JAEA, [b)]Environment and Industrial Materials Research Division, QuBS, JAEA, [c)]Ryoei Technica Corp.

Components in the vacuum vessel of the ITER, an experimental fusion reactor to be constructed under international cooperation from this year, must be replaced remotely for maintenance because neutrons created by D-T fusion reactions activate structural materials. The radiation environment during the maintenance operation is about 0.5 kGy/h and therefore, the total dose is 1 MGy if the maintenance operation takes three months. The irradiation test has been performed for the components of the ITER remote maintenance system[1, 2] and the present report describes the irradiation test of the instrumentation and operational amplifiers for strain gauges in order to examine which amplifier on the market can be used from the viewpoint of radiation-hardness. The tested amplifiers include the rad-hard products whose guaranteed acceptable dose is about 1 kGy.

Table 1 shows the list of tested instrumentation and operational amplifiers. Bipolar amplifiers were mainly selected because they are expected as rad-hard from theoretical point of view. The dose rate in the irradiation test was almost the same value as that in the real environment of the ITER maintenance operation, 0.5 kGy/h. The amplifiers were irradiated for a certain period with bias current and after that they were took out from the cell for the measurement of their electrical characteristics such as input bias current, offset voltage, gain and so on. This cycle of irradiation and measurement was repeated.

First, a preliminary irradiation test was performed with the total dose of 20 kGy for screening. As a result, three kinds of amplifiers (AD524CD, HA1-5104-2 and HS1-5104ARH-Q) still operated normally although some of characteristics were slightly out of specification. Regarding other amplifiers, AD623BR and LT1078CN8 malfunctioned at 0.25 kGy. One of rad-hard amplifiers, RH1078MH, had functioned until 2 kGy, which is higher than the guaranteed value of 1 kGy, with some of characteristics deviating from specification and malfunctioned at 9 kGy.

Next, the irradiation test was performed until 417 kGy for the three amplifiers which functioned in the preliminary test. The instrumentation amplifier, AD524CD, had functioned until 56 kGy with some of characteristics deviating from specification, and malfunctioned at 169 kGy. The normal operational amplifier, HA-5104-2, had functioned until 169 kGy with some of characteristics deviating from specification, and malfunctioned at 417 kGy. The rad-hard operational amplifier, HS1-5104ARH-Q, had functioned without deviation of characteristics from specification until the guaranteed value, 1kGy, and had continued to function from 2 kGy till 417 kGy with some of characteristics deviating from specification. Figure 1 shows the transition of the open loop gain of HS1-5104ARH-Q during irradiation. The broken and dotted lines show the reference sample and specification, respectively. The gain showed the minimum value around 10 kGy, recovered after that and decreased again from 169 kGy. The deviation from specification is generally limited and therefore, this amplifier can be used until 0.4 MGy exceeding the guaranteed value, 1 kGy. The normal operational amplifier can be also used if it is replaced enough frequently. Regarding HS1-5104ARH-Q, its acceptable total dose will be investigated in the future study.

Table 1 List of tested amplifiers

Name	Provider	Type	Guaranteed Radiation hardness
AD623BR	Analog Devices	Instr.	No
AD524CD	Analog Devices	Instr.	No
HA1-5104-2	Intersil	Op.	No
HS1-5104ARH-Q	Intersil	Op.	1 kGy
LT1078CN8	Linear Technology	Op.	No
RH1078MH	Linear Technology	Op.	1 kGy

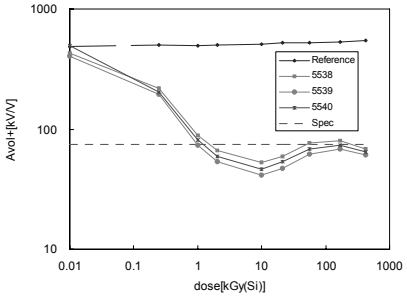

Fig. 1 Open loop gain of HS1-5104ARH-Q

References

1) K. Obara et al., JAERI-Tech 99-003 (1999).
2) K. Obara et al., J. Robot. Mechatron. Vol. 10, No. 2 (1998) pp. 121-132.

1-15 Development of Radiation Resistant O-ring for Vacuum Use

T. Ogitsu [a)], N. Kimura [a)], A. Idesaki [b)], J. Kusano [c)] and T. Tabasaki [d)]

[a)]KEK, High Energy Accelerator Research Organization, [b)]Quantum Beam Science Directorate (QuBA), JAEA, [c)]J-PARC Center, JAEA, [d)]Hayakawa Rubber Co. Ltd.

A superconducting magnet system is required for J-PARC Neutrino beam line to bent the 50 GeV 750 kW proton beam. The magnet system consists of about 150 m long vacuum vessel system to provide the thermal isolation for the superconducting magnet. The vacuum vessel system requires a lot of o-rings, of which size can be as large as 1 m diameter. Conventional o-rings, which uses the materials like fluoroelastomer (FKM), do not have sufficient resistance against radiation for long term use. High radiation resistant o-rings, such as metal o-rings, have demerits in costs or handling. Similar problems exist at the expansion joint sealants of the J-PARC accelerator tunnels. JAEA and Hayakawa Rubber Co. Ltd. jointly develop the new sealants based on the ethylene propylene diene monomer (EPDM) rubber. The new o-ring that can resist the irradiation up to 1 MGy has been developed jointly by KEK, JAEA, and Hayakawa Rubber Co. Ltd. based on the EPDM similar to that used for the expansion joint sealant. This report summarizes the irradiation tests performed for this o-ring material.

The samples were irradiated with γ ray at the Cobalt-60 irradiation facility in Takasaki Advanced Radiation Research Institute, JAEA. The irradiations were made up to 5 MGy at room temperature with air environment. The mechanical tests based on the Japanese Industrial Standard (JIS) were performed for the samples. The mechanical tests include measurements of hardness (JIS-K6253), tensile stress (JIS-K6251), and compression set (JIS-K6262). The measurement was made for the samples irradiated to 0, 1, and 3 MGy. The out gas measurements of the samples were also made for the samples irradiated to 0 and 1.25 MGy.

The measurement results of the compression set are shown in Fig. 1. The FKM sample was destroyed after 1 MGy irradiation and no data was available. All the EPDM samples show good results not only in compression set but also all the mechanical measurements, indicating that the EPDM can be used as o-rings up to 1 MGy irradiation.

The results of the out gas measurement are shown in Fig.2. The results indicate that one of the EPDM sample (517) shows a good performance. We selected the sample 517 as the final candidate from the measurement results shown here as well as the good processability. The final products use the same EPDM as 517 but with small modification of final process. The EPDM was renamed to 517LT, and were tested for both mechanical and out gas measurements. The mechanical measurements results show better performance than those of 517. The out gas measurement results were not as good as the one for 517, but still acceptable from the requirement.

The o-rings are now in the stage of mass production and will be installed in the magnet system. The magnet system will be completed in the end of 2008 and operated in 2009.

Reference

1) S. Nakatsukasa et. al., Journal of the Society of Rubber Industry, Japan Vol.79 (2006) pp 11-16

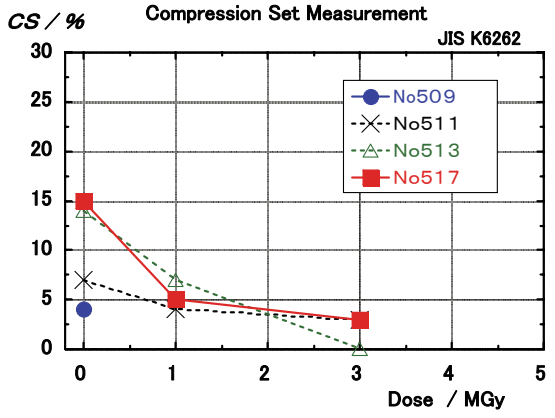

Fig.1 JIS-K6262 Compression set measurement results. No.509 is the FKM sample, which destroyed at 1 MGy irradiation. The other samples are EPDM based.

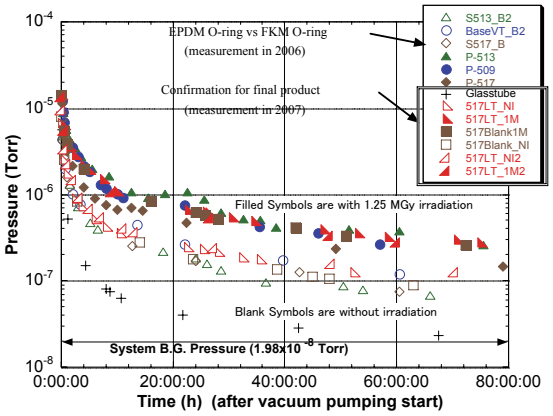

Fig.2 Out gas measurement results, BaseVT and the P-509 are the FKM, the others are EPDM. The material chosen for the final products is 517LT.

1-16 Measurement of Electrical Property Change in Commercially Available Coaxial Cable by Gamma-ray Irradiation

J. Kusano [a)], O. Takeda [a)], N. Morishita [b)], K. Takano [c)], S. Ukon [c)] and F. Suzuki [c)]

[a)]Accelerator Division, J-PARC, JAEA, [b)]Environment and Industrial Materials Research Division, QuBS, JAEA, [c)]Engineering Department, Industrial & Telecommunication Cable Division, Fujikura Ltd.

Introduction

Coaxial cable is an essential element for a communication tool in a precise measurement system because of stable characteristic impedance and electrical noise proof performance. The J-PARC[1)], a research facility complex with high-intensity proton accelerators, apply a plenty amount of coaxial cables to make good telecommunications regarding to the proton beam circumstance, the accelerator status, RF signal control and the safety issues. The proton beam power of the J-PARC is up to 1 MW on the target, which introduces the high radiation area along the proton beam line and close to the target region caused by undesirable beam loss of the accelerators. We measured the electrical property change in the commercially available coaxial cable under the high dose rate gamma-ray irradiation to confirm the reliability of the control and the data acquisition tool of the J-PARC.

Measurement

A pair of 40 m long coaxial cables (Fujikura NH-8D-SFA) was prepared as a race-track shape to compare the difference between a fresh cable and an irradiated cable. The irradiated cable is 3MGy pre-dosed by gamma-ray. Both cables are tied up and installed in the cell facing the Co-60 gamma-ray source on even dose condition, and the characteristics are measured alternatively. The dose rate of the gamma-ray is chosen 6.3 kGy/h to simulate the high radiation spot in the J-PARC. The measured items are insulation resistance, RF attenuation, phase shift, time delay, charge up and characteristic impedance.

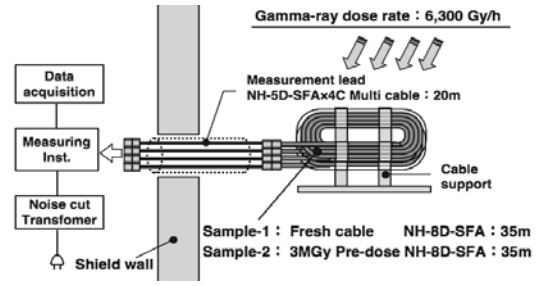

Fig.1 Coaxial cable irradiation and measurement set up. Fresh cable and 3 MGy pre-dose cable were bind up with contact and examined alternatively in same dose condition.

Result

1) No gamma-ray run as static characteristics

Slightly degradation, range of a few percent, was observed for RF attenuation, phase shift, time delay and characteristic impedance on the 3 MGy pre-dose cable caused by increasing capacitance and dielectric constant shift at the insulator material. The insulation resistance between the inner conductor and the outer conductor decreased in the pre-dose cable by 20 % of the fresh one. The absolute value of the resistance still remains at the normal use level.

2) High gamma-dose run as dynamic characteristics

In the high radiation condition, the property of the pre-dose cable shows a constant deterioration for phase shift, time delay and characteristic impedance by several percent. The RF attenuation was -40 dB/km at GHz band. The charge up phenomenon was observed both the fresh cable and the pre-dose cable. Potential difference between the inner conductor and the outer conductor was measured during the gamma-ray irradiation period. The charge up voltage fluctuated through the beginning to the several minutes after the irradiation period[2)]. These phenomena affect like a common mode noise to the control and the beam monitoring system of the J-PARC.

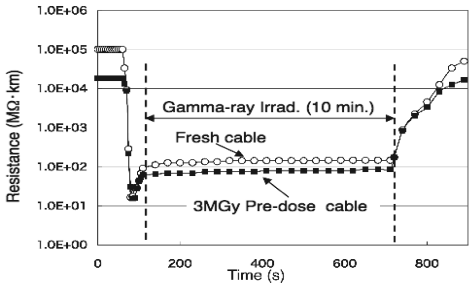

Fig.2 Insulation resistance between the inner and outer conductor behavior around 10 minutes exposure.

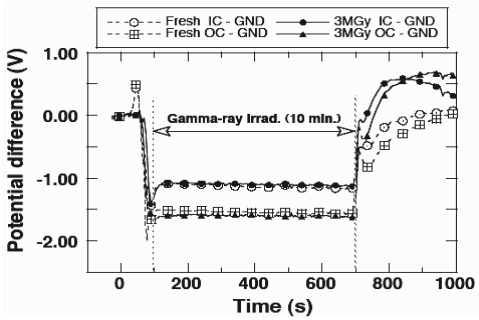

Fig.3 Potential difference behavior between the conductors and ground potential induced by charge up around the 10 minutes exposure. IC denotes the inner conductor and OC denotes the outer conductor in the figure caption.

References

1) S. Nagamiya, Proc. International Radiation Shielding (ICRS-9), J. Nucl. Sci&Technol., Supplement 40 (2000)
2) Y. Tanaka *et. al*., Proc. Annual Rep. CEIDP (1998) 629

1-17 Research on Radiation Resistance of Grease, etc. for Reprocessing Cell Equipment

N. Okamura [a)], H. Ogino [a)], Y. Arai [a)], T. Kase [a)], T. Koizumi [a)],
A. Idesaki [b)], N. Morishita [b)], T. Oshima [b)] and T. Kojima [c)]

[a)]Nuclear Cycle Engineering Department, NFCEL, JAEA, [b)]Environment and Industrial Materials Research Division, QuBS, JAEA, [c)]Department of Advanced Radiation Technology, TARRI, JAEA

In the nuclear cycle engineering department of JAEA, an innovative centrifugal contactor system has been developed for an advanced aqueous reprocessing of FBR fuel [1)]. The centrifugal contactor would be one of the key equipments to establish better reprocessing economy because of its compact size and rapid processing performance. It was already confirmed that it had a higher extraction capacity through the uranium test [2)]. Furthermore, in a cold experiment, the driving unit with ball bearing and grease had been operated continuously for 5000 hours that was equal to a term of an annual operation in the reprocessing plant. In this study, the equipment was operated under gamma-ray irradiation, and the durability of the driving unit was confirmed under the simulated reprocessing plant atmosphere with mechanical load, nitric acid and radiation.

The schematic diagram of experimental equipment is shown in figure 1. Generally, the extraction process consists of several centrifugal contactors, but this was one stage with a liquid self-circulation system because of the restriction of Co-60 gamma-ray irradiation facility. Two kinds of greases, RG-42R-1 and GK-1, were chosen from the viewpoint of radiation and heat resistance. The significant difference between them was that GK-1 contained MoS_2 as a solid lubricant to extend the lifetime. In a series of irradiation experiments, 900mL of nitric acid and 400mL of n-dodecane with the TBP concentration of 30% were poured into it. The exposure rate (72C/kg/h) in this irradiation facility was about ten times higher than that in the reprocessing cell, so the irradiation time was set 500 hours.

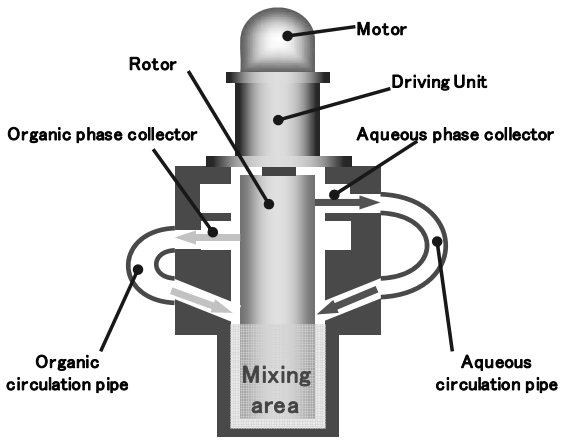

Fig.1 Schematic diagram of experimental centrifugal contactor

After these experiments, the rate of base oil, the nitric acid concentrations and the fragment concentration in grease were measured. These measured values were not different from ones in the cold endurance experiment. These results showed that the driving units by using these greases had abilities to be operated continuously and no additive damages to ball bearings and greases was caused by combining mechanical load, nitric acid and radiation.

Furthermore the differential thermal analysis was adopted to evaluate grease degradation. Previously, the gel permeation chromatography and the infrared spectroscopy were used for the evaluations, which requested all of grease left in the ball bearing after the operation. This new method had some advantages, such as a small amount of sample and a simple pretreatment. The results of measurements are shown in figure 2. It was found that the variation of GK-1 was larger than that of RG-42R-1 in molecular weight. The reason why is as follows: the base oil of GK-1 consisted of not di-alkyl tetraphenyl but tri-alkyl tetraphenyl mainly, so that it was oxidized easily by radiation. The GR-42R-1 was more suitable than the GK-1 under the reprocessing cell atmosphere.

References

1) T. Washiya et al., Proc. GLOBAL2005 (2005)
2) M. Takeuchi et al., Proc. ICONE13 (2003)

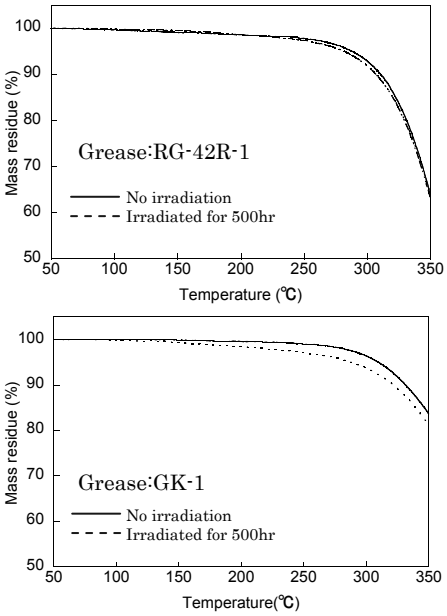

Fig.2 TG-curve measured with differential thermal analysis

1-18 Investigation of Effect of Radiation Deterioration on Confinement Capability of Glove-box

H. Abe, K. Watanabe, S. Tashiro and G. Uchiyama

Nuclear Facility Safety Research Unit, NSRC, JAEA

In the mixed-oxide (MOX) fuel fabrication facility, MOX is required to be handled in Glove-box to sustain containment of MOX into the facility. Since the Glove-box consists in some inflammable components such as plastic panel and packing, in case of fire in the facility, the static containment capability of the Glove-box may be deteriorated by pyrolysis or combustion of the components by thermal stress. Deterioration of the static confinement capability of the Glove-box may cause release of MOX to the room involving the Glove-box and to the outside of the facility and exposure of worker and public around the facility. Therefore, to confirm the safety of the facility under the fire, acquisition of fundamental data of the thermal properties of the components and establishment of quantitative evaluation method of time-course of the deterioration are very important. From this point of view, in JAEA, the thermal properties of the components have been investigated as a contract research from Japan Nuclear Energy Safety Organization (JNES)[1]. The purpose of this research is to examine exothermic and endothermic properties, such as starting temperatures, calorific values, temperature ranges and reaction rate data of the relative reactions of the components, as the pyrolysis properties by thermal analysis. Moreover, energy and mass release rates as source-term data for thermo-fluid analysis in the Glove-box and ventilation system and smoke generation rate as source-term data for clogging analysis of the ventilation filters with combustion of the inflammable components of the Glove-box have been also examined by using "Apparatus for Evaluation of Source-term under Fire Accident".

Since a large amount of MOX is handled in the MOX fuel fabrication process in the actual facility, the components of the Glove-box are irradiated by radiation from MOX and radiation deterioration of the components could be caused. In this contract research, investigation of effect of the radiation deterioration on the pyrolysis properties of the components has been started from fiscal 2006. In the first place, to verify the effect, the some components of the Glove-box were irradiated under an extremely high-dose condition, 880 kGy (=10 kGy/h×88 h), by using 6th ^{60}Co cell at JAEA Takasaki. After the irradiation, the exothermic and endothermic properties and weight change as a function of temperature of the components were measured by using Simultaneous Differential Thermogravimetric Analyzer (Shimazu DTG-60H). Figure 1 and Fig.2 show the experiment results about the effect of the radiation deterioration on the pyrolysis properties under air atmosphere condition for Polymethylmethacrylate (PMMA) and Polycarbonate (PC) as commonly used as plastic panel of the Glove-box. Initial weights of PMMA and PC were about 6 mg and 3 mg, respectively. Starting temperature of weight decrease of the irradiated PMMA was shifted to lower temperature than the non-irradiated PMMA. Moreover, endothermic peak at about 270 ℃ of the irradiated PMMA decreased than the non-irradiated PMMA and exothermic peak at about 350 ℃ appeared for the irradiated PMMA. These results mean the pyrolysis rate of the irradiated PMMA is probably faster than the non-irradiated PMMA. On the other hand, for PC, the effect of the radiation deterioration on the pyrolysis properties was not observed. In future, the more detailed investigation, for example, observation of threshold of dose affecting the pyrolysis properties, is planned.

Reference

1) H. Abe et al., JAEA-Research 2006-054 (2006.9). [In Japanese]

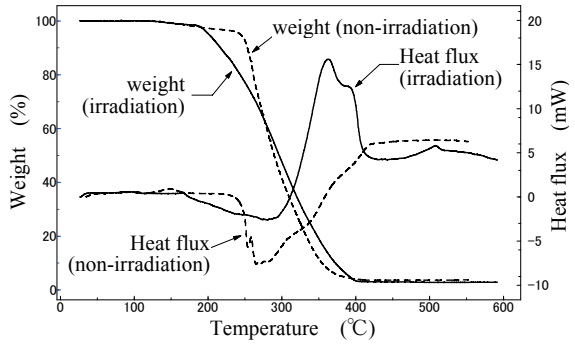

Fig.1 Experiment results of pyrolysis properties for PMMA

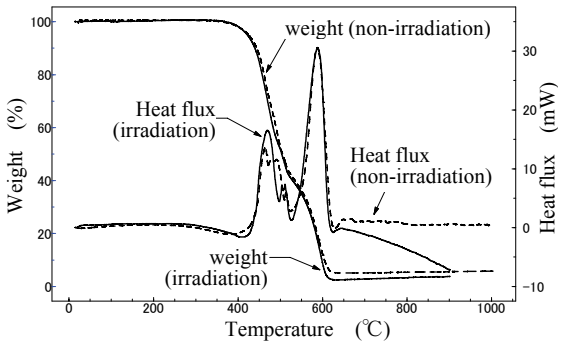

Fig.2 Experiment results of pyrolysis properties for PC

1-19 Corrosion Behavior of Type 316L Stainless Steel Ion-irradiated under Deformed Condition

K. Kondo [a)], Y. Miwa [a)], N. Okubo [a)], Y. Kaji [a)] and T. Tsukada [a)]

[a)]Division of Fuels and Materials Engineering, NSED, JAEA

Irradiation assisted stress corrosion cracking (IASCC) on austenitic stainless steel (SS) is one of the problem in reactor cores. Degradation of materials under irradiation and applied stress are important to the IASCC initiation[1)]. The objective of this work is to obtain the fundamental knowledge on the synergistic effect of residual stress and irradiation on the corrosion behavior of type 316L SS. In this paper, the correlation between the corrosion behavior and microchemistry change in irradiated specimens is discussed from a viewpoint of the effect of residual stress.

In order to examine the effects of residual stress during irradiation on corrosion behavior, flat plate specimens that were plastically deformed by bending constraint and without deformation constraint were irradiated by 12 MeV Ni^{3+} ion using the tandem accelerator and a vacuum chamber at JAEA- Takasaki. Plastic strain of the irradiation surface region in bent specimens was calculated to be about 2%. Irradiation temperature was 330 ºC. The displacement damage levels ranged from 1 to 45 dpa. The corrosion behavior of irradiated specimens was estimated by means of single-loop electrochemical potentiokinetic reactivation (SL-EPR) testing, in which the corrosion property was evaluated using the normalized charge (P_a). And, three dimensional atom probe (3D-AP) analysis was conducted on the irradiated specimens to investigate the microchemical compositional change in irradiated specimens.

The dose dependence of the values of normalized charge (P_a) is shown in Fig.1. The P_a of undeformed specimen increased rapidly with increasing dose, and saturated above 12 dpa. In case of the deformed specimens, on the other hand, the P_a below 12 dpa was much smaller than that of the undeformed specimen. At 6 dpa irradiation, the P_a for the deformed specimen was 0.01 C/cm^2, which was about 2 orders of magnitude lower than the value for the undeformed specimen, 5.7 C/cm^2. At 45 dpa irradiation, the P_a was almost the same between the deformed specimen and the undeformed specimen.

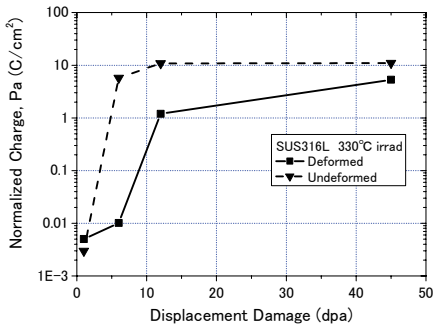

Fig.1 Dose dependence of corrosion behavior in single-loop EPR testing on deformed and undeformed specimens.

Since the significant effect of residual stress on corrosion behavior was observed in the specimens irradiated to 6 dpa, microchemical composition measurement was conducted using the 3DAP. Fig.2 shows Si atom map in the deformed specimen. Inhomogeneous distribution of Si was observed. In the Si enriched region, enrichment of Ni and depletion of Cr were observed. Chemical composition was measured in seven segregation regions. The enrichment of Si composition was 4.7±0.8 at.%, and the depletion of Cr composition was 4.5±1.4 at.% in comparison with the bulk composition. In the undeformed specimen, inhomogeneous distribution solute was also observed and the segregation behavior was similar to that in the deformed specimen. Chemical composition was measured in four segregation regions. The depletion of Cr composition was 5.2±1.5 at.%, and enrichment of Si composition was 6.6±2.0 at.%. It was, therefore, speculated that the degree of Cr depletion and Si enrichment at a sink such as dislocation was greater in undeformed specimen than in deformed specimen. And, it could be suggested that radiation induced segregation behavior of solute atoms as a consequence of diffusion and annihilation of irradiation defects at sink is affected by residual stress.

The corrosion behavior of SSs was related to the diffusion behavior of the solute atoms such as Cr. It could be speclated that, due to the suppression of the segregation of solute by residual stress, deformed specimens showed higher corrosion resistance than undeformed specimens.

Reference

1) K. Kondo et al., Proc. of 13th Int. Conf. Env. Degradation of Materials in Nuclear Power Systems – Water Reactors, 2007, to be published.

Fig.2 Three dimensional map of Si atoms in 316L irradiated at 330°C under the deformed condition. The volume is approximately 15 x 15 x 170 nm^3.

Present study is the result of "New evaluation method of material degradation considering synergetic effects of radiation damage" entrusted to Japan Atomic Energy Agency by the Ministry of Education, Culture, Sports, Science and Technology of Japan (MEXT).

1-20 Mechanical Properties of Austenitic Stainless Steel Ion-irradiated under External Stress

I. Ioka [a)], Y. Ishijima [a)], M. Futakawa [b)], H. Ogawa [a)], Y. Nakahara [a)] and T.Naoe [c)]

[a)]Division of Fuels and Materials Engineering, NSED, JAEA,
[b)]QuBS, JAEA, [c)]Graduate School of Ibaraki University

Irradiation creep has been studied extensively to provide data that can be used for component analysis of fusion, fast breeder and light water reactors. It is now generally recognized that the irradiation creep data were in agreement with an empirical equation[1)]. Moreover, there have been many irradiation experiments done under external stress to investigate stress effects on microstructural evolution. It is reported that the total nucleation rate of Frank loops was increased with increasing external stress[2)]. However, there are few studies on the effect of external stress on mechanical properties of the material under irradiation. The purpose of this study is to evaluate the mechanical properties of the irradiated material under external stress.

The material tested is a high chromium austenitic stainless steel (25Cr-35Ni-0.2Ti EHP)[3)] which is a candidate material of cladding tube for LWR of ultra high burnup. Chemical composition of the specimen is shown in Table 1. 25Cr-35Ni-0.2Ti was machined from the plate produced by the thermo-mechanical treatment so-called SAR (strained, aged and recrystallized).

Table1 Chemical composition of 25Cr-35Ni-0.2Ti (wt%)

Fe	Cr	Ni	Ti	C	N
bal.	24.55	34.99	0.18	0.0013	0.0014
O	S	Si	Mn	P	
0.0011	0.0009	<0.005	0.001	0.001	

The thickness of specimen is about 0.5 mm. It has three different cross-sections (S division:1.5 mm, M division: 1.75 mm, L division:2.0 mm in width) in order to irradiate under different stress at the same time. The surface of specimen was polished with #2400 paper.

The specimens were irradiated in triple (12 MeV Ni^{3+}, 1.1 MeV He^{+} and 380 keV H^{+}) ion beam mode at a temperature of 300 °C using the triple ion beam facility (TIARA). The temperature of the specimen was measured by an infrared thermometer (THERMAL VISION, Nikon Co.). The displacement damage in the specimen was mainly attributed to Ni^{3+} ion irradiation. The peak dose was about 10dpa around 2 μm. The He^{+} and H^{+} ions were implanted in depth ranges from 1.0 to 1.5 μm using aluminum foil energy degraders. The concentrations of He^{+} and H^{+} ions in the implanted range were 15 appmHe and 100 appmH, respectively, which correspond to LWR condition. The dose was about 5 dpa in the implanted range of He^{+} and H^{+} ions. Two specimens were irradiated. One was a stressed specimen. The other was a stress-free specimen which was prestressed at the same stress level of the stressed specimen.

The microindentation test was carried out on the surface of specimens at room temperature. A testing machine, DUH-200 (Shimadzu Co.), was used for the microindentation test. A load was applied with a loading speed of 4.4 mN/s, held 1 second and then removed. During loading, the load was continuously monitored along with the displacement with a resolution of 2 mN and 0.01μm, respectively. The Berkovich indenter was used in the microindentation test. The obtained data were converted into the relationship between load/depth and depth (L/D-D curve), and the universal hardness was calculated from these data.

Figure 1 shows the universal hardness of irradiated region at the S, M and L divisions. The vertical axis denotes the universal hardness normalized by the unirradiated ones. The result of stress-free specimen is added to Fig.1. The

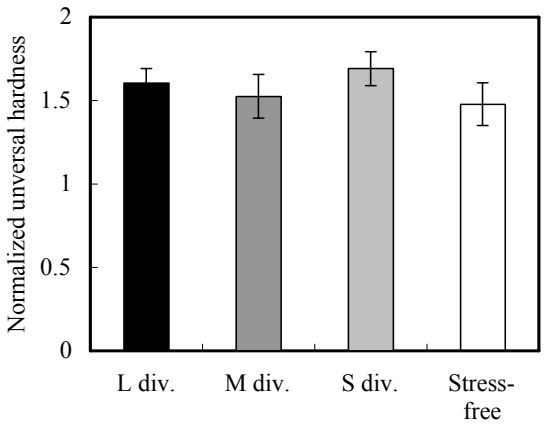

Fig.1 Comparison of normalized universal hardness after

universal hardness of the irradiated specimen was about 40-60 % higher than those of the unirradiated specimen. The irradiated specimen was hardened by irradiation and external stress. It is considered that there is little influence of external stress on universal hardness of the irradiated specimen in this test condition.

References

1) F.A.Garner et al,, J. Nucl. Mater. 251(1997)252.
2) H.Tanigawa et al., Nucl. Instru. and Methods in Phy. Resea. B 102(1995)151.
3) K.Kiuchi et al,, ICAPP, June 9-13, 2002(Florida).

1-21 Evaluation of Property Change in Ultra High Purity Austenitic Stainless Steel under BWR Condition Simulated by Triple Ion Irradiation

Y. Ishijima , I. Ioka , M. Yamamoto and J. Suzuki

Division of Fuels and Material Engineering, NSED, JAEA

1. Introduction

To prevent material degradation under corrosion and LWR condition, we developed ultra high purity (UHP) grade (C + N + O < 100 wppm) and high Cr (~25wt% Cr) austenitic stainless steel. We have evaluated corrosion behavior and change of mechanical properties of UHP grade austenitic stainless steel. Decrease of carbon concentration in stainless steel decreases receptivity of irradiation assisted stress corrosion cracking (IASCC). As a result, it is considered that segregation of small amount (~10 wppm) of B and P under BWR condition causes degradation of grain boundary corrosion resistance. However, the behavior of these elements under BWR condition is not clear. The purpose of this study is to obtain basic knowledge of behavior of small amount of impurities (B and P) under irradiation.

In this paper, triple ion irradiation that simulates BWR condition was carried out for the candidate (Fe- 25Cr- 35Ni- 0.2Ti UHP grade) and segregation of small amount of elements around grain boundary was evaluated.

2. Experimental procedures

The candidate (Fe-25Cr-35Ni-0.2Ti UHP grade) was cut to a size of 6x3x2 mm^3. Irradiated area was then mechanically and electrochemically polished to a specular finish. Triple ion irradiation simulating BWR neutron irradiation condition was performed using Ni^{3+} (12 MeV), He^+ (1.1 MeV) and H^+ (0.38 MeV) ion beams. Aluminum film degraders were used to spread He^+ and H^+ irradiated area. Irradiation temperature was 573 K. Irradiation damage and ion-implantation depth were calculated using TRIM code. As a result, He^+ and H^+ ion-implantation depth was estimated to be 1.1~1.3 μm and irradiation damage of this area to be 75 dpa. He^+ and H^+ concentrations in ion-implantation area were 3 and 30 appm/dpa, respectively.

Segregation of elements around grain boundary after ion-irradiation was evaluated using Auger electron spectroscopy (AES) in which the electron beam diameter was 25 nm. After electropolish to a depth of 1.2 μm at irradiated face, evaluation of segregation was carried out at 10 nm intervals from grain boundary.

3. Results

Figure 1 shows chemical compositions of the candidate around grain boundary after ion-irradiation by AES measurement. From this result, irradiation induced segregation of Cr was observed but segregation of small amounts of impurities (B and P) were not observed by AES measurement.

At next step, 3D-AP measurement will be used to evaluate irradiation behavior and presence state of small amount of impurities.

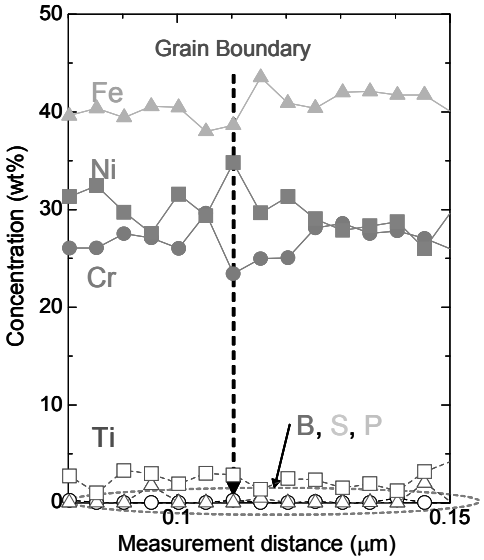

Fig. 1 result of AES measurement

1-22 Radiation Hardening of Ferrite Phase in a Dual Phase Austenitic Steel

S. Jitsukawa [a)], N. Okubo [a)] and M Ando [b)]

[a)]NSED, [b)]FRDD, JAEA

Dual phase stainless steel is widely used as the structural material for LWR core component. For example, cast stainless steel for LWR components CF8 with similar chemical composition to that of 304 stainless steel often exhibits dual phase microstructure depending on the cast condition. During the initial stage of the solidification, .Ni rich austenite phase is formed. This is followed by ferrite phase formation with lower Ni content. Although the Ni content is lower, this ferrite phase containing 2 to 6 % of Ni is expected to exhibit large hardening by neutron irradiation. Also, austenite phase containing lower level of Ni has lower phase stability tends to cause lower toughness after irradiation. Hardening is often accompanied by the reduction of toughness and increase in DBTT. Therefore, susceptibility to irradiation hardening of dual phase stainless steel is examined by ion irradiation method at temperatures from 200 ^{o}C to 350 ^{o}C to damage levels to 5 dpa.

An alloy with nominal chemical compositions of around 0.01C-1Si-0.7Mn-9Ni-19Cr containing 10% ferrite phase after solution annealing at 1050 ^{o}C is used. Yield stress, ultimate tensile stress and hardness at room temperature are 210 MPa, 490 MPa and 168 Hv (correspond to 2.1 GPa of average contact area pressure), respectively. Ultra micro-hardness value was about 4.5 GPa. Surface of the specimen for ion irradiation was finished by electro-polishing technique. Irradiation was carried out with 10MeV Fe ions to nominal damage levels of 0.1, 1 and 5 dpa at temperatures of 200, 280 and 350 ^{o}C. Hardness after irradiation was examined with ultra micro-hardness testing machine with indentation load of 1 g.

Hardness at twenty points was measured for one specimen after irradiation. Minimum distance between each point was about 10 micro-meter. Size of each indentation was about 1 micro-meter. Figure 1 (a) shows impressions on the irradiated surface with microstructure. Dark and light areas correspond to ferrite and austenite phases, respectively. Hardness was plotted in Fig. 1 (b). The hardness of the ferrite phase (red) was apparently higher than those in austenite regions, as shown in the figure. Damage level dependence of the hardness is plotted in figure 2. Plots for a reduced activation ferritc steel of F82H (a reference alloy) are also shown in the figure. Before irradiation, hardness for the dual phase alloy and F82H exhibited similar hardness of about 4.5 GPa. After irradiation to 0.1 dpa, some of the ferrite phase in the dual phase alloy hardened to 5.5 GPa, while small hardness change was obtained for austenite phase and F82H. At higher damage levels, hardness in most of the ferrite phase was continuously higher than austenite phase, and attained to 8 GPa at 5 dpa. Damage level dependence at 280 ^{o}C and 350 ^{o}C was qualitatively similar to that at 200 ^{o}C. Results clearly indicate that ferrite phase in the dual phase austenitic alloy is susceptible to irradiation induced hardening.

Acknowledgement

Some of the results are obtained from the research sponsored by JNES.

References

1)M. Ando, et. Al., J. Nucl. Mater, 307-311(2002)260

2)For example; S.Jitsukawa, et. Al., J. Nucl. Mater, 307-311(2002)179 and G.R.Odette, Philos Mag. 85-4(2005)779

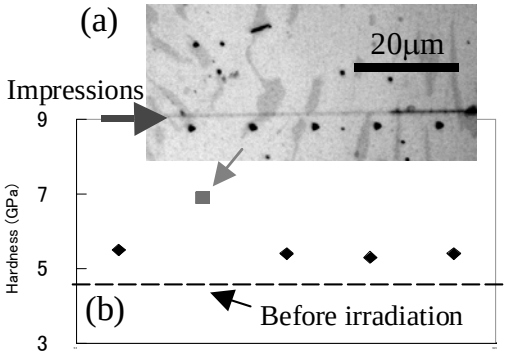

Fig. 1 Microstructure (a) and Hardness (b) after irradiation in the dual phase alloy after irradiation.

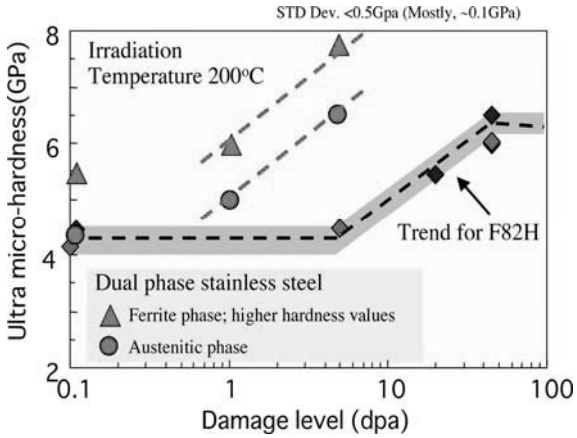

Fig. 2 Damage level dependence of hardness in the dual phase alloy. Results for F82H (a reference martensitic steel) were also shown.

1-23 Study on Irradiation Defect Generation Process and Radiation Induced Segregation in Fe-P Model Alloys

T. Tobita [a)], Y. Chimi [a)], N. Ishikawa [b)], S. Nakagawa [c)] and A. Iwase [c)]

[a)]Reactor Safety Research Unit, NSRC, JAEA, [b)]Advanced Science Research Center, JAEA,
[c)]Department of Materials Science, Osaka Prefecture University

To investigate the fundamentals of irradiation embrittlement mechanisms of Reactor Pressure Vessel steel (RPVs), we have performed electron irradiation experiments using Fe-based model alloys, such as pure Fe, Fe-Cu and Fe-P. The impurities in RPVs materials have been known to have a storing effect on the irradiation embrittlement. The Cu precipitates which grow during irradiation cause irradiation hardening, while the P segregation to the grain boundary weakens the Fe-Fe bonds. Our previous study [1)] shows the changes of electrical resistivity of Fe-Cu model alloys induced by electron irradiations at high temperature to evaluate the irradiation damage mechanisms, such as the behaviours of irradiation defect and Cu clustering in the materials.

In this paper, we measured the changes of electrical resistivity of several types of Fe-P model alloys induced by 2MeV electron irradiations at high temperature (523 K) to evaluate the irradiation damage mechanisms, such as the behaviours of irradiation defect and P segregation to the grain boundary in the materials. We tried to obtain the dose dependence and P content dependence of the electrical resistivity change.

The chemical composition of these materials is shown in Table 1. The Fe-P model alloys were fabricated as pure as possible to eliminate the effects of impurities. After the heat treatment at 950 °C for 10 min, the materials were quenched to keep the P atoms in supersaturated solid solution at room temperature. The specimens were cut into ribbons of 1mm width, 0.03 mm thickness, and the four electrodes were spot-welded. Figure 1 shows the schematic illustration of electron irradiation apparatus. 2 MeV electron irradiation was performed at dose rate 1.5×10^{-9} dpa/s. The electrical resistivity was measured at 77K in LN2. In addition to these irradiation tests, thermal aging experiments at the same temperature were performed to clarify the irradiation temperature effect.

Figure 2 shows the electron dose dependence and thermal aging time dependence of the electrical resistivity change in Fe-0.1 %P and Fe-0.04 %P, where thermal aging time and electron irradiation time were almost the same. At this temperature and dose, accumulation of irradiation defects (vacancy and interstitial) is negligible [1)]. Therefore, the decreasing of electrical resistivity change was mainly caused by behavior of P or annihilation of thermal vacancy introduced by heat treatment.

The electrical resistivity change decreases with increasing electron dose and aging time in all materials. However, the amount of decrease is in inverse proportion to P content. And furthermore, both the amount of decreasing of electrical resistivity change decreasing induced by electron irradiation and thermal aging were almost the same. It means that detection of P segregation by electrical resistivity is impossible, or P segregation was not clearly enhanced in this electron fluence. If the decreasing of electrical resistivity change was mainly caused by decreasing of thermal vacancy introduced by heat treatment, P may obstruct the migration and annihilation of thermal vacancies.

Table 1 Chemical composition of materials (wt%)

Material	Fe	P	C	Si
Fe-0.04wt%P	Bal.	0.039	<0.0005	<0.002
Fe-0.1wt%P	Bal.	0.103	<0.0005	<0.002
	Mn	S	Cu	O
	<0.01	0.0008	<0.01	0.019
	<0.01	0.0009	<0.01	0.018

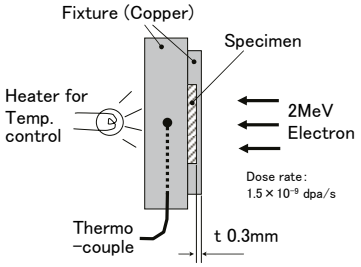

Fig.1 Schematic illustration of electron irradiation.

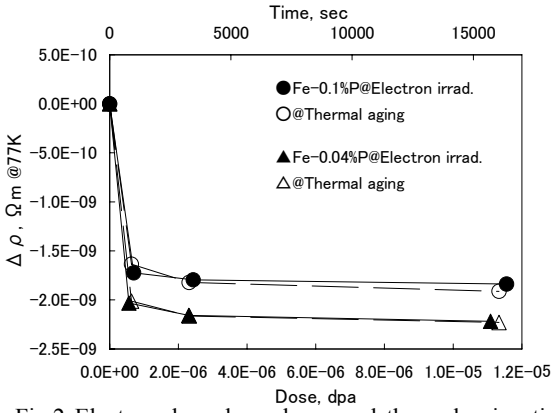

Fig.2 Electron dose dependence and thermal aging time dependence of the electrical resistivity change in Fe-0.1 %P and Fe-0.04 %P.

Reference

1) T. Tobita, Y. Chimi, N. Ishikawa, S. Nakagawa and A. Iwase, JAEA-Review 2006-042 (2007)20.

1-24 Evaluation of Radiation Damage Created via Elastic Displacements in Oxide Ceramics

N. Ishikawa

Division of Fuels and Materials Engineering, NSED, JAEA

Radiation damage is one of the important causes of degradation of thermal conductivity and serious swelling in MOX (Mixed Oxide) fuel. Understanding of radiation damage in nuclear fuel is important for controlling fuel properties during burn up and for the prediction of fuel burn up behavior. The objectives of this study are to elucidate the irradiation parameter dominating the radiation damage of ceramics by means of accelerator experiments, and to precisely evaluate their radiation damages. Especially for simulating the process of radiation damage by elastic displacements, 10MeV Ni irradiation experiment has been performed at room temperature and at high temperature, and CeO_2 target which has the same crystal structure with nuclear fuel is adopted.

Thin films of CeO_2 were prepared on Al_2O_3 single crystal substrates, and were irradiated with 10 MeV Ni ions at room temperature and at high temperature of 400 ℃. After the irradiations, fluence dependence of change of X-ray diffraction pattern was measured in the wide fluence range of 10^{12}-10^{16} ions/cm^2, in order to quantify the corresponding radiation damage. The film thickness was restricted to be about 0.3 μm which is thin enough to rule out the possibility of unrequired implantation effects.

In Fig.1 evolution of X-ray diffraction peak for different fluence is shown for CeO_2 irradiated with 10 MeV Ni at 400 ℃. It is found that the intensity of the peak monotonically decreases as increasing fluence, but in the high fluence region this tendency slows down. This reflects that the sample maintains its crystal structure even in the high fluence region, and the CeO_2 structure has high radiation resistance up to 10^{16} ions/cm^2. It is also found that the peak position shows complex fluence dependence; it moves toward high angle side in the low fluence region (<10^{13} ions/cm^2), and moves back to low angle side in the high fluence region (>10^{13} ions/cm^2). This tendency is clearly demonstrated in Fig.2, where lattice parameter change decreases in the low fluence region and increases in the high fluence region. The increment of the lattice parameter for room temperature irradiation is more prominent than that for high temperature irradiation when compared at high fluence region (10^{15}-10^{16} ions/cm^2), suggesting that the created oxygen defects are diminished by thermal energy in case of high temperature irradiation.

Present study is the result of “Research of highly accurate evaluation of radiation damage in advanced nuclear reactor fuel ceramics” entrusted to “Japan Atomic Energy Agency” by the Ministry of Education, Culture, Sports, Science and Technology of Japan (MEXT).

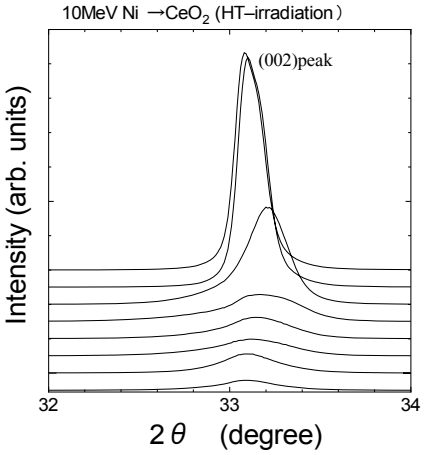

Fig.1 Evolution of X-ray diffraction peak assigned for (002) reflection of CeO_2 irradiated with 10 MeV Ni at high temperature (400 ℃). The fluence ranges from 0 (top) to 1.0x10^{16} ions/cm^2 (bottom).

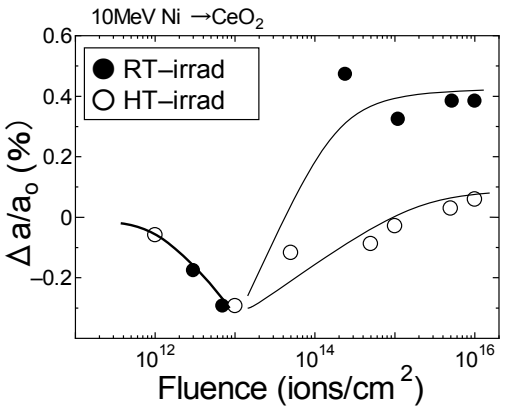

Fig.2 Fluence dependence of lattice parameter change normalized by that of unirradiated sample in CeO_2 irradiated with 10 MeV Ni at room temperature (RT: closed circles) and high temperature (HT: open circles).

1-25 Behavior of Advanced Materials under Heavy Irradiation

N. Okubo [a)], E. Wakai [a)], S. Yamashita [a)], M. Ando [a)], S. Otsuka [a)], S. Jitsukawa [a)], N. Hashimoto [b)] and S. Ohnuki [b)]

[a)]Nuclear Science and Engineering Directorate, JAEA
[b)]Hokkaido University

In the structural materials heavily irradiated in fusion reactor, next generation fast breeder reactor and IFMIF target etc., displacement damage and He accumulation simultaneously occur by high energy irradiation. The materials are degraded by the effect of superposition. Therefore, to understand dependences of behaviors of irradiation hardening and microstructural evolution on displacement damage and He concentration is important for modeling of irradiation behavior.

In this study, the behavior of irradiation hardening of the reduced activation ferritic steels F82H was evaluated in the high damage region. For oxide-dispersion-strengthened (ODS) martensitic steel, which was one of the candidate materials for fuel cladding used in the next generation fast breeder reactor, the microstructural evolution was conducted under irradiation.

Ion irradiation of 15 MeV-Ni^{4+} to the F82H (IEA Heat) was conducted at 270℃ in order to investigate the irradiation-hardening behavior up to 165 dpa. The change of the micro-hardness (ΔH) measured by nanoindentation was transformed to that of yield stress ($\Delta\sigma_y$) by relation of $\Delta H \fallingdotseq 3\,\Delta\sigma_y$ [1)] The microstructual evaluation was conducted by in-situ TEM observation under 200 keV He ion irradiation at room temperature and 550℃ for 9Cr martensitic and 12Cr ferritic ODS steels.

Dependence of irradiation hardening on the displacement damage on the F82H is shown in Fig. 1. The irradiation hardening increased gradually as increasing the damage up to 20 dpa. The slope appeared to be shelving around 40dpa and subsequently saturating. The value of power obtained from the log-log plots of $\Delta\sigma_y$ vs. dpa data was about 0.12 for the high dpa regime.

The vicinity of oxyde particles in 12Cr ODS steels observed by in-situ TEM under He irradiation (7 appm-He) is shown in Fig. 2. The He bubble formation around the boundary between oxide particle and ferrite matrix was observed as the fluence of He ions was increased. In 9Cr ODS steels, however, the bubble formation was not observed under irradiation.

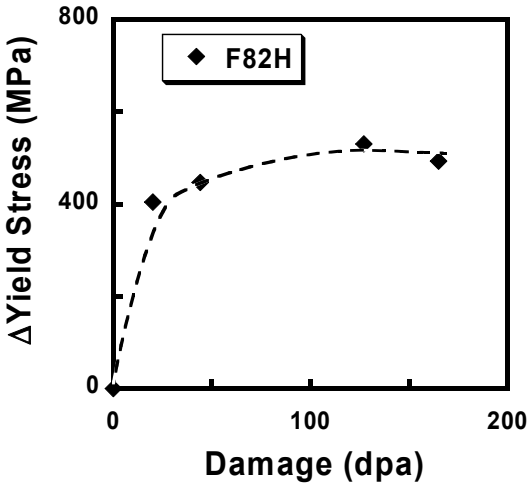

Fig.1 Dependence of irradiation hardening on displacement damage in F82H

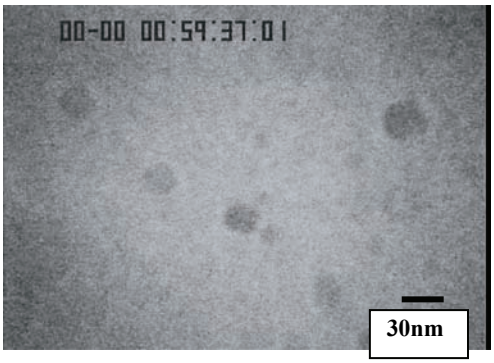

Fig.2 Vicinity of oxide particles of 12Cr ODS steels

Reference

1) J.T. Buswell, C.A. English, M. G. Hetherington, W.J. Phythian, G.D.W. Smith,G.N. Worral, Effect of radiation on materials, The 14th International Symposium (Vol II), N. H. Packan, R.E. Stroller, A.S. Kumar, Eds., ASTM STP-1046, American Society for Testing and Materials, Philadelphia, (1990)127-153.

1-26 Fundamental Radiolysis Effects Relevant to Volatile Iodine Formation during Nuclear Reactor Accidents

K. Moriyama [a)], S. Tashiro [b)], Y. Maruyama [a)] and H. Nakamura [a)]

[a)]Thermohydraulic Safety Research Group, NSRC, JAEA
[b)]Fuel Cycle Facility Safety Research Group, NSRC, JAEA

Iodine is recognized as the most hazardous radioactive material in terms of public heath impacts among those potentially released into the environment during a severe accident of light water reactors (LWRs). The chemical behavior of iodine compounds under irradiation in the containment vessel of LWRs during accidents was, thus, studied intensively for the last three decades[1]. Recently, computer programs that solve mechanistic models for the chemical kinetics of iodine compounds under LWR accident conditions were developed. To validate such models, we need fundamental radiolysis data for aqueous solutions of related materials as well as overall iodine volatility data under irradiation. We performed a series of experiments to observe changes in pure water and several kinds of aqueous solutions under gamma-irradiation for this purpose.

Table 1 summarizes the conditions of the experiments. The experiments were performed in the 7th ^{60}Co cell at JAEA Takasaki. Each solution was irradiated in a 500 mL-separable flask while stirred with ϕ11x30 mm glass stir bar at 510 rpm. The cover gas was either swept at a constant flow rate or kept stagnant with a vent path not to cause pressurization of the flask. The stagnant condition was set when the solution contained MEK or ammonia. After the start of the irradiation on the first day, sampling of about 40 mL of each solution was done with intervals of about 1.5 hours for four times. Then, irradiation continued through the night, and the last sampling was done just after the end of the irradiation on the next morning. Electrochemical probes (electrodes) for pH, NO_3^-, CO_2, I^-, and NH_3 were used to observe changes in each solution.

Figures 1 and 2 show selected results of the analysis. Pure water showed slight decrease of pH, but NO_3^- was not detected though nitric acid formation was suspected. MEK solution showed significant drop of pH. In the MEK solution, CO_2 was generated and reached the concentration about 10^{-3} M at the end of the irradiation. CsI solution showed only slight decrease of I^- concentration when pH was initially set 5 and increased slightly. While, I^- almost vanished when the initial pH was 3 which did not changed through the irradiation.

These data are to be used for verification of a mechanistic iodine chemistry model under development.[2]

Table 1 Experimental cases and conditions

Case	Solution	Cover gas	Analysis
1B-Air	Pure water	Air flow	pH/NO_3^-
2-Air	1x10^{-3}M MEK	Air stag.	pH/CO_2
2-N2	1 x10^{-3}M MEK	N_2 stag.	pH/CO_2
4A-Air (pH=5)	5 x10^{-6}M H_2SO_4 (pH~5)/1 x10^{-4}M CsI	Air flow	pH/I^-
4A-N2 (pH=5)	5 x10^{-6}M H_2SO_4 (pH~5)/1 x10^{-4}M CsI	N_2 flow	pH/I^-
4A-Air (pH=3)	5 x10^{-4}M H_2SO_4 (pH~3)/1 x10^{-4}M CsI	Air flow	pH/I^-
4A-N2 (pH=3)	5 x10^{-4}M H_2SO_4 (pH~3)/1 x10^{-4}M CsI	N_2 flow	pH/I^-
3-Air	0.1M NH_3(pH~11)	Air stag.	pH/NH_3

MEK = methyl-ethyl-ketone
flow/stag. = flow (1L/min) or stagnant cover gas
Solution initial volume: 500mL
Temperature: 17－22°C
Dose rate, time: 1.88kGy/h, 1300min

Acknowledgement
This work is a part of contract research with Japan Nuclear Energy Safety Organization (JNES).

References

1) OECD/NEA/CSNI/WGAMA, NEA/CSNI/R(2007)/1 (2007).
2) K. Moriyama et al., 2007 Annual Mtg. AESJ, C25 (2007) [In Japanese]

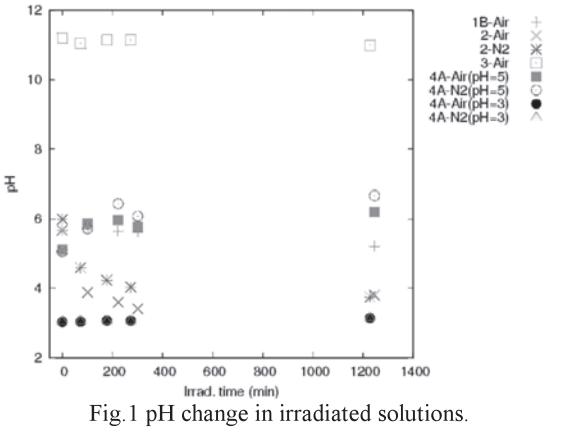

Fig.1 pH change in irradiated solutions.

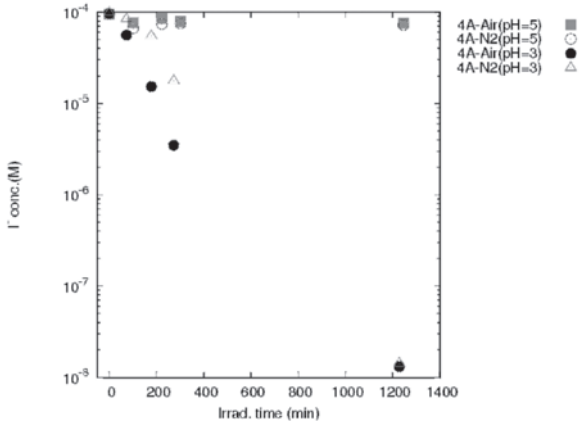

Fig.2 Decrease of iodide ion by irradiation.

1-27 Polymer Electrolyte Membranes for Fuel Cell Applications Prepared by Ion Track Technology

T. Yamaki, A. Hiroki, S. Hasegawa, H. Koshikawa, M. Asano, Y. Maekawa and M. Yoshida

Environment and Industrial Materials Research Division, QuBS, JAEA

Proton exchange membranes (PEMs) for polymer electrolyte fuel cells (PEFCs) have recently been developed by our original swift-heavy-ion based technique in addition to the γ-ray or electron-beam crosslinking and graft polymerization. The bombardment of high-energy ions produces cylindrical damage along with their trajectory in polymers. Our main focus is the use of such a localized damage area that is called a latent track. The approach using this ion track technology is being taken according to two techniques. One is the track etching and subsequent chemical modification inside the etched pores[1-3]; and the other is ion-track grafting[4], i.e., direct grafting into the activated zone. The report in the preceding issue[1] described the former attempt including the preparation methodology and proton conductivity of the resulting membranes. We present here, as an extension of this study, their other basic characteristics as a PEM.

The commercial fluoropolymer films were employed as a matrix for maintaining a reasonable mechanical and chemical stability. A 25-μm-thick poly(vinylidene fluoride) (PVDF) film was bombarded by 3.5 MeV/n ^{129}Xe from the TIARA cyclotron at the JAEA. According to the established procedure, track etching was then performed in a 9 M KOH aqueous solution at 80˚C. The pore density ranged between 3.0×10^6 and 3.0×10^9 /cm^2, which agreed with the number of actually irradiated ions per 1 cm^2. The sulfonic acid groups were introduced into the track-etched cylindrical pores of 100 μm diameter via the γ-ray-induced styrene grafting and subsequent sulfonation[1-3].

A transmission electron microscope (TEM) was used to observe the morphology of proton-conductive, hydrophilic domains in the membranes. Figure 1 is the representative TEM micrograph of a cross section of the membrane stained by ruthenium tetraoxide (RuO_4) vapor. This revealed that the stained lines with about a 100 nm width were arranged almost parallel to the through-thickness direction. Accordingly, it was confirmed that the membrane had a cylindrical electrolyte part with a diameter of about 100 nm, comparable to the size of the etched pore. In other words, we were able to prepare a novel PEM, which possessed nano-sized proton-conductive pathways extending along the ion projectile as was expected.

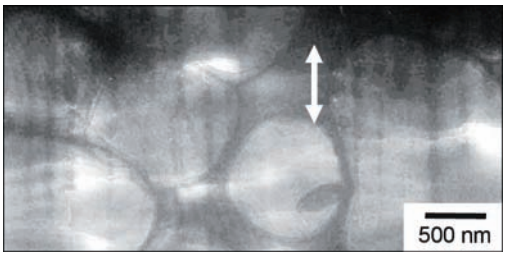

Fig. 1 Cross sectional TEM image of the RuO_4-stained membrane. The white two-headed arrow indicates the direction perpendicular to the membrane surface, i.e., the thickness direction.

Figure 2 shows a plot of water uptake, defined as: $100\times(W_w-W_d)/W_d$, where W_w and W_d are the membrane weights in the wet and dry states, respectively, as a function of the ion exchange capacity. In all cases, the water uptake of the nano-structure controlled membranes was enhanced with an increase in the ionic content. A notable result was apparent from the comparison with the properties of not only a Nafion membrane, but also the PEMs separately obtained by the usual γ-ray-induced *homogeneous* grafting (result not shown). The water uptake was lower than that of the *homogeneously*-grafted membranes in spite of the same ion exchange capacity; for example, it decreased from 36% to 23% (up to about two-thirds) at 1.6 meq/g. An inert PVDF host without any graft electrolyte chains was found to restrict the swelling of the entire membrane. It can be concluded, therefore, that our PEM is applicable for use in a PEFC, thus extending the performance beyond the limit of conventional ones.

References

1) T. Yamaki et al., JAEA Takasaki Annual Report 2005 (JAEA-Review 2006-042) (2007) 35.
2) T. Yamaki et al., ECS Transactions 3 (2006) 103.
3) T. Yamaki et al., Electrochemistry 75 (2007) 175.
4) T. Yamaki et al., GSI Scientific Report 2004 (2005) 260.

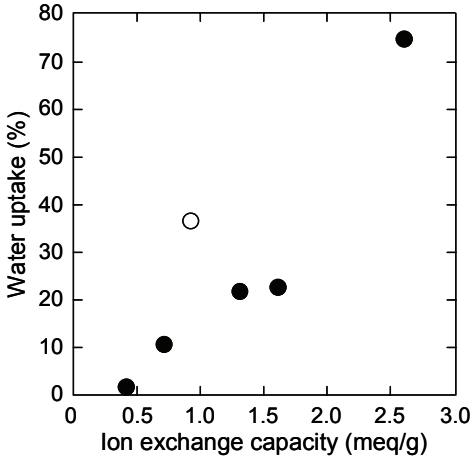

Fig. 2 A plot of water uptake versus the ion exchange capacity of the membrane (filled circle). For comparison, the result of Nafion117 is also plotted (open circle).

1-28 Hybrid Polymer Electrolyte Membranes Prepared by Radiation Grafting and Silane-crosslinking Techniques

J. Chen, M. Asano, Y. Maekawa and M. Yoshida

Environment and Industrial Materials Research Division, QuBS, JAEA

Hybrid polymer electrolyte membranes (PEM) have been widely studied for the application in intermediate temperature fuel cells[1-5]. These membranes are generally prepared by incorporating inorganic particles into organic polymer electrolytes. The inorganic particles enhance the water retention and thermal stability of PEMs. However, because of the lack of covalent bonds between the two components, the inorganic particles are easily separated out from the organic PEM.

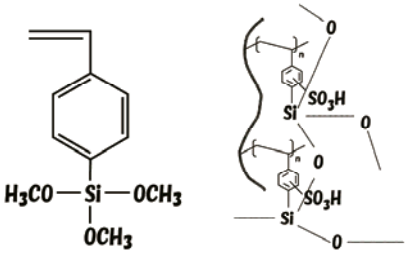

Fig. 1 Structures for the *p*-styryltrimethoxysilane (a) monomer and new hybrid PEM (b).

In this work, we attempted to combine the radiation grafting and silane-crosslinking to prepare a covalently crosslinked hybrid PEMs[1]. For this purpose, we grafted a special aromatic vinylsilane monomer, namely *p*-styryltrimethoxysilane (StSi), which has aromatic rings available for sulfonation and has trimethoxysilyl groups available for silane-crosslinking, into poly(ethylene-*co*-tetrafluoroethylene) (ETFE) base film. The StSi-grafted ETFE film was sulfonated in chlorosulfonic acid solution and then silane-crosslinked by hydrolysis and condensation in HCl solution.

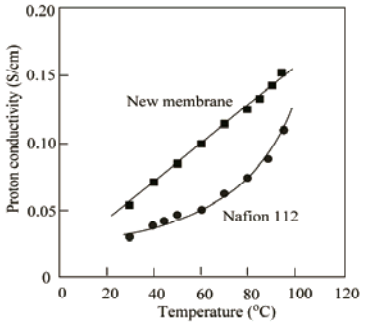

Fig. 2. Effect of temperature on the proton conductivity of the new hybrid PEM and Nafion. Relative humidity, 95%.

Figure 1 shows the structures of the monomer and the prepared new hybrid PEMs. The proton conductivity as a function of temperature is shown in Figure 2. The proton conductivity of the hybrid PEM linearly increased with increase in temperature, while for Nafion, the proton conductivity gradually increased with temperature up to 70°C, and then quickly increased in the temperature rise from 80 to 100 °C. The drastic increase in conductivity of Nafion was due to the changes in its structure. Therefore, Nafion is not appropriate for application in a fuel cell operating at temperatures above 80 °C. On the contrary, in the new hybrid PEMs, no drastic increase in proton conductivity was found over the tested temperature range, indicating the stable microstructure of this membrane and its suitability for use in higher temperature fuel cells.

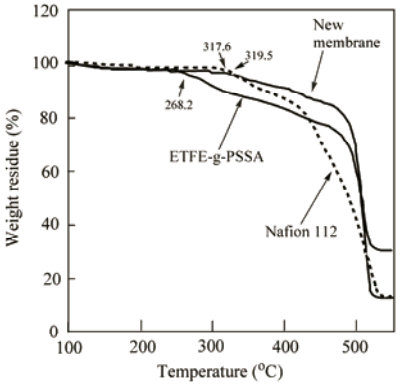

Fig. 3 Thermal stability of the new hybrid PEM, Nafion, and styrene-grafted PEM (ETFE-g-PSSA).

As seen in Figure 3, the thermal stability of the new hybrid PEMs exhibited a degradation temperature near 318°C, which was about 50 °C higher than that of the styrene-based membrane (268 °C), and was comparable to Nafion (320 °C). This enhanced thermal stability was due to the temperature tolerance of the crosslinked silicon network in the membrane. In addition, the silicon attached to the *p*-site aromatic rings enhanced the electronic density and thus increased the bond stability between aromatic rings and sulfonic acid groups. Furthermore, due to the silane-crosslinking structure introduced, the new hybrid membrane showed the high chemical stability than that of the divinylbenzene-crosslinked styrene-grafted PEMs.

References

1) J. Chen et al, J. Membr. Sci. 296 (2007) 77.
2) J. Chen et al, J. Membr. Sci. 277 (2006) 249.
3) J. Chen et al, J. Membr. Sci. 269 (2006) 194.
4) J. Chen et al, J. Power Sources, 158 (2006) 69.

2 Environment Conservation and Resource Security

2-01 Utilization of Scallop Processing Waste with Graft Adsorbent

H. Nakai [a)], T. Temma [a)], M. Tamada [b)],
T. Sawamura [c)],T. Saito [c)], T. Honma [c)] and K. Sato [d)]

[a)]Hachinohe Technical Laboratory, Aomori Industrial Research Center,
[b)]Environment and Industrial Materials Research Division, QuBS, JAEA,
[c)]Hachinohe National College of Technology, [d)]Kawasaki Plant Systems, Ltd.

Experimental equipment was assembled for removal of Cd^{2+} in mid-gut gland with the iminodiacetic acid adsorbents synthesized with radiation-induced graft polymerization. To check some effectiveness of the experimental equipment. The spatial distribution of the Cd^{2+} concentration in mid-gut gland in the basket and the removal rate of Cd^{2+} with regenerated adsorbents were investigated. As a result, a few variation in the Cd^{2+} concentrations of mid-gut gland was found in the basket. No significant difference of the adsorption performance was observed between regenerated adsorbents and fresh ones. These results indicate that our equipment is suitable for the purpose.

ホタテ貝の加工にともない廃棄されている中腸腺を肥料や飼料等の資源として有効利用することを目的とし，Cd^{2+}を除去するための中腸腺処理装置を開発した。この装置では、中腸腺からリンゴ酸溶液でCd^{2+}を溶出させるとともに、放射線グラフト重合法により作製した捕集材を通して溶液を循環させ、Cd^{2+}を効率良く捕集することができる。

中腸腺処理装置を用いて、中腸腺 30 kgを 0.1 Mリンゴ酸溶液 150 L（固液比 0.2）で処理した。リンゴ酸溶液を 30 ℃に保ち、中腸腺を入れたカゴの下方からバブリングを行なった。捕集カラムは直径 100 mm、厚さ約 0.8 mmのイミノ二酢酸型グラフト重合捕集材 800 枚を充填したもの 1 基を使用した。リンゴ酸溶液は 3 L/min（空間速度SV＝36 h^{-1}）の速度で循環させた。時間ごとにカゴの上面の中腸腺、溶出槽中の溶液、Cd^{2+}捕集カラムの通液直後の溶液を採取し、含有するCd^{2+}濃度をICP分析装置で測定した。24 時間後については、処理のバラツキを調べるため、Fig.1 に示したカゴの 18 箇所から中腸腺を採取し、Cd^{2+}残濃度を調べた。

次に使用した捕集カラムは再生装置を用いて塩酸で処理を行ない、同じようにCd^{2+}の除去実験を行った。捕集カラムの再生については、0.6 N塩酸を 1.7 L/min（SV=20 h^{-1}）で捕集カラムに通液させた後、水道水で十分に洗浄した。再生したカラムを使用して前述と同様のCd^{2+}除去実験を行った。

カゴの場所における 24 時間後の中腸腺中のCd^{2+}濃度のバラツキは平均 1.3 mg/kgで、最大で 2.3 mg/kg、最小で 0.6mg/kgであった。リンゴ酸溶液の撹拌効果が高いカゴ上面及び下面の中腸腺のCd^{2+}濃度が低く、カゴ内部及び外周で中腸腺が重なり合っている所のものは濃度が高かった。中腸腺処理装置のスケールではバラツキが大きくなると懸念されたが、バブリングにより溶液が撹拌されたためバラツキを少なくすることが出来た。

再生したカラムを使用してCd^{2+}除去実験を行った結果をFig.2 に示した。中腸腺中のCd^{2+}濃度は新品の時とほぼ同じ結果が得られた。溶出槽中の溶液、Cd^{2+}捕集カラムの通液直後の溶液についても、新品の時とほぼ同じ結果であった。捕集材の再生が正常に行われたことを示している。

以上のように、中腸腺からのCd^{2+}除去、捕集材の再生特性を調べた結果、スケールアップによる阻害要因は無く、予想通りの結果を得ることができた。

【謝辞】本研究は独立行政法人新エネルギー・産業技術総合開発機構（NEDO）の産業技術研究助成事業により実施したことを記し，感謝の意を表します。

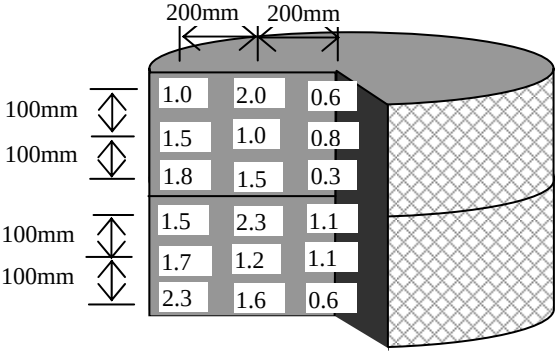

Fig.1 Spatial distribution of the Cd^{2+} concentration in mid-gut gland in the basket（after 24 hour）（concentration of Cd^{2+}: mg/kg）

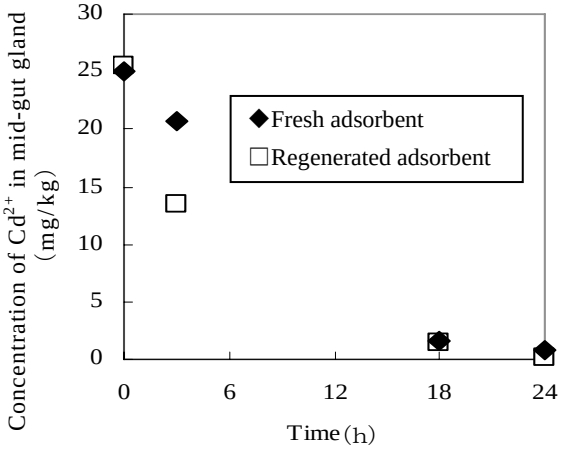

Fig.2 Change in the concentration of Cd^{2+} in mid-gut gland treated with fresh or regenerated graft adsorbents

2-02 Study on Analysis of Toxic Elements in Food with Graft Adsorbent

K. Saito [a)], A. Ogasawara [a)], J. Ichita [a)], N. Seko [b)] and M. Tamada [b)]

[a)]Hirosaki Technical Laboratory, Aomori Industrial Research Center, [b)]Environment and Industrial Materials Research Division, QuBS, JAEA

The demand for the analysis of toxic elements in food has increased because of the current problem of polluted food. To analyze toxic elements in food, the thiol-type adsorbent was developed in the present study. The adsorbent was prepared by radiation-induced graft polymerization of glycidyl methacrylate onto polyethylene fiber in aqueous medium and subsequently the modification with *L*-cystein in which active sites were blocked by zinc. When the thiol-type adsorbent was put in the cadmium solution of 10ppm, the total amount of adsorbed cadmium reached to 3.4 g/kg-adsorbent. This adsorbent is considered to have promising properties for cadmium removal.

近年､食品の有害化学物質による汚染が世界的規模で問題となったため、これまであまり問題とされなかった鉛、カドミウム、スズ、ヒ素、水銀等の有害元素の分析の要望が増えている。食品は不均質で、糖、蛋白質、脂質などの金属分析に対して妨害する成分が多いので、分析に際しては煩雑な前処理工程が不可欠であり、これが分析の迅速化や自動化の妨げとなっていた。そこで我々は、金属吸着時の選択性の高い放射線グラフト重合捕集材を食品分析における金属の分離及び定量へと応用し、食品中の金属分析の迅速化や自動化に関する検討を行ってきた。これまでの検討で、食品中の塩濃度の上昇に伴って、特にカドミウム吸着の収率低下が見られたため、より選択性の高い官能基を有する捕集材を必要としていた。

そこで本研究では､生体内において有害金属の解毒をしているメタロチオネインが、チオール基でカドミウム等を捕捉している点に着目し、新規チオール型捕集材の合成を検討した。

チオール型捕集材は、将来、食品中の有害元素除去素材にも使用するため、安全性を考慮して、チオール基を有するアミノ酸である*L*-システイン（*L*-Cys）を官能基に用い、これとグリシジルメタクリレート（GMA）母材とを結合させる合成方法を検討した。その際、a）GMAと*L*-Cysとをチオール基以外の官能基で結合させる方法、b）チオール型キレート樹脂は、使用直前にジスルフィド結合を還元処理してチオール基に戻して使用するが、これを還元処理なしで使用できる状態を保つ方法、の両方を満たす方法を検討した。その結果、亜鉛と*L*-Cysとは、中性、アルカリ性においてチオール基で結合すること[1)]、また、チオール基と亜鉛との反応性は､食品に多く含まれているナトリウム､カリウム､カルシウム、マグネシウム等よりは選択性が高く、カドミウム、鉛等と比べると選択性が低い。そのため、容易に亜鉛とカドミウムの交換反応が起こること[2)]から、先に亜鉛と*L*-Cysとをアルカリ条件下で反応させてチオール基を亜鉛で塞ぎ、これとGMA母材とを反応させる、以下の合成方法を開発した。

ポリエチレン製不織布に対して、窒素雰囲気下で 10 kGy の電子線を照射した後､グリシジルメタクリレート（GMA）及び Tween20 を純水と混合させて得られるエマルジョン溶液に入れて 40 ℃でグラフト重合を行い、GMA 母材を得た。

次に、メタノール 50 ml に粒状水酸化ナトリウムを添加して 1～10 %溶液に調製した後、酢酸亜鉛 0.22 g と *L*-Cys 塩酸塩 0.35g とを入れて加熱溶解し、これに GMA 母材 1 枚（約 0.1 g）を投入して、60 ℃で 24 時間反応させた。反応後、蒸留水で水洗した後、真空乾燥機で乾燥させて、目的のチオール型捕集材を得た。

反応した*L*-Cys量の指標として､チオール基の硫黄に着目し、波長分散型蛍光X線分析装置（WDX）により測定した結果､Fig.1 に示すように､水酸化ナトリウム濃度が 2 %付近にピークを示し、最高で 19 μg/cm^{2}の硫黄濃度を示した。

このチオール型捕集材 0.1 g と、10 mg/ℓのカドミウム水溶液 50 ml とを 100 ml バイアル瓶に入れて密栓し、25 ℃の恒温水槽中で 24 時間良く振り混ぜた後、ICP-AES によって溶液中のカドミウムの減少量を測定し、捕集量を求めた。その結果、3.4 g-Cd/kg-ad という結果が得られ、新規チオール型捕集材が、設計通りにカドミウムを捕集していることが確認できた。

References

1) Akira Sato et.al., J.Fac.Appl.Biol.Sci., Hiroshima Univ., **23** (1984) 1
2) 鈴木和夫他，微量金属の生体作用，季刊化学総説，**27**(1995)153

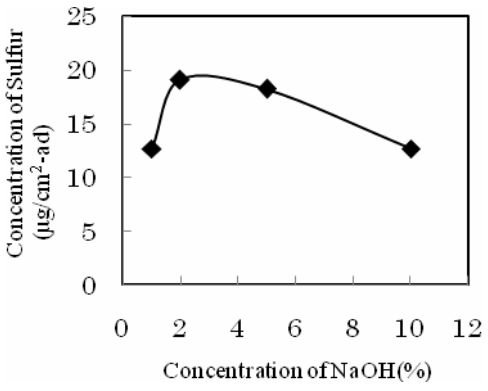

Fig.1 Effect of NaOH concentration in modification reaction on sulfur concentration in graft adsorbent.

2-03 Development of Low-loss Millimeter-wave Devices Using Fluororesin

N. Ito [a, c)], A. Mase [a)], Y. Kogi [a)], N. Tateishi [a)], N. Seko [b)], M. Tamada [b)] and E. Sakata [c)]

[a)]Art, Science and Technology Center for Cooperative Research, Kyushu University,
[b)]Quantum Beam Science Directorate, JAEA, [c)]Kyushu Hitachi Maxell, Limited

The development of high performance millimeter-wave planar antennas is essential for their application to satellite communications and imaging diagnostics which have become increasingly important. For fabricating such devices by using fluororesin as an antenna substrate, we propose two methods, i.e., (1) surface treatment of fluororesin substrate to increase the peel strength of copper foil, and (2) fabrication method using electro fine forming (EF2) technology.

Polytetrafluoroethylene (PTFE) films were irradiated with electron beam, and different degrees of grafting were achieved by immersing the irradiated films for different intervals in monomer solution. After the grafting, copper was attached on the surface of the films for measuring the peel strength between the metal and the grafted-films. Figure 1 shows the effect of grafting on the peel strength of the metal / grafted-PTFE. It is noted that a large increase in the peel adhesion strength was obtained by the graft polymerization on the PTFE surface. The increase in the adhesion strength between the metal and grafted films can be ascribed to cross-linking reaction or covalent bonding between the copper ion and the carboxyl group of an acrylic acid (AAc) introduced onto the thin surface layer of the PTFE films.

The dielectric constant measured by a cavity resonance method is shown in Fig. 2. The values of the dielectric constant were not significantly changed by the surface treatment. It suggests that the radiation grafting does not affect the composition of the PTFE surfaces.

By using a micro fabrication technology EF2, ultrafine pattern such as 15 μm line width and 6μm gap width without side edges can be formed. Applying this technology for fabrication of planar-type antennas on the fluororesin substrates, we have performed an experimental production of microwave antennas having 16 elements and millimeter-wave antennas having 240 elements. It was found from the evaluation of their radiation characteristics that they have good radiation patterns. The application of the antennas to biomedical measurement system, remote monitor of heart pulse and respiration is now in progress.

In summary, PTFE films have been modified by radiation-induced graft polymerization using AAc to develop low-loss millimeter-wave antennas. As a result of the treatment, the peel adhesion strength on the PTFE was improved to be 1.64 kgf/cm. In addition, the values of dielectric constant were confirmed not to be significantly changed, which is suitable for the antenna application.

Further investigations are necessary to realize low-loss devices, such as antennas, filters and non-linear transmission lines, by using radiating grafting and EF2 fabrication technique.

References

1) Sung R. Kim, J. Appl. Polym. Sci. Vol.77 (2000) 1913-1920.
2) Asaf A. Benderly, J. Appl. Polym. Sci. Vol.VI No.20 (1962) 221-225.
3) Shaoyu Wu, E.T.Kang, Neoh, C.Q.Cui and Thiam Beng Lim, IEEE Transactions on Advanced Packaging. Vol.23 No.3 (2000) 538-545.

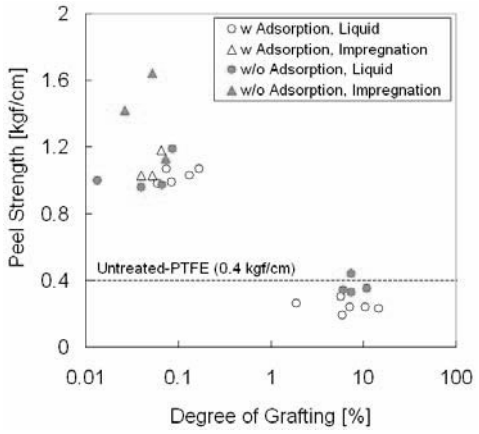

Fig.1 Peel strength of metal / AAc / PTFE as a function of degree of grafting.

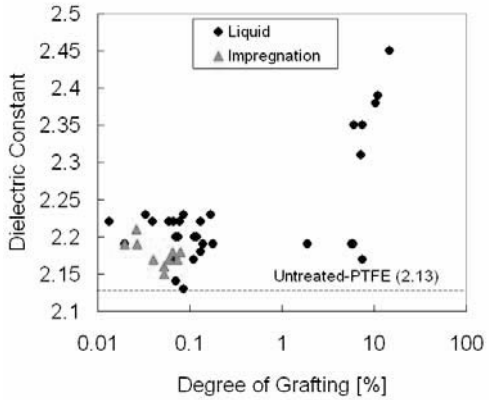

Fig. 2 Dielectric constant of the films as a function of degree of grafting.

Degree of Grafting [%] = (w2-w1) / (w1) ×100
w1 = Weight before Grafting,
w2 = Weight after Grafting

2-04 Preparation of Ampholite-immobilized Interface by Radiation-induced Grafting

A. Iwanade [a)], D. Umeno [a)], K. Saito [a)], A. Katakai [b)] and M. Tamada [b)]

[a)]Department of Applied Chemistry and Biotechnology, Chiba University, [b)]Environment and Industrial Materials Research Division, QuBS, JAEA

Three types of ampholites containing dimethylamino and carboxyl groups, *i.e.*, $N(CH_3)_2(CH_2)_nCOOH$ (n = 1-3), were introduced into an epoxy-group-containing polymer brush grafted onto a porous hollow-fiber membrane with a porosity of 70 % and pore size of 0.36 μm. Lysozyme was captured by the amphoteric polymer brush during the permeation of a lysozyme solution buffered with a carbonate buffer (pH 9.0) across the ampholite-immobilized porous hollow-fiber membranes. The $N(CH_3)_2(CH_2)_2COOH$-immobilized porous membrane exhibited a five fold higher flux for the buffer solution and a 50-fold lower binding capacity for lysozyme at a lower molar conversion of the epoxy group into the amphoteric group, up to 17 %, than the other two kinds of membranes.

1. 緒言

高分子製多孔性膜の界面に放射線グラフト重合法を用いて，両性電解質を有するポリマーブラシを固定し、リゾチーム吸着容量と透過流束とを両立できる吸着材料を作製した[1)]。両性電解質固定高分子鎖のコンホメーションは電荷の中和の度合い[2)]により支配される。そこで、本研究では電荷中和の度合いを調節するために、ジメチルアミノ基とカルボキシル基との間のメチレン基数を変化させた両性電解質を多孔性膜に固定し、その性能を評価した。

2. 実験

1) PE多孔性膜への両性電解質の固定　両性電解質固定ポリマーブラシを付与した多孔性膜の作製経路をFig. 1 に示す。ポリエチレン製多孔性中空糸膜に電子線を照射後、グリシジルメタクリレート（GMA）をグラフト重合した。化学式$N(CH_3)_2(CH_2)n$COOHによって表される両性電解質の水 / 1,4-ジオキサン溶液（v / v = 1 / 1）を用いてエポキシ基の一部を開環したのち、残存するエポキシ基をジオール基へ転化した。ここで、メチレン基の数nは 1 から 3 と変化させた。

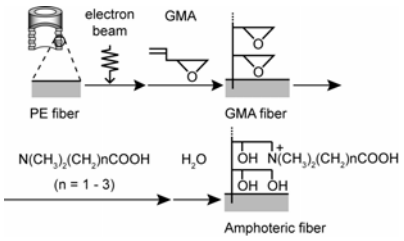

Fig. 1　Introduction scheme of ampholite into polymer brushes grafted onto a porous hollow-fiber membrane.

2) 両性電解質固定膜へのタンパク質吸着　リゾチーム（Lyと略記，p*I* 11）溶液（pH 9.0）を両性電解質固定膜の内面から外面まで一定流量で透過させた。流出液のLy濃度が供給液のそれと一致するまでLy溶液を透過させた。

3. 結果と考察

エポキシ基から両性電解質基への転化率の経時変化をFig. 2 に示す。メチレン基の数 n = 1 および 3 の最終転化率は同程度で、n = 2 はそれの約 1/3 であった。

nが異なる両性電解質固定膜のLy 平衡吸着量と緩衝液透過流束を転化率の関数として Fig. 3 に示す。n = 1 および 3 の膜の Ly 平衡吸着量は転化率が 40 %を超えると急激に増加した。Ly 吸着層数（ =（平衡吸着量）/（理論単層吸着量））の最大値を比較すると n = 1 および 3 の膜は、それぞれ 16 および 8 であった。Ly を多層に吸着できたのは、荷電中和よりも荷電反発の効果の方が強いためである。n = 1 および 3 の膜の場合、転化率 25%まで、Ly 平衡吸着量は理論単層吸着量と同程度であった。一方、n = 2 の膜の場合、理論単層吸着量の 1/50 であった。どの膜でも緩衝液透過流束の転化率依存性はなかった。ここで、n = 2 の膜は、n = 1 および 3 の膜に比べて透過流束が 5 倍高かった。n = 2 の膜ではポリマーブラシの伸長が抑えられ、他の膜に比べ荷電中和の効果が強いことが示された。両性電解質固定ポリマーブラシにおいて、転化率とメチレン基の数 n を変化させることによって、Ly 平衡吸着量を単層吸着量の 1/50 から 16 倍まで調節できることがわかった。

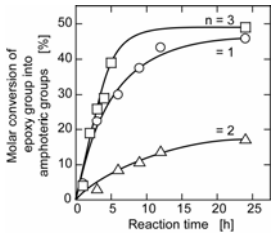

Fig. 2　Time course of molar conversion of epoxy group into amphoteric groups.

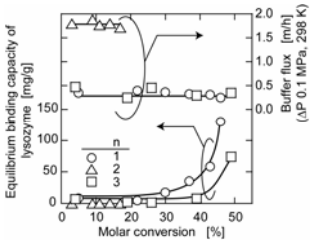

Fig. 3　Equilibrium binding capacities for lysozyme and buffer fluxes of membranes.

References

1) K. Miyoshi, et al., "Introduction of taurine into polymer brush grafted onto porous hollow-fiber membrane", J. Membr. Sci., **264**, (2005) 97.

2) R. G. Alargova, et al., "Properties of amphoteric surfactants studied by ζ-potential measurements with latex particles" Langmuir, **14**, (1998) 1996.

2-05 Hydolophilic Modification of Vulcanised Rubber by Radiation Grafting

N. Mizote [a)], A. Katakai [b)] and M. Tamada [b)]

[a)]Mitsuba Co.Ltd.,[b)]Environment and Industrial Materials Research Division, QuBS, JAEA

Rubber wiper is generally chlorinated to improve the properties such as friction, adhesion and abrasion. However, chlorination causes the degradation of wiping performance owing to the hardening of rubber surface. Thus, a novel technology of surface modification is inevitable to decrease the environmental burden of chlorination. In the present study, hydrophilic modification of vulcanised rubber by radiation grafting is evaluated as a new surface treatment for the blade rubber.

1. はじめに

加硫ゴム製品は摩擦・粘着性の低減、耐摩耗性の向上等を目的として表面処理が行われている。自動車用ワイパーゴムでは、ハロゲン処理が行われてきたが、最近、グラファイト焼付けコーティングが注目され、払拭摩擦の低減や耐磨耗性の向上に寄与している[1)]。しかし、これら表面処理によって、ゴム表面の柔軟性が低下し、ガラス追従不良による払拭性の悪化が問題となっている[2)]。本研究では放射線グラフト重合法による加硫ゴム表面の親水化について検討し、摩擦低減と払拭性の双方の向上が可能なワイパーゴム表面処理技術としての可能性を評価した。

2. 実験方法

ゴム基材として、カーボンブラックを配合した厚さ2 mmの架橋天然ゴム用いた。2-ヒドロキシエチルメタクリレート(HEMA)のグラフト重合では、水を溶媒として用い、モノマー濃度30~70 wt%、照射線量10~25 kGyの範囲で電子線同時照射グラフト重合を行った。グラフト率はグラフト前後の重量増加から算出した。加硫ゴム表面に対する水の接触角は協和界面科学製接触角計により求めた。また表面硬度は高分子計測器製マイクロゴム硬度計により求めた。なおウェット状態から乾燥状態へ移行する際の表面硬度変化は、水に濡らしたゴムにおいて、余剰水分を拭き取ってからの表面硬度の経時変化により確認した。摩擦の測定はピンオンディスク型摩擦試験機を用い、ガラスディスクとグラフトした架橋天然ゴムとの間の乾燥摩擦係数を測定した。

3. 結果および考察

電子線同時照射法により加硫ゴムにHEMAをグラフト重合したときの、グラフト率の照射線量依存性をFig.1に示した。照射線量の増加に伴いグラフト率は上昇し、またモノマー濃度が高いほどグラフト率が高くなった。この結果から、加硫ゴム表面へのHEMAのグラフト重合は照射線量とモノマー濃度により制御できることが分かった。次にHEMAのグラフト重合における接触角のグラフト率依存性をFig.2に示した。HEMAのグラフトに伴い接触角は70°まで低下した。これらの結果からHEMAの電子線同時照射グラフト重合により加硫ゴム表面の親水化が可能である事が分かった。

Fig.3にウェット状態から乾燥状態への移行に伴う表面硬度変化を示した。この図で0 minは完全に水に濡れた状態で、経過時間3 minは完全に乾燥した状態である。

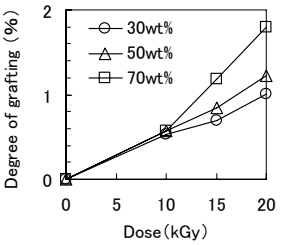

Fig.1 Dose dependence of the degree of grafting.

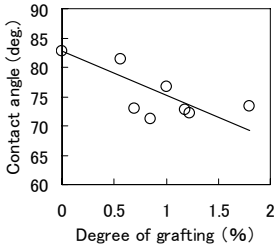

Fig.2 Relationship between the degree of grafting and the contact angle.

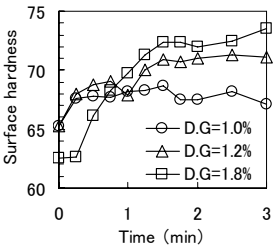

Fig.3 Change of the surface hardness due to a shift from wet to dry state.

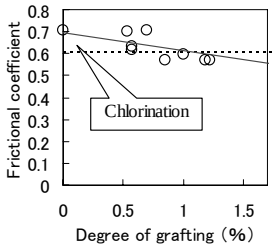

Fig.4 Relationship between the degree of grafting and the coefficient of friction.

グラフト率が1.8 %になると、加硫ゴムはウェット状態で表面硬度が低下する。またグラフト率が高くなるほどウェットと乾燥状態での表面硬度差が大きくなる事が確認できた。ウェット状態でゴム表面が軟化する事により、ワイパー雨滴払拭時のガラス追従性向上による高い払拭性が期待できる。次に電子線同時照射法により加硫ゴムにHEMAをグラフト重合したときの、摩擦係数のグラフト率依存性をFig. 4に示した。HEMAのグラフトにより摩擦係数は低下し、その値はハロゲン処理を下回ることが確認できた。これらの結果から、HEMAの電子線同時照射グラフト法はワイパーゴムの表面処理として満足できる摩擦特性が得られ、さらに従来にない摩擦低減と払拭性の双方を向上するワイパーゴム表面処理技術として有望であることが分かった。

References

1) 前川道信, 大倉重喜, トライボロジスト 50, 677 (2005).
2) 小暮勇治, 日本ゴム協会誌 65, 287 (1992)

2-06 Emulsion Graft Polymerization of Vinyl Acetate

M. Tamada [a)], N. Seko [a)], Y. Wada [b)] and H. Mitomo [b)]

[a)]Environment and Industrial Materials Research Division, QuBS, JAEA,
[b)]Faculty of Engineering, Gunma University

Grafting of vinyl acetate (VAc) on the surface of polyhydroxybutylate (PHB) film depresses the biodegradability of PHB. After saponification of grafting layer, the graft chains of VAc were converted into biodegradable polyvinylalcohol. As a result, VAc-grafted PHB recovered intrinsic biodegradability[1]. This grafting can lead that the PHB in use can not be degraded biologically and then its waste can be decomposed after alkaline saponification. Such characteristic of VAc-grafted PHB is applicable in the cabinet of household electrical appliances. To impart this property of off-on control of biodegradability, the grafting of VAc on PHB is inevitable. However, the grafting yield is so low that VAc solution more than 80 % should be used. It is found that emulsion of VAc in water could dramatically improve the grafting yield. In the present study, the reactivity in the emulsion grafting of VAc on PHB was compared with that in the methanol solvent.

PHB film, 150 μm thick, was prepared by thermal pressing of PHB powder (Mn=3.3×10^5). The film obtained was cut into the sample, 10mm×60mm, for grafting and then irradiated with 10kGy of electron beam in nitrogen gas. Irradiation of electron beam simultaneously induces the degradation of PHB. Molecular weight was reduced 45% of the initial value after irradiation of 10 kGy and 32 % at 50 kGy. The tensile strength decreased 10 % at 50 kGy[2]. Hence, the irradiation dose for grafting was restricted to 10 kGy to minimize the damage of trunk PHB.

The irradiated PHB film was put into glass reactor and 150 ml of VAc emulsion was added into the same reactor. to stabilize the VAc micelles in water at 60 ℃. VAc of 5 % was suspended in Nonion L-4 of the concentration from 0.2 to 1%. Instead of VAc emulsion, methanol and waster were used as solvents. The reactor was maintained at 60℃ to carry out the VAc grating. The grafting reaction was evaluated by degree of grafting (Dg):

$$Dg[\%]=(Wg-W_0)/W_0\times 100$$

where W_0 and Wg are weight of PHB films before and after graft polymerization, respectively.

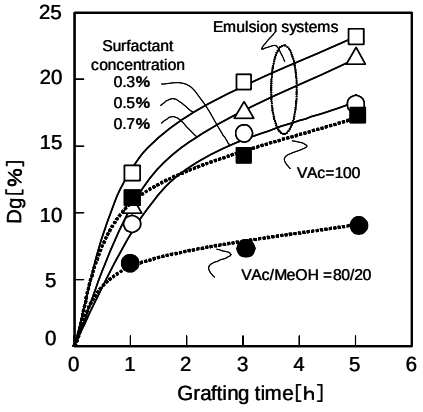

Fig. 1 Degree of grafting (Dg) in VAc emulsions, 100 % VAc and 80 % VAc in methanol. Polyoxyethylene monolaurate (Nonion L-4, NOF Co.) was used as surfactant in emulsion grafting.

Figure 1 shows the degree of grafting in VAc emulsions, 100 % VAc and 80 % VAc in methanol. In the emulsion grafting, Dg was affected by the concentration of Nonion L-4. At 0.5 %, Dg reached the maximum value of 23 % at the grafting time of 5 h. The micelle size of VAc was minimized at 0.4 μm. In the case of 80 % VAc in methanol, Dg was only 9 % at the grafting time of 5 h. This value of Dg was two fifth of the emulsion grafting. When 100 % of VAc was used, the Dg obtained was lower than those of the emulsion graftings.

The percentage of monomer consumed in the grafting was evaluated as monomer reactivity. The monomer reactivities of the grafting in water, emulsion, and methanol listed in Table 1. Since the VAc less than 2 % can be dissolved in water, the grafting data in 2 % water were compared. Monomer reactivities were 0.62 %, 1.01 %, and 0.010 % for the grafting in water, emulsion, and methanol, respectively. In the methanol, the monomer reactivity increased with the increment of monomer concentration. At 100 % VAc the monomer reactivity became 0.046 % which is lower than that in water and emulsion of 2 % VAc. The maximum reactivity was realized at emulsion grafting. The reactivities were around 1% in both VAc concentrations of 2 and 10% in the emulsion grafting.

References

1) Y. Wada et al., Radiat. Phys. Chem. 76 (2007) 1075 .
2) Y. Wada et al., J. Appl. Polym. Sci. 101 (2006) 3856.

Table 1 Monomer reactivities of the grafting in water, emulsion, and methanol in various concentrations of monomer.

Solvent	Monomer concentration [%]	Dg [%]	Monomer reactivity [%]
Water	1	2.6	0.68
Water	2	4.8	0.62
Water(emulsion)	2	7.8	1.01
Water(emulsion)	10	35.0	0.91
Methanol	2	0.1	0.010
Methanol	80	9.4	0.030

2-07 Adsorption Performance of Graft Amine Adsorbent for Au(III)

N. Seko and M. Tamada

Environment and Industrial Materials Research Division, QuBS, JAEA

To meet the demand for rare noble metals, it is necessary to reduce the amount of noble metals involved in catalysts to save the amount of such noble metals used in catalysts or increase the recycle rate of waste catalysts[1]. Recovery of these metals from waste catalysts is carried out by a wet process which comprise of dipping waste catalysts in a strong acid to dissolve the noble metals, and separating and purifying these metals from the resulting solution by an ion exchange method using chelate resin beads or by a solvent extraction method using a chelating reagent. However, the wet process has such disadvantages that diffusion of metal ions in the chelating resin beads is a rate-determining step in the recovery from low-concentrated metal solutions; the concentration efficiency is low, etc.

The objective of this study is the preparation of a new fibrous adsorbent containing amino groups for Au(III). A combination of methacrylic acid (MAA) or N-vinylacetamide (NVA) with allylamine (AAm) was co-grafted onto the nonwoven fabric (NF) using by pre-irradiation techniques[2]. The NF was irradiated with an electron beam up to 200 kGy in nitrogen atmosphere at ambient temperature. The irradiated NF was immersed in a monomer solution immediately deaerated by bubbling with nitrogen gas. The total concentration of the two monomers was set at 50 (wt/v) % in H_2O as a solvent, where the weight ratio of AAm/MAA or AAm/NVA in the monomer mixture ranged from 90/10 to 10/90. Co-grafting was performed at 313 K for a reaction time up to 8 hours. The degree of co-grafting (Dg) was calculated from the weight gain by before and after grafting. The resultant grafted-NF was referred to as AAm/MAA (x/y, Dg) or AAm/NVA (x/y, Dg) grafted-NF, where x/y and Dg designate the weight ratio of AAm/MAA or AAm/NVA in the monomer mixture and the degree of grafting, respectively.

Figure 1 shows the distribution coefficient of AAm/MAA and AAm/NVA adsorbents along with weight percent of AAm in the monomer. The D of AAm/NVA (50/50, 88) was $5x10^5$. This value was nine times higher than that of AAm/MAA (50/50, 100). The column mode study was conducted by using a column packed with the adsorbent named AAm/NVA (50/50, 88). Column-mode study was conducted by supplying a feeding solution of pH 3 containing 1 mM of Au(III) to the column at flow rates of 260, 520, or 1040 h^{-1} in space velocity (SV). These breakthrough curves are shown in Fig. 2. Although the breakthrough point slightly decreased at the extremely high flow rate of 1040 h^{-1}, there are no large differences in the bed volume (BV). The flow rate of 1040 h^{-1} is 100 times faster than that of general granular resin packed column. The breakthrough points of three flow rates were 163, 150 and 144 BV, respectively. Respective breakthrough capacities were 2.76, 2.18 and 1.95 mmol/g of Au(III) on AAm/NVA.

References

1) K. Fujiwara, Kagakukogaku. **55(1)** (1991) 21.

2) N. Seko et al., Nucl. Instr. Meth. Phys. Res. B **135** (2005) 21.

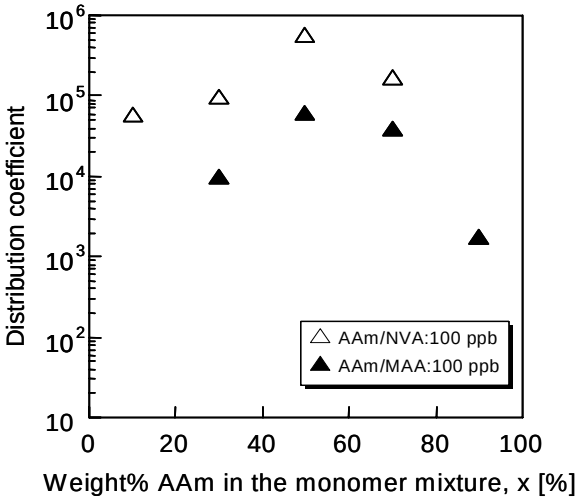

Fig.1 Distribution coefficient for Au(III) on AAm adsorbents.

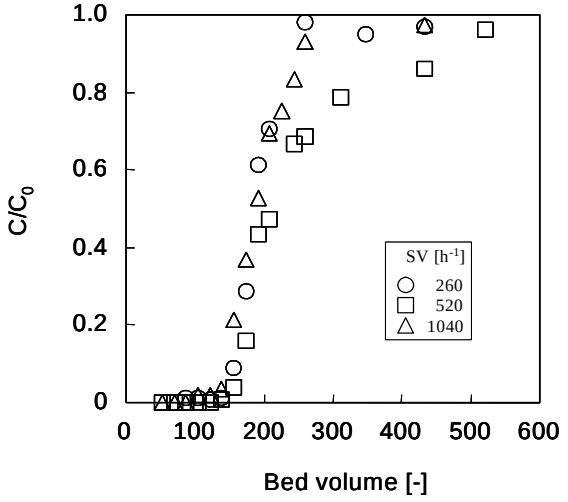

Fig.2 Effect of flow rate with 1mM Au(III) solution at pH3.

2-08 Synthesis of Graft Adsorbent with N-methyl-D-glucamine for Boron Adsorption

H. Hoshina, N. Seko, Y. Ueki and M. Tamada

Environment and Industrial Materials Research Division, QuBS, JAEA

Boron is widely distributed in the environment more often as boric acid or borate salt which is harmful to human organism, therefore WHO revised a drinking water guideline for boron in 1998. In response to this, a boron effluent standard was limited at 10 ppm in the water pollution control law in Japan. Then, it is expected that regulation for boron is more severe in near future. The most commonly used removal techniques for boron are chemical clarification and ion-exchange of granular resin having N-methyl-D-glucamine (NMDG). The chelating adsorbents having NMDG have been extensively investigated because NMDG has high affinity for boron adsorption[1]. However conventional adsorbents had a slow adsorption rate, and were difficult to adsorb a low concentration of boron efficiently. Therefore, we have been developed a new method to make more effective adsorbents for boron removal.

A non-woven polyethylene fabric as a trunk polymer purchased from Kurashiki MFG. Co. was irradiated by electron beam at voltage of 2 MeV, and current of 3 mA. Radiation induced grafting of glycidyl methacrylate (GMA) onto non-woven polyethylene fabric in aqueous medium with 0.05 wt% Tween20 as a surfactant in the presence of water was investigated. The Dg of 200 % was obtained with 5wt% GMA at 20 kGy for 60 min, which is enough for metal adsorbents. GMA-grafted fabric was chemically converted to NMDG. The maximum density 2.4 mmol/g of NMDG could be given by 5 wt% NMDG at 80 ℃ for 1 h.

To compare the boron adsorption performance of graft adsorbent with granular resin (NMDG density 2.2 mmol/g, particle size 0.8 mm), the column-mode adsorption was conducted. Column-mode adsorption was carried out by using the 10 ppm of boron solution at pH 7 at various flow rates. The characteristic of breakthrough was evaluated by plotting C/C0 which was the value of outflow concentration divided by the injecting concentration against bed volume (BV) as shown in Fig. 1. When the breakthrough point was determined at C/C0 of 0.05, the BV values at the breakthrough point were 235 and 138 of the graft adsorbent and the granular resin at SV10 h^{-1}, respectively. Figure 2 shows the effect of flow rate on BV at the breakthrough point of the graft adsorbent and the granular resin. The BV at the breakthrough point increased with decreasing flow rate. The BV at the breakthrough point of the graft adsorbent is higher than that of the granular resin at any flow rates. At the flow rate of SV50 h^{-1}, the result implied that the graft adsorbent has 4 times higher breakthrough capacity than the granular resin. The breakthrough capacity of the graft adsorbent at SV100 h^{-1} gave the same one with the granular resin at SV10 h^{-1}. This result indicates that the graft adsorbent can adsorb boron 10 times faster than the granular resin.

Reference

1) N. Kabay, I. Yilmaz, S. Yamac, S. Samatya, M. Yuksel, U. Yuksel, M. Arda. M. Saglam, T. Iwanaga, and K. Hirowatari, Reactive & Functional Polymers, 60, 163-170 (2004).

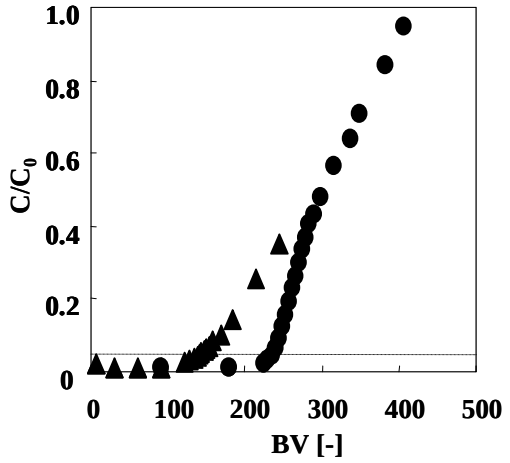

Fig.1 Breakthrough curve of graft adsorbent(●) and granular resin(▲) at SV10 h^{-1}

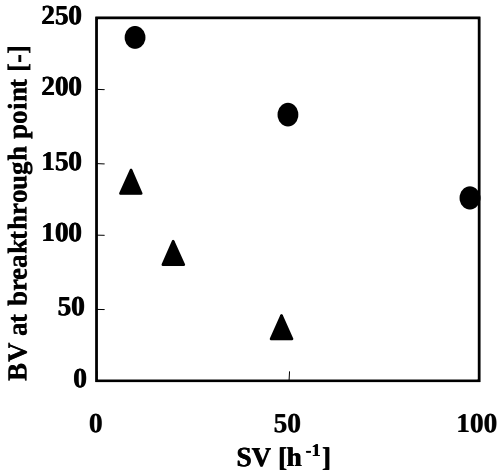

Fig.2 Effect of flow rate on BV at breakthrough point of graft adsorbent(●) and granular resin(▲)

2-09 Development of Bifunctional Iminodiacetic Acid Fiber

A. Jyo [a)], A. Ikegami [a)], H. Matsuura [a)], M. Tamada [b)], A. Katakai [b)] and N. Seko [b)]

[a)]Graduate School of Science and Technology, Kumamoto University, [b)] Environment and Industrial Materials Research Division, QuBS, JAEA

In this work, first, the monofunctional iminodiacetic acid fiber was prepared from polyethylene-coated polypropylene fiber (PPPE) grafted with vinylbenzylglycidylether (VBGE) according to Scheme 1. Electron (200 kGy) irradiated PPPE (0.9 denier, length 3.8 cm) was immersed in dimethyl sulfoxide solution of VBGE (50 weight %) for 24 h at 50 °C, and the weight increase of the resulting VBGE grafted

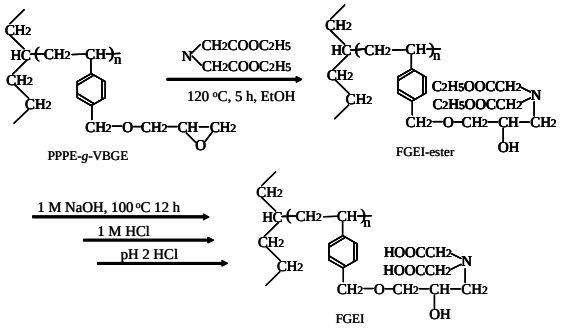

Scheme 1 Preparation of iminodiacetic acid fiber

PPPE (PPPE-*g*-VBGE) was 91% of the weight of the trunk PPPE. PPPE-*g*-VBGE was functionalized by heating in ethanol solution of diethyl iminodiacetate (67 volume %) for 5 h at 120 °C using a stainless steel autoclave. After alkaline hydrolysis of ester groups, the resulting fiber FGEI shown in Scheme 1 was finally equilibrated with a dilute hydrochloric acid of pH 2, and was dried in vacuum. Nitrogen content and acid capacity of FGEI were 1.7 mmol/g and 4.2 meq/g, respectively.

FGEI exhibited excellent performances in column-mode uptake of divalent metal ions from solutions of neutral pH. For instance, breakthrough capacity of Zn(II) is as high as ca. 0.5 mmol/g at high flow rate of 1000 h^{-1} in space velocity (SV). On the other hand, trivalent metal ions such as Fe(III) must be treated in strongly acidic solutions less than pH 2 to avoid their precipitation as hydroxides. Under such strongly acidic conditions, polymer bound iminodiacetic acid groups exist as electrically neutral or positively charged species, which interfere with uptake of trivalent cations. Then, the second purpose of this work is to resolve this problem. The introduction of sulfonate as second functional group is expected to be effective, because sulfonate exists as anionic species irrespective of pH. Negatively charged sulfonate enhances swelling of the polymer phase and also reduces the undesirable effect of positively charged species [-$HN^+(CH_2COOH)_2$]. However, the sulfonation of FGEI with chlorosulfonic acid and sulfuric acid resulted in marked weight loss of the fiber (ca. 30 %). This is probably due to cleavage of ether bonds by the strong acids. Then, we have examined the electron irradiation induced graft polymerization of sodium styrenesulfonate (SSS) onto FGEI.

FGEI-ester, FGEI in Na^+ form, and FGEI in H^+ form were irradiated by electron (200 kGy) and they were immersed in an aqueous solution of SSS (16.7 weight %) at 40 °C for a given time. FGEI-ester grafted with SSS was hydrolyzed and changed into the H^+ form (FGEIS1). The other two SSS grafted fibers FGEIS2 and FGEIS3 were also changed into the H^+ form. Results for graft polymerization of SSS are summarized in Table 1, which shows that the reactivity of SSS in the electron irradiation induced graft polymerization increases in the order FGEI-ester < FGEI(Na^+) < FGEI(H^+). However, too much SSS was introduced in cases of FGEIS2 and FGEIS3, and then the effect of grafted SSS on uptake of Fe(III) was examined by using FGEIS1. The results are shown in Fig. 1. The monofunctional iminodiacetic acid fiber FGEI can not effectively take up Fe(III) at pH 1.5. On the contrary, the bifunctional fiber FGEIS1 can take up Fe(III) even at high flow rate of 1000 h^{-1} in SV. FGEI and FGEIS1 gave breakthrough capacities of 0.09 and 0.61 mmol/g for Fe(III) at the feed flow rate of SV 50 h^{-1}, respectively. Thus, the electron irradiation induced graft polymerization is useful for preparation of bifucntional chelating fibers containing sulfonate without use of harmful acids.

Table 1 Properties of bifunctional iminodiacetate acid fibers in the H^+ form

Precursor	Objective Fiber	TG[a)] (h)	WI[b)] (%)	N content (mmol/g)	S content (mmol/g)	Acid capacity (meq/g)
PGEI-ester	FGEIS1	5	44.5	1.03	1.27	4.3
		7	60.3	0.907	1.57	4.6
PGEI(Na^+)	FGEIS2	5	112	0.764	2.34	4.5
		5	104	0.667	2.47	4.5
PGEI(H^+)	FGEIS3	3	123	0.810	2.31	4.0
		5	191	0.589	2.47	4.2

a) Time for graft polymerization. b) Weight increase

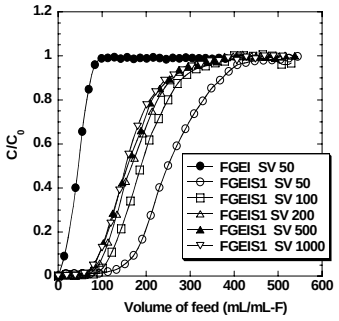

Fig. 1 Column-mode uptake of Fe(III) by FGEI and FGEIS1. Column: FGEI 1.2 mL (0.35 g), FGEIS1 1.0 mL (0.35 g). Feed: 0.001 M Fe(III) pH 1.5. SV means space velocity (h^{-1}).

2-10 Preparation of Graft Adsorbent with Ultrafine Non Woven Fabric

F. Basuki [a)], N. Seko [b)] and M. Tamada [b)]

[a)]Center for Education and Training, National Nuclear Energy Agency, BATAN,
[b)]Environment and Industrial Materials Research Division, QuBS, JAEA

The chelating adsorbent containing phosphoric group has been extensively investigated because of its unique selectivity to the metal ion. We have prepared fibrous phosphoric chelating adsorbent (FPCA) direct synthesized by radiation induced graft polymerization. It has been demonstrated that FPCA had good ability to remove toxic metals such us Pb and Cd [1)]. This adsorbent also had 200 times higher distribution coefficient for uranium than that of a commercial adsorbent al low pH [2)]. Although the FPCA was successfully prepared for industry application, the optimum grafting condition (200 kGy dose, 20 % monomer, 10/90 wt% methanol-water, 12 h reaction time at 60 ^{o}C which degree of grafting reached 250 %) need to be improved. In the present study we have made improvement by using ultrafine non woven fabrics to get optimum condition of grafting.

Polypropylene coated polyethylene (PPPE, diameter was 15 μm) and Polyethylene non-woven fabrics (UFPE, diameter was 2 μm) were cut into rectangular shape (3 cm x 5 cm) and placed into polyethylene bag. After de-aerated with nitrogen gas, samples were irradiated with electron beam in dry ice condition. The irradiated samples were contacted with phosphoric acid monomer solution (2-hydroxyethyl methacrylate phosphoric acid (HMPA) in SDS/methanol-water) in de-aerated glass ampoule and maintained at desired reaction time and temperature in water bath. At the completion of grafting, the graft copolymer was washed by methanol.

The ability of grafting between PPPE and PE polymer is shown in Fig 1. Radiation dose used was 100 kGy, 30 % monomer, 60 ^{o}C reaction temperature. The degree grafting (Dg) for UFPE reached 750 % for 6 hours and for PPPE the highest Dg was 93 %. In graft reaction, because the total surface area increased with decreasing the diameter of fiber Dg increased. The Dg in 2 % SDS solution was higher than methanol and no homo-polymerization observed. So 2 % SDS can be replaced of previous condition. Since the grafting rate of UFPE was high, grafting conditions could be optimized to 50 kGy of dose, 20 % monomer, 60 ^{o}C and 3 hours. From the FTIR spectra, the grafted samples have a very strong band at 1732 cm^{-1}, which were characteristic of carbonyl group, and the peaks at 1262 cm^{-1} and 1151 cm^{-1} correspond to P=O and O-P-O bonds in phosphoric group, respectively. In the SEM photos, the average diameter of UFPE of non-grafting, Dg of 59, 110, 168, 189, 299, and 479 % were 2.3, 2.6, 2.8, 3.0, 3.2, 3.4 and 3.6 μm, respectively. As a conclusion, by using UFPE the optimum grafting condition had been improved as follows; the dose was 50 kGy, 20 % monomer-2 %SDS in water solution, 60 ^{o}C and 3 hours which Dg reached 230 %.

References

1) Basuki F. Seko N, Tamada M, Sugo T, Kume T, J. Ion Exchange,14A, 209 (2003).
2) Seko.N, Tamada M, Yoshii F, Nucl. Instr. Meth Phys. Res. B, 236, 21 (2005).

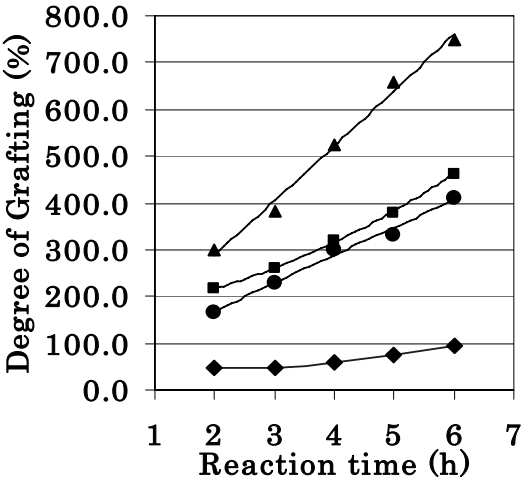

Fig.1 Dg of HMPA at various reaction times.
▲:PE/100 kGy/30 %monomer/2 %SDS,
◆:PPPE/100 kGy/30 %monomer/2 %SDS,
■:PE/100 kGy/30 %monomer/10 %MeOH,
●: PE/50 kGy/20 %monomer/2 %SDS

2-11 Synthesis of Graft Adsorbent with Amine Groups onto Polylactic Acid Nonwoven Fabric

L. D. C. Nayanajith [a)], Y. Ueki [b)], N. Seko [b)] and M. Tamada [b)]

[a)]Industrial Technology Institute, Sri Lanka, [b)]Environment and Industrial Materials Research Division, QuBS, JAEA

1. Introduction

Graft adsorbents, which can rapidly remove and effectively recover metal ions from water resources, are attracting a lot of attention as sophisticated metal adsorbents. However, the most of them were synthesized from petroleum materials[1)]. If plant-derived polymer, such as polylactic acid (PLA), is used as trunk polymer for graft polymerization, the consumption of petroleum can be reduced, and besides the reduction of environmental burdens is brought because of biodegradable property of themselves. In the present study, the preparation of PLA-based metal adsorbent was eagerly attempted by using radiation-induced graft polymerization.

2. Expermental

PLA nonwoven fabrics (a basis weight of 120 g/m^2) were irradiated with a certain dose of electron beam in nitrogen atmosphere. The grafting was carried out by immersing the irradiated fabrics into the aqueous emulsion solution consisting of 4-chloromethylstyrene (CMS), Tween 20 (surfactant) and deionized water. After grafting, the CMS-grafted samples were further treated with 50 wt% ethylenediamine (EDA) in isopropyl alcohol (IPA) at 60°C. The degree of grafting (Dg) was estimated by the increased weight after grafting, and the amine group density was defined by the nitrogen content of EDA-modified adsorbent, respectively. The metal adsorption capacity was individually evaluated through the batch adsorption experiments. The batch adsorption tests were carried out by dipping the adsorbent of 30 mg into 50 mL of each metal ion solution of 100 ppm at 25 °C for 24 h.

3. Results and Discussion

In this work, irradiation dose of 100 kGy, CMS concentration of 3 wt%, Tween 20 concentration of 0.3 wt% and reaction temperature at 40 °C were optimum conditions for CMS grafting onto PLA. As shown in Fig. 1, the Dg of PLA nonwoven fabric can be controlled in the range of up to 115 % under the optimal graft polymerization conditions. However, the optimal graft polymerization time was determined for 4 hours because the homopolymerization of CMS was occurred after 4 hours, and then the Dg at 4 hours reached about 80 % (2.8 mmol-CMS/g-adsorbent).

In the modification process of CMS-grafted PLA with EDA, PLA was readily hydrolyzed by EDA, and its mechanical strength decreased. Therefore, to prepare PLA-based metal adsorbents with adequate performance and sufficient mechanical strength, the effect of composition of modification solvent on the introduced functional groups was investigated. As a result of trial and error, 50 wt% EDA in IPA was found to be the optimum condition, and then its EDA group density was 3.0 mmol/g-adsorbent.

The EDA-modified adsorbent showed higher affinity to Cu^{2+} and lower affinity to Cd^{2+}, Pb^{2+} and Zn^{2+}. As seen in Fig. 2, this adsorbent could effectively capture metal ions from weak acid and neutral solutions, and then the equilibrium adsorption amounts for Cu^{2+} at pH 5.2 and Cd^{2+}, Pb^{2+} and Zn^{2+} at pH 7 were 2.5, 0.37, 0.23 and 0.21 mmol/g-adsorbent, respectively.

Reference

1) N. Seko, M. Tamada and F. Yoshi, *Nucl. Instr. Meth. Phys. Res. B*, **236** (2005) 21–29.

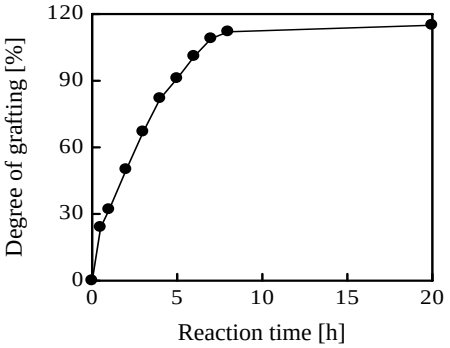

Fig.1 Effect of reaction time on Dg.

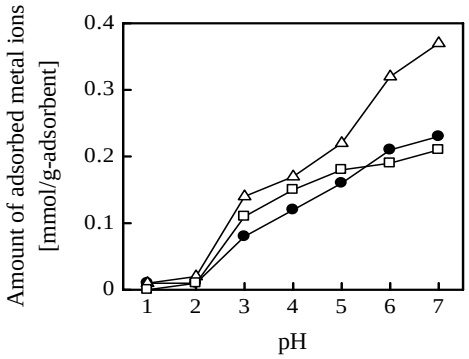

Fig.2 Effect of pH on adsorption of Cd^{2+} (△), Pb^{2+} (●) and Zn^{2+} (□) on EDA-modified adsorbent (3 mmol-EDA/g-adsorbent).

2-12 Preparation of New Adsorbent Containing Hydroxamic Acid Groups by Grafting for Metal Adsorption

S. Phiriyatorn [a)], H. Hoshina [b)], N. Seko [b)] and M. Tamada [b)]

[a)]Thailand Institute of Nuclear Technology,
[b)]Environment and Industrial Materials Research Division, QuBS, JAEA

Introduction

Hydroxamic acid groups can form complexes with various metal ions such as Cd^{2+}, Fe^{2+}, Fe^{3+}, Zn^{2+}, Pb^{2+}, Ni^{2+}, Hg^{2+}, Au^{3+}, Ag^{+}, Cu^{2+}, Co^{2+}, Cr^{3+}, and UO_2^{2+} [1-3)]. In the present work, a new adsorbent containing hydroxamic acid groups was synthesized by radiation-induced graft copolymerization of methyl acrylate (MA) onto nonwoven fabric composed of polyethylene-coated polypropylene fiber. Graft copolymerization was carried out in MA emulsion containing sodium dodecyl sulfate (SDS) as an emulsifier in the presence of water. Grafting polymerizations were studied with regard to various parameters of importance: dose, concentration of MA, reaction time, reaction temperature, and concentration of SDS. Conversion of the ester groups of the grafted copolymer into the hydroxamic groups was performed by treatment with an alkaline solution of hydroxylamine (HA).

Experiment

The trunk polymer fabrics were packed in a polyethylene bag under nitrogen atmosphere. After irradiation, fabrics were placed into a glass ampule and were evacuated. The deaerated MA solution was transferred into the ampule. The grafted copolymers were reacted with hydroxylamine in a methanol-water mixture at 75 ºC to convert the ester groups of grafted copolymer to hydroxamic acid groups. The percentage conversion was determined by elemental analysis.

Result and Discussion

Degree of grafting increased with increasing dose, MA concentration, reaction temperature, and reaction time and decreased with an increasing SDS concentration. The grafted copolymer produced with 2 % MA, 0.1% SDS wt/v water, dose 20 kGy, reaction time 1 h, and reaction temperature 40 ºC gave degree of grafting 120 % (6.33 mmol/g of MA group) (Fig.1). The maximum percentage conversion of the ester groups of the grafted copolymer into the hydroxamic groups was 60 % at optimum condition: 20 % HA in methanol-water ratio (5:1), pH 13, reaction time 1 h, and 1 g of trunk polymer. The FTIR spectrum of grafted copolymer shows a new characteristic absorption band of an ester at 1725 cm-1 due to C=O stretching mode in addition to the same adsorption bands of trunk polymer as shown in Fig. 2 while the FTIR spectrum of modified copolymer shows the characteristic absorption bands of hydroxamic acid (C=O at 1711 cm-1) and amide (N-H at 1629 cm-1). Adsorbent containing hydroxamic acid groups can adsorb 99 % of UO_2^{2+}, 98 % of V^{5+}, 97 % of Pb^{2+}, and 96 % of Al^{3+} at pH, 5, 4, 6, and 4, respectively after contacted with 100 ppb metal solution for 24 h.

References

1) H. L. Yale, Chem. Rev., 33, 209 (1943).
2) R. M. Mendez, V.N. Sivasankara Pillai, Talanta, 37, 591 (1990).
3) Y. K. Agrawal, H. Kaur, S.K. Menon, React. Funct. Polym., 39, 155 (1999).

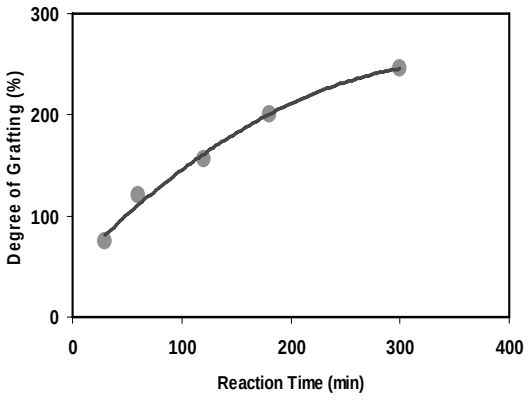

Fig 1. Effect of reaction time on degree of grafting.

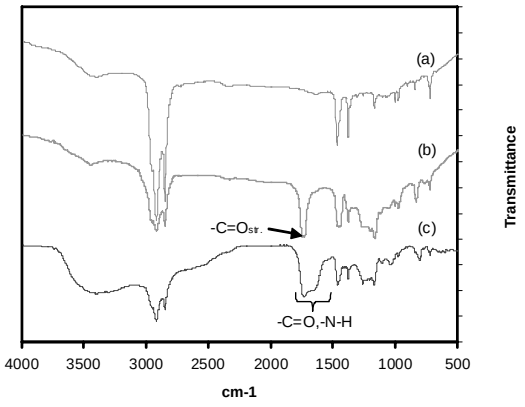

Fig 2. FTIR spectrum of (a) trunk polymer, (b) grafted copolymer, (c) adsorbent .

2-13 Preparation and Characterization of Polylactic Acid Nonwoven Fabric-based Metal Adsorbent

Y. Ueki, N. Seko, H. Hoshina and M. Tamada

Environment and Industrial Materials Research Division, QuBS, JAEA

1. Introduction

The graft adsorbent has been attracting attention as a sophisticated metal adsorbent because the adsorption rate is 10–100 times higher than that of a commercially available particulate resin[1)]. However, these adsorbents are originated from petroleum resources[2)]. If plant-derived polymer, such as polylactic acid (PLA), is used as a trunk polymer, the dependence on petroleum resource and the amount of industrial waste can be decreased to some extent. In the present study, the preparation of PLA-based metal adsorbent was attempted by using radiation-induced graft polymerization, and the metal adsorption capacity and the selectivity for various metal ions were evaluated.

2. Expermental

PLA nonwoven fabrics (fiber diameter: 18 μm) were irradiated with a certain dose of electron beam in nitrogen atmosphere at dry ice temperature. The graft polymerization was carried out by immersing the irradiated samples into the aqueous emulsion solution consisting of GMA, Tween 20 (surfactant) and deionized water at the desired reaction temperature. After grafting, the GMA-grafted samples were further immersed in 0.5 M of disodium iminodiacetate (IDA-Na) solution at 80 °C. The degree of grafting (Dg) was estimated by the increased weight after grafting, and the IDA group density of the adsorbent was estimated by the equilibrium adsorption capacity for Cu^{2+}, respectively. The metal adsorption capacity of the adsorbent was individually evaluated through the batch adsorption experiments. The batch adsorption tests were carried out by dipping the adsorbent of 30 mg into 50 mL of each metal ion solution of 100 ppm at 25 °C for 24 h.

3. Results and Discussion

The optimum grafting conditions were basis weight of 120 g/m^2, dose of 50 kGy, GMA concentration of 4 wt%, Tween 20 concentration of 0.1 wt%, reaction temperature at 40 °C, and the Dg can be controlled in the range of up to 200 % (4.7 mmol-GMA/g-grafted PLA) (Fig.1).

Figure 2 shows the effect of methanol (MeOH) concentration in the modification medium on the IDA group density. The IDA group density increased with the increase of the MeOH concentration. However, at the same time, the PLA was also damaged by the IDA groups themselves, and its mechanical strength was deteriorated. The IDA group density of PLA-based metal adsorbent, which had adequate metal adsorption capacity and sufficient mechanical strength, was about 500 μmol/g-adsorbent.

The order of metal ion selectivity of the graft adsorbent was $Cu^{2+} > Pb^{2+} > Ni^{2+} > Zn^{2+} > Cd^{2+} > Co^{2+} > Ca^{2+} > Mg^{2+}$ and the equilibrium adsorption capacities for each metal ion were 488, 423, 418, 317, 284, 207, and 111 μmol/g-adsorbent, respectively. Although this selectivity was in the same order of that of a commercially available particulate resin (DIAION CR11), its adsorption capacities for heavy metal ions were within the range from 30 to 80 % of those of the DIAION CR11. This difference of the adsorption capacities was caused by the lower conversion rate, below 25 %, of the GMA-grafted chains in order to maintain the sufficient mechanical strength of the fabrics.

References

1) S. Aoki, K. Saito, A. Jyo, A. Katakai and T. Sugo, *Anal. Sci*., **17 Suppl**. (2001) i205–208.
2) N. Seko, M. Tamada and F. Yoshi, *Nucl. Instr. Meth. Phys. Res. B*, **236** (2005) 21–29.

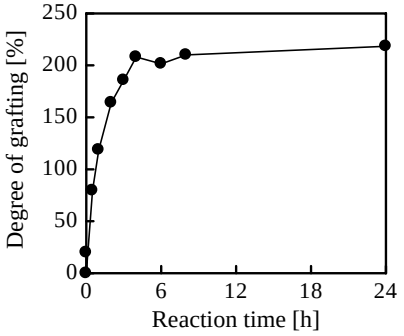

Fig. 1 Effect of reaction time on Dg.

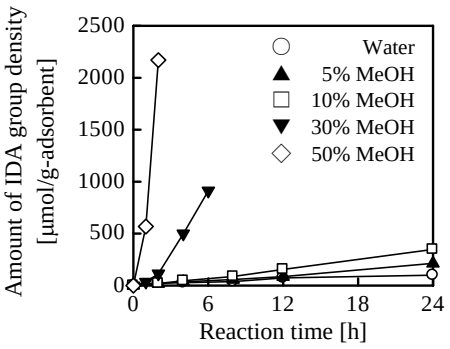

Fig. 2 Effect of MeOH concentration on IDA groups density.

2-14 Metal Adsorption of Blend Hydrogels Based on Carboxymethyl Cellulose and Carboxymethyl Chitosan

A. Hiroki [a)], H. T. Tran [b)], N. Nagasawa [a)], T. Yagi [a)] and M. Tamada [a)]

[a)]Environmental and Industrial Materials Research Division, QuBS, JAEA,
[b)]Dalat Nuclear Research Institute, VAEC

It is well known that hydrogels of carboxymethyl cellulose (CMC) and carboxymethyl chitosan (CMCts) are produced by gamma or electron beam irradiation with their high concentrated aqueous solution [1)]. The hydrogels adsorb metal ions such as Cu and Ca due to the carboxyl group and amino group on the side chain of CMC and CMCts [2)]. In the present report, we report metal adsorption of blend hydrogels prepared by γ-irradiation with the mixtures of CMC and CMCts. The adsorption of Pb and Au ions onto the blend hydrogels were controlled with the composition of the CMC and CMCts.

CMC and CMCts, which were purchased from Daicel Co. Ltd, Japan and Koto Chemicals Co. Ltd, Japan, respectively, have a degree of substitution of 0.91, and CMCts has a degree of deacetylation of 84%. The CMC/CMCts aqueous solution of 30 wt.% (blend ratio of CMC/CMCts: 100/0, 75/25, 50/50, 25/75, 0/100) were sealed in polyethylene nylon bags for air-free conditions after degassing using vacuum apparatus. The irradiations were carried out using ^{60}Co γ-ray source at the Takasaki Advanced Radiation Research Institute, Japan Atomic Energy Agency. The samples of paste state were irradiated to a total dose of 20 to 200 kGy (a dose rate: 10 kGy/h) at room temperature to obtain blend hydrogels. The gel fraction of the obtained hydrogels was determined gravimetrically by measuring the insoluble part after extraction of sol. The metal ion concentration in a solution was measured by Inductively Coupled Plasma Mass Spectrometer, and then the adsorption rate of Pb and Au ions with the hydrogels was calculated.

Figure 1 shows the gel fraction of CMC/CMCts blend hydrogels as a function of irradiation dose. The gel fraction increased sharply up to 30 kGy and reached a constant value in the range of 100-200 kGy. An increase in the ratio of CMC raised the gel fraction of blend hydrogel. According to gel permeation chromatography, the molecular weight of CMC and CMCts was 5 x 10^5 and 6 x 10^4, respectively. Therefore, crosslinking of CMC is easier to occur than that of CMCts in the same condition because of entanglement between the polymer chains, resulting in the increase in the gel fraction of the obtained hydrogels.

The nitrogen content in the blend hydrogels was determined by means of elemental analysis. The nitrogen content in the obtained hydrogels was proportional to the ratio of CMCts in the mixture, which was almost equal with theoretical ones. This indicates that the obtained hydrogels were constructed at the initial ratio of CMC/CMCts.

The relationship between the composition of CMC/CMCts in the blend hydrogels and the adsorption rate of Pb and Au ions is shown in Figure 2. The adsorption rate of metal ions increased with increasing the composition of CMCts. The adsorption rate of Pb ions increased from 55 % to about 75-80 % in the presence of CMCts. On the other hand, in the case of Au ions, the increases in the adsorption rate appeared clearly. Although the adsorption rate with CMC/CMCts (100/0) blend hydrogel was slightly 10 %, it reached 60 % at 75/25 of ratio and increased gradually to 90 %. Therefore, it suggests that the metal adsorption with the CMC/CMCts blend hydrogels was significantly influenced by amino group on the CMCts.

References

1) F. Yoshii, et al., *Nucl.Instr. and Meth. B*, **208**, 320-324 (2003).
2) N. Nagasawa, et al., *JAEA-Review 2006-042*, 52 (2007).

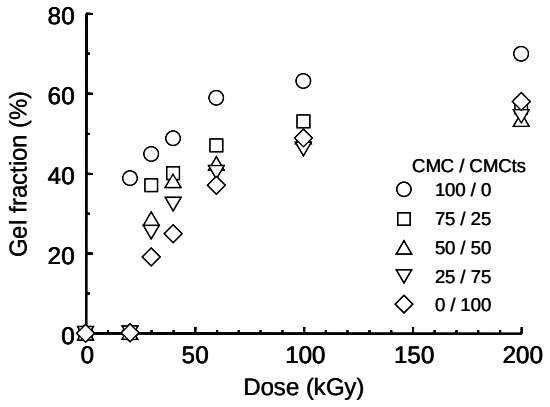

Fig. 1. Effect of dose on the gel fraction of CMC/CMCts blend hydrogels.

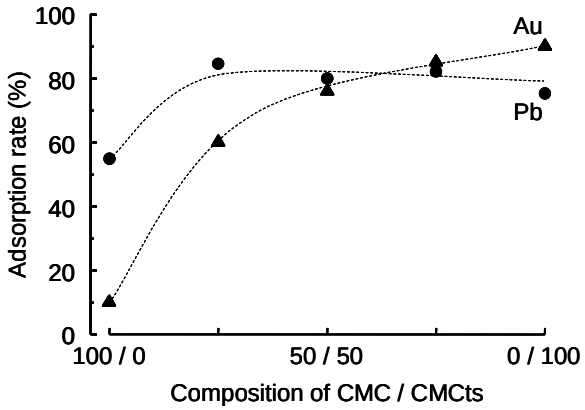

Fig. 2. Adsorption rate of Pb and Au ions with the CMC/CMCts blend hydrogels.

2-15 Improvement of Physical Properties of Poly(butylene terephthalate-*co*-adipate) / Poly(lactic acid) Blend Film by Radiation Crosslinking

N. Nagasawa [a)], P. H. Sarath Kumara [b)], T. Yagi [a)] and M. Tamada [a)]

[a)]Environment and Industrial Materials Research Division, QuBS, JAEA,
[b)]Rubber Research Institute of Sri Lanka

Poly (lactic acid) (PLA) is a biodegradable polymer produced by condensation polymerization of lactic acid obtained by fermentation of starch, which resources are renewable. The variety of PLA applications include food packaging, bottles, medical and pharmaceutical products result from very favorable properties of PLA such as high transparency, strength, biodegradability, biocompatibility, and barrier properties. Nonetheless, the brittleness, low deformation at break and the lack of flexibility limit its applications. Modification of PLA by blending with biodegradable aromatic polyesters to improve its mechanical properties has not been reported. The present attempt was made to modify PLA by blending with another biodegradable aromatic flexible polymer namely poly(butylene terephthalate-*co*-adipate) (PBTA) shown in figure 1. Triallyl isocyanurate (TAIC) as a polyfunctional monomer has been found to be the most effective crosslinking agent for PLA to improve heat-resistance in a previous study.[1,2)] The effects of electron beam (EB) irradiation in the presence of TAIC on heat-resistant and mechanical properties of the blends was investigated.

PLA, PBTA and TAIC used in the experiments were supplied as LACEA® H100 by Mitsui Chemicals Co., Japan, Ecoflex® by BASF and by Nippon Kasei Chemical Co Ltd., Japan, respectively. The blends of polymers were mixed at different ratios at 180 ºC for 10 minutes in a Laboplastomill model 50C150 (Tokyo Seiki Ltd, Tokyo, Japan) at a rotor speed of 60 rpm. TAIC was incorporated into the mixture before mixing in the plastomill. The films from the blends were hot-pressed at 180 ºC for 5 min and then cooled with running water to room temperature for 5 min to form a film with thickness of 0.5 mm. The films were enclosed in radiation resistant polyethylene / nylon bags and vacuum sealed before irradiation at different doses from 20 kGy up to 200 kGy by using an EB accelerator with a dose rate of 10 kGy pass^{-1}. Gel fractions and mechanical properties of crosslinked PBTA / PLA blend films were measured by chemical methods and tensile measurements.

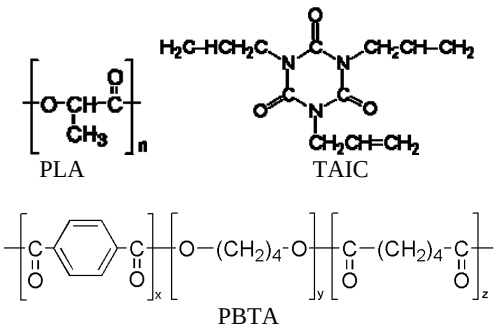

Fig. 1 Structure of PLA, PBTA and TAIC

Figure 2 shows gel fraction of PBTA / PLA blend film with different concentration of TAIC irradiated in EB accelerator at 50 kGy versus PLA content. PBTA / PLA blend film without TAIC didn't form gel. However, PBTA / PLA blend film with over 1 parts per 100 parts resin (phr) TAIC began to form gel at all PLA contents. Gel fraction of blend film mixed with 3 or 5 phr of TAIC increased steeply with increasing content of PLA in blend. It was found that TAIC at upward of 3 % concentration is necessary to promote gelation of PBTA / PLA blend.

The elongation at break of blend films was measured and showed PLA has improved point of hard but brittle at room temperature. As a result, elongation of crosslinked PLA with 5 phr TAIC EB-irradiated at 50 kGy was about 3 %, that crosslinked PBTA / PLA (8/2) blend with 5 phr TAIC increased approximately 300 %. Furthermore, the blend film was found to keep the shape by heating at 170 ºC. The brittleness and heat-resistance of PLA were improved by the blending with PBTA and the radiation crosslinking with addition of TAIC.

References

1) H. Mitomo, A. Kaneda, T. M. Quynh, N. Nagasawa, F. Yoshii, *Polymer*, **46**(3), 4695 (2005)
2) N. Nagasawa, A. Kaneda, S. Kanazawa, T. Yagi, H. Mitomo, F. Yoshii, M. Tamada, *Nucl. Instrum. Methods Phys. Res., Sect. B*, **236**(1-4), 611 (2005)

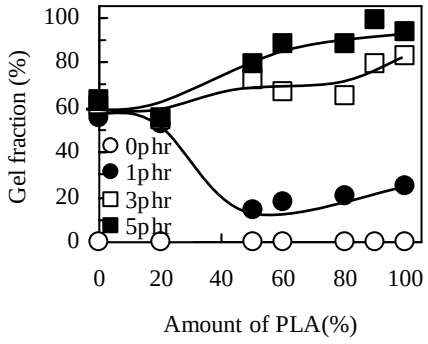

Fig. 2 Crosslinking behavior of PBTA / PLA blend films, which involve different TAIC amount, formed by EB-irradiation at 50 kGy.

2-16 Modification of Elastic Poly(lactic acid) by Radiation-induced Crosslinking

S. Kanazawa [a)], N. Nagasawa [b)], T. Yagi [b)] , T. Hayasaki [a)] and M. Tamada [b)]

[a)]Sumitomo Electric Fine Polymer Inc., [b)]Environment and Industrial Materials Research Division, QuBS, JAEA

Poly(lactic acid), PLA was irradiated using electron beams in the presence of triallyl isocyanurate at 5 phr concentration as crosslinking agent. The crosslinked PLA, of which heat resistance was improved, is applied on flexible and elastic materials by addition of plasticizer or immersion in plasticizer. The elastic PLA material has several advantages such as high holding plasticizer, heat resistance at 80 ºC and transparency. It can be concluded that crosslinking technology is beneficial to expanding application of soften PLA.

.

植物原料由来のポリ乳酸は、地球温暖化防止の観点から廃棄燃焼処理により大気中の二酸化炭素増加を招く石油由来プラスチックの代替材料として実用化検討が進められている。しかし、ポリ乳酸は耐熱性・耐衝撃性等の点で汎用プラスチックに劣り、実用化の妨げになってきた。原子力機構では、多官能性モノマーであるトリアリルイソシアヌレート(TAIC)の添加と放射線照射によるポリ乳酸の橋かけに成功しており[1)]、その耐熱性向上効果、形状記憶効果を利用した熱収縮材への適用等を住友電工FPとともに行ってきた[2)]。さらなる実用化検討の結果、放射線橋かけの可塑剤担持性向上効果を応用した、弾性ポリ乳酸の開発に成功した。

三井化学社製ポリ乳酸（レイシア H-440）に融点以上の温度（180 ºC）で TAIC を 5 質量部添加して混練した後、同温の熱プレス機にて 500 μm 厚のシートを作製した。電子線を 2 MeV、90 kGy 照射した後に、理研ビタミン社製可塑剤リケマール PL-710 および PL-019 の液中に 120 ℃で２時間浸漬・膨潤させ、可塑剤担持量（可塑剤質量／全体質量×100）が各々40 %、35 %の「弾性ポリ乳酸」を得た。弾性ポリ乳酸の可塑剤維持性を評価するために、80 ºC の恒温槽内に静置し、可塑剤の析出による重量減少の度合いを見た。さらに、可塑剤とポリ乳酸の複合化状態を見るために、透過電子顕微鏡（TEM）による微細構造の観察を行った。

Figure 1 に 80 ºC 恒温槽内での重量変化を示す。放射線橋かけポリ乳酸は、30 %を超える高い可塑剤担持状態を 80 ºC で 15 日間に亘って維持した。これは、同じ可塑剤 30 %を、加熱溶融したポリ乳酸に練り込んだ場合には常温でも数時間後に多くが析出する事を考えると、極めて高い保持力である。

コントロールとして、①電子線を照射しないシート、②TAIC を配合しないシートを作製したが、①と②のいずれも、可塑剤への浸漬工程で可塑剤の浸潤が起こらず白色化した。白色化は膨潤工程の熱で再結晶化したものと考えられた。以上の結果から、ポリ乳酸において可塑剤を高率に担持した状態を達成・維持するためには放射線橋かけ技術は非常に有効な手段だと考えられる。

Figure 2 に開発品の TEM 写真を示す（ポリ乳酸は白部分、可塑剤は黒部分に相当）。橋かけポリ乳酸の形態は 20 nm 程度のナノサイズの結晶凝集体を起点としたポア構造となっており、可塑剤はこのポリ乳酸のポア中に含有されていると考えられる。

本技術は、エラストマー様な弾力性の感触を有したポリ乳酸を開発しており、「ポリ乳酸は硬く脆い」という従来の一般認識を大きく変えるものであり、具体的な実用化についての検討を今後進める計画である。

References

1) H.Mitomo et al., Polymer, 46, 4695(2005)
2) N.Nagasawa et al., Nucl. Instr. and Meth. in Phys. Res., B, 235, 616(2005).

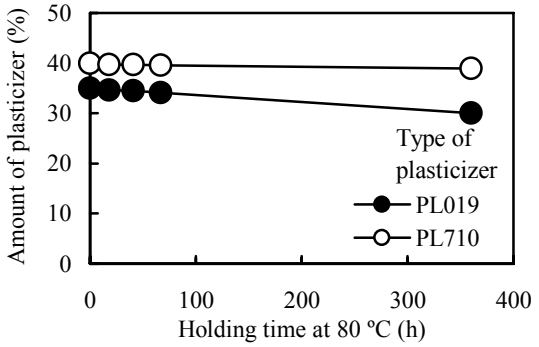

Fig. 1 Amount of plasticizer in the crosslinked PLA by EB-irradiation at 90 kGy as a function of holding time at 80 ºC.

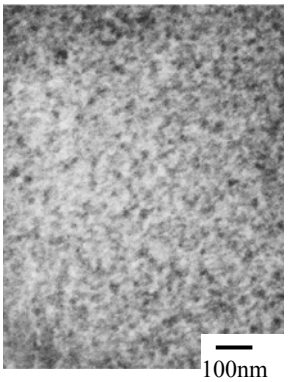

Fig. 2 TEM photograph of the crosslinked PLA with 35 % plasticizer. White area: PLA, Black area: plasticizer (PL-710)

2-17 Radiation Crosslinking of Poly(L-lactic acid) / Poly(D-lactic acid) Stereocomplex

T. M. Quynh [a)], D. Nagai [a)], N. Nagasawa [b)], T. Yagi [b)], M. Tamada [b)] and H. Mitomo [a)]

[a)]Graduate School of Engineering, Gunma University,
[b)]Environment and Industrial Materials Research Division, QuBS, JAEA

Poly(L-lactic acid) (PLLA) is produced by condensation polymerization of lactic acid obtained by fermentation of starch, which resources are renewable. Therefore, PLLA is a typical chemically synthesized and sustainable biodegradable thermoplastic, which is expected wide usage in the near future replacing many non-biodegradable engineering plastics. The applications of PLLA include food packaging, bottles, medical and pharmaceutical products which require high thermal stability. The poly(D-lactic acid) [PDLA] and PLLA blend can co-crystallize to form stereocomplex (sc-PLA), with melting point (220 ºC) that is about 50 ºC higher than for both PLLA and PDLA. Therefore, this blend was intensively studied as a potential material with high heat stability[1)] and triallyl isocyanurate (TAIC) has been proved as an effective crosslinker for PLLA[2,3)]. In this study, the properties of crosslinked sc-PLA / TAIC films by radiation with different content of TAIC and radiation doses were investigated

The melt mixture of commercial PLLA and PDLA (Mw, Mw/Mn was 9.98×10^4, 1.6 and 28×10^4 and 1.57, respectively) were hot-pressed at 230 ºC for 5 min and then cooled to room temperature for 5 min to form a film with thickness of 0.5 mm. The films were EB irradiated at different doses with the same dose rate of 10 kGy pass^{-1}. Gel fractions, thermal and mechanical properties of crosslinked sc-PLA films were measured by differential scanning calorimetry (DSC), thermomechanical analyzer (TMA) and tensile measurements.

The crosslinking structures are formed in irradiated sc-PLA films with TAIC. Gel fraction of the sc-PLA films represented to the crosslinking density increased with TAIC content and radiation dose. Gel fraction seems to saturate at dose higher than 30 kGy.

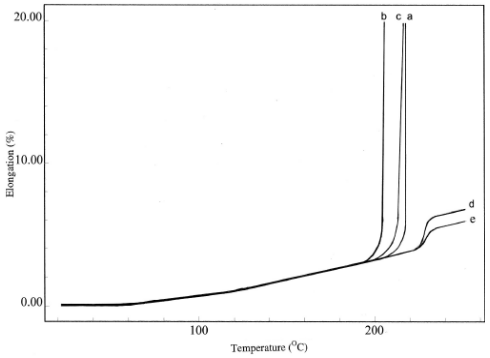

Fig. 1 TMA heating curves of crosslinked sc-PLA by EB-irradiation at 50 kGy. a)sc-PLA, b)sc-PLA / 0.5 % TAIC, c)sc-PLA / 1 % TAIC, d)sc-PLA / 3 %TAIC, e)sc-PLA / 5 % TAIC

DSC measurements of crosslinked samples irradiated at 50 kGy show typical crosslinking in sc-PLA mixed with more than 3 % TAIC. Neither crystallization peak nor melting peak of homo crystals (crystals of PLLA, PDLA) can be observed in DSC of sc-PLA / 3 % TAIC irradiated at dose higher than 30 kGy like non-irradiated sc-PLA film.

Figure 1 shows TMA data of the sc-PLA containing different amount of TAIC and irradiated at 50 kGy. Extension of all samples increases at 60 ºC with very small extension rate to around 200 ºC, then sc-PLA and irradiated sc-PLA films with TAIC below 1% quickly elongate and break. However, the crosslinked films containing more than 3 % TAIC withdrew the load at temperature over 250 ºC with low extension.

Figure 2 shows the stress-strain curves of sc-PLA containing 3 % TAIC irradiated at different doses. At low radiation doses, the curves of irradiated samples are similar to non-irradiated sample (curves (a)~(c)). At higher radiation doses (above 30 kGy), the mechanical properties of crosslinked samples are considerable higher than that of sc-PLA.

Our research proved that the crosslinking density increased, crosslinking network became tighter resulted in a higher young's modulus. The crosslinked samples became harder and more stable. The combination of stereocomplex formation and radiation crosslinking caused significant improvement of heat stability of PLA material.

References

1) Y. Ikada, et al., *Macromolecules*, **20**:904(1987)
2) H. Mitomo, et al., *Polymer*, **46**(3), 4695 (2005)
3) N. Nagasawa, et al., Nucl. Instrum.
4) Methods Phys. Res., Sect. B, **236**(1-4), 611 (2005)

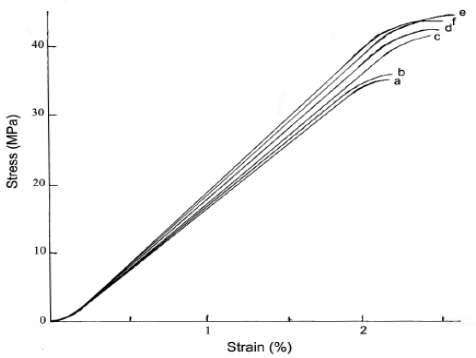

Fig. 2 Stress-strain curves of crosslinked sc-PLA with 3 % TAIC by EB-irradiation at various doses. a)Unirradiated, b)10 kGy, c)20 kGy, d)30 kGy, e)50 kGy, f)100 kGy

2-18 Novel Elastic Gel Derived from Plant-resource and Its Utilization

M. Takigami [a)], N. Nagasawa [b)], H. Amada [a)], T. Yagi [b)], N. Kasai [b)], F. Yoshii [b,c)] and M. Tamada [b)]

[a)]Gunma Industry Support Organization, [b)]Environment and Industrial Materials Research Division, QuBS, JAEA, [c)]Industrial Collaboration Promotion Department, JAEA

Carboxymethylcellulose (CMC) gel was formed by addition of acid to CMC (CMC-acid gel). Gel fraction (weight of insoluble part/initial CMC weight) was calculated after removing uncrosslinked CMC by immersing the CMC-acid gel in water. The amount of gel increased with acid concentration. Mechanism of CMC-acid gel formation was elucidated by aggregation of CMC molecules as a result of replacement of sodium in carboxyl group with hydrogen. Gels could be prepared by three different procedures; (1) mixing of CMC and acid, (2) immersion of CMC or γ-irradiated CMC pastes in acid, and (3) γ-irradiation of CMC-acid gel. Gels with different elasticity and hardness were prepared by changing degree of substitution of CMC, molar mass of CMC, type of acid, concentrations of acid and CMC, and application of γ-irradiation.

カルボキシメチルセルロース(CMC)[1)]、カルボキシメチルデンプン[2)]、カルボキシメチルキトサン[3)]等の水溶性多糖誘導体が 10 %以上のペースト状態で放射線橋かけし、水に不溶な化学ゲルに調製でき、乾燥ゲル 1 g で水を約 100～400 倍吸水する高分子吸収体になることを見出している。この技術を基に地域産学官が連携して申請した群馬県地域結集型共同研究開発プログラム「環境に調和した地域産業創出プログラム」において、平成 18 年 1 月から放射線橋かけしたセルロースゲルによる家畜廃棄物処理に関する研究を進めている。

この研究を通して、ペースト状の CMC に放射線照射と酸への浸漬処理を組み合わせることにより、これまで作製できなかった弾力性を付与した CMC ゲルを作製できることを初めて見出した。CMC 弾性ゲルは、①CMC のペーストに放射線を照射後に酸水溶液中に浸漬する、②CMC と酸水溶液とを混練する、③上記②に γ 線照射するといった 3 つの方法で調整することが可能である。CMC の濃度、酸の種類や濃度を変化させることにより、様々な硬さを有するゲルを作製できることから、様々な用途に応用可能である。

ダイセル化学工業社製の CMC（置換度 : 1.36）と蒸留水とを脱泡式ミキサーで混練した。混練した CMC ペーストをポリエチレン／ナイロンバックに入れ、脱気後、室温で γ 線照射し、酸処理を行った。作製した CMC ゲルを水に浸漬し、橋かけしていない CMC を除去し、ゲル分率（不溶化した CMC の割合）および吸水量（CMC ゲル 1g が吸収した水の重量）を算出した。CMC ゲルの力学的な物性として圧縮弾性率を測定した。また、ゲル構造変化について、フーリエ変換赤外吸収（FT-IR）測定及びエネルギー分散型蛍光Ｘ線分析装置（EDX）測定で評価した。

CMC の濃度 20 %で作製したペーストにγ線を照射し、1M の塩酸、リン酸、クエン酸水溶液に 4 日間浸漬したときのゲル分率の変化を調べた結果、強酸である塩酸とリン酸では、放射線橋かけした CMC でも、未橋かけの CMC でも、ゲル分率が 80 %になる事が分かった。弱酸性の有機酸であるクエン酸では、線量の増加とともに、ゲル化が促進された。また、塩酸の濃度によるゲル化促進効果を調べた結果、放射線橋かけした CMC ゲルに対して 0.1 M 以上の濃度でゲル化を促進し、未橋かけの CMC ペーストでも 0.5 M 以上の濃度があれば、ゲル化が促進した。これらのことから酸処理によって放射線橋かけ CMC ゲルのゲル化を促進することがわかった。放射線橋かけ CMC ゲルは、乾燥ゲル 1g に対して約 400 倍吸水するが、脆く壊れやすい性質を有する。しかし、酸処理すると吸水性が約 10 倍程度に低下するが、壊れにくく弾性を有する。そこで、放射線橋かけゲルと酸処理したゲルの圧縮弾性率を測定した結果、放射線橋かけゲルは 50%圧縮すると壊れてしまうが、酸処理したゲルは圧縮しても壊れず、荷重を外すと元の形状に戻ることがわかった。また、塩酸の濃度が濃くなるにつれ、50 %圧縮時の最大応力が増加した。

酸処理は、未橋かけCMCペースト又は放射線橋かけしたCMCゲルに弾性を付与できることから、フーリエ変換赤外吸収（FT-IR）測定及びエネルギー分散型蛍光Ｘ線分析装置（EDX）測定の結果よりゲル形成メカニズムを考察した。20 %濃度のCMCペーストにγ線を 10 kGy照射したゲルと塩酸（0.5 M）で処理したゲルのFT-IRスペクトルを比較すると、処理前のカルボキシラートイオンに起因する 1600 cm^{-1}の吸収が、酸処理後、C=O伸縮に起因する 1730 cm^{-1}の吸収に変化した。EDX測定では、放射線橋かけゲル中のNa濃度が 8.79 wt %であったが、0.5 M塩酸で処理すると 3.22 wt%に減少することが分かった。これらの結果から、CMCゲルを酸で処理することにより、CMCのカルボキシル基の対イオンとして存在していたNaがHに置き換わり、カルボキシル基の解離が押さえられ、CMC分子鎖内あるいは分子鎖間の静電的反発が減少して、CMC分子鎖が凝集すると考えられる。硬くて脆いという従来の放射線橋かけCMCゲルに弾性を付与でき、広範囲での応用が期待され、具体的な実用化について検討を進めている。

References

1) B. Fel, et al., J. Appl. Polym. Sci., **78**, 278(2000).
2) N. Nagasawa, et al., Carbohydr. Polym., **58**(2), 109-113 (2004)
3) L. Zhao, et al., Carbohydr. Polym., **51**, 169-175 (2003)

2-19 Preliminary Study on the Suitability of Carboxymethylated κ-Carrageenan for Radiation Crosslinking

C. T. Aranilla [a)] , N. Nagasawa [b)], A. Dela Rosa [a)] and M. Tamada [b)]

[a)]Philippines Nuclear Research Institute, [b)]Environment and Industrial Materials Research Division, QuBS, JAEA

Many polysaccharide derivatives have been prepared by carboxymethylation reactions in order to increase the range of potential applications of these natural polymers[1)]. Recently, it was established that carboxymethylated polysaccharides such as carboxymethyl cellulose, carboxymethyl starch, carboxymethyl chitin and carboxymethyl chitosan, predominantly undergo crosslinking reactions when are irradiated as highly concentrated aqueous solution in paste-like state[2)]. κ-Carrageenan is a sulfated anionic polymer consisted of alternating units of galactose and 3,6-anhydrogalactose[3)]. κ-Carrageenan is one type of carrageenan that is capable of forming thermo-reversible gels, however it typically undergoes chain scission reactions when is exposed to high-energy radiation. This study attempts for the first time to synthesize carboxymethylated κ-carrageenan (CMkC) and determines its suitability for radiation crosslinking.

κ-Carrageenan was slurried in isopropyl alcohol / water (80/20) and alkali-activated using 40 % aqueous NaOH at 40 ºC. After 1 h, monochloroacetic acid was added and allowed to react for 3 h. Carboxymethylation was confirmed by degree of substitution (DS), Fourier transform infrared spectroscopy (FTIR) and ^{13}C nuclear magnetic resonance analysis (NMR). For crosslinking experiments, concentrated aqueous solutions of carboxymethyl κ-carrageenan were prepared using a hybrid mixer to obtain 10-40 % (w/w) in paste-form. The samples were packed and vacuum-sealed in polyethylene / nylon bags. Gamma irradiation was conducted in ^{60}Co facility until dose of 100 kGy, in air and ambient temperature. Crosslinking was assessed in terms of gel fraction.

DS of obtained carboxymethyl κ-carrageenan derivative measured by potentiometric back-titration was 1.20. From FTIR analysis peaks due to $-COO^-$ and $-CH_2$ vibrations of the carboxymethyl group were observed. ^{13}C NMR analysis revealed the occurrence of carboxymethylation in the three hydroxyl groups of κ-carrageenan disaccharide unit.

Crosslinking of carboxymethyl κ-carrageenan was successfully done and proved to be promising as shown in Fig. 1. The samples irradiated at different concentrations exhibited different degrees of crosslinking as a function of dose. Gel fractions were obtained for CMkC aqueous solution at 30-40 % concentration while no gel content was exhibited by aqueous solutions at 10-20 % concentration. The highest gel content reached 39 % at 100 kGy for the 40 % aqueous solution. Concentration effect on crosslinking dose was also evident from the graph. Increase in concentration resulted in decrease of crosslinking dose. A gel fraction of about 30% was attained at 30 kGy for 40 % of CMkC aqueous solution, while the same gel fraction at 50 kGy for 30 %. These gels were immersed in distilled water for 48 hours to estimate swelling ratio. The swelling capacity of hydrogels decreased with increase in dose, as well as with increase in polymer concentration. This can be attributed to dependence of swelling on crosslink densities of the hydrogels.

References

1) Silva, D. A.,et al., Carbohydr. Polym., 58, 163 (2004).
2) F. Yoshii, et al., Nucl. Instrum. Methods Phys. Res., Sect. B. 208, 320 (2003).
3) Velde van de, F., Biopolymers. 6, 245 (2002).

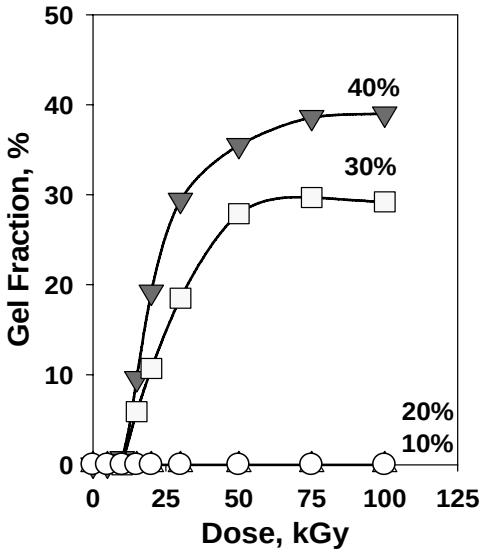

Fig.1 Gel fraction of carboxymethyl κ-carrageenan hydrogels as a function of dose. The DS of carboxymethyl κ-carrageenan is 1.20.

2-20 Effect of Radiation Crosslinking on Stability of Bent Polyethylene Pipe

N. Kasai [a)], F. Yoshii [a)] and J. Yuasa [b)]

[a)]Environment and Industrial Materials Research Division, QuBS, JAEA
[b)]Sekisui Chemical Co.Ltd

Recently polyethylene (PE) has been widely used for water and sewage pipes because of its high strength and corrosion resistivity. Bent PE pipes, which are necessary to construct pipe lines, are usually produced by bending of straight pipes at high temperatures around the melting point of PE. When such bent pipes are used for long time , change in the bending angle takes place, which is regarded as a serious problem. In this article, the effects of radiation crosslinking on the stability of bent PE pipes are investigated.

Electron irradiation was carried out at 2MV, 2mA with a dose rate of 10 kGy/pass to induce crosslinking structure for straight high density PE pipes with 60 mm diameter (thickness 5.5 mm). The PE pipes were irradiated on both sides at doses of 30 – 100 kGy. γ-ray irradiation was done for high density PE pipes with 180 mm diameter (thickness 16.4 mm) at 80 kGy with a dose rate of 10 kGy/hr.

After irradiation, straight PE pipes heated at around the melting point were set in form to bend at the angle 90° for given time and cooled down to form bent PE pipes. The angle of fabricated PE pipes was measured with on angle meter and the appearance of the pipe surface after bending at high temperatures was also examined.

Figure 1 shows changes of the angle of PE pipes bent at 135℃ after electron irradiation in a dose range of 30 – 100 kGy . For the PE pipes irradiated at 50 kGy and 80 kGy, change in the angle is small, 2 – 3°, while irradiation of PE pipe at 30 kGy and 100 kGy gives large deviations. No significant change in the surface morphology was observed between irradiated PE pipes and the original sample (before irradiation). Small angle deviations within 3° are desired in the practical application of bent PE pipes. Thus, electron irradiation at 50 – 80 kGy is preferable to fabricate stable bent pipes. As an acceleration test, the stability of bent PE pipes was examined at 60℃ for 24 hrs, the results of PE pipes γ-irradiated at 80 kGy are shown in Figure 2. Irradiated pipes exhibit smaller change in the angle than that of the unirradiated one. PE pipes bent at above the melting point, 133℃ after irradiation indicate small deviation of only 2°. Moreover, the appearance of the PE pipe surface after bending at high temperatures was investigated. PE pipes bent at 133° for partial melting were rough in comparison with that bent at 126℃. From these findings, it can be concluded that crosslinking is effective to improve the stability of PE pipes bent at high temperatures around the melting point of PE.

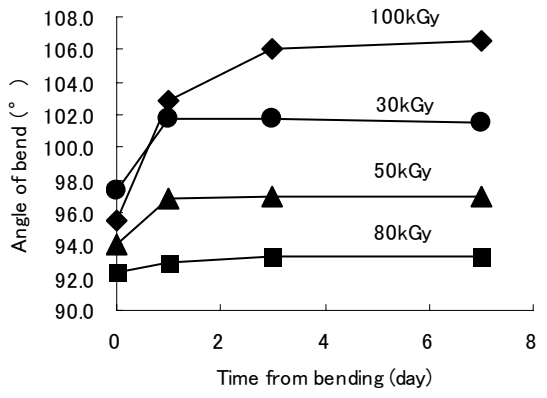

Fig. 1 Change in the angle of PE pipes bent at 135° after electron irradiation at 30,50,80 and 100kGy.

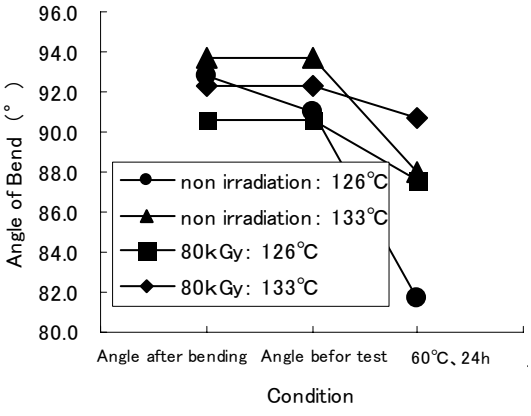

Fig. 2 Change in the angle of γ - irradiated PE pipes when they were kept at 60℃.

2-21 Development of Decomposition Technology for Formaldehyde in Air by Electron Beam

A. Shimada and K. Hirota

Environment and Industrial Materials Research Division, QuBS, JAEA,

The sterilization of clean rooms has been performed using a mixture of formalin/air generated by the vaporization of a commercially available formalin solution containing about 37 % formaldehyde (HCHO) and 5-10% methanol (CH_3OH). The mixture in clean rooms needs to be treated after sterilization. For instance, in some food packaging factories, sterilization gas is treated by circulating through heat-catalyst reactor. It takes 2 or 3 days to complete the treatment. To improve the productivity of such factories, the development of effective treatment methods is strongly required. Electron beam is expected to be one of the alternative methods for treating organic pollutants because they can effectively be oxidized by active species (OH, O, N, O_3 and so on) generated in air by electron beam irradiation. In the previous study, we estimated that formalin/air mixture (air with HCHO and CH_3OH) at the HCHO concentration of 1200 ppmv in a clean room of 2000 m^3 can be treated by electron beam within about half of a day[1]. In this study, HCHO/air mixture (air with HCHO, without CH_3OH) is irradiated to examine the decomposition process of HCHO.

Air mixture containing 100-1060 ppmv HCHO and 1 % water were irradiated with electron beams at absorbed doses of 5-80 kGys. The change in the concentration of HCHO as a function of dose is shown in Fig.1. The concentration decreased exponentially with dose. From the initial slope of the curves in Fig.1, the decrease in the HCHO concentration per 1 kGy was estimated to be 19, 35, 50, 64 ppmv / kGy for 100, 280, 480, 1060 ppmv of HCHO, respectively. These values are much larger than that of OH radical generated by electron beam, i.e., 10 ppmv / kGy. These results can be explained in terms that HCHO is decomposed by a chain reaction.

The irradiation of HCHO produced HCOOH, CO, and CO_2, as shown in Fig.2. Almost all decomposition products in the irradiation of HCHO were identified. The concentrations of CO and CO_2 gradually increased in a dose range of 2.5-10 kGy. On the other hand, the increase of the HCOOH concentration was suppressed above 5 kGy. It indicates that the active species like OH radicals reacted with not only HCHO but also with HCOOH. Carbon balances in the HCHO irradiation showed that 104, 93, and 95 % of reacted HCHO were recovered at absorbed doses of 2.5, 5, and 10 kGy, respectively. It was found that HCOOH, CO, and CO_2 were main products in the irradiation of HCHO.

Reference

1) Shimada, A.; Hakoda, T.; Kojima, T., *J. Chem. Eng. Jpn.*,Vol.39, No.9 (2006)

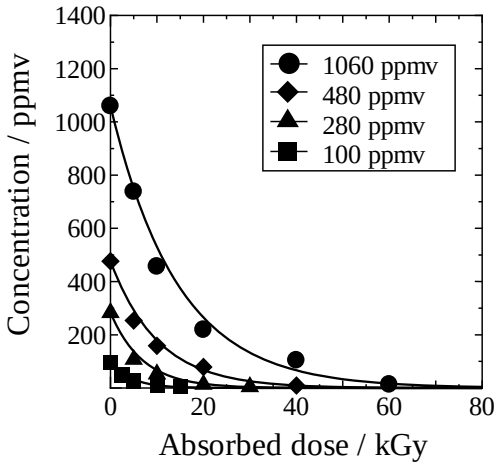

Fig.1 Concentration of HCHO in air mixture as a function of dose

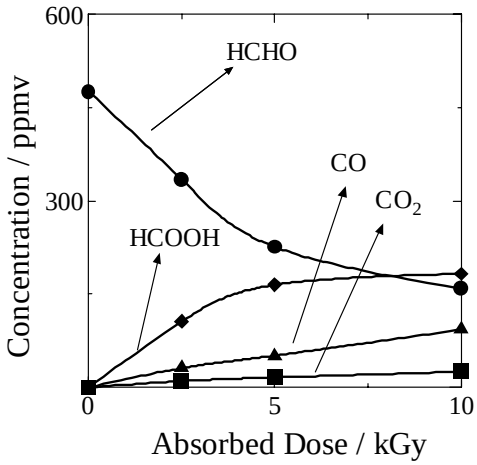

Fig.2 Concentration of HCHO and irradiation products as a function of dose

2-22 Development of PCDD/Fs Treatment Technology by Gamma-ray Irradiation

K. Hirota and C. Zhao

Environmental and Industrial Materials Research Division, QuBS, JAEA

1. Introduction

The emission of dioxins to the environment was about 330 g-TEQ/yr in 2005, which was decreased by 90% compared to those in 1999[1]. On the other hand, the amount of dioxin in analytical wastes has risen in laboratory due to a high demand on dioxin analysis. It can be much burden to store the wastes as similar to Polychlorinated biphenyl (PCB) in Japan. PCB has been treated by incineration, dechlorination, and hydrothermal oxidation etc at five facilities in Japan[2]. However, to construct sort of facilities requires residence's agreement and corporation, and is costly. Ionizing radiation technology is expected to be one of the economical methods for treating the dioxin wastes because we can use existing irradiation facilities without additional equipments. It can treat the wastes with a simple process. No additive or temperature control is required. Nuclear waste can also use as radiation source.

2. Experiments

Experiments on the treatment of dioxin wastes were carried out using octachlorodibenzo-*p*-dioxin (OCDD) (Cambridge Isotope Laboratory, Inc.) because it can be handled with lower toxicity and purchased as a crystal. The samples prepared in toluene, n-nonane, and ethanol solvents (Wako Pure Chemical Industries, Ltd.) were irradiated with gamma-ray at a dose rate of 10 kGy/h. The concentration of OCDD/F and other isomers were measured before and after irradiation using GC/HRMS (JEOL JMS-700).

3. Results and Discussion

Decomposition profile for OCDD in the three solvents is shown in Fig 1. The decomposition rate of OCDD in the three solvents increased with an absorbed dose. The highest rate was obtained from OCDD in ethanol, followed by in nonane and in toluene. This decomposition order is essentially same as G-value for the formation of solvated electron in the three solvents (ethanol:1.7, n-nonane: 0.12, toluene: 0.09)[3, 4]. This suggests that solvated electron is associated with the decomposition of PCDD. The reactions of solvated electrons with dioxins are based on the reduction by dechlorination, namely the dissociation of Cl-substituents on the aromatic rings of dioxin, leading to form lower chlorinated congeners such as hepta- and hexachlorodibenzo-*p*-dioxin (HpCDD and HxCDD). Thus, the decomposition behavior for chlorodibenzo-*p*-dioxin having from zero to eight Cl-substituents (PCDDs) was investigated and the result is shown in Fig.2. The decomposition rate for PCDDs was quit lower than that for OCDD, indicating that OCDD was dechlorinated to from lower chlorinated congeners through reactions with the solvated electrons. Although the decomposition rate for OCDD in n-nonane was higher than that for toluene, PCDD in n-nonane was less decomposed compared to PCDD in toluene. To clarify the phenomena, the dechlorination profile of OCDD was examined and found that 80 % and 20-30 % of reacted OCDD were dechlorinated in n-nonane and toluene, respectively. These values did not much change up to 160 kGy. The concentration of HpCDD formed by the dechlorination of OCDD increased in n-nonane with an absorbed dose, while reached a maximum in toluene at a dose of 50 kGy. Dechlorination is a dominant reaction for the treatment of dioxin in n-nonane. Dioxin is mainly oxidized in toluene solvent[5]. It was found that ethanol is a good solvent for treating dioxin using an ionizing radiation.

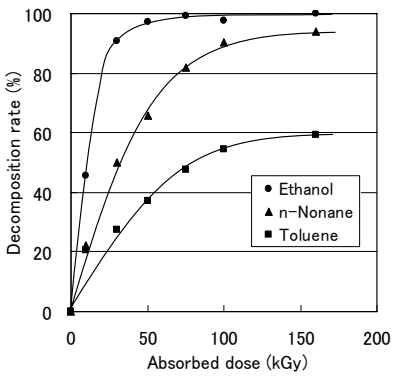

Fig.1 Decomposition of OCDD in solvents by gamma-rays

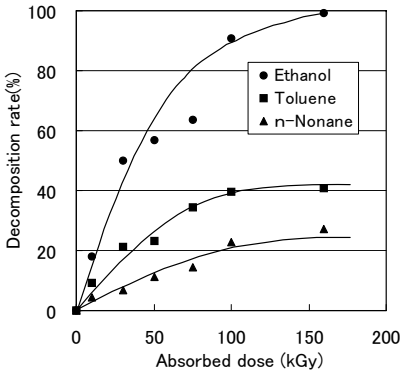

Fig.2 Decomposition of PCDD in solvents by gamma-rays

References

1) Ministry of the Environment. *Dioxin Emission Inventory.* http://www.env.go.jp/press/press.php?serial=7782 (in Japanese).

2) JESCO. *Project for the Treatment of PCB Wastes* http://www.jesconet.co.jp/business/index.html (in Japanese).

3) Spinks, J. W. T., Woods, R. J. W.: An Introduction to Radiation Chemistry, 3rd ed.; John Wiley & Sons: New York, 1990.

4) Sun, G. S., Qin, X., Fang, X., and Wang, W. *Radiat, Phys. Chem.*, 55 (1999) 409.

5) Zhao, C., Hirota, K., Taguchi, M., Takigami, M., and Kojima, T. *Radiat. Phys. Chem*. 76 (2007) 37.

2-23 Study on the Treatment of Endocrine Disrupting Chemicals in Wastewater by Ionizing Radiation

A. Kimura [a] , M. Taguchi [a], Y. Ohtani [b], H. Hiratsuka [c], T. Kojima [d] and K. Hirota [a]

[a]Environment and Industrial Materials Research Division, QuBS, JAEA, [b]Gunma Prefectual Institute of Public Health and Environmental Sciences, [c]Gunma University, [d]Department of Advanced Radiation Technology, TARRI, JAEA

1. Introduction

Endocrine disrupting chemicals (EDCs) in the environmental water give serious influence to aquatic animals such as mimicking the estrogen and disrupting the endocrine system in living bodies. This study is to give the validity of ionizing radiation for the treatment of trace amounts of EDCs in the environmental water. Decomposition of 17 β-estradiol (E2) and *p*-nonylphenols (NPs) in aqueous solution were studied using ^{60}Co γ-ray because they have higher estrogen activities in the environmental water. Real wastewaters containing some EDCs were also irradiated. The cost for the treatment of wastewater containing EDCs by ionizing radiation was estimated based on the experimental results obtained in present studies.

2. Experimental

Real wastewater samples were obtained from secondary effluents downstream from the activate sludge system in water treatment plants. Model wastewater samples were prepared by adding E2 at 1.8 nmol dm^{-3} or NPs at 20 μmol dm^{-3} to wastewater having no estrogen activity. The samples were irradiated with γ-rays at 298 K. The concentrations of the EDCs with biological activities in the samples were measured before and after irradiation by chemical analyses and biological assays. Estrogen receptors of human and medaka were used for the yeast two hybrid assay to estimate estrogen activities, which are hereinafter defined as hEA and mEA, respectively.

3. Results and Discussion

E2 in the model wastewater was decreased as a function of dose as shown in Fig. 1. The reduction rate of E2 concentration decreased with an increase in the amount of TOC. Coexistents should influence to the decomposition of E2. The same inclination was obtained for the decomposition of NPs in the model wastewater.

The change in estrogen activity of the real wastewaters by γ-ray irradiation is shown in Fig. 2. The curves of estrogen activity have a maximum, indicating that estrogen active products were formed in the decomposition process. To eliminate the endocrine disrupting property against the human body requires an expose to the samples at about 200 Gy to reach the estrogen activity less than 1 ng dm^{-3}. Since E2 at an estrogen activity of 500 ng dm^{-3} in pure water was decomposed at a dose of 50 Gy, the requirement of higher doses for the decomposition of EDCs in the real wastewaters was due to the consumption of OH radicals through reactions with coexisting organic substances having no estrogen activities.

The initial investment for electron-beam system was found to be 15 yen m^{-3} to treat secondary effluent in sewage treatment plants with a capacity of 10,000 m^3 day^{-1} on the basis of 15-years operation. The consumption of electricity for an operation of the electron accelerator is estimated to be 2 yen m^{-3}. Ionizing radiation is expected to be one of the promising methods for treating EDCs in water[1].

Reference

1) A. Kimura et al., Radiat. Phys. Chem., 76, 699-706 (2007).

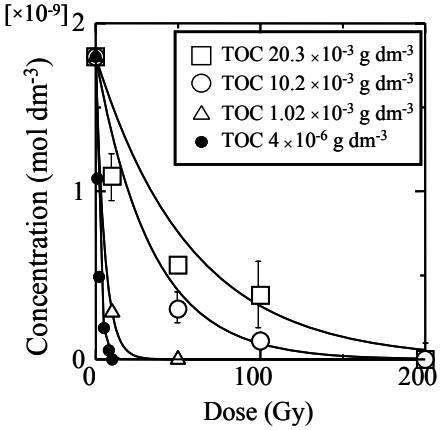

Fig. 1 Concentration of E2 in model wastewater at each TOC concentration as a function of dose.

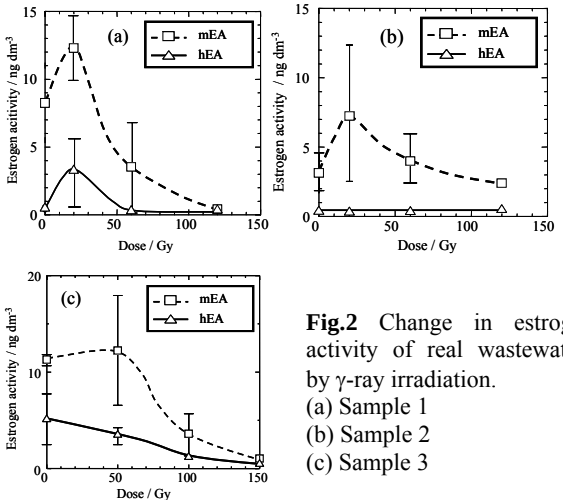

Fig.2 Change in estrogen activity of real wastewaters by γ-ray irradiation.
(a) Sample 1
(b) Sample 2
(c) Sample 3

This is a blank page.

3 Biotechnology and Medical Application

This is a blank page.

3-01 Detection of Ion-beam-induced Mutations Using Positive Selection Marker Genes in Arabidopsis

Y. Hase, R. Yoshihara, Y. Yokota and I. Narumi

Radiation-Applied Biology Division, QuBS, JAEA

The extensive analyses using model plant Arabidopsis showed that the ion beams have higher mutagenic effects compared to low-LET radiations[1]. It was also shown that the ion beams frequently induce deletion-type mutations[2]. Furthermore, application of the ion beams for mutation breeding demonstrated that the ion beams have wide mutation spectrum and that the ion beams can induce mutants without undesirable defects[3]. However, there are still unsolved points in mutagenic effects of ion beams, that is, (1) relationship between the property of ion beams and the mutation frequency or spectrum, (2) relationship between the material tissue type and the mutagenic effect, and (3) mechanism for why the recessive homozygous-like mutants, such as chlorophyll deficient mutants, were obtained in the irradiated generation. In order to clarify these points, we are analyzing the mutagenic effects of ion beams using positive selection marker genes as described below. In this year, we prepared the transgenic plant materials and determined the radiation sensitivity of them to the ion beams and gamma rays.

ribosomal protein S12 (*rpsL*)

The *rpsL* gene that encodes ribosomal S12 protein confers streptomycin-sensitive phenotype when it is transformed into *Escherichia coli*. Based on the plasmid rescue method, we can detect only the mutated genes as streptomycin-resistant colonies[4]. Since this method can detect large number of somatic mutations in a short time, we will analyze the mutagenic effects of ion beams with the emphasis on the difference of material tissue types.

cytosine deaminase (*codA*)

The *codA* gene product of *E.coli* deaminates 5-fluorocytosine (5-FC) into 5-fluorouracil (5-FU). Since 5-FU leads to depletion of dTTP for DNA synthesis, the plants having *codA* gene can not grow on a selection medium supplemented with 5-FC[5] (Fig. 1). The wild type Arabidopsis ecotype Columbia was transformed with *codA* gene under the control of CaMV 35S promoter. We have selected T3 plants that are homozygous for *codA* gene based on the segregation ratio on 5-FC medium. This method can be thought to detect any types of heritable mutations including large deletions.

We have determined the sensitivity of the seeds of transgenic plants for carbon ions and gamma rays (Fig. 2). The shoulder dose was 930 Gy for gamma rays, 240 Gy for 320-MeV carbon ions, and 180 Gy for 220-MeV carbon ions.

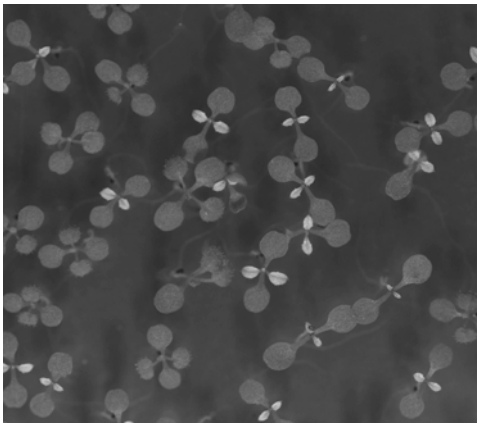

Fig. 1 Selection of transgenic *codA* plants on 5-FC-supplemented medium. T2 plants obtained by a self-pollination of transgenic plants heterozygous for *codA* gene were grown on 5-FC medium. *codA* plants (sensitive) and wild-type (resistant) plants were segregated in a ratio of 3 : 1.

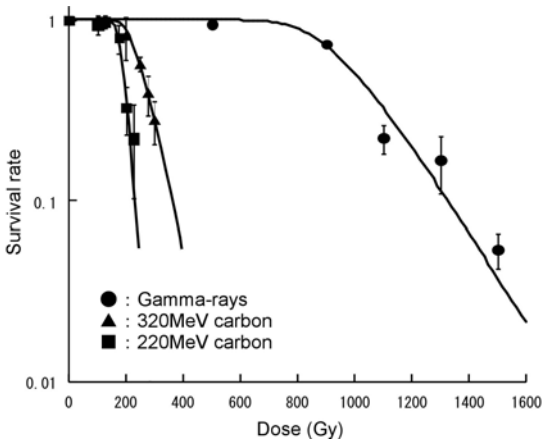

Fig. 2 Survival curves for the seeds of *rpsL* transgenic plants exposed to ion beams and gamma rays.

References

1) N. Shikazono et al., Genetics 163 (2003) 1449.
2) N. Shikazono et al., Genetics 157 (2001) 379.
3) M. Okamura et al., Nuc. Instr.Meth. B 206 (2003) 574.
4) J. Stougaard, Plant J. (1993) 755.
5) R. Yoshihara et al., Radiat. Res. 47 (2006) 223.

3-02 Mutation Induction in Orchids Using Ion Beams

A. H. Affrida [a)], A. Sakinah [a)], A. Zaiton [a)], B. Mohd Nazir [a)], A. Tanaka [b)], I. Narumi [b)], Y. Oono [b)] and Y. Hase [b)]

[a)]Agrotechnology and Biosciences Division, Malaysian Nuclear Agency,
[b)]Radiation-Applied Biology Division, QuBS, JAEA

Orchid is the main export for Malaysia's floriculture industry. Due to the increasing demand for orchid pot plants and cut flowers, new commercial varieties with new characteristics such as colour, shape and longer shelf life of flower are needed. The use of hybridization for orchid breeding is restricted by sexual incompatibility, sterility problems and long breeding time. Mutation induction by ion beam provides an alternative for improvement of orchids. In this study, we tried to produce mutants with new flower colour, shape and shelf life.

The protocorm-like bodies (PLBs) of two orchid species; *Dendrobium mirbellianum* and *Dendrobium crumenatum* were placed on 6-cm sterile petri dishes containing half strength MS (Murashige & Skoog, 1962) media. The samples covered with a Kapton film (8-μm-thick polyimide film) were irradiated with 320 MeV $^{12}C^{6+}$ ion beams at various doses ranging from 0 to 12.0 Gy[1)] from the TIARA AVF cyclotron (JAEA, Takasaki). After irradiation, cultures were subcultured on to fresh ½ MS media every 4 weeks for multiplication and regeneration. The number of regenerated shoots from each dose was recorded after 2 months.

Mutation effects of carbon ions on both species were observed at tissue culture stage. In *D. mirbellianum,* chlorophyll mutation was detected in one of cultures irradiated at 0.4 Gy (Figure 1). The PLBs from which these plantlets originated were subcultured to obtain more of the mutants. Attempt has been made to harden one of these mutant plantlets but it could not survive the glasshouse condition. The plantlets were grown for a longer period in tissue culture environment to increase the chance of survival during hardening.

More tissue culture plantlets were transferred from time to time to the glasshouse for screening. Plantlets of *D. mirbellianum* are growing very slow and have not reached flowering stage.

Fig.1 Chlorophyll mutation observed in *D. mirbellianum* cultures irradiated at 0.4 Gy.

Meanwhile, variations were also observed in some of *D. crumenatum* cultures. Some of the variations are shown in Figure 2. In Figure 2a, 2b and 2c are culture irradiated at 2 Gy. Figure 2a shows variations in leaf shape while elongation of stem is shown in Figure 2b. The rest of 2 Gy cultures look as a culture in Figure 2c. Slow growing culture was observed in a 0.2 Gy population (Figure 2d). The control is as shown in Figure 2e.

Differently from *D. mirbellianum*, *D. crumenatum* plants have started to flowering. The length of blooming period was recorded. This is for comparison with the control that only blooms for one day. Data are still currently collected. However, no morphological change in terms of flower colour and shape was observed.

Tissue culture seedlings were constantly transferred to the glasshouse to screen for color variation in the growing plants.

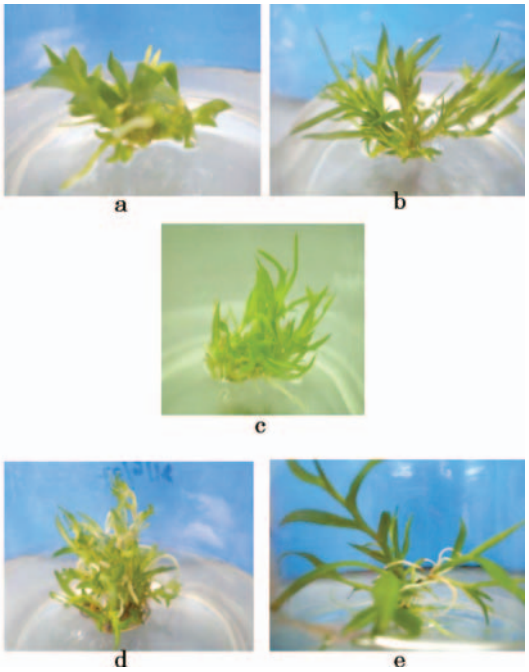

Fig.2 Cultures of *D. crumenatum* which show some abnormalities compared to the control: a,b and c (2 Gy), d (0.2 Gy), and e (control).

Reference

1) B. Mohd Nazir et al., TIARA Ann. Rep. (2005) 45.

3-03 Tobacco BY-2 Cells Have a Transient and Leaky DNA-Damage Checkpoint at G_2/M Phase after Gamma-ray Irradiation

Y. Yokota [a)], T. Funayama [a)], S. Wada [b)], Y. Hase [a)], Y. Kobayashi [a)], M. Inoue [c)], A. Tanaka [a)] and I. Narumi [a)]

[a)]Radiation-Applied Biology Division, QuBS, JAEA, [b)]Department of Veterinary Medicine, Kitasato University, [c)]Graduate School of Agriculture, Kyoto Prefectural University

Many types of higher plants including herbaceous plants show high radiation-tolerance at both levels of individual and cell [1)], however the tolerance mechanism is unclear in large part. By quantifying the initial yields and the repair kinetics of DNA double-strand breaks (DSBs), we found that tobacco BY-2 protoplasts can tolerate 5-times more DSBs per cell than Chinese hamster ovary CHO-K1 cells [2)] although they have a similar efficiency of DSB repair.

In this study, we analyzed cell cycle phase distribution by flow cytometry and measured micronucleus (MN) induction rate in tobacco BY-2 cells irradiated with gamma rays.

As a result, the fraction of G_2/M-phase of the cells irradiated with 40-Gy gamma rays was more than that of the unirradiated cells at 24 h of post-irradiation culture, and the difference was disappeared at 48 h (Fig. 1). This result indicates that the DNA damage checkpoint of BY-2 cells transiently functions at G_2/M phase. Additionally, the percentages of the cells having at least one MN were greater in irradiated cells than in unirradiated cells (Fig. 2), suggesting that the DNA damage checkpoint of BY-2 cells is leaky. In the irradiated cells, the percentage of the cells having at least one MN peaked at 48 h after irradiation and thereafter decreased over time. This is because MN is induced through at least one cell division after irradiation, and the MN induction rate per division decreases gradually.

This unstable genome maintenance seems to be unreasonable for organism at first glance, but may be admissible for life style of higher plants: most of them must grow quickly within a limited life span for acquiring sunlight more than competitors, even if the genomes of somatic cells become unstable.

References

1) Y. Yokota et al., Int. J. Radiat. Biol. 79 (2003) 681.
2) Y. Yokota et al., Radiat. Res. 163 (2005) 520.

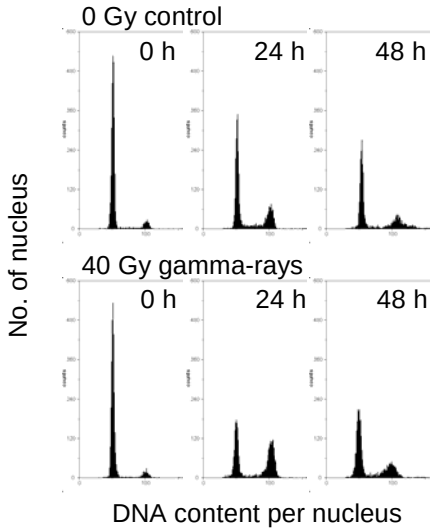

Fig. 1 Analysis of cell cycle phase distribution after gamma-ray irradiation in tobacco BY-2 cells. In each histogram, the time of post-irradiation culture was shown, and the left and right peaks and the area between their peaks indicate G_0/G_1-, G_2/M- and S-phase cells respectively.

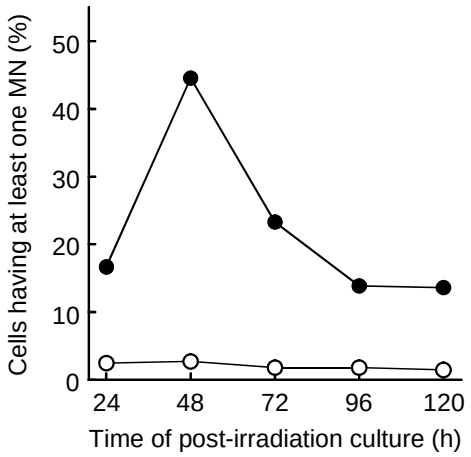

Fig. 2 Percentage of tobacco BY-2 cells having at least one MN after gamma-ray irradiation of 40 Gy (closed circle) or 0 Gy (open circle).

3-04 Effect of Ion Beam Irradiation for Microspores of Eggplant (*Solanum melongena L.*)

Y. Saiki [a)], K. Takata [a)], Y. Uchimura [a)], K. Hirashima [a)], T. Nakahara [a)], Y. Hase [b)], Y. Yokota [b)] and A. Tanaka [b)]

[a)]Department of Agricultural Biotechnology, Fukuoka Agricultural Research Center,
[b)]Radiation –Applied Biology Division, QuBS, JAEA

To get thornless eggplant, microspore of eggplant 'AE-P11' (***Solanum melongena L.***) were irradiated with $^{12}C^{6+}$・320 MeV beams ranging from 0.5 to 20 Gy by AVF cyclotron in JAEA. The number of calli formed from irradiated microspores decreased with increasing dosage. The rate of them compared with non-irradiated treatment was 91 % at 0.5 Gy, 80 % at 1 Gy, 48 % at 2 Gy, 12 % at 5 Gy, 5 % at 10 Gy and 3 % at 20 Gy. At present about four hundred calli were formed from irradiated microspores with various doses. Regenerants from the calli will be screened for thornless.

ナスの萼や葉柄にあるトゲは、作業時の怪我や果実を損傷する問題があることから、トゲがない品種が望まれている。このため、小胞子培養とイオンビーム突然変異育種を組み合わせ、トゲのない変異体の早期作出を図った。

小胞子培養の利点は、半数性細胞であるため、得られた半数性変異体の染色体数を倍加することにより、照射当代で遺伝的に固定し、短期間で目的形質を備えた純系の選抜ができることである。

今回は、ナス系統‘AE-P11’(*Solanum melongena L.*)の変異体を効率的に作出するため、その小胞子へのイオンビーム照射線量がカルス形成率に及ぼす影響を調査した。

供試したナス系統‘AE-P11’は、独立行政法人、野菜茶業研究所が育成した単為結果性系統で、受粉作業を省力化できる有望な系統である。

小胞子の単離と調整は、高田ら[1)]の方法を一部改変して、以下のように行った。すなわち、表面殺菌した蕾から葯を取り出し、滅菌水を加えシリンジで押しつぶして、単離した。滅菌水中で35 ℃、3日間の高温処理後、40 %と60 %パーコールの密度勾配遠心分離を行い、境界層の小胞子を回収した。回収した小胞子は、パーコールを滅菌水で洗浄後、0.4 mg/l 2,4-D、0.2 mg/l BA、2 % sucrose、0.2 % ゲランガムを加えたNLN培地に、2×10^5 個/ml に調整した。その培地を、直径35 ㎜シャーレに1 mlずつ分注して包埋し、カプトン膜で覆った。

$^{12}C^{6+}$・320 MeVイオンビームの小胞子への照射は、日本原子力研究開発機構イオンビーム照射研究施設（TIARA）のAVFサイクロトロンで行った。照射線量は0.5, 1, 2, 5, 10および20 Gyとした。照射後、試料に1 mlのNLN液体培地を加え、25 ℃、暗黒条件下で培養し、4週間後にカルス形成数を調査した。

無照射でのカルス形成数に対する各照射線量のカルス形成率をFig.1に示した。照射線量0.5 Gyでは91 %、1 Gyで80 %、2 Gyで48 %、5 Gyで12 %、10 Gyで5 %、20 Gyで3 %と、照射線量が増加するに従って、カルス形成率は低下した。本実験の結果、単為結果性ナス系統‘AE-P11’小胞子のカルス形成に対する$^{12}C^{6+}$・320 MeVイオンビーム照射のLD_{20}は1 Gy、LD_{50}は2 Gy付近であることが明らかとなった。

現在、$^{12}C^{6+}$・320 MeVイオンビームを0.5~20 Gy照射した小胞子からカルスが約400個形成し、カルスから倍加半数体を再生中である。今後、これらの再生植物体について、トゲのない変異体を選抜する予定である。

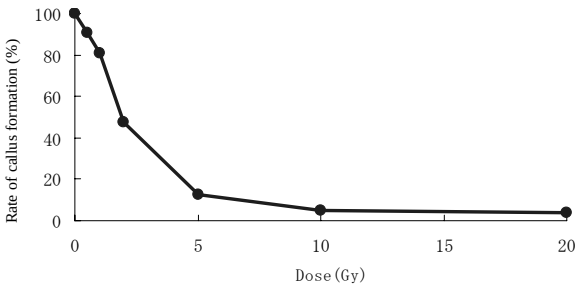

Fig.1 Effect of $^{12}C^{6+}$・320 MeV ion beam on the callus formation from microspores. The number of calli was counted at 4 weeks after irradiation. The average of 3 petri dishes at one experiment were expressed as a percent of non- irradiated control.

Reference

1) K.Takata, et al., TIARA annual report 2005 (2006) 48.

3-05 Development of Commercial Variety of Osteospermum by a Stepwise Mutagenesis by Ion Beam Irradiation

M. Iizuka [a], Y. Kimura [a], Y. Hase [b] and A. Tanaka [b]

[a]Gunma Agricultural Technology Center, [b]Radiation-Applied Biology Division, QuBS, JAEA

Introduction

Osteospermum is one of the composite perennials, and characterized by a long flowering time. Recently, the production of Osteospermum has increased as potted plants and flowerbed materials. Besides the ordinary mating, bud mutation has been used for the breeding of new varieties. However, the development of new and more efficient mutagenesis techniques with an artificial manner is expected at production fields. Previously, we irradiated Osteospermum 'Mother Symphony' with ion beams, and selected 37 flower-color and morphological variants out of approximately 3,000 individuals[1]. Among them, an unprecedented pastel color variant was applied to the variety registration as 'Vient Flamingo (tentative name)' in March 2007[2]. Besides, many petal color variants such as white and orange could be obtained from irradiated 'Mother Symphony' that has yellow petals. Usually, Osteospermum has different colors between the upper side and under side of the petals. Interestingly, the irradiated variants included orange- and yellow-isochroous variants. However, we could not obtain a white-isochroous variant that has a potentially high market value. Therefore, in an effort to obtain a variant with white-isochroous petals, we irradiated again the white petal variant of 'Mother Symphony' with ion beams.

Materials and methods

(1) *Preparation of re-irradiation material*

Leaf sections (quadrilateral pieces with 0.5 to 1 cm in size) of the white variant OM7 of Osteospermum 'Mother Symphony' were put on 1/2 MS medium supplemented with 0.1 mg/L NAA and 1.0 mg/L BA. After irradiation and post-cultivation, the re-differentiated individuals were obtained.

(2) *Examination of irradiation conditions*

Samples covered with Kapton films were irradiated with 320 MeV carbon ion beams ($^{12}C^{5+}$) at various doses (0 to 12 Gy).

(3) *Selection of variants using the optimized dose*

Leaf disc sections were irradiated with carbon ions ($^{12}C^{5+}$ and $^{12}C^{6+}$) at a range of 0.1 to 5 Gy. After 24 hr, the leaf disc sections were transferred to fresh 1/2 MS medium supplemented with 0.1 mg/L NAA and 1.0 m /L BA to induce adventitious buds. After about 1 month, grown adventitious buds were transplanted on fresh 1/2 MS medium, and cultivated to obtain plantlets. The resultant plantlets were acclimatized and then grown in a greenhouse to investigate flower color and morphological changes.

Results and Discussion

The leaf disc sections of re-irradiated variant OM7 exhibited higher sensitivity to ion beams than those of 'Mother Symphony'. The adventive bud differentiation did not occur in variant OM7 over 8 Gy of $^{12}C^{5+}$ (Fig. 1). For this reason, the optimized irradiation dose for the selection of variants from OM7 was determined to be 0.1 to 5 Gy. Up to now, several thousands of plantlets were grown, and 13 distinctive individuals were selected in terms of flower color and morphology. Among them, color variations at the upper side of petals included purple and pale orange. On the other hand, color variations at the under side of petals included pale yellow and orange. However, isochroous variant was not obtained in this experiment. Other mutations in petals and stalks included dwarf, multi-petals and petal deformations.

As mentioned above, the white petal variant OM7 was derived from irradiated 'Mother Symphony' that originally has yellow petals. Second irradiation of OM7 resulted in acquisition of variants such as purple and multi-petals that did not appear in first irradiation experiment, suggesting that re-irradiation induced a stepwise mutation in pigment synthesis and morphogenesis pathways.

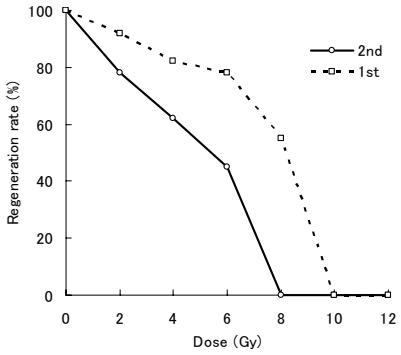

Fig. 1 Sensitivity of Osteospermum to ion beams.

References

1) M. Iizuka et al., TIARA Ann. Rep. 2004 (2005) 50.
2) M. Iizuka et al., JAEA Takasaki Ann.Rep.2005 (2006) 81.

3-06 Comparison of the Mutation Inducing Effect between Ion Beams and Gamma-rays - Guineagrass and Sorghum-

H. Nakagawa [a)], M. Inafuku [b)], M. Kusaba [c)], H. Yamaguchi [d)], T. Morishita [a)], R. Morita [a)] ,M. Nishimura [c)], S. Hoeman [e)], Y. Yokota [f)], Y. Hase [f)] and A. Tanaka [f)]

[a)]Institute of Radiation Breeding (IRB), NIAS, [b)]Okinawa Prefectural Livestock Research Center, [c)]University of Tokyo, [d)]National Institute of Floricultural Science, NAFSO, [e)]BATAN, Indonesia, [f)]Radiation-Applied Biology Division, QuBS, JAEA

Radio sensitivity to gamma (γ) ray and carbon (C) ion beam irradiation were estimated in apomictic tetraploid guineagrass (*Panicum maximum* Jacq.) and diploid sexual sorghum (*Sorghum bicolor* (L.) Moench.). We irradiated the seed of cv. "Natsuyutaka (NY)" guineagrass and "Zhengzu (ZZ)" and "Durra (DU)" sorghum with γ rays and C ion beams at varying dosages and observed the germination rate, survival rate and seed fertility of M_1 plants to identify the optimum dosage of the irradiation. Gamma ray irradiation was conducted at 50, 100, 200, 300, 400, 500, 600, 800, 1000 Gy to NY seeds at the IRB, Japan and sorghum seeds in National Nuclear Energy Agency (BATAN) and compared to the control (0 Gy). The C ion beam irradiation (220 MeV) was conducted at 10, 20, 30, 40, 50, 60, 80, 100, 150, 200 Gy to NY seeds and 50, 100, 150, 200, 300 Gy to sorghum seeds at Takasaki Ion Accelerators for Advanced Radiation Application (TIARA).

The survival rate of NY by γ ray irradiation was not decreased up to 400 Gy but gradually decreased to near 100% lethality at 1,000 Gy (Fig. 1). The survival rate by ion beam irradiation rapidly diminished at 30 Gy with near 100% lethality at 200 Gy (Fig. 2). These data suggested that LD_{50} of NY is 600 – 800 Gy for γ rays and 40 – 50 Gy with C ion beam irradiation. Figure 3 illustrates the seed fertility of NY M_1 plants following irradiation with C ion beams. The NY became seed sterile at 150 Gy and the dosage to induce 50 % seed sterility is estimated as 50 – 60 Gy which differs slightly from the LD_{50}.

The LD_{50} of ZZ sorghum by γ ray irradiation is estimated as 350 -500 Gy. On the contrary, the LD_{50} of ZZ and DU by C ion beam irradiation is estimated at 30 and 50 – 60 Gy, respectively, and a difference of irradiation sensitivity is suggested (Fig.4). It is assumed that the larger sorghum seeds reduced the degree of radiation penetrance allowing some survival at 300 Gy.

We hope these data will be useful in our knock-out mutation studies focused on estimating the influence of apomixis genes in guineagrass[1)] and inducing unique mutant of sorghum for bio-fuel production.

Reference

1) Nakagawa, H. Breeding Research 9 (2007) 3 (in Japanese)

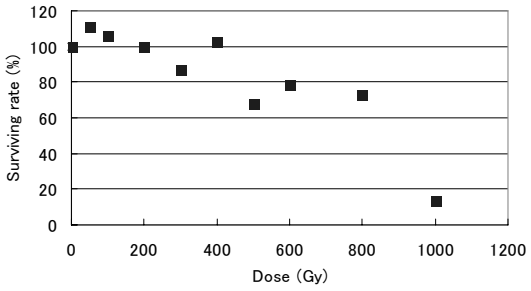

Fig. 1. Survival rate of "Natsuyutaka" at varying dosages of gamma ray irradiation.

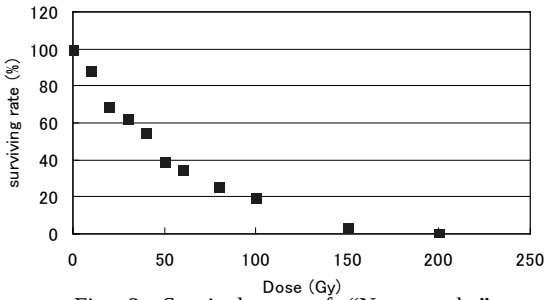

Fig. 2. Survival rate of "Natsuyutaka" at varying dosages of C ion beam irradiation.

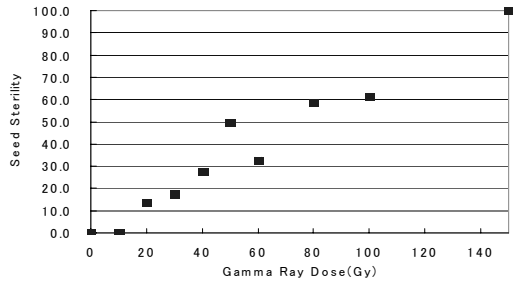

Fig. 3. Seed sterility of "Natsuyutaka" at varying dosages of C ion beam irradiation.

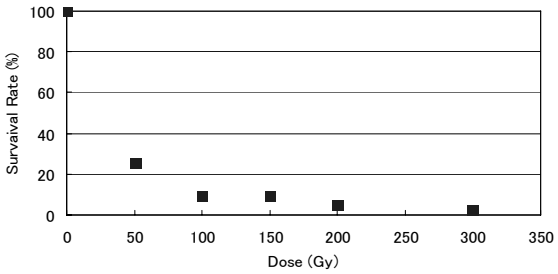

Fig. 4. Survival rate of "Zhengzu" at varying dosages of C ion beam irradiation.

3-07 The Optimum Dose of Ion Beam Irradiation for Growth of Sugarcane

F. Tohjima [a)], Y. Takenoshita [a)], T. Shirao [a)], T. Nagatani [a)], M. Ooe [a)], K. Ueno [a)], Y. Hase [b)] and A. Tanaka [b)]

[a)] Kagoshima Biotechnology Institute, [b)] Radiation-Applied Biology Division, QuBS, JAEA

Sugarcane cultivar "Ni17" has hard and harmful hair on its leaf sheath. We have intended to induce hairless or few hair mutants using ion beam irradiation to tissue cultured of leaf explants. In this study, we studied on growth of sugarcane using JAEA AVF cyclotron. The efficiency of regeneration from callus, the mutation ratio of nursery plants and the selection ratio in field were observed. We have selected 20 few hair mutants among the 5,787 regenerated plants in 2006. The optimum doses on growth were 2～3 Gy of $^{12}C^{6+}$ at 320 MeV. Furthermore, we have continued characteristic investigation and field test of the selected mutants.

サトウキビ品種“Ni17”は株出し適性が高く、耐風性も強い[1)]。しかし、葉鞘部に着生する毛群（第57毛群）が粗剛であるため、収穫や採苗時の作業に支障をきたしている。我々は、イオンビームを利用した変異誘発によって毛群の少ない優良系統の育成を行っており、今回、サトウキビのほ場生育を指標としたイオンビーム照射線量を検討した。

“Ni17”の幼葉組織の切片を2,4-D濃度 0.5～1 mg/l のカルス誘導培地に置床し、約一週間後に炭素イオンビーム（320 MeV・$^{12}C^{6+}$，以下C320）を照射した。照射は時期を変えて6回実施し、照射線量は1，2，3，4，5，8，10 Gyの7水準とした。

照射後、カルス，不定胚を経由し再生させた植物体を発根処理し、順化を行った。2005年8月～2006年4月に鉢上げしたイオンビーム照射個体（5,787個体，無照射を含む）から、主として毛群の有無を基準とするガラス室内での幼苗検定により188個体を初期選抜した。選抜個体は、2006年6月1日及び5日にほ場に定植した。ほ場は厚層腐植質黒ボク土壌で畦間1.2m，株間0.4 m，施肥法，栽培管理は慣行に従い、施肥量は窒素成分量で2 kg/aとした。その後11月上旬に最長仮茎長，茎径（最長茎における地上60 cm高さの稈直径），茎数，毛群の発生程度を調査した。

幼苗検定により初期選抜した188個体について、ほ場での毛群及び生育調査を行い、毛群が少なく生育の良好な有望個体20個体を選抜した（Table 1）。これらは現在もさらに生育特性に関して選抜中である。

イオンビーム照射によるサトウキビのほ場生育への影響を検討したところ（ほ場試験への供試個体数が少なかった8，10 Gyはグラフから省略）、仮茎長は1Gyでは無照射区と有意な差がなく、2 Gy以上では短くなった（Fig. 1）。茎径も同様に1 Gyでは無照射区と有意な差がなく、2 Gy以上では細くなった（Fig. 2）。一方、茎数については，照射によって茎数が増加した個体が観察された（データ未掲載）。5Gy照射個体群は仮茎長，茎径，茎数ともに個体間差が大きく、仮茎長，茎径の平均値が無照射区より劣ったことから生育への影響が大きいと考えられた。また、毛群については、各照射区において無照射区よりやや少なくなった個体が出現したが、無毛の個体は出現しなかった。

C320を照射した培養葉片が順化個体に再生する個体再生率は、材料による差はあるが、2 Gy以上の照射線量において低下が認められ、4 Gyの照射線量で25 %以下となることを報告した[2)]。今回ほ場生育を指標としたイオンビーム照射線量を検討した結果、2 Gy以上の線量において仮茎長や茎径の減少、不良変異の発生が認められた。以上のことから品種“Ni17”の葉片への照射に炭素イオンビーム（C320）を利用する場合、有用変異体作出に適するイオンビーム照射線量は、2～3 Gy程度であると考えられた。

Table 1 The number of tested and selected plants in 2005~2006

Ion	Energy	Dos	No. regenerated plants	No. of plants at open field	No. selected plants at open field	Selection rate
	(MeV)	(Gy)				(%)
		0	1,50	44	3	0.2
		1	1,09	26	2	0.2
		2	1,38	35	3	0.2
		3	1,36	60	11	0.8
$^{12}C^{6+}$	320	4	206	4	0	0.0
		5	215	15	0	0.0
		8	13	1	1	7.7
		10	16	3	0	0.0
		Total	5,78	188	20	0.3

Fig. 1 Effect of ion beam Irradiation on stem length

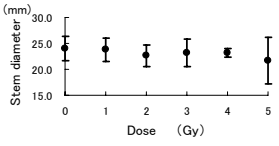

Fig. 2 Effect of ion beam Irradiation on stem diameter

References

1) M. Takemure et al., 鹿児島県農業試験場研究報告 32 (2004) 81.

2) F. Tohjima, et al., JAEA Takasaki Annual Report. 2005（JAEA-Review 2006-042）83.

3-08 Ion Beam Breeding of Chrysanthemum Cultivar 'Sanyo-ohgon'

T. Shirao [a)], K. Ueno [a)], K. Minami [b)], A. Tanaka [b)], S. Imakiire [b)], Y. Hase [c)] and A. Tanaka [c)]

[a)]Kagoshima Biotechnology Institute,[b)]Kagoshima Prefectural Institute for Agricultural Development Flower Division,[c)]Radiation-Applied Biology Division, QuBS, JAEA

We worked on the ion beam breeding aimed to reduce lateral buds, or to improve flower size of Chrysanthemum cultivar 'Sanyo-ohgon'. In the individual selection of the first year, various flower shapes and days for flowering were observed in the mutation, and 45 individuals were then selected from 6,186 regenerated plants. Also, a decrease in the amount of DNA was observed in the mutants with increasing the dose of ion beam irradiation. After vegetative propagation, the line selection was performed by flowering in November or March, and two lines were then selected. Moreover, it was indicated that the re-irradiation of the ion beam was effective in additional improvement of 'Sanyo-ohgon'.

黄系秋輪ギク「山陽黄金」は、鹿児島県の主力品種であるが、側枝発生数が多く摘芽・摘蕾作業に労力を要し、花がやや小さいなどの欠点がある。我々は、白系秋輪ギク「神馬」において、葉片にイオンビームを照射し、不定芽経由の再生個体から無側枝性に優れた変異個体を選抜し[1)]、品種登録を行った。また、育成した品種に再度イオンビームを照射することにより、新たに低温開花性の特性を付与した個体の作出に成功している[2)]。今回、「山陽黄金」について、「神馬」と同様の手法を用いて無側枝性や花の大型化を目標としたイオンビーム育種に取り組んだ。

選抜系統で県内に供給されている「山陽黄金１号」の無菌植物の葉片（2×4 ㎜）に、原子力機構高崎研のAVFサイクロトロンにより発生させたイオンビーム（220 Mev・$^{12}C^{5+}$, 320 MeV・$^{12}C^{6+}$）を1～3 Gy照射し、不定芽経由により再生個体を得た。これらの変異個体は初年目に12月開花の作型に供試し、生育調査とDNA量測定を行い、無側枝性や花容草姿に優れる個体を選抜した。次年度は選抜個体の系統選抜試験を実施し、11月開花と3月開花の作型により、選抜特性の保持状況を調査した。また、選抜した優良系統はイオンビームの再照射（320 MeV・$^{12}C^{6+}$：0.5～3 Gy）による無側枝性や花容草姿の再改良に供試した。

初年目の個体選抜試験では、供試した6,186個体から、45個体を選抜した。選抜率は0.7%で、特にボリューム，無側枝性，花容の3点ともに優れる個体は4個体であった。「山陽黄金」の花形は剣弁で、内側への抱え込みが少ないが、再生個体の中には、より顕著な剣弁咲きや丸弁，抱え咲きなど様々な花形の個体が観察された。DNA量を測定した結果、不定芽を経由しない茎頂培養由来の個体はDNA量の変化が認められなかったが、変異誘発個体は照射によるDNA量の減少が認められた。DNA量の減少は220 MeV-Cイオンで顕著に現れ、照射線量の増加に伴ってDNA量の減少した個体の割合も増加した。320 MeV-Cイオンの照射区は、DNA量の減少傾向は緩やかで、3 Gy照射区で220 MeV-Cの1～2 Gy照射区と同程度であった。

次年度の系統選抜試験に供試した45系統については、到花日数は、11月開花及び3月開花とも「山陽黄金１号」と大きな差は認められなかった。無側枝性は、「山陽黄金１号」の側枝消失率が11月開花で12 %，3月開花で14 %であったのに対し、供試系統は11月開花で9～69 %、3月開花で０～77%と系統による特性の差が現れていた。小花数についても系統間差が大きく、11月開花で219～415枚、3月開花で150～324枚であった。無側枝性や花容草姿、ボリュームから2系統（＃10，＃22）を選抜した（Table 1，2）。

DNA量が減少していない選抜系統の＃22に再度イオンビームを照射して変異誘発個体を育成し、12月開花の作型に3,215個体を供試した。これらの個体は供試した元系統の特性を引き継ぎ、7割以上が栄養繁殖が困難になる強無側枝性を示した。しかし、イオンビーム照射により、＃22より側枝数の増加した個体も一定割合で出現し、無側枝性が再度改変可能な特性であることが明らかとなった。これらの中から花容草姿の優れる30個体を選抜したが、選抜個体の側枝消失率は30.1～88.1 %で、小花数が増加した個体が観察された。これらのことから、当品種においてもイオンビームの再照射による選抜個体の再改良が有効であると考えられる。

Table 1 Characteristics of the selected lines by flowering in November

line	number of days to flowering	plant height (cm)	weight of 90cm (g)	number of disbudding	rate of lost lateral buds (%)	number of florets
#10	57	109	64	37	41	290
#22	53	106	76	17	58	260
Sanyo-ohgon No1	52	97	82	52	12	298

The dose of carbon ion beam irradiated at individual selections were 220MeV ・3Gy(#10) or 320MeV ・2Gy(#22).

Table 2 Characteristics of the selected lines by flowering in March

lin	number of days to flowering	plant height	weight 90cm (g)	number of disbudding	rate of lateral buds (%)	lost number of florets
#10	55	101	72	11	34	238
#22	57	96	81	6	53	209
Sanyo-ohgon No1	52	90	65	20	14	210

References

1) K. Ueno et al., TIARA Ann. Rep. 2002 (2003) 52.
2) K. Ueno et al., TIARA Ann. Rep. 2004 (2005) 60.

3-09 Induction of Mutations by the Ion Beam Irradiation to the Bulb-scales of *Lilium* cv. Acapulco.

M. Kondo [a)], Y. Koike [a)], Y. Hase [b)], Y. Yokota [b)] and H. Kobayashi [a)]

[a)]Department of Biotechnology, Niigata Agricultural Research Institute
[b)]Radiation-Applied Biology Division, QuBS, JAEA

We have been working on producing marketable blue lilies. It has been impossible to produce blue lilies by crossbreeding or mutation, because they lack flavonoid 3',5'-hydroxylase (F3'5'H), which is necessary for synthesis of the blue pigment, delphinidin. Therefore, we developed an *Agrobacterium*-mediated transformation system for lilies to transfer the F3'5'H gene[1)]. For the marketing of the transformed blue lilies, we have to regulate the spreading of the pollen to prevent them from crossing with other lilies, because they are genetically modified plants. The aim of this study is to produce of male-sterile lilies. In the present study, we exposed bulb-scales of lilies to $^4He^{2+}$ beams from the AVF cyclotron and investigated the effects on the bulb-scales.

Bulbs of the Oriental hybrid lily, *Lilium* cv. Acapulco, were cultured under a 16 hr light/8 hr dark cycle at 25 °C on bulb propagation medium, which consisted of modified MS medium-1/2 NH_4NO_3 and KNO_3, 40 g/l sucrose, and 3 g/l gellan gum. The diameter of the *in vitro* grown bulb was about 10 mm or more. The penetration range of 50 MeV $^4He^{2+}$ was 1.45 mm. Therefore, we sliced the scales to about 1.0 mm thickness. The sliced 10 scales were placed on a regeneration medium which consisted of modified MS medium-1/2 NH_4NO_3 and KNO_3, 30 g/l sucrose, 5 g/l gellan gum, 0.1 mg/l picloram, and 0.01 mg/l 6-benzylaminopurine and covered with sterilized Kapton polyimide film (7.5 μm in thickness, 45 mm square in size, Toray-Dupon, Japan). The scales were exposed at total doses of 0 Gy – 2.0 Gy of 50 MeV $^4He^{2+}$ beams from the AVF cyclotron.

The exposed scales were transferred to the same fresh medium and cultivated for 4 months. The culture were performed under a 16 hr light/8 hr dark cycle at 25 °C. The scales were maintained by subculturing every 2 months onto the same fresh medium under the same condition. Regenerated shoots were transferred to bulb propagation medium and cultivated for 2 months. The number of regenerated plants was counted 6 months after the ion beam exposure.

It has been suggested that the irradiation doses that suppressed the proliferation rate to 50-90% were effective in induction of mutations in cultured plant tissues [2), 3)]. In the irradiation of 50 MeV $^4He^{2+}$, the doses of 0.2-0.8 Gy suppressed the regeneration rate to 50-90 % of the non-irradiated control (Fig. 1). We assumed from this result that the doses of 0.2–0.8 Gy of 50 MeV $^4He^{2+}$ were appropriate for obtaining mutants. In the irradiation of 50 MeV $^4He^{2+}$, the doses of 0.2-0.6 Gy suppressed the proliferation rate of the calluses to 50-90 % of the non-irradiated control [4)]. These results suggest that scales are more insensitive to ion beams than calluses.

At present, the ion beam irradiation, regeneration, acclimatization and planting to a field are in progress to select male-sterile mutants of lilies (Fig. 2).

References

1) Y. Hoshi et al., Plant Cell Rep. 22 (2004) 359.
2) M. Okamura et al., Nucl. Instr. Meth. B 206 (2003) 579.
3) S. Nagatomi et al., TIARA annual Rep. 1995 (1996) 50.
4) M.Kondo et al., JAEA Takasaki Annual Rep. 2005 (2007) 8.

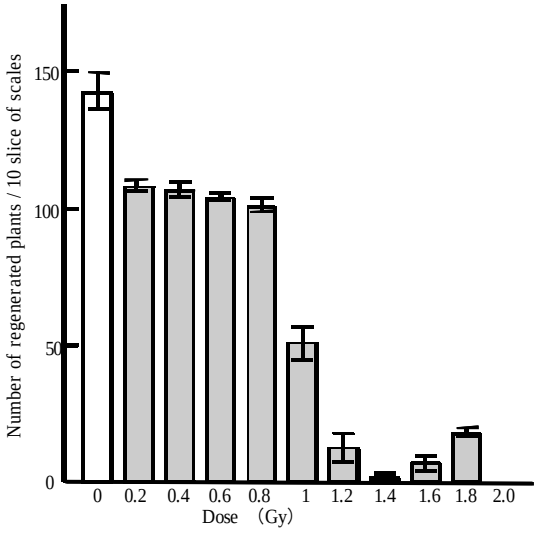

Fig.1 Effects of 50 MeV $^4He^{2+}$ exposure on the regeneration from scales. Values represent the means of 3 experiments. (Bar = standard error)

Fig.2 Ion beam-irradiated plants of "Acapulco" were planted and grown in a field in order to investigate the pollen fertility.

3-10 Development of New Commercial Strains in Functional Mushroom by Ion Beam Irradiation

Y. Kawashima [a)], Y. Hase [b)] and Y. Yokota [b)]

[a)]Gunma Prefectural Forestry Experiment Station,[b)]Radiation-Applied Biology Division,QuBS,JAEA

In *Pleurotus osutreatus* and *Lyophyllum decastes*,the increase in dose causes the reduction of mycelial growth. So we examined the mutagenic effect of ion beams on *Pleurotus eringii*,*Ganoderma lucidum* and *Grifora flondosa*. As in *Pleurotus osutreatus* and *Lyophyllum decastes*,we found that the increase in dose causes the reduction of mycelial growth. The regeneration rate went down at 600 Gy in $^{12}C^{6+}$ beams and few spores germinated at 700 Gy in $^{12}C^{6+}$ beams. However, no morphological changes were observed in the fruit bodies.

近年、植物育種における変異原として、量子ビームの利用が花卉をはじめ果樹、野菜などに広まり、成果がみられる。しかし、きのこ類においては紫外線やγ線を変異原とした報告はいくつかみられるのみである[1),4)]。

きのこ類の生産は群馬県などの中山間地域の主要な産業のひとつである。しかし、大手企業の参入、消費者ニーズの多様化、輸入量の増加などによりきびしい状況にある。

そこで、きのこ類の育種に量子ビームを利用して、突然変異を誘発することにより新品種を開発するために、致死線量の把握及び栽培試験を行った。

1. 実験方法

当場保有のエリンギGPLE-15菌株、マンネンタケGGL-5菌株及びマイタケGGF-7,33菌株の２核菌糸体を供試体として用いた。直径３ ㎜のコルクボーラーで打ち抜いた２核菌糸体を直径50 ㎜プラスチックシャーレのPDA培地上に置床して、イオンビームまたはγ線を照射し、菌糸成長量を測定した。照射線量はイオンビームが100～1000 Gyとした。

イオンビーム（加速粒子$^{12}C^{6+}$、320 MeV）の照射は、高崎量子応用研究所にあるイオン照射施設「TIARA」のAVFサイクロトロンで行った。

照射後に菌糸成長が認められたエリンギ及びマイタケの供試体については、栽培に供して子実体の形状における突然変異体の出現及び胞子形成の有無を観察した。培地基材はブナオガコ、培地添加物は生コメヌカまたはホミニーフィードとし、容積比で10：２に混合し、含水率を65%に調整した後、ＰＰ製容器に詰め込んだ。滅菌は高圧滅菌とし、培地内温度が120℃に達した後40分間行った。培養温度は22 ℃とし、培養した後に温度15～17℃、湿度90 %の発生室に移動し、子実体の発生を促した。

2. 結果及び考察

エリンギ及びマンネンタケ菌糸体について菌糸成長量とイオンビーム線量の関係を図－１及び２に示した。照射した試験区はいずれもコントロールに比べて成長量は少ない傾向がみられたものの、600 Gyにおいても菌糸が成長することがわかった。なお、700 Gy以上を照射した試験区については、菌糸の成長は認められなかった。これらの結果はハタケシメジ及びヒラタケとほぼ同様であり[2),3)]、きのこ類の２核菌糸においては、イオンビーム照射の致死線量は700 Gy前後であることが推察された。

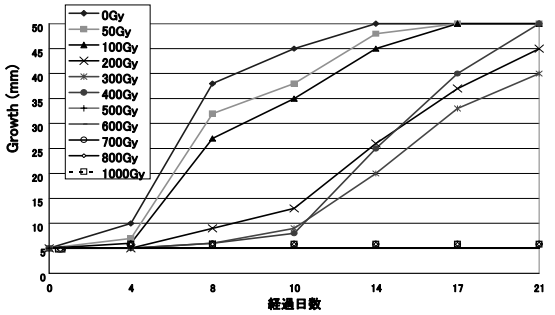

Fig.1 Effect of ion beam irradiation on mycelia growth of *Pleurotus eryngii*.

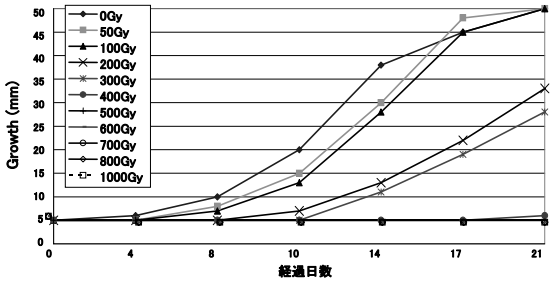

Fig.2 Effect of ion beam irradiation on mycelia growth of *Grifora flondosa*.

エリンギとマイタケの栽培試験の結果においては、子実体の形状の突然変異及び胞子欠損は認められなかった。しかし、ヒラタケにおいては突然変異の出現がみられており[3)]、イオンビームの照射はきのこ類の突然変異の誘発に有効な手段であると思われる。

References

1)S.Nagatomi, Ins. Radiat. et al., Breeding Technical News 50 (1995).
2)Y.Kawashima et.al., TIARA Ann.Rep.2004 (2005) 96.
3)Y.Kawashima et.al., JAEA Takasaki Ann Rep.2005 (2006) 91.
4)Y.Obatake,et al., Mycoscience 44 (2003) 33.

3-11 Mutation Induction of Asiatic Hybrid Lily and *Lilium* × *formolongi* Hort. Using Ion Beam Irradiation

N. Chiba [a)], K. Arakawa [a)], S. Nakamura [a)], S. Suzuki [a)], Y. Yokota [b)], Y. Hase [b)] and I. Narumi [b)]

[a)]Miyagi Prefectural Agriculture and Horticulture Research Center
[b)]Radiation-Applied Biology Division, QuBS, JAEA

We investigated mutants of Asiatic hybrid lily and *Lilium* × *formolongi* Hort. induced by ion beam irradiation. Six flower color mutants were observed in M_1 generation of Asiatic hybrid lily, and Two pollenless mutants were observed in M_2 generation of *L.* × *formolongi* . Carbon ion irradiation seemed to be more effective than Helium ion to induce mutants of Asiatic hybrid lily.

１．はじめに

スカシユリ（Asiatic hybrid lily）は、赤，桃，橙，黄等の花色で球根により繁殖し、シンテッポウユリ（*Lilium* × *formolongi* Hort.）は白花で種子繁殖性の園芸植物である。本試験では品種改良を目的に、スカシユリとシンテッポウユリに対して、イオンビームによる突然変異を誘発し、花の諸形質における遺伝的変異の拡大をねらった。

２．実験方法

無菌培養で増殖したスカシユリの２品種ロリーポップ（花色：赤白）とチャンティ（花色：桃）のりん片に炭素$^{12}C^{6+}$(320 MeV)またはヘリウム$^{4}He^{2+}$(100 MeV) を照射した。その後にりん片から再生した個体をM_1世代とし、ほ場で栽培し開花時に変異の有無を調査した[1)]。

シンテッポウユリについては、品種オーガスタの種子に炭素$^{12}C^{6+}$ (320 MeV) を照射処理しM_1世代を育成した。M_1世代の自殖により変異した遺伝子座をホモ化し、得られたM_2世代をほ場で栽培し開花時に変異の有無を調査した。

３．結果及び考察

スカシユリでは花色に関する６系統の変異体が得られた。ロリーポップの変異体４系統は全てFig. 1(B)に示した花の白色化であった。チャンティではFig. 1(D)に示した花色の変異体と、花被片の先端が白い変異体が得られた。ロリーポップにおいて、炭素イオンとヘリウムイオンの効果を同線量で比較した場合、突然変異率は、炭素イオンが高い傾向であった（Table 1）。シンテッポウユリのM_1世代では、変異体が観察されなかった。M_2世代では花色等の変異は無かったが、花粉が生産されない２系統の変異体を得ることができた（Table 2）。

Table 1 Number of observed mutants and estimated mutation rates in Asiatic hybrid lily by ion beam irradiation.

Cultivar	Ion	Dose (Gy)	No. of M_1	No. of Mutants	Mutation Rate (%)
Lolly pop	$^{12}C^{6+}$	0.5	90	1	1.1
		1.0	40	1	2.5
	$^{4}He^{2+}$	0.5	336	0	0
		1.0	232	2	0.86
Chanty	$^{12}C^{6+}$	0.5	75	2	2.7

Table 2 Number of observed mutants and estimated mutation rates in *L.*× *formolongi* by carbon ion irradiation.

Cultivar	Ion	Dose (Gy)	No. of M_2	No. of Mutants	Mutation Rate (%)
Augusta	$^{12}C^{6+}$	1	445	1	0.22
		2	521	1	0.19

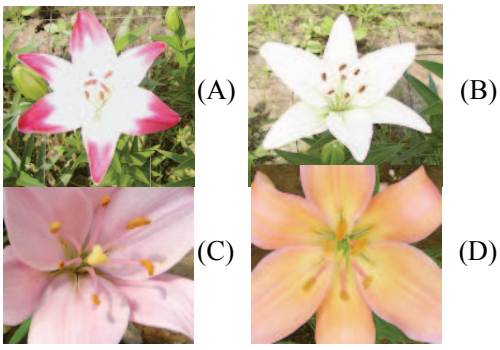

Fig. 1 Mutation of flower color in Asiatic hibrid lily.
Normal (A) and Mutant (B) of cultivar 'Lolly pop'.
Normal (C) and Mutant (D) of cultivar 'Chanty'.

Reference

1) N. Chiba et al., TIARA annual report 2005 (2007) 92.

3-12 Dose Response and Mutation Induction by Ion Beam Irradiation in Chrysanthemum

A. Matsumura [a)], N. Furutani [a)], Y. Hase [b)], Y. Yokota [b)] and A. Tanaka [b)]

[a)]Kyoto Prefectural Institute of Agricultural Biotechnology,
[b)]Radiation-Applied Biology Division, QuBS, JAEA

Recently irradiation of ion beam has become a new method for mutation breeding of chrysanthemum. This study was conducted to investigate the effect of ion beam irradiation on mutant induction of chrysanthemum cultivars (‘H13’ and ‘Shiroyamate’). Irradiation of ion beam induced flower colour changing; that is, yellow mutant was successfully obtained from ‘Shiroyamate’, and vermilion and white/red mutants were also induced from ‘H13’. These results suggest that the ion beam irradiation would be valuable for mutation induction in chrysanthemum flower.

盆コギクは、仏花として出荷期が決まっているが、天候による開花変動が大きく、産地では危険分散のために多くの品種が作付けされている。

こうした中、京都府では開花変動の少ない赤色系統‘H13’（赤紫色）を育成した。しかし、盆コギクとしては赤・白・黄の3色セットが望まれる。そこで、イオンビームを用いた突然変異育種法に取り組むこととした。イオンビームは、ガンマ線やX線などの放射線を用いた育種と比較して幅広い変異を示すことが知られており[1)]、キクでは花色変異品種をはじめ、多くの品種が育成されている。

本研究では、‘H13’及び在来白色品種‘白山手’から、イオンビーム照射と培養により白色や黄色等に変化した品種を育成するために、花弁あるいは葉片にイオンビームを照射し、変異体の作出を試みた。

‘白山手’の花弁を3～5 mmに調製し、NAA 10 mg/lとBA 3 mg/lを添加したMS培地を10ml含む60 mmシャーレに置床した。一方、‘H13’は葉片を3～5 mmに調製し、NAA 0.1 mg/lとBA 0.5 mg/lを添加したMS培地を10ml含む60 mmシャーレに置床した。次に、日本原子力研究開発機構 (高崎市) イオン照射研究施設のAVFサイクロトロンを用いて、これらサンプルに加速粒子$^{12}C^{5+}$、エネルギー220 MeVで0～32 Gyの範囲で照射し、培養によりシュートを再生させた。順次、順化・育苗した後、‘白山手’はビニールハウスに定植、H13は４号ポットに鉢上げしてガラス温室内で栽培し、開花調査を実施した。

‘白山手’では、イオンビームの線量が高くなるに伴い、黄色花及び無花粉株の出現率が高くなった（Table 1 and Fig. 1）。また、葉の波打ちや矮化などの変異率も高まり、8 Gy以上では半数以上の個体に変異が現れた。これら結果から、‘白山手’の花弁に照射するイオンビームの線量は4 Gy以下が適すると考えられた。

‘H13’への照射では、濃赤色、朱色、桃色などの花色変異体が得られた（Fig. 1）。また花形や花房にも変異が認められた。現在、これら再生植物体をほ場に定植し、慣行法により栽培を行っている。今後、花色や草型等の特性を調べ、有望系統を選抜するとともに、得られた花色変異株に再度イオンビームを照射し、さらに花色変異の幅を広げていきたいと考えている。

Table 1 Mutation induction in ‘Shiroyamate’ by $^{12}C^{5+}$ ion beam irradiation

Does (Gy)	No. of plants	Flower mutation [a] (%)	Pollen sterility (%)	Leaf mutation [b] (%)	Dwarf (%)
Cont	30	0	0	-	-
0	126	0.8	4	0	0
1	482	2.3	1	6.8	5
2	424	4	3.8	10.1	5.4
4	443	7.4	2.7	23.3	12.2
8	360	9.7	11.1	28.9	7.5
16	88	1.1	0	10.2	0
32	46	6.5	0	8.7	0

[a] Flower mutation indicates yellow mutants
[b] Leaf mutation indicates that leaf shape was mutated from serrated to round

Fig. 1 Selected mutants from ‘Shiroyamate’ and ‘H13’
A: ‘Shiroyamate’ (Normal)
B: Yellow variety from ‘Shiroyamate’
C: ‘H13’ (Normal)
D: Vermilion variety from ‘H13’
E: Red/white variety form ‘H13’
F: Cylinder-shaped variety from ‘H13’

Reference

1) S. Nagatomi, et al., TIARA Annual Report 1997 (1998) 41.

3-13 Induction of Thornless Yuzu Mutant by Heavy Ion Beam Irradiation

Y. Matsuo[a)], Y. Hase[b)], Y. Yokota[b)], I. Narumi[b)] and E. Ohyabu[a)]

[a)] Saga Prefectural Agricultural Research Center, [b)] Radiation-Applied Biology Division, QuBS, JAEA

Yuzu (*Citrus junos*) tree bears long thorns that deteriorate fruit quality. We are trying to produce thornless mutant of Yuzu by carbon-ion irradiation. Cut surface of lower hypocotyls were exposed to carbon ions with a total energy of 320 MeV. Based on the shoot regeneration rate, we determined less than 8 Gy is appropriate for our culture system. We successfully obtained completely thornless mutant together with several mutant plants with weak thorns or lesser number of thorns. We grafted these mutant plants into rough lemon (*Citrus jambhiri*) to grow up quickly, and will examine their thornless traits.

ユズは樹体に長いトゲが発生するため、栽培管理上障害となっている。さらに、トゲによる刺し傷はキズ果や腐敗果の発生など果実の商品性を低下させる。そこで、ユズ実生の胚軸断面からシュートを再生させる培養系に重イオンビームを照射しトゲ消失変異体の作出を試みた。今回はシュート再生率などを指標とした照射条件や変異体作出に最適な線量の検討を行うとともに、再生シュートを育成し、トゲ消失変異個体を得たので報告する。

試験１　ユズ（*Citrus junos* Sieb.ex Tanaka)種子を1/2ＭＳ培地に播種後、３週間目に胚軸を２cm程度残し切断した。さらに、１週間後に切断面より発生したカルスに重イオンビームを照射した。照射線種はＣイオン（$^{12}C^{6+}$　総エネルギー320 MeV）を用い、照射線量は１ Gy、２ Gy、４ Gy、８ Gy、16 Gy、32 Gy、64Gy、128Gy、256Gyの９線量区とした。照射施設は原子力機構高崎量子応用研究所のAVFサイクロトロンを用いた。照射後、再分化個体数及び根の伸長量を調査した。

試験２　試験１の結果を踏まえ、線量を１Gy、２Gy、４Gy、８Gyの４線量区で照射を実施し、再分化を確認後、馴化培地へ継代培養した。さらに、培土に鉢上げし、トゲの発生が見られない個体についてはラフレモン等に寄せ接ぎを行い伸長促進を図りトゲの発生状況を確認した。

試験１　２週間後の再分化シュートの発生率は、２Gy以下では100 %以上であり、また８ Gyでも60 %は再分化した。なお、シュートの発生率が100 %を越えるのは１胚軸より複数発生したものである。照射線量が32 Gy以上の場合シュート発生は認められなかったが、根の伸長は確認できた。根の伸長量については、照射線量が増加しても顕著な影響は見られなかった。これは、重イオンではＸ線等とは異なり、到達深度が浅いため、根の発生阻害が起こりにくいものと考えられ、照射時には植物体根部（地下部）の保護は必要ないと言える。以上の結果より、ユズ実生に重イオンビームを照射する線量は８ Gy以下で検討していくこととした。

試験２　各線量区とも200個体前後に照射を実施した結果、２ Gy区で完全無刺個体を獲得することができた。また、トゲの発生がほとんど見られない個体は１ Gyを除き各線量とも出現した。これらの個体以外に、初期生育が緩慢で判断がつかない個体もあったため、ラフレモン等に寄せ接ぎを実施し確認を急ぎたい。

Table 1. Shoot regeneration rate from hypocotyls irradiated with carbon ions.

Dose	No. of irradiation	1 week after irradiation		2 week after irradiationr	
		No. of shoots	Regeneration rate	No. of shoots	Regeneration rate
(Gy)			(%)		(%)
0	10	11	110	15	150
1	10	10	100	12	120
2	10	10	100	11	110
4	10	10	100	9	90
8	10	8	80	6	60
16	10	1	10	2	20
32	10	0	0	0	0
64	10	0	0	0	0
128	10	0	0	0	0
256	10	0	0	0	0

Table 2. Effects of carbon ion irradiation on root growth.

Dose	No. of irradiation	3 week after irradiation		4 week after irradiation	
		No. of roots	Root length	No. of roots	Root length
(Gy)			(mm)		(mm)
0	10	8	12.3	8	28.7
1	10	6	12.4	7	24.9
2	10	7	13.3	6	25
4	10	6	9.9	6	30
8	10	7	11.7	6	20.6
16	10	4	15	5	24.6
32	10	6	10.6	8	17.8
64	10	8	11.3	8	21.5
128	10	6	7.7	4	15.3
256	10	4	10.4	4	22.6

Figure 1. (a) Thornless Yuzu mutant. (b) Normal shoot with long thorns that is regenerated from the same hypocotyls.

3-14 Producing New Gene Resources in Fig by Using Ion-beam Irradiation

I. Asami [a)], S. Fukuta [a)], S. Kuroyanagi [a)], T. Ooya [a)], Y. Hase [b)], Y. Yokota [b)] and I. Narumi [b)]

[a)]Aichi-ken Agricultural Research Center, [b)]Radiation-Applied Biology Division, QuBS, JAEA

The goles of our study are to produce new gene resources in fig by mutation induction with ion-beam irradiation, because the breading by varietal crossing in fig is very difficult. As the first paper of our study, we report the influences of carbon ion beams and soft X-rays irradiation to in vitro lateral buds on mutation induction in fig 'Masui-dorfin'. In vitro buds were irradiated with carbon ion beams (320 MeV $^{12}C^{6+}$) at various doses of 0 – 40 Gy at TIARA, and with soft X-rays (100 KVp, 5 mA, 191 Gy/Hr) at Aichi Agric.Res.Ctr. at various doses of 0 – 160 Gy. The efficiency of survival rate of buds, the fresh weight and the length of lateral shoots, and the rate of shoot that grows over 1 cm were observed. The optimum doses for carbon ion beams and soft X-rays were 5 Gy of 320 MeV $^{12}C^{6+}$ and 60 Gy of soft X-rays, respectively.

日本のイチジク産地で栽培されている品種は、そのほとんどが“桝井ドーフィン”であり、遺伝子資源としては非常に限られたものになっている。さらに、日本の湿潤気候での栽培に適したフィッグ型イチジク品種はほとんど単性花（雌花）しか着生しない[1)]ことから他品種との交雑育種は困難であり、これまで遺伝子資源の拡大はされてこなかった。そこで本課題では、イオンビームを利用して高品質でかつ特徴のあるイチジク新品種開発につながる遺伝子資源を創成する。本年度はイチジクへの適切な照射方法を確立するために、培養苗腋芽への炭素イオンビーム及び軟Ｘ線の照射効果を調査する。

無菌培養したイチジク“品種：桝井ドーフィン”の茎頂部と葉を切除した茎部を節ごとに切断し、６㎝径プラスチックシャーレ内にＭＳ液体培地（ショ糖３％、ホルモン無し）を含ませた生け花用オアシス（発砲フェノール樹脂）を入れ、腋芽の向きを上に揃えて挿した。同シャーレ内の試料に加速した炭素イオン粒子（320 MeV・$^{12}C6^{+}$、LET：86 keV／μm）を種々の線量で照射した。また、比較のため愛知農総試保有の軟Ｘ線照射装置（ソフテックス株式会社製M-100 WE型：100 KVp、5 mA、191 Gy／Hr）を用いて同様の方法で照射した。照射済試料はＭＳ液体培地（ショ糖３％、ホルモン無し）を含ませた育苗用オアシス（Oasis5710）に挿し、プラントボックス内で育てた。培養は25 ℃、16時間日長で行い、培養60日後の腋芽の生存率、10 mm以上伸長した腋芽の割合、腋芽の茎長及び腋芽重量を調査した。試験はそれぞれ２回ずつ行い、各試験区ごとに腋芽30～40節を供試した。

炭素イオンビームを５ Gyから40 Gyまで段階照射したところ、15 Gy以上で生存する腋芽の割合が低下し始め、30 Gy以上では全て枯死した。また、10 mm以上伸長する腋芽の割合、伸長した腋芽の茎長及び腋芽重量は５ Gy照射で非照射区（０Gy）の平均値に対して50 %程度にまで低下した。腋芽が生存しても伸長しなければ選抜に用いることができないことから、10 mm以上伸長する腋芽がわずかに残る10 Gyが限界であると考えられた（Fig.１）。

軟Ｘ線を10 Gyから160 Gyまで段階照射したところ、80 Gy以上になると腋芽生存率が低下した。生存はしたものの腋芽の伸長が抑えられることが多く、10 mm以上伸長した腋芽の割合が50 %を切るのは40 Gyから80 Gyの間であった（Fig.２）。

それぞれ２回目の試験を行ったところ、腋芽の生育が非照射区の50 %程度に低下する線量は、炭素イオンビームで５ Gy、軟Ｘ線では60 Gyあった（データ未掲載）。

以上の結果、両線種について腋芽の生育に同程度の影響が現れる線量を比較すると、炭素イオンビームは軟Ｘ線の十分の一以下であった。

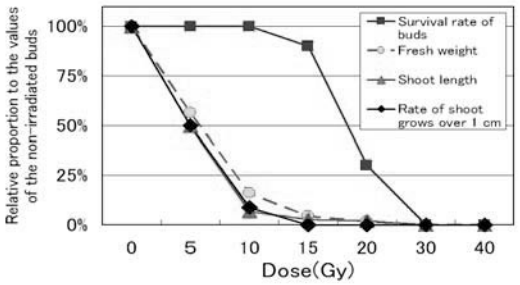

Fig.1 Influence of 320 MeV carbon ion beam irradiation to on growth of *in vitro* lateral buds in Fig‘Masui-dorfin’.

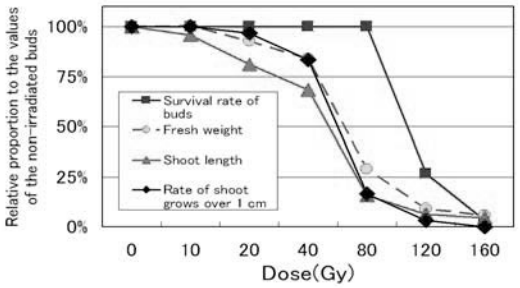

Fig.2 Influence of soft X-ray irradiation on growth of *in vitro* lateral buds in Fig‘Masui-dorfin’.

Reference

1）平田尚美.農業技術体系-果樹編５,東京,農文協.イチジク,基29（1993）.

3-15 Induction of New Color Variation by Irradiation of Ion Beams to Light Yellow 'Jinba'

T. Toyoda [a)], H. Watanabe [b)], K. Emoto [a)], S. Yoshimatsu [b)], Y. Hase [c)] and S. Kamisoyama [a)]

[a)]Paddy Farming Research Institute, Oita Prefectural Agriculture, Forestry and Fisheries Research Center, [b)]Floriculture Research Institute, Oita Prefectural Agriculture, Forestry and Fisheries Research Center, [c)]Radiation-Applied Biology Division, QuBS, JAEA

'Jinba' is a white chrysanthemum. In 2002, we found a light yellow variant of 'Jinba' at south area of Oita prefecture. So, we have intended to induce deep yellow 'Jinba' using ion beam irradiation($^{12}C^{6+}$:320MeV,1･2･3 Gy) to this light yellow 'Jinba'. Leaves or petals were cut and cultured on the regeneration MS medium and irradiated. Five mutants (2 Gy:2 mutants,3 Gy:3 mutants) which showed deep yellow at flower bud time were obtained. But their petals gradually became white toward flowering.

秋輪ギク「神馬」(白)は、大分県南部の佐伯市を中心に多く栽培されている。しかし、「神馬」の栽培特性に類似した高品質の黄色品種がなく、黄色品種を多く生産できないことが、生産・販売戦略上大きな障害となっている。また、花き研究所では、平成 14 年度に佐伯市蒲江町で発見された「神馬」淡黄色系統について、系統選抜を行い、濃黄色系統を選抜してきたが、開花時に退色する欠点を改善されていない。

そこで、「神馬」淡黄色系統に対して花色変異に有効なイオンビーム照射を行い、花色変異の誘発を試みた。

供試材料は、「神馬」淡黄色系統（以下元株）無菌培養中の葉片及び花弁を用いた。葉片は 2×5mm、花弁は 2×5～7mm 程度に切断し、不定芽形成培地〔MS 培地+NAA2.0mg/L+BA1.0 mg/L(ショ糖 3%、寒天 0.8%、pH5.8)〕に置床し、1 週間程度培養したものに、8 月 21 日にイオンビームを照射した。照射後、同じ不定芽形成培地へ継代し、3～4 週間培養後、不定芽伸長培地〔MS 培地+NAA0.01 mg/L+BA0.05 mg/L(ショ糖 3 %、寒天 0.8 %、pH5.8)〕へ移植した。照射は、TIARA 内の AVF サイクロトロンを利用し、$^{12}C^{6+}$：320 MeV、1、2、3 Gy を 15 シャーレ照射した [1)]。

再生した植物体は順次発根、順化、鉢上げを行い、開花させて花色の確認を行った。色彩値（Hunter b 値）は色彩色差計（CR-321、MINOLTA）で測定した。

その結果、葉片からの再生個体数は、1・2 Gy を照射したものは同程度だったが、3 Gy を照射したものは、1・2 Gy と比較して半分程度であった(Table1)。

花弁から伸長したシュートは、照射線量に関係なくビトリフィケーションが多く発生したが、発根培地にフロリアライトを利用することにより、約 1 カ月後には、症状はほぼ改善され、鉢上げが可能となった。

鉢上げした再生個体の開花は、早い個体で 1 月下旬から始まった。この中から元株よりも黄色の濃い個体を、3 Gy 照射により得られた個体から 3 個体、2 Gy 照射により得られた個体から 2 個体(以下濃黄化個体)を選抜したが、全て葉片由来のものであった。また、再生個体数との関係から、線量が強い方が濃黄化個体が得られやすい傾向があった。

選抜した 5 個体は、元株と比較して切り前時の黄色が濃くなり(b 値)、黄色スプレーギクと同等の濃さであっが、開花時に外弁が退色するため、黄色品種として利用することは困難だと思われた(Table2,Fig.1)。今後も、再生個体の開花処理と調査を継続するとともに、選抜濃黄化個体への再照射を検討していきたい。

Reference

1)鹿児島県バイオテクノロジー研究所成績概要書 (2000～2002)

Table 1. The number of regenerated and selected plants

Tissue	No. of plants	$^{12}C^{6+}$:Dose(Gy) 1	2	3	Total
Leaf	Regenerated plants	520	492	233	1,245
	Selected plants	0	2	3	5
Petal	Regenerated plants	23	41	73	137
	Selected plants	0	0	0	0

Table 2 . Changes of color indices b

Individual	Dose (Gy)	Bud	Full bloom Inside	Outside
Light yellow 'Jinba'	-	30.84	23.67	1.57
No.8	3	37.25	35.49	1.40
No.10	3	40.61	37.30	2.80
No.11	3	43.33	34.78	10.27
No.12	2	43.07	25.94	16.47
No.13	2	37.94	31.07	4.61
'Jinba'	-	11.16	2.02	2.41
Yellow chrysanthemum of spray type	-	41.09	38.12	34.82

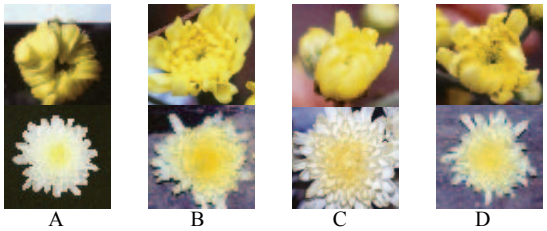

A B C D

Fig.1 Selected flower color mutants

A : Light yellow Jinba B : No.11 C:No.12 D:No.13

Upper : Bud Lower : Flower

3-16 Ion Beam Breeding of Flower Color Variations in Transgenic Plants with Multi-Disease Tolerance

M. Okamura [a)], A. Shimizu [a)], S. Watanabe [a)], Y. Hase [b)], I. Narumi [b)] and A. Tanaka [b)]

[a)]Plant Research Center, Kirin Agribio Co., LTD., [b)]Radiation-applied Biology Division, QuBS, JAEA

1. Introduction

Ion beams have different effect from that of electron beams on mutation generation of crops and have great impact on plant seed and seedling business. New carnation variety series with 10 flower color variations have been developed by ion beam breeding in the joint R&D between Kirin Agribio Co., LTD. and JAEA. They have been commercialized in Japan and Europe [1)].

We are trying to develop an advanced application system of ion beams to produce color variations or to add improvements in transgenic plants that have acquired useful characteristics such as tolerance to multi-diseases by recombinant DNA techniques.

2. Materials and Methods

Agrobacterium-mediated transgenic chrysanthemum plants (*Dendranthema grandiflora*) expressing double-stranded RNA-specific ribonuclease gene (pac1) derived from *Schizosaccharomyces pombe* were used as materials for ion beam breeding. Leaf segments were placed in petri dishes containing Murashige and Skoog medium supplemented with 0.05 mg/l NAA and 0.1 mg/l BA, 30 g/l sucrose and 7 g/l agar. The samples covered with Kapton film were irradiated with 220 MeV or 320 MeV carbon ion beams from the TIARA AVF cyclotron (JAEA, Takasaki). *In vitro* plants derived from ion beam irradiation have been acclimatized and cultivated in the greenhouse and their flower color and shape were investigated.

3. Results and Discussions

Transgenic chrysanthemum plants expressing pac1 gene showed tolerance against Chrysanthemum Stunt Viroid (CSVd) and Tomato Spotted Wilt Virus (TSWV) [2)]. The tolerance of pac1 transgenic chrysanthemum to CSVd is shown in Figure 1.

Thus fur 400 plants derived from 3 Gy to 10 Gy irradiation of 220 MeV or 320 MeV carbon ion beams have been cultivated in the greenhouse and flowered. Flower color mutants such as pale pink, dark pink, salmon etc. have been obtained (Figure 2).

The control of viroid disease has been very difficult because factors essential for viroid survival are indispensable to the host plants. Viruses belonging to the genus *Tospovirus* including TSWV are very serious pathogens not only in chrysanthemum but on other horticultural plants. Ion beam breeding is effective to produce color variations, once the transgenic plants with virus- and viroid-resintance have been acquired.

From these results we confirmed that the advanced application system of ion beams will contribute to the development of variety series of ornamentals with high quality at lower cost, as compared with the method to introduce useful characteristics into several varieties with different flower color by transformation one by one.

Figure 1. Symptoms by CSVd infection. (from left to right) Non-transgenic without infection, non- transgenic with CSVd infection, transgenic without infection, transgenic with CSVd infection

Figure 2. Flower color mutants obtained from ion beam breeding of transgenic chrysanthemum plants with multi-disease tolerance. (from left to right) parent, dark pink, salmon, light pink

References

1) Okamura M. et.al. Floriculture, Oranamental and Plant Biotechnology Vol.I, Global Science Books (2006) p.619

2) Ogawa T. et.al. Breeding Science 55 (2005) 49.

3-17 Mutation Induction on Oriental Hybrid Lily Irradiated with Ion Beams

S. Chinone [a)], A. Ishizawa [a)], K. Tokuhiro [a)], K. Nakatsubo [a)], M. Amano [a)], Y. Hase [b)], I. Narumi [b)] and A. Tanaka [b)]

[a)]Kaneko Seeds CO., LTD., [b)]Radiation-Applied Biology Division, QuBS, JAEA

To obtain mutants of Oriental hybrid Lily, we investigated the influences of ion beams irradiation to bulb scales *in vitro*. Survival rates of scales irradiated with 320 MeV carbon and 50 MeV helium ion decreased at 0.2 and 1.5Gy, respectively. The suitable dose was estimated to be around 0.2-0.4Gy in carbon ion and 1.5-2.0 Gy in helium ion. Leaf color mutations which chlorophyll were defected partly or wholly were observed.

ユリ属においてイオンビーム照射によって誘発された変異体としては、アジアティックハイブリッド系ユリで花色や花型の変化、花被片の斑点の減少が報告されている[1)]。本研究ではオリエンタルハイブリッド系ユリの花色，雄性不稔，八重化および草姿などにおいて特徴のある変異体獲得を目的としてイオンビーム照射を行った。

無菌的に培養しているカネコ種苗㈱育成のオリエンタルハイブリッド系ユリ‘LC96-005-11’の小球根のりん片を、小球根形成培地を分注した60 ㎜シャーレに向軸面を上にして置床し、約1週間後に照射を行った。イオンビーム照射は日本原子力研究開発機構イオンビーム照射研究施設（TIARA）のAVFサイクロトロンを用いて，炭素イオン（$^{12}C^{6+}$，320 MeV）を0.1，0.2，0.4，0.6および0.8 Gy，ヘリウムイオン（$^{4}He^{2+}$, 50 MeV）を0.5，1.0，1.5，2.0および2.5 Gyで照射した。照射後新しい小球根形成培地に移植し、1～2ヶ月後に生存率や小球根形成数などについて調査した。形成された小球根は直径が10 mm前後の大きさになるまで培養し、順次定植した。

照射したりん片の生存率や生育量は無照射のりん片に比べて低下し、その影響は$^{12}C^{6+}$照射の方が$^{4}He^{2+}$照射より大きかった（データ略）。

$^{12}C^{6+}$照射による生存率は0，0.1および0.2 Gyの線量までは90 %以上であったが、0.4 Gyでは80 %に低下し、0.8 Gyになると著しく低下した（Fig.1）。小球根形成数は0.2Gyまでは線量とともに増加したが、それ以上の線量になると減少した。シュートおよび根の生育は0.6 Gy以上では著しく抑制され、発根しない球根も認められるようになった。

$^{4}He^{2+}$照射による生存率は0～2.0 Gyの間では80～100 %であったが、2.5 Gyになると60 %に低下した（データ略）。小球根形成数は1.5Gyで最も多くなり、2.5 Gyでは著しく減少した。2.0 Gyより線量が強くなるとシュートや根の生育が遅く、形成がみられない個体も観察された。無照射のりん片では基部に直接小球根が形成されたが、照射りん片ではカルスが形成されるものが多く、そのカルスから小さな球根が多数形成された。

これらのことから$^{12}C^{6+}$での適正線量は0.2～0.4 Gyに、$^{4}He^{2+}$では1.5～2.0 Gy付近にあると推察された。

$^{12}C^{6+}$照射したりん片から形成された小球根を817個体、$^{4}He^{2+}$では641個体を定植したところ、クロロフィルが完全にまたは部分的に欠損している個体が観察された（Table.1，Fig.2）。今後は球根養成を行い花色，花型や雄性不稔等の特性について調査する予定である。

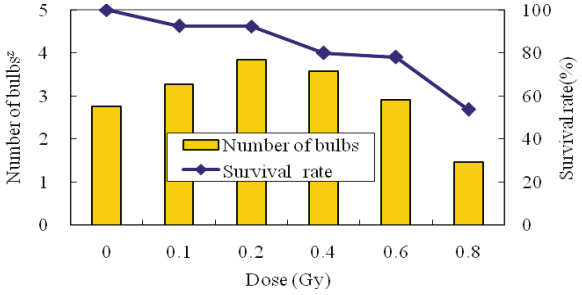

Fig.1. Influence of 320 MeV carbon ion beam irradiation to bulb scale on survival rate in Lily.

Table.1. The number of leaf color mutants induced by ion beam irradiation.

Dose(Gy)		No. of bulbs	No. of leaf mutants	Dose(Gy)		No. of bulbs	No. of leaf mutants
Control		28	0	Control		32	0
$^{12}C^{6+}$	0.1	200	0	$^{4}He^{2+}$	0.5	126	0
	0.2	245	4		1.0	146	0
	0.4	143	1		1.5	176	0
	0.6	142	0		2.0	119	1
	0.8	59	0		2.5	42	0

Fig.2. Leaf color mutants induced by ion beam irradiation

Reference

1) N. Chiba, et al., TIARA Annual Report 2005 (2006) 92.

3-18 Mutation Breeding on the Ornamental Plants of *Gypsophila* and *Gentiana* Species

S. Tsuji [a)], M. Miyamoto [a)], T. Okabe [a)], Y. Hase [b)], Y. Yokota [b)] and I. Narumi [b)]

[a)]Oita General Service Co., Ltd.,[b)]Radiation-Applied Biology Division, QuBS, JAEA

Gypsophila paniculata and *Gentiana trifida* var. *japonica* are the important ornamental crops for cut flower use in Japan. In an attempt to induce mutation for breeding use, shoots of such plants on LS medium were irradiated with carbon ion beams using the JAEA AVF cyclotron. Irradiation experiments were conducted two times, and survival rates of the regenerated plants were evaluated when they were transplanted to the pots. The doses suitable for mutation induction are estimated to be 2-4 Gy for *Gypsophila* and 0.5-1 Gy for *Gentiana*. Apparently, *Gentiana* is more susceptible to ion beam irradiation than *Gypsophila*.

花き類の宿根かすみそう・りんどうは切花用として栽培・出荷され、日本での作付面積は各々355および508ヘクタールであり、農林統計において花き品目中5および4位に位置する重要な作物である。これらの花き作物について、イオンビーム照射による新たな有用変異の誘発の可能性についての知見を得ることを目的とする。

有用変異誘発のための適正線量を検討するため、宿根かすみそう（品種「ブリストルフェアリー」）・りんどう（在来系統）のLS培地上の茎頂培養植物に、2006年4月12日および6月12日の2回にわたり、日本原子力研究開発機構イオンビーム照射研究施設（TIARA）のAVFサイクロトロンを用いて、炭素イオンビーム（$^{12}C^{6+}$, 320 MeV）の照射を行なった。照射後、培養を継続し、発根培地への植え継ぎ、ハウスへの順化、およびポットへの鉢上げを実施した。順化の際に、茎葉の奇形・生育不良などの異常率および生存率を調べた。また、ポットへの鉢上げ時にも生存率を測定し、照射線量との関係について調査した。

宿根かすみそうにおける第1回の照射（線量0.5～128 Gy）では、順化時の観察で8 Gy以上から徐々に奇形・生育不良などの異常率が増加した。32 Gy以上の照射でポットへの鉢上げまでに生存する個体はなかった。第2回照射（線量0.5～28 Gy）でも同様な結果が得られた(Fig. 1)。これらの照射試験で、順化および鉢上げ時において、8 Gyまでは高い生存率を維持していたが、16 Gyで急激に低下していた。したがって、有用変異の誘発のためには、2～4 Gy照射が適正であると考えられた。このことは、すでに報告されている線量とも対応する[1)]。

りんどうへの第1回の照射（線量0.5～128 Gy）で、培養期間中において、4 Gy以上の線量で低下していき、それにともない、形態および葉緑体の異常率が明らかに高くなる傾向が認められた。8 Gy以上になると順化時までに枯死した。第2回照射（線量0.25～8 Gy）でも同様な結果が得られた(Fig. 1)。有用変異誘発には0.5～1 Gy照射が適正であると結論した。

今回の研究で、りんどうは、宿根かすみそうと比較して、イオンビーム照射に対して感受性がより高いことが明らかとなった。

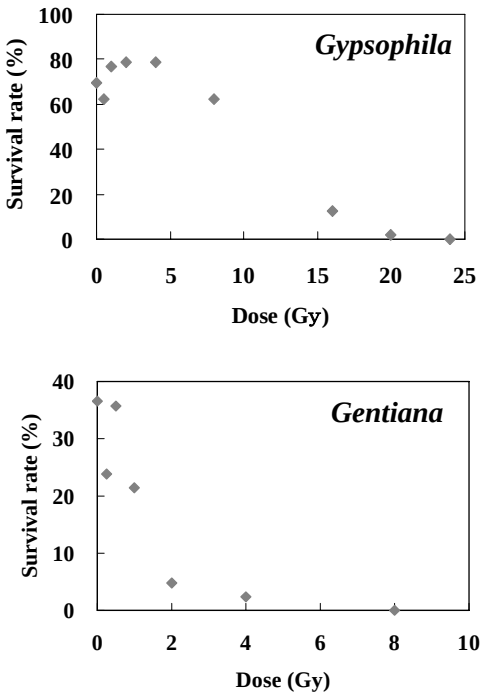

Fig.1 Survival rates of the plants regenerated from carbon ion irradiated shoots of *Gypsophila* and *Gentiana* plants, measured when they were transplanted to pots.

Reference

1) M. Okamura et al. 2006 Ann. Rep. Res. Project with Heavy Ions at NIRS-HIMAC (2007) 75.

3-19 Breeding New Varieties of Miniature *Cymbidium* Using Ion Beam Irradiation

S. Yuki [a)], S. Araki [a)], T. Suzuki [a)], T. Ohsuga [a)], K. Katayama [a)], Y. Hase [b)] and Y. Yokota [b)]

[a)]Central Research Institute, Ishihara Sangyo Kaisha, Ltd.,
[b)]Radiation-applied Biology Division, QuBS, JAEA

The protocorm like bodies (PLBs) of two novel varieties of miniature hybrid *Cymbidium*, which were bred by crossing *Cymbidium hybrida* with *Cymbidium goeringi*, were irradiated with 320 MeV $^{12}C^{6+}$ ions at various doses ranging from 0 to 128 Gy. Irradiated PLBs were cultured at 25 °C with a 16 hr photoperiod. After 12 months of culture, the efficiency of regeneration from the PLBs was evaluated. In both varieties, it was drastically decreased at 16 Gy or more. Based on this result, we irradiated PLBs of three varieties of miniature hybrid *Cymbidium* at doses of 0-12 Gy in a mutation breeding experiment.

はじめに

シンビジウムは、ファレノプシスやデンドロビウムと共に、我国で最も重要なラン科園芸植物の一つとなっている。しかし、近年、業務用花卉需要の減少を受け、大型鉢物中心のシンビジウム市場は減少傾向にある。この市場の改善を目指し、石原産業㈱では、シンビジウムとシュンランの交配により育種された数種の小形シンビジウムを導入し、生産・販売することを検討している。この小形シンビジウムは、その大きさのため、交配による育種には制約がある。そこで、さらなる品種拡充のため、花弁育種で実績が高く、また、シンビジウムでの変異体作出の報告[1)]のある、「イオンビーム育種」の本花弁への適用の検討を始めた。

材料および方法

感受性検定試験１

2種の小形シンビジウム（S-26-9及びS-27-1）より調製したPLB（直径2～3 mm）をメスで2分割し、寒天培地上へ置床した。約1週間、25 ℃、16 hr照明下で培養後、炭素イオン（$^{12}C^{6+}$、320 MeV）を照射した。照射線量は、0、0.5、1、2、4、8、16、32、64及び128 Gyとし、一群50個の切片に照射した。照射サンプルは、新しい培地へ移植し、12ヶ月間培養した。その間に、出芽・発根したPLBを再分化したPLBとしてカウントし、0 Gy照射群の再分化PLB数で除した値を各群の再分化率とした。

感受性検定試験２

4種の小形シンビジウム（S-26-1、S-26-9、S-27-1及びS-27-6）のPLBから厚さ1 mm程度の切片を調製し、寒天培地上へ置床した。1～5日間培養後、試験1と同様に炭素イオンを照射し、培養した。

変異誘発試験

3種の小形シンビジウム（S-27-1、S-27-6及びS-39-2）のPLBから厚さ1 mm程度の切片を調製し、寒天培地上で3～4日間培養後、炭素イオンを照射した。照射線量は、0、0.25、0.5、1、2、4、6、8、10及び12 Gyとし、一群100個の切片に照射した。

結果及び考察

感受性検定試験１

2種の小形シンビジウム共に、1 Gy以上の照射で、明確な線量依存的な生育抑制が観察された（データなし）。また、再分化率に関しては、8 Gyまでは僅かな低下のみだったが、16 Gy以上で大きく低下した（Fig.1）。ただし、128 Gyでも、約10%のPLBが再分化しており、本試験においては、照射サンプルの厚さにバラツキがあり、イオンビームが完全に透過していないサンプルが生じたことが想定された。

感受性検定試験２

試験１において、サンプルの厚さに懸念が生じたため、試験２においては、サンプル調製時に、2分割ではなく、削ぎ切りで厚さを1 mm程度に調整した。また、照射前の培養期間も短縮し、品種も2種追加した。これらの照射サンプルは、現在経過観察中であるが、これまでのところ、試験１とほぼ同様な経過を示している。ただし、やや感受性高くなっていると思われる。

変異誘発試験

感受性検定試験の結果から、変異誘発のための照射線量は16 Gy未満が適当と推定された。そこで、3種の小形シンビジウムのPLBに対して、12 Gy以下の10段階の線量で照射を実施した。今後、これらの照射サンプルから再分化した個体を開花期まで栽培し、優良品種の選抜を試みる予定である。

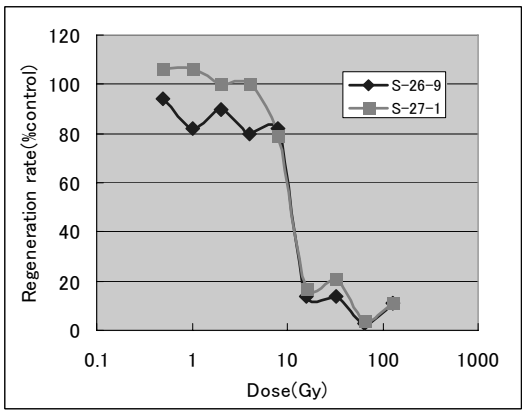

Fig.1 Effect of ion beams on regeneration rate of PLBs

Reference

1) K. Furukawa, et al., イオンビーム育種研究会第2回大会要旨集.(2005)

3-20 Study of Molecular Mechanism of Carbon Ion Beam Induced Mutations in the *Saccharomyces cerevisiae*

Y. Matuo [a)], S. Nishijima [a)], Y. Hase [b)], A. Sakamoto [b)], Y. Yokota [b)], I. Narumi [b)] and K. Shimizu [c)]

[a)]Graduate School of Engineering, Osaka University,
[b)]Radiation-applied Biology Division, QuBS, JAEA,
[c)]Radioisotope Research Center, Osaka University

The carbon ion beams were widely used as the mutagen for breeding technology and also used for cancer therapy. However, precise effect of ion beams to DNA molecules has not been elucidated.

The molecular mechanism of the mutagenesis caused by carbon ion beams was studied. The mutation sites caused by ion beams were determined and the mutation spectrums were compared with those induced by gamma ray.

S. cerevisiae strains used in this study were S288C (RAD^+), *rad50* and *rad52*. RAD50p is a component of the nonhomologous end joining repair pathway. RAD52p is a component of the homologous recombination repair pathway.

The yeast cells were irradiated with carbon ions ($^{12}C^{5+}$; 220 MeV) with the dose 10 to 300 Gy, and LET was 107 keV/μm. Carbon ion beams were generated from AVF cyclotron in JAEA. The survival rates following irradiation were determined on the basis of colony-forming ability. And, selection of *ura3* cells was accomplished by plating the cells on the media containing 5-fluoroorotic acid[1)]. The mutation sites of *ura3* mutants were determined by DNA sequencing.

Figure1 shows the survival rates of several strains exposed to $^{12}C^{5+}$ ion. *rad50* and *rad52* cells showed high sensitivity to ion-beam (Fig.1).

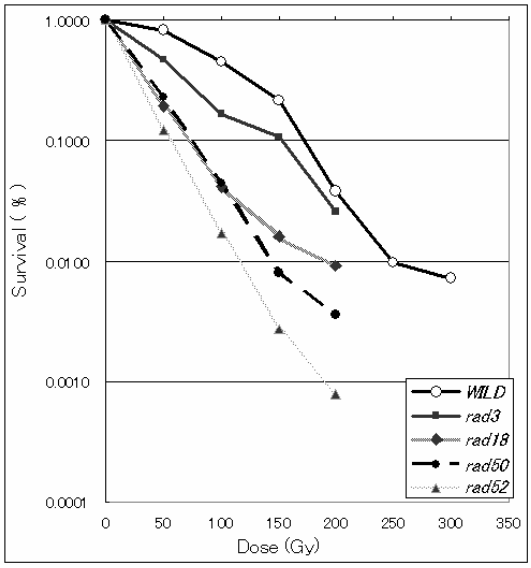

Fig. 1. Survival curves for yeast strain S288c after irradiation with carbon ion beams.

The *URA3* regions (804 bp) were sequenced. Fig.2 shows the mutational spectrums of irradiation ion beam and gamma ray. The remarkable feature of mutations in *wild* type cells induced by carbon ions was that the mutations sites were localized near the linker regions of nucleosomes[2)]. On the contrary, the mutations were induced in the DNA region which combined with the histone-protein in *rad50* or *rad52* strain (Fig.2). This difference may result from the repair pathway which operates in mutant strains.

Moreover, the GC → TA transversion was largely observed. It suggests that the mutations by ion beams resulted from oxidative damage such as formation of 8-oxodGTP mainly[2-3)]. To elucidate the ion beam effect on the budding yeast, we are going to analysis *ogg1* and *msh2* mutant strains which are deficient in oxidized purine base lesion DNA N-glycosylase activity and mismatch repair activity, respectively.

References

1) D. Burke, et al., Cold Spring Harbor Laboratory Press (2000) pp7-15
2) Y. Matuo et al., Mutat. Res. 602 (2006) pp7-13.
3) P. M. Girard et al., Carcinogenesis. 19 (1998) pp1299-1305

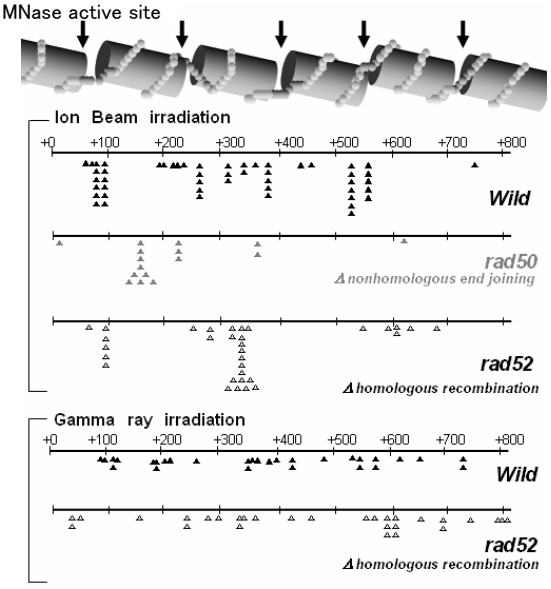

Fig. 2. Mutational spectrum of irradiation ion beam (above) and gamma ray (below).

3-21 Mutation Induction in Azalea Using Ion Beam Irradiation and Its Gene Analysis

N. Kobayashi [a], S. Sakamoto [a], A. Nakatsuka [a], Y. Hase [b] and I. Narumi [b]

[a]Faculty of Life and Environmental Science, Shimane University
[b]Radiation-Applied Biology Division, QuBS, JAEA

1. Introduction

In this study, ion beams were irradiated to azalea seeds and cultured leaf segments to induce flower color and shape mutation. Additionally, we try to research the key genes of ion beam induced mutations as a final purpose; anthocyanin biosynthesis genes related to flower color mutation and homeotic genes related to flower shape and organ mutation that we already isolated [1),2)].

2. Materials and Methods

2-1. Seeds of *Rhododendron kaempferi*, *R. ripense, R. japonicum* and *R. matternichii* var. *brevitolium* were irradiated with carbon ion beam (220 MeV $^{12}C^{5+}$) at 0 to 50 Gy (Fig. 1). After the irradiation, seeds were sowed on sphagnum moss bed in pot. The germination rate was evaluated after 6 weeks.

2-2. Young leaves of potted *R.*×*pulchrum* 'Sen-e-oomurasaki' were excised, sterilized and used as explants materials as previous study[3)]. The leaf segments were cultured on modified 1/2 Murashige and Skoog's medium supplemented with 2 μM NAA and 9 μM TDZ in the test tube[4)]. The explants were transplanted on the high concentration agar medium in the tissue culture dishes and covered with Kapton film. The transported samples were irradiated with carbon ion beam (220 MeV $^{12}C^{5+}$) at various doses (0 to 128 Gy, Fig. 2). The leaf segments were transplanted on the initial medium and cultured at 22±1 °C with 16 hours-photoperiod after the irradiation. The regeneration rates of callus, shoot primordia and shoot were investigated after 2 months.

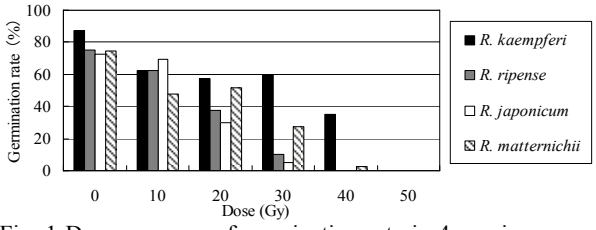

Fig. 1 Dose response of germination rate in 4 species at 6 weeks after sowing.

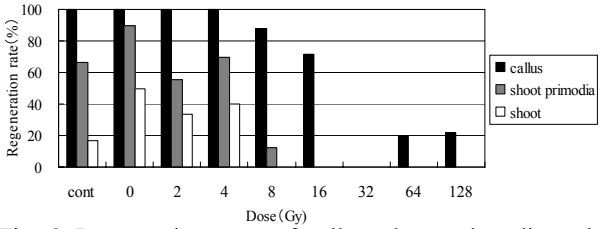

Fig. 2 Regeneration rates of callus, shoot primordia and shoot from *R.*×*pulchrum* 'Sen-e-oomurasaki' leaf segments at 2 months after irradiation.

3. Results and Discussion

3-1. In preliminary experiment, seeds of 5 species were irradiated with carbon ion beam at ranges from 0 to 100 Gy[5)]. These seeds were difficult to germinate with ranges more than 60 Gy irradiation. Therefore, the second irradiation was applied narrow doses (0 to 50 Gy) in the same condition (Fig. 1). The germination rates were strongly downed at the ranges from 30 to 50 Gy and different depending species. The optimal irradiation doses for seeds considering from median germination decrease may be 30 to 40 Gy for *R. kaempferi*, 20 Gy for *R. ripense*, 10 to 20 Gy for *R. japonicum* and 20 to 30 Gy for *R. matternichii* var.*brevitolium*.

3-2. The regeneration rate of callus decreased according to the ion beam strength from 8 Gy irradiated leaves (Fig. 2). While, shoot primordia and shoot were not able to regenerate with more than 8 to 16 Gy irradiation (Fig. 2, 3). The effective conditions to obtain irradiated mutants were thought to be from 4 to 8 Gy exclusive for *R.*×*pulchrum* 'Sen-e-oomurasaki' leaves. Mutation research will determine plants regenerated from these shoot primordia and shoot of ion beam irradiation.

4. References

1) D. Mizuta et al. 2007. Abst. Chugoku-Shikoku Br., Japan. Soc. Hort. Sci. 46 (2007) 44 (In Japanese).
2) M. Ohtani et al. Hort. Res. (Japan) 6 Suppl.1 (2007) 458 (In Japanese).
3) N. Kobayashi et al. JAEA-Review 2006-042 (2007) 96.
4) S. Sakamoto et al. J. Japan. Soc. Hort. Sci. 74 Suppl.2 (2005) 310 (In Japanese).
5) S. Sakamoto et al. Abst. Chugoku-Shikoku Br., Japan. Soc. Hort. Sci. 46 (2007) 39 (In Japanese).

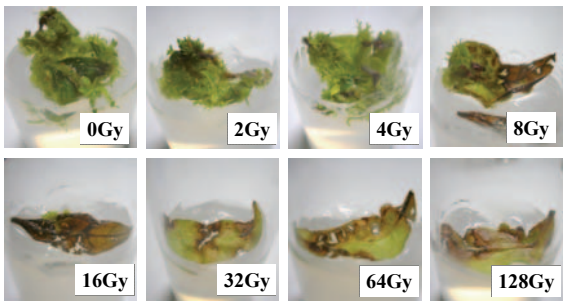

Fig. 3 Dose response of regeneration from *R.*×*pulchrum* 'Sen-e-oomurasaki' leaf segments at 2 months after irradiation.

3-22 Effects of Ion Beam Irradiation on Plant Growth and Morphology in Soybean

A. Kanazawa [a)], J. Abe [a)], Y. Hase [b)] and A. Tanaka [b)]

[a)]Research Faculty of Agriculture, Hokkaido University,[b)]Radiation-Applied Biology Division, QuBS, JAEA

Soybean (*Glycine max*) is an important crop in terms of production of food, oil, and forage. However, existing mutant lines of soybean ave very limited, which is a constraint on performing genetic study and breeding of this plant. One of the reasons for the small number of mutant lines in soybean appears to be associated with difficulty in production of a mutant and to duplication of genomic segments. This plant is considered to have derived from ancestral plant(s) that have a tetraploid genome, and as a consequence, more than 90 % of nucleotide sequence in the soybean genome is duplicated[1), 2)]. It is conceivable that such a duplicated nature of the genome brought about a low frequency of mutant production by conventional methods for mutagenesis such as γ-ray or X-ray irradiation as well as chemical treatments. In these circumstances, we have started to examine whether ion beam irradiation is effective in producing a mutant in soybean because ion beam irradiation is expected to cause genomic changes that are more drastic than those induced by conventional mutagenesis.

Dried seeds of soybean were exposed to the 320 MeV carbon ions with a range of 0.2-25 Gy. In order to irradiate at an equal dose on seeds, seeds were fixed on a plastic dish in which meristem tissues were positioned on the top (Fig. 1). The irradiated seeds were sown on soil and plants were grown for three weeks in a green house. A prominent decrease in plant height was observed depending on the dose in the range of 5-25 Gy (Fig. 2), but not in the range lower than 5 Gy (0.2, 0.5, 1.0, and 2.0 Gy; data not shown), indicating that doses higher than approximately 5 Gy affect plant growth rate.

In addition to the inhibition of plant growth, morphological changes were also induced by irradiation. One of the prominent changes in morphology was detected in the primary leaves in which a narrow portion was generated in the central part of a leaf. This type of change was detected in 15 plants per 66 plants irradiated at 5 Gy, and in 4 plants per 56 plants irradiated at 2 Gy. The other prominent morphological change was unscheduled generation of stem(s) from the node where cotyledons were formed (Fig. 3). This type of change was detected in 8 plants per 66 plants irradiated at 5 Gy, and in 2 plants per 56 plants irradiated at 2 Gy. Both types of change were not detected in plants irradiated at the doses lower than 1 Gy.

Based on the observed effects of irradiation at various doses on plants, we concluded that irradiation at 2-5 Gy is most appropriate for producing mutant population in our material. We subsequently performed a large-scale irradiation to soybean seeds at the doses of 5 Gy and 2.5 Gy to 3,200 seeds and 3,320 seeds, respectively, and grew them in the field of Hokkaido University. We are currently analyzing the effects of irradiation using field-grown plants.

References

1) R. C. Shoemaker et al., Genetics 144 (1996) 329.
2) H. Zhu et al., Plant Physiol. 137 (2005) 1189.

Fig. 1 Soybean seeds placed on a dish for irradiation.

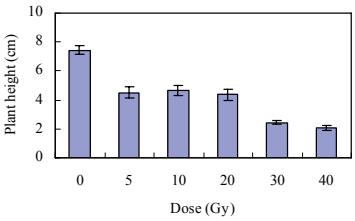

Fig. 2 Growth of plants after irradiation at the doses of 5-40 Gy. Average ± SE are shown.

Fig. 3 An altered phenotype of plants as a consequence of irradiation. Left, control plant; right, plant exhibiting altered morphology.

3-23 Mutation Induction by Carbon Ion Beam Irradiation in Banana (*Musa* spp.)

W. O. Reyes-Borja [a)], I. Sotomayor [b)], I. Garzón, D. Vera [b)],M. Cedeño [b)], A. Tanaka [c)], Y. Hase [c)], Y. Sekozawa [a)], S. Sugaya [a)] and H. Gemma [a)]

[a)]Life and Environmental Sciences, University of Tsukuba,
[b)]Estación Experimental Tropical Pichilingue, Ecuador,
[c)]Radiation-Applied Biology Division, QuBS, JAEA

In Banana (*Musa acuminata* AAA), most research focuses on generating cultivars tolerant/resistant to black Sigatoka disease caused by *Mycosphaerella fijiensis* Morelet which is the most dangerous disease distributed worldwide. Ion beams radiation breeding permitted us to select some candidates plants at the nursery condition showing some tolerance against to this disease; however, others interesting characteristics were also observed.

The irradiation was conducted at the Takasaki Ion Accelerators for Advanced Radiation Application (TIARA), Japan Atomic Energy Agency (JAEA). Carbon ion beams irradiation was applied on *in vitro* explants of banana cultivars 'Cavendish Enano' and 'Williams' with the dose of 0, 0.5, 1, 2, 4, 8, 16, 32, 64 and 128 Gy. Recorded data were: survival rate (%), relative DNA content (by flow cytometry), leaf disc necrotic area (LDNA-%) under the juglone toxin inoculation, disease development period (DDP-days) and infection index (II-%) by using the fungus of *Mycosphaerella fijiensis* Morelet for inoculation.

Regarding to the survival rate (%) in general terms, the higher irradiation dose resulted in higher mortality rate, but doses of 8 Gy and lower did not seem to have any effect on survival rates. The flow cytometer analysis detected hexaploid cells among the samples (Fig. 1A). 'Cavendish Enano', and 'Williams' reported 5 and 1 hexaploid plants, respectively at 4 Gy. This could be a way of causing chromosome duplication, efficiently and fast, especially on improved diploids possessing resistance that could be used as parental lines for banana breeding. A fast growing plantlet (Fig. 1B) was also observed among the irradiated cultivar which is a very important characteristic as it may result in earliness of fruit harvesting.

For selecting tolerant/resistant plants to black Sigatoka, the variables DDP-days, II-% and LDNA-% were combined by linear regression to categorise the response to black Sigatoka in the irradiated materials. LDNA-% regression versus II-% showed high significance ($p \leqq 0.01$) compared with LDNA-% versus DDP-days, and DDP-days versus II-% that were significant at the 5% level ($p \leqq 0.05$) in 'Williams' (Fig. 2). Six plants in 'Williams' and two plants in 'Cavendish Enano' were selected as candidates with increased tolerance to black Sigatoka disease. Regarding the complete assessment of the candidate plants, field experiments based on the whole plant cycle are necessary to evaluate not only the response to black Sigatoka disease but also fruit quality, potential production and post-harvest parameters as valuable components for final selections.

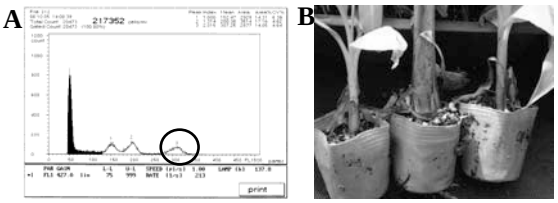

Fig 1. A. Hexaploid cells (encircled) in 'C. Enano' produced by ion beam dose 4 Gy. B. 'C. Enano' at 4 Gy showing a fast growth (in the center).

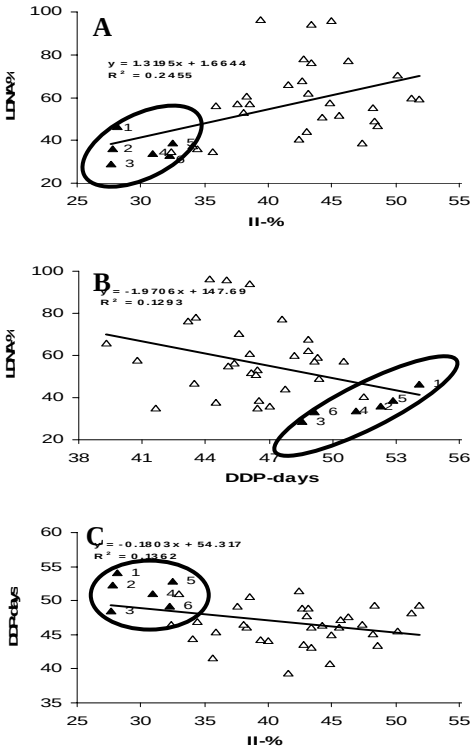

Fig. 2. LDNA-% regression versus II-% (A), LDNA-% regression versus DDP-days (B) and DDP-days regression versus II-% (C) in 'Williams'. Encircled bold and numbering triangles belong to the selected candidate plants that clearly show relationships.

3-24 Effect of $^{12}C^{6+}$ Beam Irradiation on Callus Formation and Shoot Regeneration from Isolated Cultured Cells in *Lavandula* x *intermedia* Emeric.

M. Tsuro [a], S. Daimyo [a], T. Takeda [a], Y. Yokota [b] and Y. Hase [b]

[a]Faculty of Agriculture, Meijo University
[b]Radiation-Applied Biology Division, QuBS, JAEA

In order to develop a new lavandin, *Lavandula* x *intermedia* Emeric., plant with different fragrance from original plant, effect of several doses of $^{12}C^{6+}$ beam on callus formation and shoot regeneration from isolated cultured cells was analysed. Growth index (GI) of callus proliferation was decreased with increase of irradiation dose. RD_{50} in GI of callus proliferation was estimated between 64.0 to 128.0 Gy. On the other hand, RD_{50} in shoot formation rate was determined among 2.0 to 4.0 Gy, lower than that in GI of callus proliferation. These results suggested that RD_{50} in GI of callus proliferation and shoot formation rate were different. However, any regenerated plants were not obtained from shoots. Further analysis is now conducted to obtain regenerated plants from shoots.

ラベンダーのエッセンシャルオイルは多くの化合物で構成されており、その成分比の違いにより香調が大きく変化することから新しい香りの創出が期待されている。

本研究では、$^{12}C^{6+}$ビームの照射により、エッセンシャルオイル成分比が親植物体と大きく異なり香調が変化した変異体の作出を目的として、$^{12}C^{6+}$ビームの線量がラベンダー培養細胞の増殖および不定芽の形成に及ぼす影響を調査した。

植物材料としてラバンジン（真正ラベンダーとスパイクラベンダーとの雑種）品種‘スーパーセビリアンブルー’を用いた。0.2 mg/*l* 2,4-Dと0.2 mg/*l*カイネチンを添加したMS固形培地で誘導した葉由来カルスを同組成の液体培地で振盪培養し、得られた懸濁培養細胞を細胞密度が2×10^5個/mlとなるように調整した。カルス培養と同組成の固形培地を入れた直径6 cmのプラスチックシャーレに細胞懸濁液を0.5 ml分注し、320 MeV $^{12}C^{6+}$ビームを0, 0.5, 1.0, 2.0, 4.0, 8.0, 16.0, 32.0, 64.0および128.0 Gyの線量で照射した。照射後、25℃、暗条件で培養を行い、4週間後に増殖したカルスの大きさを0から5の6段階で評価した。評価後、カルスを1mg/*l* BAを添加したMS固形培地に移植して25℃、明条件で培養し不定芽の誘導を試みた。実験は4回反復で行った。

培養１ヶ月間後のカルスの増殖程度を評価したところ、0 Gy区ではカルス形成が見られない培地は認められなかったものの、増殖指数(GI)は1から5までとばらつきが見られ平均指数は2.7であった。0.5 Gy区および1.0 Gy区も0 Gy区とほぼ同様の指数を示していたが、2.0 Gy以上では全くカルスの形成が認められないシャーレも見られ、線量の増加に伴って平均指数が低下した。さらに、128.0 Gy区では細胞のカルスの形成が全く認められず、ラバンジン培養細胞では64.0 Gy～128.0 Gyの間に致死線量があることが推察された。カルス増殖指数を指標した増殖反応曲線をもとに0 Gyの半分程度の増殖指数を示す線量（半増殖線量（RD_{50}））を探索したところ、16.0 Gyから32.0 GyにRD_{50}があることが示唆された（Fig.1）。

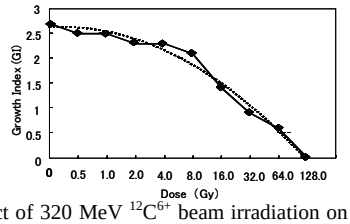

Fig.1 Effect of 320 MeV $^{12}C^{6+}$ beam irradiation on proliferation of cultured isolated cells in lavandin. (■); Average number of GI on a given dose, (…) ; Fitted curve for line graph.

一方、増殖したカルスをシュート誘導培地に移植した後、約1ヶ月培養をしたとき、カルスからシュートの形成が認められた。Table 1にシュート誘導培地で1ヶ月間培養したときのカルスの生存率およびシュート形成率を示した。0 Gy区では、12.5%のカルスがシュートを形成しており、2.0 Gyまで同程度のシュート形成率で、1.0 Gy区において、24.1%と最も高いシュート形成率が認められた。2.0 Gyを超える線量では、カルス増殖と同様に線量の増加に伴ってシュート形成率が低下し、32.0 Gyおよび64.0 Gyのカルスからは全くシュートが形成されなかった。このことから、0～2.0 Gy区での平均シュート形成率を基準としたときの半シュート形成線量（RD_{50}）は、2.0 Gy～4.0 Gyの間にあることが推察された。しかしながら、全ての線量区で誘導されたシュートの多くが、伸長途中に枯死したため、効率的な変異体獲得には今後より詳細な培養条件の検討が必要であると思われる。

Table 1. Influence of 320 Mev $^{12}C^{6+}$ beam irradiation on shoot formation from isolated cells-derived callus in lavandin

Dose (Gy)	No. of cultured callus	No. of survived callus (%)	No. of shoot formed callus (%)
0	56	28 (50.0)	7 (12.5)
0.5	59	36 (61.0)	6 (10.2)
1.0	58	39 (67.0)	14 (24.1)
2.0	59	35 (59.0)	8 (13.6)
4.0	51	27 (53.0)	4 (7.8)
8.0	51	29 (57.0)	4 (7.8)
16.0	47	28 (60.0)	2 (4.3)
32.0	21	1 (5.0)	0 (0)
64.0	3	0 (0)	−

3-25 Screening of Higher Astaxanthin Producing Mutants of a Green Unicellular Alga *Haematococcus pluvialis* by Ion Beam Irradiation

T. Kakizono [a)], T. Sugiura [a)], R. Yoshihara [b)], Y. Hase [b)], I. Narumi [b)] and A. Tanaka [b)]

[a)]Department of Molecular Biotechnology, AdSM, Hiroshima Univ, [b)]Radiation-Applied Biology Division, QuBS, JAEA

A highly anti-oxidative ketocarotenoid, astaxathin has been produced by culturing a unique green unicellular alga *H. pluvialis* in large-scale photobioreactors at rich solar energy areas such as Hawaii islands. Since it seems disadvantageous to carry out the algal culture phototrophically in a commercial basis in Japan, we have applied heterotrophic cultivation for the alga. In the dark condition, the alga was found to have a very limited carbon source specificity, namely acetate, and produce astaxanthin about one-third of the phototrophic condition (20 mg-astaxanthin/*l*) as the cellular content basis (2% w/w). In this study, we have examined the possibility of ion beam irradiation technology for the alga to obtain higher astaxanthin producing mutants, and also high tolerant mutants to acetate. Firstly, the dose effect of ion beam was studied for two culture conditions. In addition, several algal cell preparation techniques including filtration on paper, glass wool, or nitrocellulose, and spreading directly on agar were tested for the better cell recovery.

高度に抗酸化力を有するアスタキサンチン(以下ASX)は、ほとんどの種類の甲殻類，サーモンの肉色，タイの体表皮など海洋生物に広く分布するケトカロテノイドである。近年、体内で必然的に発生する活性酸素が種々の疾病，老化，発ガン作用に関与するとの報告があるので、食品やサプリメントとして抗酸化作用が注目され、特にASXについては、疲れ目予防，ローション，健康飲料など様々な用途に利用されるようになった。

微細緑藻 *H. pluvialis*は分裂増殖する栄養細胞(Fig.1左)においてカロテノイド色素は少量であるが、栄養条件の悪化とともにシスト細胞と呼ばれる胞子嚢細胞(同,右図)へ形態変化し、ASXを細胞重量比で2-3%の著量に生成する[1)]。

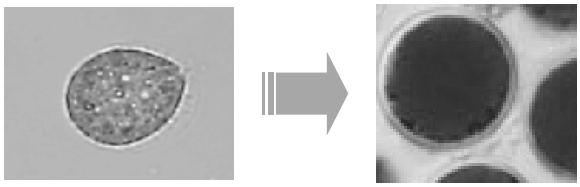

Fig.1 Morphological change from vegetative cells (left) to cyst cells (right) of *H. pluvialis,* and massive astaxanthin formation in cyst cell.

太陽光を用いた大規模培養が、年間を通して良好な晴天が得られる地域（米国ハワイ諸島，中国昆明等）で行われているが、閉鎖系・開放系を問わず、雑菌汚染，温度・日照時間変動など農業に類似する問題があり、安定な生産系ではない。

そこで、われわれは本緑藻が、太陽光に依らずに暗所で酢酸を炭素源に従属栄養的に増殖し、ASX生成を行いうることに着目し、その大規模生産の可能性を検討すべく、形態変化を伴わせたASX生産条件、および基質種と濃度効果を調べた。その結果、ASX含量は光培養系に匹敵するものの、細胞濃度が上がらず、また基質には酢酸とピルビン酸しか使えないことが明らかとなった。さらに、基質である酢酸は50mMを越えると増殖阻害が起きるので、細胞の高濃度化の障害となる。そこで、イオンビーム変異導入法により、緑藻ゲノム(近縁種の*Chlamydomonas* では110Mb)に染色体レベルの分断と再編成をもたらすことによって、従属栄養条件で旺盛に増殖し、ASXを高含量に生成する変異株または、酢酸耐性変異株等を広範囲にスクリーニング・単離することを目的に、イオンビームの線量について、様々な培養条件で調製した栄養細胞，シスト細胞を、ろ紙，あるいはグラスウールフィルタを用いてろ過下細胞、または寒天培地に直接細胞を高濃度に塗布したものを照射試料として、変異致死率(Fig.2)、変異細胞調製と細胞回収の効果を検討してきている。

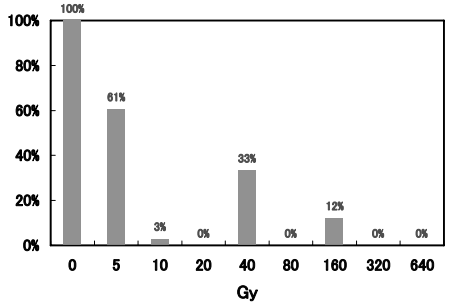

Fig.2 Effect of ion beam irradiation on the green algal colony formation.

References

1) 杉浦俊浩ら “単細胞緑藻*Haematococcus pluvialis*の従属栄養培養におけるアスタキサンチン生成の検討”, 第59回日本生物工学会大会要旨集 ID10-3, p60 (2006).

2) Kobayashi, M *et al.* “Enhanced carotenoid biosynthesis by oxidative stress in acetate–induced cyst cell of a green unicellular alga, *Haematococcus pluvialis.,*”., Appl. Environ. Microbiol. **59**, 867–873 (1993).

3-26 Role of LexA2 in Radiation Response Mechanism of *Deinococcus radiodurans*

K. Satoh [a)], H. Ohba [a)], H. Sghaier [a), b)] and I. Narumi [a)]

[a)]Radiation-Applied Biology Division, QuBS, JAEA, [b)]Department of Biological and Chemical Engineering, Faculty of Engineering, Gunma University

Introduction

RecA and LexA proteins in *Escherichia coli* play important roles in the inducible DNA damage response and repair mechanism (the SOS system). Following DNA damage, RecA is activated by binding to single-stranded DNA which is generated by DNA damage. The interaction of activated RecA and LexA results in the proteolytic cleavage of LexA. RecA-mediated cleavage of LexA inactivates LexA as a repressor. Consequently, various DNA repair genes controlled under LexA are derepressed, thereby the intracellular levels of various DNA repair proteins including RecA are transiently increased.

Although the radioresistance bacterium *Deinococcus radiodurans* possesses LexA1 protein which resembles *E. coli* LexA protein, LexA1 is not involved in induction of DNA repair proteins following DNA damage[1)]. Bioinformatic analysis of the *D. radiodurans* genome sequence showed that the genome encodes a second, diverged copy of LexA1, named LexA2. In an effort to gain an insight into the role of LexA2 in the radiation response mechanism, *recA*, *lexA1* and *lexA2* disruptant strains were generated, and the sensitivity to γ-rays, the expression of radiation inducible DNA repair gene and the changes in intracellular level of protein following irradiation were investigated.

Experimental procedures

Gene disruptants were generated using directed insertional mutagenesis technique that was developed by our group[2, 3)]. *D. radiodurans* cells were resuspended in 10 mM sodium phosphate buffer. The cell suspension was irradiated with ^{60}Co γ-rays at dose rates from 0.1 to 5 kGy/h at Food Irradiation Facility, JAEA. The gene expression and the changes in intracellular level of protein were analyzed by dual luciferase assay[4)] and western blotting method[5)], respectively.

Results and discussion

Like LexA1, LexA2 was cleaved by activated RecA to produce two breakdown products. The intracellular level of LexA2 in the *recA* disruptant strain did not change following γ irradiation, indicating that RecA is the sole protein required for LexA2 cleavage.

RecA induction following γ irradiation was also observed in the *lexA2* disruptant and *lexA1 lexA2* double-disruptant strains, clearly indicating that neither LexA1 nor LexA2 is involved in RecA induction. Interestingly, as shown in Fig. 1, the *lexA2* disruptant and *lexA1 lexA2* double-disruptant strains exhibited a much higher resistance to γ-rays than the wild type and *lexA1* disruptant strains. Since the decrease in the intracellular LexA1 level reflects the co-protease activity of activated RecA, the recovery to a basal level of LexA1 indicates the inactivation of RecA. The inactivation of RecA was faster in the *lexA2* disruptant strain than in the wild type strain. Given that the inactivation of RecA is associated with the completion of DNA repair, the DNA repair capacity might be enhanced in the *lexA2* disruptant strain relative to the wild type strain.

Furthermore, *pprA* promoter activation was enhanced in the *lexA2* disruptant strain following γ irradiation. The *pprA* gene encoding the novel radiation-inducible protein PprA plays a critical role in the radioresistance of *D. radiodurans*[6)]. The increase in radioresistance of the *lexA2* disruptant strain is explained in part by the enhancement of PprA functions[7)].

References

1) I. Narumi et al., J. Bacteriol. 183 (2001) 6951.
2) T. Funayama et al., Mutat. Res. 435 (1999) 151.
3) H. Nishida et al., Microbiology 148 (2002) 2911.
4) H. Ohba et al., Gene 363 (2005) 133.
5) K. Satoh et al., J. Biochem. 131 (2002) 121.
6) I. Narumi et al., Mol. Microbiol. 54 (2004) 278.
7) K. Satoh et al., Microbiology 152 (2006) 3217.

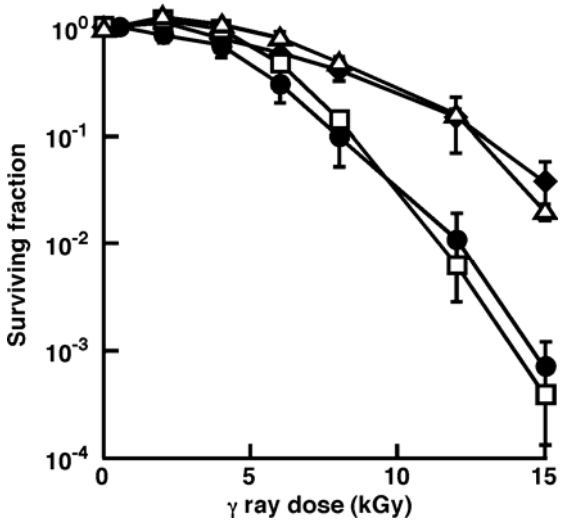

Fig. 1 Survival curves for γ rays. Symbols: closed circles, wild type; open squares, *lexA1* disruptant strain; open triangles, *lexA2* disruptant strain; closed lozenges, *lexA1 lexA2* double-disruptant strain.

3-27 Analysis of Mutagenic Effect Induced by Ion Beams for Breeding of *Aspergillus oryzae*

Y. Toyoshima [a)], T. Akagawa [a)], T. Yamazaki [a)], K. Satoh [b)], Y. Hase [b)] and I. Narumi [b)]

[a)]Soy Sauce Laboratory Manufacturing Division, YAMASA CORPORATION, [b)]Radiation-Applied Biology Division, QuBS, JAEA

In this study, we investigated the mutagenic effect induced by ion beams for breeding of *A. oryzae*, which is used in the manufacture of traditional Japanese fermented foods, such as soy sauce, sake and miso. We irradiated *A. oryzae* with 220 MeV carbon ions by AVF cyclotron at the doses of 300-700 Gy. Mutation rate was measured by counting the number of selenic acid resistant colonies whose mutation relates to *sB* and *sC* genes that are involved in sulfur incorporation. These analyses indicated the suitable dose for obtaining variants to be 400 Gy. Furthermore, PCR analysis suggested 57 % of these variants carry a deletion with *sC* or *sB* gene under this condition.

【緒言】

麹菌（*Aspergillus oryzae*）は醤油、清酒、味噌などの醸造産業において利用される重要な微生物である。そのため古来より麹菌の育種が精力的に行われてきた。

近年、植物などの育種においてイオンビームが注目されており、その変異効果が従来の変異原に比べて高く、変異スペクトルも様々であることが報告されている。そこで我々は、麹菌育種の新しい手段としてイオンビームの利用を検討することとした。麹菌へのイオンビーム照射についてのデータはまだ少数であることから、まず、照射条件や変異効果について検討した。

【実験方法】

・サンプル調製および照射条件

A. oryzae（niaD300）の分生子を凍結乾燥し、照射サンプルとした。照射はTIARAのAVFサイクロトロンを用いて加速した$^{12}C^{5+}$（220 MeV, 107 keV/μm）により行った。

・生存率と変異率

生存率はイオンビームを300～700 Gy 照射したサンプルを栄養培地に播種し、生育したコロニー数から生存率を求めた。

イオンビーム照射サンプルをメチオニン 30 ppm, セレン酸 0.1 mM を含む最少培地に播種し、得られたセレン酸耐性株の数から変異率を求めた。

・変異箇所の探索

硫黄の取り込みに関与する*sB*遺伝子、*sC*遺伝子が変異することによりセレン酸耐性になることが知られている[1)]。*sB*、*sC*の前半、後半領域の各断片を増幅するプライマーを設計し、遺伝子欠損の有無についてPCRにより検討した。

【結果】

生存率については線量が大きくなるに従って低下した。また、線量ごとの変異率は 400 Gyで最大を示した（Fig. 1）。次に、得られた変異株の変異パターンを解析した。変異株のゲノムを抽出しPCRを行ったところ、遺伝子の前半領域のみ、もしくは後半のみが増幅されるもの、両方とも増幅されないものなど、欠損変異を示唆するデータが得られた。これらの株の割合を求めたところ、全耐性株の 27%ほどを占め、高い確率で遺伝子欠損株が得られることが示唆された。また、400 Gy照射区では欠損変異を示唆する株の割合が57%であり、他の照射区に比べ極めて高い割合であった（Table 1）。

以上のことから、凍結乾燥処理を行った麹菌のイオンビーム照射では 400 Gy程度の線量で高い変異効果が期待でき、遺伝子の欠損変異が高い割合で生じていることが示唆された。

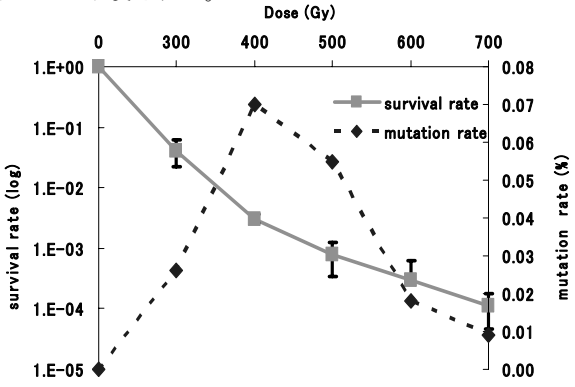

Fig. 1 Survival rate and Mutation rate of conidia after irradiation with ion beams in *A.oryzae*.

Table 1 Difference in mutagenic effect at various doses of ion beams in *A.oryzae*.

Dose (Gy)	0	300	400	500	600	700
Survival rate (%)	100	4.13	0.31	0.08	0.03	0.01
Mutation rate (%)	0	0.026	0.070	0.055	0.018	0.009
No. of variants (cfu)	0	12	21	11	5	2
No. of deficient strain (cfu)	0	1	12	1	0	0
Percentage of deficient strain per variants (%)	0	8.3	57.1	9.1	0	0

Reference

1) O. Yamada et al., Biosci. Biotechnol. Biochem. 61 (1997) 1367.

3-28 Mutation Breeding of Koji Mold Induced by Ion Beam

K. Ito [a)], J. Takeichi [a)], Y. Hanya [a)], K. Satoh [b)], Y. Hase [b)] and I. Narumi [b)]

[a)]R&D Division, Kikkoman Corp., [b)]Radiation-Applied Biology Division, QuBS, JAEA

Introduction

Koji molds, *Aspergillus sojae* and *Aspergillus oryzae*, are industrially important microorganisms which is used for brewing of soy sauce. The various mutagens have been used for mutation breeding of koji molds for many years. However, there are problems in usual mutagens, for example UV, NTG and X-rays lead to much inconvenient mutation such as slow growth rate and poor conidiation. Consequently, most mutants simultaneously have these traits, even if target trait was acquired. Therefore, we focused on mutation by ion beam. It is known that this method induces targeted mutations with smaller number of inconvenient mutation. We previously reported that survival rate and mutation frequency of *A. sojae* IFO4241 following irradiation of ion beams and determined optimal irradiation conditions[1)]. In this report, we investigated whether ion beams induce deletion mutations in *A. sojae* IFO4241 as well as higher plants. A defect in the *wA* gene of *Aspergillus* species is associated with the loss of conidial pigmentation and the conidial color of this mutant will turn to white from green[2)]. To investigate the deletion mutation frequency, the pigmentless-conidium mutants were obtained and the *wA* gene of these mutants were analyzed.

Materials and Methods

(1) *Isolation of pigmentless conidium-mutants*

The suspension containing 10^6 conidia (*A. sojae* IFO4241) were spread on Malts agar plate and incubated at 30 ºC for 6 hr for germination. Germinated conidia were irradiated with 220 MeV $^{12}C^{5+}$ (121.8 keV/μm) ion beam accelerated by AVF cyclotron at TIARA with the dose of 100, 150 and 200 Gy. Irradiated conidia were cultured at 30 ºC for 3 days. The pigmentless-conidium mutants were picked up and purified three times by single conidium isolation on Malts agar plate containing 0.25 % Triton X-100. UV irradiation was performed as previously described[1)]. Only one mutant was picked up from each irradiated plate.

(2) *DNA analysis of* wA *gene of pigmentless-conidium mutants*

The full length of genomic *wA* gene from pigmentless conidium mutants and/or their internal regions were amplified by PCR using various primer sets. The amplified DNA fragment size was compared with that of wild type on 0.8 % agarose gel. Southern blot analysis was performed using DIG labeling Kit (Roche). The PCR fragment of *wA* gene was used as a probe for southern analysis.

Results and Discussion

The number of pigmentless-conidium mutants from irradiated plates with ion beam and/or UV was 114 and 38, respectively (Table 1). The full-length *wA* gene (8.0 kb) of pigmentless-conidium mutants was amplified by PCR using primer F1 and R2 (Fig. 1). We evaluated the deletion mutation of *wA* gene if the PCR fragment was not amplified (Fig. 1 (B)-(D)) or the amplified PCR fragment size was smaller than that of wild type (Fig. 1 (A)). Out of 114 pigmentless-conidium mutants with ion beam irradiation, 38 mutants were deletion mutant (Table 1). On the other hand, all pigmentless-conidium mutants with UV irradiation were not due to deletion mutation. These results indicated that deletion mutation frequency with ion beam irradiation was higher than that with UV irradiation. PCR analysis of 38 deletion mutants revealed that the deletion mutation was classified into four patterns (Table 2 (A)-(D)). The loss of whole *wA* gene of pattern C mutants was confirmed by southern blot analysis (data not shown). This result revealed that an 8.0-kb chromosomal region could be deleted with ion beam irradiation in *A. sojae* IFO4241. The large deletion mutation might be occurred in *A. sojae* IFO4241 as well as higher plants.

Table 1 Comparison of deletion mutation frequency between ion beam irradiation and UV irradiation.

	Number of irradiated plates	Number of pigmentless mutants	Number of deletion mutants	Deletion mutants per pigmentless-conidium mutants (%)
Ion beam	144	114	38	33
UV	120	38	0	0

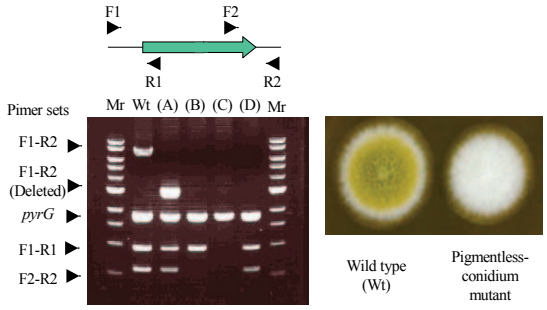

Fig. 1 PCR analysis of the *wA* gene of deletion mutants. The *pyrG* gene was amplified as a positive control. The lane Mr is DNA size marker.

Table 2 The mutation pattern of *wA* gene in deletion mutants.

Mutation pattern		Number of mutants
(A)	Deletion of internal region	22
(B)	Deletion of 3' region	7
(C)	Deletion of full genomic region	2
(D)	Translocation, inversion etc.	7

References

1) K. Ito et al., JAEA Annual Report 2005 (2006) 98.
2) M. E. Mayorga et al., Genetics 126 (1990) 73.

3-29 Deletion of Minor Enzyme Activities of *Rhizomucor miehei* by Heavy Ion Beam Irradiation

K. Sakai [a)], H. Kobayashi [a)], A. Oshima [a)], S. Kato [a)], K. Satoh [b)] and I. Narumi [b)]

[a)]Tokyo Research Laboratory, Meito Sangyo Co., Ltd., [b)]Radiation-Applied Biology Division, QuBS, JAEA

1. Introduction

Cheese is one of the major dairy product and various kind of cheese are produced in the world. Rennet, which breaks kappa-casein and induces coagulation of milk, is originated from veal of lactating calf or lamb stomach or produced by fermentation of *Rhizomucor (Rh.) miehei*. *Rh. miehei* also produces various minor enzymes such as lipase and these enzymes usually cause production of undesirable flavors during maturation of cheese. For this reason, acidification and chemical treatments are employed to improve the property. However, these treatments also cause loss of coagulation activity. Therefore, breeding a strain of lipase-less or very low lipase activity is expected for improving the productivity and quality of cheese.

The survival rate of sporangiospore was about 1% following 200 Gy irradiations of $^{12}C^{5+}$ at 220 MeV and $^{20}Ne^{8+}$ at 350 MeV. On the other hand, He and Ar ions had lower effect on survival rate than those of C and Ne ions. In 2006, lipase-less mutant strain separation was performed by irradiation of C and Ne ions at doses of 100 and 200 Gy to spore.

2. Materials and Methods

Sporangiospore of two parent mutants of *Rh. mihei* obtained by chemical and γ-ray mutagenesis was harvested from plate cultivation and was spread on a petridish as previously reported. Spore was dried over silica gel, conditioned over saturated NaCl solution, and covered with polyimide film for the beam irradiation. The beam irradiation of C-220 MeV and Ne-350 MeV was performed at AVF cyclotron of TIARA.

Irradiated spore was resuspended in sterile water, spread over glucose-yeast extract agar plate, and cultivated at 37 ˚C for three days. A mutation rate was determined by a frequency observation of red-pigmented colony that was caused by the mutation in AMP-synthesis pathway and accumulation of polyribosyl-aminoimidazole during cultivation at 37 ˚C [1)].

After mutation rate determination, the colonies were transfer to agar plate containing milk to detect secreted rennet activity from colonies. Coagulation activity was detected by formation of clear zone on the milk agar plate. After contacting with the milk agar plate overnight, the colonies were transferred onto agar plate containing olive oil to detect lipase activity secretion. Colonies those formed inarticulate clear zone on each medium were cultivated to confirm the coagulation and lipase activity production by a tube cultivation with a medium that was consisted of soybean flower and soluble starch. Lipase activity was determined by an alkali-titration released fatty acid from olive oil. Coagulation activity was determined by comparing clotting time (time for initiating coagulation of milk) with a standard enzyme using skimmed milk solution as a substrate.

3. Results and Discussion

Mutation rate varied from 0.06 to 0.99 %. A mutagenesis effect of neon ions was lower than that of carbon ions as shown in Table 1.

After observation of the mutation rate, colonies were transferred onto milk-agar and then oil-agar medium to select a deficient mutant by an inarticulate clear zone formation. All mutants isolated on agar media excreted lipase in tube cultivation. Among them, some mutants showed several times smaller activities than that of the parent strain (Table 2). These mutants might be heterozygous and further purification is necessary.

A mutant strain with low coagulation activity was also found and its culture product showed a different chromatographic profile from that of parent (data not shown).

Table 1 Mutation rate by irradiation of heavy ion beams. Irradiated spore was spread on agar plate medium and cultivated for 3 days at 37˚C. Mutation rate is defined as the ratio of red-pigmented colonies in total colony.

Parent	Irradiation	Total colony	Mutation rate
B	C-100 Gy	252	0.40%
	C-200 Gy	1,313	0.99%
	Ne-100 Gy	1,805	0.06%
D	C-200 Gy	406	0.49%

Table 2 Mutants with low lipase activity.

Mutant strains were isolated from the parent strain B and D irradiated with neon and carbon ions at a dose of 200 Gy. Enzyme activity was shown as a proportional value to the activity of each parent.

Mutant	Coagulation activity	Lipase activity
B-14 (Ne-200 Gy)	95%	23%
B-43 (Ne-200 Gy)	102%	21%
D-57 (C-200 Gy)	35%	75%

Reference

1) F. J. Jin et al., Biosci. Biotechnol. Biochem. 68 (2004) 656.

3-30 Spectral Analysis of DNA Damages Induced by He^{2+} Ion Beam Compared to Those of ^{60}Co γ-rays

K. Akamatsu [a], S. Wada [b] and Y. Kobayashi [c]

[a]Division of Environmental and Radiation Sciences,NSED, JAEA, [b]Laboratory of Veterinary Radiology and Radiation Biology, Kitasato University School of Veterinary Medicine, [c]Radiation-Applied Biology Division, QuBS, JAEA

1. Introduction

Information in relation to chemical structures and their distribution on DNA is quite important to clarify following biological repair procedures. In case of ionizing radiations, especially, it is expected that three-dimensional distribution of DNA damages is diversified as well as their chemical structures, and the diversity makes investigations of physicochemical processes in radiation effects difficult. In fact, double-strand breaks produced by high linear energy transfer (LET) alpha particles are more difficult to rejoin in living cells than those produced by low LET ^{137}Cs γ-rays[1]. To investigate difference of DNA damage spectrum between radiations, we have developed new methodology to analyze strand break-termini and nucleobase lesions using snake venom phosphodiesterase (SVPD), calf intestinal alkaline phosphatase (CIAP) and piperidine[2]. In this report, the results of the DNA damage spectra induced by He^{2+} ion beams and ^{60}Co γ-rays are demonstrated. The He^{2+} ion beams used was obtained from TC-1 port of 3 MV tandem accelerator in TIARA at Takasaki Advanced Radiation Research Institute. The ^{60}Co γ-rays, as a standard radiation source, were irradiated in the second cell in the first building of γ-irradiation facility at the same institute.

2. Materials and Methods

Linear formed pUC19 plasmid DNA digested with *Sma*I, (pUC19/*Sma*I) was used. pUC19/*Sma*I aqueous solution was mounted on a silicon plate and dried thoroughly in vacuum under P_2O_5. For γ-irradiation, the dried DNA sample on a plate was put into a glass tube sealed in vacuum to achieve secondary electron equilibrium. Each sample was irradiated at a dose (dose rate) of 40 (0.333), 100 (0.833), 400 (3.33), 900 (7.50), and 1,800 kGy (15.0 kGy/h) at r.t., respectively. For He^{2+} beams, the DNA-mounted plate was fixed in a cylindrical chamber (39 mmϕ, hight: 22 mm) with a Kapton® window (8 μm) under argon gas. Each sample was irradiated with ~ 200 keV/μm of the beam just under the Bragg-maximum, which was controlled using a depth-tunable cell irradiation equipment, at a dose (dose rate) of 100 (1.068), 400 (1.068) and 900 kGy (1.068 kGy/pass) at r.t.. The irradiated DNA samples were recovered by water at 0°C to be 0.32 μg/μL.

The new method for DNA damage analysis is indroduced in previous paper in detail[2]. In brief, the solution dissolving irradiated DNA was treated directly by SVPD, or was treated by SVPD following to CIAP pretreatment, to produce 5'-deoxynucleotides (pdNs) from 3' termini without phosphate for 15 min at 31.4 °C. The pdNs were quantified by HPLC after dephosphorylation to be 2'-deoxynucleosides by additional CIAP treatment. Furthermore, the irradiated DNA sample was pretreated by piperidine, to convert a variety of nucleobase damages and abasic sites into 3' termini with phosphate. The increase of 3'termini with phosphate by piperidine treatment reflects the amount of piperidine-labile nucleobase lesions and abasic sites. Based on the series of the experiments, the yields of total 3'termini, those of 3'termini with or without phosphate, and piperidine-labile lesions were calculated. (Table 1).

3. Results and Discussion

Table 1 shows the yields of DNA lesions calculated. Additionally, the yields of unaltered nucleobase release are also demonstrated as a reference. In case of the strand break patterns, the yields of them for He^{2+} were almost the same as those for γ-rays. In general, 3' termini with phosphate were predominantly produced compared with those without phosphate. On the other hand, in case of piperidine-labile lesions, the yields of them for He^{2+} were twice as large as those for γ-rays. This tendency was shown also in case of unaltered nucleobase release. Although the yields of nucleobase lesions for high-LET radiations would be larger than those for low-LET radiations according to the data from the table, it is also possible that piperidine-labile sites are susceptible to be produced in the high-LET radiation field. Anyway, more investigation additionally using base-excision enzymes should be needed to clarify the difference between the radiations. Moreover, the differences in DNA spectrum between on and off peaks of the Bragg-maximum, and between some degrees of hydration of DNA molecule are to be investigated.

Table 1 Yields of DNA lesions for He^{2+} ion beam and ^{60}Co γ-rays

Category of lesions	Yield (μmol/J, x 10^{-9} $Gy^{-1}Da^{-1}$)	
	^{60}Co γ-rays	He^{2+} (~ 200 keV/μm)
Total 3' termini	0.102	0.092
3'termini without phosphate	0.024	0.024
3'termini with phosphate	0.078	0.068
Piperidine-labile lesions	0.084	0.183
Unaltered nucleobase release (ref.)	0.018	0.034

4. Acknowledgments

We would like to gratefully thank Dr. Y. Hase at Gene Resource Research Group in Takasaki Advanced Research Institute for maintaining and operating the TC-1 beamline.

References

1) C. M. deLala et al., Radiat. Res. 144 (1995) 43.
2) K. Akamatsu, Anal. Biochem. 362 (2007) 229.

3-31 DNA Damage Yields in Hydrated DNA after Carbon Ion-irradiation

T. Ushigome [a)], H. Tauchi [a)], A. Yokoya [b)], N. Shikazono [b)], K. Fujii [b)] and A. Urushibara [b)]

[a)]Department of Environmental Sciences, Faculty of Science, Ibaraki University, [b)]Advanced Science Research Center, JAEA

Ionizing radiation causes various types of DNA lesions, such as strand breaks, base lesions and, in particular, biologically relevant complex damage known as cluster damage sites, which consist of two or more elemental lesions within one or two helical turns of DNA [1)]. Clustered DNA damage sites are considered to be less readily repaired than isolated lesions and therefore may induce deleterious and serious genetic changes in cells. The complexity of clustered damage is proposed to increase on increasing the ionizing density of the radiation (LET). It has been demonstrated that the direct effect of low LET radiation produces 30-40 % of the lesions in cells[2)]. This value is shown to reach 70 % when cells are irradiated with α-particles[2)]. However, few investigations have been systematically undertaken to elucidate the nature of lesions produced by the direct effects of radiation with varying ionizing density.

To gain insights on the nature of lesions induced by the direct effect of the radiation, yields of single- and double-strand breaks (ssb's and dsb's), and base lesions for hydrated plasmid DNA were measured after exposure to carbon ion particles with varying LETs. The use of hydrated DNA eliminates the indirect effect of radiation arising from irradiation of bulk water. Base lesions were detected as additional strand breaks after treatment of irradiated DNA with two glycosylases, Nth and Fpg proteins, which convert the oxidative base lesions into an ssb.

The yield of prompt ssb after exposing hydrated plasmid DNA to carbon ion particles with a LET of 87 keV/μm was 6.2 X 10^{-11} ssb/Gy/Da (Fig. 1). The yields were found to be fairly similar for carbon ion particles with LETs of 122, 342 and 507 keV/μm. This value of around 6 X 10^{-11} ssb/Gy/Da is comparable to that obtained after γ- irradiation [3)]. While the yield of prompt ssb does not alter with varying LET values from 87-507 keV/μm, the yield of prompt dsb appears to increase as the LET increases (Fig. 2). Consequently, the ratio of prompt ssb to dsb tends to decrease as the LET increases, indicating that strand breaks in close proximity, which would produce dsb's, are more readily induced at higher LET.

Results of enzymatically induced ssb/dsb revealed that the amount of base lesions susceptible to cleavage by Nth and/or Fpg becomes less as the LET gets higher (Fig. 1 and Fig. 2). Although we cannot fully disregard the possibility that the number of damaged bases is actually reduced at higher LET, we favor the interpretation of base lesions being clustered and thus becoming less readily cleaved by the glycosylases. Inhibition of excision of damaged bases within a cluster has been indeed demonstrated using purified enzymes[4)]. It should be noted that the yields of prompt and enzymatically induced DNA damage after exposing to carbon ion particles with a LET of 87 keV/μm were lower than those of helium ion particles with a LET of 95 keV/μm[5)]. This result suggests that the LET is not fully sufficient a parameter to describe the nature of damage clustering and that rather the actual density of ionization should be taken into account.

In summary, our results indicate that DNA lesions in hydrated plasmids become more readily clustered on increasing ionizing density of the radiation.

References

1) Goodhead, D. T. Int. J. Radiat. Biol. 65 (1994) 7.
2) de Lara, C. M., et al. Radiat. Res. 144 (1995) 43.
3) Yokoya, A., et al. J. Am. Chem. Soc. 31 (2002) 8859.
4) Weinfeld, M., et al. Radiat. Res. 156 (2001) 584.
5) Urushibara, A., et al. Radiat. Prot. Dosimetry 122 (2006) 163.

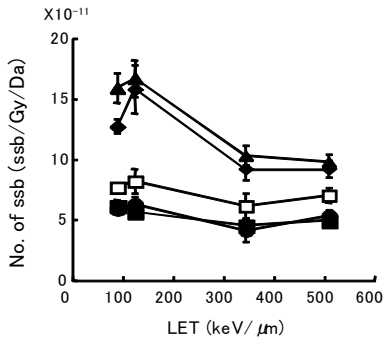

Fig.1 Number of prompt and enzymatically induced single strand breaks as a function of LET (keV/μm). Prompt (■), Mock treatment of enzymes (●), Fpg treatment (□), Nth treatment(◆), Fpg+Nth treatment (▲)

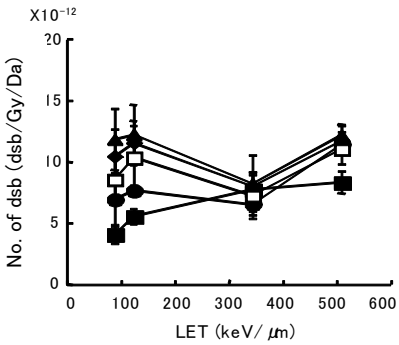

Fig.2 Number of prompt and enzymatically induced double strand breaks as a function of LET (keV/μm). Prompt (■), Mock treatment of enzymes (●), Fpg treatment (□), Nth treatment(◆), Fpg+Nth treatment (▲)

3-32 Analysis of Cellular Effects and Local Damage Induced by High LET Heavy Ions

S. Wada [a), b)], T. Funayama [b)], T. Sakashita [b)], K. Fukamoto [b)], N. Hamada [a), b)], T. Hara [a), b)], T. Kakizaki [c)], M. Suzuki [b)] and Y. Kobayashi [a), b)]

[a)]Department of Quantum Biology, Division of Bioregulatory Medicine, Gunma University Graduate School of Medicine, [b)]Radiation-Applied Biology Division, QuBS, JAEA, [c)]Department of Veterinary Medicine, Kitasato University

Introduction

High linear energy transfer (LET) radiation, such as heavy ion beam, has greater biological effectiveness than low LET radiation. Higher biological effectiveness of high LET radiation is probably a consequence of local damage like clustered DNA damages that contain locally multiple oxidized bases, single strand breaks and double strand breaks (DSB), because it is considered that the clustered DNA damage is non-repairable or more difficult to repair than a lesion sparsely induced. On the other hand, mammalian cells efficiently detect and repair DNA damage. Especially, mammalian cells have evoked two pathway for repairing DSB, homologous recombination (HR) and non-homologous end joining (NHEJ). The major pathway in mammalian cells is NHEJ. Many proteins are involved in NHEJ which include Ku70/80 heterodimer, DNA-PKcs, XRCC4 and ligase IV. First, Ku bind to the ends of a DSB and DNA end binding by Ku initiates a cascade of molecular events that leads to joining of the broken DNA ends. In addition to DNA repair, Ku protein plays a role in multiple nuclear processes, such as chromosome maintenance and transcription regulation. However, much less is known about the yield and reparability of clustered DNA damages.Recently we suggest that the number of non-repairable DSB by Ku–dependent DSB repair system increases with increasing LET. In this study, to investigate non-repairable DSB by Ku–dependent DSB repair system we analyzed behavior of Ku protein to DNA damage induced by high LET heavy ions.

Material and Methods

We transfected pGFP-Ku80 into xrs-5 cells (mutated in Ku80). This cell was grown in MEM-alpha medium supplemented with 10 % serum and were incubated at 37 ℃ in a humidified atmosphere of 5 % carbon dioxide and 95% air. Accelerated ions of 220 MeV C^{5+} (108 keV/μm), 460 MeV Ar^{13+} (1610 keV/μm) were provided by the AVF cyclotron at TIARA JAEA-Takasaki. Cells were irradiated with ion beams. To evaluate DNA damage and NHEJ pathway induced by heavy ion beams, we carried out immunohistochemical detection of phosphorylated histone H2AX (γ-H2AX). Cells were attached on the CR-39 film that is a particle track detector. After post-irradiate incubation of 10-30 min, the cells were fixed by 1 % paraformalehyde in PBS. Then, the cells were incubated with anti-γH2AX antibody for detecting DNA double strand break sites *in situ*. Thereafter, the cells were counter-stained with DAPI and the opposite side of the CR-39 film was etched with KOH-ethanol solution at 37 °C. Using a conforcal microscope, we took images of the cells (γH2AX and GFP-Ku80) and the etched pits on the CR-39 film at a same field of view. By merging all images together, the position of hit-ions, γH2AX and GFP-Ku80 were simultaneously detected. Additionally, because Ku70/80 and DNA-PKcs formed complex in NHEJ pathway, *in situ* localization of DNA-PKcs was also analyzed.

Results and Discussion

In xrs5 -GFP-Ku80 cells, the site of γH2AX foci and the site of etched pits were coincident. In addition, GFP-Ku80 foci co-localized with those of γH2AX. These observations show that Ku80 proteins localize to DNA damages induced by ion beam irradiation, indicating that Ku80 protein can recognize and bind to DNA damages induced by heavy ion irradiation. The GFP-Ku80 foci were observed in the samples of 10 min to 30 min after C ion irradiation, and, at the same moment, DNA-PKcs also were localized to DNA damage sites. This observation suggests that the damage induced by C ion irradiation is repairable by Ku-dependent DNA repair pathway. On the contrary, the foci of GFP-Ku80 were observed in 10 min after Ar ion irradiation, but they disappeared in 20 min or later (Fig.1). In addition, co-localization of GFP-Ku80 and DNA-PKcs was not clear even in 10 min after Ar ion irradiation. These results indicate that Ku80 can bind to DNA damage induced by high LET heavy ion like Ar, but cannot form a complex with DNA-PKcs, resulting in failure of NHEJ repair of induced DNA damages.

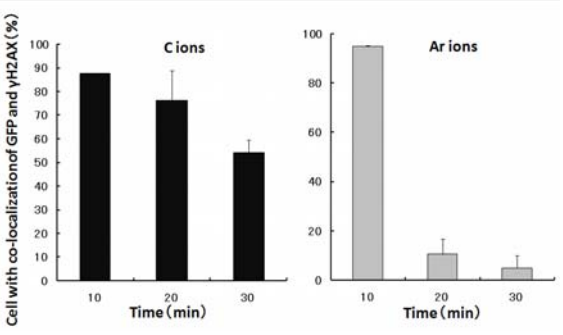

Fig.1. Cell with co-localization signal of GFP-Ku80 and γH2AX after C ion and Ar ion irradiation.

3-33 Analysis of Molecular Mechanisms for Radiation-induced Bystander Effects Using Heavy Ion Microbeams

H. Matsumoto [a)], M. Hatashita [a)], M. Tomita [b)], K. Otsuka [b)], T. Funayama [e)], T. Sakashita [e)], N. Hamada [c,d,e)] and Y. Kobayashi [c,d,e)]

[a)]Faculty of Medical Science, University of Fukui, [b)]Central Research Institute of Electric Power Industry, [c)]Gunma University Graduate School of Medicine, [d)]The 21st Century Center of Excellence Program for Biomedical Research Using Accelerator Technology, [e)]Radiation-Applied Biology Division, QuBS, JAEA

The objective of this project is to elucidate molecular mechanisms of the bystander effect using heavy ion microbeams in JAEA. We found that the foci of γH2A.X and pNBS1 were formed in the unirradiated cells in the target colony including the irradiated cell 6 h after irradiation with 460 MeV ^{40}Ar beams and that this formation of the foci was almost completely suppressed by the addition of DMSO or Lindane. Also we found that the foci of γH2A.X and pNBS1 were formed in the unirradiated cells in the untargeted colonies 6 h after irradiation and that this formation of the foci was almost completely suppressed by the addition of aminoguanidine or c-PTIO. Our findings strongly suggested that ROS and NO are initiators/mediators for evoking heavy ion microbeam-induced bystander effects.

低線量／低線量率放射線に対して生物が示す特異的な応答様式の一つに放射線誘発バイスタンダー効果がある[1)]。我々は、日本原子力研究開発機構において開発された重イオンマイクロビーム細胞照射システム（細胞局部照射装置）を用いて、この放射線誘発バイスタンダー効果の分子メカニズムを明らかにすることを計画した。

1. 実験方法

(1)細胞：ヒト正常線維芽細胞(AG1522 細胞)を用いた。

(2)培養：開孔（径 12 mm）35 mmディッシュの内面中央に 20 mm四方のCR-39をパラフィンで固定したものを使用した。またCR-39 の表面をcollagenコートして細胞を培養した。2×10^5 cells/mlの細胞懸濁液 5 µlをCR-39 樹脂上に 5 箇所スポットし(1000 cells/colony)、15~20 時間培養したものを照射実験に供した。

(3)照射：Funayamaら[2)]の方法に従って、中央にスポットしたコロニーの細胞 1 個に 5 粒子の 460 MeV $^{40}Ar^{13+}$をHZ1 ポートにおいて照射した。また対照実験として 460 MeV $^{40}Ar^{13+}$をHY1 ポートにおいても照射した。

(4)細胞の蛍光免疫染色：照射後、細胞を 37°Cで培養し、0.5 および 6 時間後にメタノールで固定し、リン酸化型H2AX（γH2AX）抗体およびリン酸化型NBS1（pNBS1）抗体を用いた蛍光抗体染色法により染色し、蛍光顕微鏡下で観察した[3)]。標的細胞を含む正方形枠（250 x 250 µm; C）内、そこから右方向に設定した 2 個の正方形枠（250 x 250 µm; AおよびB）の内部、および遠隔に存在するサテライトコロニーの中心部の正方形枠（250 x 250 µm; S）内のフォーカス形成頻度を測定した。

2. 結果および考察

(1)標的細胞でのγH2AXおよびpNBS1のフォーカス形成：Ar線マイクロビームの照射により、照射された細胞においてγH2AX および pNBS1 のフォーカス形成が認められ、それらは同所局在していた。

(2)バイスタンダー細胞における γH2AX および pNBS1 のフォーカス形成：Ar 線マイクロビーム照射により、バイスタンダー細胞においてもγH2AXおよび pNBS1 のフォーカス形成が認められ、それらは同所局在していた。従って標的細胞から分泌された可溶性低分子物質（バイスタンダー因子）によりバイスタンダー細胞に DNA 二本鎖切断が誘発されていることが示唆された。またバイスタンダー細胞におけるこれらのフォーカス形成は標的細胞から離れるに従ってその頻度は減少した。

(3)バイスタンダー因子の種類に依存したバイスタンダー効果の発現：Ar 線マイクロビーム照射により、バイスタンダー細胞における γH2AX および pNBS1 のフォーカス形成がDimethylsulfoxide（DMSO, 0.1%）、Lindane（40 µM）、Aminoguanidine（AG, 10µM）およびcarboxy-PTIO（c-PTIO, 10 µM）によって抑制された。DMSO は ROS の消去剤、Lindane は細胞間のギャップ結合の阻害剤、AG は nitric oxide (NO)ラジカル合成酵素の阻害剤、c-PTIO は NO ラジカルの消去剤である。DMSO による抑制は、C および A において顕著であり、それ以外の部位では抑制効果は認められなかった。Lindane による抑制効果は C においてのみ顕著であった。AG および c-PTIO による抑制効果は、A、B および S において認められたが、特に S において最も顕著であった。

以上の結果よりギャップ結合を移行しているバイスタンダー因子および標的細胞近隣の細胞に培地を介して作用しているバイスタンダー因子は活性酸素種（ROS）であることが示唆された。一方、遠隔的に作用しているバイスタンダー因子は活性窒素種（RNS）、特に NO ラジカルであることが示唆された。

References

1) H. Matsumoto, et al., J. Radiat. Res., **48**, 97 (2007)
2) T. Funayama, et al., Radiat. Res. **163**, 241 (2005).
3) A. Takahashi, et al., Cancer Res. **64**, 8839 (2004).

3-34 Exposure of Normal Human Diploid Fibroblasts to Heavy Ions Facilitates Differentiation in Their Progeny

N. Hamada [a,b], T. Hara [a,b], T. Funayama [b], T. Sakashita [b] and Y. Kobayashi [a,b]

[a]Department of Quantum Biology, and The 21st Century COE Program, Gunma University Graduate School of Medicine, [b]Radiation-Applied Biology Division, QuBS, JAEA

Radiation-induced genomic instability encompasses a variety of delayed effects that occur in the progeny of survivors multiple generations after the initial insult. LET dependence of these effects is incompletely characterized; however, we have previously found that delayed reductions in clonogenicity can be most pronounced at LET of 108 keV/μm. To gain insight into potential cellular mechanisms underpinning LET-dependent delayed loss of clonogenicity, we investigated morphological changes in colonies arising from normal human diploid fibroblasts exposed to ^{60}Co γ-rays (0.2 keV/μm) or carbon ions (18.3 MeV/amu, 108 keV/μm). Carbon ions were fourfold more effective at inactivating cellular clonogenic potential and produced more abortive colonies containing reduced number of cells per colony than γ-rays. Second, colonies were assessed for clonal morphotypic heterogeneity. The yield of differentiated cells was elevated in a dose- and LET-dependent fashion in clonogenic colonies, while differentiated cells dominated to a comparable extent irrespective of irradiation in abortive colonies. The incidence of giant or multinucleated cells was also increased but much less frequent than that of differentiated cells. All together, our results indicate that carbon ions facilitate differentiation more effectively than γ-rays. Accelerated differentiation may account for dose- and LET-dependent delayed loss of clonogenicity in normal human diploid cells, and could be a defensive mechanism that averts further expansion of aberrant cells.

重粒子は、線エネルギー付与(LET)の低い光子に比べ、生物学的効果比(RBE)が高く、線量分布の集中性にも優れていることから、がん治療に利用されている。しかし、がん病巣の内部や周囲には正常細胞が混在しているため、放射線治療の際に正常細胞への照射は避けられない。このことから、重粒子がヒト正常細胞に及ぼす生物効果を詳細に解析する必要がある。長い間、放射線の生物効果は、核が照射された細胞にのみ認められると考えられてきたが、近年では、細胞質が照射された細胞、さらには、照射子孫細胞(遺伝的不安定性)や照射周囲の細胞(バイスタンダー効果)にまで及ぶことが明らかになってきた[1)]。放射線照射子孫細胞には、照射後の分裂を経た後に、増殖死や染色体異常などが遅延的に誘発されることが知られている。我々は、これまでに、放射線誘発遅延的増殖死のLET依存性に関して、2次コロニー形成能(1個の照射細胞に由来して形成される1次コロニーを回収・再播種させた場合の細胞のコロニー形成能)の喪失を指標としたRBEが108 keV/μmで最大になることを報告してきた[2)]。本研究では、1次コロニーを構成する細胞の形態変化を解析することにより、照射子孫細胞に遅延的に誘発される応答と、LET依存的な2次コロニー形成能喪失の機序を細胞レベルで明らかにすることを目的とした。

細胞周期による感受性のばらつきを軽減させるため、そして、細胞間相互作用はストレス応答に重要な役割を果たしている[3)]ことから、ヒト正常二倍体線維芽細胞AG01522を1x10^4 cells/cm^{2}の密度で播種後、4・7・9日目に培地交換し、11日目に放射線照射実験に使用した。^{60}Co γ線(0.2 keV/μm)、または、TIARAにて炭素線(18.3 MeV/amu、108 keV/μm)を照射後1時間以内に再播種し、13日間培養し、形成されたコロニーを固定・染色した。顕微鏡下で、コロニーあたりの細胞数を計数するとともに、細胞の形態を観察した。生存率は50細胞以上のコロニー数から算出した。

γ線の10%生存線量に対する炭素線のRBEは3.9であった。線量とLETに依存して、コロニーあたりの細胞数は減少し、特に2-7細胞のコロニーの割合が著しく増加した。形態変化を起こした細胞の割合は、50細胞以上のコロニーでは線量とLETに依存して増加したが、50細胞未満のコロニーでは照射の有無に依らずほぼ一定であった。コロニー内には巨細胞や多核化細胞も認められたが、観察された形態変化の大半を占めたのは、分化が進行した細胞であった。分化した細胞、巨細胞、多核化細胞のいずれもコロニー形成能を喪失していると考えられるため、照射子孫細胞への形態変化の誘導は、2次コロニー形成能喪失の機序である可能性とともに、異常を蓄積した細胞の増殖を抑制するための防御機構である可能性が示唆された[4)]。また、分化した細胞の誘発頻度が線量依存的に増加したことから、DNA損傷が一因となり分化の誘導を促進することが考えられる。放射線照射後に観察されるクロマチンの構造変化[5)]などに由来して形成されるゲノム上の潜在的不安定領域が恒常的な酸化ストレスにより再活性化され、照射子孫細胞に遅延的にDNA損傷が誘発されると考えられている。このことから、照射細胞に誘発されるDNA損傷が起因となって子孫細胞に遅延的に誘発されるDNA損傷が、チェックポイントを活性化することにより遺伝的不安定性の形質が永続的に発現すると考えられる。今後は、重粒子線誘発遺伝的不安定性の分子機序を明らかにしていきたい。

References

1) N. Hamada et al., J. Radiat. Res. 48 (2007) 87.
2) N. Hamada et al., Radiat. Res. 166 (2006) 24.
3) N. Hamada et al., Carcinogenesis 24 (2003) 1723.
4) N. Hamada et al., Mutat. Res. (2007) in press.
5) N. Hamada et al., Radiat. Res. 166 (2006) 31.

3-35 Radiation Induced Apoptosis in *Drosophila* Cells

H. Kawamura [a)], K. Tatei [b)], T. Nonaka [a)], H. Obinata [b)], T. Hattori [b)], A. Ogawa [b)], H. Kazama [a)], N. Hamada [c, d)], T. Funayama [d)], T. Sakashita [d)] Y. Kobayashi [c, d)], T. Nakano [a)] and T. Izumi [b)]

[a)]Department of Radiation Oncology, [b)]Department of Molecular Biochemistry, [c)]Department of Quantom Biology, Gunma University Graduate School of Medicine, [d)]Radiation-Applied Biology Division, QuBS, JAEA

Extracellular stresses including radiation were reported to increase intracellular ceramide concentration in mammalian cells. Cell-permeable ceramide, such as C_2 ceramide which has shortened fatty-acyl chain, was able to induce apoptosis in many cell lines. These results suggested that ceramide acts as a signaling molecule in radiation-induced apoptosis of mammalian cells. Ceramide is generated either by de novo synthesis or sphingomyelin degradation catalyzed by sphingomyelinases. The sphingomyelin degradation pathway was reported that the major source for generating ceramide in radiation-induced apoptosis. There are three classes of sphingomyelinase based on their optimal pH, acid, neutral. Both acid sphingomyelinase (aSMase) and neutral sphingomyelinase were reported to be activated during apoptosis. The mechanisms that control radiation-induced activation of SMases are not well defined. It has been shown that key components in apoptotic pathway are well conserved between *Drosophila* and mammals.

We examined whether ceramide level is regulated during radiation-induced apoptosis in *Drosophila* Schneider line 2 cell (SL2). Three-fold increase in ceramide was observed 5 hours after UV-C irradiation. Addition of cell permeable ceramide, C_2 ceramide, to SL2 cells increased Caspase 3/7 activity. Furthermore, overexpression of ceramidase that hydrolyzes ceramide caused reduction of Caspase 3/7 activity.

We carried out RNA interference experiment to clarify the ceramide-generating enzyme(s) during the apoptosis. Caspase 3/7 activity was decreased only by adding the ds RNA for neutral sphingomyelinase homolog. Other ds RNAs including acid sphingomyelinase homolog, and sphingolipid Δ4-desaturase had no significant effect. (Fig1)

These results suggested that ceramide have an important role in radiation-induced apoptosis and neutral sphingomyelinase homolog might affect the regulation of ceramide synthesis.

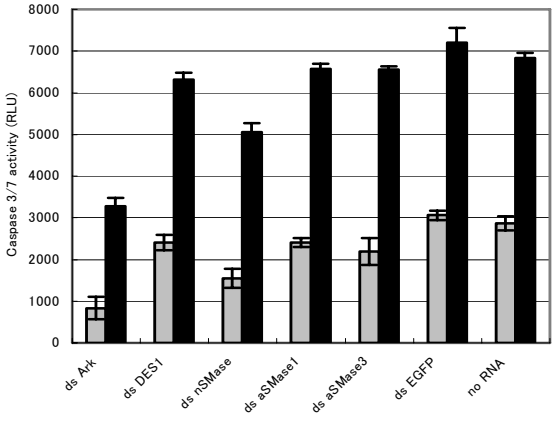

Fig 1. Effects of various dsRNAs for sphingomyeline-related genes on the hea

Double strand (ds) RNA was added to SL2 and incubated for 3 days to allow for turnover of the protein. To induce apoptosis cells were irradiated with heavy ion. DEVD-luciferin and luciferase was added to the cell lysate after 55 hours of irradiation, followed by measurement of Caspase 3/7 activity with luminometer. Filled bar: irradiated with 40 Gy of C^{5+} ion, Gray bar: no irradiation, Ark: Apaf-1 related killer, DES: sphingolipid Δ4-desaturase, aSMase1: acid sphingomyelinase homolog-1, aSMase3: acid sphingomyelinase homolog-3, EGFP: enhanced green fluorescent protein

3-36 Pathological and Immunohistochemical Findings of a Human Glioblastoma Cell Line (CGNH-89) after X-ray and Heavy-ion Beam Exposure

T. Oishi [a,e], A. Sasaki [a], N. Hamada [b,e,f], T. Funayama [e,f], Y. Kobayashi [b,e,f], S. Ishiuchi [c,e], Y. Nakazato [a,e] and T. Nakano [d,e]

[a]Departments of Human Pathology, [b]Quantum Biology, [c]Neurosurgery, [d]Radiation Oncology, and [e]21st Century COE program, Gunma University Graduate School of Medicine, [f]Radiation-Applied Biology Division, QuBS, JAEA

Purpose

It has not been elucidated whether heavy-ion beam irradiation modulates the biology of glioblastoma at the cellular level. Our project is designed to investigate whether heavy-ion beam exposure is effective against glioblastoma cells. We examined a human glioblastoma cell line (CGNH89[1]) by morphological and immunohistochemical techniques after X-ray or heavy-ion beam exposure.

Method

For X-ray and heavy-ion beam exposure, CGNH89 cells were divided into 3 groups; control, 5 Gy and 10 Gy exposure. For each group, cells were fixed at the same time-points. Hematoxylin-Eosin (HE) and immunohistochemical staining were done in formalin-fixed cells. For electron microscopy, cells were fixed in fixative (1 % glutaraldehyde, 10% formaldehyde). These samples were postfixed with osmium and embedded in Quetol 812. Ultrathin sections were examined under a transmission electron microscope.

Results and Discussion

After the exposure, both living cells and mitotic cells decreased in cell number. In the HE staining, nuclear condensation and apoptotic bodies increased after exposure. MIB-1 labeling index decreased in the early stage after exposure, but increased in later stages. It is suggested that cell cycle arrest and induction of apoptosis was induced by X-ray and heavy ion-beam exposure in CGNH89 cells. Ultrastructurally, the nuclei and cytoplasm after exposure showed a tendency to increase in size. Cellular swelling seems to depend on the swelling of mitochondria, increase of cellular organelles, cytoskeleton, and secondary lysosome (Fig.1,2). However we did not find out either apoptotic body or necrotic change. We conclude that X-ray and heavy ion-beam exposure might trigger the same morphological changes in the surviving CGNH-89 cells.

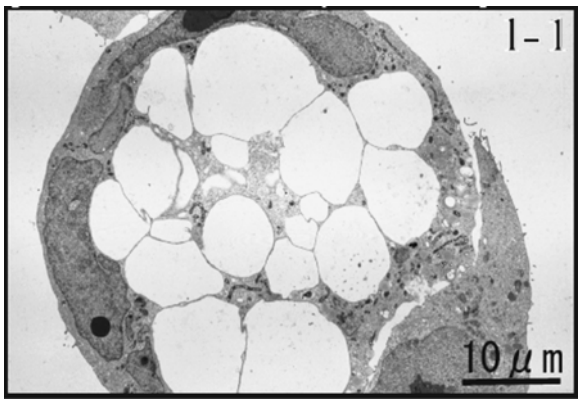

Fig. 1 Electron micrograph of the cell after exposure showing enlarged cytoplasm with vacuolar change.

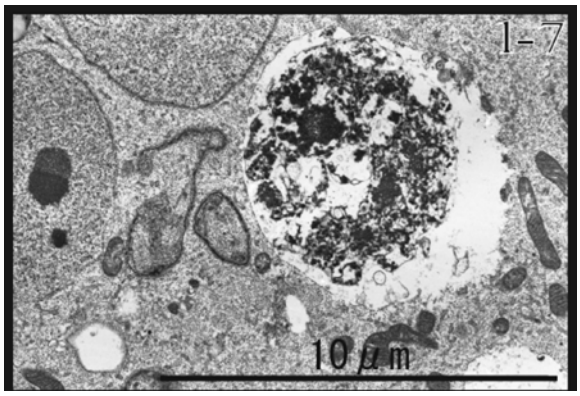

Fig. 2 Ultrastructurally, the cell exhibits the swelling of mitochondria and the increase of secondary lysosome.

Reference

1) Ishiuchi S et al, Nature medicine 8 (2002) 971.

3-37 Bystander Killing of Human Lung Cancer Cells by Heavy Charged Particle Irradiation

K. Harada [a)], T. Nonaka [a)], N. Hamada [b,c)], T. Funayama [c)], H. Sakurai [a)], T. Sakashita [c)], S. Wada [b,c)], T. Kakizaki [c)], M. Hasegawa [a,d)], Y. Kobayashi [b,c)] and T. Nakano [a)]

[a)]Department of Radiation Oncology, [b)]Department of Quantum Biology, Gunma University Graduate School of Medicine, [c)]Radiation-Applied Biology Division, QuBS, JAEA, [d)]Department of Radiation Oncology, Nara Medical University School of Medicine

We have here examined clonogenic survival of confluent human lung cancer A549 cells exposed to X-rays or 220 MeV $^{12}C^{5+}$ charged particles. Targeted exposure of 0.001-0.005 % of cells within the confluent population were resulted in 7-14 % reduction of surviving fraction. However, this reduction was diminished when cells were treated with the inhibitor of gap junction. These results suggest that gap junctional intercellular communication plays an essential role in heavy charged particle irradiation-induced bystander effects.

1. はじめに

これまでのわれわれの検討から、ブロードビームを用いた実験で$^{12}C^{5+}$の細胞生残曲線は直線的であったが、X線および$^{12}C^{5+}$のD_0（37%生存線量）／D_{10}（10 %生存線量）はそれぞれ1.59 Gy／4.00 Gy、1.23 Gy／2.39 Gyであった。この重イオンビーム照射による細胞死の機序にバイスタンダー効果が関与していることが知られているが、本研究では細胞間のギャップ結合に注目し、重イオンビーム照射後の細胞生残率について検討を行った。

2. 実験方法

細胞はヒト肺癌由来の細胞株A549を用いた（p53 statusは野生型）。重イオン照射は原子力機構TIARAのマイクロビームにて行った（220 MeV ^{12}C、108 keV/μm）。照射後の細胞生存率はコロニー形成法で検討した。細胞を高密度（コンフルエント）と低密度に培養した状態で照射するため、照射2日前に底面に固体飛跡検出材（CR-39）を貼付した35mmのグラスベースディッシュ上に細胞を準備した（高密度群では$5x10^5$個、低密度群では$5x10^4$個）。標的細胞はディッシュ中の1-25個の細胞をランダムに選択し、照射するイオンの数はひとつの細胞あたり1-10個とした。照射後は60 mmのディッシュに至適個数の細胞をtriplicateでまきなおし、14日後に細胞を固定・染色した後、コロニー数をカウントし、非照射細胞の生存率を対照とし細胞生存率を検討した。また、高密度に培養した細胞ではギャップ結合の促進剤（8-Br-cAMP：シグマ社製：照射の48時間前に添加し1mMに調節）、および阻害剤（Lindane：シグマ社製：照射の2時間前に添加し0.1mMに調節）を加えて照射し細胞生残率を求め、ギャップ結合の関与について検討した。

3. 結果および考察

コンフルエントな状態の細胞のうち選択的に1つの細胞にのみイオンを照射した際の細胞生存率は非照射細胞とほぼ同様であった。照射細胞数をディッシュ内の5-25個、また各細胞への照射イオン数を5-10個とすると照射していない細胞の生存率に比較し7-14 %低下した（P<0.05：データの提示なし）。一方、低密度に細胞を培養し、細胞間のコンタクトをなくした状態でディッシュ内の細胞を選択的に照射したときの細胞生残率は非照射の細胞と同様であった（データの提示なし）。コンフルエントに培養した細胞でギャップ結合を促進(＋cAMP)するとバイスタンダー効果が促進される傾向にあった(p=0.07)が、ギャップ結合を阻害(＋lindane)するとバイスタンダー効果が有意に抑制された(P<0.05、Fig.1）。

本実験ではディッシュ全体の細胞のうち0.001-0.005 %という極少数の細胞を重イオンビームで照射した時、ディッシュ全体の細胞生存率が有意に低下する結果が得られたが、細胞間のコンタクトをなくした状態で照射するとこの現象は認められなかった。またギャップ結合阻害剤を細胞に接触させることにより照射後の細胞生残率低下は抑制された。これらより重イオン照射による細胞死に照射細胞から非照射細胞へのバイスタンダー効果が関わっており、また、そのシグナル伝達経路にギャップ結合が深く関与していることが示唆された。

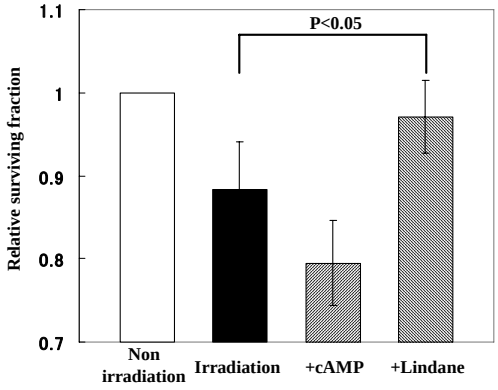

Fig.1 Relative surviving fraction of confluent density-inhibited culture of A549 cells where 25cells were irradiated with 5 carbon ions with or without treatment with lindane or cAMP. The surviving fraction of the nonirradiated A549 control was normalized as 1. The plating efficiency of control was 46-57 %.

3-38 Effects of Heavy-ion Irradiation on the Expression of Cellular and Viral Genes

N. Shimizu [a)], A. Oue[a)], T. Ohtsuki [a, b)], T. Mori [a, b)], S. Wada [b c)], N. Hamada [b)], T. Funayama [c)], Y. Kobayashi [b, c)] and H. Hoshino [a, b)]

[a)]Department of Virology and Preventive Medicine, and [b)]21st Century COE Program, Gunma University Graduate School of Medicine, [c)]Radiation-Applied Biology Division, QuBS, JAEA

Introduction

Heavy-ion irradiation, a new tool for cancer therapy and radiation biology, is expected to cause different responses on human cells from those by X-rays. The expression of some cellular genes is possibly induced by heavy-ion radiation. The aim of this study is to identify such genes using the susceptibility of human cells to human immunodeficiency virus type-1 (HIV-1) as an indicator. We have found that the susceptibility of human cells to HIV-1 is enhanced by heavy-ion irradiation. This enhancement was not detected in cells irradiated with X-rays. The mRNA expression of various cellular factors that are involved in HIV-1 replication, DNA damage or DNA repair were examined. Effects of various drugs on the mRNA expression of cellular factors were determined.

1. Materials and Methods

Human glioma cells transduced with CD4 and CCR5 genes, NP-2/CD4/CCR5 [1)], and NP-2/CD4/CCR5 cells transduced with green fluorescence protein (GFP) gene driven by HIV-1 LTR, NP-2/CD4/CCR5/LTR-GFP, were used in this study. NP-2/CD4/CCR5 cells were irradiated with carbon (C) ion or X-ray at different doses (0.5, 1.0, 2.0, and 4.0 Gy). Then, NP-2/CD4/CCR5 cells were exposed to a CCR5-using (i.e. R5-tropic) HIV-1 strain, Ba-L, 48 hour after irradiation. The susceptibility of NP-2/CD4/CCR5 cells to HIV-1 was determined by PCR to detect reverse-transcribed env DNA 24 and 48 hour after infection. Irradiated NP-2/CD4/CCR5 cells were exposed to HIV-1 at 4 ℃ for one hour and HIV-1 bound on the cells was detected by RT-PCR. The mRNA expression of various cellular factors was detected by RT-PCR using total RNA isolated from NP-2/CD4/CCR5 cells 48 hour after irradiation. Induction of GFP expression was detected in NP-2/CD4/CCR5/LTR-GFP cells treated with drugs.

2. Results and discussion

An amount of the reverse-transcribed env DNA was increased in NP-2/CD4/CCR5 cells infected with HIV-1 after heavy-ion irradiation at 0.5 and 1.0 Gy, suggesting that the susceptibility of the cells were enhanced by the radiation (Fig. 1). However, enhancement of the HIV-1 susceptibility could not be detected in NP-2/CD4/CCR5 cells irradiated with heavy-ion at 2.0 and 4.0 Gy. An amount of HIV-1 bound on NP-2/CD4/CCR5 cells irradiated with heavy-ion at different doses was similar, suggesting that the radiation has little effect on the efficiency of HIV-1 binding on the cell surface. The enhancing effects of heavy-ion irradiation on the susceptibility of NP-2/CD4/CCR5 cells to HIV-1 may be caused by increased incorporation or genomic reverse-transcription of HIV-1.

Expression of CD133 (Prominin-1) and NF-kB mRNA was detected to be increased in NP-2/CD4/CCR5 cells irradiated with heavyion. Expression of histon deacetylase, Ku80, and poly-ADP ribose polymerase mRNA was decreased in NP-2/CD4/CCR5 cells irradiated with heavyion. However, a relationship between the enhancing effect of heavy-ion irradiation on the susceptibility of NP-2/CD4/CCR5 cells to HIV-1 and the altered expression levels of these cellular factors has not been elucidated well.

Not only inducers of apoptosis, G2/M arrest of cell cycle, and acidic stress, but also inhibitors of HDAC and N-glycosylation failed to enhance the susceptibility of NP-2/CD4/CCR5/LTR-GFP cells to HIV-1. Therefore, none of these effects induced possibly by heavy-ion irradiation in human cells may be involved in the enhancement of HIV-1 susceptibility of NP-2/CD4/CCR5/LTR-GFP cells.

The susceptibility of NP-2/CD4/CCR5 cells to HIV-1 was upregulated when the cells were pretreated with 5-azacytidine, neuraminidase or Wortmannin, suggesting that chromosomal demethylation, inhibition of PI3-kinase, or modification of glycosylation of cell membrane factors may have a role in the enhancing effects of heavy-ion irradiation on the susceptibility of NP-2/CD4/CCR5 cells to HIV-1.

Effects of heavy-ion irradiation on expression and activities of other cellular factors should be analyzed to elucidate its biological effects on human cells.

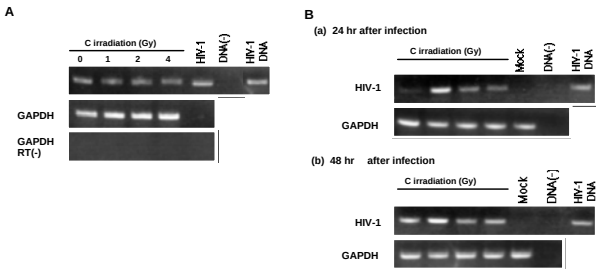

Fig. 1. The susceptibilities of NP-2/CD4/CCR5 cells to HIV-1 after heavy-ion irradiation. (A) Effects of heavy-ion irradiation on binding of HIV-1 to cells. NP-2/CD4/CCR5 cells were irradiated with heavyion at different doses and exposed to HIV-1 Ba-L strain for one hour at 4℃. HIV-1 bound on the cells was detected by RT-PCR. Expression of GAPDH mRNA was detected by RT-PCR as controls. (B) Reverse-transcription of HIV-1 in irradiated NP-2/CD4/CCR5 cells. Reverse-transcribed HIV-1 DNA was detected by PCR after 24 and 48 hour after viral exposure.

Reference

1) Y. Soda et al., Biochem. Biophys. Res. Comm. 258 (1999) 313.

3-39 Morphological Study on the Effects of Heavy Ion Irradiations to the Isolated Muscle Fibers of SJL Mice

H. Yorifuji [a,b], M. Hino [a,b], S. Wada [c], Y. Tajika [a], Y. Morimura [a], N. Hamada [b,c,d], T. Funayama [c], T. Sakashita [c], T. Kakizaki [c] and Y. Kobayashi [b,c,d]

[a]Department of Neuromuscular and Developmental Anatomy, and [b]The 21st COE Program, Gunma University Graduate School of Medicine, [c]Radiation-Applied Biology Division, QuBS, JAEA, [d]Department of Quantum Biology, Gunma University Graduate School of Medicine

Muscular dystrophy is a hereditary disease characterized by progressive muscle wasting and degeneration. Although many genes affected by the disease have been elucidated, there remains a wide gap between the mutations of the genes and the development of the disease. We are trying to use irradiations of heavy ion beams to skeletal muscle cells to understand the pathophysiology of the disease.

In a major subgroup of muscular dystrophy, products of the affected genes are localized in or around the plasma membrane. Their absence is supposed to cause the fragility of the membrane, which leads to the degeneration of the muscle fibers. In a previous study[1,2], we found that the irradiation of heavy ion microbeams on isolated single fibers of the skeletal muscle caused the damage of the sarcolemma, which induced irregular protrusions and invaginations of the plasma membrane, in addition to the changes of the cytoplasmic structures such as disarrangement of the myofilaments, enlargement of the cisternae of sarcoplasmic reticula containing flocculent matter and increase of autophagy.

Here, we report the results of heavy ion irradiation to the isolated single fibers of SJL mice, which have a mutation in dysferlin gene and are the model animal of limb-girdle muscular dystrophy type 2B and Miyoshi muscular dystrophy.

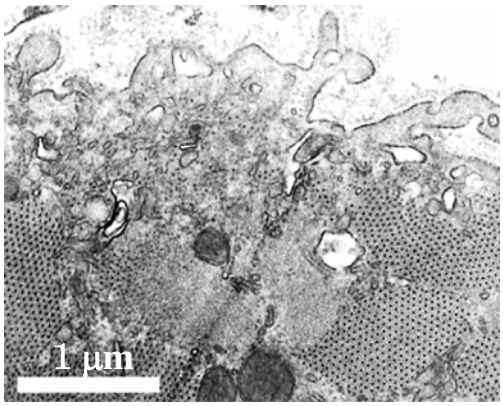

Fig. 1 Isolated single fiber of SJL mouse irradiated with ^{20}Ne-microbeam. Irregular protrusions and invaginations of sarcolemma, disarrangement of thick filaments, and enlargement of cisternae of endoplasmic reticula were observed. Some autophagic vacuoles were also seen.

Single fibers of SJL mice were isolated by collagenase treatment and plated on CR-39 plastic cover slips. Specimens were irradiated with either microbeam (^{40}Ar: 11.2 MeV/amu or ^{20}Ne: 12.8 MeV/amu) or broadbeam (^{40}Ar: 460 MeV or ^{20}Ne: 260 MeV, total 1-10 Gy). After irradiation, the muscle fibers were fixed at various time points and processed for electron microscopy.

The irradiated fibers of SJL mice showed the same change as those found in control ICR mice (Fig. 1), namely irregular protrusions and invaginations of plasma membrane, disarrangement of thick filaments, distended cisternae of endoplasmic reticula containing flocculent matter, and increase of autophagy. In addition, vesicles of unknown origin and autophagic vacuoles intermingled with disarranged thick filaments were observed in some areas under the sarcolemma (Fig. 2). These vesicles may be concerned with the disturbed turnover of the membrane system, as dysferlin, which is absent in SJL mice, is proposed to be involved in the event.

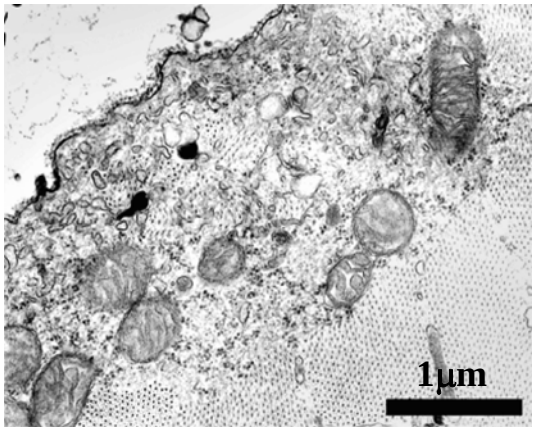

Fig. 2 Isolated single fiber of SJL mouse irradiated with ^{20}Ne-broadbeam (1 Gy). Undulation of the sarcolemma and disarranged thick filaments under the plasma membrane were observed. Vesicles of unknown origin and autophagic vacuoles intermingled with disarranged thick filaments.

References

1) M. Hino et al., Cell Struct. Funct. 32 (2007) 51-56.
2) H. Yorifuji et al., JAEA Takasaki Ann.Rep. 2006 (2007) 106.

3-40 Relative Biological Effectiveness of Carbon Beams on Cell Neurons; Approach Using Growth Cone Collapse Assay

W. S. Al-Jahdari [a,c)], Y. Yoshida [a,c)], N. Hamada [b,c,d)], T. Funayama [d)], T. Sakashita [d)], Y. Kobayashi [b,c,d)] and T. Nakano [a, c)]

Departments of [a)]Radiation Oncology and [b)]Quantum Biology, Gunma University Graduate School of Medicine, [c)]The 21st Century Center of Excellence Program for Biomedical Research Using Accelerator Technology, [d)]Radiation-Applied Biology Division, QuBS, JAEA

The relative biological effectiveness (RBE) on neurons are believed to be difficult to be evaluated due to the complexity for culturing them alone, which has meant that their radio-sensitivity has not been well investigated. The growth cone collapse (GCC) assay has been reported as a useful means of quantifying the effects of various factors on cultured explants of nervous tissue [1-2)]. Here, we used the GCC assay to determine the RBE of carbon beams to X-rays on the cell neurons.

Dorsal root ganglia (DRG) and sympathetic ganglion chains (SYMP) were isolated from day-16 (mature) and day-8 (immature) chick embryos and cultured for 20 h [3)]. Thereafter, neurons were exposed to graded doses of X-rays, or high-LET ^{12}C ions (18.3 MeV/amu, 108 keV/μ m). Morphological changes of the neurons were examined quantitatively by GCC assay. Apoptosis induction was examined using TUNEL assay (Fig. 1).

Carbon beams induced GCC and neurite destruction in a time and dose–dependent manner (Fig. 2). Day-8 neurons were more radiosensitive than day-16 neurons ($p=0.01$). At 12 h post-irradiation, 20 Gy carbon beams and 30 Gy X-rays induced about 65% and 25% apoptosis, respectively. The simple regression analysis revealed that the carbon beams RBE at day-8 DRG and SYMP using the GCC data were 4.6 and 4.2, respectively. Whilst, at day-16 DRG and SYMP were 3.4 and 3.3, respectively. However, the RBE at day-8 DRG and SYMP for apoptosis induction was 4.1 and 3.7, respectively, whereas that at day-16 DRG and SYMP was 4.2 and 3.7 respectively. The carbon beams were 3.3-4.6-fold more effective than X-rays for inducing GCC and apoptosis on neurons. Our implication is that attention should be considered when estimating the therapeutic dosage of carbon beams clinically. GCC assay could be beneficial in *in vitro* radiobiological investigations.

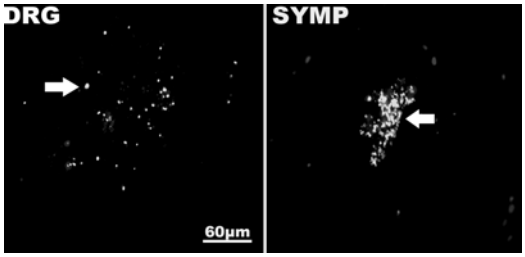

Fig. 1 Day-16 for both DRG and SYMP after exposure to 10 Gy. Some apoptotic cells (TUNEL-positive) were indicated by arrow and has gleaming appearance, and non apoptotic cells were shown as gloomy spots. Number of ganglia used n = 16. Scale bar = 60 µm

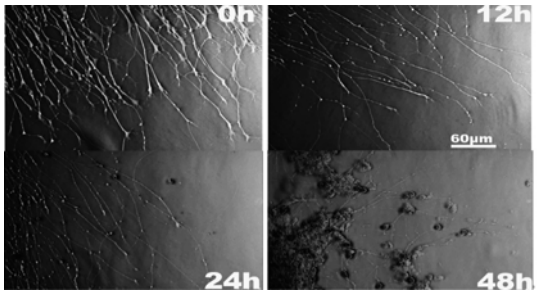

Fig. 2 Growth cones and neurites' morphological appearance. (0 h) before exposure, 12, 24 and 48 h after exposure with 10 Gy carbon beams.

References

1) Raper et. al., Neuron; 4 (1990) 21.
2) Saito et al., Neurosci. Lett. 229 (1997) 73.
3) Bottenstein et al., Exp Cell Res 125 (1980) 183.

3-41 Cell-killing Effect in Bystander Cells Induced by Carbon-ion Microbeams

M. Suzuki [a)], Y. Furusawa [a)], T. Funayama [b)], N. Hamada [b,c)], C. Tsuruoka [a)], T. Sakashita [b)], T. Kakizaki [b)], T. Hara [b,c)], K. Fukamoto [b)], Y. Yokota [b)] and Y. Kobayashi [b,c)]

[a)]Research Center for Charged Particle Therapy, NIRS, [b)]Radiation-Applied Biology Division, QuBS, JAEA, [c)]Department of Quantum Biology, Gumma University Graduate School of Medicine.

A central paradigm in radiation biology has been that only cells "hit" by a track of radiation would be affected to induce radiobiological consequences, and cells "not hit" should not be. This paradigm is the basis for the current system for risk estimation of radiobiological effects. Also, the risk of radiation-induced cancer after high and moderate doses is relatively well known, based on the data from detailed epidemiological studies of the Japanese atomic bomb survivors in Hiroshima and Nagasaki[1)]. However, it recently has been challenged by so called non-targeted effects, such as genomic instability, adaptive response and bystander effect, and such radiation-induced non-targeted effects may have important implications for risk evaluation of low dose / low dose rate radiations.

This year, we have begun to investigate cellular bystander responses in normal human fibroblasts induced by carbon-ion microbeams. Carbon-ion microbeams ($^{12}C^{5+}$, 220 MeV) were generated with the HZ1 port at TIARA. Approximately 6 x 10^5 exponentially growing cells were inoculated into each of microbeam dish, which was constructed with an aluminum ring of 36 mm diameter and attached 7.5 μm-thick polyimide film on the bottom of the ring, 2 days before irradiation. One day after plating, half of the dishes were treated with a specific inhibitor of gap-junction mediated cell-cell communication (40 μM of γ -isomer of hexachloro-cyclohexane). At the irradiation period, cultures were confluent. Cell cycle distribution of the confluent cultures were analyzed using a flow cytometory and around 95% of the cells were G_1- or G_0-phase. Irradiation was carried out using a 256 (16 x 16)-cross-stripe method (Fig.1). Microbeams of 20 μm in diameter were irradiated in each point with 8 delivered ions.

Figure 2 showed cell-killing effect, which was detected with a colony-forming assay as a reproductive cell death, in microbeam-irradiated dishes (IR) and microbeam-irradiated dishes with a specific inhibitor of gap-junction mediated cell-cell communication (IR+L). The percent cell survival in microbeam-irradiated dishes was ranging from 83% to 94%, while from 97% to 100% in microbeam-irradiated dishes with a specific inhibitor of gap-junction mediated cell-cell communication. In our microbeam-irradiation method, we estimated that the percent of C-ion direct hit cells was ranging from 0.08% to 0.2% of all cells in the dish. The results showed a higher cell-killing effect in the microbeam-irradiated cell population than that with a specific inhibitor of gap-junction mediated cell-cell communication. Our studies provide clear evidence that microbeam-irradiated cells can induce a bystander lethal response in neighboring cells, which are not directly hit by C ions and gap-junction mediated cell-cell communication play an important role in the bystander effect.

Reference

1) D.A.Pierce and D.L.Preston, Radiat. Res., 154 (2000) 178.

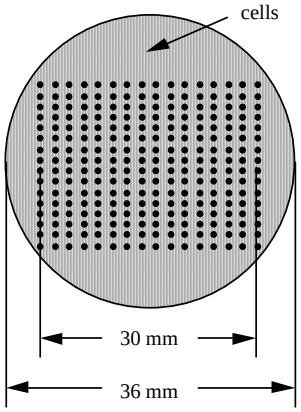

Fig.1 Microbeam-irradiation procedure of normal human fibroblasts using a 256 (16 x 16)-cross-stripe method. A microbeam dish was constructed with an aluminum ring of 36 mm diameter and attached 7.5 μm-thick polyimide film on the bottom of the ring.

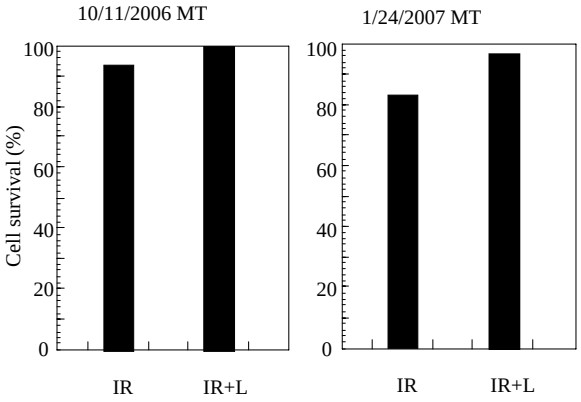

Fig.2 Representative cell-killing effects in normal human fibroblasts irradiated with C-ion microbeams treated with (IR+L) / without (IR) a specific inhibitor of gap-junction mediated cell-cell communication (40 μM of γ -isomer of hexachloro-cyclohexane) of 2 independent beam times.

3-42 Ion Beam Irradiation Has Different Influences on Glutathione Peroxidase of Cultured Human Retinal Vascular Endothelial Cells Exposed to L-dopa among ^{20}Ne, ^{12}C and ^{4}He

K. Akeo [a,b], N. Hamada [c,d], Y. Kobayashi [c,d], T. Funayama [c], T. Sakashita [c], K. Kawada [a] and Y. Akeo [a]

[a]Akeo Eye Clinic, [b]Department of Ophthalmology, Keio University School of Medicine, [c]Radiation-Applied Biology Division, QuBS, JAEA, [d]Department of Quantum Biology, Division of Bioregulatory Medicine, Gunma University Graduate School of Medicine

It is well-known that the damage of retinal endothelial (RE) cells is one of causes as pathogenesis in senile macular degeneration and diabetic retinopathy. Glutathione peroxidase (GPX), a selenium-dependent and lipid peroxide-scavenging enzyme that effectively reduces lipid peroxides with the concomitant oxidation of glutathione is distributed in mitochondria [1]. Faucher et al. measured the expression of two bcl-2 family members, bax and bcl-2, in a human endothelial like cell-line overexpressing the organic hydroperoxide-scavenging enzyme GPX, in the absence of any apoptotic/oxidant stimulus, and showed that overexpressing an antioxidant gene such as GPX in endothelial cells is able to change the basal mRNA and protein bax levels without affecting those of p53 and bcl-2. This phenomenon could be useful to antiatherogenic therapies which use antioxidants with the aim of protecting the vascular wall against oxidative stress injury [2]. The irradiation is known to result in a dose-dependent decline in the activities of GPX in the skin of mice [3]. The gamma ray (^{60}Co) causes ionization uniformly in the whole irradiated tissue. We found out that high dose of gamma irradiation prevented programmed cell death regulated by p53 and bcl-2 genes in the ciliary body dissected from living body, and was useful for preservation of organ after culture by the protective influence of inflammatory reaction [4]. Deficiency of L-dopa causes degeneration of the substantia nigra in the brain and L-dopa is used in the treatment of Parkinson's disease. We proved that L-dopa produced NO and superoxide, and had the cytotoxic effects on the retinal pigment epithelial cells [5]. L-dopa injected into the vitreous of the rats dilated the vena in the ciliary body [6]. We wondered if RE cells could be exposed to oxidative stress by administrated L-dopa. We already reported that oxidative stress such as hyperoxia [7] augmented the cytotoxicity of the aortic endothelial cells by L-dopa. We investigated how L-dopa influenced GPX in mitochondria and the cytoplasm of the RE cells that prevented from damage of phospholipid of cell membrane. We applied the ion beams as the induction of the oxidative stress that influenced GPX against in the RE cells, and measured the expression GPX with LightCycler system as a real time-reverse-transcriptase polymerase chain reaction (RT-PCR).

Established human RE cells in vitro incubated with L-dopa (250 μM) for 2 hrs were exposed to an ionization radiation that is induced by acceleration of the ionizing atom of 350 MeV ^{20}Ne, 220 MeV ^{12}C, and 50 MeV ^{4}He. We obtained the RE cells after 0, 4, 8, 24 hr of the irradiation and extracted total cellular RNA and cDNA was synthesized. We used the Primer3 website to design the primers for RT-PCR amplification of the cDNA of GPX and 18S RNA. The reactions were carried out at the following temperature: 95 ℃, for denaturation; 60 ºC, for annealing; and 72 ºC, for extension for 17–27 cycles. After mixing the cDNA, primer, and SYBR green, the expression of 18S RNA and GPX was measured using the LightCycler system. The technology of this system is extremely innovative and enables rapid and simultaneous evaluation PCR experiments. Fluorometric analysis of the formed PCR products was performed as a real-time measurement either continuously or at specifically defined time points during each PCR cycle.

Exposure to L-dopa inhibited the expression of GPX in RE cells. Ion beam irradiations both of ^{4}He and ^{12}C decreased more remarkably than ^{20}Ne. The expression of GPX in RE cells incubated with L-dopa decreased significantly after 8 hrs of exposure to ^{4}He, and after 4 and 24 hrs of exposure to ^{12}C. On the contrary, ion beam irradiation of ^{20}Ne increased the expression of GPX in RE cells incubated with L-dopa after 4 hrs of the exposure of the irradiation significantly. We considered the different accumulation of the energy irradiated at a point by various ions could be concerned with the effects on the expression GPX in RE cells incubated with L-dopa.

References

1) K. Watanabe, Tran.Soc Pathology Jpn 76 (1986) 39.
2) K. Faucher et al., Mol Cell Biochem. 277 (2005) 81.
3) J.G. Chandra et al., Clin Chim Acta 332 (2003) 111.
4) K. Akeo et al., Exp. Animals. 55 (2006) 375.
5) K. Akeo et al., Pigment Cell Res. 13 (2000) 80.
6) S.A. Amaki et al., Pigment Cell Res. 14 (2001)256.
7) K.Akeo et al., Exp. Eye Res. 49 (1989) 335.

3-43 Analysis of Lethal Effect Induced by Ion Beams in Canine Spontaneous Tumor Cells

S. Wada [a)], T. Ito [a)], T. Kakizaki [a)], T. Funayama [b)], T. Sakashita [b)], Y. Kobayashi [b)] and N. Ito [a)]

[a)]Department of Veterinary Medicine, Kitasato University, [b)]Radiation-Applied Biology Division, QuBS, JAEA

Due to the recent understanding of animal diseases and preventive medication including vaccination and premedication, companion animals can live much longer than before. These changes made it possible to reduce severe infectious diseases, and then made diseases of companion animals shifts from infectious diseases to the aging-related metabolic disorders and neoplasm (cancer) formation. Radiotherapy is considered to be one of the good choices for the medical treatment against cancer. In human medicine, new radiotherapy such as high-LET heavy-ion beam radiotherapy has been introduced, because of its higher lethal effect than that of low LET radiation such as X- rays and γ-rays. However, in veterinarian medicine, there is still limited data on X-ray and γ-ray radiotherapy to dogs and cats, and needless to say, no study on ion beam radiotherapy. Therefore, to establish a proper protocol for radiotherapy on the animals, we investigated the fundamental aspects of the radiation effects on cancer cells of companion animals.

Even in the human medicine, the protocol for heavy ion radiotherapy still cannot be say well optimized, and the investigation for its establishment is still undergone. Of course, the dose per fraction of heavy ion therapy may become lower than that of X-ray therapy, because of its higher lethal effect. However the effects of low dose radiation has only been estimated by extrapolation from the data obtained by the higher dose radiation and not considered a concept of low dose specific biological responses such as adaptive response, radiation induced bystander effects, and low dose radio-hypersensitivity. Because the effect of those phenomenons cannot be estimated by extrapolation from the data obtained by high dose exposure, we also investigated lethal effects induced by low dose/dose-rate radiation that is considered to be important on heavy ion radiotherapy.

Cell lines used for this experiment were melanoma cell from spontaneously generated canine tumor. The cells were irradiated with 20 MeV H^+ ions (2.7 keV/μm), 220 MeV $^{12}C^{5+}$ ions (108 keV/μm) or X-rays at a dose rate of 0.8 Gy/min at a room temperature and replated on tissue culture dishes at a given density to measure the rates of the surviving cells. About 8 days after the irradiation, colonies of the cells were stained and counted. The survival rates against the given doses were plotted and fitted to a linear-quadratic model.

The survival curves of carbon ion irradiation showed almost linear in logarithmic scale and had no shoulder, but the curves of proton and X-ray irradiation showed to have shoulders. The lethal effect was highest by carbon ion irradiation among three types of radiation. The relative biological effectiveness (RBE) of proton and carbon ions calculated from the dose required to give 10 % of survival rate was 1.32 and 2.82, respectively. These results indicate that the lethal effect increase a with LET value of ion beams.

The low dose survival rates measured by proton and X ray irradiation showed good agreement to the extrapolated curve from the data of high dose irradiation. On the other hand, low dose survival rates by carbon ion irradiation were less than the estimated value from extrapolated curve of the high dose irradiation (Fig. 1). This result indicates that the lethal effect by low dose carbon ion irradiation is higher than estimated effect based on higher dose irradiation data. Additionally, we observed the treatment with DMSO, a radical scavenger, after low dose carbon ion irradiation restored the rate of survival to the value that is extrapolated from high dose irradiation (Fig. 2). This result indicates there is some participation of radicals in killing effects of low-dose carbon irradiation. In conclusion, the application of carbon ion radiotherapy to malignant melanoma therapy on companion animals would lead high therapeutic effects.

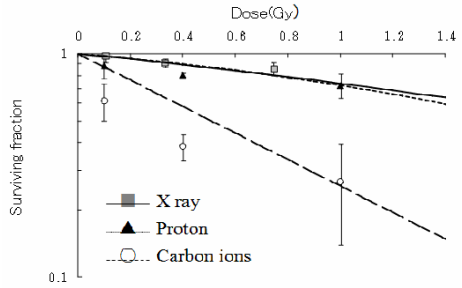

Fig. 1 Rate of survival of canine melanoma cell lines after low dose exposure. Lines of survival curves were extrapolated from 1-8 Gy irradiation data.

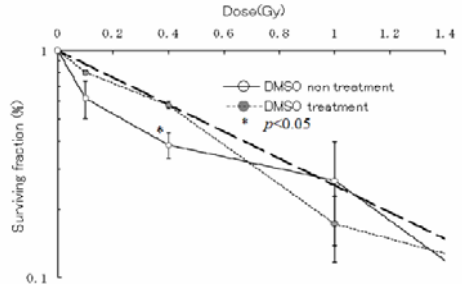

Fig. 2 Comparison of lethal effect by treatment with or without DMSO after low dose carbon ion irradiation. Dashed line was extrapolated from 1-4 Gy irradiation data.

3-44 Food-NaCl Associative Learning in Response of *C. elegans* to Gamma-ray Irradiation

T. Sakashita [a)], M. Suzuki [a)], K. Fukamoto [a)], T. Funayama [a)], S. Wada [a, b)], Y. Kobayashi [a, b)], D. D. Horikawa [c)] and A. Bolige [d)]

[a)]Radiation-Applied Biology Division, QuBS, JAEA, [b)]Department of Quantum Biology, and The 21st Century COE Program, Gunma University Graduate School of Medicine, [c)]Graduate School of Science, University of Tokyo, [d)]United Graduate School of Agricultural Science, Iwate University

Learning impairments following ionizing irradiation as well as DNA damages is an important potential risk for astronauts[1)]. We used *Caenorhabditis elegans* as a neuronal model organism, and previously reported that ionizing radiation affected food-NaCl associative learning behavior only at the transition stage of learning conditioning, which induced additional decreases in chemotaxis to NaCl immediately after irradiation. In the present study, we investigated the effects of gamma-ray irradiation on the time-course and chemotaxis to benzaldehyde.

We used well-fed adults grown on the plate containing 10 ml of the nematode growth medium agar[3)] and spread with the *E. coli* at 20 ˚C in all experiments. Using the method of Saeki et al.[2)] with some modifications, we evaluated the chemotaxis to NaCl. Animals move freely for 15 min on the 6-cm diameter assay plate with a gradient of NaCl concentration. When animals reach to the test spot or control spot, they were paralyzed by NaN_3. The test spot is the place with highest concentration (100 mM) of NaCl in the plate. The control spot is 4 cm away from the test spot. The chemotaxis index (CI) was calculated as the following equation; CI = { (number of animals within 1.5 cm diameter of the test spot) – (number of animals within 1.5 cm diameter of the control spot) } / (total number of animals on the assay plate). For the benzaldehyde assay, we used the 10-cm plates, in which 1 µl of ethanol or 0.5 % vol/vol benzaldehyde in ethanol was spotted at the control or test spot, respectively. The test spot was 6 cm away from the control spot, and NaN_3 was spotted to the both.

To test the effects of gamma-rays on the time-course, animals on the NaCl-conditioning plates (food-/NaCl+) were exposed to gamma-rays from ^{60}Co sources, Japan Atomic Energy Agency (JAEA). We measured chemotaxis at the time points of immediately after irradiation, 1, 3, 5 h after irradiation. NaCl-conditioning was continued during the post irradiation. As shown in Fig. 1, animals exposed to gamma-rays showed significant decreases in chemotaxis immediately after irradiation and complicated responses on post-irradiation. Animals exposed to the dose of 118 or 332 Gy showed almost the same level in CI 5 h after irradiation, whereas the CI of animals exposed to the highest dose increased up to the about 0.4.

Gamma-ray irradiation during the stage of conditioning for associative learning induced the significant decrease in CI of *C. elegans*, and then did show the complicated responses. We had the question whether other functions of the nervous system were also affected by gamma-ray irradiation. Thus, we examined the chemotaxis to benzaldehyde of animals with same conditioning and exposure as the previous result (Fig. 1). The CIs for chemotaxis to benzaldehyde were 0.84 ± 0.04 (0 Gy), 0.82 ± 0.03 (481 ± 32 Gy) immediately after irradiation, and 0.81 ± 0.02 (0 Gy), 0.81 ± 0.03 (481 ± 32 Gy) 5 h after irradiation. There was no significant difference in CI. Thus, animals exposed to gamma-rays did show the normal chemotaxis to benzaldehyde, whereas chemotaxis to NaCl was affected at the transition stage of associative learning.

These results may suggest the specific effects of gamma-rays on functions of the nervous system in *C. elegans*.

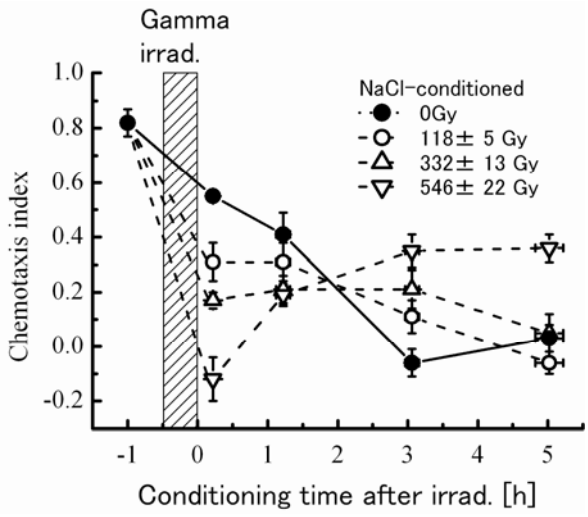

Figure 1. Time course of CI in NaCl-conditioned and exposed animals during the post irradiation. The error bars indicate the standard error of mean (SEM) from 5 or more experiments.

References

1) Koike et al., Acta Astronautica 56 (2005) 367.
2) Saeki et al., J. Exp. Biol. 204 (2001) 1757.
3) Brenner, S., Genetics 77 (1974) 71.

3-45 Food-NaCl Associative Learning in Response of *C. elegans* to High-LET Carbon Ion Beam Irradiation

T. Sakashita [a)], M. Suzuki [a)], T. Kakizaki [a)], T. Funayama [a)], N. Hamada [a, b)], S. Wada [a, b)] and Y. Kobayashi [a, b)]

[a)]Radiation-Applied Biology Division, QuBS, JAEA, [b)]Department of Quantum Biology, and The 21st Century COE Program, Gunma University Graduate School of Medicine.

Learning impairments following ionizing irradiation is an important potential risk for astronauts as well as DNA damages[1)]. Using *Caenorhabditis elegans* as a neuronal model organism, we previously showed that ionizing radiation affected food-NaCl associative learning behavior only at the transition stage of learning conditioning, which induced additional decreases in chemotaxis to NaCl immediately after irradiation. In the present study, we investigated the effects of high-LET carbon ion beam irradiation on the ability of associative learning and chemotaxis to benzaldehyde.

Well-fed adults grown on the plate containing 10 ml of the nematode growth medium agar[2)] and spread with the *E. coli* at 20 ˚C were used in all experiments. Chemotaxis to NaCl was measured by the method of Saeki et al. [3)] with some modifications. Animals (*C. elegans*) move freely for 15 min on the 6 cm diameter assay plate with a gradient of NaCl concentration. When they reach to the test spot or control spot, they were paralyzed by NaN_3. The test spot is the place with highest concentration (100 mM) of NaCl in the plate, and the control spot is 4 cm away from the test spot. The chemotaxis index (CI) was calculated as the following equation; CI = { (number of animals within 1.5 cm diameter of the test spot) – (number of animals within 1.5 cm diameter of the control spot) } / (total number of animals on the assay plate). For the benzaldehyde assay, we used the 10 cm plates. 1 µl of ethanol or 0.5 % vol/vol benzaldehyde in ethanol was spotted at the control and test spots, respectively. The test spot was 6 cm away from the control spot, and NaN_3 was spotted to the both.

To test the effects of carbon ions on the ability of associative learning, animals on the mock-conditioning plates (food-/NaCl-) were exposed to ^{12}C (220 MeV, 113.3 keV/µm) delivered from the azimuthally-varying-field cyclotron installed in the Takasaki Ion Accelerators for Advanced Radiation Application (TIARA) facility, Japan Atomic Energy Agency (JAEA). Immediately after irradiation, animals were transferred to the NaCl-conditioning plates (food-/NaCl+) and placed for 4 hours to perform the conditioning for the food-NaCl associative learning. Subsequently, the chemotaxis assays were carried out. As shown in Fig. 1, there was no significant difference in CI between exposed and non-exposed animals. Thus, the result suggests that exposure to carbon ions dose not induce the decrease of the ability of food NaCl associative learning in *C. elegans*. This result is in accordance with that of animals exposed to ^{60}Co gamma rays.

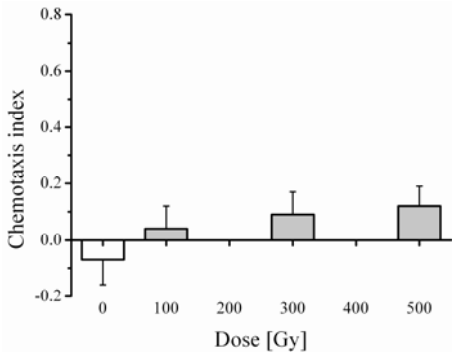

Fig. 1. Dose response of the ability of associative learning. The error bars indicate the standard error of mean (SEM) from 4 experiments.

We have been reported that carbon ion irradiation during the stage of conditioning for associative learning induce the significant decrease in CI of *C. elegans*. The finding raises the question whether other functions of the nervous system are also affected by carbon irradiation. Thus, we examined the chemotaxis to benzaldehyde of animals with same conditioning and exposure as the previous report. There was no significant difference in CI (Fig. 2). Thus, animals exposed to carbon-ions showed the normal chemotaxis to benzaldehyde, whereas chemotaxis to NaCl was affected at the transition stage of associative learning. These results suggest that the carbon ion irradiation did not affect all functions of the nervous system in *C. elegans*.

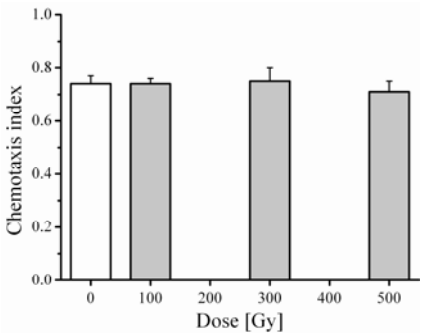

Fig. 2. Dose response of chemotaxis to benzaldehyde. The error bars indicate the standard error of mean (SEM) from 4 experiments.

References

1) Koike et al., Acta Astronautica 56 (2005) 367.
2) Brenner, S., Genetics 77 (1974) 71.
3) Saeki et al., J. Exp. Biol. 204 (2001) 1757.

3-46 Effect of Energetic Heavy-ion Irradiation on Gene Expression in *Caenorhabdits elegans*

A. Higashitani [a)], C. Mori [a)], T. Kimura [a)], T. Ikenaga [a)], T. Takanami [a)], T. Sakashita [b)], S. Wada [b,c)], N. Hamada [b,c)] and Y. Kobayashi [b,c)]

[a)]Graduate School of Life Sciences, Tohoku University, [b)]Radiation-Applied Biology Division, QuBS, JAEA, [c)]Department of Quantum Biology, and The 21st Century Center of Excellence Program, Gunma University Graduate School of Medicine

Heavy ion irradiation, which is more effective than γ irradiation in inducing DNA damage and gene mutation, has been used for cancer therapy to kill tumor cells. Masumura et al.[1)] reported that carbon particles induce deletions, generally greater than 1,000 base pairs in size, whereas γ-rays induce base substitutions and deletions of less than 100 base pairs. Other different effects of heavy ion irradiation are not well understood. We, therefore, study the effect of heavy ion and γ irradiation on gene expression with DNA microarray analysis of entire genome in *Caenorhabditis elegans*.

As a model organism *C. elegans* is easy to handle and genetically well-characterized, and its development and life cycle are well understood. In addition, the transcriptional profiles of individual cells or tissues at different developmental stages have been previously reported[2)]. Here, we compared the transcriptional profiles of nematodes that were exposed to either $^{12}C^{5+}$ ion broad beam (220 MeV) delivered from the AVF cyclotron or ^{60}Co γ-rays using the whole genome *C. elegans* GeneChip array (Affymetrix, Santa Clara, CA).

To prepare the RNA for microarray analysis, N2 bristol wild-type hermaphrodites were synchronously cultured on *Escherichia coli* OP-50 NGM plates at 20 ℃. Young adult hermaphrodites (24 h after the L4 larval stage) were exposed to 100 Gy of $^{12}C^{5+}$ ion beam and γ-rays, and were collected 4 h later. Total RNA in each 10^3 worms was isolated with the TRIzol Reagent (Invitrogen Corporation, Carlsbad, CA) and was used as a template for generating probes using the One-Cycle Target Labeling and Control Reagents package (Affymetrix, Santa Clara, CA). Transcriptional alterations between heavy ion irradiated samples, 100 Gy γ-irradiated samples and non-irradiated controls were measured. Following heavy ion irradiation, 297 transcripts (approximately 1.3 % of the total transcriptome) were upregulated 2 fold or greater (Fig. 1). 388 transcripts were reduced at least 2 fold (Fig. 1). On the contrary, 187 transcripts were upregulated 2 fold or greater and 358 transcripts were down regulated at least 2 fold after γ-ray irradiation (Fig. 1). Interestingly, there were only 51 (upregulated) and 54 (down regulated) transcripts that were similarly affected by both irradiations (Fig. 1).

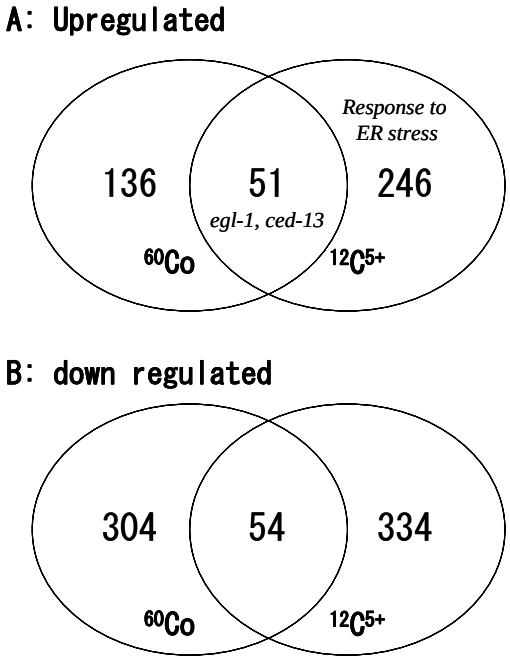

Fig.1 Alterations of gene expression by irradiation of either heavy ion particles or γ-ray radiations.

We further characterized the transcripts which were upregulated following treatment according to gene function. The expression levels of genes related to apoptotic inducer containing BH3 domain, *egl-1* and *ced-13*, and glutathione S-transferase genes, *cdr-2*, *cdr-3*, *gst-5* and *gst-6*, were significantly upregulated by either irradiation. It suggests that apoptosis and oxidative stress are similarly induced by 100 Gy of $^{12}C^{5+}$ ions and γ-rays.

In contrast to γ-rirradiated worms, certain genes mediating response to endoplasmic reticulum (ER) stress were significantly and specifically induced in heavy ion-irradiated worms. These results suggest that the heavy ion irradiation may efficiently cause both DNA damage and ER stress. It has been known that heavy ion particle irradiation efficiently causes apoptotic cell death[3, 4)]. All together, ER stress induced by heavy ion particle irradiation may be a direct trigger of apoptotic induction.

References

1) K-I. Masumura et al., Environ. Mol. Mutagen. 40 (2002) 207
2) SJ. McKay et al., Cold Spring Harb. Symp. Quant. Biol. 68 (2003) 159
3) A. Takahashi et al., Int. J. Radiat. Oncol. Biol. Phys. 60 (2004) 591.
4) M. Aoki et al., J. Radiat. Res. 41 (2000) 16.

3-47 Radiation Tolerance Linked to Anhydrobiosis in *Polypedilum vanderplanki*

Y. Nakahara [a)], M. Watanabe [a)], T. Kikawada [a)], A. Fujita [a)], D.D. Horikawa [a,b,d)], T. Okuda [a)], T. Sakashita [b)], T. Funayama [b)], N. Hamada [b,c)], S. Wada [b,c)] and Y. Kobayashi [b,c)]

[a)]Anhydrobiosis Research Unit, National Institute of Agrobiological Sciences, [b)]Radiation-Applied Biology Division, QuBS, JAEA, [c)]Department of Quantum Biology, Gunma University Graduate School of Medicine, [d)]Graduate School of Science, The University of Tokyo

The larvae of the sleeping chironomid, *Polypedilum vanderplanki*, are able to withstand almost complete desiccation during which they enter a state of suspended animation[1)], this phenomenon is known as anhydrobiosis[2)]. The anhydrobiotic larva can tolerate various extreme conditions including high doses of radiation[3,4)]. Since physiological status is drastically changed during entry into anhydrobiosis[5)], it is of great interest to know how the desiccating larvae gain radiation tolerance.

We first examined effects of high-LET radiation on 4 kinds of larvae (Fig. 1): normal hydrated larva (W-low), intermediates between the anhydrobiotic and normal hydrated state (W-mid), almost completely dehydrated (anhydrobiotic) larvae (D-high), and immediately-rehydrated larvae that are assumed to have a similar molecular profile to anhydrobiotic larvae (W-high)[6)]. These samples were exposed to 1 to 4500 Gy of 50 MeV ^{4}He (LET_∞=16.2 keV/μm) ion beam delivered from the azimuthally- varying-field cyclotron at TIARA. Irradiated larvae were supplied with distilled water and diet. Larvae that moved their pharyngeal plunger were considered to be survivors.

At doses between 3500 and 4500 Gy, differences in radiation effects became pronounced, depending on the physiological state of the larvae (Fig. 2). For all doses studied, survival period after radiation was greatest in D-high, followed by W-high, W-mid, and finally W-low. This result indicated that radiation tolerance increased as anhydrobiosis progresses. We previously thought that tolerance against various stresses in *P. vanderplanki* larvae is achieved by a complete desiccation. However, radiation tolerance was increased even in hydrated larvae as well, suggesting the protection mechanisms different from what we have speculated in desiccated state.

It is possible that trehalose itself has radioprotective effects in hydrated larvae of *P. vanderplanki*[3)]. However, high-LET radiation mainly causes harmful damage to DNA by direct action, which is not reduced by protective agents. Therefore, it could not be determined whether trehalose inhibits a direct action of high-LET radiation in *P. vanderplanki*. Alternatively, we assume that DNA repair capacity is increased in desiccating larvae[4)]. We reexamined the EST (expresses sequence tag) database from desiccating *P. vanderplanki*[5)] and found that fragments annotated as antioxidation enzymes such as thioredoxin reductase and glutation peroxidase, and DNA repair enzymes such as DNA photolyase and TFIIH, increased during dehydration. Full-length cDNA cloning awaits further studies.

Damage from radiation shares common traits with desiccation damage: e.g. oxidative stress and DNA break. Many anhydrobionts seem to cope with that challenge by antioxidative defense and DNA repair systems. Prompt repair of DNA upon rehydration can be achieved by provision of efficient repair systems during entry into anhydrobiosis. Therefore, the increased radiation tolerance in *P. vanderplanki* presented here is probably due to cross-protective effects caused by anhydrobiosis[6)].

References

1) Hinton, Proc. Zool. Soc. Lond. 121 (1951) 371.
2) Keilin, Proc. R. Soc. Lond. 150B (1959) 149.
3) Watanabe et al., Int. J. Radiat. Biol. 82 (2006) 587.
4) Watanabe et al., Int. J. Radiat. Biol. 82 (2006) 835.
5) Kikawada et al., Biochem. Biophys. Res. Commun. 348 (2006) 56.
6) Watanabe et al., J. Insect Physiol. 53 (2007) 573.

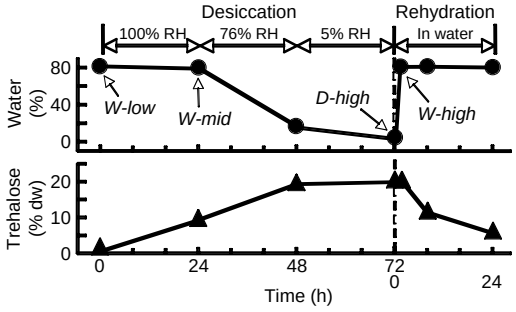

Fig. 1 Preparation of larvae with different physiological conditions. Intact larvae (W-low) were incubated at 100% relative humidity (RH) for 24 h (W-mid), and further 76% RH, and 5% RH, each for a day (D-high). D-high larvae were rehydrated in distilled water for 1 h (W-high).

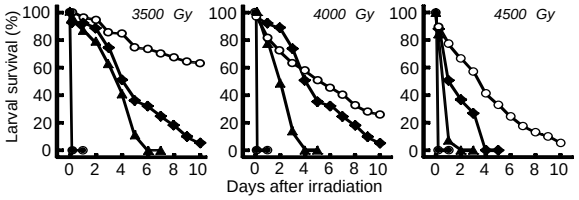

Fig. 2 Temporal changes in survival after high-LET radiation in *P. vanderplanki* larvae. Closed circle: W-low, triangle: W-mid, diamond: W-high, open circle: D-high.

3-48 Study on Regeneration Mechanism of the Heavy-ion Irradiated Hemopoietic Organ of the Silkworm, *Bombyx mori* -Timing of Degradation and Regeneration of the Irradiated Organ -

K. Shirai [a)], T. Sakata [a)], S. Tsuchiya [a)], K. Kiguchi [a)], K. Fukamoto [b)], T. Sakashita[b)], T. Kakizaki [b)], T. Funayama [b)], Y. Yokota [b)] and Y. Kobayashi[b)]

[a)] Faculty of Textile Science and Technology, Shinshu University, [b)] Radiation-Applied Biology Division, QuBS, JAEA

Our previous studies elucidated that, in *Bombyx mori*, the hemopoietic organ disrupted by the heavy-ion irradiation, would regenerate at wandering stage. This observation is a interesting phenomenon to investigate the hemopoietic stem cells in *B. mori*. However, the detailed mechanisms for degradation or regeneration on the irradiated organs have been obscured. In this study, the morphological changes of the hemopoietic organs after irradiation with 100Gy of carbon-ions at day 0 of 4th instar were observed. In addition, the stage-specific marker proteins were also identified by 2-D electrophoresis followed by peptide-mass fingerprinting (PMF).

The timings of degradation and regeneration of the organ irradiated at day 0 of 4th instar occurred at almost identical stages to those of the organs irradiated at day 3 of 4th instar. These results predict that the developmental condition in larva, including the hormonal condition, might influence the timing for the degradation and regeneration of the irradiated organ.

Two prominent protein spots were detected in the sample from the organs being disrupted (at day 2 of 5th instar) by 2D electrophoresis. Those two proteins, estimated as soluble alkaline phosphatase and eIF 2 alfa kinase by PMF, would be involved in the degradation process of the organ.

ほ乳類の細胞と比較して、一般に昆虫細胞は放射線照射に極めて耐性である。例えばカイコ幼虫の真皮細胞では表面線量400 Gyで炭素イオンを照射しても細胞死は認められない。その中で造血器官中の血球前駆細胞は、線量100 Gyで同じ炭素イオンを照射するとほとんど全ての細胞が致死・崩壊する比較的感受性の細胞である。ところが著者らは、炭素イオン照射により崩壊した造血器官が、その後、再生することを発見した。

本研究は重イオン照射されたカイコ幼虫造血器官の崩壊と再生の分子メカニズムを明らかにすることを目的にしている。これまでの研究では、重イオン照射後の造血器官の崩壊と再生の過程を調査し、さらにこの過程に体液中の循環血球が関与することを明らかにしてきた。平成 18 年度は、さらに詳細な分子メカニズムを明らかにするため、今後の研究に必須となる造血器官再生のタイムテーブルの作製とステージ特異的な分子マーカーの探索を行った。

実験には著者らの研究室で継代飼育している着色非休眠系統のカイコ幼虫を供試した。重イオン照射は原子力機構TIARAで行った。照射に用いたイオン種および線量は、炭素イオン($^{12}C^{5+}$、18.3 MeV/u、水中飛程：約1.1 ㎜)で、線量は100 Gyである。照射はカイコ幼虫の造血器官に局部照射した。

照射後、一定時間ごとに造血器官を採取し、電子顕微鏡試料を作製し内部の細胞を観察した。また、採取した造血器官中のタンパク質成分を調査するため、一部の器官からタンパク質成分を抽出し成分を2次元電気泳動で分離・分析した。特に顕著に変化が認められた成分については、トリプシンで消化後、MALDI-TOF/MSを利用したpeptide-mass fingerprintingにより同定を試みた。

まず4齢day0の幼虫造血器官に重イオンを照射し、その後の造血器官の再生過程を経時的に観察した。その結果、以前報告した4齢催眠期（day3）幼虫に照射した場合とほぼ同じ過程が確認された。すなわち、照射を受けた造血器官は、一旦崩壊し、その後再生した。

当初、本実験は照射する幼虫の発育ステージを3日間早め、造血器官再生に十分な時間を確保することで、再生造血器官から産出される血球種を追究する予定であった。しかし、予想に反し、照射造血器官の崩壊・再生は大きく遅延し、照射時期を3日間早めたにも関わらず、4齢day3幼虫に照射した場合とほとんど同時期であった。この結果は、造血器官の再生が照射後の経過時間ではなく、幼虫の発育ステージに影響されることを示唆する。

次に、造血器官の再生過程をさらに詳細に研究する上で、必須と思われる各ステージ特異的な分子マーカーを得るため、重イオン照射造血器官のタンパク質成分の経時的変化を2次元電気泳動で分析した。その結果、血球前駆細胞が致死・崩壊するステージである5齢day 2幼虫から得た試料中で照射サンプルのみ大きくその量が増大する2つの成分が認め、peptide-mass fingerprintingによる同定を試みた。その結果、これらの成分は可溶型のアルカリフォスファターゼおよびeIF2αキナーゼと推定された。

現在、得られた結果をもとに、さらに詳細な重イオン照射造血器官の崩壊と再生のタイムテーブルを作製中である。また、得られたステージ特異的マーカーについて、その関与を確認するとともに、造血器官崩壊期における役割について追究する予定である。

3-49 Influence of Local Irradiation with Heavy-ion Microbeam on the Incidence of Somatic Mutation Arising on the Larvae in Embryo and Yolk in the Egg of the Silkworm, *Bombyx mori*

T. Furusawa [a)], E.Suzuki [a)], S. Nagaoka [b)], H. Suzuki [c, d)], N. S. Ishioka [d, e)], N. Hamada [f, g)], S. Wada [f, g)], Y. Kobayashi [f, g)], T. Sakashita [f)], T. Kakizaki [f)], T. Funayama [f)] and K. Fukamoto [f)]

[a)]Center for Bioresource Field Science, Kyoto Institute of Technology, [b)]Fujita Health University, [c)]Japan Space Forum, [d)]Graduate School of Med. And Dental Sci, Kagoshima University, [e)]Japan Aerospace Exploration Agency, [f)]Radiation-Applied Biology Division, QuBS, JAEA, [g)]Department of Quantum Biology, and The 21st Century Center of Excellence Program, Gunma University Graduate School of Medicine

Irradiation of diapause eggs (heterozygote) with heavy ion beam induces somatic mutation appearing as white spots on the black integument during larval stage. The incidence of the somatic mutation was clearly estimated as individual level dependently on both dose and LET[1)]. The sensitivity was the highest level during the first 2 days after resumption of embryonic developments in the eggs, which terminated diapause status. Low dose irradiation with 2 mGy could induce the mutation [2)].

It remains unclear whether the somatic mutation would be induced by direct hit of the heavy particles to embryo, or indirect hit to yolk surrounding the embryo by bystandar effect. This leads us to examine the incidence of the somatic mutation by local hit of heavy ion particles to embryo or yolk in *Bombyx* eggs.

The eggs (P^S/p) were kept at 25 ℃ for first 10 days after oviposition, and then at 5 ℃ for 70 days to terminate diapasuse. These diapause-terminated eggs were transferred again to 25 ℃ for resumption of embryonic development. Carbon ion beam (3.0 Gy and 6.0 Gy) was irradiated to the 3-day old eggs after the resumption, and locally to 20μm^2 of the center (yolk) of the egg at 112 keV/μm and embryo at 119 keV/μm. After irradiation, the newly hatched larvae were reared on an artificial diet throughout all stages, and we counted the number of larvae with white spots on the black integument to examine the incidence of the somatic mutation.

For local irradiation, 10 eggs were lined up on vertical and horizontal line in 1 cm length each, namely 98 eggs were placed on 1 cm^2 of plastic film. But we did not place eggs at left corner on the first upper line and at right corner on the 10th lowest line to set fix points on the coordinate. The location of abdominal and caudal portion of embryo in each egg was determined under microscope, and was input in PC. According to this data, carbon ion-beam was hit on the definite location on each egg.

We set up two controls, one is placed at Kyoto and the other is carried to TIARA to check the influence of transport.

The incidence of the somatic mutation was 5 % in control of Kyoto, and 12 % in TIARA (Fig. 1). However, the irradiations of 3 Gy and 6 Gy to the center of egg did not result in the significant incidence of mutation between Kyoto and TIARA (Fig. 1).

In contrast, irradiation of 3 or 6 Gy to abodomen near caudal portion of embryo induced 63 % and 80 % of somatic mutation, respectively (Fig. 1).

In addition, irradiation of carbon beam to head had the almost same level in the incidence of somatic mutation as the control (non-irradiation), but the irradiation of 5 Gy to abdomen of embryo
induced 80 % of the incidence (Fig. 1). The white spots appeared near the location which was hit by ion-beam.

From these results, it is not said that somatic mutation was resulted by bystander effect.

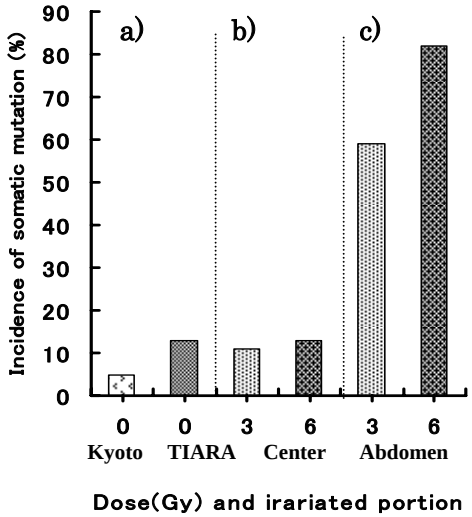

Fig. 1. Local irradiation of carbon beam to the silkworm egg and the incidence of somatic mutation. a) non-irradiated control of Kyoto(left) and TIARA (right), b) Center of egg, c) abdomen near caudal portion of embryo.

References

1) E. Kotani et al., J. Radiat. Res. 43, (2002) S193.

2) T. Furusawa et al., Proceeding of the 48th Annual Meeting of the Japan Radiat Res. Society, The 1st Asia Cong. of Radiat. Res.(2005) 145.

3-50 Functional Analysis of Root Elongation Zone in Hydrotropism in *Arabidopsis* Using Heavy-ion Microbeam

Y. Miyazawa [a)], T. Sakashita [b)], H. Negishi [a)], A. Kobayashi [a)], T. Kaneyasu [a)], A. Ooba [a)], K. Morohashi [a)], T. Kakizaki [b)], T. Funayama [b)], N. Hamada [b, c)], S. Wada [b, c)], Y. Kobayashi [b, c)], N. Fujii [a)] and H. Takahashi [a)]

[a)]Graduate School of Life Sciences, Tohoku University, [b)]Radiation-Applied Biology Division, QuBS, JAEA, [c)]Department of Quantum Biology, and The 21st Century Center of Excellence Program, Graduate School of Medicine, Gumma University

Previous studies on root hydrotropism suggest the importance of auxin response at elongation zone, however, there has been no functional confirmation of these necessities in this response. To determine the responsible tissue for root hydrotropism, it is necessary to inactivate the cell at desired position. Laser ablation of a specific cell can be used for similar purpose, and in fact, it has been used to dissect the functional role of root cap cells in gravitropism[1]. Although this cell ablation is a powerful technique for understanding the function of certain cells, it is still difficult to determine the role of elongation zone, since application of this method to this tissue leads the root to be snapped and become unsuitable to monitor the root curvature. To solve this problem, we used heavy-ion microbeam irradiation for nondestructive cell inactivation method. Although irradiation with charged particles induce activation of specific genes in mammalian cells, irradiation of heavy charged-particles with relatively high linear energy transfer is thought to cause cell inactivation through induction of DNA double strand breaks[2]. Recently, a device for heavy-ion microbeam irradiation with high precision has been established, and used to determine the effect of irradiation on root gravitropism[3]. However, the interpretation of the effect of irradiation had been ambiguous, because, to the best of our knowledge, no report has demonstrated that irradiation of heavy-ion beam inactivates cellular processes by monitoring gene expression of interest in plant cells. In this study, we investigated the positional effect of cell inactivation by heavy-ion microbeam irradiation with root hydrotropism, together with the confirmation whether irradiation of heavy-ion beam suppresses auxin-inducible gene expression in plant species.

First, we tested whether heavy-ion beam irradiation could inactivate the cell, by investigating the alteration of auxin-responsive gene expression by exogenously applied auxin. In the following experiments, we used cold-run seedlings (seedlings without irradiation) as control samples to exclude the possibility that the experimental procedure itself affects the gene expression levels and the phenomenon. When control *Arabidopsis* seedlings were treated with 10^{-6} M indole acetic acid (IAA), 43.3-fold increase in the abundance of mRNA for auxin-responsive gene, namely *IAA5*, was observed as compared with mock cultures. On the other hand, when *Arabidopsis* seedlings were systemically irradiated by 220 MeV $^{12}C^{5+}$ ion at a dose of 500 Gy, only 8.3-fold induction in the abundance of mRNA for *IAA5* was observed, which is far less than control. This indicates that the heavy-ion beam irradiation causes the dull responsiveness to exogenously applied auxin.

Next, we monitored the positional effect of heavy-ion beam irradiation on root hydrotropic response by irradiating with 220 MeV $^{12}C^{5+}$ ion at a dose of 500 Gy. We chose 180 μm aperture for irradiation so as to irradiate the whole part of elongation zone proximal to root tip. Control *Arabidopsis* seedling roots responded to water potential gradient and developed orthotropic curvature. When cells at elongation zone proximal to root tip were exposed to heavy-ion microbeam irradiation, hydrotropic response is significantly repressed especially at the early phase of the hydrotropic response (data not shown). Our present results indicate that elongation zone profoundly affects the development of hydrotropic curvature, probably involving *de novo* auxin-responsible gene expression.

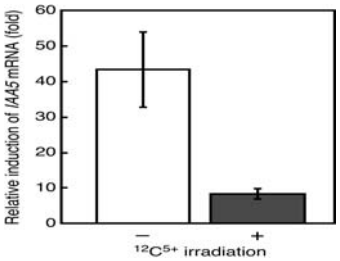

Figure 1. Effect of heavy-ion beam irradiation on auxin responsiveness.

Total RNA extracted from either $^{12}C^{5+}$-irradiated or non-irradadiated samples was subjected to quantitative reverse transcription PCR. The amount of *IAA5* transcript was normalized with *ACT2* transcript level, and expressed as relative value where the normalized *IAA5* transcript level in auxin omitted samples was set as one. Open bars indicate non-irradiated samples, whereas grey bars indicate irradiated samples. Data are the means of three independent experiments ± SD. Note that statistically significant difference was observed between two samples as calculated using Student's two-tailed *t*-test ($P < 0.05$).

References

1) Blancaflor et al. *Plant Physiol*. 116 (1998): 213
2) Blakely *Radiat. Environ. Biophys*. 31 (1992) 181
3) Tanaka et al. *J. Exp. Bot.* 53 (2002) 683

3-51 Differences in Circadian Rhythms of Resistance to γ-rays and Heavy-ion Beam in *Euglena*

A. Bolige [a)], T. Sakashita [b)], T. Kakizaki [b)], T. Funayama [b)], N. Hamada [b, c)], S. Wada [b, c)], Y. Kobayashi [b, c)] and K. Goto [d)]

[a)]United Graduate School of Agricultural Science, Iwate University, [b)]Radiation-Applied Biology Division, QuBS, JAEA, [c)]Department of Quantum Biology, and The 21st Century Center of Excellence Program, Gunma University Graduate School of Medicine, [d)]Laboratory of Biological Rhythms, Obihiro University of Agriculture and Veterinary Medicine

The algal flagellate *Euglena gracilis* (Klebs Z) displays circadian rhythms in resistance to γ-rays and heavy-ion beams: they persist for several days under continuous darkness at a constant temperature, and the most resistant phases occur 2-4 h before subjective mid-days, at which circadian rhythms in UV resistance and anti-oxidative capacities become maximal. We report here how these rhythms are related to each other. First, irradiation temperatures influenced neither survival after exposure to UV, γ-rays, nor C ions, whereas the incubation at high temperatures (25˚C) after irradiation considerably lowered the survival particularly after γ irradiation, but not after UV irradiation at all. Secondly, although the antioxidants β-carotene and dimethylsulfoxide (DMSO) increased the survival of the alga at the least resistant phase after UV-C and UV-B irradiation, respectively, to the level of the most resistant alga, none of these were not so effective for γ- or C-ion-irradiation. Instead, GSH, GSH-ethylester, l-cysteine and l-histidine increased the resistance to γ-irradiation, while the other set of antioxidants did so for the resistance to C-ions. Particularly interesting was that the antioxidants l-ascorbate, N-acetyl-l-cysteine, rutin, trolox increased the latter but not the former resistance. Finally, FITC-dextran was incorporated into the alga only after C-ion irradiation but not γ irradiation, suggesting that C-ions may perforate cell membranes to kill the alga.

概日リズムは恒常環境の下ではその生物に固有な周期性（約２４時間；ユーグレナで２６時間）を表すとともに、昼夜の周期環境に同調して環境適応する。ユーグレナ（*Euglena gracilis* Z）では、UVC耐性やUVB耐性、及び抗酸化能の全般（脂溶性and/or水溶性の一重項酸素消去能・ヒドロキシルラジカル消去能）が主観的真昼に最大となるよう概日リズムによって制御され、真昼に最大化する光酸化ストレスに対する予知的な防衛機能を果たしている。γ線や220 MeV 12Ｃイオン（以下Ｃイオン）に対してもユーグレナは同様の概日リズムを示すが、その最大耐性は主観的真昼にはなく、2～4時間ほど先行した形をとる。この放射線耐性リズムと同一位相で走る抗酸化能リズムも振幅は小さいながら認められる。

実験にはユーグレナを6～8万細胞/mL になるまで25 ℃、6 klx 恒明（白色蛍光灯）で培養し、恒暗に移す。恒暗中の様々な時点でγ線や220 MeV 12Ｃイオン（以下Ｃイオン）を照射し、中性赤を用いて生死判別を行った。その生存率をもって耐性の基準とした（Ｃイオンは照射直後、γ線は一日後）。

γ線とＣイオン照射を行う温度（0、25 ℃）は生存率に影響しない。これはＵＶ照射の場合も同様である。これに対し、照射後に低温（4 ℃）放置した場合には、25℃で保存した場合より10～60 %ほど高い生存率を示し、温度依存的な生命活動が死を促進する可能性が示された。このことは、γ線照射の場合により顕著に認められる。ＵＶ照射の場合は細胞死はすべて照射中及び直後にのみ生起するので、この点については比較対照外である。γ線耐性増強には還元型グルタチオン、GSH－エチルエステル、システイン、ヒスチジンなどが有効であった。また、β―カロテンやリコピンも少なからず有効であった。

Ｃイオン耐性増強に有効であったのはシステイン、N－アセチルシステイン、ルチン、アスコルビン酸、還元型グルタチオン、GSH－エチルエステル、トロロックス、β―カロテンやリコピンなどの抗酸化剤である。したがって、γ線耐性やＣイオン耐性には水溶性や脂溶性のラジカル消去能と一重項酸素消去能が総合的に関与しているものと考えられる。ただし、両耐性は互いに異なる抗酸化機作も関係している。例えば、γ線耐性増強に有効な抗酸化剤はＣイオン耐性増強にも有効であったが、逆にＣイオン耐性増強に有効なアスコルビン酸、N－アセチルシステイン、ルチン、トロロックスなどはγ線耐性増強には殆ど無効だからである。また、還元型グルタチオン、システインやβ―カロテンを含む抗酸化剤の組み合わせ投与により、600 Gy程度の低線量照射の場合、γ線耐性もＣイオン耐性も非酵素的な抗酸化能だけで説明できるが、高線量照射の場合には、抗酸化能以外の要因も関係している可能性が示された。更に、分子量の異なるFITC－デキストランを用い、放射線によるユーグレナの死滅に細胞膜の物理的損傷の有無を調べたところ、γ線照射の場合には高線量でもFITC－デキストランを透過させるほどの損傷は生じないことが明らかになった。これに対し、Ｃイオン照射の場合には1,500 Gy 以上の線量でFITC-デキストランの取り込みが顕著に確認された： 10 kDのもので50 %のユーグレナに, 20 kDで10-15 %のユーグレナに取り込まれる。したがって、Ｃイオン照射による致死作用には物理的生体膜損傷が関与していると考えられる。この致死作用に抗酸化剤は殆ど無効である点も、高線量Ｃイオン耐性には抗酸化能は無縁であるという上記事実と符合している。

3-52 Detection of Damage Using ESR Method to Irradiated Wheat Flour

M. Ukai [a)], M. Matsuura [a)], S. Ogawa [a)], T. Kume [b)], M. Kikuchi [c)], T. Sakashita [c)], T. Funayama [c)] and Y. Kobayashi [c)]

[a)]Hokkaido University of Education, [b)]TARRI, JAEA, [c)]Radiation-Applied Biology Division, QuBS, JAEA

Irradiation of food is a non-thermal treatment and a method of cold pasteurization. This pasteurization technique retains the quality of foods as prepared and harvested. Recently, the use of this sterilization technology by irradiation through various electromagnetic waves or rays of elementary particles is gaining wide applications. Since irradiation induces free radicals, consumer believes that irradiated foods can be the threatening of public health.

Electron spin resonance (ESR) spectroscopy has been applied for the evaluation of irradiation on the wide variety of foods. We have reported on a new ESR protocol for the analysis for irradiated foods[1)].

In the present study, we will report on the radiation-induced radicals containing in wheat flour using ESR spectroscopy. We shall describe new radical species in the irradiated wheat flour by comparison with non-irradiated wheat flour. Attempts have been made on the irradiation damage of radicals.

The flour sample of wheat was the products of Gumma, Japan. The nutritional contents of the wheat flour consist of starch (70 wt %) and protein (14 wt %). In order to avoid the anisotropic EPR spectral dependence by the microcrystalline of grain in wheat flour, we employed a separation method of powder sizes of less than the 200 meshes. Thereby, the identical ESR signals were detectable irrespective of the sample tube rotation. The specimens were irradiated at the JAEA Takasaki at room temperature (ca. 20 ºC). The dosage level of the gamma ray was controlled by the irradiation period. We selected the three dose levels, i.e., 10, 30 and 50 kGy.

ESR measurements were carried out using an ESR spectrometer (Jeol, JES-FE1XG and JFS-FA200). All the ESR spectra were recorded at the X-band (9.3 GHz). In order to detect full view of all the radical species of wheat flour, we employed two kinds of field sweep, 250 ± 250 mT and 320 ± 100 mT.

The ESR spectrum of wheat flour before irradiation consists of a sextet centered at g = 2.0 and a singlet signal at the same g-value position (Fig.1). The first one is attributable to a signal with hyperfine (hf) interactions of Mn^{2+} ion (hf constant: 7.4 mT). The second is originated from carbon-centered radical.

Upon gamma ray irradiation, however, a new signal with two triplet lines at the low and high field ends was detected in wheat flour on top of the Mn^{2+} sextet lines (Fig.2). We analyzed the triplet ESR lines as powder spectra (rhombic g-tensor symmetry) with nitrogen (^{14}N) hyperfine interactions. This indicates that a new organic radical was induced in the conjugated protein portion of wheat flour by the gamma ray irradiation. Intensity of the organic free radical at g = 2.0 detected in irradiated wheat flour increased with the degree of irradiation.

Reference

1) M. Ukai, et al. Appl. Magn. Reson., 24 (2003) 1.

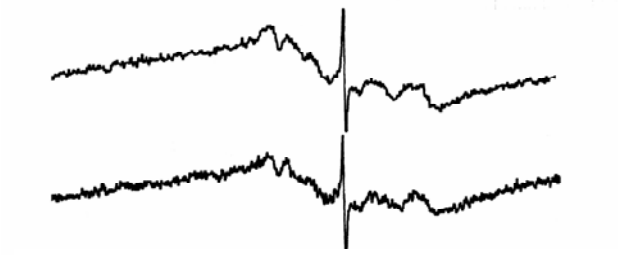

Fig.1 Anisotropic ESR spectra from wheat flour before irradiation. Different signals were observed by the rotation of ESR sample tube containing wheat flour.

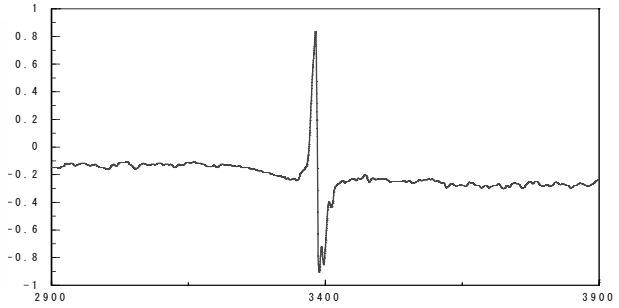

Fig.2 ESR signal of irradiated wheat flour (50k Gy).

3-53 Preparation of Acellular Arteries by Gamma Irradiation

T. Fujisato [a)], M. Kikuchi [b)], T. Sakashita [b)], T. Funayama [b)], Y. Kobayashi [b)], S. Funamoto [c)], T. Kimura [c)], A. Kishida [c)] and T. Yamaoka [d)]

[a)]Department of Biomedical Engineering, Osaka Institute of Technology,
[b)]Radiation-Applied Biology Division, QuBS, JAEA,
[c)]Institute of Biomaterials and Bioengineering, Tokyo Medical and Dental University,
[d)]Department of Biomedical Engineering, National Cardiovascular Center Research Institute

Synthetic materials, such as ePTFE or Dacron are not suitable for reconstructing the small-diameter arteries. In contrast, tissue engineering (TE) graft has been attracting great attention recently. One of the promising approaches of TE grafts is using acellular tissues. The acellular scaffold may have the same structure and characteristics as the natural tissue and can be replaced with the host tissues. In this study, we prepared the acellular scaffold using gamma irradiation, which is expected to induce the apoptosis of the cells.

現在、我が国において人工心臓弁は年間１万個、人工血管は５万本が使用されている。屍体から提供されるヒト心臓弁や血管も組織バンクを通じて臨床使用されているが、年間数十件程度に過ぎない。米国では商業利用によって、年間数千件のヒト組織が使用されている。人工素材から作製される移植用組織は生体にとっては異物であり、自己組織と置き換わることはない。また、小児患者においては体の生育に伴った成長性が欠如しているという欠点もある。近年、移植後の拒絶反応を避けるために、自己組織と置換される素材を用いた組織再建が臨床応用され始め、東京女子医大グループによる生体内分解吸収性材料を用いた再生型血管や、ドイツ・フンボルト大学グループによるブタ脱細胞化組織を用いた再生型心臓弁が報告されている。我々は、放射線照射によって細胞を除去した生体組織をバイオスキャホールド（細胞足場材料）として用いた再生型移植用組織の開発を行っている。

移植組織片は以下のようにして作製した。生後４ヶ月、体重約10 kgのクラウン系ミニブタ（㈱ジャパンファーム、鹿児島）から清潔下にて下行大動脈を採取した。PBSによる洗浄後、PBSを満たした滅菌容器に封入し、10, 30, 100, 300, あるいは1000 Gyのガンマ線を高崎量子応用研究所のCo-60照射施設を用いて照射した。吸収線量率は、それぞれ100, 300, 100, 300, 1000 Gy/hである。照射後、PBSをベースとする洗浄液にて２週間洗浄した。洗浄液は、適宜交換した。Wisterラット（７週令）の皮下部位に上記脱細胞化ミニブタ大動脈を埋入し、２週間後に取り出し、ヘマトキシリンーエオジン（HE）染色、マクロファージに対するCD68免疫染色にて組織学的検討を行った。

種々のガンマ線量による組織脱細胞化の基礎的検討を残存DNA定量試験、力学試験にて行った結果、残存DNA定量試験では、100あるいは300 Gy以上の照射では大幅なDNA減少傾向が見られた。また、力学特性は、破断強度並びに弾性率とも大きな影響は見られなかった。すなわち、300 Gy以上のガンマ線を照射後、洗浄処理することによって、循環器系組織内の細胞はほぼ完全に除去できると思われた。

次に、ガンマ線照射によって作製した脱細胞化ミニブタ大動脈の有効性を、ラット皮下への埋入試験により、組織学的、免疫組織学的検討を行った。ガンマ線未照射ミニブタ大動脈の場合、ラット由来の血管の流入が認められた。一方、1000 Gyのガンマ線照射脱細胞化ミニブタ大動脈では、血管の流入は確認されなかった。HE組織染色結果からは、ガンマ線未照射ミニブタ大動脈では、組織反応による細胞の浸潤が見られたが、1000 Gyのガンマ線照射脱細胞化ミニブタ大動脈では、細胞浸潤は認められなかった。

また、移植片を免疫染色によって評価した結果、未処理血管では、マクロファージ陽性を示すCD68陽性部位が多く見られるのに対して、ガンマ線照射脱細胞化血管では、炎症部位の減少が示された。これら染色画像について画像解析ソフトを用いてCD68陽性細胞面積を計測した。その結果、未処理血管では、炎症細胞が多く存在していたが、ガンマ線照射の組織では炎症細胞が有意に減少していた。

3-54 Molecular Imaging by Using Positron Emitting Tracer Imaging System (PETIS) to Study Plant Physiology; Parametric Imaging of Photosynthesis

N. Kawachi, S. Fujimaki, S. Ishii, N. Suzui, N. S. Ishioka and S. Matsuhashi

Radiation-Applied Biology Division, QuBS, JAEA

Radionuclide-based imaging techniques enable us to obtain images of the kinetics of the transport of water and nutrients in plants, and hence determine plant physiology. In particular, by using the positron-emitting tracer imaging system (PETIS), which was designed for studying plant physiology and agriculture, many experiments have been performed for the imaging of the distribution and translocation of the nutrients using positron emitting tracers. The kinetics of ^{11}C make it a potential candidate for estimating the physiological function parameters of photosynthesis. By using $^{11}CO_2$, the kinetics of photoassimilation and of the flow of sucrose, which is synthesized as a photosynthate, through sieve tubes have been obtained as movies comprising serial images. We have analyzed the exchange of carbon compounds inside and outside a test leaf, based on the ^{11}C-labeled tracer kinetics in the compartmental model. An analytical solution of the carbon tracer balance was obtained by the following equation; as follow;

$$L(t) = K1 \bullet C_i(t) \otimes e^{-(k3+\lambda)t} \qquad \text{(Eq. 1)}$$

where, *L(t)* is the leaf response time-activity curve, which indicates the time variation of ^{11}C concentration in leaf; *Ci(t)*, the input time-activity curve; λ, the physical decay of ^{11}C; and $\otimes$, the convolution integral. Further, photoassimilation (K1) and the sucrose export (*k3*) rate constant were estimated by kinetic analysis[1].

In order to produce parametric images of photosynthetic functions from the PETIS movie data, we performed a pixel-by-pixel analysis by the present compartmental method. To construct the images depicting photoassimilation and the sucrose-export images from the estimated values of the parameters *K1* and *k3*, approximately 10,000 pairs of time-activity curves were fitted to the Eq. 1 by the nonlinear least squares method. By this analytical method, 2 bioactive distribution images were produced from a single movie data.

Shown in Fig. 1 are the parametric images of 2 photosynthetic processes namely, photo-assimilation and sucrose export. The *K1* image indicates that photoassimilation was distributed uniformly over the entire leaf. In contrast, the *k3* image indicates that sucrose export was not distributed uniformly. The sucrose export ability at the tip was greater than that at the base. This seems attributed to the well-known fact that the base of the leaf is the region of growth. It implies that sucrose produced at the base of the leaf was probably consumed there itself for the growth, and that produced at the tip was mainly transported to the other parts of the plant.

In summary, we have performed imaging using PETIS and kinetic analysis for studying the processes of plant physiology, such as photosynthesis in living systems mainly in response to the environment, and processes involved in the anisotropic maturation of leaf tissues [2].

References

1) N. Kawachi et al., IEEE Trans. Nucl. Sci., 53 (2006) 2991.
2) N. Kawachi et al., IEEE Nucl. Sci. Symp. C. R., 5 (2006) 151.

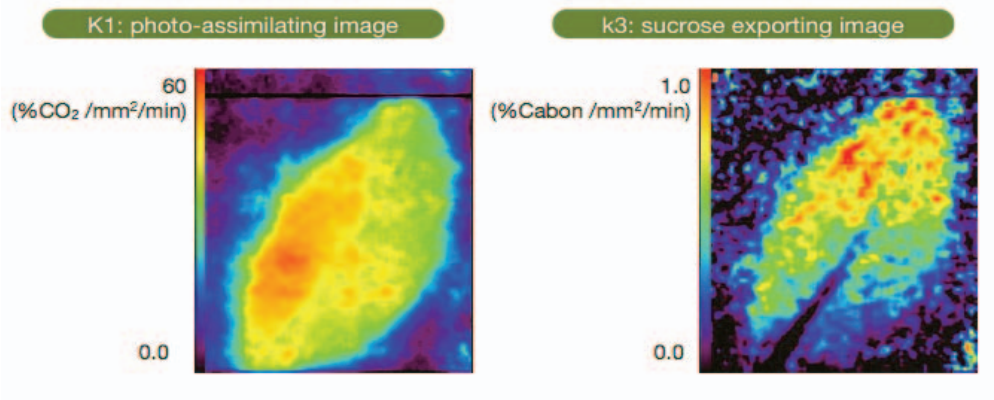

Fig. 1 Parametric images of photosynthetic functions. The left image on the left indicates the distribution of photo assimilation (*K1*) and the image on the right indicates the distribution of sucrose export in different regions of the leaf (*k3*).

3-55 Non-invasive Estimation of Phloem Flow Velocity under Cadmium Stress Using the Positron Emitting Tracer Imaging System

N. Suzui [a)], N. Kawachi [a)], S. Ishii [a)], S. Nakamura [b)], S. Matsuhashi [a)] and S. Fujimaki [a)]

[a)]Radiation-Applied Biology Division, QuBS, JAEA,
[b)]Faculty of Bioresource Sciences, Akita Prefectural University

Cadmium (Cd) is a major environmental pollutant, which accumulates in agricultural soils, and is a toxic element to all organisms. In plant, the most sensitive symptom of Cd toxicity is stomata closure, followed by the inhibition of photosynthesis. However, it has been reported that Cd treatment increases carbohydrate content of source organ. This contradictory result could be due to the inhibition of translocation of photoassimilates by Cd. However, direct evidence has not been reported.

In this study, we estimated a phloem flow under Cd stress using the positron emitting tracer imaging system (PETIS), quantitatively and non-invasively. In an experiment, $^{11}CO_2$ was supplied to leaves of rice plants and the translocations of ^{11}C- photoassimilates were monitored.

Rice plants (*Oryza sativa* L. cv Nipponbare) were germinated and grown hydroponically in nutrient solution (without Cd) for 4 weeks. Plants were transferred to the nutrient solution containing 0 (control), 1, 10 and 100 μM of Cd, and cultured for 1 day before PETIS experiment.

Five to six of Cd-treated plants were placed between a set of PETIS detectors in a growth chamber. The upper half of the largest expanded leaf of each plants was inserted into a "gas-cell", a clear acrylic box for feeding $^{11}CO_2$ (100 MBq) gas (Fig.1). Time course of ^{11}C-radioactivity (Time-Activity Curve) in the basal region was generated from the serial images of each rice plant (Fig.1). The value of the x-axis intercept of approximated line was defined as ^{11}C-arrival time to basal region.

We performed 6 sets of PETIS experiments using 5 ~ 6 different rice plants treated with 0, 1, 10, 100 μM of Cd. The arrival times of ^{11}C-photoassimilates to the basal region of each plant were analyzed (Fig. 2). Phloem flow velocities were also estimated using the ^{11}C-arrival time and the distance from the bottom of gas-cell to the basal region.

Arrival time of 100 μM Cd-treated plants was significantly different from that of control and 10 μM Cd-treated plants ($p < 0.05$). This result indicates that Cd exposure for 1 day causes the decrease of phloem flow velocity in rice plant. Now we are also examining the rate of photoassimilation in source leaf and the concentration of photoassimilates in phloem sap under Cd stress. These data will provide the basis of Cd toxicity to plant.

This study indicates the utility of estimation of phloem flow velocity using PETIS and simple data analysis. This method can be applied for studying influences on phloem transport against other environmental conditions.

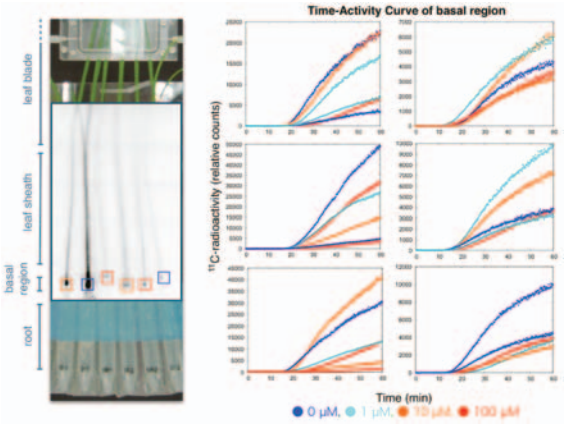

Fig.1 Time-Activity Curve for accumulation of ^{11}C-photoassimilates in the basal region of rice plants treated with 0, 1, 10, 100 μM of Cd. The figure on the left shows the image of ^{11}C-radioactivity captured by PETIS and the picture of tested plants.

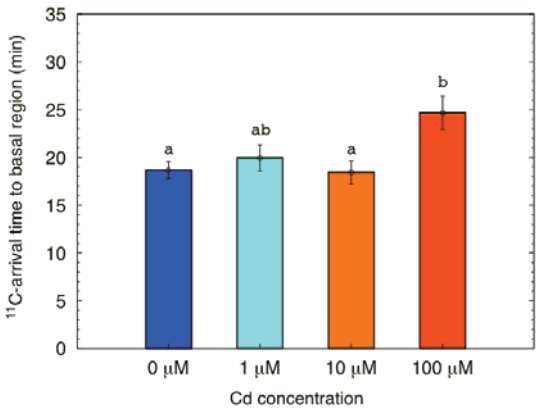

Fig.2 Effect of Cd stress on ^{11}C-arrival time to basal region. Means with the same letter are not significantly different ($p < 0.05$). n=7~8

3-56 The Imaging of Translocation of Major Nutrition Using the Positron Emitting Tracer Imaging System

S. Ishii, N. Kawachi, N. Suzui, S. Fujimaki and S. Matsuhashi

Radiation-Applied Biology Division, QuBS, JAEA

Nitric acid and ammonium absorbed by the roots, and carbon dioxide fixed on the leaves, are metabolized, distributed and accumulated into the plant organs. Correlation between carbon assimilation and nitrogen assimilation is one of the important factors regulating plant growth [1, 2].The Positron-Emitting Tracer Imaging System (PETIS) and tracers of major nutrition have been an available system to obtain movies of tracer in short-term distribution non-invasively. Therefore, we tried to visualize the movement of carbon and nitrogen nutrition in a whole plant.

Soybean (*Glycine max* [L.] Merr. cv. Enrei) plant inoculated with rhizobium had been hydroponically cultured with MS medium for 25 days, and was used for the PETIS experiment (Fig.1). Three tracers, $^{11}CO_2$, $^{13}NO_3^-$ and $^{13}NH_4^+$ were produced by bombarding targets ($^{11}CO_2$: nitrogen gas, $^{13}NO_3^-$: pure water, $^{13}NH_4^+$: pure water with a small amount of ethanol) with proton beam delivered from the TIARA AVF cyclotron. Soon after approximately 30 MBq of $^{11}CO_2$ was fed to the leaves, PETIS images were acquired for 2 hours. After first imaging, 100 MBq of $^{13}NO_3^-$ was fed to the roots and PETIS images were acquired for 90 min. Subsequently, 16 MBq of $^{13}NH_4^+$ was fed to the roots and images were acquired for 90 min. The interval of each imaging was about 30 min to allow radioactivity to decay at the background level.

As a result, a movie of distribution of ^{11}C-labeled photoassimilates in the plant organs and nodules, and movies of translocations with $^{13}NO_3^-$ and $^{13}NH_4^+$ were acquired (Fig.2). In other words, the real time imaging of translocation of ^{11}C labeled carbon source and ^{13}N labeled nitrogen in an intact nodulated soybean plant was demonstrated.

Furthermore, nitrogen fixed by nodule was important factor regulating plant growth in soybean plant. An imaging experiment on N_2 fixation of nodule and fixed nitrogen translocation in soybean is currently in progress by using PETIS and $^{13}N_2$ gas.

References

1) H. Fujikake et al. J Exp Bot. 2003 May; 54 (386) 1379
2) S. Ito, N. Ohtake, K. Sueyoshi and T. Ohyama
Soil Science and Plant Nutrition 52 (2006) 438

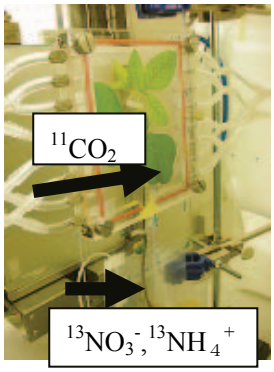

Fig.1 Setting of PETIS experiment.
Soybean plant was fixed on acrylic plate. $^{11}CO_2$ was fed to leaves covered with acrylic gas cell. The roots were soaked in hydroponic solution in plastic bag. $^{13}NO_3^-$ $^{13}NH_4^+$, were mixed with hydroponic solution.

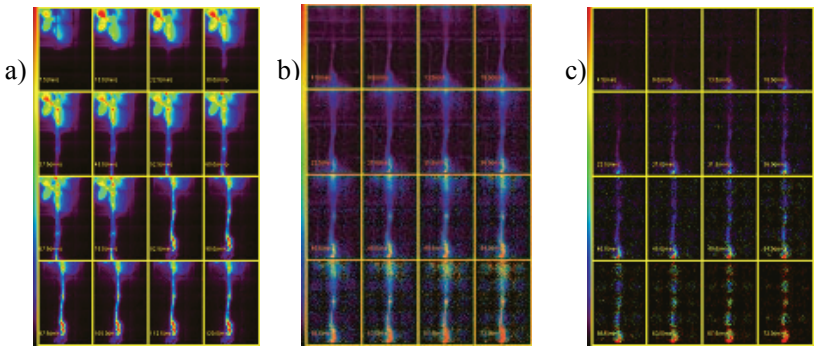

Fig.2 The Serial images from the PETIS experiments.^{11}C scan sequence was 7.5 min and ^{13}N scan sequence was 4.5 min. All images were corrected for the radioactive decay of each tracer. Images were arranged sequentially from left to right and top to bottom. a) $^{11}CO_2$ exposure to leaves. b) $^{13}NO_3^-$ absorption by root. c) $^{13}NH_4^+$ absorption by root.

3-57 Non-invasive Imaging of Cadmium Long-distance Transport in Higher Plants

S. Nakamura [a)], N. Suzui [b)], N.S. Ishioka[b)], N. Kawachi [b)], M. Chino [a)], S. Matsuhashi [b)] and S. Fujimaki [b)]

[a)]Faculty of Bioresource Sciences, Akita Prefectural University,
[b)]Radiation-Applied Biology Division, QuBS, JAEA

Cadmium (Cd) is a harmful heavy metal element. It causes various obstacles in the human body when it is taken in via the food. Cd is also famous as a causative substance of the itai-itai disease. Recently, there is the international movement which makes the reference level of cadmium content in the food harsh. It has become national urgent business to establish the agricultural technology which decreases the cadmium content in the farm products.

In order to decrease the cadmium content in the farm products, two technologies are focused recently. One is called “phytoremediation” which cleans up the cultivation soil using absorption by special plants. The other is to modify the crop plants not to accumulate cadmium in their edible parts. However, these technologies are not practical yet. For realization of these technologies, it is necessary to elucidate the mechanism of transport of Cd in the plant body.

In this research, we visualized Cd transport in the plant body by using Positron Emitting Tracer Imaging System (PETIS). We tried to elucidate the mechanism of Cd transport in the whole plants by analyzing the experimental data which is obtained by PETIS.

^{107}Cd which is positron-emitting nuclide was used for PETIS experiment. Production method of ^{107}Cd was established by Ishioka et al.[1)]. Sorghum plants (*Sorghum vulgare* L.) and oilseed rape plants (*Brassica napus* L.) were grown hydroponically for two weeks after sowing. PETIS experiment was performed inside the growth chamber where we can control growth conditions of plants completely. After setting plants inside the chamber, PETIS experiment was started by adding purified ^{107}Cd in hydroponic solutions. Time-series images of the ^{107}Cd distribution in the aerial part and upper part of the roots of plants were obtained with the PETIS apparatus. Time courses of the absorption of water and the tracer (^{107}Cd) by plants were also monitored. Time-activity curves, temporal changes of the tracer amount in specific regions of interest (leaves, stems, and so on) were generated from PETIS data. These data were combined and analyzed.

We succeeded to obtain fine serial images of Cd transport in sorghum plants (Fig. 1) and oilseed rape plants (Fig. 2). We could observe that ^{107}Cd signals arrive in the aerial parts of both plants in a few hours after the start of the experiment. Patterns of accumulation of ^{107}Cd signals in sorghum plants were similar to those in rice plants[2)]. Strong signals of ^{107}Cd were seen in the basal region of the shoot, which consists of a short stem, nodes and meristems. Interestingly, ^{107}Cd also accumulated in the node strongly in oilseed rape plants although these two plants have different structure as a monocot and a dicot. The analysis of time-activity curves revealed that pattern of accumulation of ^{107}Cd changes in development in the oilseed rape plants.

References

1) N. S. Ishioka et al., JAEA Takasaki Ann.Rep. 2005 (2006) 162.
2) S. Fujimaki et al., JAEA Takasaki Ann.Rep. 2005 (2006) 127.

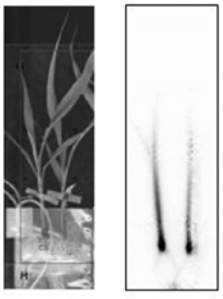

Fig. 1 Accumulation of ^{107}Cd signals in sorghum plants. This image is integration of 15 original frames, corresponding to 1 hour (From 23 hour to 24 hour after the start of the experiment).

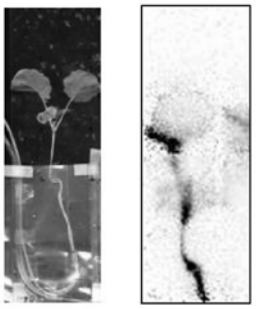

Fig. 2 Accumulation of ^{107}Cd signals in oilseed rape plants. This image is integration of 15 original frames, corresponding to 1 hour (From 23 hour to 24 hour after the start of the experiment).

3-58 Imaging of Translocation and Spatial Distribution of the Assimilated Carbon and Nitrogen in the Host–root Parasite System by PETIS

H. Sekimoto [a)], N. Kawachi [b)], S.Honda [a)], Y. Yamaguchi [a)], S. Kato [a)], K. Yoneyama [a)], S.Fujimaki [b)], N. Suzui [b)], S. Ishii [b)], S. Watanabe [b)], N. S. Ishioka [b)], H. Sutoh [b)] and S. Matsuhashi [b)]

[a)]Faculty of Agriculture, Utsunomiya University
[b)]Radiation-Applied Biology Division, QuBS, JAEA

Translocation and distribution of $^{11}CO_2$, ^{13}N-nitrate or ^{13}N-ammonium in the red clover (*Trifolium pratense* L.) parasitized by small broomrape (*Orobanche minor* Sm.) was examined by PETIS. The PETIS images acquired periodically after $^{11}CO_2$ exposure indicate that *Orobanche* is a big 'sink' of the assimilated $^{11}CO_2$ by host plant. Accumulation of ^{13}N applied as $^{13}NH_4^+$ in *Orobanche* tubercles was higher than that applied as $^{13}NO_3^-$, indicating that $^{13}NH_4^+$ stay longer in *Orobanche* tubercles than $^{13}NO_3^-$. The differences in the accumulation may be due to the rapid metabolism of ammonium to amino acids.

Sharing photoassimilates and absorbed nitrogen-compounds with host plants is of primary importance for the survival of root parasites. Direct imaging of translocation and spatial distribution of the assimilated carbon and nitrogen in the host–parasite system is the most convincing approach for the study of host–parasite interactions. However, each host-parasite system is unique and may be different from others, and therefore, it is quite difficult to obtain reproducible results. Consequently, a noninvasive and repeatable imaging system using the radioactive nuclides having short half-lives is needed. The positron-emitting tracer imaging system (PETIS), designed for the use in plant science to study the translocation and distribution of nutrients by using radioisotope tracers (^{11}C, ^{13}N, etc), allows us to perform noninvasive, repeatable, and quantitative analyses of nutritional sharing between host plants and root parasites. In the present study, translocation and distribution of $^{11}CO_2$, ^{13}N-nitrate or ^{13}N-ammonium in the red clover (*Trifolium pratense* L.) parasitized by small broomrape (*Orobanche minor* Sm.) was examined by PETIS.

The PETIS images acquired periodically after $^{11}CO_2$ exposure indicate that *Orobanche* is a big 'sink' of the assimilated $^{11}CO_2$ by host plant (Fig.1). Based on the image analysis of the ^{11}C radioactivity in the host–parasite system, 15% of the carbon assimilated by host plant accumulated in *Orobanche* 30 to 40 min after the $^{11}CO_2$ exposure. In addition, It seemed that *Orobanche* tubercles absorbed $^{13}NH_4^+$ more strongly than $^{13}NO_3^-$, indicating that $^{13}NH_4^+$ stay longer in *Orobanche* tubercles than $^{13}NO_3^-$ (Fig.2). However, relative ratios of radioactivity in *Orobanche* tubercles to that in the root area were very similar in both the $^{13}NO_3^-$- and $^{13}NH_4^+$-fed host–parasite systems, suggesting that *Orobanche* tubercles absorb $^{13}NH_4^+$ and $^{13}NO_3^-$ with similar affinities. The differences in the accumulation may be due to the rapid metabolism of ammonium to amino acids.

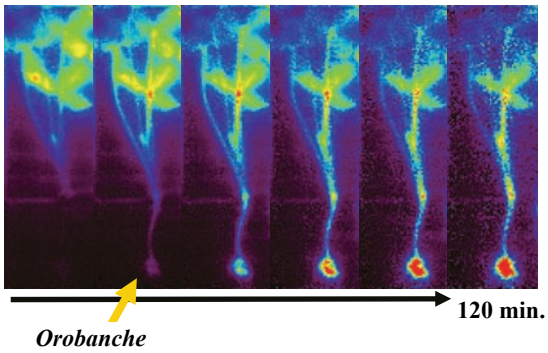

Fig.1 $^{11}CO_2$ translocation and distribution in the *Orobanche* infected plants

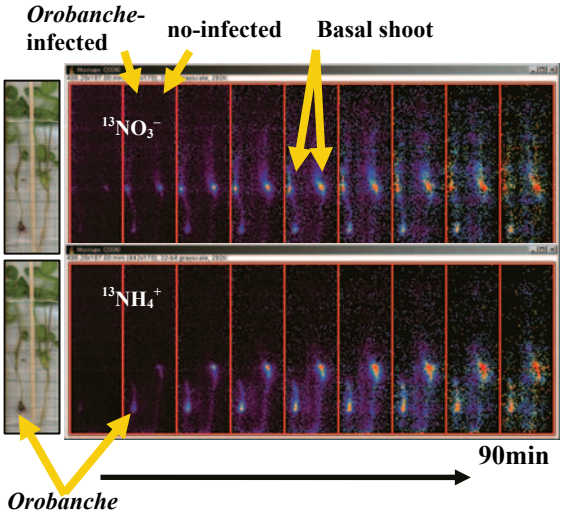

Fig.2. $^{13}NO_3^-$ (above) and $^{13}NH_4^+$ (below) translocation and distribution in the *Orobanche* infected plant

3-59 ^{52}Fe and ^{62}Zn Translocation from the Roots to the Shoots of Rice Monitored by Positron Emitting Tracer Imaging System (PETIS)

H. Nakanishi [a)], T. Tsukamoto [b), c)], S. Watanabe [c)], S. Matsuhashi [c)], N. K. Nishizawa [b)] and S. Mori [a)]

[a)]Department of Applied Biological Chemistry, The University of Tokyo, [b)]Department of Global Agricultural Sciences, The University of Tokyo, [c)]Radiation-Applied Biology Division, QuBS, JAEA,

1. Introduction

Iron (Fe) and zinc (Zn) are essential nutrients for plants. However, little is known how Fe and Zn are translocated in rice plants especially to the ear after absorption from roots. In addition, the real-time measurement of translocation of Fe and Zn has not been documented in plants. To study the pathway of Fe and Zn to the ear, we traced ^{52}Fe and ^{62}Zn in rice plants (*Oryza sativa* L. cv. Nipponbare) of 3 weeks after flowering by positron emitting tracer imaging system (PETIS).

2. Experimental procedure

Rice (*Oriza sativa* L. cv. Nipponbare) were hydroponically cultured in a growth chamber under a mixture of incandescent and fluorescent lamps with a 14 h light (30 °C)/10 h dark (25 °C) regime and a photon flux density of 320 μmol m^{-2} s^{-1}. The nutrient solution was renewed once a week. The absorption experiments were performed about 3 months after germination and 3 weeks after flowering. A rice plant was supplied with 20 mL of culture solution in polyethylene bags. The plants and the bags were fixed an acrylic board and placed between a pair of PETIS detectors in a chamber at 30 °C under 65 % humidity and a light density of 320 μmol m^{-2} s^{-1}. $^{52}Fe^{3+}$-deoxymugineic acid (DMA) (about 2 MBq) or $^{62}Zn^{2+}$ (about 20 MBq) were added to culture solution. The shoots were monitored by PETIS for 14 h.

3. Results and discussion

In order to clarify the pathway of Fe and Zn from the roots to the ear of rice, $^{52}Fe^{3+}$-DMA or $^{62}Zn^{2+}$ was fed to roots of a rice plant, and translocation of ^{52}Fe or ^{62}Zn was monitored using PETIS method. ^{52}Fe and ^{62}Zn was translocated to shoots within 14 h (Fig. 1, Fig. 2). In particular, the nodes were strongly labeled. Both ^{52}Fe and ^{62}Zn were preferentially accumulated in the lower node until 2 h and 5 h after absorption, respectively. However, the radioactivity of upper node was higher than that of lower node in the last results. It was reported that the nodes contained the elliptical, diffuse and anastomosing vascular bundles, and the xylem transfer cells were found in the elliptical bundles[1)]. Therefore, ^{52}Fe and ^{62}Zn might be transferred from xylem to phloem in the nodes.

Reference

1) S. Y. Zee et al., Aust. J. Bot. 20 (1972) 41.

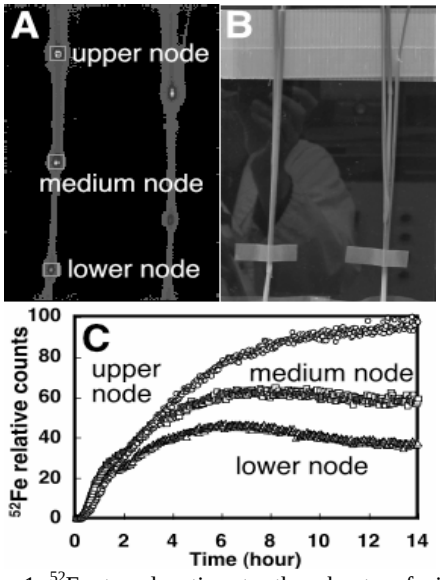

Fig. 1 ^{52}Fe translocation to the shoots of rice. (A) Accumulative PETIS image. (B) Gross image of rice plant. (C) Time course of radioactivity of ^{52}Fe in the nodes.

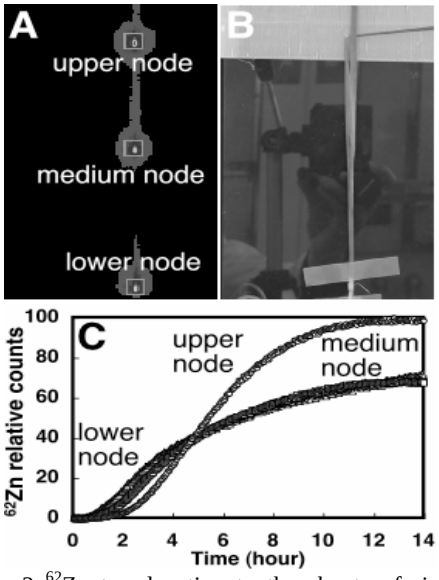

Fig. 2 ^{62}Zn translocation to the shoots of rice. (A) Accumulative PETIS image. (B) Gross image of rice plant. (C) Time course of radioactivity of ^{62}Zn in the nodes.

3-60 Impact of Aluminum on the Photosynthesis and Translocation of Photoassimilats in Rice Seedling. -Imaging-based Analysis by PETIS-

T. Furuichi [a)], S. Fujimaki [b)], N. Kawachi [b)], N. Suzui [b)], S. Ishii [b)], N. S. Ishioka [b)], H. Sutoh [b)], S. Matsuhashi [b)], M. Sokabe [a)] and Y. Yamamoto [c)]

[a)]Graduate School of Medicine, Nagoya University
[b)]Radiation-Applied Biology Division, QuBS, JAEA
[c)]Research Institute for Bioresources, Okayama University

Accumulation, translocation and distribution of ^{11}C-labeled photoassimilates in the rice (*Oriza sativa*. cv. Nipponbare) seedling treated with or without aluminum (Al) was examined by PETIS. The PETIS images acquired periodically after $^{11}CO_2$ exposure indicate that the long-term exposure promote the accumulation of ^{11}C-labeled photoassimilates and its translocation toward roots. In contrast, the short-term exposure attenuate both. Similar results were observed in the seedlings of tobacco, suggest that Al-dependent modulation on the rate of photosynthesis and the following translocation of ^{11}C-labeled photoassimilates is the common feature of land plants.

Thirty to 40 % of arable land in the world has been estimated to be acidic soils. In addition global industrialization has triggered huge exhaustion of acidic compounds into the atmosphere, which expanded the area of acidic soils in all over the world. In the regions where acidic soils are prominent, most of the crops or pastures are disturbed their growth and development. Aluminum (Al), the most abundant metal element in soils, is solubilized as free ions under acidic conditions and exhibits toxicity to plants. A variety of plants can grow in acidic soils by secretion of organic acids from root apices, which excludes and/or detoxifies Al ion in the apoplast. To support the efflux of organic acid from root apecies under al stress, sugars should be transported to the root apecies, but how the rate and amount of sugar-translocation are regulated is still obscure.
To understand that, $^{11}CO_2$ was applied to the entire seedlings which settled in a air-tight clear-acrylic box (inside dimensions: 8 cm in length, 5 cm in width, 1 cm in depth), and the box was positioned in the middle of the PETIS detectors. In rice seedlings, a major crop of monocots, were pre-treated with Al, ^{11}CO2 fixation and sugar translocation toward roots were enhanced by the long-term exposure (31.5 h) to $AlCl_3$ (100 μM) in acidic condition. In contrast, relatively short-term exposure (25.5 h) attenuate those and those were recovered in transition state (28.5 h), as observed in tobacco seedlings (reported in the previous report)(Fig.1). These results suggest that the stimulation of photosynthesis in leaves by Al exposure to roots and subsequent translocation of photoassimilates toward root part is a common feature of both dicots and monocots.

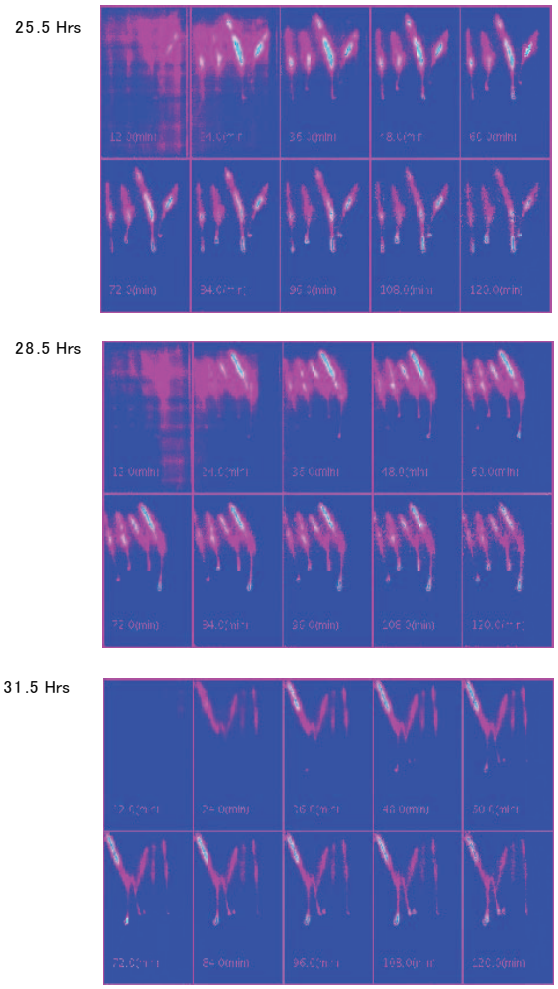

Fig.1 Aluminum-dependent modulation of photoassimilates-distribution in rice seedlings. Hydropotonically-grown rice seedlings (20-day old) were treated without (control, right two in each panel) or with 100 μM $AlCl_3$ (+Al, left two in each panel) in modified Ruakura medium (pH 4.3) for the indicated dulations. Then the entire seedlings were expose to $^{11}CO_2$, and the distribution of ^{11}C-labeled photoassimilates was monitored for 120 min. The radioactive counts integrated for every 12 min from a start till 120 min are shown.

3-61 Cyclotron Production of PET Radionuclide: No-carrier-added Bromine-76 with Protons on Natural SeO_2 and KBr Targets

N.S. Ishioka [a)], Sh. Watanabe [a)], Y. Iida [b), c)], H. Suto [a)], H. Hanaoka [b), c)], H. Yoshioka [c), d)], N. Suzui [a)], K. Endo [c), d)] and S. Matsuhashi [a)]

[a)]Radiation-Applied Biology Division, QuBS, JAEA, [b)]Bioimaging Information Analysis, Gunma University Graduate School of Medicine, [c)]The 21st Century COE Program for Biomedical Research Using Accelerator Technology, [d)]Diagnostic Radiology and Nuclear Medicine, Gunma University Graduate School of Medicine

In recent years Positron Emission Tomography (PET) has become established as particularly attractive tracer for cancer detection using positron-emitter. The increasing use of PET for clinical diagnosis, drug development and biological research has prompted many chemists to develop new labeling and purification methods. The PET radionuclides such as ^{11}C, ^{13}N, ^{15}O and ^{18}F have been used for imaging agent, which are short half-lives; ^{18}F with the longest half - life is 110 minutes. On the other hand, the positron-emitter with a longer half-life that can be applied to the PET diagnosis based on a nuclear characteristic is proposed besides above-mentioned nuclides. ^{76}Br is of potential interest in nuclear medicine: ^{76}Br has been suggested as a halogen label with a convenient half-life ($T_{1/2}$ = 16.1 h) and a sufficient β-branching ratio (57.2 %) in PET. Here we present the development of a direct and an indirect production methods for ^{76}Br.

^{76}Br was produced from the direct and indirect nuclear reactions ($^{76}Se(p,n)^{76}Br$, $^{79}Br(p,4n)^{76}Kr$ ($T_{1/2}$: 4.6 h)→^{76}Br). In the direct method, 6 ml of SeO_2 solution with the natural isotope composition was irradiated for 20-30 minutes with proton beams (20 MeV) of 1μA. The generated ^{76}Br was separated from the irradiated solution by anion exchange method. In the indirect technique, 1.2 g of NaBr pellet (10 mmφ) with the natural isotope composition was irradiated for 5-10 minutes with proton beams (65 MeV) of 0.5-1μA. The irradiated pellet was dissolved in 10 ml of H_2O. After dissolving the pellet 5 ml of 10 % H_2SO_4 was added in the solution. The resulting ^{76}Kr was transported to the upper vial with H_2 carrier gas and trapped in the 5 ml of H_2O (Fig. 1). After the decay of ^{76}Kr the generated ^{76}Br was collected. The ^{76}Br produced by both methods was measured with the high-pure Ge detector in each solution.

The production of ^{76}Br with proton induced reactions on natural SeO_2 and NaBr targets can be accomplished. These ^{76}Br yields are summarized in Table 1. The production yields were found to be 21-24 kBq/μA・min with SeO_2 target and 126 MBq/μA・min with NaBr target (EOB). In addition, the maximum production yield was calculated using the value of maximum beam current and irradiation time at TIARA AVF cyclotron. It was estimated that the amount of ^{76}Br was about 240 MBq in the use of SeO_2 target, and was about 360 MBq in the use of NaBr. In the comparison of production yields, an indirect method is more advantageous.

In a clinical application of ^{76}Br, it is necessary to be sufficient radioactivity for subsequent labeling. Further research into the development of the production method using enriched ^{76}Se target is currently underway.

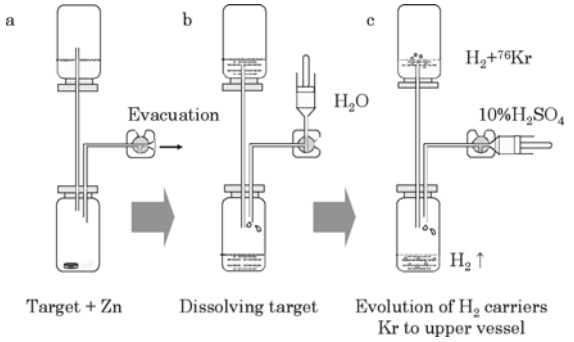

Fig. 1 Separation of Kr from NaBr. (a) Evacuation of the closed system containing target + 0.2 g Zn powder. (b) Target dissolved in water. (c) Hydrogen gas is evolved and carriers the Kr gases to the collection vial containing 5 ml of ultra-pure water.

Table 1
Recovery yields of ^{76}Br with SeO_2 and NaBr targets and maximum activity using TIARA AVF cyclotron

Nucler reaction	Beam energy	Target	^{76}Br yield (kBq/μA・min)	Irradiation condition	^{76}Br Activity (calculated)
$^{76}Se(p,n)^{76}Br$ (direct method)	20 MeV	0.1% SeO_2	21	5 μA×16 h	120 MBq
		10% SeO_2	24		
$^{79}Br(p,4n)^{76}Kr$-^{76}Br (indirect method)	65 MeV	NaBr	126	3 μA×16 h	360 MBq

3-62 Production of Radioisotopes for Nuclear Medicine Using Ion-beam Technology and Its Utilization for Both Therapeutic and Diagnostic Application in Cancer

Y. Iida [a)], H. Hanaoka [a)], T. Katabuchi [b,d)], S. Watanabe [b,d)], N. S. Ishioka [d)], S. Watanabe [d)] S. Matsuhashi [d)], T. Higuchi [c)], N. Oriuchi [c)] and K. Endo [c)]

[a)]Department of Bioimaging Information Analysis, [b)]21st Century COE Program and [c)]Department of Diagnostic Radiology and Nuclear Medicine, Gunma University Graduate School of Medicine, [d)]Radiation-Applied Biology Division, QuBS, JAEA

PET is superior in quantitative measurement, so ^{18}F-FDG-PET is most valuable tool for tumor diagnosis. Although several positron emitters have been used for PET, their uses are limited for their short half-lives. Compared with these radionuclides, ^{64}Cu and ^{76}Br have appropriate properties (^{76}Br: $T_{1/2}$ = 16.1hr, ^{64}Cu: $T_{1/2}$ = 12.7hr) and they may have great potentials for PET utility. In this study, we synthesized monoclonal antibody (mAb) labeled with ^{64}Cu or ^{76}Br and evaluated their potential for tumor diagnosis with PET. The results of tumor localization studies show that ^{64}Cu or ^{76}Br labeled mAb were highly accumulated to tumor. From these data, the use of ^{64}Cu and ^{76}Br has great advantage for PET utility.

PET（ポジトロン断層画像撮像法）はSPECT（シングルフォトン断層画像撮像法）、シンチカメラに比べ定量性、解像度の点で優れており、有用な画像診断法として注目されてきた。しかしながらPETに用いられる放射性核種（RI）はいずれも半減期が短く（^{18}F：110分、^{15}O：2分、^{13}N：10分、^{11}C：20分）、その利用にはサイクロトロンの設置が必要になるなど費用がかかるため、普及が制限されていた。近年、がん診断における^{18}F標識グルコース（^{18}F-FDG）の有用性が明らかになるとともに[1)]製薬企業による^{18}F-FDGの供給が開始され、PETの普及は大きく進展したが、一方でやはり^{18}F標識薬剤では安定したPET用製剤の供給に限界がある。そこで本研究では製薬企業からの供給が可能な程度の半減期（現在臨床で広く用いられている^{123}Iの半減期は約13時間）を有するPET用RIを利用し、がん診断を目的とした放射性薬剤の開発を行うことを計画した。

新しいPET診断用RIとして半減期：12.7時間の^{64}Cuおよび半減期：16.1時間の^{76}Brの製造を計画した。^{64}Cuは金属RIであることから化合物への導入にキレート結合部位を必要とするが、比較的安定な放射性薬剤を得ることが可能である。^{64}Cuの製造は^{64}Ni(p,n)^{64}Cu反応により行った。得られた^{64}Cuをモノクローナル抗体（NuB2）に標識し、マウスを用いてそのがん診断薬としての有効性を評価した。抗体とRIの結合には1,4,8,11-tetraazacyclotetradecan-1,4,8,11-tetraacetic acid (TETA)を用いた。

一方^{76}Brは^{18}Fや^{123}Iと同じハロゲンであり、これまでに開発されたがん診断、脳機能診断などに有効な^{18}Fあるいは^{123}I標識放射性薬剤をベースとした放射性薬剤の開発に適したRIであると考えられる。^{76}Brの製造は^{76}Se(p,n)^{76}Brあるいは^{79}Br(p,4n)^{76}Kr→^{76}Brにより行った。分離精製後、^{76}BrをNuB2に直接標識し、^{64}Cuと同様の方法により動物体内動態を評価した。

^{64}Cu-TETA-NuB2の標識率は約90%、精製後の放射化学的純度は99%以上であった。がんを移植したマウスに^{64}Cu-TETA-NuB2（約1μCi/匹）を投与したところ、腫瘍への高いRI集積を認めた[2)]（投与２日後で約13%dose/g、Fig.1A）。一方^{76}Br-NuB2の標識率は約10%と低く、精製後の放射化学的純度は約95 %であった。^{64}Cu同様、担がんマウスに^{76}Br-NuB2（1～4μCi/匹）を投与し、その体内動態を調べた結果、^{76}Br-NuB2も腫瘍へ高く移行することを認めた[3)]（投与２日後で約10%dose/g、Fig.1B）。

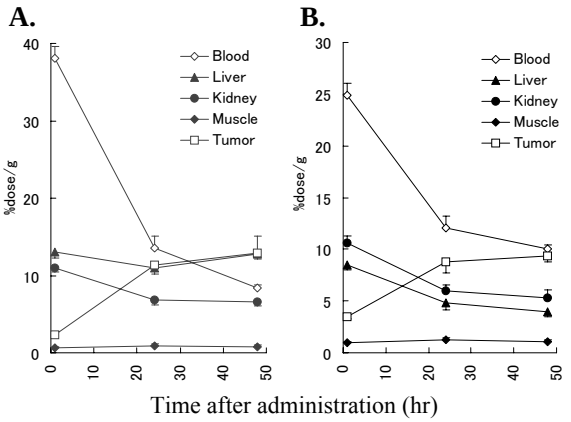

Fig.1 Biodistribution of (A) ^{67}Cu- TETA-NuB2 and (B) ^{76}Br-NuB2 in SCID mice bearing B-cell lymphoma RPMI1788 tumor xenografts. For each time point, data were acquired from five animals.

以上の結果より、新規PET用RIを用いたがん診断薬剤の有効性が示された。

References

1) Endo K, et al., Int. J. Clin. Oncol. 11, 286 (2006).
2) IIDA Y., et al., Proc. Mol. Imaging 5, 361(2006), The Big Island of Hawaii, USA.
3) IIDA Y., et al., Proc. World Journal of Nuclear Medicine 5, suppl1 S189(2006), Seoul, Korea.

3-63 Incident Energy Effect of the Production Yield of Endohedral ^{133}Xe-Fullerene by Ion Implantation

S. Watanabe, N. S. Ishioka and S. Matsuhashi

Radiation-Applied Biology Division, QuBS, JAEA

Endohedral fullerenes encapsulating a radioisotope within a fullerene cage have a possibility of being new radiopharmaceuticals. We have prepared endohedral ^{133}Xe-fullerenes by ion implantation[1]. Xenon-133 ($T_{1/2}$ = 5.243 d) would be useful for cancer therapy because it emits 0.346-MeV β^- rays (maximum range in water: 1.0 mm) followed by 81-keV γ rays and conversion electrons associated with the γ transition. However, we could not obtain efficient production of endohedral ^{133}Xe-fullerene. To achieve more efficient production, conditions of the ion implantation, especially incident energy, has to be studied. In the present paper, we describe incident energy effect on the production yield of endohedral ^{133}Xe-fullerene.

Fullerene targets for ion implantation were made by vacuum evaporation of C_{60} on Ni foils. Implantation of $^{133}Xe^+$ ions into the targets was carried out with an isotope separator at acceleration energies of 30 keV. For retardation of incident energy, the high voltage of 15kV was supplied from a retardation power supply to the fullerene targets: incident energy became 15 keV. Doses were in the rage of $1x10^{12}$ to $1x10^{14}$ cm^{-2}. After ion implantation, the fullerene part on the target was dissolved in *o*-dichlorobenzene. The solution was filtered through a membrane filter to remove insoluble materials. The filtrate was analyzed by high performance liquid chromatography (HPLC) with a Cosmosil Buckyprep column. Elution was done with *o*-dichlorobenzene at a flow rate of 1 ml/min. The concentration of fullerene in the effluent was continuously monitored by a UV detector. The effluent after UV measurement was collected in glass vials each for 1 min until 20 min and the ^{133}Xe radioactivity in each vial was measured by γ-ray spectrometry.

Figure 1 shows elution curves of ^{133}Xe and C_{60} obtained from the sample bombarded with ^{133}Xe ions of 15 keV at a dose of $2.0x10^{12}$ cm^{-2}. The strong correlation observed between the C_{60} and ^{133}Xe peaks corroborates the formation of ^{133}Xe@C_{60}. HPLC data obtained from the other samples also corroborate the formation of ^{133}Xe@C_{60}. In order to evaluate the efficiency of the formation of ^{133}Xe@C_{60}, the yield of ^{133}Xe@C_{60} was defined as a percentage of the radioactivity of ^{133}Xe@C_{60} to that of ^{133}Xe implanted into the target. The radioactivity of ^{133}Xe@C_{60} was obtained from the sum of the ^{133}Xe radioactivities in the fractions from 3 to 10 min. The yields of ^{133}Xe@$C_{60,}$ each of which is derived from one experiment, were plotted as a function of ^{133}Xe dose in Fig. 2. The solid and broken straight lines in those figures, which were fitted by the method of least-squares on log-log scales, are y=(10.18±0.09)-(0.842±0.007)x and y=(9.6±0.8)-(0.80±0.06)x on 15 and 30 keV, respectively. For both dose studied, the yields of ^{133}Xe@C_{60} were found to decrease with increasing dose. Because an increase of the dose leads to an increase of the number of damaged fullerene molecules as reported by Kastner *et al.*[2] from their Raman spectra measurements of fullerene targets bombarded with energetic-ions, those dose dependences of the production yields can be ascribed to amorphization of ^{133}Xe@C_{60}.

From comparison between both lines one can note that the yield of 15 keV is about 25% larger than that of 30 keV for the same dose in the rage of $1x10^{12}$ to $1x10^{14}$ cm^{-2}. Those energy dependences of the production yields can be also ascribed to the amorphization of ^{133}Xe@C_{60}. The yields of the ^{133}Xe@C_{60} should be more increased by decreasing incident energy.

References

1) S. Watanabe *et al.*, J. Radioanal. Nucl. Chem., 255 (2003) 495.
2) J. Kastner *et al.*, Appl. Phys. Lett. 65 (1994) 54.

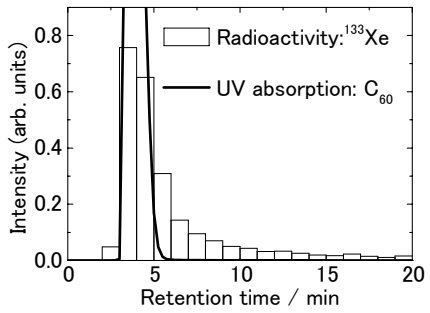

Fig.1 HPLC elution curves of ^{133}Xe and C_{60}.

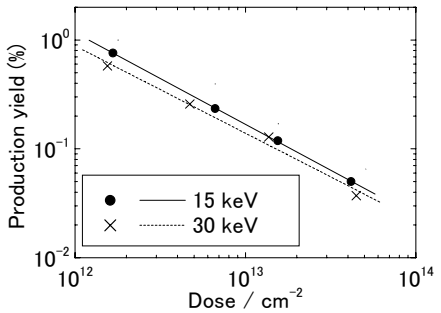

Fig.2 The yield of ^{133}Xe@C_{60} as a function of ^{133}Xe dose.

3-64 Analysis of Elements in Tumors and Normal Tissues following Irradiation by Micro-PIXE

M. Hasegawa [a,c,d], H. Sakurai [a,c], S. Ishiuchi [b,c], T. Tamamoto [d], I. Asakawa [d], M. Shin [a,c], M. Oikawa [c,e], T. Satoh [e], T. Kamiya [c,e], K. Arakawa [c,e] and T. Nakano [a,c]

Departments of [a]Radiation Oncology and [b]Neurosurgery, and [c]21st Century COE Program, Gunma University Graduate School of Medicine, [d]Department of Radiation Oncology, Nara Medical University, and [e] Department of Advanced Radiation Technology, TARRI, JAEA

The distribution of elements at the cellular level can be imaged by an in-air micro-particle-induced X-ray emission (micro-PIXE), but its application at the tissue level has been very limited. We compared the distribution of elements in tumors and normal tissues examined by the micro-PIXE with light-microscopic findings [1]. Furthermore, we analyzed the changes in the distribution of elements caused by cell death before and after irradiation.

Human ependymoblastoma, glioblastoma, and small cell lung cancer (SCLC) subcutaneously transplanted into male nude mice and normal organs (spleens, livers, kidneys, and testes) of mice were examined. X-ray irradiation (10 or 20 Gy) was administered, and the tumors or normal tissues were excised 3, 4.5, 6, 24, and 72 hours after irradiation. Frozen sections produced with a thickness of 5 and 10 micrometers were fixed by rapid drying and examined using an in-air micro-PIXE. After the examination, the samples were stained by hematoxylin-eosin, and observed by light microscopy to compare the distribution of elements and histological findings.

In the control (non-irradiation) groups, phosphorus (P), potassium (K), chlorine (Cl), and sulfur (S) were observed in the regions, corresponding to viable cells of the 3 tumors and normal tissues, and these elements seemed to be distributed in the nuclei and cytoplasm. In homogeneous areas of cells, these elements were homogeneously distributed, agreeing well with the morphological findings by light microscopy. But, the resolution of light microscopy was clearly higher than that of the micro-PIXE method. There were no significant correlations between the distribution of calcium (Ca), silicon (Si), or iron (Fe) and morphological findings. In the control groups of glioblastoma and SCLC, small necrotic areas were observed, and P, K, Cl, and S were significantly decreased in these lesions.

In the irradiation groups, a high incidence of TUNEL-positive apoptosis was detected in the ependymoblastoma and spleen 3-6 hours after 10 or 20 Gy irradiation by light microscopy. The incidence peaked 6 hours after, and decreased 24 hours after irradiation. In all ependymoblastoma and spleen samples with a thickness of 5, 10, or 20 micrometers, no significant differences between the irradiation and control groups were detected by the micro-PIXE, and the findings were almost the same as those in the control group or slightly inhomogenous in some samples (Fig.1). In the irradiation groups of glioblastoma and SCLC, small necrotic areas were detected at all excision times, and marked decreases in P, K, Cl, and S were observed in the regions, corresponding to the necrosed lesions and tissue defects. But, there was no significant difference in this change observed in the necrosed lesions between the irradiation and non-irradiation groups. No significant changes of elements were observed in the kidneys, livers and testes by the micro-PIXE, though a few apoptotic spermatogonia were found in the testes. There were no significant changes in the distribution of Ca, Si, and Fe in all tumors and normal tissues.

The light-microscopic morphology of the 3 different types of tumors and 4 organs examined in this study markedly differed, but examination by the micro-PIXE demonstrated almost no differences among the tumors and organs if they do not have necrotic areas. The resolution of light microscopy was clearly higher than that of the micro-PIXE.

In this study, we evaluated the applicability of an in-air micro-PIXE method to analyze of the distribution of elements at the tumor and normal tissue levels, and found that necrotic lesions could be imaged, suggesting the usefulness of this method in biological and medical fields. However, since the resolution of this method is much lower than that of light microscopy and apoptotic cell death was not detected, its improvement is required for evaluating the involvement of elements in microscopic changes.

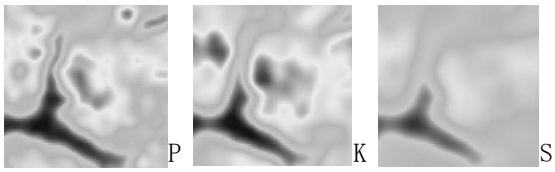

Fig.1 Spleen; 6hours after 20Gy irradiation.

Reference

1)Hasegawa M, Sakurai H, Ishiuchi S, Tamamoto T,Asakawa I, Shin M, Oikawa M, Satoh T, Kamiya T, Arakawa K, Nakano T. Analysis of radiation-induced cell death in vivo by micro particle-induced X-ray emission (micro PIXE). JAEA-Review 2006-42, 168 (2007).

3-65 Investigation of Cisplatin Sensitivity in Esophageal Squamous Cancer Cell Lines and the Localization of Pt Using In-air Micro-PIXE

N. Tanaka [a)], H. Kimura [a)], T. Asao [a)], H. Kuwano [a)], T. Sakai [b)], M. Oikawa [b)], T. Satoh [b)] and T. Kamiya [b)]

[a)] The 21st Century program, Graduate School of Medicine, Gunma University
[b)] Department of Advanced Radiation Technology, TARRI, JAEA

The purpose of this study was to elucidate the involvement of CDDP(cis-diammine dichloroplatium) in ESCC(esophageal squamous cell carcinoma) using in air-micro PIXE (Particle Induced X-ray Emission). Two human ESCC cell lines–TE-2 and TE-13–were examined for their response to CDDP. TE-2 cells were more highly sensitive to CDDP than TE-13 cells in MTT assay. Dynamic state of element and intracellular metabolism were measured in CDDP treated cancer cells using air PIXE. Using air PIXE, we observed distribution of P and K were localized at cytoplasm, and Br was localized at nuclear site. Air PIXE may be one of the new methods to measure CDDP combined with existing methods. Intracellular concentration of Pt was measured using air PIXE, unfortunately we cannot confirm the difference of distribution of intranuclear Pt in two cells at this moment. Air PIXE may have role in application to predict CDDP sensitivity in cancer cells. Our results using air PIXE has limitation, since it only can be presented by the imaging semi quantitative data. Future study will be needed to establish a new method for precise quantitative data.

近年、様々な癌において数多くの遺伝子の研究が行われているが、いまだに不明な点が多く、特に元素動態や分布などのレベルにおいては殆ど知られていない。そこで我々は、大気マイクロPIXEを用いて、食道扁平上皮癌におけるシスプラチン(Pt)の取り込みの検討を行った。食道癌は独特な生物学的特徴を有する癌である[1)]。化学放射線療法が効果的な癌の一つであり、そのresponderとnon-responderを選別することは、個別化治療において重要な課題になっている。我々は分子生物学的アプローチによる食道癌患者における化学放射線療法の感受性評価法を検討し報告している[2)]。我々は既存の感受性評価法にPIXEの技術を融合させることにより、さらに精度の高い感受性評価法を開発できないかと考えた。我々はこれまでの検討で、シスプラチン処理した食道癌細胞株を試料として、PIXEを用いた測定により、細胞内プラチナ元素の検出が可能であることを見出した。続いて、感受性の相違によるシスプラチン投与後の細胞内元素動態を比較するため、基礎実験としてシスプラチン感受性試験食道癌細胞株を用いてシスプラチン感受性試験(MTT assay)を行い、高感受性株(TE-2)と低感受性株(TE-13)を見出した。この差異につき細胞周期およびアポトーシスの面からも、FACSやDNA fragmentation assayを行い確認している。様々なシスプラチン投与濃度と時間を組み合わせ、試料作成を行い、PIXEを用いたシスプラチン感受性評価における試料の最適化を目指した。シスプラチンを細胞内のPt分布として評価するには、感受性評価に用いられるIC50より、かなり高濃度での投与が必要であった。ただし、この濃度での長時間投与ではほとんど全ての細胞がviabilityを失うため、高濃度短時間投与、具体的には、マイラー膜上に細胞を生着させ、2.0 mMのシスプラチン含有メディウムで1時間培養し、洗浄後凍結乾燥したサンプルにて、比較的短時間の照射でPt分布の安定した検出が可能であった。また、シスプラチンは核内に作用することに着目し、細胞培養の段階でBrdU

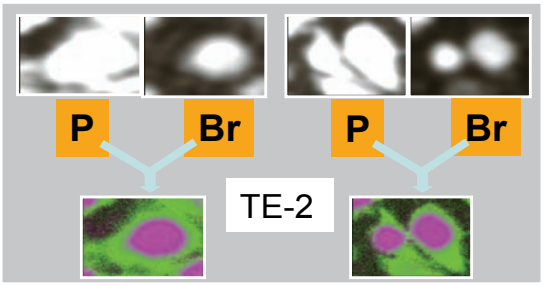

Fig. 1. Cell lines (TE-2) was cultured in medium including BrdU for 24 hours. The cellular configuration was identified by phosphorus (P). The nuclear localization in cell was identified by bromine (Br). The T/N ratio shows a marked tendency to high.

を用いることで、細胞内における核の局在を確認した。PIXEの実験では、カリウム(K)とリン(P)の分布より細胞質の形態の確認を行った。Fig. 1に細胞の形態を表すPと核の局在を表すBrの2次元分布画像と、それを合成したカラー画像を示す。PIXE分析の結果、高感受性株(TE-2)において細胞内のPtカウントが2488、核内が894であった。現在は、高感受性株のみ核内のPt分布の半定量化を行ったところであるが、今後はシスプラチン低感受性株(TE-13)においても同様の検討を行い、両者の比較検討を行っていく予定である。

References

1) Kuwano H., et al., Ann Thorac Cardiovasc Surg. 2003 Feb; 9(1): 6-13.
2) Sohda M., et al., Int J Cancer, 2004. 110(6): 838-44.

3-66 Direct Visualization and Quantification of Cis-platinum in a Human Lung Cancer Cell Using Micro-PIXE Analysis

H. Sakurai [a)], M. Okamoto [a)], M. Hasegawa [b)], T. Satoh [c)], M. Oikawa [c)], T. Kamiya [c)], K. Arakawa [c)] and T. Nakano [a)]

[a)]Department of Radiation Oncology, Gunma University Graduate School of Medicine, [b)]Department of Radiology, Nara Medical University, [c)]Department of Advanced Radiation Technology, TARRI, JAEA

We established an imaging method of intracellular CDDP, and also established the method of quantification of intracellular CDDP in a human lung cancer cell line using air micro-PIXE. For the purpose of nuclear labeling, the cells were incubated with 10 μM BrdU. After the pulse labeling of BrdU, the cells were exposed to CDDP at a concentration of 1 mM for 30 min to 24 hr. Analyses were performed with an in-air micro-PIXE system at the division of Takasaki ion accelerator for advanced radiation (TIARA). For 24 hr exposure of CDDP, there was unclear Pt signal detected at dose of 1-100 μM. However, significant Pt signals were seen dose at 1 mM. The Pt image quality by micro-PIXE was considered adequate if both the nucleus and cytoplasm could be visualized well enough to allow performance of the procedure. The stronger signals were detected in the intracellular nucleus rather than in the cytoplasm. For time course study, longer exposure time of CDDP shows more uptake of the drug in the cells. The elemental analysis using air micro-PIXE can be applied for biomedical samples. Intracellular distribution of CDDP can be visualized with very fine resolution, and individual intracellular concentration of CDDP can be measured using our system.

シスプラチンは現在，頭頸部腫瘍から肺癌，消化器癌，婦人科癌にまで幅広い領域でkey drugとなっている．また，シスプラチンはこれらの腫瘍に対し，放射線治療と併用して，有効な増感効果をもたらすとされている．しかし，臨床ではシスプラチンによる治療効果には，患者ごとに明らかな感受性の差がある．もし，個々の癌細胞の取り込んだシスプラチンが画像化，定量化できれば，シスプラチン感受性やシスプラチン耐性機構の解析のために，重要な情報をもたらすと考えられる．一方，大気マイクロPIXE（Particle Induced X-Ray Emission）は数MeVに加速したプロトンを試料に照射し，放出される特性X線を検出することにより，試料中に含まれる多くの元素を1 μmの分解能で解析できる装置である．個々の癌細胞の取り込んだシスプラチンを画像化，定量化できれば，シスプラチン感受性やシスプラチン耐性機構の解析において，重要な情報をもたらすと考えられる．

大気マイクロPIXEによるPtの定量性を確認するために，標準試料（Pt濃度を変化させた寒天を20 μmに薄切し凍結乾燥したもの）を作成し，測定を行った．細胞はヒト肺腺癌細胞であるA549を用いて，10 μM のBrdUでパルスラベルした対数増殖期の細胞を5 μm厚のマイラーフィルム上で培養し，生着したことを確認した後，1 mMのシスプラチンを接触させた．接触時間は30分から24時間とした．薬剤に接触後，THAMバッファーで６回洗浄した後，急速凍結乾燥した．解析は日本原子力研究開発機構高崎量子応用研究所の大気マイクロPIXE測定装置を用いた．

標準試料を用いた解析では，試料内のシスプラチン濃度と測定されたPtの間に直線性が明らかであった（Fig. １）．培養細胞試料では，P，K，Clなどの細胞の局在を示す元素，BrdUでラベルした核内Brおよび細胞に取り込まれたPtが検出可能であった．シスプラチン接触時間の延長とともに，細胞内Ptおよび核内Ptのカウントの増加が観察された（Fig２）が，生物実験に応用可能なPt濃度での検出は困難であった．

大気マイクロPIXEによるPtの細胞内可視化，定量化が可能であった．生物試料に応用可能であるが，検出感度をあげる工夫が必要と考えられた．

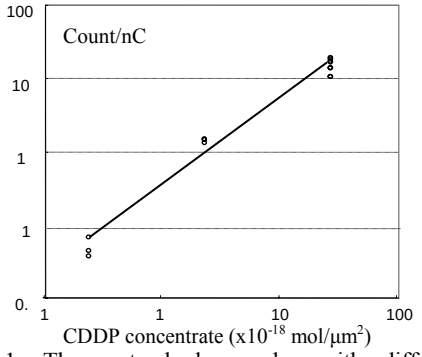

Fig.1. Three standard samples with different CDDP concentration was analyzed by in-air micro-PIXE

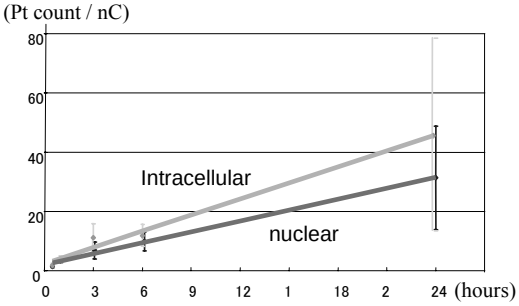

Fig.2. Intracellular and nuclear platinum count / nC according to CDDP exposure time

3-67 Analysis of Trace Metal of HCV Replicon by In-air Micro- PIXE and ICP-MS

K. Yuasa, H. Takagi, E. Saito, D. Takizawa, T. Ichikawa, S. Kakizaki, K. Sato, and M. Mori

Department of Medicine and Molecular Science, Gunma University Graduate School of Medicine

We had reported that zinc was a negative regulator of HCV replication. The distribution of trace metal in HCV replicon (HCV-O) using in-air micro-PIXE and ICP-MS was analyzed. In-air micro-PIXE revealed more zinc in nucleus than in cytoplasm and no significant difference was observed in HCV-O and control (Huh7). On the contrary, ICP-MS proved that zinc bound-metallothionein was higher in HCV-O than in be needed to elucidate this discrepancy.

1. はじめに

我々は微量金属の亜鉛が C 型肝炎ウイルス(HCV)に対して一定の抗ウイルス効果を有する事を報告してきた[1,2,)].しかし、亜鉛の HCV に対する作用は十分解明されてはいない。今回我々は in vitro HCV 産生細胞である HCV replicon を用い、micro PIXE 及びその他の定量系により HCV と微量金属、特に亜鉛の関係を調べた。

2. 実験方法

HCV replicon(HCV-O)は岡山大学加藤宣之教授より供与された。本細胞は人肝癌細胞株 Huh7 に full length の HCV を感染させて樹立された。Huh7 をコントロールとして、無刺激、Zn、interferon (IFN)、両者の併用による影響をみた。1) micro PIXE を用い細胞内微量金属を測定した。2) ICP-MS により細胞内 Zn、Cu、メタロチオネインの濃度を測定した。3) メタロチオネインは免疫染色、CdHem assay によっても測定した。

3. 結果

1) micro PIXE によって得た P と Br の分布から、細胞、核の contour を同定し得た。さらにそれに基づき細胞の Zn の分布を HCV-O と Huh7 で比較したところ差は無く、Zn、IFN, 両者の併用でも著明な差は見られなかった（Fig 1)。2) ICP-MS による測定では、無刺激状態では HCV-O は Huh7 に比し Zn は少ないが、Zn 刺激によって Huh7 より高まり、それは metallothionein (MT)結合型であった（data not shown)。3) MT の染色では、いずれも亜鉛添加によりコントロールに比し MT は増加したが、HCV-O でより強く増加した（Fig 2)。IFN と亜鉛併用でその傾向はより強くなった。

4. 考察

micro PIXE による細胞個々の微量元素の分布を HCV-O において測定したのは今回が始めてであり、Zn の核への局在は確認された。しかし、Huh7 との違い、刺激による変化を見出すことはできなかった。微量定量系である ICP-MS では Zn 刺激により HCV-O は MT 結合型の Zn をより多く、細胞内に取り込むことが判明し、MT 染色でも確認された。定量的には HCV は明らかに Zn の動態に影響を与えているが、micro PIXE ではその違いを捉えられないという結果であった。今後は micro PIXE での定量の可能性と、Zn 変化のメカニズムについて検討したい。

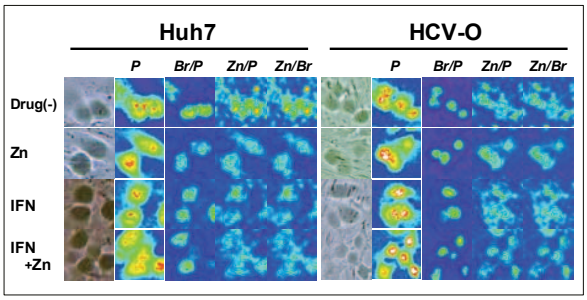

Fig 1. P, Br and Zn distribution map of Huh7 and HCV-O. Both cells were stimulated with Zn, IFN and both. P map represents whole cell figure and Br does nucleus as a background of Zn map. Zn and Br exist in the same area.

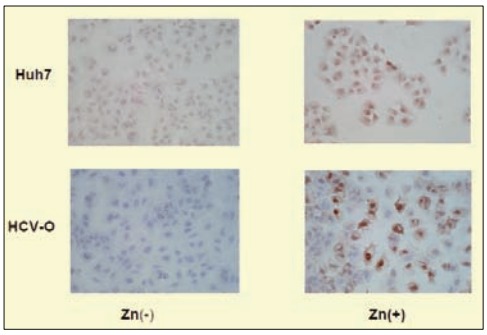

Fig 2. Huh7 and HCV-O are immunostained for metallothionein. Each cell was stimulated with Zn, and HCV-O showed higher expression of metallothionein than Huh7.

References

1).Takagi H, et al. J Viral Hepatitis. **8**:367-371(2001)

2).Yuasa K, et al. Liver Int. **26**:1111-8, (2006)

3-68 Improved Radiosensitive Liquid-core Microcapsules for Targeting of Chemotherapeutic Agents

S. Harada [a)], S. Ehara [a)], K. Ishii [b)], H. Yamazaki [b)], S. Matsuyama [b)]
T. Satoh [c)], M. Oikawa [c)], T. Kamiya [c)], K. Arakawa [c)] and K. Sera [d)]

[a)]Department of Radiology, Iwate Medical University
[b)]Department of Quantum Science and Energy Engineering, Tohoku University
[c)]Department of Advanced Radiation Technology, TARRI, JAEA
[d)]Cyclotron Center of Iwate Medical University

We have reported that microcapsules consisting of alginate and hyaluronic acid can decomposed by irradiation, and releases their core contents. These microcapsules have been generated by spraying a mixture of alginate and hyaluronic acid into $CaCl_2$ solution for more than 30 min. However, the use of Ca results in the hardening of the alginate, and the long polymerization time of more than 30 min results in the formation of microcapsules with thick outer shells. These factors prevent the efficient release of core contents from microcapsules[1)].

During microcapsule development, we observed that yttrium (Y) prevents the regular polymerization of alginate by calcium (Ca), thereby allowing easy rupture of the microcapsules. Moreover, sonication of a mixture of alginate and hyaluronic acid results in shorter polymerization time that in turn results in the formation of microcapsules with thin outer shells[2)]. In this study, the effect of Ca-Y polymerization and sonication of materials were tested, using micro-PIXE camera.

A 0.2% (w/v) alginate solution and 0.1% (w/v) hyaluronic acid were mixed in an agar pestle; these percentages were determined in our previous experiment[1, 2.] To this mixture, 0.2 mmol carboplatin (a platinum (Pt)-containing anticancer drug) was added. A droplet of this mixture was sonicated using an ultrasound disintegrator and atomized to yield a 4.34% solution of $CaCl_2$ that was supplemented with Y at concentrations ranging from 0% to 0.01%. Resulting microcapsules was irradiated with single doses of 0.5, 1.0, 1.5, or 2 Gy ^{60}Co γ-radiation. Then a frequency of microcapsules' rupturing were tested by micro PIXE camera.

The distribution of the microcapsular core contents (carboplatin) was imaged using a micro PIXE camera that detected platinum (Pt) signals (Fig. 1 a–h). The contours of the microcapsules were identified by detecting the distribution of Ca and ion beam-induced charge (IBIC) (Fig. 1(b), (d), (f), and (h)). Prior to irradiation, the microcapsule contours were clearly detected, and Pt was observed to be distributed within the capsules (Fig. 1(a), (b), and (d)). After irradiation, microcapsules with unclear Ca or Y distribution and with heterogeneous distribution of Pt (Fig. 1 (a)–(c) and (e)–(g)) were observed. We determined that these types of microcapsules had released their core contents upon irradiation. The frequency of microcapsules' rupturing were shown Fig.-2. The increment in the frequencies of microcapsule decomposition was dependent on the final concentrations of the added Y (Fig. 2). When the concentration of the added Y exceeded 3.0×10^{-3}%, the frequency of decomposition increased significantly (Fig.2). Significant increases in these frequencies were also observed when the radiation dose exceeded 1.0 Gy (Fig. 2). The maximum decomposition frequency was observed when the final concentration of the added Y was 5.5×10^{-3}% with 2.0-Gy irradiation. 2.0-Gy is the dose that is used in the conventional fractionated radiotherapy. Therefore, our microcapsules have a great possibility to be used in combination with clinical radiotherapy.

References

1) S. Harada *Nucl. Instrum. Methods. B* In press.
2) S. Harada *IJ PIXE* In press.

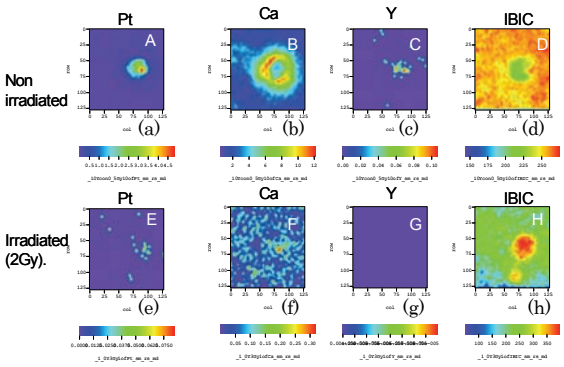

Fig.-1

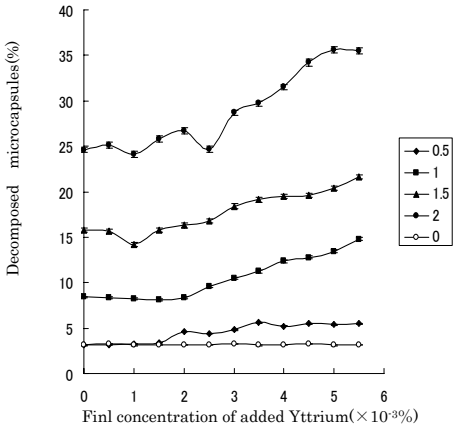

Fig.-2

3-69 Fluorine Uptake into Enamel around Fluoride-containing Materials during pH-cycling

H. Komatsu [a)], Y. Matsuda [a)], H. Yamamoto [b)], Y. Iwami [b)], S. Ebisu [b)], M. Nomachi [c)], Y. Sugaya [c)], K. Yasuda [d)], T. Satoh [e)], M. Oikawa [e)] and T. Kamiya [e)]

[a)]Department of Oral Health Science, Hokkaido University Graduate School of Dental Medicine, [b)]Osaka University Graduate School of Dentistry, [c)]Osaka University Graduate School of Science, [d)]The Wakasa Wan Energy Research Center, [e)]Department of Advanced Radiation Technology, TARRI, JAEA

Introduction

It is well established that the fluorine (F) is a possible agent for caries prevention. Also, the fluoride that contained some restorative material was demonstrated as a great benefit for preventing dental caries. The purpose of this study was to determine fluorine (F) uptake into enamel around fluoride-containing materials during pH-cycling[1)] using proton induced gamma-ray emission or PIGE technique[2)].

Material and Methods

Class I cavities in the buccal surfaces of 6 extracted human teeth were drilled and filled with fluoride-containing materials; “Fuji IX (GC)” (FN) and “UniFil flow (GC)” with “MEGA bond (KURARAY)” (UF), and nonfluoride-containing material; “SOLARE (GC)” (SO). Four 300-μm sections through the material were obtained from each tooth. All specimens were polished to a thickness of 120 μm. All tooth surfaces, except outer surface of enamel, were coated with a wax. In order to simulate daily acid challenges occurring in the oral cavity, the pH-cycling (pH 7.0-pH 4.5) was carried out for 0, 1, 3 and 5 weeks, separately[1)]. After pH-cycling, F distribution of the outer lesion in each specimen was evaluated using PIGE technique[2)]. The amount of F in the outer 125 μm of the lesion was calculated. Two-way ANOVA and Bonferroni test were used for the analysis ($p<.05$).

Results

F distribution of the specimens clearly showed the F uptake from FN into only enamel adjacent to the material, while the F uptake from UF and SO were not detected. The enamel adjacent to only FN remained the area as caries inhibition zone in wall lesion. For FN, the amount of F uptake into the outer lesion increased during pH-cycling (Fig. 1). The amount of F uptake in 5-week pH-cycling had significantly higher value comparing to those in 1- and 3-week pH-cycling. For UF and SO, there were no significant differences among the duration of pH-cycling (Fig. 2 and 3).

Discussion

For fluoride-containing UF, the F uptake into cavity wall was not detected. This indicated the bonding layer between the tooth and fluoride-containing material interfered with the F absorption into the tooth. Therefore, there was not the area as caries inhibition zone in wall lesion. It was confirmed that the amount of F uptake from FN increased during pH cycling. In a pH of 5.5-4.5, hydroxyapatite dissolves and, by supplying fluorine, precipitation of fluorapatite (FA) occurs because of the continuing supersaturation of FA. This suggests that FN operated as a resource for supplying fluorine when the pH was in the low range.

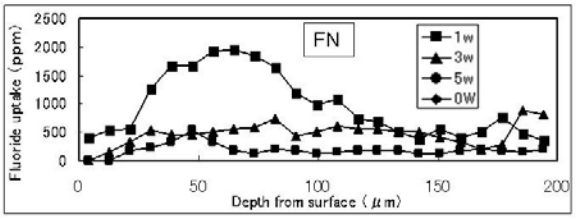

Fig. 1 Fluorine uptake from FN into the outer lesion during pH-cycling.

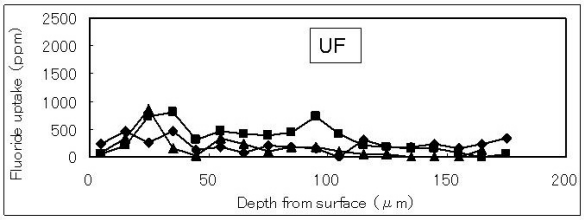

Fig. 2 Fluorine uptake from UF into the outer lesion during pH-cycling.

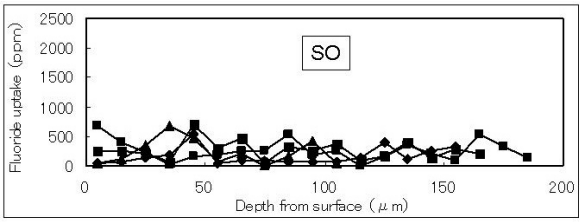

Fig. 3 Fluorine uptake from SO into the outer lesion during pH-cycling.

Conclusion

Among fluoride-containing materials, there existed some differences in the F uptake with increasing pH cycling.

References

1) Y. Matsuda et al., Dent. Mater. J. 24 (2006) 280.
2) H.Yamamoto et al., Nucl. Instr. Meth. B 210 (2003) 388.

This is a blank page.

4 Advanced Materials, Analysis and Novel Technology

This is a blank page.

4-01 SiC-based Membrane for Gas Separation Synthesized by EB Curing of Precursor Polymers

R.A. Wach, S. Yamamoto, M. Sugimoto and M. Yoshikawa

Environment and Industrial Materials Research Division, QuBS, JAEA

1. Introduction

SiC thin layer ceramics are expected to surpass the performance of polymeric, silica and carbon membranes. Beside superior mechanical behavior, they exhibit high oxidation resistance. Production of SiC coatings usually includes techniques where the substrate component is an inorganic SiC. However employment of organometallic polymer precursor, such as polycarbosilane (PCS) deposited from solution followed by pyrolysis is a simple and convenient method for SiC production. Recently we applied PCS and/or polyvinylsilane (PVS) derived SiC-base coatings on γ-Al_2O_3 substrate, as membranes for gas separation. Nevertheless, thermal stability of the substrate limits pyrolysis temperature to relatively low, 850°C[1)]. Present report describes combination of two deposition methods, i.e. pulsed laser deposition (PLD) and polymer derived coating.

2. Experimental Procedure

α-Al_2O_3 was used as a substrate. Initially, PLD system was used with a SiC target at argon atmosphere and 500°C. Subsequently, a blend of PCS (Mn 2600) and PVS (Mw 2800, Mn 960) in cyclohexane solution was spin coated onto PLD surface. Samples were cured (or not) by EB, typically to dose of 1.2 MGy at a dose rate of 1.2 kGy/s, under dry air atmosphere. In order to transform the polymeric coating into an inorganic SiC-based one, samples were pyrolyzed in Ar atmosphere up to 850 °C using controlled heating ramp. Nitrogen and hydrogen gas permeation tests were conducted with samples of effective permeation area of 1.0 cm^2 by a vacuum method.

3. Results and Discussion

While considering fabrication methods of membranes for selective gas permeation, controlling of pore diameter is the crucial issue. Surface of PLD and PCS/PVS (80/20wt%) derived SiC deposited on alumina substrate is presented in Fig. 1. A rough surface resulted from PLD deposition (5h) does not provide satisfying membrane parameters: N_2 permeance was measured as $2.5x10^{-7}$ mol·$sec^{-1}m^{-2}pa^{-1}$ and H_2/N_2 separation of 3.7 (Knudsen diffusion).

However, it provides proper support for polymer deposition. γ-alumina substrates with PLD originated SiC coated by preceramic polymer after pyrolysis shows relatively smooth surface. Thus we expect that such two-step technology of membrane preparation will be beneficial for its performance. Permeance of hydrogen and nitrogen was measured, and it was in the range 10^{-10} - 10^{-8} mol·sec^{-1}·m^{-2}·pa^{-1} depending on fabrication parameters. Accordingly, H_2/N_2 perm- selectivity was usually better than that characteristic for Knudsen diffusion. As an example, H_2/N_2 separation is presented in Fig.2. It was found nearly independent of PLD time, but strongly dependent on the polymer derived film. Here, one and two coating, irradiation, firing sequence is shown. Separation ratio is better, about 20, for twice coated substrate. So far, this separation ratio is smaller than that measured for membranes fabricated by four times polymer deposition[1)]. Therefore the combination technique presented here should be further developed.

References

1) R.A. Wach, M. Sugimoto, M. Yoshikawa, J. Am. Ceram. Soc. 90, 275 (2007).

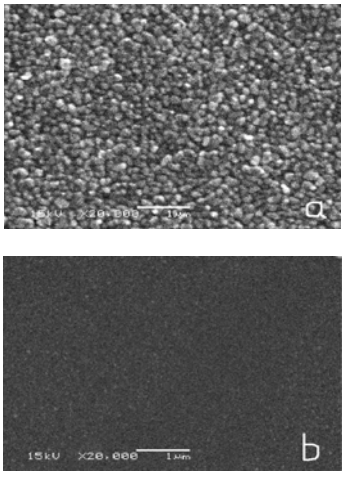

Fig.1. Surface of (a) PLD and (b) Polymer derived SiC.

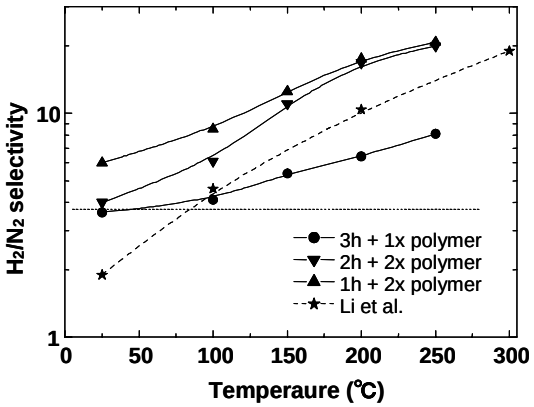

Fig.2. Perm-selectivity of N_2 and H_2. PLD followed by polymer deposition: PCS 80/20 PVS, 3% cyclohexane, spin coated at 1000rpm, irradiated at 1.2 MGy, fired at 850°C in Ar.

4-02 Effect of Ion Beam Irradiation on SiC Thin Film for Gas Separation

M. Sugimoto, R. A. Wach, S. Yamamoto, A. Inoue and M. Yoshikawa

Environment and Industrial Materials Research Division, QuBS, JAEA

1. Introduction

SiC thin film synthesized from Si-based polymer as a ceramic precursor by firing has an excellent thermal and corrosion resistance, and the structure is amorphous with nano-hole which has gas permeability [1]. Therefore, the SiC thin film is expected as a hydrogen separation filter that can be used in the severe environment. However, the improvement of the amount of the hydrogen penetration and the separation ratio is required. In this research, the possibility of controlling the gas penetration of the SiC thin film was examined by the methods of ion implantation to form the hydrogen catalyst layer in the SiC film and of making nano-hole structure by passing high energy ions.

2. Experimental Procedure

The polycarbosilane (PCS) concentration of 2.5% in cyclohexane solution was spin coated at 1000 rpm onto porous alumina substrates, and the coated substrates were cured by thermal oxidation at 453K, and then fired in Ar at 1023K to transform the polymeric film into an inorganic SiC ceramic-based one. The SiC thin film with 0.5μm thickness was synthesized by repeating these process five times. Subsequently, the hydrogen and nitrogen permeation of the samples at 373 and 473K were measured by differential pressure method. The samples exhibiting the gas separation function by the molecular sieving mechanism were irradiated with several kinds of ions with energies enough to pass through the SiC thin film. After irradiation, nitrogen and hydrogen gas permeation tests were conducted with samples exhibiting effective permeation. Moreover, the SiC thin films of 0.2 and 0.4 μm in thickness were formed on the silicon substrate using similar process, and the change in the film thickness by the ion beam irradiation was examined.

3. Results and Discussion

Figure 1 shows the permeation ratios of hydrogen and nitrogen at 573K before and after irradiation of various ions at $1x10^{12}$ion/cm^2. The permeation of nitrogen was not changed significantly by ion irradiation, but that of hydrogen decreased in 0.8 or less compared with that before irradiation, and the separation ratio of hydrogen/nitrogen became small. Moreover, when the ion fluence was increased up to $1x10^{14}$ion/cm^2, the nitrogen permeation also decreased to 0.9 compared with un-irradiated samples.

Figure 2 shows the thickness change of the SiC thin film according to the ion irradiation of Ni 15 MeV. The thickness decreased over 20% at $1x10^{15}$ ion/cm^2. It is likely that the decrement of the film thickness was in proportion to the initial thickness. Therefore the surface of the film was not reduced by ion sputtering, but by the shrinking of the film in the thickness direction. The SiC thin film has amorphous ceramic structure fired at low temperatures compared with ceramic structural materials such as SiC fiber, and thus it has shrunk easily by ion beam irradiation as well as shrinkage of the amorphous silica film [2]. The size of the nano-hole in which only hydrogen penetrates by the molecular sieve mechanism is about 0.3nm, and the number of the holes depends on the density of the SiC films. Therefore, the number of holes decreases by shrinkage, leading to a decrease in the amount of the gas permeation.

In the case of 0.5 MeV Pt irradiation, the projected range was estimated to be 0.14 μm below the SiC film thickness, and therefore the shrunk part was less than those of the other samples irradiated by high energy ions. However, the Pr irradiated film showed the smallest values of hydrogen and nitrogen permeation. According to the results of Rutherford Backscattering Spectrometry, the thin layer containing Pt was formed in the SiC film. It suggests that the formation of such thin layer reduces the number of nano holes, leading to the decrease of hydrogen and nitrogen permeation. Further investigations are necessary to clarify the mechanisms behind Pt irradiation.

References

1) R.A. Wach, et.al. J. Am. Ceram. Soc. 90, 275 (2007).
2) E. Snoeks, et.al. Appl. Phys. Lett., 65, 19, 7 (1994).

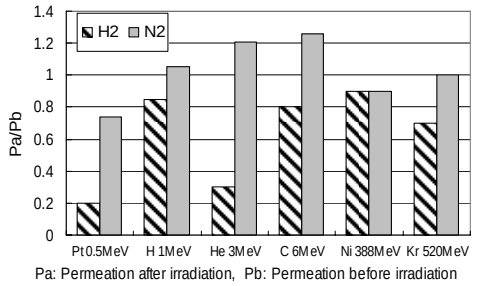

Fig. 1. Change in the hydrogen and nitrogen permeation ratios at 573K after irradiation of a variety of ions at $1x10^{12}$ion/cm^2.

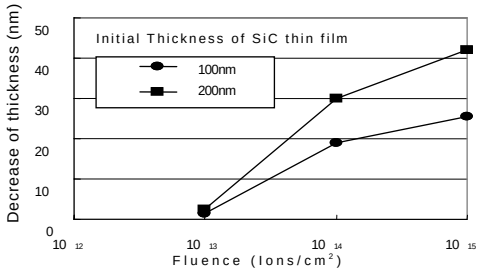

Fig. 2. Thickness change of the SiC thin film according to irradiation of Ni 15MeV.

4-03 Formation of Si Nano-crystals and Control of the Spatial Distribution in Si-thermal Oxides

H. Aiba [a)], Y. Ohki [a)], M. Nakamura [b)], H. Nishikawa [b)], T. Iwayama [c)], Y. Ishii [d)] and T. Kamiya [d)]

[a)]Waseda University, [b)]Shibaura Institute of Technology, [c)]Aichi University of Education, [d)]JAEA

Si nano-crystals attract much interest because of their unique electrical and optical properties. The formation of Si nano-crystals and control of spatial distribution are important in industrial devices. In this work, Si nano-crystals are fabricated in Si –thermal oxide film by ion implantation and thermal annealing. We have measured the dependence of the size and photoluminescence (PL) spectra of Si nano-crystals on the implantation doses. With increasing Si doses, the size of Si nano-crystals and the intensity of PL are increased, and the peak energy of PL is red shifted. This result indicates that size and PL of Si nano-crystals are controllable by Si implantation dose.

半導体ナノ結晶は量子サイズ効果による特異な電気的特性や光学的特性を持つため、多くの注目を集め、光･電子デバイスへの適用が検討されている。特に、その発光性や電荷蓄積機能を利用したエレクトロルミネッセンス(EL)素子およびメモリ機能への適用は多くの注目を集めている。また、自然界に大量に存在するため環境負荷が小さく、半導体や集積回路において広く利用されているシリコンのナノ結晶は産業用途においても重要である。本研究の目的は、シリコンナノ結晶の形成と、その空間的な配置制御である。そのため、シリコン熱酸化膜(膜厚600 nm)に対してシリコンイオン注入(Si^+, エネルギー200 keV, 照射量:3-7×10^{16} ions/cm^2)を行い、シリコンナノ結晶形成のためのイオン注入条件を検討した。さらに空間的配置制御のため、電子あるいはイオンビーム照射によるシリコン結晶析出が可能なシード基板の作成条件についても検討した。

実験では、窒素雰囲気中、1050 ℃において1時間の熱処理を行い、熱酸化膜中にシリコンナノ結晶を凝集させた[1)]。その後HFエッチングにより試料の表層300 nm程度のSiO_2を除去した後、原子間力顕微鏡(AFM)による表面観察を行った。また、顕微フォトルミネッセンス(PL)による光学特性評価(室温、488 nm励起)を行った。

イオン注入後のシリコン熱酸化膜を熱処理後にエッチングし、AFMにて表面状態を観察した。イオン注入していない試料では、表面に析出物は観測されなかったのに対し、イオン注入した試料では、エッチング後の試料表面にシリコンナノ結晶の析出が観測された。イオン注入量に対するシリコンナノ結晶の高さ及び幅をFig.1に示す。注入量が増加するにつれて析出するシリコンナノ結晶の高さと幅が共に増大した。Fig.2にイオン注入及び熱処理後の試料のPLスペクトルを示す。イオン注入量の増加と共に、PL強度が増大し、ピーク波長は600 nmから690 nmにレッドシフトした。発光強度の増大はFig.1に示すシリコンナノ結晶の粒径の増大と共に、発光種が増加したためと考えられる。それと共に、量子サイズ効果あるいは界面の変化が生じ、発光種が変化することで、ピーク波長がシフトしたと考えられる。

電子ビームあるいはMeVイオンビーム照射効果を利用したシリコンナノ結晶析出のためのシード基板をシリコンイオン注入にて作製した。熱処理により凝集したシリコンナノ結晶をAFM及びPL測定により観測し、作製した試料がシード層として利用可能であることを確認した。シリコンナノ結晶の大きさとPLスペクトルの強度は注入量の増加と共に増大し、ピーク波長はレッドシフトした。この結果から、注入量を制御することでシリコンナノ結晶の大きさと発光を制御できることが確認できた。今後は、本シード基板に対して電子線や高エネルギープロトンビームの照射を行い、局所的にシリコンナノ結晶を析出させる予定である。

Reference

1) T. Shimizu-Iwayama, et al., Nucl. Instrum. Methods B 230, 203 (2005).

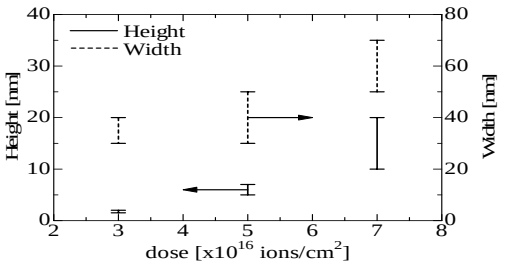

Fig.1 Height and Width of Si nano-crystals observed by AFM. Solid lines and dashed lines are height and width of Si nano-crystals, respectively.

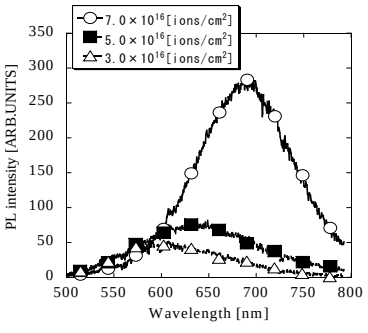

Fig.2 Photoluminescence spectra of Si nano-crystals induced by ion implantation and thermal annealing.

4-04 Radiation Oxidation of Silicon-based Polymer Blends

A. Idesaki, R. A Wach, M. Sugimoto and M. Yoshikawa

Environment and Industrial Materials Research Division, QuBS, JAEA

We have developed silicon carbide (SiC) coating for hydrogen gas separation membrane from a polymer blend of polycarbosilane (PCS) and polyvinylsilane (PVS). As one of the processes for synthesis of SiC coating, the PCS-PVS polymer blend is coated on the substrate, cured by irradiation in air, and pyrolyzed in an inert gas atmosphere. It has been found that the PCS-PVS polymer blend can be cured by the irradiation in air with dose as half as pure PCS. However, the mechanism of radiation oxidation curing of the PCS-PVS polymer blend has not been cleared. In order to clear the mechanism, it is useful to investigate the radical behavior of the PCS-PVS polymer blend because the radicals cause the oxidation and/or crosslinking of the molecules. In this work, the radical behavior of the PCS-PVS polymer blends was investigated.

Figure 1 shows the chemical structure of PCS and PVS. The PCS is a solid polymer at room temperature and its number average molecular weight is 2000. The PVS is a viscous liquid polymer at room temperature and its number average molecular weight is 960.

The PCS-PVS polymer blends were irradiated by gamma rays with dose of 0.2 MGy at liquid nitrogen temperature (77 K) in vacuum, and then the radicals in PCS-PVS polymer blends were measured by an electron spin resonance (ESR). The ESR measurements were also conducted for the PCS-PVS polymer blends irradiated by gamma rays with dose of 3 MGy at room temperature in air.

Figure 2 shows the relationship between the radical concentrations in PCS-PVS polymer blends and the PVS content after the irradiation of gamma rays at 77 K in vacuum. The radical concentration decreased linearly with increase in the PVS content. This suggests that the PVS does not affect on the production of the radicals in PCS-PVS polymer blends. Figure 3 shows the relationship between the radical concentration in PCS-PVS polymer blends and the PVS content after the irradiation of gamma rays at room temperature in air. Comparing with the result in Fig. 2, the radical concentration in the PCS-PVS polymer blends irradiated in air was low by a factor of 10^2. This means that the produced radicals were decayed during the irradiation at room temperature in air. Furthermore, a tendency that the radical concentrations in PCS-PVS polymer blends were below the straight line that links the points of 0 % PVS and 100 % PVS was shown.

The decay of radicals in case of the irradiation in air is considered to be attributed by the recombination of the radicals (partly crosslinking) and production of peroxides (-OOH). So, the radicals in the PCS-PVS polymer blends may decay easily due to characteristics of the PVS such as liquid, low molecular weight, and rich Si-H bonds, that is, high mobility of molecules and high reactivity of Si-H bonds with oxygen. However, we can not distinguish clearly the recombination of radicals or the production of peroxides as a reason to cause the decay of radicals for the moment. Further investigation is necessary to know the radiation effects on the PCS-PVS polymer blends in detail.

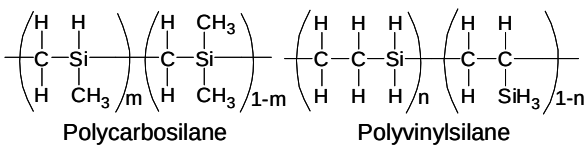

Fig.1 Chemical structure of polycarbosilane (PCS) and polyvinylsilane (PVS).

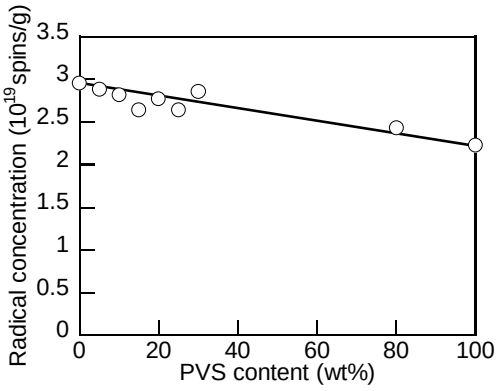

Fig.2 The relationship between the radical concentrations in PCS-PVS polymer blends and the PVS content after the irradiation of gamma rays at 77 K in vacuum.

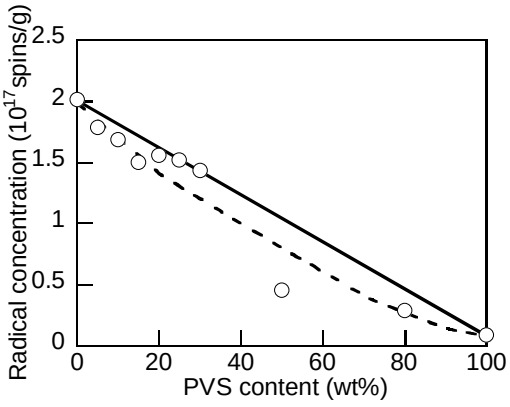

Fig.3 The relationship between the radical concentration in PCS-PVS polymer blends and the PVS content after the irradiation of gamma rays at room temperature in air.

4-05 Possibility of Silicon Carbide Micro-tube Synthesis from Polycarbosilane-silicone Oil Blend Precursors

K. Kita [a)], M. Narisawa [a)], H. Mabuchi [a)], M. Itoh [b)], M. Sugimoto [c)] and M. Yoshikawa [c)]

[a)]Division of Materials Science, Graduate School of Engineering, Osaka Prefecture University
[b)]Fukushima National College of Technology
[c)]Environment and Industrial Materials Research Division, QuBS, JAEA

A blend polymer of 85 mass% polycarbosilane (PCS) and 15 mass% poly-hydro methylsiloxane (H-oil) was prepared as ceramic fiber precursor. Viscosity measurements on the blend polymer indicated that the blend polymer was sufficiently melt-spinnable at temperatures of 543 and 573 K. Optical microscope observation indicated that the fiber spun at 543 K was turbid, while the fiber spun at 573 K was transparent. IR spectra revealed that HS Low fiber (PCS – H-oil blend fiber melt spun at 543 K) maintained original H-oil content during melt spinning process, while the H-oil content in HS High fiber (PCS – H-oil blend fiber melt spun at 573 K)decreased. After thermal oxidation or radiation curing and pyrolysis at 1273 K, fibers with continuous pore structures were obtained. Continuous pore structure depends on spinning and curing conditions.

当研究グループではポリカルボシラン（PCS）と異種のポリマーをブレンド紡糸、放射線照射不融化、焼成することにより、より細い直径を有するSiC系繊維の合成などを行ってきた。この場合、PCSにブレンドされる前駆体は、PCSに良好な相溶性を示す一方、極めて高価、稀少であることが多い。近年、我々は、より低廉であり、一般的に入手しやすいシリコーンオイルについてPCSとのブレンド時の挙動、繊維化について検討を開始した。

シリコーンオイル、シリコーン樹脂には極めて多くの種類があるが、一次元的な構造を有する通常のシリコーンは、セラミックス収率が極めて低い。繊維原料としてPCSに混合し、分散状態や不融化過程を制御することにより、繊維内部にナノレベルの細孔を形成できる可能性がある。

しかし、今までにこのような組み合わせについて、相溶性、紡糸性、不融化法の適否、微細構造変化の傾向について、系統的な検討を行った例は無い。当研究ではこのようなテーマの追求を主体に、電子線照射、ガンマ線照射、および不融化時の雰囲気制御を組み合わせて、研究を遂行中である。

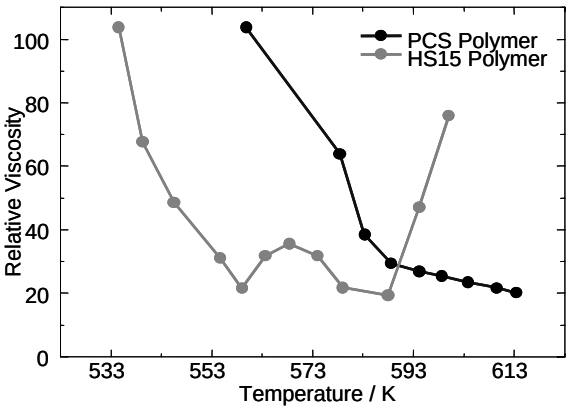

Fig.1 Relative viscosity of PCS-H-oil polymer blend with temperature rising.

Fig. 1に一例として、PCSに対して、Si-H基を側鎖に有するタイプのシリコーンオイルをブレンドし、加熱時の溶融粘度測定を行った結果を示す。粘度は単純に下方にシフトするのではなく、粘度が減少を始める温度自体が低温側に移動していることが分かる。これはシリコーンオイルがPCSに対して、一部は相溶し、軟化剤として働いていることを示している。しかし543Kでの紡糸では、繊維は不透明な白色の外観を呈し、全てのオイルが相溶しているわけではないことも示された。相溶の限界はおおよそ10mass%程度と見積もられた。

低温紡糸により、わずかにオイルリッチなドメインを残した状態で電子線照射による不融化を行い、焼成後に繊維断面の観察を行った結果をFig.2に示す。オイルリッチ成分とPCSリッチな部位との間に三日月状の孔としてサブマイクロレベルの細孔が存在していることが分かる。ただし、放射線照射不融化がオイル自体にも働いてしまうため、細孔の形成が見られないケースもあり、良好な線量を選定する必要性を示している。

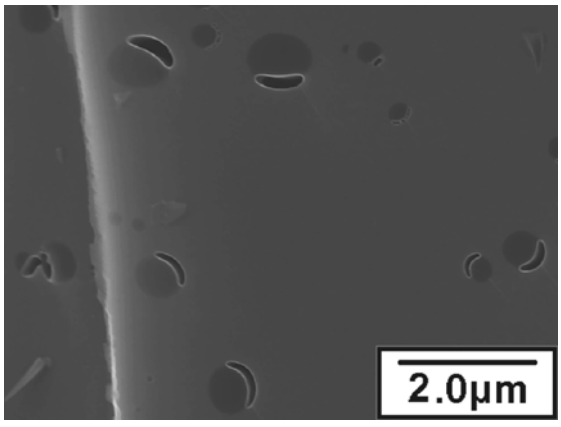

Fig.2 Small crescent pores observed on the cross section of HS15 Low fiber cured with electron beam curing for 1.5h.

4-06 Effects of Ion Irradiation on Microstructural Change of SiC Nanotubes

T. Taguchi [a)], Y. Yamada [a)], K. Kodama [a)], S. Yamamoto [b)], H. Yamamoto [a)] and S. Shamoto [a)]

[a)]Neutoron Material Research Center, QuBS, JAEA, [b)] Environment and Industrial Materials Research Division, QuBS, JAEA

Since the discovery of carbon nanotubes (CNTs) in 1991, significant numbers of researches have prepared new one-dimensional nanostructured materials such as nanotubes, nanorods and nanowhiskers for potential applications. Some of them report that many nanomaterials such as TiC, NbC, BN, C/C/N, SiO_2 and GaN nanostructures are synthesized from CNTs as the template materials. We reported that the C-SiC coaxial nanotubes, which were CNTs sheathed with SiC, were formed. Furthermore, the single-phase SiC nanotubes were successfully synthesized by heating the C-SiC coaxial nanotubes in air. SiC is the most important semiconductor and has the excellent mechanical properties at high temperature. These SiC nanotubes are expected to be electrical devices and reinforcement materials used in radiation environments due to their excellent stability against radiations. Until now, there have been many researches about the effects of irradiation on the microstructural change of SiC bulk materials. However, the effects of irradiation on the microstructural change of the SiC nanostructure materials with peculiar shape such as SiC nanotubes in this study have not been investigated. The purpose of this study is, therefore, to investigate the effects of ion irradiation on the microstructural change of SiC nanotubes.

CNTs (GSI Creos Corporation, Tokyo, Japan) as the template materials and Si powder (The Nilaco Corporation, Tokyo, Japan) were used. The C-SiC coaxial nanotubes were synthesized by the reaction CNTs with Si powder at 1200 °C for 100h in a vacuum. Single-phase SiC nantoubes were formed by the heat treatment of C-SiC coaxial nanotubes at 600 °C for 2h in air. Thin films of single-phase SiC nanotubes were prepared by embrocating with the single-phase SiC nanotubes dispersed in ethanol on the alumina plates. These thin films of single-phase SiC nanotubes were irradiated by 3.0-MeV Si^{2+} ions at 300 °C and 900 °C. The irradiation dose was $6.4x10^{20}$ ions/m^2.

The results of X-ray diffraction measurements revealed that no change was observed by the ion irradiation at 300 °C and 900 °C .

The XPS spectra of the C 1s bands for the SiC nanotubes before and after ion irradiation at 300 and 900 °C are shown in Fig.1. There are two peaks representing Si-C and C-C in all specimens before and after ion irradiation. The energy difference between the peaks representing Si-C and C-C decreased with increasing the irradiation temperature. This result indicates that the binding state of SiC nanotubes changed by the ion irradiation at higher temperature. Similarly, the results of XPS measurements of the Si 2p bands for the SiC nanotubes before and after ion irradiation indicated that the peak representing Si-C existed in all specimens. The peak representing $Si-O_2$ also existed in the specimen before ion irradiation. However, the peaks representing Si-O and $Si-O_2$ disappeared by the ion irradiation.

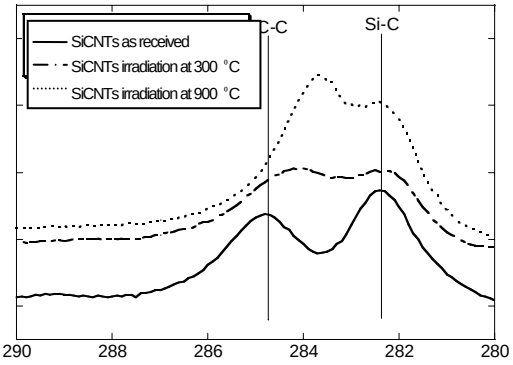

Fig.1 XPS of C 1s in the SiC nanotubes before and after 3.0 MeV Si^{2+} ion irradiation at 300 and 900 °C.

The TEM observation revealed that the SiC nanotubes before ion irradiation were composed of the SiC grains with the size of a few nm to a few ten nm. Several single crystalline SiC nanotubes were formed by the ion irradiation at 900 °C. The result can be explained by the assertion that the grain growth of SiC nanotubes was enhanced by the ion irradiation at such high temperature.

References

1) T. Taguchi, N. Igawa, H. Yamamoto, S. Jitsukawa, J. Am. Ceram. Soc. 88 [2] (2005) 459-461.
2) T. Taguchi, N. Igawa, H. Yamamoto, S. Shamoto, S. Jitsukawa, Physica E 28[4] (2005) 431-438.

4-07 Fabrication of Blue-light Emitting Fused-silica Substrates by Using Si-ion Implantation

K. Miura [a], T. Tanemura [a], O. Hanaizumi [a], S. Yamamoto [b], K. Takano [b], M. Sugimoto [b] and M. Yoshikawa [b]

[a]Faculty of Engineering, Gunma University, [b]Environment and Industrial Materials Research Division, QuBS, JAEA

Introduction

Various works on silicon (Si) based luminescent materials utilizing the quantum confinement effect, such as Si nanocrystal (Si-nc), have been reported. Typical fabrication methods of Si-ncs are co-sputtering of Si and SiO_2 [1,2], laser ablation [3], and Si-ion implantation into SiO_2 plates or thermal oxidized Si wafers [4,5]. Pavesi et al. reported that their samples including Si-ncs formed by using Si ion implantation exhibited photoluminescence (PL) and a large optical gain of $100cm^{-1}$ in a wavelength range from red to infrared after annealing at 1100 °C [4]. The optical gain is nearly equal to that of III-V semiconductors. Therefore, it has recently been anticipated that light emission devices composed of Si-nc-containing materials could be realized. In this work, we fabricated Si-nc including fused-silica substrates by using the Si-ion implantation method and annealing, and evaluated their PL properties.

Fabrication and Evaluation

Si ions were implanted into a fused-silica substrate (10 mm x 10 mm x 1 mm^t) at room temperature in TIARA. The implantation energy was 80 keV, and the implantation amount was 1 x 10^{17} ions/cm^2 [4]. The Si implanted substrate was cut into four pieces (0.5 mm x 0.5 mm x 1 mm^t) using a diamond-wire saw and they were annealed in air for 25 min at 1100, 1150, 1200, and 1250°C by using a siliconit furnace. PL spectra were measured at room temperature with excitation using a He-Cd laser (λ=325 nm). A monochromator, a photomultiplier, and a lock-in amplifier were used in our measurements. Figure 1 presents the PL spectra of the four samples generated at room temperature. Blue PL spectra having peaks around a wavelength of 400 nm were observed from all the samples. The peak wavelengths of the blue PL spectra of the samples are almost the same in spite of the varying annealing temperature. In our experiments, the blue PL peak had a maximum intensity after annealing at 1200 °C, and the intensity was 4.2 times higher than that of the peak of the longer wavelength band of the sample annealed at 1100 °C.

Discussion

Liao et al. reported that a blue PL having a peak wavelength of 470 nm was observed from Si-ion-implanted SiO_2 films and stated that the blue-light emission may have originated from an oxygen-defect level in SiO_2 [5]. However, the emission origin seems to differ from that of our samples owing to the difference of the PL peak wavelengths. In addition to a blue PL peak, a PL peak around a wavelength of 800 nm in a wavelength range from red to infrared was observed for the sample annealed at 1100°C. In our experiments, the Si-ion-implant conditions were almost the same as those reported in ref. 4 and the annealing temperature of 1100 °C is common to ref. 4, therefore it seems that Si-ncs are also formed in this sample. There may be a common origin of blue-light emission in these samples and Si:SiO_2 co-sputtered films [1]. The SiO_x layer located at the interfacial region of Si nanoclusters and surrounding SiO_2 medium may contribute to such emission. Blue-light-emitting materials are expected to be useful as light sources for optical pick-up systems. Therefore, we are trying to optimize the conditions of Si-ion implantation and annealing to improve the emission intensity and evaluate optical gains of the Si-implanted samples.

References

1) O. Hanaizumi et al., Appl. Phys. Lett. 82 (2003) 538.
2) O. Hanaizumi et al., Jpn. J. Appl. Phys. 41 (2002) L1084.
3) Y. Yamada et al., Jpn. J. Appl. Phys. 35 (1996) 1361.
4) L. Pavesi et al., Nature 408 (2000) 440.
5) L. S. Liao et al., Appl. Phys. Lett. 68 (1996) 850.

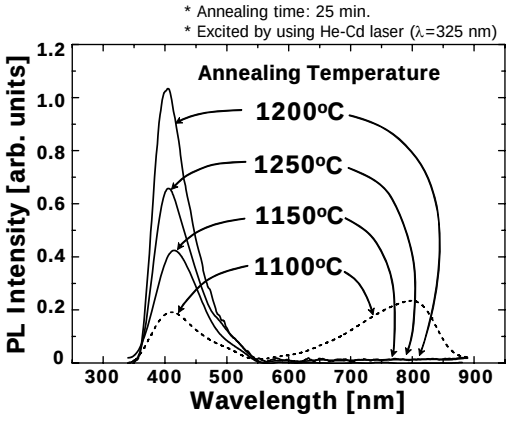

Fig.1 Measured PL spectra. PL peaks around a wavelength of 400 nm were observed from all the samples. The longer-wavelength peak was reduced after annealing above 1150 °C.

4-08 Effect of Impurity Co-implantation on Hydrogen Surface Exfoliation

H. Iwata [a,c], M. Takagi [b,c] and Y. Tokuda [a]

[a]Department of Electronics, Aichi Institute of Technology, [b]Department of Mechanical Engineering, Aichi Institute of Technology, [c]Research Institute for Industrial Technology, Aichi Institute of Technology

SOI (silicon on insulator) fabrication has become an attractive technology for low power, low voltage and high-speed electronics. Much attention has been given to the hydrogen exfoliation method introduced by Bruel [1] in comparison with other SOI fabrication techniques. This method involves the micro slicing process of silicon by high-dose hydrogen implantation and has advantages of greater uniformity of thickness and higher crystal quality of the silicon layer than other processes [1,2]. Although this unique and useful process has been extensively developed in industrial applications during the past few years, the fundamental phenomenon and the underlying mechanism are still not completely understood [3]. Behaviors of exfoliation on the surface were mainly examined by in-situ microscopic experience. From these results, we attempt to explain the relation between the defects distributions and the exfoliation phenomena, and report the effects of impurities (boron or fluorine) co-implantation.

Hydrogen ion implantation was performed in p-type Cz-grown (100) oriented silicon. The implantation energy was 80keV and hydrogen dose was 8×10^{16} H/cm^2. After the hydrogen implantation, boron ion was implanted with 140keV. The projection rang (Rp) of boron is same depth with the Rp of hydrogen.

These specimens were annealed at in-situ heating optical microscopy (OM) experience. Annealing was carried out till 700° C. Defects distribution was estimated using cross sectional transmission electron microscopy (XTEM). Exfoliated area of surface were evaluated by scanning electron microscopy (SEM) and OM, and the depth of exfoliation was obtained with scanning prove microscopy (SPM). The damaged layer caused by hydrogen ion implantation is located in the region from 600nm to 800nm depth from the surface. Increasing the doses of boron bellow 3×10^{14} B/cm^2, the thickness of the damaged layer became narrower. Bellow 3×10^{14} B/cm^2 dosage, the number of exfoliated pieces was proportional to the boron dose, and average exfoliated diameter was proportional to the hydrogen dose. The total exfoliated area was maximized at 3×10^{14} B/cm^2 dosage. Over the 3×10^{14} B/cm^2 dosage, the number of exfoliated pieces was inverse proportional to the boron dose, and average exfoliated diameter was inverse proportional to the hydrogen dose. The total exfoliated area was maximized at 3×10^{13} B/cm^2 dosage. However, from XTEM observation, long crack was observed in the damaged layer of as implanted specimen. Using this condition, exfoliation with no annealing was observed.

Fluorine ion was implanted with 300keV. The projection rang (Rp) of fluorine is almost coincident with the Rp of 80keV hydrogen. After the fluorine implantation, the defect distributions were observed by XTEM.

In a fluorine dose range from 1×10^{16} F/cm^2 to 5×10^{16} F/cm^2, a thick amorphous layer is formed in the surface vicinity. However, no differences were seen in the thickness of amorphous layer.

In the case of H and F co-implantation (as shown in Fig.1), crystal layer was found in the surface side. After the 700° C annealing, it was found that the thickness of crystal layer was proportional to the hydrogen dose. The result that hydorgen has an important role of impeding the amorphization

References

1) M. Bruel, Electronics letters 31 (1995) 1201,
2) Q.Y. Tong, R.W. Bower, MRS Bulletin 23 (1998) 40
3) M.K. Weldon, et al., J. Vacuum Science Technology B 15(1997) 1065

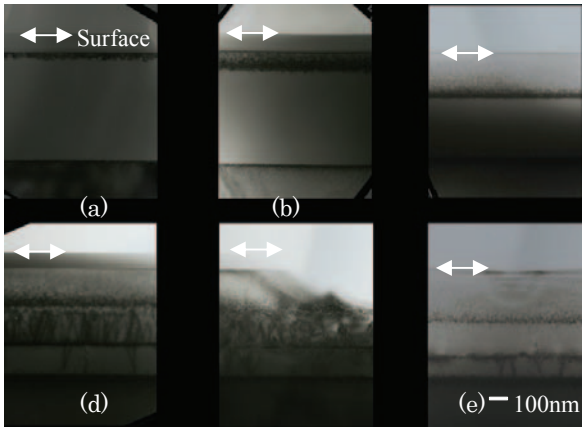

Fig.1 Damage layers obtained by cross-sectional TEM. (a): (H 1×10^{16} + F 1×10^{16}) / cm^2 as implanted. (b): (H 3×10^{16} + F 1×10^{16}) / cm^2 as implanted. (c): (H 8×10^{16} + F 1×10^{16}) / cm^2 as implanted. (d): (H 1×10^{16} + F 1×10^{16}) / cm^2 as annealed. (e): (H 3×10^{16} + F 1×10^{16}) / cm^2 as annealed. (f): (H 8×10^{16} + F 1×10^{16}) / cm^2 as annealed.

4-09 Improvement of Gasochromic Properties in Tungsten Oxide by Ion Irradiation II.

K. Takano [a)], A. Inouye [b)], S. Yamamoto [a)], A. Miyashita [a)] and M. Yoshikawa [a)]

[a)]Environment and Industrial Materials Research Division, QuBS, JAEA,
[b)]School of Engineering, Tohoku University

Tungsten trioxide, WO_3, has gasochromic coloration in that the color changes from yellow to dark blue in hydrogen atmosphere. Fiber-optic hydrogen gas sensors using a gasochromic WO_3 film have been studied to support the safe utilization of hydrogen as a clean energy source for the environment in recent years[1,2)]. One of the subjects of the investigation in the WO_3 film is large extent of the gasochromic coloration for satisfying the specifications of hydrogen sensors. The gasochromic properties are considered to relate to oxygen vacancies or defects in the tungsten oxide[3)]. In our study, ion beam irradiations have been tried to make oxygen vacancies in WO_3 thin films, and a possibility of the improvement in the gasochromic coloration has been investigated.

WO_3 thin films with the thickness of 0.4 μm were prepared on quartz glass substrates by reactive rf magnetron sputtering method with argon and oxygen mixture. After the deposition, the films were annealed at the temperature of 400 ºC during 1 hour. The films were confirmed to have crystal peaks by the measurement of x-ray diffraction. The crystal structure was assigned to be monoclinic plane of WO_3[4)]. To investigate the gasochromic coloration of the films, a reduction of the intensity transmitted 630-nm-wavelength light was measured with an exposing of 1 % hydrogen diluted with argon gas. The typical reduction of the intensity at the exposure time of 600 seconds, that is, the extent of gasochromic coloration, R_0, was 15 %. $^4He^+$ irradiations were performed in the fluence range from $5x10^{14}$ to $1x10^{17}$ ions/cm^2 at room temperature using the ion implanter at JAEA/Takasaki. The incident energy was selected 40 and 350 keV. After the irradiations, the extent of gasochromic coloration, R, was measured with the same procedure to the case of R_0.

In the previous report with x-ray photoelectron spectroscopic analysis[5)], 20 % of the tungsten atoms in WO_3 film changes to oxygen-deficient tungsten caused by the 350 keV He^+ irradiation at the fluence of $1x10^{17}$ ions/cm^2. Here, it is supposed that the oxygen vacancies of $1.1x10^{22}$ number/cm^3 are created at the fluence of $1x10^{17}$ ions/cm^2, as the theoretical density of oxygen atom in WO_3 is 5.7 $x10^{22}$ number/cm^3. In the case of 40 keV irradiation, the amount of the oxygen vacancy is expected to be 8.2-fold of that in 350 keV from a calcuration[6)] with theoretical density of monoclinic WO_3, 7.29 g/cm^3. Assuming that the amount of oxygen vacancy is proportion to the fluence of 40 and 350 keV irradiation, the oxygen vacancy dependence of the gasochromic coloration is shown in Fig. 1. The value of R increases with increasing of the oxygen vacancy. At the amount of oxygen vacancy from $1x10^{22}$ to $5x10^{22}$ number/cm^3, which is equivalent from 1 to 9 % of oxygen atoms in the WO_3 film, R has the maximum to be more than 3-fold of R_0. However, in the range above $5x10^{22}$ number/cm^3, R returns to R_0. From this result, it is concluded that the optimum number of oxygen vacancy for high extent of the gasochromic coloration in WO_3 films exists.

Ion irradiation to WO_3 films was found to improve their gasochromic coloration by introducing oxygen vacancies, and expected to achieve high performance of gasochromic hydrogen sensor based on the WO_3 films.

References

1) K. Ito and T. Ohgami, Appl. Phys. Lett. 60 (1992) 938.
2) K. Takano, et al., Trans. Mater. Res. Soc. Jpn. 31 (2006) 223.
3) A. Georg, et al., Thin Solid Films 384 (2001) 269.
4) B. O. Loopstra and P. Boldrini, Acta Cryst. 21 (1966) 158.
5) K. Takano et al., Trans. Mater. Res. Soc. Jpn. 32 (2007) 159.
6) J. P. Biersack and L. Haggmark, Nucl. Instr. and Meth., 174 (1980) 257.

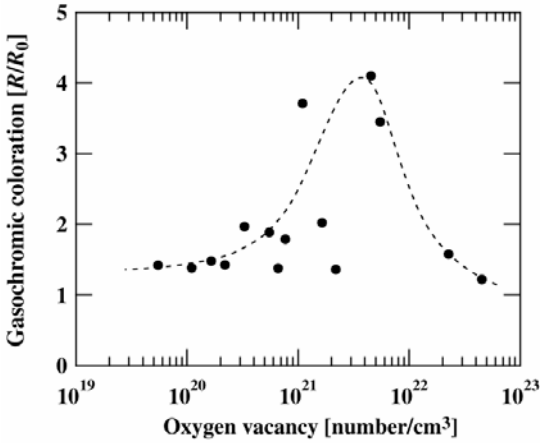

Fig.1 Oxygen vacancy dependence of gasochromic coloration on WO_3 film with He^+ irradiations. R_0 and R is the extent of gasochromic coloration for the unirradiated and irradiated film, respectively.

4-10 Structural Change of Gasochromic WO_3 Films by Hydrogen Incorporation

A. Inouye [a), b)], S. Yamamoto [b)], S. Nagata [c)], K. Takano [b)], M. Yoshikawa [b)] and T. Shikama [c)]

[a)]School of Engineering, Tohoku University
[b)]Environment and Industrial Materials Research Division, QuBS, JAEA
[c)]Institute of Materials Research, Tohoku University

Structural change of the gasochromic WO_3 films by hydrogen incorporation was investigated. (0 1 0)-oriented monoclinic WO_3 films were prepared by a sputtering method on SiO_2 substrates. When the light green color of Pd coated WO_3 films turned to dark blue by exposure of 1 % H_2-N_2 gas, the monoclinic WO_3 structure changed to a tetragonal structure. The results of elastic recoil detection analysis (ERDA) and Rutherford backscattering spectroscopy (RBS) revealed that the hydrogen concentration increased 0.2 H/W in the samples during hydrogen exposing. These results indicate that the coloration of the WO_3 by hydrogen gas is caused by incorporation of hydrogen, with formation of hydrogen tungsten bronze (H_XWO_3).

パラジウム（Pd）などの触媒を表面に担持させた三酸化タングステン（WO_3）は、水素と反応することで着色する特性（ガスクロミック特性）を示す。この着色メカニズムとして、触媒によって解離した水素原子がWO_3の結晶格子中に侵入し、タングステンブロンズ（H_XWO_3）が形成されて着色するモデル[1)]と、或いは水素により酸素欠損を形成されて着色するモデル[2)]など、いくつかのモデルが提案されている。しかし、着色メカニズムは十分には理解されていない。そこで本研究では、結晶配向性酸化タングステン膜を用いて着色前後における結晶構造変化と水素挙動の関連性を調べ、着色メカニズムを追求した。

試料作製には反応性RFマグネトロンスパッタ法を用いた。アルゴン/酸素混合ガス中で金属タングステンターゲットをスパッタし、600 ℃に保持した石英基板上に酸化タングステン膜（約 550 nm厚）を堆積した。その表面に約 15 nmのPdを蒸着したものを試料とし、1 %の水素を含んだ窒素ガス（1%H_2-N_2）に曝して着色させた。着色前後における結晶構造をX線回折法（XRD）により評価し、水素濃度の定量にはラザフォード後方散乱法（RBS）および反跳粒子検出法（ERDA）を用いた。

作製試料の着色前後におけるX線回折パターンをFig.1 に示す。着色前では、2θ=23.6°付近に単斜晶系WO_3（0 2 0）に由来する回折ピークが観測された（Fig.1(a)）。これは作製試料の結晶構造が単斜晶系WO_3（0 1 0）に一軸配向していることを示している。この試料を1%H_2-N_2に 20 分間さらし着色させると、X線回折パターンは変化し正方晶系$H_{0.23}WO_3$（JCPDS No.42-1261）に対応した（Fig.1(b)）。

Fig.2 は、着色前後における膜中水素の深さ分布を示す。着色前における試料のスペクトル形状およびピーク強度から、膜中には水素が一様に含まれており、その濃度は 0.6 H/W（13at.%）と見積もることができた。着色後では、膜中の水素濃度は約 0.2 H/W 増加した。

以上のことから、酸化タングステン膜のガスクロミック着色は、膜中への水素の侵入が伴っており、正方晶系タングステンブロンズの形成と深く関係していると考えられる。したがって、酸化タングステンの水素による着色メカニズムとしてH_XWO_3の形成によって着色するモデルを支持する。

References

1) S. H. Lee, et al., Electrochimica Acta 46 (2001) 1995-1999.
2) A. Georg, et al., Solid State Ionics 127 (2000) 319-328.

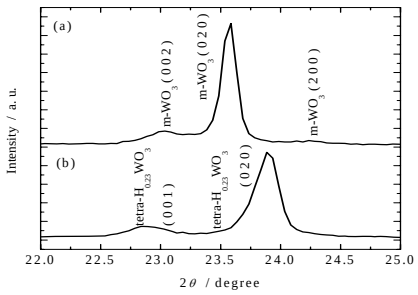

Fig. 1. XRD patterns of the oriented WO_3 films (a) as-prepared and (b) colored states.

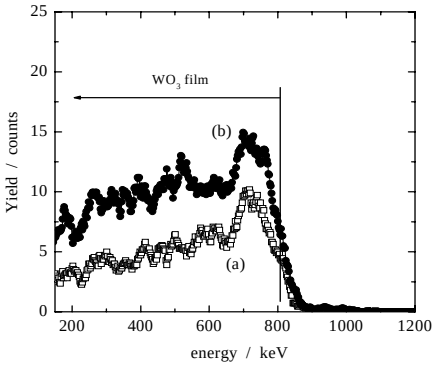

Fig. 2. Hydrogen depth profiling in the oriented WO_3 films (a) as-prepared and (b) colored states.

4-11 Effect of Annealing Temperature of Palladium Oxide Films on Hydrogen Detection

S. Yamamoto [a)], K. Takano [a)], A. Inouye [a), b)] and M. Yoshikawa [a)]

[a)]Environment and Industrial Materials Research Division, QuBS, JAEA,
[b)]School of Engineering, Tohoku University

The fast detection of hydrogen leaks below the lower explosive limit (LEL) of 4 % by volume ratio of hydrogen in air is an important technology. Hydrogen sensors based on electrical properties of metal oxides have been developed. However, a hydrogen sensor, which can safely detect at room temperature, with a low cost and lightweight, is desirable. Recently, the gasochromic materials, coloration by gases, have considerable promise as the optical hydrogen sensing films. Palladium oxide films coated with noble metal (Pd, Pt) catalysts were expected to have gasochromic coloration, since it is known to exhibit optical absorbance changes due to the reduction with hydrogen.

Palladium oxide films are prepared by thermal oxidation of polycrystalline Pd films deposited on quartz substrates using an rf magnetron sputtering. The Pd films were annealed at temperatures range from 300 to 900 °C in air. For the gasochromic coloration measurements, the transmittance of palladium oxide films coated with Pd catalyst (15 nm thickness) was measured using a spectrometer with a fiber optics at a wavelength of 645 nm from a light-emitting diode. To confirm the detection of hydrogen less than LEL, the samples were exposed in 1 % H_2/Ar flow of 100 sccm. The composition of palladium oxide films was determined by the RBS using a 3 MV single-stage-accelerator at JAEA/Takasaki.

Figure 1 shows optical response curves of gasochromic coloration for the palladium oxide films with 32 nm thicknesses annealed at 600 °C, (a) coated with Pd catalyst, and (b) without Pd catalyst, respectively. The transmittance T at a wavelength of 645 nm was measured as a function of exposure time of hydrogen. T_0 is the transmittance at the beginning of the measurements. The normalized transmittance T/T_0 of the film with Pd catalyst is rapidly decreased down to 0.1 within 2 min. The result shows that the Pd catalyst on palladium oxide film causes gasochromic coloration for hydrogen at room temperature.

The dependence of gasochromic performance on annealing temperature of polycrystalline Pd films is shown in Fig 2. The T/T_0 of the films on quartz substrates was taken after exposure 20 min in 1 % H_2/Ar. The T/T_0 of the films is decreased with increasing annealing temperatures and reaches to a minimum at 600°C. This result indicates that the palladium oxide film with superior gasochromic performance for hydrogen was obtained by annealing at 600°C in air. It is found that the gasochromic coloration of palladium oxide films for hydrogen is strongly influenced by annealing temperature. The composition of the palladium oxide films with different annealing temperatures was examined by the RBS. Polycrystalline Pd films (64 nm thickness) were annealed at temperatures range from 200 to 600°C in air for 1h. The results of RBS indicate the Pd phase remains up to at 200 °C and begins to oxidize at around 250 °C and then becomes completely oxidized at 450 °C with formation of PdO phase. Palladium oxide film with PdO phase obtained by annealing at 600°C in air shows the appropriate gasochromic performance for hydrogen detection.

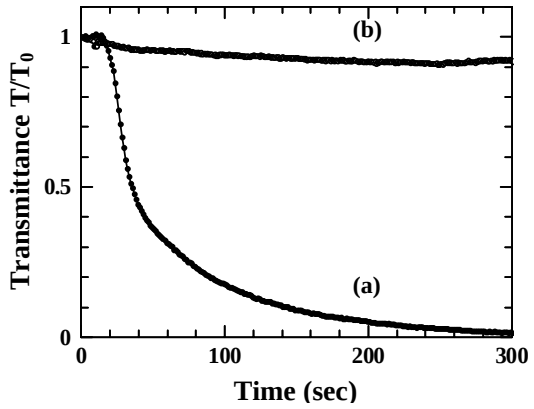

Fig. 1 Optical response of the coloration for the palladium oxide films in 1 % H_2/Ar. (a) with Pd catalyst and (b) without Pd catalyst.

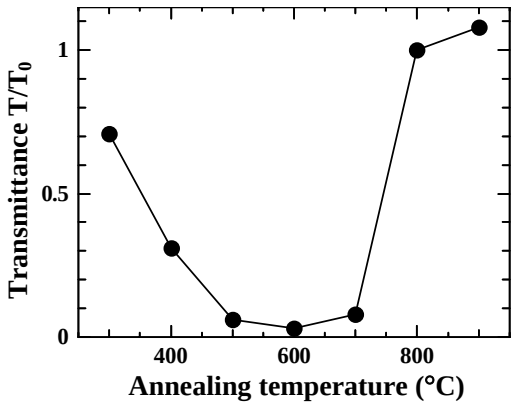

Fig. 2 The dependence of gasochromic performance on annealing temperature of polycrystalline Pd films.

4-12 Improvement of Hydrogen Storage Characteristics of Palladium by Ion Irradiation

H. Abe [a)], S. Aone [b)], R. Morimoto [b)], H. Uchida [b)] and T. Ohshima [a)]

[a)]Environment and Industrial Materials Research Division, QuBS, JAEA
[b)]Department of Applied Science, Graduate School of Engineering, Tokai University

In previous studies, the induction of vacancy in palladium (Pd) was found to be effective for an increase in the hydrogen absorption rate[1, 2]. Regarding the hydrogen storage in metals, it was reported that the absorption concentration of hydrogen atoms and the hydrogen absorption rate depend strongly on the surface state of metals[1]. For the surface modification of materials, ion implantation with low energy is known to be a quite useful method. These facts give the possibility that the hydrogen absorptivity in Pd is improved by surface modification using ion irradiation.

In this study, we perform chromium (Cr) ion irradiation into Pd, and the hydrogen absorption rate of ion irradiated Pd was evaluated. Based on the obtained results, we discuss the correlation among ion irradiation, work function and hydrogen absorption in Pd.

The samples used in this study were Pd sheets (99.99 % purity, 7.5 x 7.5 x 0.1 mm^3). Prior to ion irradiation, all samples were annealed in nitrogen atmosphere for an hour at 1173 K. Cr ion (Cr^+) irradiation onto the Pd samples was made at room temperature using the ion implanter at TIARA. The acceleration energy of Cr^+ and the maximum fluence were 350 keV, and 1 x 10^{17} /cm^2 respectively. The hydrogen absorption rate of the irradiated Pd was investigated using an electrochemical method. Pd was used as a cathode, and an Hg/HgO was used as the reference electrode. Details of the electrochemical measurements have been reported elsewhere[3].

Figure 1 shows the hydrogen absorption curves of Pd samples before and after 350keV-Cr^+ irradiation. With increasing Cr^+ fluence, the hydrogen absorption rate increased. The sample irradiated at a dose of 1 x 10^{17} /cm^2 exhibited a much higher rate than the others, and the hydrogen absorption rate of the Pd became five times higher than that of un-irradiated Pd. Since vacancy type defects are introduced by irradiation and such vacancies might act as hydrogen trapping sites, the enhancement of the hydrogen absorption rate obtained in this study can be interpreted in terms of an increase of hydrogen trapping sites near the surface region due to irradiation of Cr^+ into Pd.

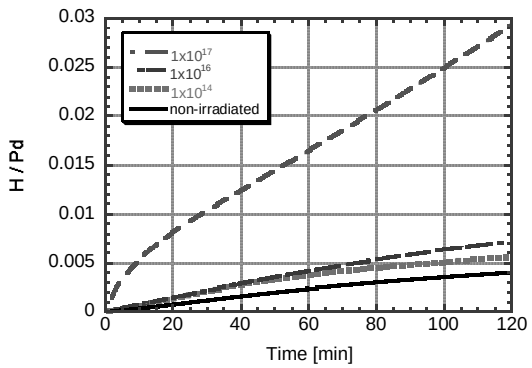

Fig.1. Hydrogen absorption, 5 cycles, curves of Pd irradiated with 350keV Cr^+ at doses from 1x10^{14} /cm^2 to 1x10^{17} /cm^2.

Figure 2 shows the relationship between the work function of Pd ($\Delta\phi$) and the hydrogen absorption rate before and after Cr ion irradiation. The value of $\Delta\phi$ is depicted as a shift from un-irradiated sample. The shift of the $\Delta\phi$ is estimated from $\Delta\phi = V_E / (\Delta V - 1)$, where V_E is the peak-to-peak output voltage and ΔV represents the voltage difference between the probe tip and Pd sample. By Cr^+ irradiation, $\Delta\phi$ shifts to the negative side. As for the hydrogen absorption rate, the value increased with increasing fluence of Cr ions. These results imply that the value of $\Delta\phi$ decreases and the hydrogen absorption rate increases with increasing vacancy concentration.

In summary, Cr ion irradiation with energies of hundred keV is useful for the improvement of the hydrogen absorption rate of Pd.

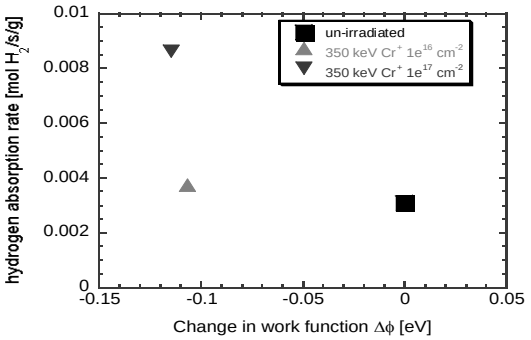

Fig.2. Relationship between the work function of Pd ($\Delta\phi$) and the hydrogen absorption rate before and after Cr ion irradiation.

References

1) H. Abe, A. Uedono, H. Uchida, A. Komatsu, S. Okada and H. Itoh, Mat. Sci. Forum, 363-365 p. 156 (2001).
2) H. Abe, H. Uchida, Y. Azuma, A. Uedono, Z. Q. Chen and H. Itoh, Nucl. Inst. and Meth. B, 206 p. 224 (2003).
3) H.H. Uchida, Y. Watanabe, Y. Matsumura and H. Uchida, J. Alloys Comp., 231 p. 679 (1995).

4-13 Gamma-ray Irradiation Effect on Lattice Defect Centers Detected from the Tsurukawa Fault Gouge, Japan

T. Fukuchi and D. Tanaka

Department of Earth Sciences, Graduate School of Science and Engineering, Yamaguchi University

A well-known method for the assessment of fault activity (i.e., seismicity) is the ESR (electron spin resonance) dating method using lattice defect centers detected from intrafault material (fault gouge)[1]. Clay minerals such as smectites in fault gouge are considered to be produced at almost the same geological time as the fractures of host rocks during fault movements, so that ESR ages obtained from the clay minerals may directly show the ages of fault movements. In this report, we investigate γ-rays irradiation effect on ESR centers detected from the fault gouge along the Tsurukawa fault, which is distributed from Yamanashi to Kanagawa Prefecture, and consider whether or not the ESR centers can be used for ESR dating of fault movements. The experimental fault gouge samples were collected from an outcrop along the Kaisawa River, Tabayama Village, Yamanashi Prefecture. At this outcrop, a black fault gouge layer (T-3) has been formed along the fault plane that may have been most active at the latest fault movement, and dark gray gouge layers (T-2, T-4) are positioned on both sides of the black fault gouge. Furthermore gray gouge layers (T-1, T-5) are distributed outside the dark gray gouge layers. The source rock of these fault gouge samples is pelite.

The γ-irradiation was carried out using a ^{60}Co source in the 6 cell irradiation facility, Takasaki Advanced Radiation Research Institute, JAEA. The dose rate and time of irradiation are 23.7 C/kg/h (0.97 kGy/h) and 0~10 hours. ESR measurements were carried out using an X-band ESR spectrometer with a 100 kHz modulation field (JEOL RE-3X) in Yamaguchi University. As a result of ESR measurements, paramagnetic Fe^{3+} and Mn^{2+} ions signals are detected from all the fault gouge samples. In addition, ESR signals (g=2.0123, 1.9973) intrinsic to smectites, an E' center (g=2.0015) derived from oxygen vacancies, an organic radical center (g=2.0039), and an unknown ESR signal (g=2.0041) are detected especially from T-3 or T-4 sample. Figure.1 shows variations of ESR spectra obtained from T-3 and T-4 samples before and after γ-irradiation. As shown in the figure, the ESR signals intrinsic to smectites regularly increase with γ-irradiation. This result means that the ESR signals of smectites are applicable to ESR dating of fault movements. On the other hand, the E' and organic radical centers irregularly change by γ-irradiation. There have been hardly experimental data on the γ-irradiation effect on organic radical centers. Our result indicates that the organic radical centers are not available for ESR dating. Furthermore, the unknown ESR center at g=2.0041 clearly increases with γ-irradiation, so that it may be applicable to ESR dating of fault movements. According to X-ray diffraction analysis, this unknown center may be derived from another clay mineral such as illite. To identify this unknown center, we need to carry out more detailed experiments such as comparison with ESR signals detected from standard clay minerals.

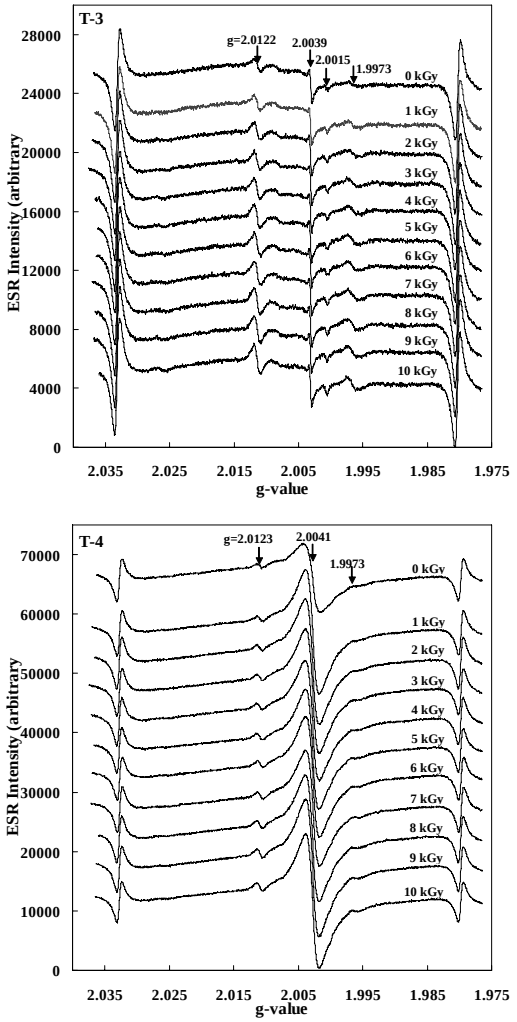

Fig.1 Variations of ESR spectra obtained from the Tsurukawa fault gouge samples (T-3 and T-4) by γ-rays irradiation. The dose rate of irradiation is 23.7 C/kg/h. The irradiation time is 0~10 hours.

Reference

1) T. Fukuchi (2004) ESR dating method of fault movements- Its principle and practice. Fukadaken Library, No.63, 45pp.

4-14 Provenance Study of Eolian Deposits Using Electron Spin Resonance Signal Intensity and Crystallinity of Quartz

R. Tada [a)], Y. Isozaki [a)], Y. Sun [b)] and K. Nagashima [c)]

[a)]Department of Earth and Planetary Sciences, Graduate School of Science, University of Tokyo, [b)]Institute of Earth Environment, Chinese Academy of Sciences [c)]Institute of Observational Research for Global Change, Japan Agency for Marine-Earth Science and Technology

Inland desert areas of western China such as Taklimakan and Gobi are special for their distribution in higher latitudes, and it has been suggested that uplift of Himalaya and Tibet is a cause of their formation based on paleoclimatic model simulations. Thus, specification of the timing and mode of formation of these deserts is critical to test the potential linkage among the uplift of Himalaya-Tibet, the evolution of Asian monsoon and the formation of deserts in inland Asia. Then, we aim to reconstruct past provenance changes of aeolian deposits in East Asia in order to examine the timing of formation of these deserts and the evolution of Asian monsoon. In order to estimate the provenance of aeolian deposits, we focused on Electron Spin Resonance (ESR) signal intensity and crystallinity index of quartz, which are powerful methods to constrain on the provenance of dust deposits. Here we first determine the procedure of gamma-ray irradiation for ESR analysis.

ヒマラヤ・チベットの隆起に伴ってアジア内陸部（タクラマカン、ゴビ砂漠域）が乾燥化すると共にアジア・モンスーンが強化されたとする仮説は古くから提唱されてきた。しかしながら、ヒマラヤ・チベットの隆起時期や様式、アジア・モンスーンの強化時期や発達の様式に関する地質学的証拠が不十分であったため、この仮説は十分検証されていない。そこで本研究の目的は、アジア内陸部の乾燥化やアジア冬季モンスーンの開始時期・発達過程を調べ、ヒマラヤ・チベットの隆起に伴う乾燥化およびアジア・モンスーン強化の可能性を検証することにある。そのために、冬季モンスーン風および偏西風によりアジア内陸部の乾燥域から運ばれる風成塵に注目し、風成塵の起源とその時代変遷を復元して、アジア内陸部の乾燥化およびアジア・モンスーン強化の時期や様式を検証する。

風成塵の供給源推定に際して注目したのが、石英の電子スピン共鳴(Electron Spin Resonance; ESR)信号強度および結晶化度である。石英のESR信号強度は、母岩の形成年代を反映する指標と考えられている[1)]。一方、石英の結晶化度は、石英の生成環境を反映する指標と考えられている[2)]。そこで我々はこれらの指標を組み合わせて、風成塵の供給源推定を行う。

本研究は平成18～20年度の3年間で行われ、初年度である平成18年度は、中国黄土高原の風成堆積物を用いて、ESR信号強度の測定条件の検討を行った。ここでは、ESR分析に際して行うγ線照射の条件設定のための予備実験結果について簡単に述べる。

ESRとは物質中の不対電子が静磁場中でマイクロ波を吸収する性質を利用して、不対電子を検出する手法である。本研究では石英中に生成されるE_1'中心と呼ばれるESR信号に注目した。E_1'中心とは、結晶中の酸素空格子に、１つの不対電子が捕らえられている状態である。E_1'中心のESR信号強度とは、この格子欠陥をESRによって測定したものである。E_1'中心の信号強度は、石英を過熱すると300 ℃までは増加する。これは電子を2個とらえ安定な状態で存在する酸素空格子が、加熱によって放出された電気的ホールを１個とらえ、常磁性のE_1'中心に変化するためであると考えられている[3)]。つまり事前にγ線を照射し、石英中に十分な量の電気的ホールが存在する状態で過熱を行えば、電気的ホールが酸素空格子へ移動し、石英中のすべての酸素空格子がE_1'中心として存在するようになる。沖縄で採取された花崗岩を用いた先行研究[3)]では、約1 kGyのγ線照射と加熱によって、E_1'中心のESR信号強度が飽和に達することが示されているが、東アジアの風成堆積物の場合、1 kGyで飽和に達するのか否かが明らかになっていない。そこで中国の黄土高原から採取された7つの風成堆積物試料について、それぞれ1kGyと2.5 kGの2通りの照射を行い、ESR信号強度の差を検証した（Fig.1）

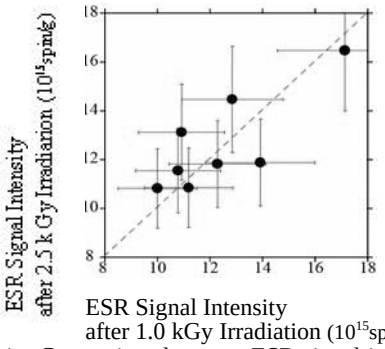

ESR Signal Intensity
after 1.0 kGy Irradiation (10^{15}spin/g)

Fig.1 Comparison between ESR signal intensity for samples irradiated 1kGy and 2.5kGy.

その結果、照射量を変えてもESR信号強度には有意の差が見られず、1 kGyで飽和に達していること、また照射量を増やしても（少なくとも2.5 kGyまでは）人工的なE_1'中心の生成は起こっていないことが明らかになった。以上の結果から、1-2.5 kGyの範囲でのγ線照射は、我々の目的に沿うものであることがわかった。

References

1) S.Toyoda, Ph. D. Thesis, 106pp., Osaka University (1992).
2) K. Murata and M. Norman, Am. J. Sci., 276, 1120-1130 (1976).
3) S. Toyoda and W. Hattori, Applied Radiation and Isotopes, 52, 1351-1356 (2000).

4-15 Preparation of Anisotropic Conductive Membranes Using Ion Beam Irradiation

H. Koshikawa and Y. Maekawa

Environment and Industrial Materials Research Division, QuBS, JAEA

The damaged region created along the path of swift heavy ions in polymers is susceptible to a proper etchant, resulting in the formation of through-holes with nanometer-to-micrometer diameters. This so-called ion track membranes of thermally and mechanically stable polymers have been developed for applications to electronic devices through hybridization with metals and semiconductor alloys by electroplating[1,2]. In this study, anisotropically conducting membranes were prepared by electrochemical deposition of copper (Cu) wires into the cylindrical pores in the polyimide (PI)-based ion track membrane. We report here the conductivity of PI/Cu composite films with low fluence Cu wires.

Commercially-available PI films (Kapton, thickness: 12 μm) were irradiated by 450 MeV $^{129}Xe^{23+}$ with fluences of 3×10^3 and 3×10^5 ions/cm^2 from the AVF cyclotron at the TIARA facility. According to the established procedure[3], the PI ion track membranes with 0.5 – 2.0 μm diameter cylindrical pores were then prepared by the etching in a aqueous sodium hypochlorite (NaClO) solution at 60°C. Successive layers of gold (25 nm) and Cu (20 μm) were coated on one side of the ion track membranes as a cathode[4]. The Cu wires were deposited within the pores of the ion track membranes onto the Cu cathode by electrochemical plating in a pH1 aqueous solution of 1.3 M copper sulfate ($CuSO_4$). The dot of Au electrodes with 0.3 - 0.5 mm in diameter was deposited on the other side of the Cu cathode to connect with copper wires of the PI/Cu composite films. The Au dot electrodes were connected to two terminals of milliohmmeter via Au wires, then electrical conductivity of the PI/Cu composite films was measured.

The electric resistances of the ion track membranes with pores of 0.5 μm in diameter and a fluence of 3.0 x 10^5 ions/cm^2 were measured using the dot electrodes in 8 places on the PI/Cu composite films. The measured (B) and theoretical (A) resistances and these ratios (B/A) were shown in Table 1. Theoretical resistances were given by the next equation,

$$R = 1/S = \frac{\rho L}{\pi(d/2)^2 AF}$$

where ρ is a resistivity of copper (1.67x10^{-6} Ωcm), L is length of copper wires, d is a diameter of the copper wires, A is an area of the electrode, and F is a particle fluence.

Somewhat lower conductivity of the PI/Cu composite films compared with the theoretical value is likely to result from the defects in copper wires during the electroplating preparations, influence of the interfaces between copper wires and the pore surfaces of PI, and/or the contact resistances between the Au dots and the top of copper wires.

Table 1 Resistance that calculated the area of each electrode and the magnification to the theoretical resistances of measurements

	Area of the electrode cm^2	Theoretical resistance, A mΩ	Measured resistance, B mΩ	Ratio (B/A)
1	1.2 x10^{-3}	2.8	23	8.3
2	2.7 x10^{-3}	1.3	7.2	5.7
3	2.3 x10^{-3}	1.5	8.3	5.6
4	2.8 x10^{-3}	1.2	11.8	9.8
5	3.1 x10^{-3}	1.1	8.4	7.7
6	4.2 x10^{-3}	0.8	6.9	8.5
7	3.5 x10^{-3}	1.0	7.2	7.5
8	3.3 x10^{-3}	1.0	7.2	7.0

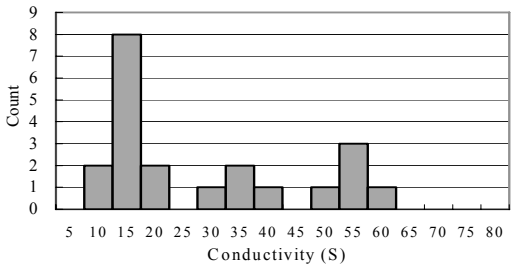

Figure 1 The histogram of the distribution of 21 points of the measured conductivity in the composite films with the copper wires; fluence: 3x10^3 ion/cm^2, diameter: 2μm.

Thus, we used the samples with low density of Cu wires (3x10^3 ion/cm^2) with low resistance of each wire (2μm in diameter) in order to obtain the resistivity information of single wire.

Figure 1 shows the histogram of the distribution of the measured conductivity of 21 points of the PI/Cu composite films with pores of 2 μm and a fluence of 3x10^3 ion/cm^2. There was three distributions with peaks at conductivities of 15, 35 and 55 S with the equal intervals. These peak conductivities are in good agreement of the integral multiple of the theoretical conductivity of one copper wire of about 17 S. It was considered that the copper nanowires in the composite membranes formed by using the ion track films had the conductivity equal with the bulk. However, lower conductivity of the PI/Cu composite films with pores of 0.5 μm in diameter should results from some of the wires are not connected to the Au dot electrodes.

References

1) C.Trautmann et al., Nucl. Instr. Meth. B111 (1996) 70.
2) T.Molares et al., Adv. Matter., 13 (2001) 62.
3) Y. Maekawa et al., Polymer, 45 (1996) 2291.

4-16 Development of Optical System for Direct Observation of Behavior of Transient Species under Pulsed-heavy Ion Irradiation

M. Taguchi [a)], A. Kimura [a)], K. Hirota [a)], S. Kurashima [b)], G. Baldacchino [c)] and Y. Katsumura [d)]

[a)]Environment and Industrial Materials Research Division, QuBS, JAEA, [b)]Department of Advanced Radiation Technology, TARRI, JAEA, [c)]Laboratoire de Radiolyse, DSM/DRECAM/SCM/URA331CNRS, CEA/Saclay, [d)]Department of Nuclear Engineering and Management, School of Engineering, The University of Tokyo

1. Introduction

High energy heavy ion irradiation induces characteristic chemical reactions in water, which are considered to be caused by high concentrations and heterogeneous reactions of radicals in track. Hydroxyl(OH) radical is the most important radical for oxidations in water. We reported the dependence of the differential *G*-values of OH radicals on the energy and mass of the incident ions, and on the elapsed time by the product-analysis method[1)]. In order to understand precisely the reactions in track, direct observation method is more useful and informative. We construct the optical system under the pulsed heavy ion irradiation.

2. Experimental

Carbon ion with 220-MeV energy was selected to evaluate and improve the specification of the constructed optical system. As shown in Figure 1, C ion beam from an ion source was bunched by a chopper to obtain the short pulse with a width of several μs to 1000 μs, which was controlled by a pulse generator. Time profile and charge of the pulse were directly measured by Faraday cup set at the upper stream of the beam in vacuum. Sample cell was horizontally set on the optical stage under the window for extracting the ion from vacuum. The sample cell has two glass windows with 50-μm thickness for the ion irradiation and optical measurement on the top and bottom. Probe light was introduced into the sample cell with an angle of 30 degree against the ion beam axis, and reflected by mirror under the cell. Light intensities observed by a photodiode with and without irradiation are defined as I and I_0, respectively. Absorbance due to produced radicals is estimated by Lambert-Beer equation ($OD=\log(I_0/I)$). Improving optical system and reducing electric noise make possible to measure a small absorbance less than 10^{-4}.

KSCN dissolved in water was used as sample solution, because its reaction mechanism is well known and primary radical has a large extinction coefficient.

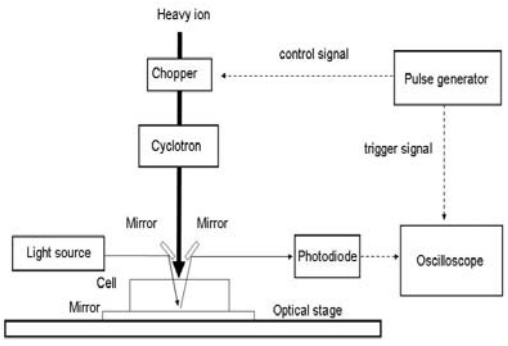

Fig. 1 On-line optical measurement system for pulsed heavy ion irradiation.

3. Results and discussion

Time dependent absorbance was recorded at 447 nm for aqueous KSCN solution irradiated with C ion as shown in Figure 2. OH radicals produced in the track react with solute to produce $(SCN)_2^-$, and absorbance shown in Figure 2 is assigned to $(SCN)_2^-$. Rise time of absorbance from time 0 is completely the same as the irradiation pulse width. Increase in absorbance with pulse width implies that $(SCN)_2^-$ is relatively stable and its concentration increases. Saturation observed for the longer pulse irradiation demonstrates the competition between the formation and decomposition of $(SCN)_2^-$.

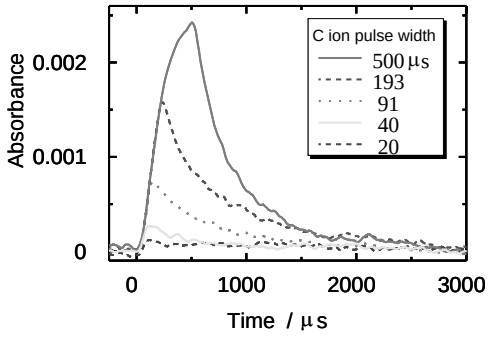

Fig. 2 Time dependent absorbance for 10-mM aqueous KSCN solution irradiated with C ions having different pulse widths.

Reference

1) M. Taguchi and T. Kojima, Nuclear Science and Techniques, 18 (2007) 25.

4-17 LET Effect on Irradiation of Hydroxymaleimide in Alcohol Solution

S. Nakagawa [a], N. Ohta [b], M. Taguchi [c] and K. Hirota [c]

[a]TMITRI, [b]Hiroshima Univ.,
[c]Environment and Industrial Materials Research Division, QuBS, JAEA

Hydroxymaleimide was irradiated in 2-propanol and methanol solutions with 350 MeV Ne-ion, 220 MeV C-ion, 100 and 50 MeV He-ion beams from the AVF cyclotron in the TIARA Facility. The differential G-values of the reduction of hydroxymaleimide decreased with increasing LET. The LET dependence by He-ion shifted from heavier ions. This effect clearly appeared in methanol solution.

＜はじめに＞　マレイミド($C_2H_2(CO)_2NH$)は、光化学重合反応の開始剤として研究が行われてきた。一方、ヒドロキシマレイミド($C_2H_2(CO)_2NOH$)を2-プロパノールおよびメタノール中でγ線照射したところ、溶媒分子のラジカルが付加した化合物やダイマーが生成することがわかった。そこで、アルコール溶媒中でヒドロキシマレイミドのイオン照射を行い、ＬＥＴ効果について検討する。

＜実験方法＞　ヒドロキシマレイミドを2-プロパノールおよびメタノールに溶かした（0.1モル%）試料に原子力機構ＴＩＡＲＡ施設内ＡＶＦサイクロトンのＮｅイオン(350 MeV)、Ｃイオン(220 MeV)およびＨｅイオン(100 MeV,50 MeV)を照射した。また、試料の上にアルミ箔を置き、入射イオンのエネルギーを変化させ、ＬＥＴ依存性を調べた。生成物およびヒドロキシマレイミドは、液体クロマトグラフ・質量分析計（カラムＯＤＳ、移動相アセトニトリル:水＝50：50、イオン化法：ＥＳ-ＮＣＩ）で分析した。分析試料は、真空乾燥した残留物をアセトニトリルで溶解したものを用いた。

＜結果および考察＞　吸収線量あたりのヒドロキシマレイミドの減少割合から分解効率を求めた。得られた分解効率をイオンの入射エネルギーあたりで規格化すると、見かけのＧ値が得られる。Fig.1に2-プロパノール中での分解での初期エネルギーに対する見かけのＧ値をプロットする。初期エネルギーの増加に伴い、Ｇ値は増加した。これより、ＬＥＴの増加に伴い微分Ｇ値が減少すると推測される。これは、溶媒分子のラジカルなど、生成物の反応に関与する活性種の生成量のＬＥＴ依存性に対応すると考えられる。

アルミ箔によるＬＥＴ増加の各ステップで微分Ｇ値が一定と仮定して、見かけのＧ値から微分Ｇ値を概算した。2-プロパノールおよびメタノール中での照射で得られた微分Ｇ値をFig.2-3に示す。Ｈｅイオン照射では、50MeVと100MeVで得られた微分Ｇ値はほぼ直線関係にあるが、ＣイオンやＮｅイオンの重イオン照射で得られた値とずれている。Ｈｅイオン照射において、イオン種効果があるものと考えられる。これは、メタノール溶媒中で、より明確に現れた。

今後は、添加物を入れた系で、活性種の生成機構とＬＥＴの関係について、γ線照射と比較して検討していく予定である。

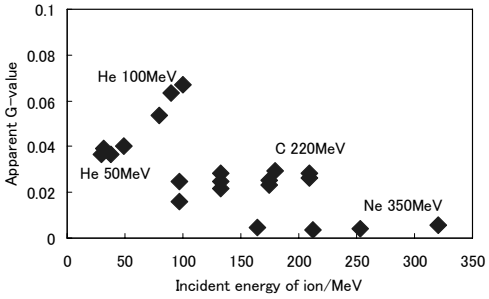

Fig.1　Apparent G-value depending on the incident energy of ion in 2-propanol.

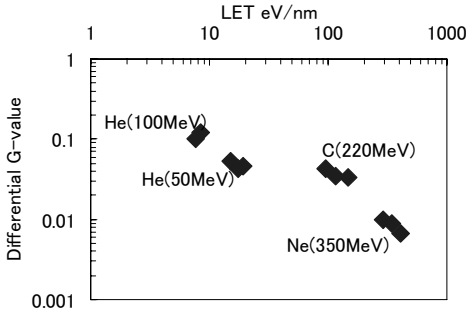

Fig.2　LET dependence of differential G-value obtained by ion irradiation in 2-propanol.

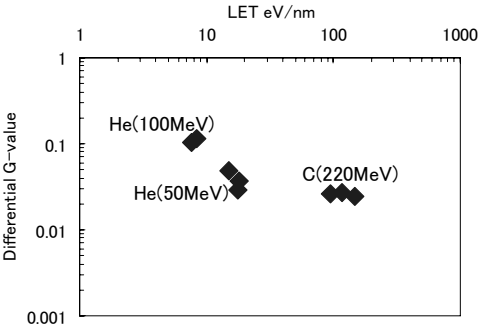

Fig.3　LET dependence of differential G-value obtained by ion irradiation in methanol.

4-18 Transient Absorption of a Cation Radical of Pyrene Induced by Heavy Ion Beam Pulses

T. Kondoh [a)], J. Yang [a)], K. Kan [a)], Y. Yoshida [a)], H. Shibata [b)], M. Taguchi [c)] and T. Kojima [c)]

[a)]ISIR, Osaka University, [b)]Faculty of Engineering, Kyoto University, [c)]Eenvironment and Industrial Materials Research Division, QuBS, JAEA

The heavy ion beam is a high LET radiation. Ion beam can excite materials high densely. The characteristic of this ion beam was used to develop the new technology such as the material and the medical application. Ion beam pulse radiolysis is developing for elucidation of the initial process of ion beam induced chemical reaction. Our unique measurement method is developing using a scintillator and the photon counting method. Transient optical absorption of the Pyrene's cation radical which was induced by irradiation of 220MeV C^{5+} ion was measured. A decay time of cation radical of pyrene in ion beam case was faster than that in electron beam case.

高速重イオンビームは高LET放射線であり、物質中を直進し一定の深さで大きなエネルギーを与えるので物質を局所的に高密度励起できる。イオンビームの特性を利用した新規プロセスを開発し、材料、医学等の領域へ応用されている。しかし、応用技術を発展させるにはイオンビームが誘起する化学反応の機構を明らかにする必要がある。イオンビームによって生成される短寿命活性種の挙動を明らかにし、イオンビーム初期過程を解明する。高密度励起効果は、活性種の分布や減衰過程に反映される。活性種が高密度にできるため、再結合や化学反応が、非常に短い時間領域で起こることが予測される。本研究では、イオンビームによる固体シンチレーター発光を分析光とすることにより高感度なフォトンカウンティング法と組み合わせて、イオンビームの励起構造に適した過渡吸収実験を考案した。この方法では、イオンビームが通過した微小領域でのみ、分析光が発生し活性種が誘起され、過渡光吸収を測定できる。TIARAのパルス性能を活用した時間分解分光法を開発し、ナノ・ピコ秒時間領域のイオンビーム誘起反応初期過程の解明を行っている。

本研究の吸収分光測定システムをFig.1に示す。本実験では、AVFサイクロトロンからの220 MeV C^{5+}イオンを用いた。ビームはチョッパーで間引かれ、イオンビームは、金属箔窓と試料間に設置されたシンチレーターを通過し試料に入射した。シンチレーターの発光を分析光とし、光ファイバーを通して光測定系に導いた。シンチレーターはCaF_2(Eu)(940 ns, 435 nm)を用いた。イオンビームの効果を解明するために、電子線パルスラジオリシスも行い比較検討した。電子線照射と測定は阪大産研で行った。測定する波長領域で、吸収も発光もない塩化メチレンにピレンを溶解し、イオンビームが誘起した活性種をピレンの活性種として測定し時間挙動を調べた。

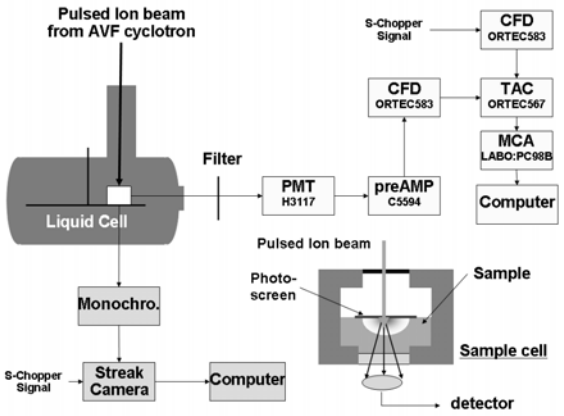

Fig.1 Measurement system of ion beam induced optical absorption

Fig.2に220 MeV C^{5+}イオン照射により誘起した100 mMピレン塩化メチレン溶液の440 nmでの過渡光吸収を

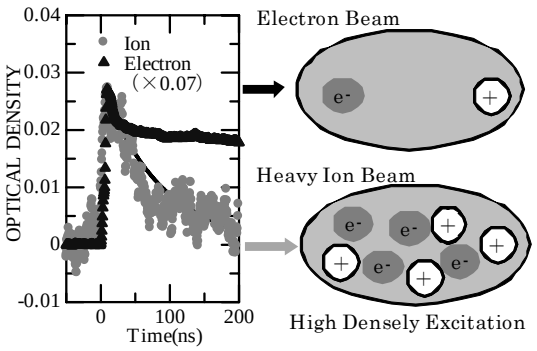

Fig.2 Transient Optical absorption of 100mM Pyrene-CH_2Cl_2 solution at 440nm induced by Ion beam (Gray dots) and electron beam (Black triangle dots)

灰色ドットで示した。27 MeV電子線の場合を黒三角で示した。比較すると減衰特性に違いが見られた。電子線励起の場合長寿命成分があるのに対し、高速重イオンビームでは、単純な指数関数減衰ではないが、簡単のために指数関数を仮定すると約85 nsの時定数で減衰した（黒実線）。電子線励起の場合に比べて明らかに速く減衰している。右に示したように、高速重イオン励起では、ピレンカチオンラジカルと消滅する電子も同時に高密度に生成されるために、電子線励起の場合と比較して短時間で消滅すると思われる。ピレン濃度依存性を1 mM, 10 mM, 100 mMで調べた。過渡吸収強度はピレン濃度に依存して増加したが、高濃度ではピレン濃度に単純比例しなかった。イオンビームが生成するピレンカチオンラジカル濃度の飽和が起こっている可能性がある。

4-19 Basic and Application Studies on Chemical Responses to Quantum Beams in Heterogeneous Systems

R. Nagaishi [a], R. Yamada [a], N. Aoyagi [a] and Y. Sugo [b]

[a]Division of Environment and Radiation Sciences, NSED, JAEA, [b]Division of Fuels and Materials Engineering, NSED, JAEA

From the standpoints of utilization of radioactive wastes, and of sophistication of separation process of spent fuels, we have been investigating promotion or inhibition of radiation-induced reactions in immiscible heterogeneous systems: solutions coexisting/contacting with solid oxides, solvent system with aqueous and organic phases, etc.. We have recently report that the reactions of reduction of metal ions and of hydrogen production in aqueous solution were promoted by adding oxide particles to the solution [1], and that the radiolysis of amides in n-dodecane was dependent on aqueous solution contacting with the n-dodecane [2]. In this report, we illustrate recover of platinum-group elements from aqueous solution, and non-toxic treatment of chrysotile asbestos using ionizing radiations as the experimental results found in fiscal 2006.

The samples of Pt-group element ions and asbestos were irradiated at ambient temperature and pressure using the electron beams (initial energies: 0.5-0.8 MeV) and γ-ray (avrg. one: 1.25 MeV) at JAEA-Takasaki: the dosimetry was made by using the CTA-film and/or solution dosimeters. After the irradiation, ions/molecules formed in the solution part of sample were measured by using spectrophotometry, liquid chromatography and ICP-AES; the gas part such as H_2 gas by using gas chromatography; the solid part such as precipitates formed in solution or adsorbents on solid oxides by using electron or X-ray spectrometry.

A large amounts of Pt-group elements, especially Pd, Re and Ru, were contained in high level wastes discharged from power reactors, and expected to be recovered from there. Figure 1 shows the radiation-induced reductions involving Pt-group elements. When considering the recover of elements by using radiations, Pd(II), Rh(III) and Pt(IV) ions were effectively reduced and solidified in the presence of a small amount of oxide particles without using reducing agents such as alcohol radicals, which can be formed by adding alcohols to the solution, although not in the absent (a); the solidified ones were dispersed on the particles and recovered. When using the recovered particles, Ce(IV) ion was reduced more effectively than the original ones.

Asbestos is discharged from general/industrial wastes in large amounts. Since it is so toxic due to its needle-shape and to its resistance to heat and chemicals, a novel method for the non-toxic treatment without using high-temperature heat and harmful chemicals is expected. Figure 2 shows results for asbestos irradiated in aqueous solutions. While the dried asbestos did not change before and after irradiated, its change from needle- to particle-shape (a) and dissolution into the solution rapidly proceeded with the increasing the absorbed dose and acidity in the solution when it was immersed into the solution. During the morphological, H_2 gas was produced from the solution (b): the yield in the presence of asbestos was much larger than those in the absence of asbestos or in the presence of oxide particles [3].

References

1) R. Nagaishi et al., Radiat. Phys. Chem. 75 (2006) 1051.
2) Y. Sugo et al., Radiat. Phys. Chem. 76 (2007) 794.
3) N. Aoyagi et al., Chem. Lett. 36(7) (2007) 890.

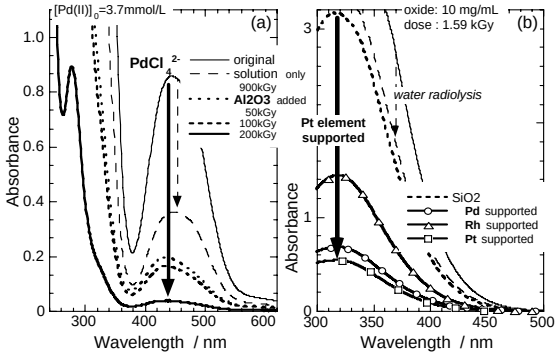

Fig. 1 The radiation-induced reductions involving Pt-group elements in aqueous solutions. (a) The recovering of Pd: when adding oxide particles adding to the solution, Pd(II) ion was effectively dispersed on the particles. (b) When using the dispersed particles, Ce(IV) was reduced more effectively than the original ones.

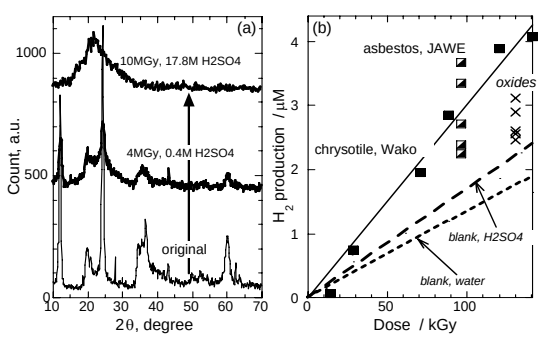

Fig. 2 Morphological change of needle-shaped asbestos and H_2 production in aqueous solutions. (a) The XRD peak at 24° indicating the crystalline asbestos decreased with increasing the dose and acidity. (b) The yield of H_2 produced in the presence of asbestos was much larger than those in the absence of asbestos or in the presence of oxide particles.

4-20 Effect of Ion-irradiation and Annealing on Pinning Property of PLD Prepared YBCO Tapes

K. Nakashima [a, b], N. Chikumoto [b], A. Ibi [b], S. Miyata [b], Y. Yamada [b], T. Kubo [c], A. Suzuki [c] and T. Terai [c]

[a]Department of Quantum Engineering and Systems Science, The University of Tokyo, [b]Superconductivity Research Laboratory, ISTEC, [c]Department of Nuclear Engineering and Management, The University of Tokyo

The change in pinning properties of YBCO tapes prepared by pulsed laser deposition (PLD) method was investigated after ion-irradiation and thermal annealing treatment in order to confirm that ion-irradiation is effective for the J_c enhance in the practical material. In this study, YBCO tapes (2 mm×2 mm×0.5 mm) were irradiated with 400 MeV Kr^{18+}, 450 MeV Xe^{23+} or 500 MeV Au^{31+} from 1.0×10^{10} to 1.5×10^{12} ions/cm^{-2}. As a result of ion-irradiation, the enhancement of J_c was observed especially at high applied magnetic field in 77 K. After the ion-irradiation, the samples were annealed at the temperature of 473 K or 673 K in the oxygen atomosphere for 2 h. From the post –annealing experiment, it was clarified that oxygen vacancies and interstitial atoms in the irradiated YBCO tapes can be recovered at the temperarure of 473 K and 673 K, respectively.

1986年に銅酸化物における高温超伝導が発見されて以来、液体窒素温度である77 Kにおける超伝導応用へ向けて種々の研究開発が行われている。HTSCは第2種超伝導体であるため、磁場中では量子化された磁束(Vortex)がHTSC内へ部分的に進入する。Vortexが超伝導電流により駆動されると電気抵抗が発生してしまうことから、Vortexをピン止めする必要が生じる。ピニングセンターとなるものは超伝導体中の欠陥や不純物などであり、高い臨界電流密度（J_c）を実現することのできる効果的な導入方法の開発が進められている。量子線照射は、製作過程によらず、照射条件を変化させることで超伝導体内のピニングセンターの形状・密度を制御できる利点がある。そこで本研究においては、重イオンビーム照射を用い、現在開発が進められている超伝導線材であるPulsed laser deposition法（PLD法）により作成されたYBCO線材(Y系PLD線材)へ照射欠陥を導入し、J_cなどの超伝導特性の変化を調べた。

重イオン照射による欠陥は中心にアモルファス構造を有する円柱状となるが、その際、電子的阻止能S_e[KeV/Å]が大きいほど、欠陥の直径が大きくなることが報告されており[1)]、過剰フルエンス照射では欠陥が重なるために超伝導特性は低下してしまう。しかし、適当な熱アニールにより低下した特性が回復するという報告がなされている[2)]。以上のことから、本研究ではY系PLD線材に照射フルエンス、イオン種を変えた重イオンを照射し、超伝導特性の変化を調べると共に、照射後アニールを行い、アニールによる超伝導特性および結晶構造の変化を評価し、試料の特性向上条件を調べた。

照射用試料は(財)国際超電導産業技術研究センター超電導工学研究所において作製されたY系超伝導線材を2 mm×2 mm×0.5 mm程度に切り出して作製した。高エネルギー重イオン照射にAVFサイクロトロンを使用した。照射は保護層であるAg層(5 μm)側からYBCO層(0.5 μm)に垂直に照射した。照射イオン種はYBCO層を貫通する条件として、400 MeVのKr^{18+}、450 MeVのXe^{23+}、500 MeVのAu^{31+}を選択し、照射フルエンスは1×10^{10} ～ 1.5×10^{12} [ions/cm^2]の範囲とした。PPMS（Quantum Design社製）を用いた磁化測定により、転移温度(T_c)、臨界電流密度(J_c)等の評価を照射前後で行った。照射後アニールは、照射試料を酸素雰囲気中で目的の温度、時間で保持した後に銅板上で急冷しその影響を調べた。

温度77K、印加磁場2Tにおける照射フルエンスとJ_cの関係をFig.1に示す。どのイオン種でも5×10^{11} [ions/cm^2] 程度のフルエンスで最もJ_cが向上した。また、J_cが最も向上するイオン種はXeイオンであるが、この理由は結晶性を大きく損なわずに有効な円柱状欠陥を多数導入できるためであると考えられる。

照射後アニール実験は473Kおよび673Kについて2時間行った。473 Kでは酸素欠陥が、673 Kでは格子間原子が、それぞれ過剰フルエンス照射の場合に特に大きく回復することが分かった。

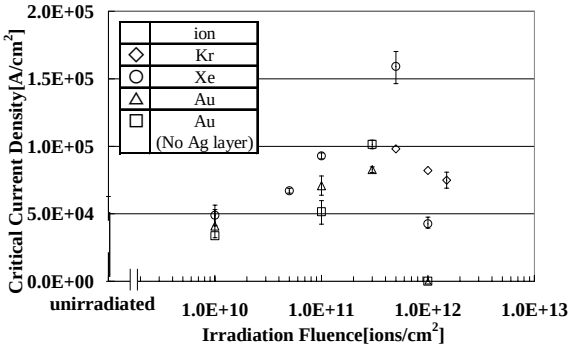

Fig.1 The relationship between fluence and J_c.

本研究の一部は超電導応用基盤技術開発業務の一環として新エネルギー・産業技術総合開発機構（NEDO）の委託により実施された。

References

1) Y. Zhu *et al.*, Phys. Rev. B **48,** 6436 (1993).
2) T. Terai *et al*., Physica C **282-287**, 2285 (1997).

4-21 Damage Evaluation by Means of Electrical Resistivity Measurement in Oxide Irradiated with MeV Electrons

N. Ishikawa [a], S. Yamamoto [b], Y. Chimi [c], H. Sugai [a], T. Kato [a] and A. Iwase [d]

[a]Division of Fuels and Materials Engineering, NSED, JAEA [b]Environment and Industrial Materials Research Division, QuBS, JAEA, [c] LWR Long-term Reliability Research Unit, NSRC, JAEA [d]Department of Materials Science, Osaka Prefecture University

One of the well-known standards for describing radiation damage density in solids irradiated with high energy (keV-MeV) particles is called dpa (displacements per atom). Radiation damage created by different radiation conditions can be compared respectively with the common standard, if dpa is adopted. Especially when the target material is a simple metal, this evaluation method is widely used. This is because relatively simple defects are created in an irradiated simple metal which consists of one atom species. Moreover, elastic displacement is the only origin of the defect formation for simple metal, and this facilitates the estimation of the dpa value.

However, it is not established for oxide ceramics materials that this method can be simply applied for the estimation of damage density, and there is a significant possibility that complicated defect formation or annihilation can take place. Moreover, for oxide ceramics, the method for experimentally evaluating radiation damage has to be re-examined in the first place.

In this study electrical resistivity measurement is adopted for evaluating radiation damage in oxides as it is widely used for the evaluation of radiation damage in metals. Electron irradiation of TiO_{2-x} and in-situ electrical resistivity measurement were performed. The energy range is restricted in the range of 1.0-2.5 MeV, since in this energy range the irradiation with electrons is known to cause elastic displacements of target atoms, and relatively simple defects are created.

Thin films of TiO_{2-x} were deposited on $SrTiO_3$ (100) single crystal substrates, and were irradiated with 1.0 MeV and 2.5 MeV electron beam. The thickness of the films was about 0.3 μm which is thin enough for the electrons to pass through. The irradiations were performed at room temperature (280-283K), and the fluence dependence of electrical resistivity was measured in-situ at a fixed temperature of 280K by means of the conventional four probe method.

In Fig.1 the electrical resistivity as a function of fluence is shown for TiO_{2-x} irradiated with 1.0 MeV and 2.5 MeV electrons. The monotonic decrease of the electrical resistivity is found for both irradiations in contrast to the monotonic increase found for high-energy ion irradiations. The decrease in electrical resistivity probably originates from increase in carrier concentration which may be related to displacements of oxygen atoms. For high fluence region ($>1x10^{15}$ cm^{-2}) the electrical resistivity can be described by the linear function of the logarithm of fluence. In this fluence range, the calculated atomic displacements are in the order of ppm, and the mutual interaction between created defects is not intense. Moreover, the change in mobility due to increase in scattering center for conduction electrons is probably very small.

The slopes of the curve shown in the figure are almost the same, and the defect creation cross section for 2.5 MeV electron irradiation is higher than for 1.0 MeV electron irradiation, indicating that the energy increase contributes to enhancement of defect creation cross section. The investigation over wider energy range is necessary to describe more precise energy dependence of the resistivity behavior.

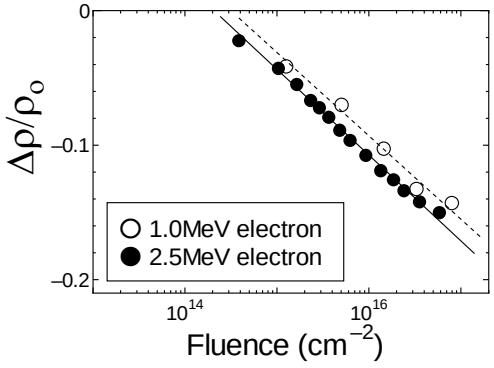

Fig.1 Fluence dependence of the change in electrical resistivity normalized by the value before irradiation ($\Delta\rho/\rho_o$) in TiO_{2-x} irradiated with electrons. Closed circles are the data for 2.5 MeV electron irradiation, and the open circles are for 1.0 MeV electron irradiation.

4-22 Lattice Defects Induced by Electron Irradiation in FeRh Alloys

A. Iwase [a)], A. Ishii [a)], F. Hori [a)], Y. Zushi [a)] and N. Ishikawa [b)]

[a)]Department of Materials Science, Osaka Prefecture University,
[b)]Division of Fuels and Materials Engineering, NSED, JAEA

FeRh alloys were irradiated with 0.80 -MeV and 2.0 -MeV electrons, and the defect structure was studied by means of a positron annihilation technique. The experimental result shows that the electronic structure around irradiation-induced vacancy-type defects depends on the energy of electrons.

Fe-50%Rh は B2 構造を有する金属間化合物であり、室温付近で強磁性状態から反強磁性状態に磁気相転移を起こす合金である。最近我々は、この合金を高速重イオン照射することにより、本来反強磁性を示すべき低温でも、強磁性が発現することを、磁化測定で明らかにしてきた。イオン照射の場合は、ターゲット試料の原子に与えるエネルギーが大きいため、Fe 原子も Rh 原子も区別なく弾き出されてしまう。これに対して、電子線照射はターゲット原子へ与えるエネルギー値が弾き出しエネルギーと近いため、電子線のエネルギーを選ぶことによって、Fe 原子のみを弾き出したり、Fe 原子、Rh 原子とも弾き出したりすることができる。従って、電子線照射を用いて、Fe 原子のみを弾き出した場合と Rh 原子も同時に弾き出した場合に、試料中に生ずる格子欠陥,、あるいは磁性状態がどのように違うか、という点が興味深い。以前の実験により、電子線のエネルギーが 0.5 MeV 以下のときは Fe 原子、Rh 原子とも弾き出しは起こらず、0.5-1.0 MeV の時には、Fe 原子だけが弾き出され、エネルギーが 1.0 MeV を超えると、Fe 原子に加えて Rh 原子の弾き出しも起こる、ということがわかっている。そこで、TIARA シングルエンド加速器により Fe-50%Rh に 0.8 MeV, 2.0 MeV の電子線を照射し、陽電子消滅法によって試料中の格子欠陥を調べた。

試料は Fe-50%Rh のインゴットから切り出し熱処理を行った。照射条件は上で述べた通りである。陽電子消滅測定は全て室温で陽電子寿命とドップラー拡がり測定を行った。

Fig. 1 に陽電子消滅同時計数ドップラー拡がり測定から得られたS-Wパラメータの相関図を示す。一般にSパラメータの変化は空孔の濃度およびサイズに依存し、Wパラメータの変化は陽電子消滅位置周囲の原子種に反映される。そのため、この図から横軸の変化から電子線照射により0.8、2 MeVいずれの場合も空孔型欠陥が導入された事がわかる。陽電子の金属結晶中での消滅が飽和するのはおよそ100at.ppm程度であることを考えると、未照射での空孔型欠陥量は数ー数10 ppm程度で、照射によってー100 ppm程度に増加している事がわかる。

この欠陥量は照射量から計算される値が1.95×10^{17} (0.8 MeV)、7.6×10^{17} (2 MeV)程度である事を考えると妥当である。

一方で導入された欠陥の形態を考えた場合、0.8 MeVと2 MeVではSの値がほぼ同じであるのに対し、W値が異なっている。このことはこの２つの照射で導入された空孔の周囲の電子状態に違いが生じた事を示す。すなわち、この合金系で考えられる空孔はFe空孔(V_{Fe})とRh空孔(V_{Rh})の２種類であり、照射によってV_{Fe}とV_{Rh}との濃度比に偏りが生じていると考えられる。これまでの結果と比較して考えると、2 MeV照射では両空孔が均一に入るが0.8 MeVでは鉄原子のみが弾き出され、V_{Fe}のみが照射によって導入された事を示している。

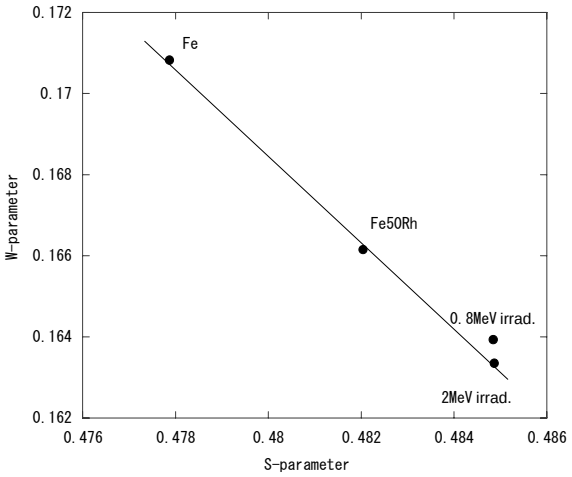

Fig. 1 Relationship between S-parameter and W-parameter for FeRh alloys irradiated with 0.8 MeV electrons and 2 MeV electrons. Data for pure Fe and unirradiated Fe-50Rh alloy are also shown in the figure.

4-23 Study of Mass-transport Process in Noncrystalline Films Using Ion Beam Technique

H. Naramoto [a)], K. Narumi [a)], S. Sakai [a)], Y. Maeda [a, b)], T. Motooka [c)], Y. Ikoma [c)], S. Munetoh [c)] and X-q. Cheng [c)]

[a)]Advanced Science Research Center, JAEA, [b)]Faculty of Engineering, Kyoto University, [c)]Department of Materials Science, Kyusyu University

The energetic ions have been employed for the position-sensitive materials processing and also for the depth-sensitive analysis of elements and defects[1]. These features are typically suitable for the study of atomistic mass transport process in the near surface region, which can not be complemented by other techniques.

The mass-transport processes in crystalline solids are mostly initiated through the thermal activation of the relevant atoms bound to the surrounding atoms with the periodic nature. The recent progress in nanoscience/nanotechnology has opened the new interests in the transport process in the noncrystalline and/or the inhomogeneous atomistic environment[2].

In the present report, two kinds of mass-transport related studies are described on the noncrystalline layer of Ag(40nm)/C_{60}(100nm)/Co_4C_{60}(40nm)/C_{60}(100nm) on MgO(100) substrate, and on ion-irradiation-amorphized Si.

The noncrystalline layers were prepared with a conventional evaporation technique using Knudsen cells by keeping the exact stoichiometry of Co_4C_{60} mixture because the Co-C_{60} mixtures can be easily phase-separated above the stoichiometric ratio[3, 4]. The Ag top layer was deposited to avoid the influence of oxygen attack on the transport of Co atoms in the Co_4C_{60} mixture. The mass-transport features were characterized *in-situ* by Rutherford Backscattering Spectrometry (RBS) equipped with a heating stage under the ultra high vacuum.

The amorphization of Si was induced by 200keV Ar ion irradiation up to the appreciable dose of 2×10^{16}/cm^2 to RBS. The additional irradiation with 10keV Ar^+ ions was performed to introduce the possible bending strain in the near surface region by changing the doses systematically.

Figure 1 illustrates the typical profile changes of the layered films characterized by 2MeV $^4He^+$ RBS. After annealing at 397K, there induced the considerable profile changes at the Ag top layer and also at the Co_4C_{60} mixture layer. The temperature range observed coincides with that in which the compound is relaxed into more stable form as evidenced by the detailed Raman analysis[4]. Further annealing at 483K induced the definite change of Co profile moving toward deeper. This result is totally different from that caused by the thermal diffusion with the broadening nature towards both sides. The inward change of Co atoms could be associated with the peculiar nano-structure together with the possible bending strains.

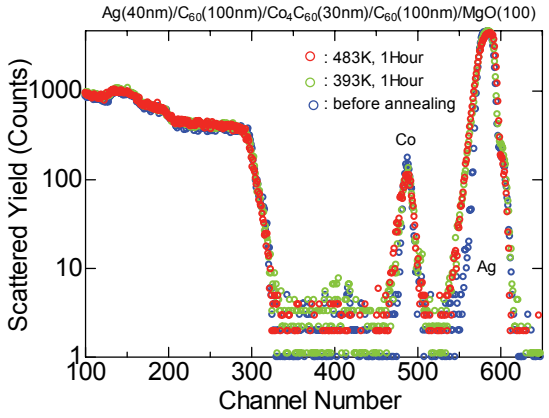

Fig. 1 2MeV $^4He^+$ ion RBS spectra from the multi-layer of Ag/C_{60}/Co_4C_{60}/C_{60}/MgO(100) annealed in the temperature range between 300K and 483K.

The effect of strain on the implanted Ar distribution in amorphized Si was examined by implanting the 10keV Ar ions additionally. In this case, the compressive strains can be induced in the amorphized region below the surface.

The results obtained are not shown here for the simplicity, but the conclusions are listed below.

*The transportation of implanted 200keV Ar atoms toward the surface region was observed clearly at the higher dose of 10keV Ar ions more than 5×10^{16}/cm^2.

*The influence seems to be localized in the shallower region than the peak depth of implanted profile.

*The redistribution of implanted Ar atoms does not induce the crystallization of amorphized region.

*The systematic analysis on the observed phenomena is in progress by changing the strain parameters and the implanted species.

References

1) H. Naramoto et al., Nucl. Instr. & Meth. 161 (2000) 534.
2) M. J. Demkowicz and A. S. Argon, Phys. Rev. B 72 (2005) 245205.
3) S. Sakai et al., Mater. Trans. 46 (2005) 765.
4) S. Sakai et al., Thin Solid Films 515 (2007) 7758.
5) V. Lavrentiev et al., Chem. Phys. Lett. 423 (2006) 366.

4-24 Carbon-concentration Analysis of Si Surfaces Bombarded with 10- to 100-keV C_{60} Ions

K. Narumi [a)], H. Naramoto [a)] and Y. Maeda [a, b)]

[a)]Advanced Science Research Center, JAEA, [b)]Department of Energy Science and Technology, Kyoto University,

Our previous study shows that sputtering is one of the most important radiation effects of 10-to-100-keV C_{60} ions[1-4]. It is so strong that it can affect any other radiation effect of C_{60} ions. Carbon deposition or implantation by C_{60} irradiation is one of such effects. Carbon content in the surface layer is sensitive to the sputtering; thus, analysis of carbon concentration could be helpful to understand the strong sputtering effect of C_{60} irradiation. We will report here the analysis of carbon concentration of Si surfaces bombarded with 10-, 50- and 400-keV C_{60} ions.

A piece cut from a Si(100) wafer was irradiated with C_{60} ions. Before the irradiation, the samples were cleaned with a wet chemical treatment to reduce carbon contaminants on the surface. A part of the sample was covered with a mask, so that one sample had both irradiated and unirradiated areas. After the C_{60} bombardment, carbon concentration in the surface layer was evaluated with a nuclear reaction $^{12}C(d, p)^{13}C$ using 1.2-MeV D. Examples of the observed energy spectra are shown in Fig. 1. Signals at lower energies correspond to the primary D scattered from Si nuclei, while those at higher energies are attributed to protons produced in the nuclear reaction. Integrated proton yields reflect overall carbon content in the surface layer. Since the proton signals in the spectrum for an unirradiated area originates from residual carbon contaminants on the sample, the difference between the proton yields of bombarded and unirradiated areas is caused by the C_{60}-ion bombardment.

Figure 2 shows the fluence dependence of the carbon concentration in the surface layer of C_{60}-bombarded Si. The number of ^{12}C nuclei per cm^2 was evaluated with the use of the cross section measured by Kashy et al.[5] A solid line in the figure shows carbon concentration estimated from the ion fluence. The experimental results are inconsistent with this line: At lower fluence, measured carbon concentration is higher than the value estimated from the ion fluence, while at higher fluence the increase rate of carbon concentration decreases. The former could be attributed to carbon implantation by C_{60}-bombardment-induced recoil of the surface contaminants. On the other hand, the latter reflects the strong sputtering effect of the C_{60} bombardment. This conclusion can be explained by the following scenario: The carbon concentration in the surface layer is determined by the competition between the sputtering and the carbon deposition or implantation by the C_{60} bombardment. Under this competition, the higher the carbon concentration, the more carbon atoms are sputtered; thus, the increase rate of the concentration decreases with the ion fluence. It could be expected that the carbon concentration reach a certain value determined by the sputtering yield.

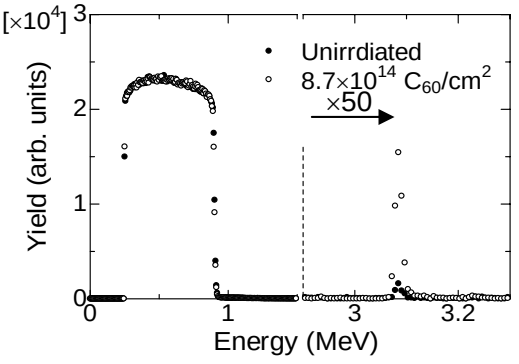

Fig.1 Example of energy spectra measured when 1.2-MeV D was incident on a Si sample bombarded with 50-keV C_{60}^+ ions. Energy spectrum measured on an unirradiated part of the sample is also shown.

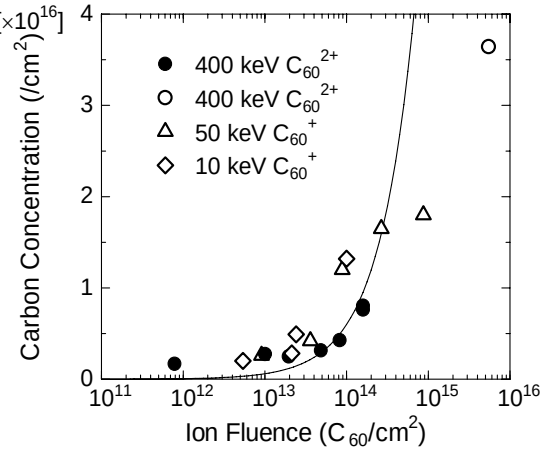

Fig.2 Fluence dependence of the carbon concentration at Si surfaces bombarded with 10-, 50- and 400-keV C_{60} ions. Solid line shows areal density which is 60 times as much as C_{60} ion fluence.

References

1) H. Naramoto et al. TIARA Annual Report 2002, JAERI-Review 2003-033 (2003) 225.
2) H. Naramoto et al. TIARA Annual Report 2003, JAERI-Review 2004-025 (2004) 211.
3) H. Naramoto et al. TIARA Annual Report 2004, JAEA-Review 2005-001 (2006) 271.
4) H. Naramoto et al. Takasaki Aannual Report 2005, JAEA-Review 2006-042 (2007) 149.
5) E. Kashy et al. Phys. Rev. 117 (1960) 1289.

4-25 1-D Crosslinked Polymer Nanowires Prepared by Single Particle Nanofabrication Techniques

S. Seki [a)], M. Sugimoto [b)], T. Sato [b)], M. Oikawa [b)] and T. Sakai [b)],

[a)]Graduate School of Engineering, Osaka University
[b)]Quantum Beam Science Directorate, Japan Atomic Energy Agency

Recently we have successfully produced 1-D nanowires by the crosslinking reactions of polymer molecules within an ion track along the particle trajectory. The present nano-scaled negative tone imaging technique (single particle nano-fabrication technique: SPNT) shows a striking contrast to the conventional nuclear track technique, providing the direct formation of nanowires based on a variety of polymeric materials with fairly controlled sizes. Effective crosslinking reactions of the polymers are the unique requirement of SPNT. Thus nanowires reflecting the properties of the target polymer materials have been successfully realized by the simple one-step procedure of SPNT, giving conducting, light-emitting, ceramic, protein, hydrogel nanowires as well as the multi-functional nanowires /nanoparticles by the combination of the polymer materials. The formation process of ultra-fine optical nano-fibers by SPNT is discussed in the present letter based on silsesquioxanes (SSQ) as the target polymer material which is optically clear and suitable to the organic-inorganic conversion reactions by subsequent sintering processes.

High energy particle beam at low fluence without overlapping ion tracks produces single-ion events in the target materials, yielding a cylinder-like nanofiber in the thin film. Fig. 1 shows the AFM images of the SSQ nanofiber observed on Si substrates. The nanowires were clearly produced by all high energy particles used, and the thickness of the cross-section depends strongly on the parameters of the incident particles. The relationship between radial distribution of deposited energy released by an incident particle and induced crosslinks of polymer molecules has been precisely investigated in the previous studies, resulting in the changes of the radius of cross section of the cylindrical nanofiber. The radial distribution was characterized by the linear energy transfer (LET) of the incident particle which reflects the averaged energy density per unit length in a particle trajectory. The initial radial distribution of the released energy and the subsequent radial diffusion of the energy and/or reactive intermediates determine the cylinder-like area where gelation occurs, thus the size increased considerably with an increase in LET of the particles. Radii of the cross-section of the nanofibers were measured as 10.1, 8.7, and 6.3 nm, respectively under irradiation of 450 MeV Xe, 400 MeV Kr, and 388 MeV Ni ion beams. The values of LET of these particles are calculated as 4800, 2700, and 1800 eV/nm, respectively in SSQ thin films,[13] which shows a striking coincidence with the values of radii. In spite of the relatively small molecular weight of SSQ (Mw = 1.2 $\times 10^3$), the thicker nanofibers in comparison with the size observed for the other polymeric materials were observed. It has been already revealed that the radial size of the cylinder-like area depends also on the efficiency of the crosslinking reaction (*G(x)*). The vinyl groups in the side chain promote efficiently the crosslinking reactions, and this is the case giving considerable increase in the radius of nanofiber based on SSQ. The nanofibers based on the other silsesquioxanes were also successfully prepared by the same scheme. Sintering of the nanofibers at 1000 K caused no change in the number density of the nanofibers based on all the polymeric materials. The shrinking of the sizes was observed for the nanofibers giving 30-40 % reduction in the radii, however there was almost no change in the length of the nanofibers. The interaction at the interface restricts the axial shrinking, hence radial shrinking dominates in the present case. The successful organic–inorganic conversion by this sintering process provides the ultrafine SiO_2 optical nanofibers as demonstrated in the present study.

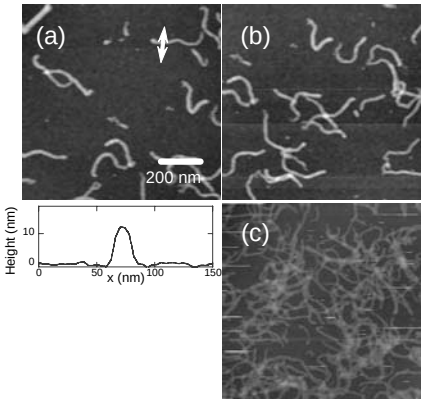

Fig. 1. AFM micrographs of nanofibers based on SSQ produced by SPNT. Images (a) – (c) were observed in the thin films of SSQ at 300 nm thick after irradiation of 450 MeV Xe, 400 MeV Kr, and 388 MeV Ni ion beams at the fluence of 2.9×10^9 ions cm^{-2}(a,b) or 1.1×10^{10} ions cm^{-2} (c), respectively. Superimposed figure is the profile of cross section of a nanowire at the point represented by an arrow in (a).

References

1) S. Seki, et al., *Adv. Mater.*,**13** (2001) 1663.
2) S. Seki, et al., *J. Phys. Chem. B*, **103** (1999) 3043.
3) S. Seki, et al., *Macromolecules*, **38** (2005) 10164.
4) S. Tsukuda, et al, *J. Phys. Chem. B*, **110** (2006) 19319.
5) S. Seki, et al., *Macromolecules*, **39** (2006) 7446.
6) S. Tsukuda, et al., *Appl. Phys. Lett.*, **87** (2005) 233119.
7) S. Seki, S. Tagawa, *Polymer J.*, **39** (2007) 277.

4-26 Analysis of Light Elements in Carbon Materials

Y. Horino [a)], Y. Mokuno [a)], A. Chayahara [a)], H. Yasui [b)], K. Awazu [b)],
S. Yamamoto [c)], K. Narumi [d)] and H. Naramoto [d)]

[a)]National Institute of Advanced Industrial Science and Technology
[b)]Industrial Research Institute of Ishikawa
[c)]Environment and Industrial Materials Research Division, QuBS, JAEA
[d)]Advanced Science Research Center, JAEA

Carbon materials are well known for their excellent properties and many applications are being under intense study. The plasma enhanced chemical vapor deposition (PECVD) using hydrocarbon gas is the most used method to synthesize carbon materials. But hydrogen will be involved during processing and they will influence properties of carbon materials. In order to investigate the influences, we examine the distribution of hydrogen at near surface region in some carbon materials by a nuclear reaction analysis (NRA). We have checked the system by using a hydrogen-implanted silicon wafer. We could obtain a profile of the implanted hydrogen which was consistent with one calculated with the TRIM code. It was found that the amount of hydrogen in poly-type diamonds was 0.2-1 at %. However, it was difficult to determine the amount of hydrogen in single crystal diamonds due to a poor S/N ratio of the analyzing system.

ダイヤモンドなどの炭素系薄膜材料が、炭化水素系のガスを用いた気相合成で作製された場合、水素が含有され[1,2]、材料特性に影響する。そのため、水素の量・分布を評価することは炭素系新奇材料の創製･利用に不可欠なものとなっている。しかし、特に数十ppmオーダーの微量の水素の定量分析は非常に困難で、材料特性に対する影響の詳細な研究は行われていないのが現状である。

本研究では、炭素系材料に対する水素の影響を検証するために、炭素系薄膜材料中の水素分布を定量的に測定し、材料特性との関連を調べることを目的とする。そのため、エネルギー6～8 MeVの^{15}N（窒素同位体）と水素との共鳴核反応法（NRA）を利用した。水素分布を定量的に測定し、本方法の定量下限や深さ分解能を評価する。また、水素の吸着量や深さ分布と材料特性との関連を明らかにする。

測定に用いた共鳴核反応は、^{1}H(^{15}N, α γ)^{12}Cで、共鳴エネルギー（ER）=6.385 MeV、共鳴幅＝1.8 keVである。試料に入射したプローブイオン（^{15}N）が試料中でエネルギーを失いながら進行し、エネルギーがERになると水素との核反応が起こり、約4.4MeVのガンマ線が放出される。エネルギー損失量が水素の存在する深さ、検出されるガンマ線が水素量の情報を有し、プローブイオンのエネルギーをスキャンすることで深さ方向の水素分布を得ることができる。共鳴幅が非常に狭いため、深さの分解能は主に^{15}Nイオンのエネルギー拡がりで決まり、今回は約5nmであった。

Fig.1に、Siウェハに2 keV Hイオンを5×10^{15} ions/cm^{2}注入したもの（■）、多結晶ダイヤモンド（▲）、およびダイヤモンド単結晶（○）を分析した結果を示す。いずれの場合も約6.49 MeV近傍にピークが観察された。これらは材料表面に吸着している水素に相当する。図中のエネルギーは使用した加速器の表示をそのまま用いている。そのため実際のエネルギーより数10 keV程度のずれがある。

Siの場合、表面吸着水素と注入水素の分布が明瞭に分かり、TRIMで計算した飛程44 nmとほぼ一致した。ダイヤモンドの場合も表面での水素の吸着が観察された。そのため表面の影響を受けないように、入射プローブのエネルギーを選んで、いくつかのダイヤモンド中の水素量の分析を行った。多結晶ダイヤモンドの場合、水素量は約0.2～1at%となり、製造方法によりばらつきが見られた。一方、単結晶ダイヤモンドの場合、測定限界以下で定量は困難であった。S/N比を向上することが必要であり、現時点で、使用した分析システムの定量限界は100 ppmオーダーであることが分かった。

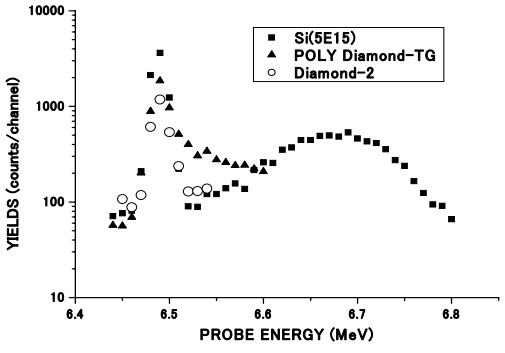

Fig.1 Hydrogen profiles measured by the NRA. The samples were a silicon wafer implanted with 2-keV H with a dose of 5×10^{15}ions/cm^2 (■), a polycrystalline diamond (▲) and a single-crystalline diamond (○).

References

1) Y. Horino, et al., New Diamond and Frontier Carbon Technology 16 (2006) 63-69.
2) Y. Mokuno, et al., Diamond and Related Materials 15 (2006) 455-459.

4-27 Structural Change in Si Induced by Ion Bombardments and Its Application for Nano-Fabrication

T. Motooka [a)], Y. Ikoma [a)], S. Munetoh [a)], X.Q. Cheng [a)], H. Naramoto [b)], K. Narumi [b)], S. Sakai [b)] and Y. Maeda [b, c)]

[a)]Department of Materials Science, Kyusyu University, [b)]Advanced Science Research Center, JAEA, [c)]Faculty of Engineering, Kyoto University,

Energetic ion bombardments can induce various kinds of effects on inorganic crystalline materials through the electronic excitations and nuclear collisions depending on the incident ion energies. The electronic excitations along a single ion passage can generate a heat pulse which results in the shear stress extending to the surface. The nuclear collisions can be influential through the generation of point defects and the associated directional flow. This process can be also employed to change the shape of the relevant samples.

In the present study, the main concern has been focused on the structural change in silicon. For the possible applications for nanopore devices [1)], silicon-on-insulator (SOI) samples with μm-size holes made by focused-ion-beam (FIB) irradiation were prepared for the irradiation experiment. Through this experiment, the irradiation chamber was kept to be free from the carbon contamination by cooled shrouds surrounding the samples. Ar^+ and Si^+ ions were chosen to avoid the chemical influences on the irradiation effects. The incident ion energies are high enough to generate the displaced atoms.

Figures 1 and 2 show the transmission electron microscopy (TEM) photographs obtained from the SOI samples before and after the ion irradiation. The structural changes induced by ion bombardments were analyzed based on the dark field (DF) and bright field (BF) images combined with the selected area diffraction (SAD) patterns. The shape of each hole was determined by using the BF image, while the Si crystallinity of the hole region was judged by the DF image using the Si(004) diffraction spot and by using the SAD patterns with the resolution of approximately 500 nm. Main results are summarized as follows:

1)In the case of the irregular shaped hole (see Fig. 1), Si looks to be damaged before ion irradiation probably due to the FIB process, and no remarkable ion-bombardment effects can be observed.

2) In the case of the round hole (see Fig. 2), the hole region is crystalline before ion irradiation, but after ion irradiation the hole region is changed to amorphous resulting in an approximately 10 % reduction of the hole size.

3)The observed shrinking effect may be attributed to dilation of crystalline Si upon amorphization induced by ion beam bombardments.

Further studies on the ion-beam-induced shrinking effects of the holes as well as a new method to form nanopores on SOI [2)] are currently underway.

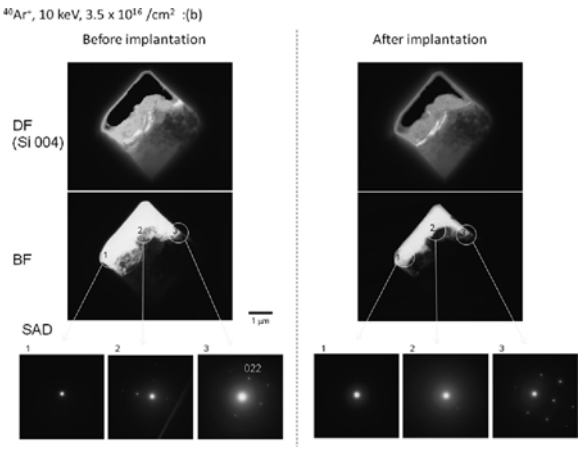

Fig. 1: TEM photographs from the SOI sample with a irregular hole before and after irradiation with 3.5×10^{16} $/cm^{-2}$ 10 keV $^{40}Ar^+$ ions.

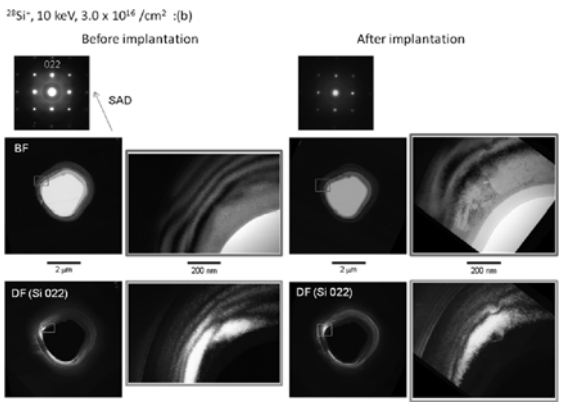

Fig. 2: TEM photographs from the SOI sample with a round hole before and after the irradiation with 3.0×10^{16} $/cm^{-2}$ 10keV $^{28}Si^+$ ions.

References

1) C. Dekker, Nature Nanotechnology, (2007)209.

2) Y Ikoma et al., abstract of the 6th International Conference on Thin Film Physics and Application (TFPA2007) (Sept. 25-28, 2007, Shanghai, China), p. 27 (2007).

4-28 Ion-induced Self-organized Ripple Patterns on Graphite and Diamond Surfaces

K. Takahiro [a)], K. Ozaki [a)], K. Kawatsura [a)], S. Nagata [b)], S. Yamamoto [c)], K. Narumi [d)] and H. Naramoto [d)]

[a)]Department of Chemistry and Materials Technology, Kyoto Institute of Technology, [b)]Institute for Materials Research, Tohoku University, [c)]Environment and Industrial Materials Research Division, QuBS, JAEA, [d)]Advanced Science Research Center, JAEA

The irradiation with heavy ions leads to various morphological evolutions of material surfaces as a result of a balance between roughening and smoothing processes. It is known that self-organized ripple patterns are formed on the surfaces in the case of off-normal incidence of ions. We concentrate on the study of ripple formation on surfaces of carbon allotropes after irradiation under identical conditions. According to the linear erosion theory developed by Bradley and Harper[1)], similar features should be observed for all different carbon materials since all surfaces become amorphous already after low fluence irradiation. Very recently, Takahiro et al.[2)] experimentally showed that different features appeared on graphite, diamond and amorphous carbon surfaces. In the present work, highly oriented pyrolytic graphite (HOPG) and single crystalline diamond were irradiated under identical conditions in order to investigate the allotropic effect on ripple pattern formation.

The HOPG (0001) sample ($1\times1\times0.1$ cm^3 in size), manufactured by Molecular Device Tools for Nano Technology, Russia, was cleaved with a Scotch tape just before irradiation. The diamond (001) sample ($0.3\times0.3\times0.05$ cm^3) is a commercially available Ib-type diamond. The samples were irradiated with Xe^+ ions of 5–30 keV at an incident angle of 60° with respect to the sample normal at room temperature. The ion current density and ion fluence were 2–4 $\mu A\cdot cm^{-2}$ and 2×10^{17} $Xe^+\cdot cm^{-2}$, respectively. The surface topography of the eroded sample surfaces was examined with an atomic force microscope (AFM) in a contact mode. Raman spectroscopy was performed by backscattering from the sample using an Ar laser operating at 514.5 nm.

Figures. 1 (a) and (b) show AFM images taken for HOPG and diamond irradiated with 30-keV Xe^+. Ripples are clearly seen on the irradiated HOPG and diamond surfaces, and they are aligned perpendicular to the ion-beam projection. The averaged ripple spacing for HOPG is found to be approximately 170 nm, much larger than that for diamond (100 nm). The line profile analysis reveals that the amplitudes of ripples, defined as height differences between hills and valleys, are typically 60 nm and 30 nm for HOPG and diamond, respectively. Thus, large differences in ripple wavelength and amplitude between HOPG and diamond were recognized. The top surface layers of Xe^+-irradiated HOPG become amorphous as shown in Fig. 2. The SRIM simulation predicts that the crystalline diamond surface is transformed into amorphous due to sputter erosion. Further experiments under various irradiation conditions will reveal more detail in the mechanism for rippling of carbon materials. Such experiments are now in progress

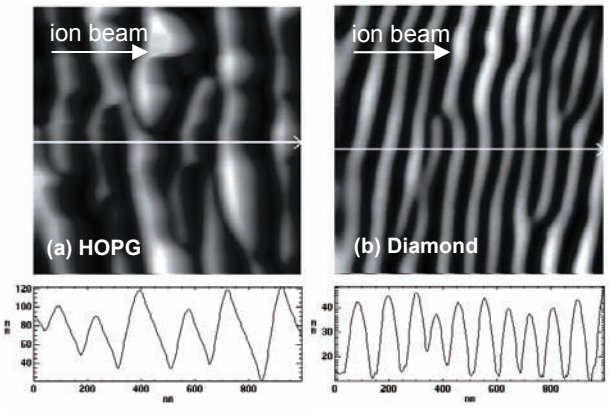

Fig. 1 AFM images (upper panels) of (a) HOPG and (b) diamond irradiated with 30-keV Xe ions at 60° to 2×10^{17} cm^{-2}. Cross sectional line profiles (lower panels) are also shown. Arrows indicate the projection of ion-beam direction.

References

1) R. M. Bradley and J. M. E. Harper, J. Vac. Sci. Technol. A 6 (1988) 2390.
2) K. Takahiro et al., Nucl. Instr. Meth. B 256 (2007) 378.

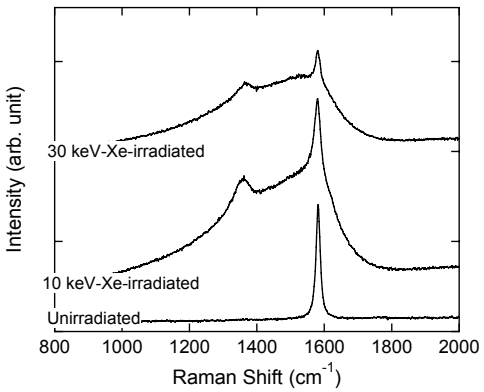

Fig. 2 Raman spectra of HOPG before (bottom) and after irradiation with 30-keV (top) and 10-keV (intermediate) Xe ions to a fluence of 2×10^{17} cm^{-2} at an incident angle of 60° with respect to the sample normal.

4-29 Optical Property Modifications of Diamond and Sapphire by Ion Implantation and Heat Treatment

Jae-Won Park [a)], Hyung-jin Kim [a)], Dong-Hwa Oh [b)] and Young-Chool Kim [c)]

[a)]Korea Atomic Energy Research Institute, [b)]Sung Kyun Kwan University, [c)]Hanmi G. I. Laboratory

Introduction

In order to modify the optical properties of sapphire and diamond materials, a method of the ion-implantation and subsequent annealing was employed. To understand the change in optical properties, calculation of the band structure using density functional theory (DFT) and characterizations of surface chemical properties before and after the ion implantation and subsequent annealing were conducted.

Experimentals

100 keV Co and B ions using 400 keV ion accelerator and 1 MeV H ions using 3 MV Tandem accelerator were implanted into the sapphire and diamond samples with a dose of about 10^{17} ions /cm^2 for all samples, followed by post-irradiation annealing at 600 ℃ – 1200 ℃ both in air and in vacuum atmosphere for 2 ~ 24 hours. Once certain modifications in the optical properties of the treated diamond and sapphire specimens were visually observed, the relevant samples were analyzed with X-ray photoelectron spectroscopy (XPS) and FTIR to understand the mechanisms of the modifications. In order to examine the band gap variation in the doped diamond and sapphire, calculations by first-principles density-functional theory (DFT) were done [1)].

Results and discussion

The N-ion-implanted diamond showed only black even after post-implantation annealing, but the diamond implanted with proton (H^+ ion) and subsequent annealing at 600 ℃ in vacuum emitted the purple-red color.

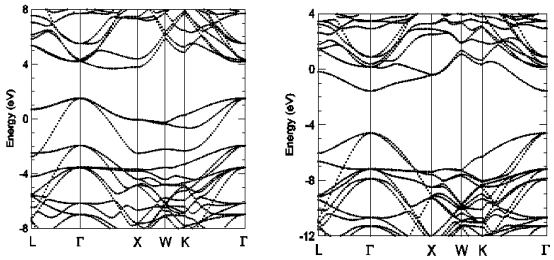

(a) **(b)**

Fig. 1. The band gap of N-doped diamond is reduced by 1.12 eV as compared to the band gap of the clean diamond (a), but the band gap of H-doped diamond is reduced by 1.96 eV (b).

Since the DFT calculation shows a significant difference in the band gap between N and H doped diamonds (Fig. 1), the different elemental doping should play a major role in the optical property change.

The transparent sapphire implanted with Co ions shows sky-blue colors after post-implantation annealing at 900 ℃ in air for 6 hours. XPS analysis shows that. Co2p peak at 778.7 eV [2)] which denotes metallic Co is clearly seen along with Co-Al-O peak at 782.2 eV [2)] in the as-implanted sapphire (Fig. 2a) while the peak corresponding to metallic Co disappeared in the post-implantation annealed sample (Fig. 2b). Therefore, it can be concluded that the formation of Al-Co-O compound is responsible for the sky-blue color emission. On the other hand, the sapphire implanted with H, B, N showed nothing but black or white even after annealing at 900 ℃.

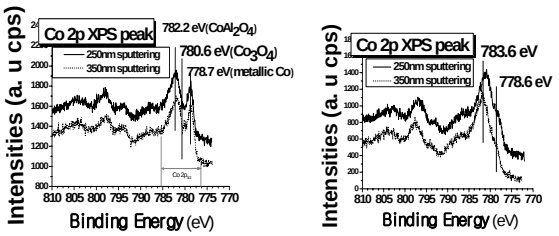

(a) **(b)**

Fig.2. Co2p XPS peaks obtained from as-implanted (a) and post-implantation annealed (b) sapphire samples.

FTIR spectra for the sky-blue colored sapphire implanted with Co ions followed by annealing show broad absorption band in the range of 588 nm to 626 nm wavelength which seems to be affected by Co ion implantation.

References

1) J. Y. Lee, J. Park, and J. H. Cho, Appl. Phys. Lett. 87, 011904 (2005)

2) Haifeng Xiong, Yuhua Zhang, Kongyong Liew, Jinlin Li, Journal of Molecular Catalysis A: Chemical 231, 145–151 (2005)

4-30 Change in Curie Temperature in Fe-Ni and Fe-Ni-Mn Alloy Thin Films Irradiated with Energetic Ions

Y. Chimi [a)], N. Ishikawa [b)], A. Iwase [c)] and F. Ono [d)]

[a)]LWR Long-term Reliability Research Unit, NSRC, JAEA, [b)]Division of Fuels and Materials Engineering, NSED, JAEA, [c)]Department of Materials Science, Osaka Prefecture University, [d)]Department of Physics, Okayama University

We have studied effects of high-energy heavy-ion irradiation on the magnetic properties in Fe-Ni invar alloys, and have already found that T_C increases by the irradiation[1,2]. This result suggests that the local ferromagnetic regions can be induced by the irradiation in the paramagnetic phase above T_C for the matrix of Fe-Ni invar alloy. In general, high-energy heavy-ion irradiation of materials induces electronic excitation continuously along with the ion path. The induced ferromagnetic region in the irradiated Fe-Ni alloy, therefore, may have linear shape. However, it still remains uncertain whether the origin of the effect is electronic excitation or elastic displacement, because in our previous study[1,2] we used bulk specimen in which the energy of the incident ions decreased with the depth. In the present work, we investigate the change in T_C in Fe-Ni[3] and Fe-Ni-Mn alloy thin films irradiated with several kinds of energetic ions and the dominant irradiation parameter for the modification.

Specimens of Fe-Ni and Fe-Ni-Mn alloy thin films (~500 nm in thickness) were prepared on MgO(100) single crystal substrates by means of rf magnetron sputtering at ambient temperature with target materials of Fe-32at.%Ni and Fe-28at.%Ni-7at.%Mn alloys, respectively. The specimens were annealed at 1273 K for 1 h in a vacuum below ~3.5×10^{-4} Pa. After this thermal treatment, the crystal structure of the Fe-Ni specimen changed from bcc to fcc, which was the same structure as the bulk material of Fe-Ni invar alloy. The specimens were irradiated at room temperature with 1.0-MeV ^{1}H, 1.5-MeV ^{4}He, 5.0-MeV ^{12}C and 12.0-MeV ^{35}Cl ions by using the 3-MV tandem accelerator of TIARA at JAEA-Takasaki, and 200-MeV ^{197}Au ions by using the 20-MV tandem accelerator at JAEA-Tokai. In order to detect the irradiation effect precisely, a half area of the specimen was unirradiated by means of a masking technique, and thus both irradiated and unirradiated regions were produced in the same specimen. After the irradiation, measurements of AC-susceptibility of the specimen were performed in the temperature range from room temperature to ~550 K. The value of T_C for the specimen was derived from the temperature dependence of the AC-susceptibility.

Although a large increase in T_C with increasing the ion fluence was observed for ^{1}H, ^{4}He, ^{12}C, and ^{35}Cl ion irradiations, no change in T_C was detected in the case of 200-MeV ^{197}Au ion irradiation. This result suggests that the dominant energy transfer process for the increase in T_C is the elastic displacement. In Fig. 1, the values of ΔT_C for all irradiations are plotted against the total energy deposited by the elastic displacement, $\Phi\times S_n$, where Φ is the incident ion fluence, and S_n the nuclear stopping power for the incident ion. This result implies that the density of the elastic energy deposition is a dominant irradiation parameter for the increase in T_C in Fe-Ni alloy. In the case of Fe-Ni-Mn alloy, the modification seems to be more susceptible to the elastic energy deposition than that for Fe-Ni alloy.

References

1) F. Ono et al., Nucl. Instr. and Meth. B 206 (2003) 295.
2) F. Ono et al., Mater. Res. Soc. Symp. Proc. 792 (2004) 441.
3) Y. Chimi et al., Nucl. Instr. and Meth. B 257 (2007) 388.

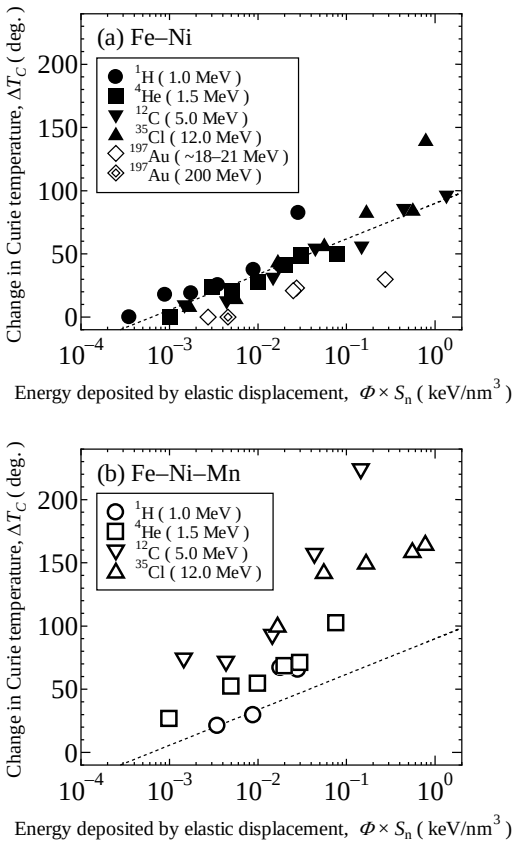

Fig.1 Change in Curie temperature, ΔT_C, plotted against total energy deposited by elastic displacement, $\Phi\times S_n$, for (a) Fe-Ni alloy, and (b) Fe-Ni-Mn alloy. Dotted lines are guides for the eye.

4-31 Effects of Multi-ion Beam Irradiation on Microstructural Changes in Li_2TiO_3

D. Yamaki, N. Okubo, T. Aruga, T. Nakazawa, S.Jitsukawa

Division of Fuels and Materials Engineering, NSED, JAEA

Li_2TiO_3 is regarded as one of the most suitable candidates for the solid tritium breeder material of D-T fusion reactors. Simulation of the fusion reactor environment and hence the study of a synergistic effect of atomic displacement damage in Li_2TiO_3 are presumed to be approached by a simultaneous irradiation with "triple" ion beams which consist of O^{2+}, He^+ and H^+ ion beams. In this study, the results of the FT-IR photoacoustic spectroscopy (PAS) with Li_2TiO_3 samples irradiated with the single ion beam, with the triple ion beams simultaneously and with the triple ion beams sequentially were analyzed for investigation of microstructral changes.

The characteristics of the Li_2TiO_3 samples and the experimental parameters used in this experiment were described in ref[1]. The characteristic peaks in FT-IR PAS spectra for non-irradiated Li_2TiO_3 sample were observed around 680, 780, 880, 1090, 1430, 1480, 1570, 3150 and 3450-cm^{-1}. In comparison to the reported spectra of TiO_2 and Li_2TiO_3, 680- and 780-cm^{-1} peaks are identified from Ti-O bond, 1570-, 3150- and 3450-cm^{-1} peaks are from the O-H bond in hydroxyls adsorbed on or near the surface, and others are from C=O bond in Li_2CO_3 formed on or near the surface by reaction with CO_2 in the atmosphere[1].

Among the observed peaks, irradiation effect is clearly found for 780-, 1090- and 3450-cm^{-1} peaks. In the previous study, the radiation-dose dependence of the areas of these peaks indicates that TiO_2, hydroxyl and Li_2CO_3 are formed near the surface by irradiation, and the amount of each was found to be strongly affected by displacement per atom (dpa). Among them, the amount of the formed hydroxyl is affected not only by dpa but also by the method of irradiation, that is, the single, the simultaneous triple or the sequential triple irradiation. This may suggest that H^+ implantation after irradiation degrades the generation of hydroxyl (-OH) group near the surface by trapping hydrogen in the irradiation defects or radiolytic products[2,3].

To verify the effect of H^+ implantation on the generation of -OH group, the results of irradiation with O^{2+} ions (about 8 dpa) or He^+ ions (about 1 dpa) with simultaneous, with sequential or without H^+ implantation were compared. The results so far are summarized in Table 1. The results should be interpreted cautiously, since they are by no means complete. However, it likely supports the previous suggestion that H^+ implantation, especially in the sequential irradiation, suppresses the –OH group generation near the surface.

Under the fusion reactor operation, these microstructural changes may strongly affect the tritium release behavior from Li_2TiO_3, durability of Li_2TiO_3, and compatibility of Li_2TiO_3 with other components of the breeder blanket such as structural materials. Further study of the irradiation effects on these microstructural changes is needed to enhance the reliability of the related materials.

References

1)D.Yamaki et al, J.Nucl.Mater. 329-333 (2004)1279-1282.
2)D.Yamaki et al, JAEA-Review 2005-01 (2006) 212-214.
3)D.Yamaki et al, JAEA-Review 2006-042 (2007) 26.

Table 1. Summary of the effects of H^+ implantation on the 3450- cm^{-1} peak, which is due to the O-H bond. Notation as "A+B" means simultaneous irradiation of the beams A and B, and "A->B" means that irradiation with the beam B was performed after closing of irradiation with the beam A.

Dpa	≈8		
Irradiated Ions	O^{2+}	$O^{2+} + H^+$	O^{2+}-> H^+
Peak Area (arb. unit)	(not measured)	571	362

Dpa	≈1		
Irradiated Ions	He^+	$He^+ + H^+$	He^+-> H^+
Peak Area (arb. unit)	380	387	276

4-32 Structural Phase Transition of One-dimensional in Wire on Si Surface Studied by Reflection High-energy Positron Diffraction

M. Hashimoto [a)], Y. Fukaya [a)], A. Kawasuso [a)] and A. Ichimiya [a,b)]

[a)]Advanced Science Research Center, JAEA, [b)]Faculty of Science, Japan Women's University

When one monolayer of In atoms is deposited on a Si(111)-7×7 surface, In/Si(111)-4×1 super-structure is formed (see Fig. 1). From various studies, this super-structure is considered to be a quasi-one-dimensional metallic chain, which is composed of the upper and lower In atoms having two different heights. The 4×1 structure is transformed into the 8×2 structure below 130 K, accompanying the metal-insulator transition[1)]. This transition is considered to be a Peierls transition with the formation of charge-density wave from angle-resolved photoelectron spectroscopy[1)]. However, the mechanism of the phase transition between the 4×1 and 8×2 structures is not fully clarified because the atomic configuration of the 8×2 phase is still unknown. In this study, on the basis of the rocking curve analyses using reflection high-energy positron diffraction (RHEPD), we will report on the atomic displacement of the quasi-one-dimensional metallic chains due to the phase transition.

The RHEPD experiments were carried out in a UHV chamber equipped with a ^{22}Na positron source and electro magnetic lenses[2)]. The positron energy was set at 10 keV. Two azimuthal angles were chosen to measure the rocking curves; (1) 7.5°-off oriented from the [$11\bar{2}$] direction (one-beam condition) and (2) the [$1\bar{1}0$] direction (chain-parallel). The rocking curves were obtained by rotating the sample from 0.3° to 6.0° with an interval of 0.1°.

We measured the rocking curves at 210 K (4×1 phase) and 60 K (8×2 phase) under the one-beam condition, where the curve mainly depends on the vertical position of the surface atoms. The profiles of the rocking curves do not change with temperature (60 K and 210 K). To determine the vertical positions of the In atoms, we calculated the curves based on the dynamical diffraction theory. Two different vertical positions of the In atoms (d_1 and d_2 in Fig. 1) were used as a parameter on the basis of the structure model determined by SXRD[3)]. The measured rocking curves are in good agreement with the optimized curves at both temperatures[4)]. The vertical distances of the In atoms were determined to be d_1 = 0.98±0.09 Å and d_2 = 0.54±0.09 Å at 210 K, and d_1 = 0.99±0.09 Å and d_2 = 0.55±0.10 Å at 60 K[4)]. We found that the vertical positions of the In atoms do not change during the phase transition.

Figure 2 displays the rocking curves measured for the In/Si(111) surface at 53 K (8×2 phase) and at room temperature (4×1 phase) at the [$1\bar{1}0$] direction. The rocking curves change with temperature. We calculated the rocking curves at the [$1\bar{1}0$] direction using the zigzag chain structure determined by SXRD[3)]. The measured rocking curve at room temperature is in good agreement with the curve obtained by calculation, as shown in Fig. 2. On the other hand, the feature of the experimental results at low temperature can not be reproduced by the calculation using the zigzag chain structure and even using the trimer structure[5)]. We found that the rocking curve calculated using the hexagon structure[6)], which was recently proposed by the theoretical calculations, is in good agreement with the experiment as shown in Fig. 2. In conclusion, the metal-insulator transition of the In/Si(111) surface at 130 K occurs with the displacements of the In atoms from the zigzag chain to the hexagon structures.

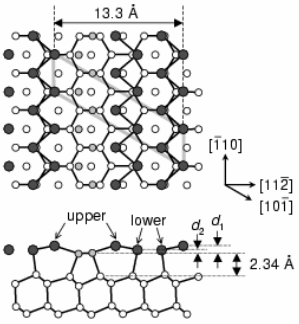

Fig. 1. Top and side views for In/Si(111)-4×1 surface. The large black circles represent the topmost In atoms. Gray and white circles indicate the Si atoms in the first and the deeper layers, respectively.

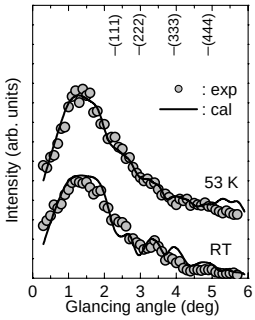

Fig. 2. RHEPD rocking curves for the In/Si(111) surface at the [$1\bar{1}0$] direction at 53 K and RT. The circles and the solid lines show the measured and calculated curves, respectively.

References

1) H.W. Yeom *et al.*, Phys. Rev. Lett. **82**, (1999) 4898.
2) A. Kawasuso *et al.*, Rev. Sci. Instrum. **75**, (2004) 4585.
3) O. Bunk *et al.*, Phys. Rev. **B 59**, (1999) 12228.
4) M. Hashimoto *et al.*, Surf. Sci. (2007), in press.
5) X. López-Lozano *et al.*, Phys. Rev. **B 73,** (2006) 035430.
6) C. González *et al.*, Phys. Rev. Lett. **96**, (2006) 136101.

4-33 Reflection High-energy Positron Diffraction Study on Surface Structures and Dynamics

Y. Fukaya [a)], M. Hashimoto [a)], A. Kawasuso [a)] and A. Ichimiya [a,b)]

[a)]Advanced Science Research Center, JAEA, [b)]Faculty of Science, Japan Women's University

The surface atoms reconstruct to reduce the surface energy and hence the super-structures, which are different from the bulk, are formed on the surface. To investigate the surface structure and properties in detail, the surface-sensitive tool is needed. Thus, we tried to apply positron diffraction to the surface study[1)]. The positrons are the antimatter of electrons and have a positive charge. When the positrons are incident on the surface at grazing angle, the total reflection takes place due to the presence of positive barriers of crystals[2)]. The diffracted positrons under the total reflection condition are very sensitive to the topmost surface. We studied the surface structure and the dynamics of super-structures fabricated on the crystal surface, by using the reflection high-energy positron diffraction (RHEPD).

The experiments were carried out in an ultra-high vacuum chamber equipped with a ^{22}Na positron source and electromagnetic lenses[3)]. The intensity of the diffraction patterns were enhanced using a micro-channel plate with a phosphor plane and recorded by a CCD camera. The accelerating voltage of positron beam was set at 10 kV. To measure the rocking curve, the glancing angle was changed from 0.5˚ to 6˚ by rotating the sample.

By depositing one monolayer of In atoms on the Si(111) surface at 673 K, one-dimensional structure of 4×1-In is formed. The 4×1 phase is transformed into 8×2 phase below 130 K. The phase transition is considered as Peierls transition. However, the phase transition is still in debate because the surface structure of the 8×2 phase is unknown. The circles in Fig. 1(a) shows the rocking curves measured from the 8×2 phase at the [$1\bar{1}0$] direction. From the analyses based on the dynamical diffraction theory, we found that the 8×2 structure consists of hexagons, not trimers. This result supports the recent theoretical calculations. We also confirmed that the 4×1 structure corresponds to the zigzag chain model. Consequently, the 8×2-4×1 phase transition is accompanied by the large displacements of the In atoms.

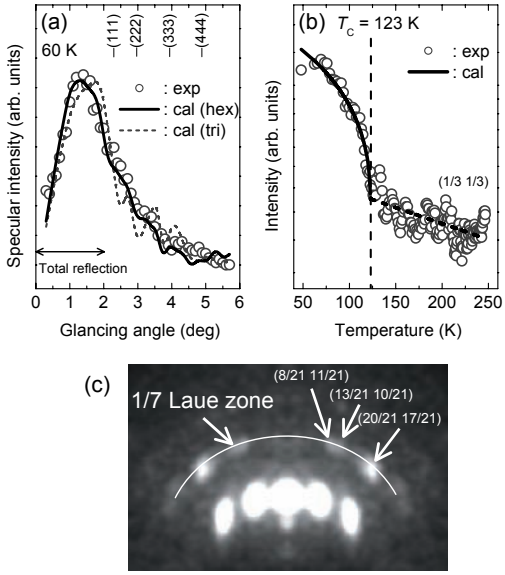

Fig.1 (a) RHEPD rocking curve for the Si(111)-8×2-In surface, (b) Temperature dependences of the total reflection intensities for the Si(111)-√3×√3-Ag surface, and (c) RHEPD pattern for the Si(111)-√21×√21-Ag surface.

When one monolayer of Ag atoms is deposited on the Si(111) surface at 773 K, the super-structure of √3×√3-Ag is formed. The phase transition from one √3×√3 to another √3×√3 phase takes place at 123 K. Although the √3×√3-Ag surface has been studied by various techniques, the phase transition remains unresolved. Figure 1(b) shows the temperature dependences of the total reflection intensities. We observed that at below 123 K, the (1/3 1/3) spot intensity drastically increases with decreasing temperature. By the intensity analyses, we found that the intensity change can be completely explained by considering the order-disorder phase transition[4)].

By depositing small amounts of the Ag atoms on the √3×√3-Ag surface at 110 K, the super-structure of √21×√21-Ag phase is formed accompanied by drastic increase of the surface conductivity. Although several structure models were proposed by many researchers, there is no consensus. From the results of the rocking curve analyses, the five different structures were selected for a possible structure from candidates for the models. Finally, from the line profile of the 1/7th Laue zone (see Fig. 1(c)), we found that the additional Ag atoms are situated on the large Ag triangle of the substrate with triangular shape at the corner of the unit cell[5)].

References

1) A. Kawasuso and S. Okada, Phys. Rev. Lett. **81** (1998) 2695.
2) A. Ichimiya, Solid State Phenom. **28&29** (1992) 143.
3) A. Kawasuso et al., Rev. Sci. Instrum. **75** (2004) 4585.
4) Y. Fukaya, A. Kawasuso, and A. Ichimiya, Phys. Rev. B **75** (2007) 115424.
5) Y. Fukaya, A. Kawasuso, and A. Ichimiya, Surf. Sci. **600** (2006) 3141.

4-34 Characterization of Ion Beam-induced Buried Oxide Layer Using a Slow Positron Beam

M. Maekawa and A. Kawasuso

Advanced Science Research Center, JAEA

For the high-power silicon carbide (SiC) devices, SiC-On-Insulator (SiC-OI) structure is suitable. Ion implantation is one of the methods to make the SiC-OI structure[1]. However, the properties of radiation defects have not been fully clarified. We attempted to investigate the defects in the SiC-OI structure using the positron annihilation spectroscopy which is suitable to detect vacancy-type defects.

Samples were formed by the oxygen implantation to the *n*-type 4*H*-SiC substrate with the energy of 200 keV to dose of $1x10^{18}$ cm^{-2}. High temperature implantation was carried out for avoiding the amorphization. After implantation, samples were annealed in argon ambient tat 1400 °C. The Doppler-broadening of annihilation quanta was measured as a function of incident positron energy (E). The obtained Doppler broadening spectra were characterized by S-parameters which are enhanced by the positron trapping at the vacancy defects.

Figure 1(a) shows S parameters of as-implantation sample of various implantation temperatures. The mean implantation depth of E = 4~8 keV corresponds to the oxygen implanted region. After implantation, S paremter increases in the whole energy range. This indicates that vacancy defects are formed by ion implantation. A remarkable increase of S paramter in the top SiC layer (E=1~3keV) is observed. This indicates that larger vacancy clusters are created in this region. The well-defined SiO_2 layer is not necessarily formed because S parameters of the oxygen implanted region (E=7keV:S=1.05) is apparently lower than those of SiO_2 bulk value (S = 1.15) [2]. This is attributed to the existence of competitive trapping centers, such as vacancy defects which give relatively low S parameters [3]. Even if the implantation temperature increased, the clear SiO_2 layer was not appeared. In the top-SiC layer (E=1~3 keV), a remarkable increase of S parameter is observed. S parameter increases with implantation temperature. This indicates that larger vacancy clusters are easily created at higher temperature.

Figure 1(b) shows the S parameters obtained after annealing at 1400 °C. S parameters at E > 10 keV decreases to the bulk value(S=1) suggesting the recovery of defects. At the region of E = 5~10 keV, a shoulder appears. To determine the electron momentum distribution more in detail, coincidence Doppler-broadening (CDB) measurement was performed. Ratio curve of E=7 keV to the SiC bulk obtained from the specimen implanted at 800 °C are shown in Fig.2. The obtained ratio curve resembles the annihilation at the interface layer of the SiO_2/SiC interface

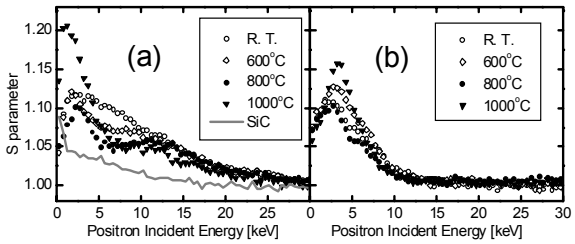

Fig.1. S parameters for the bulk SiC and oxygen-implanted SiC of (a) as-implanted state and (b) after annealing at 1400 °C. S parameters are normalized to these for bulk SiC.

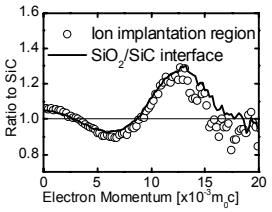

Fig.2. Ratio curve of E=7keV to the bulk SiC obtained from the specimen implanted at 800°C after annealing at 1400 °C.

produced by conventional oxidation as shown on solid line in Fig.2 [2]. That is, the oxygen implanted layer contains vacancy defects with oxygen dangling bonds. In the top-SiC layer, S parameters are still high even if the thermal annealing was performed. This indicates that microvoids were formed.

In summary, defects in SiC-OI structure formed by oxygen implantation were probed by positron annihilation spectroscopy. The defective SiO_2 layer seems to be formed in the oxygen-implanted region. Radiation defects are hardly removed even if higher implantation temperatures were applied. In the top-SiC layer, larger vacancy clusters are created. From this study, it is suggested that more advanced techniques should be developed in order to obtain a defect-free SiC-OI structure by ion implantation method.

References

1) N. P. Barradas, C. Jeynes and S. M. Jackson, Nucl. Instrum. Meth. B136-138, 1168 (1998).
2) M. Maekawa, A. Kawasuso, M. Yoshikawa, A. Miyashita, R. Suzuki and T. Ohdaira, Phys. Rev. B73, 014111 (2006)
3) M. Maekawa, A. Kawasuso, M. Yoshikawa, A. Miyashita, R. Suzuki and T. Ohdaira, Physica B: Condensed Matter, **376-377**, 354-357 (2006).

4-35 Development of 2-Dimentional Nuclear Reaction Micro-analysis Technique of Boron-doped Materials

H. Shibata [a)], Y. Kohno [b)], T. Satoh [c)], M. Oikawa [c)], J. Haga [c)] and T. Sakai [d)]

[a)]Graduate School of Engineering, Kyoto University, [b)]Department of Materials Science and Engineering, Muroran Institute of Technology, [c)]Department of Advanced Radiation Technology, TARRI, JAEA, [d)]Policy Planning and Administration, JAEA

The microanalysis of trace amount of boron has been carried out using 1 μm proton microbeam from 3MV single ended electrostatic accelerator of TIARA facility. Steel specimens containing 20-100 ppm boron have been bombarded by 1.7 MeV proton beam for gamma ray detection and 1.32MeV H_2^+ beam for alpha particles. In 2006 the maps of boron distribution have been measured by detecting 3.7 MeV alpha particles from the ^{11}B (p, α) ^{8}Be nuclear reaction mainly. As a result of imaging, segregation of several microns sized boron precipitates, which has been already observed by detecting gamma ray, could be clearly seen in this method.

鉄鋼材料に微量のホウ素を添加することにより強度特性を良くすることは経験的に知られているが、鉄鋼中でのホウ素の振舞いについては殆ど解明されていない。これは鉄鋼中に限らず、ホウ素の局所的かつ定量的な元素分析が、SIMS、EDXA、EELS などの分析方法を用いても、難しいことによる。

ホウ素の局所的（三次元的）な定量元素分析ができるようになれば、ホウ素添加鉄鋼材料の強度特性とホウ素の分布の関係を明らかにすることができ、ホウ素分布を最適化するような熱処理法等の開発を可能にする。これは、ホウ素の効率的な処理によって、クロム、モリブデンなどの鋼中合金元素を必要とすることなく所要強度の実現を可能にするものであり、生産コストの低減化、省資源化、そして環境に優しいリサイクルマテリアルを可能とする。

材料中に含まれる微量のホウ素の分布を空間的、定量的に精度良く調べるために、陽子マイクロビームとホウ素との核反応を利用した分析法を採用し、新たな分析手法の確立を目指すのが本研究テーマの目的である。

2006 年度は TIARA の大気マイクロ PIXE のポートを用いて、陽子とホウ素の核反応で放出されるα粒子の二次元分布測定を試みたので報告する。

ホウ素の定量的な分布を求めるために、2004 年度より ^{10}B(p, α ' γ)^{7}Be の核反応によって放出されるγ線を、半導体検出器を用いて測定を行ってきた。さらに 2005 年度には新たに製作したアニューラ型半導体検出器（Raytech 社製）を用いたα線検出を試みた。図 1 に測定の概念図を示す。検出器にはビーム貫通穴が空いており、真空チャンバー内（約 1x10^{-3} Pa）に置かれている。試料はγ線検出の場合と同じチャンバーのサンプルホルダー窓に取り付けられていて、γ線とは反対のビームが照射される側で計測する。^{11}B (p, α) ^{8}Be の核反応で放出される 3.7 MeV のα粒子を測定することでγ線と同じようにホウ素の分布を測定できる。この核反応は約 800 keV にピークを持つ半値幅約 400 keV の幅広い共鳴反応である。そのため、用いたビームは 1.6 MeV の水素分子ビームで、固体内に進入した直後には 0.8 MeV のエネルギーを持つ 2 個の陽子になることを利用した。Raytech 社製の検出器が不調であったので、2006 年度は Canberra 社製のアニューラ型半導体検出器（ANFD 300-20-300RM）を用い、二次元検出に成功した。

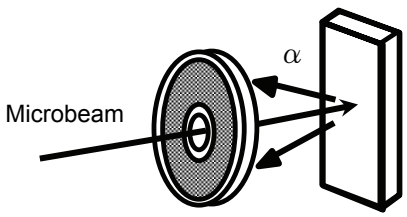

Fig.1. Schematic view of experimental setup for α-particle measurements.

試料として34 ppmのホウ素を含んだ鉄の板（10x10x1 mm）を用いた。ホウ素を含む試料はその量とその他の含有物によっていくつかの種類に分けられるが、今回準備された試料では、Bの他、C, Si, Mn, P, S, N, Cr, Vを含む。2005年度までのγ線検出の実験で、鉄鋼中にあるホウ素は直径10ミクロン位の粒状になって分布しているのが観察されている。

2006年度では^{11}B (p, α) ^{8}Beの核反応によって放出されるα粒子ついて測定し、図２のようにγ線と同様な分布を得ることができた。この試料には添加物として微量のクロムやバナジウムが添加してあり、これらの添加物がホウ素の凝集に関係していることが考えられる。また鉄鋼中にあるホウ素は粒界に凝集しているといわれており、一様に分布するホウ素よりはるかに密度が高いと思われるので 20 ppmでもγ線測定が可能だと考えられる。残念ながらこの測定では鉄の粒界の状況がわかからないので、ホウ素が鉄鋼中にどのように分布しているかはわからない。また定量性についても、まだγ線やα粒子の収量に対する較正がなされていないのでこれからの課題であるが、BN試料の収量と比較することで定量性を出すことを考えている。

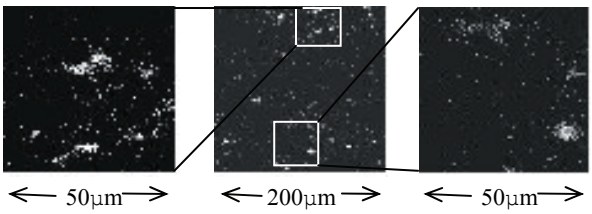

Fig.2. A typical α -particle image of 34 ppm boron contained in a steel specimen bombarded by 1.32 MeV molecular hydrogen microbeam.

4-36 Three-dimensional Measurement of Density in Minute Biological Samples by STIM

T. Satoh, M. Oikawa, J. Haga, T. Kamiya and K. Arakawa

Department of Advanced Radiation Technology, TARRI, JAEA

When samples which have thickness variation and internal constitution are analyzed with an in-air micro-PIXE system[1], X-ray yields have to be corrected using X-ray production cross sections and linear attenuation coefficients. For that purpose in the case of biological samples, it is necessary to measure the three-dimensional distribution of carbon, hydrogen, and oxygen, which are the matrix of cells. Because it is difficult to measure them with spatial resolution of a few microns by micro-PIXE analysis by itself, we used Scanning Transmission Ion Microscopy (STIM)[2], which can measure it easily using a particle detector located just behind the sample in the atmosphere.

In our previous study[3], the elemental map by micro-PIXE for a spherical sample could be corrected by STIM under the assumption the ratio of major elements in the sample was constant. Thus X-ray yields from symmetric and uniform samples can be fully corrected by STIM only. But if there are projection maps by STIM in all directions, the tomograms can be acquired in the same way as CT scan. This method is called STIM-CT[4]. We attempted in-air STIM-CT of plant cells to get three-dimensional shape, and the good tomogram of the sample was acquired in 2005[5]. In 2006, we could get the tomogram of an insect's head. Since it has generally hollow shape, it is necessary to measure the internal structure using STIM-CT.

In this series of study, the 3MV single-ended accelerator and the micro-PIXE system at the TIARA were used. The 3 MeV proton microbeams were scanned over a target. The diameter of the microbeam was about 1 μm. Polycarbonate foil 5 μm thick was used as a beam extraction window. A target was glued on the needle just behind the extraction window, and was rotated by 180° at intervals of 15°. A surface barrier detector was placed behind the target.

Figure 1 is a photograph of the test sample. It was a head of a tiny insect. Figure 2 shows the projected image of the sample and Figure 3 is the tomogram reconstructed using the back projection method with the Shepp&Logan filter. Using all tomograms such as Fig. 3, three-dimensional reconstruction of the sample could be realized as in Fig. 4.

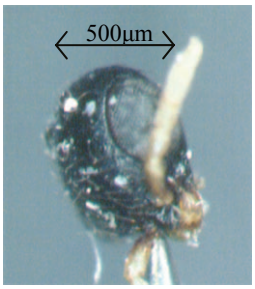

Fig 1. Optical microscope image of an insect's head, which glued on a metal needle.

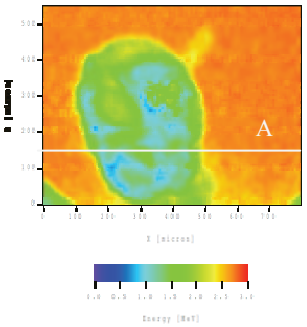

Fig 2. Projected image of the insect's head obtained using STIM.

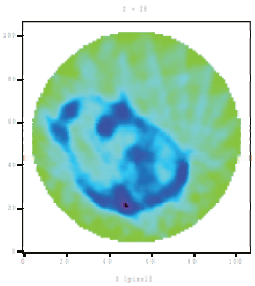

Fig 3. Tomogram at line A in Fig. 2.

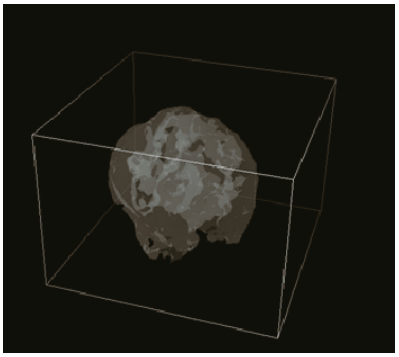

Fig 4. Three-dimensional image of an insect's head. This image was reconstructed from tomograms such as Fig. 3.

References

1) T. Sakai et al., Int. J. PIXE Vol. 10 Nos. 3 & 4 (2000) 91.
2) J. C. Overley et al., Nucl. Instr. Meth. B 30 (1988) 337.
3) T. Satoh et al., Nucl. Instr. Meth. B 249 (2006) 234.
4) C. Michelet et al., Nucl. Instr. Meth. B 150 (1999) 173.
5) T. Satoh et al., JAERI-Review 2006-042 (2007) 167.

4-37 In-air Micro-PIXE Analysis of Asbestos in Asbestos Exposed Lung

Y. Shimizu [a)], K. Dobashi [a)], T. Kusakabe [a)], T. Nagamine [a)], M. Oikawa [b)], T. Satoh [b)], J. Haga [b)], T. Ookubo [b)], Y. Ishii [b)], T. Kamiya [b)], K. Arakawa [b)] and M. Mori [a)]

[a)]The 21st Century Program, Graduate School of Medicine, Gunma University
[b)]Department of Advanced Radiation Technology, TARRI, JAEA

Asbestos were causative agents of pulmonary fibrosis and cancer. To identify inhaled asbestos in lung, lung tissues from asbestos exposed patients were analysed by in-air micro-PIXE (Particle Induced X-ray Emission). The localization of asbestos body composed by silica, iron, and magnesium were identified in the lung, and other metals of titanium and aluminium were also observed. In-air micro-PIXE was considered as useful to identify asbestos in lung tissue.

アスベストとは、天然の鉱物繊維で長さは約8 μm, 幅約0.1 μm、断熱性、耐火性、防音性、耐腐食性に優れており、建築用製材として多く用いられてきた。クリソタイル（白石綿）、クロシドライト（青石綿）、アモサイト（茶石綿）などがある。アスベスト吸入は肺に炎症を惹起し、肺線維症や肺癌発症と関係があるといわれている。このアスベストの肺内における局在とアスベスト組成を大気中マイクロPIXE（Particle Induced X-ray Emission）分析を用いて解析することを試みた。

対象患者：Asbetos group：Asbestos吸入歴があり、肺癌を合併した患者肺の癌以外の部分とControl group：Asbestos吸入歴がない肺癌を合併した患者肺の癌以外の部分の肺組織の凍結切片を作成し、それを表面にPIXE用の高分子フィルムを張ったスライドグラス上に載せて乾燥させた。肺組織を含むフィルム膜とともに肺切片を切り出しサンプルフォルダに固定し、3 MeVのプロトンビームを照射して、大気中マイクロPIXE分析を行った。[1)]

結果：Si, Mg, Feおよびそれらが混ざったアスベストを検出できた。得られたマイクロPIXE画像をFig. 1に示す。正常肺では組織中少量のSiを測定できたが、Mgや、Feはほとんど検出されなかった。一方、アスベスト肺組織中からは、無数のSiが検出されると同時に、その部位にMgやFeも一緒に検出され、無数のアスベストが肺に沈着している様子が明らかとなった。さらに、今回検出されたアスベストは、Chrysotile （白石綿, $Mg_3Si_2O_5(OH)_4$：わずかに鉄を含む）もしくはAmosite（茶石綿，$(Mg, Fe)_7Si_8O_{22}(OH)_2$）が考えられ、Crocidolite（青石綿, $Na_2(Fe^{2+}{}_3Fe^{3+}{}_2)Si_8O_{22}(OH)_2$）では無かった。また、アスベスト小体は組織間隙に刺さったようになっている様子が2次元的に観察できた。以上のように、大気マイクロPIXEによる観察で、アスベストの種類や、組織内での存在部位が、明らかになった。

【考察】アスベスト暴露歴のない肺では、わずかなSiしか見られないが、アスベスト肺では、Siが、密度濃く、広範囲に一様に分布している像が見られ、明らかに多量のSiを吸入していることがわかる。さらに、アスベスト暴露歴のない肺のSiは、その部位にほとんど金属を含まないが、アスベスト肺のSiの部位には、Mgなどの金属が同時に存在しており、その違いは明らかであった。この成分の違いが、アスベスト患者の癌発症率の高さに関与するか今後の検討課題である。

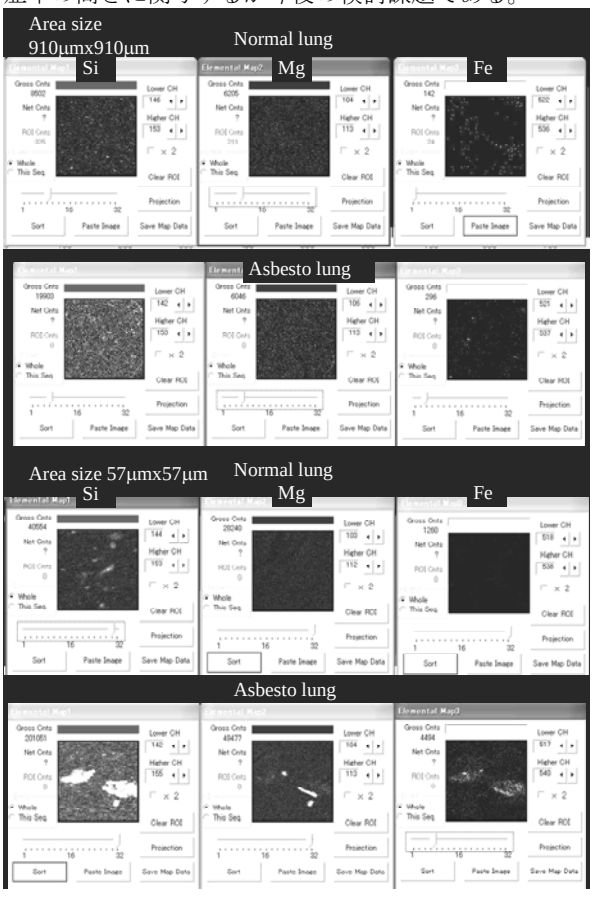

Fig. 1. Micro-PIXE images of elemental distributions of Mg, Si and Fe in normal lungs and asbestos lungs.

References

1) T. Kusakabe, K. Nakajima, K. Suzuki , K. Nakazato, H. Takada, T. Satoh, M. Oikawa, K. Kobayashi, H. Koyama, K. Arakawa, T. Nagamine, The changes of heavy metal and metallothionein distribution in testis induced by cadmium exposure. Biometals, 2007 Apr 19; [Epub ahead of print].

4-38 The Present Situation and Problems of the Analysis of Boron Micro-distribution in Tumor Cells Using Micro-PIXE and PIGE

K. Endo [a)], Y. Shibata [a)], T. Yamamoto [a)], K. Nakai [a)], A. Matsumura [a)], T. Sato [b)], M. Oikawa [b)], K. Arakawa [b)], T. Kamiya [b)] and K. Ishii [c)]

[a)]Department of Neurosurgery, Institute of Clinical Medicine, University of Tsukuba
[b)]Department of Advanced Radiation Technology, TARRI, JAEA
[c)]School of Engineering, Tohoku University

We have applied micro particle induced X-ray emission (micro-PIXE) to determine inter- and intracellular distribution of boron (^{10}B). Because the energy of micro-PIXE from ^{10}B is too low, we employed a method to detect gamma-ray produced from the nuclear reaction of ^{10}B(p, α γ)^{7}Be, namely particle induced gamma-ray emission (PIGE). We showed the results of inter and intracellular distribution of boron elements in tumor tissue using micro-PIGE. However, we analyzed many background too and still can not detect the true boron elements. So further investigation is necessary to obtain higher spatial resolution and the optimization of the measurement time or the improvement of the sampling methods should be investigated. In future, this method will be applied to analyze the intracellular micro-distribution of the capture element and development of new drugs for NCT.

悪性脳腫瘍に対する放射線治療法の一つとして硼素中性子捕捉療法(BNCT)の臨床研究が進められているが、その効果は硼素元素の細胞内分布状態に大きく影響を受けると考えられている。これまでにも硼素元素の腫瘍内での分布やその動態の研究が報告されてきたが、画像的に明らかにしたものはなかった[1,2)]。

本研究の目的は腫瘍細胞内での硼素元素の分布状態を測定・画像化することである。そのためTIARAのSingle-ended acceleratorを用い、特にγ線の測定によるparticle induced γ-ray emission (PIGE)法を用いることでまず硼素10(^{10}B)の画像化に成功した。今回はその後の現状と課題について報告する。

はじめにIn vivo実験として脳腫瘍にBSHが集積していることを確認、細胞レベルでの分布状態を明らかにするために、まずラット脳に９L腫瘍細胞を移植しこれを２週間生育した。２週間後にBSHを静脈投与し、その数時間後にこれを安楽死させ脳腫瘍及び正常脳組織を採取した。これを厚さ20μmに切載しマイラー膜上に固定。正常脳、脳腫瘍組織・細胞における硼素元素の分布状態を比較した。

図1左は正常脳組織の厚さ20μm切片をマイラー膜上に固定し、燐(P)や硫黄(S)の分布を指標に測定画像化したもの、また右は硼素元素(^{10}B)チャンネルにおける測定分布図である。しかし硼素元素は測定スペクトル上ピークとして認められず周辺バックグランドと同等レベルであり、これらのドットはほとんどがバックグランドと考えられた。また図2左は脳腫瘍組織の厚さ20μm切片を同様にPやSの分布を基に画像化したもの、また右は硼素元素分布図である。脳腫瘍組織では測定スペクトル上硼素元素チャンネルにおいてピークを形成し、脳腫瘍組織からは硼素元素が測定された。これは脳腫瘍組織にはBSHが集積していることを示している。

しかしながら本来の目的である細胞レベルでの硼素元素分布の明確な画像化は困難であった。それは脳腫瘍を採取する際にある程度の組織破壊を伴っている可能性があること、また摘出した脳腫瘍を急速凍結する際に組織内での凍結速度にギャップが生じることが予想され、これに伴う細胞内・細胞間での元素の移動の可能性が考えられること、さらにこれを10～20μmの厚さに薄切するのは困難であり、その際に腫瘍組織・細胞の破壊を伴っている可能性が考えられる、などのためである。そのため図1，2とも細胞分布は不明瞭な形態を呈しており、固定過程で生じたと思われる亀裂らしい跡も認められている。当然細胞内容の移動、偏移も生じているものと想像され、図2の如く硼素元素は測定されたものの、バックグランドの問題とともに細胞レベルでの分布状態は不明瞭な結果であった。

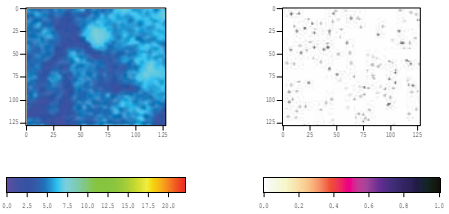

Fig.1 Distribution of normal cells(P) and ^{10}B

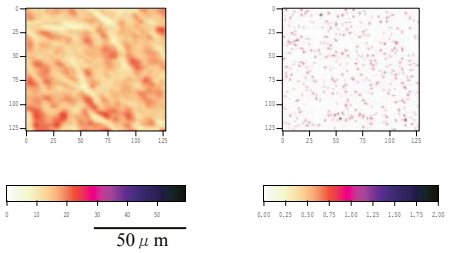

Fig.2 Distribution of tumor cells(P) and ^{10}B

これらの問題点を改善するために、ある程度の大きさ、体積のある試料の急速凍結方法、また組織・細胞破壊をできるだけ伴わない薄切方法及びその固定方法などの新たな開発・検討が今後必要と考えている。

References

1) Coderre JA, et al., Radiat Res 149 (1998) 163-170.
2) Wegden M, et al., Nucl Instr and Meth in Phys Res B 219-220 (2004) 67-71.

4-39 Standard Reference Material for Determination of Trace Elements in Biological Materials by Micro Beam PIXE

Y. Iwata [a)], T. Konno [a)], K. Ishii [b)], M. Fukuda [c)], T. Kamiya [c)], T. Satoh [c)] and M. Oikawa [c)]

[a)]Department of Chemistry, Faculty of Education and Human Studies, Akita University,
[b)]Department of Quantum Science and Engineering, Graduate School of Engineering, Tohoku University, [c)]Department of Advanced Radiation Technology, TARRI, JAEA

Standard Reference Material (SRM) is indispensable to the calibration of apparatus and the evaluation of the accuracy and precision of analytical technique. Previous work, we showed utilities of several macro porous anion and cation-exchange resins for micro PIXE analysis. In this work, we made SRM containing the known amount of Ca^{2+} and trace amount of essential elements for living matter, such as Fe^{3+}, Ni^{2+} and Zn^{2+} in cation-exchange resin. Macro porous anion-exchange resin, Macro-Prep 25S (BioRad) was suspended in 0.01 M HNO_3 and added the known amount of standard solutions. The concentration of trace elements in the resin was 20-60 ppmv. Individual particle of the resin was subjected to 3 MeV proton bombardments by micro beam system of TIARA. It was found the macro porous nature of the resin (pore size; 72.5nm) allows cation to access the exchange sites located throughout the matrix. This SRM is similar to biological cell because it is spherical in shape and its matrix elements are carbon, oxygen and hydrogen. This SRM made of macro porous resin has a possibility for use as SRM for determination of trace elements in biological samples by micro beam PIXE.

PIXE分析を含め、ほとんどの機器分析において、装置の校正や分析結果の相互比較のために標準物質(SRM)は、不可欠である。 これまで、粒径が25から100 μmで球状の陽イオン交換樹脂に、微量元素を付着させたSRMを作成し、TIARAマイクロPIXEシステムで、生体試料分析に対する有効性を報告してきた。この検討では、TIARAにおける Cu、Zn等の生体必須元素の画像化の下限値（5 ppm程度）を求めた[1)]。また粒径25ミクロンの多孔質の構造を持つマクロポーラス型陽イオンおよび陰イオン交換樹脂に、微量の金属陽イオンを球体全体に均一に付着させた粒子状試料の作成に成功し、分析感度、分解能、照射安定性において優れたSRMになりえることを示した[2)]。

本研究では、生体中の微量元素として、Fe、Ni、Cuを選び、これらを同時にマクロポーラス型陽イオン交換樹脂に添加した。元素添加量と特性X線強度について検討し、生体中の微量元素分析用標準物質としての有用性を報告する。

実験　樹脂への金属イオンの吸着　純水中で懸濁させたマクロポーラス型陽イオン交換樹脂Macro Prep 25S（スルホン基型 粒径25 μm、BIORAD）を、メスピペットで吸い上げ、樹脂の体積を測定した。樹脂を含む懸濁液に、Ca^{2+}、Fe^{3+}、Ni^{2+}およびCu^{2+}を含む標準溶液を加え、振とうした。樹脂体積あたりの含有量は、Ca^{2+}は400 ppmvの一定量とし、Fe^{3+}、Ni^{2+}およびCu^{2+}は、0、20、40、および60 ppmvとした。

マイクロPIXE分析　ターゲットホルダー上に、樹脂の懸濁液を付着させ、こよりで水分を吸い取った。顕微鏡下で、樹脂が重なり合わないように、樹脂をばらまいた。マイクロPIXEシステムにより3MeV pビームをサブミクロンに絞った。スキャンエリアを30 x 30 μmとし、大気中200-300 nCの照射を行った。

結果と考察　標準物質の調製　一定体積の樹脂と目的元素の標準溶液を混合するだけで、簡便に調製することができた。Fe^{3+}イオンの加水分解を防ぐために0.1M硝酸酸性下で振とうした。この陽イオン交換樹脂の吸着反応は、分配現象としてよく研究されており、大部分の+2、+3の陽イオンに適用が可能である。

標準物質のマイクロPIXE像　一粒のマクロポーラス型イオン交換樹脂について、添加した微量元素（Ca, Fe, Ni, Cu）ならびにイオン交換基に含まれるSの画像化に成功した。SとCaの分布は、樹脂が球体とした場合とよく一致しており、樹脂内にイオン交換基が均一に分布し、その交換基と金属イオンが反応することが確かめられた。生体中で微量であるFe, NiおよびCuについては、その添加量を20から60 ppmvと変化させたが、いずれの場合も樹脂内の元素分布を画像化できた。

微量元素の定量感度　標準物質の使用目的で最重要課題は、機器の校正、すなわち分析感度の定量化である。樹脂に一定量添加したCaからの特性X強度に対するFe, Ni, Cuの強度をプロットした(Fig１)。Fe, Ni, Cuの添加濃度に対して原点を通る直線となり、定量性も優れていることが確かめられた。以上の検討から、生体試料の画像化の精緻化における微量元素分布の定量化への有効であることが確かめられた。

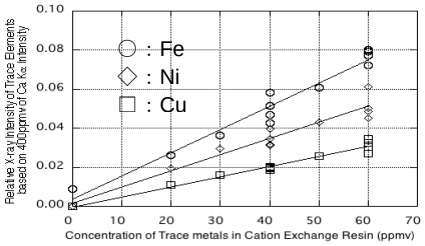

Fig.1 Relationship of Concentration Trace Elements and Relative X-ray Intensity of based on Ca Kα

References

1) Y. Iwata et al., TIARA annual report 2004 (2005) 320.
2) Y. Iwata et al., JAEA Review 2006-042 (2007) 171.

4-40 Measurement of BrdU in Mouse Brain by In-air Micro PIXE Analysis

E. Sakurai [a)], K. Yanai [a)],K. Ishii [b)], R.Oyama [b)], M. Sakamaki [b)], H.Hiromichi [b)], S.Matsuyama [b)],T. Kamiya [c)], T. Satoh [c)], J. Haga [c)], M. Oikawa [c)] and K. Arakawa [c)]

[a)]Department of Pharmacology, Tohoku University School of Medicine,
[b)]Department of Quantum Science and Energy Engineering, Tohoku University,
[c)] Department of Advanced Radiation Technology, TARRI, JAEA

1. Introduction

There are many reports that trace elements might be related to cerebral nerve diseases, such as Alzheimer's disease[1)]. To examine changes of spatial distributions of trace metal elements in cells, organs or tissues using various kinds of disease model, it is useful to establish a new pharmaco-therapeutics.

In this study, we developed a method to analyze elements in brain slices using histamine receptor gene knockout mice on the basis of Micro-PIXE analysis.

2. Experimental method

1) Target preparation of brain samples for PIXE analysis

We examined 4 target preparations: ① brains were removed and stored at –80 ℃, ② brains were removed and immediately quick-frozen in 2-methylbutane cooled in liquid nitrogen, ③ brains were removed and treated with sucrose solution and stored at –80 ℃, ④ brains were removed and immediately quick-frozen in dry ice to –40 ℃.

The target preparation of ④ was most suitable for this study. Trace metal elements were difficultly detected in the frozen conditions of ① and ③. In the condition of ②, the brains were delicate and it was difficult to make their slices.

2) Histamine receptor gene knock out mice and their neurogeneses

Histamine H1 receptor gene knock out mice (H1-KO) and their wild type mice were bred in our laboratory. 5-bromo-2'-deoxyuridine (BrdU) of 75 mg/kg were injected into mice 4 times at 2-hour intervals. Each brain was cryosectioned sagittally at 16μm thickness. The brain slices were mounted on polycarbonate films, which were processed with 5N sulfuric acid. The brain slices were examined by the micro-PIXE analysis with 3 MeV-proton micro-beams of beam currents of ~ 120 pA.

3. Results and discussion

H1 receptor antagonists are widely used to such as a medicine for a cold or to relieve itching. However it is well known that sedative antihistamines induce cognitive decline in human through blockage of H1 receptor. H1KO mice showed impaired leaning and memory than their wild type (C57BL/6) mice. It was recently reported that newborn cells within 24 hours in the hippocampus are related to the cognition. BrdU labeling hippocampal neurogeneses were observed in the brain slices of H1KO and their wild type mice by the use of micro-PIXE analysis. Figures 1 and 2 show the beam irradiation image of a brain slice and the distribution image of bromine in the region of 100 × 100μm ^{2} in the brain slice of Fig 1.

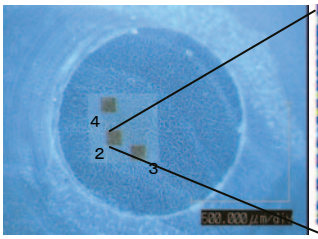

Fig. 1 Beam irradiation image of brain slice of wild type mouse.

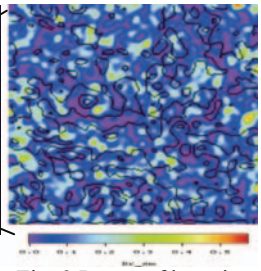

Fig. 2 Image of bromine (100 × 100μm ^{2})

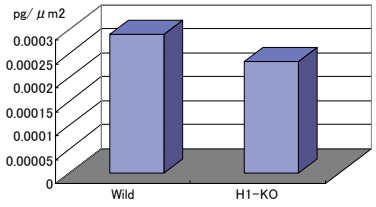

Fig. 3 Amount of bromine in 1μm ^{2} of brain slices

The amounts of bromine in the slices of wild type mice and H1KO mice are shown respectively in Fig. 3.
The amount of Bromine in the case of H1KO mice is small compared with that of wild type mice. This result is accord with the results of other physiological studies using H1-KO and their wild type mice[2)].

Here, we presented the difference of accumulation of BrdU in the brain of H1-knock out mouse from that of its wild type mouse by the use of micro-PIXE which can be used to clarify the roles of trace elements in psychotic diseases such as depression, schizophrenia and Alzheimer's disease.

4. References

1) Okamura N *et al.* Br. J. Pharmacol., 129, 2000.
2) Dai H *et al*. Neurosci. Res., 57, 2007.

4-41 Monte-Carlo Particle Trajectory Simulation Study on Classification of Structure of 3-MeV C_3 Cluster Ion

M. Adachi [a)], Y. Saitoh [a)], A. Chiba [a)], K. Narumi [b)], K. Yamada [a)] and T. Kaneko [c)]

[a)]Department of Advanced Radiation Technology, TARRI, JAEA, [b)]Advanced Research Center, JAEA,[c)]Department of Applied Physics, Okayama University of Science.

We have studied interaction of swift cluster ion beam with matter. The interaction is well described by the nuclear collision of projectiles and target atoms with the many body effect, as far as the projectile speed is lower than the Bohr speed $v_B \cong 2.19 \times 10^6$ m/s. When the speed exceeds v_B, the interaction of the swift cluster ion is caused mainly by the electronic collision, and the interaction mechanism has not yet been revealed. The interaction caused through the electronic collision involving a many body effect of projectile itself suggests us necessity for revealing the relation between a projectile charge state and time interval of irradiation between each constituent ion or a cluster spatial structure. We have therefore developed a measurement system[1)], which realizes simultaneous observation of charge states and a planar pattern of cluster constituent ions.

The Coulomb explosion imaging technique is utilized in order to expand the space size of the 3-MeV C_3^+ ion from angstrom- to millimeter-size in our system, which is consisted of the thin carbon foil and a screen of a luminous type of multi-channel plate. It was required to evaluate a mixing degree of cluster structures of triangular one and linear one by the scattering effects inside the foil, in order to estimate the structure. We developed, for performing that evaluation, a Monte-Carlo particle trajectory simulation code. Initial positions of each constituent ion are assumed to follow a lateral straggling distribution, by the scattering effects inside the foil, with two dimensional Gaussian distribution with 0.4 angstrom in half width at half maximum on the rear-surface of the foil. The lateral straggling distribution is experimentally measured using 1-MeV C^+ ion beam for the foil. In case of a C_3 cluster, centre points of distributions compose a straight line or an equilateral triangle with the same atomic separation distances of 1.2 angstrom. It is also assumed that the cluster plane of triangular cluster and the chain of linear one are perpendicular to the incident direction of the cluster.

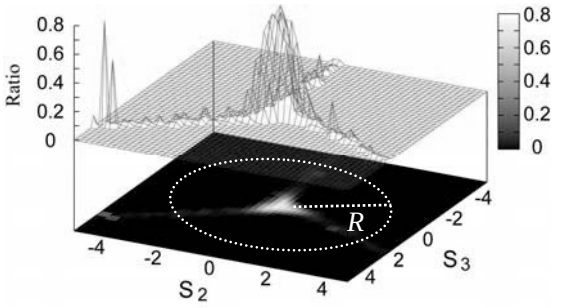

Fig.1. A distribution of the ratio of triangular structure to all data points is plotted in S_2-S_3 plane.
The distribution is constructed form all calculated data points for all charge state combination, +1 ~ +4, with a charge fraction measured in our experiment.

Figure 1 shows distribution of the ratio of triangular ions toward the sum of both ions on a screen, 190 mm away from the foil, with a reduced relative length S_2 and S_3: ,

$$(S_2, S_3) = \begin{cases} \left(\frac{1}{\sqrt{2}}\left(\frac{d_1}{d_2} - \frac{d_2}{d_3}\right),\ \frac{1}{\sqrt{6}}\left(2\frac{d_3}{d_1} - \frac{d_2}{d_3} - \frac{d_1}{d_2}\right)\right) \\ \left(\frac{1}{\sqrt{2}}\left(\frac{d_3}{d_1} - \frac{d_1}{d_2}\right),\ \frac{1}{\sqrt{6}}\left(2\frac{d_2}{d_3} - \frac{d_1}{d_2} - \frac{d_3}{d_1}\right)\right) \\ \left(\frac{1}{\sqrt{2}}\left(\frac{d_2}{d_3} - \frac{d_3}{d_1}\right),\ \frac{1}{\sqrt{6}}\left(2\frac{d_1}{d_2} - \frac{d_3}{d_1} - \frac{d_2}{d_3}\right)\right) \end{cases}$$

where d_i is a respective distance from a barycentre of three constituent ions to i-th constituent ion positions. This reduction enables us to classify structure in a unite plane for all charge state combinations. Value zero in the distribution indicates that there is no data point for the triangular structure in that region. Unity indicates only triangular ions exist, and smaller value corresponds to a larger fraction of linear ions. We, from the calculation, obtained the tendency that the triangular ions are concentrated into a centre position on this plane, and the linear ions are dispersed toward three edge regions, even if different charge states contains in a combination. This characteristic enables us to classify each structure inside or outside of the circular regions with radii R.

The dependence of the accuracy on the radii was also calculated and applied for the decision of the radii. We, finally, evaluate the accuracy of our measurement as 70 % and 90 %, for triangular and linear structures respectively, when R_{in} = 0.67 and R_{out} = 1.75 for triangular and linear structures, respectively.

In conclusion, we developed the evaluation method for our charge state and cluster structure measurement system, based on the Monte-Carlo particle trajectory simulation. The calculation results also provide us a criterion for the structure classification, R, with accuracy. The relation between the charge state and the structure, classified using these radii, qualitatively agrees with the one theoretically predicted by Kaneko[2)].

References

1) A. Chiba, Y. Saitoh and S. Tajima, Nucl. Instrum. Meth. B **232** (2005) 32.
2) T. Kaneko, Phys. Rev. A, **66** (2002) 052901.

4-42 Study of Secondary Ion Emission from HOPG Target Bombarded by Fast Cluster Ion Beams

H. Shibata [a)], H. Tsuchida [a)], A. Itoh [a)], Y. Saitoh [b)], A. Chiba [b)], M. Adachi [b)], T. Kamiya [b)], W. Yokota [b)] and K. Narumi [c)]

[a)]Graduate School of Engineering, Kyoto University, [b)]Department of Advanced Radiation Technology, TARRI, JAEA, [c)]Advanced Science Research Center, JAEA

Recently the interaction of fast (MeV) cluster ions with solids has attracted attention in basic physics and application fields. Fast cluster ion bombardment causes nonlinear effect or synergetic effect, which is unusual for single atom collision with solid targets. A time of flight (TOF) mass spectrometer combined with pulsed fast cluster ion beams which were produced by the TIARA tandem accelerator was used for a secondary ion measurement. In this report we present some results of positive and negative secondary ion measurement from a highly oriented pyrolytic graphite (HOPG) target bombarded with carbon, aluminum and gold cluster ions.

高速（高エネルギー）クラスターイオンと物質との相互作用では単原子イオンの数の集合体として線形的に振る舞うのではなく、個数以上、あるいは個数以下の非線形的な効果を与える。二次荷電粒子放出の収量や二次イオン放出スペクトルの測定を通して、高速クラスターイオン照射の特徴を調べることが本研究の目的である。H18 年度は直線飛行時間型(TOF)質量分析器を用いて炭素、アルミニウム及び金クラスターイオンと HOPG (Highly Oriented Pyrolytic Graphite: 高配向性熱分解炭素) 標的との衝突で放出される正負の二次イオン測定を行ったので報告する。

本実験に用いたクラスターイオンはエネルギー0.5 MeV/atom（ー42 keV/u）のC_1^+ーC_8^+イオン、0.675 MeV/atom（ー25 keV/u）のAl_1^+ーAl_4^+イオン及び 1.67 MeV/atom（ー8.5 keV/u）のAu^+ーAu_3^+イオンである。同種のクラスターイオンで核子当たりのエネルギーを広範囲に変えることができることが望ましいのであるが、加速器の制約上不可能なので、加速可能な粒子を変えることで核子当たりのエネルギーを変更し比較した。

標的試料にはHOPGを用いた。HOPG試料は層状に剥がすことができ新しい表面を測定に使えるので他の試料に比べて不純物の吸着が少ないと考えられる。それでも相当不純物（例えば、水、ナトリウムなど）が観測されるので、ECRイオン源からのArビーム照射により表面のクリーニングを行ったTOFスペクトルの計測はイオンビームをパルス化し、TAC（時間波高変換）を用いる方法により行われた[1)]。核子当たりのエネルギーはBohr速度（ー25 ｋeV/u）とその前後を選び、放出正負二次イオンの全収量（水素を除く）の入射クラスターサイズに対する依存性を比較した。AlやAuクラスターイオン照射に対して放出二次イオン質量スペクトルはそれほど変わらず、あまり大きなサイズの放出クラスターイオンは観測されていない。一方、Cクラスターの場合では、大きなサイズのクラスターが正、負二次イオン共に観測されており、炭素-炭素衝突における特異性が考えられる。 図１はC（左図）、Al（中央）及びAuクラスターイオン（右図）をHOPGに照射した際に放出された二次イオンで水素を除いた正負イオンの全収量のC_1^+、Al_1^+　及びAu_1^+イオン照射における正イオン全収量に対する比をプロットしたものである（C_1^+、Al_1^+及びAu_1^+照射における正イオン放出の全収量をそれぞれ１とした）。図中のLinear relationは収量がクラスターの個数に比例している場合である。

図からわかるように三者の入射粒子について比較してみると、Au の場合、正負イオンの収量はクラスターサイズに余り依存せずほぼ一定で、負の非線形性を示している。一方、C 及び Al の場合はクラスターサイズに対し、ほぼ指数的に増加し、正の非線形性を示している。すべての入射クラスターについて、負イオンの収量は正イオンの数倍から数 10 倍になっていて、この傾向はエネルギーに関わらず同様である。この理由は未だ明らかではない。

二次イオン放出現象においては、イオンの速度がBohr速度以下の低速領域では、核的衝突が支配的でクラスターイオンでは負の非線形性が、またBohr 速度以上の高速領域では電子的衝突が支配的で正の非線形性が表れることが理論的に知られており[2)]、今回の実験では定性的には理論と同じ結果になっている。

References

1) Shibata et al., TIARA Annual Report 2005 (2007) 177.
2) P.Sigmund et al., Nucl. Instrum. Meth. **B112** (1996) 1.

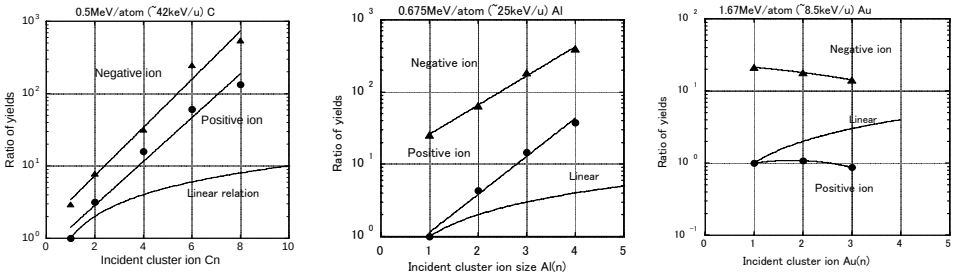

Fig.1. The ratio of yields of positive (●) and negative secondary ions (▲) emitted from HOPG target bombarded with carbon (left hand side), aluminum (middle) and gold (right hand side) incident ions. The yield of positive secondary ions bombarded by with C_1^+, Al_1^+ or Au_1^+ ion is unity.

4-43 Secondary Ion Emission from Polycarbonate upon Cluster Ion Impacts

K. Hirata [a)], Y. Saitoh [b)], A. Chiba [b)], M. Adachi [b)], K. Narumi [c)] and W. Yokota [b)]

[a)]National Institute of Advanced Industrial Science and Technology (AIST), [b)]Department of Advanced Radiation Technology, TARRI, JAEA, [c)]Advanced Science Research Center, JAEA

Secondary ions are ejected from the surface when the primary ions bombard the target. Cluster ion bombardments give different secondary ion emission yields from those for monoatomic ions because of their peculiar irradiation effect. We have developed a time-of-flight (TOF) secondary ion mass spectroscopy using cluster ion impacts, and applied it to various samples[1-3]. In this paper, we report secondary ion emission from polycarbonate (PC) upon cluster ion impacts.

Positive secondary ion (P-SI) TOF measurements for amorphous PC films with a thickness of 100 μm were performed with a linear type TOF mass analyzer using pulsed monoatomic and cluster ion beams produced by a 3 MV tandem accelerator of the TIARA[1-3]. A schematic diagram of the experimental arrangement is shown in Fig. 1. Pulsed 0.5 MeV/atom-C_1^+ and C_8^+ beams were injected into the sample with an incident beam angle of 45° relative to the sample surface. P-SIs accelerated between the sample and a TOF drift tube flew in the tube before hitting a 40mm-diameter microchannel plate (MCP). The TOF spectra recorded in a multi-channel analyzer (MCA) were transferred to a computer. Several improvements were made in the TOF system detailed in our previous paper[1] : (1) the mass resolution was improved by shortening a half-width of the pulsed incident ion beam to *ca.* 0.1μs and extending a length of the TOF drift tube, (2) the SI transmission efficiency of the analyzer was enhanced by inserting an electrostatic lens with transmission grids between an extractor grid and the MCP. The TOF measurements were performed at a pressure below 3×10^{-8} Torr and a fresh sample was used for each measurement.

Figure 2 shows the P-SI TOF spectra from *m*/*z* (mass to charge ratio)=20 to 60 of PC for (a) 0.5 MeV C_1^+ (0.5 MeV/atom C_1^+), and (b) 4.0 MeV C_8^+ (0.5 MeV/atom C_8^+), respectively. The major peaks observed in Fig.2 can be attributed to hydrocarbon fragments $C_2H_m^+$ ($C_2H_3^+$: *m*/*z*=27, and $C_2H_5^+$: *m*/*z*=29), $C_3H_m^+$ ($C_3H_3^+$: *m*/*z*=39, $C_3H_5^+$: *m*/*z*=41, and $C_3H_7^+$: *m*/*z*=43), and $C_4H_m^+$ ($C_4H_3^+$: *m*/*z*=51, $C_4H_5^+$: *m*/*z*=53, $C_4H_7^+$: *m*/*z*=55, and $C_4H_9^+$: *m*/*z*=57).

We note that the relative intensities of the fragments are different between C_1^+ and C_8^+ impacts although the PC samples are bombarded with the primary ions of the same element with the same velocity. Implanted ions lose their kinetic energy by interaction with the target. Depending strongly on the local density of energy deposited by the implanted ion, the target molecule may be fragmented and a fraction of the fragments is emitted as secondary ions. The local density of the energy deposited at the near surface due to C_8^+ impact is larger than that due to C_1^+ impact because constituent atoms originating from the same cluster simultaneously transfer their kinetic energy to a small area of the target surface. The higher deposited energy density makes the fragmentation process for C_8^+ different from that for C_1^+; this difference provides the different positions and relative intensities of some fragments between the C_1^+ and C_8^+ impacts.

In conclusion, the cluster ion impact provides different relative P-SI intensities for PC from those for the impact of the monoatomic ion with the same element and velocity.

References

1) K. Hirata, Y. Saitoh, A. Chiba, K. Narumi, Y. Kobayashi, and K. Arakawa, Appl. Phys. Lett., **83**, (2003) 4872.
2) K. Hirata, Y. Saitoh, A. Chiba, K. Narumi, Y. Kobayashi, and Y. Ohara, Appl. Phys. Lett., **86**, (2005) 044105.
3) K. Hirata, Y. Saitoh, A.Chiba, K. Narumi, Y. Kobayashi, and T. Kamiya, JAERI-Review, **2006-042** (2007) 179.

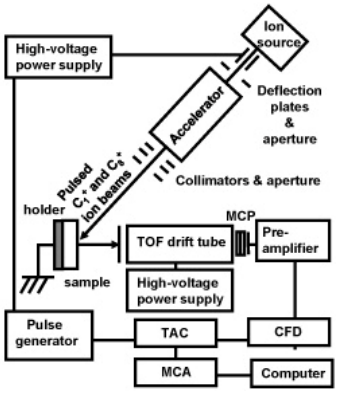

Fig. 1 Schematic diagram of the set-up.

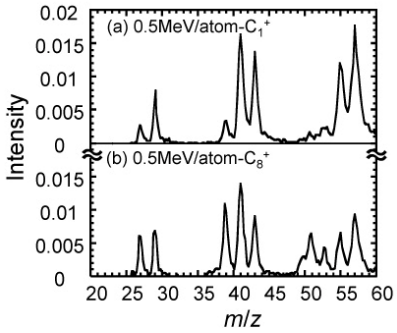

Fig. 2 P-SI TOF spectra of PC for (a) 0.5 MeV C_1^+ (0.5 MeV/atom C_1^+), and (b) 4.0 MeV C_8^+ (0.5 MeV/atom C_8^+).

4-44 Amorphization of Si Single Crystals by Au Cluster-ion Irradiation

A. Iwase [a)], T. Nakatani [a)], F. Hori [a)], R. Oshima [b)], Y. Saitoh [c)] , A. Chiba [c)] , K. Narumi [d)] and M. Adachi [c)]

[a)]Department of Materials Science, Osaka Prefecture University,
[b)]Osaka Nuclear Science Association,
[c)]Department of Advanced Radiation Technology, TARRI, JAEA
[d)]Advanced Science Research Center, JAEA

Si single crystals were irradiated with Au cluster ions, and the amorphization of the crystal was observed by means of a transmission electron microscope. The experimental result shows that the degree of amorphization strongly depends on the size of Au cluster ions.

原子が複数個の化学結合状態を形成して電荷を帯びた、いわゆるクラスターイオンを高エネルギーに加速して物質に照射すると、単原子イオンを同じ個数だけ照射した場合と異なる効果が期待される。それは、ある領域に原子複数個に対応するエネルギーが同時に散逸されるためである。前報では、Si単結晶をAu_2、Au_3クラスターイオンで照射し、透過型電子顕微鏡（TEM）で欠陥集合体を観察した結果を示した。それによると、Au原子の個数を同数照射したにもかかわらず、クラスターサイズが増加するにつれて観察される欠陥集合体の数やサイズが増加することが示された。これらの結果は、クラスターイオン照射量が少ない場合の結果である。今回は、照射量が多いとき、Siにどのようなクラスター効果が現れるかを調べた。

ターゲットには１１１方位のSi単結晶を用いた。あらかじめTEM観察用に薄膜化した試料をTIARAタンデム加速器により、１原子あたり 1.66 MeVのAu_1イオン、Au_2イオン、Au_3イオンを室温で照射した。クラスター効果をクリアに見るために、照射されたAu原子の個数が一定になるような照射量を用いた。TEMにより照射後の試料の電子回折パターンを観測した。照射量が比較的小さい$1x10^{13}Au/cm^2$の場合では、Au_1、Au_2イオンを照射したときはSi結晶の乱れは回折パターンからは観察されなかったが、Au_3クラスターイオン照射では、結晶の一部が非晶質化したことを示すハローが見られた。照射量が$2x10^{13}Au/cm^2$と少し多くなるとAu_3クラスターイオンだけでなくAu_2クラスターイオン照射の場合でも非晶質化が起こった。この結果を図１に示す。照射量をさらに多くして$6x10^{13}Au/cm^2$とすると、クラスターサイズによらず、すべての照射で非晶質化が見られた。

本実験の結果は、予測したように、クラスターイオンは物質のある領域へ高密度のエネルギー付与を起こし、今回の場合は、それは、単原子イオン照射の場合よりも低照射量での非晶質化をもたらしたと考えられる。

Reference

1) A.Iwase et al., JAEA-Review 2006-042 (2007) 178

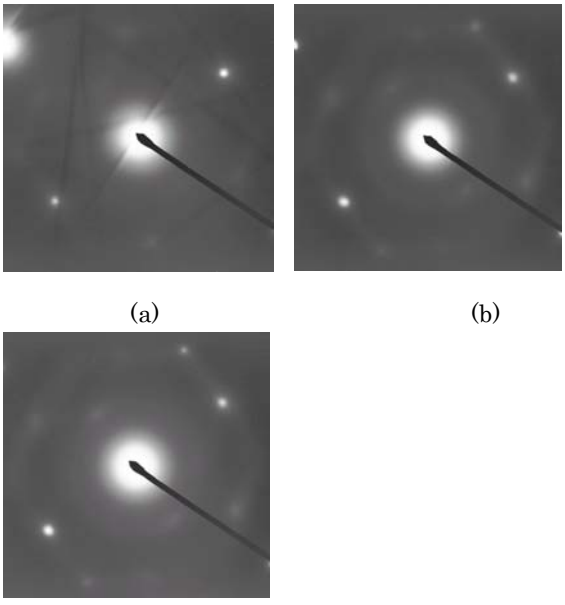

Fig.1 Electron ditfraction patterns for Si single crystals irradiated with Au clster ions (a)Au_1, (b)Au_2, (c)Au_3. Irradiation fluence is $2 \times 10^{13}Au/cm^2$

4-45 Double Differential Cross Section for Neutron Production of Beryllium

Y. Iwamoto [a)], N. Matsuda [a)], Y. Sakamoto [a)], K. Ochiai [b)], Y. Nakane [c)], H. Nakashima [c)] and T. Shibata [c)]

[a)]Nuclear Science and Engineering Directorate, JAEA, [b)]Fusion Research and Development Directorate, JAEA, [c)]J-PARC Center, JAEA

For boron neutron captured therapy (BNCT), there is a candidate as a accelerator neutron source for the use of Fixed Field Alternating Gradient (FFAG) ring, in which protons with the energy of about 10 MeV are circulated. In this source, thin beryllium will be used as a target material. Neutron production yields, its energy spectra and angular distributions from the thin beryllium bombarded by protons of about 10 MeV have not been measured systematically and there is no simulation code to estimate exactly these items. In this work, neutron spectra and its angular distributions from the beryllium target bombarded by protons were measured for the characterization of neutron source intensity, source term of shielding calculation and development of simulation code including of PHITS code.[1)]

Measurements were performed at the No.1 heavy ion irradiation room of AVF cyclotron in TIARA. Neutron energy spectra were obtained by the time-of-flight method using the two NE213 organic liquid scintillation detectors with 5.08-cm-diameter and 5.08-cm-thickness. The thickness of beryllium target in the vacuumed chamber is 15 μm which is corresponding to the energy loss of 940 keV for 10 MeV protons. The neutrons and photons emitted from a beam dump, in which the transmitted protons through the target are stopped, are shielded by iron and paraffin blocks settled between detectors and the beam dump.

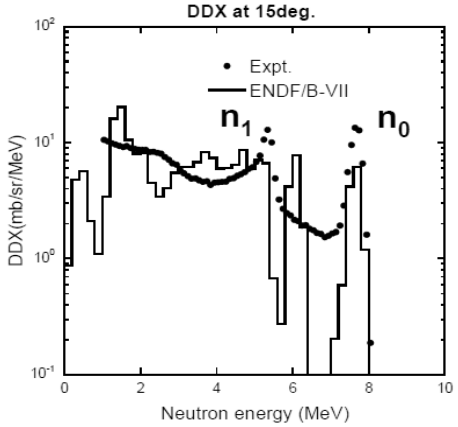

Fig.1 Double differential cross section for neutron production toward 15 degree from thin beryllium bombarded by 10 MeV protons. Bold line presents the evaluated values in ENDF/B-VII.

Figure 1 shows the neutron production double differential cross section for the energy above 0.8 MeV toward 15 degree direction compared with values of Evaluated Nuclear Data File, ENDF/B-VII. Peak energies and values of the cross section are the almost same between measured and evaluated ones. Two peaks in the measurements are corresponding to the energy levels of the ground state and the first excited state, 2.4 MeV level.[2)] For the evaluated spectrum, there is a level corresponding to energy of 1.4 MeV, but such a peak is not appeared in observation. Similar tendency is observed in the neutron spectra of other direction angles.

Figure 2 shows the angular dependence of neutron production yields. The term of “Two peaks” presents the integrated neutron yield with the energy region above 4 MeV including two peaks, “Low energy” presents that with the energy region below 4 MeV, and “Total” presents the sum of “Two peaks” and “Low energy”. As three types of neutron production yields get sharply decreasing with backward angles above 45 degree, the irradiation position of the patients should be forward direction below 45 degree to secure the neutron intensity for radiation therapy.

References

1) H. Iwase, et al., J. Nucl. Sci. Technol. **39** (2002) 1142.
2) M.W.McNaughton, et al., Nucl. Instrum. Method **130** (1975) 555.

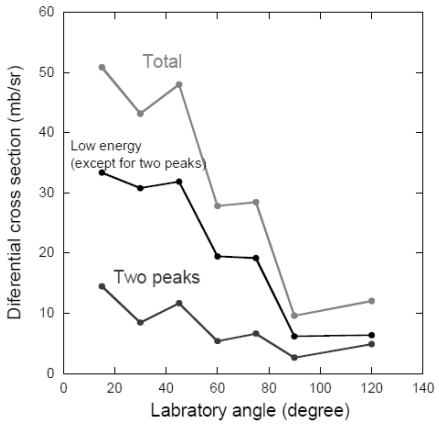

Fig.2 Angular dependence of integrated neutron yield with three different energy regions.

4-46 Development of Dose Monitor Applicable to Wide-energy Neutron

A. Endo [a)], T. Sato [a)], D. Satoh [a)] and H. Kaneko [b)]

[a)]Division of Environment and Radiation Sciences, NSED, JAEA, [b)]Department of Advanced Radiation Technology, TARRI, JAEA

Workers in high-energy accelerator facilities, such as J-PARC, are potentially exposed to high-energy neutrons, photons and muons because of their high penetrability in radiation shielding. Measurement of doses given by these particles is therefore of great importance for assuring radiation safety in the accelerator facilities. None of the existing survey instruments is however able to measure doses given by all of these particles. The authors have developed a new radiation dose monitor, designated as DARWIN (Dose monitoring system Applicable to various Radiations with WIde energy raNges), for real-time monitoring of doses in workspaces and surrounding environments of high-energy accelerator facilities[1)]. In the fiscal year 2006, we have measured doses in various radiation fields in order to demonstrate the applicability of DARWIN.

Figure 1 depicts the time-dependence of neutron dose rates measured with DARWIN in the Light Ion Room No.3 of TIARA, together with that of the beam current of the cyclotron. Quasi-monoenergetic neutrons of 60MeV were generated by the ^{7}Li(p, n) reaction in the LC0 course and then transported to the Light Ion Room No.3. The time profile of neutron dose rates measured by DARWIN is consistent with that of the beam current. It was confirmed that the measured dose rates agree with the estimated dose rates from the neutron spectrum in the field. These results indicate the rapid response and reliability of DARWIN.

Figure 2 shows the measured dose rates with DARWIN in comparison with the corresponding estimated values in various fields. The measurements were performed in 1) TIARA, 2) HIMAC at the National Institute of Radiological Sciences, 3) Los Alamos Neutron Science Center (LANSCE), and 4) the neutron fields of ^{252}Cf and ^{241}Am–Be sources in the Facility of Radiation Standard (FRS) at JAEA. Natural background dose rates of neutron from cosmic-rays were also measured in Tokai-mura and Los Alamos and then compared with the estimated values calculated by EXPACS[2)], EXcel-based Program for calculating Atmospheric Cosmic-ray Spectrum. Excellent agreement can be found between the measured and estimated dose rates over wide dose rates.

For further investigation concerning the sensitivity of DARWIN, the background neutron dose rates in Tokai-mura were measured simultaneously with DARWIN and a conventional rem-counter (TPS-451, Aloka). It was found that DARWIN needs only 20 min to obtain the data with a statistical error within 10%, while the rem-counter needs ~ 5 h. This result clarifies that one order of magnitude for difference in the sensitivity for neutron radiation lies between DARWIN and the rem-counter. With this property, DARWIN enables us to monitor small fluctuations of neutron dose rates near the background level.

References

1) T. Sato et al., J. Nucl. Sci. Technol. 42 (2005) 768.
2) http://www.jaea.go.jp/04/nsed/ers/radiation/rpro/
3) EXPACS/expacs.html

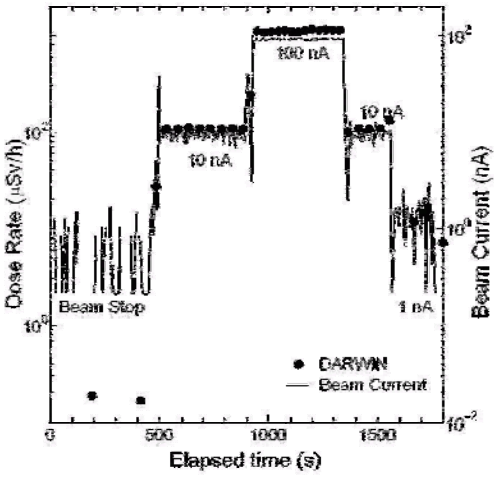

Fig.1 Relation between the dose rates measured with DARWIN in the Light Ion Room No.3 of TIARA and the beam current of the cyclotron.

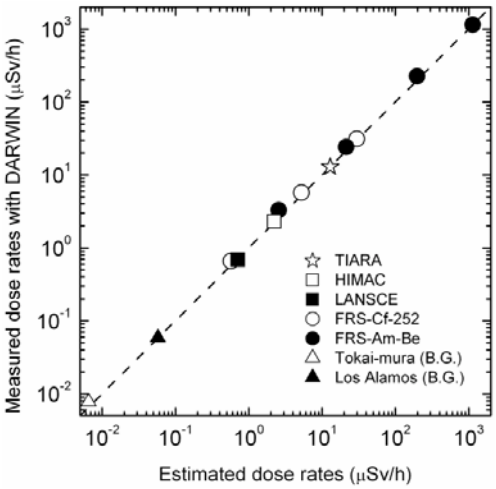

Fig.2 Measured dose rates with DARWIN in comparison with the corresponding estimated values in various radiation fields.

4-47 Development of a Detector for Absolute Measurement of Neutron Fluence in Quasi-monoenergetic Neutron Calibration Fields of High Energies

Y. Shikaze [a)], Y. Tanimura [a)], J. Saegusa [a)], M. Tsutsumi [a)], Y. Yamaguchi [a)], H. Harano [b)], T. Matsumoto [b)] and H. Kaneko [c)]

[a)]Department of Radiation Protection, NSRI, JAEA, [b)]National Metrology Institute of Japan, National Institute of Advanced Industrial Science and Technology, [c)]Department of Advanced Radiation Technology, TARRI, JAEA

In facilities of high intensity proton accelerator, it is important for radiation control to measure the dose for high energy neutrons penetrating the shielding materials. High energy neutron calibration fields are necessary for accurate dose measurements to appropriately calibrate the monitor and the dosemeter used there. For the neutron fields above 20 MeV, however, the international standards for the neutron fields and relevant calibration techniques have not been established. Therefore, by using the quasi-monoenergetic neutron irradiation fields of several tens of MeV at TIARA[1)] of Takasaki Advanced Radiation Research Institute, Japan Atomic Energy Agency (JAEA), the development of the calibration fields for such high energies has been in progress toward the standard fields. Neutron fluence of peak region is one of the most important characteristics of the calibration fields with quasi-monoenergetic spectrum. For absolute measurement of the peak neutron fluence, a proton recoil telescope (PRT) has been developed.

The PRT consists of a Si semi-conductor detector to measure ionization energy loss (ΔE) and an organic liquid scintillation detector to measure full energy (E) of recoil protons. The Si detector has the sensitive area of 3000 mm^2 with a fully depletion layer of 300-μm. The liquid scintillator (BC-501A type) has the sensitive volume of 7.62-cm both in diameter and in length. Its performance was tested in the neutron fields, where neutrons were produced in the nuclear reaction of ^{7}Li targets with 50, 65 and 80 MeV protons. The proton energies correspond to neutrons with the peak energy of 45, 60 and 75 MeV, respectively. The measurement is based on the detection of the recoil protons produced in a polyethylene converter by the incident neutrons. For the precise measurement of the peak fluence based on the n-p elastic scattering cross-section, the unwanted protons from carbon in converter material (C(n,xp)) must be subtracted. Therefore, measurement with graphite converter was also performed. The PRT was set on the neutron beam axis at the two different distances from the target (5.585 and 12.905 m). The brass shadow bar (8-cm in dia., 50-cm in length) was used to avoid the neutrons directly incident to the detector. The thin annular converters with inner diameters of 8.8-cm were applied. Since the collimated neutron irradiation fields at TIARA enlarge with increasing distance from the target[2)], outer diameters of the annular converters were appropriately selected to use the irradiation fields effectively.

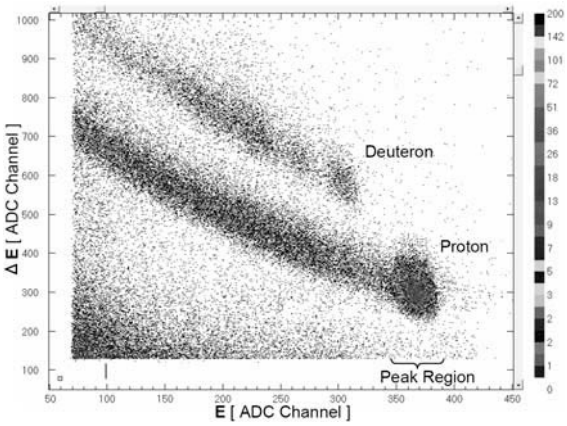

Fig.1 Energy loss (ΔE) measured by the Si detector v.s. Energy (E) measured by the organic liquid scintillation detector for measurement with polyethylene converter (neutrons with 45 MeV peak).

Recoil protons were clearly identified in the obtained ΔE v.s. E distribution as shown in Figure 1. Energy resolution of the Si detector was 24.7 % for recoil protons corresponding to peak neutrons with 45 MeV, and was enough for the separation of protons from background deuterons. By selecting the recoil protons, energy spectra of the recoil protons were obtained for the two different converter materials. After the compensation for the backgrounds from carbon and air nuclei, the recoil proton energy spectra only for n-p elastic scattering were derived. From the results for the three neutron fields with 45, 60 and 75 MeV peak, it was confirmed that detection efficiency was enough for the absolute measurements of peak neutron fluence both at 5.585 and 12.905 m from the target.

References

1) M. Baba et al., Nucl. Instr. Meth. A 428 (1999) 454.
2) Y. Shikaze et al., JAEA-Review 2005-001 (2006) 337.

4-48 Development of Focusing High-energy Heavy Ion Microbeam Technology and Its Application

T. Kamiya [a,b], T. Satoh [a], M. Oikawa [b,a], S. Okumura [a], S. Kurashima [a], N. Miyawaki [a], H. Kashiwagi [a], W. Yokota [a], T. Funayama [c], T. Sakashita [c], S. Wada [c], T. Hirao [d], S. Onoda [d], K. Mishima [d], Y. Kobayashi [c,b] and T. Ohshima [d]

[a]Department of Advanced Radiation Technology, TARRI, JAEA, [d]21st Century COE program Graduate school of medicine, Gunma University, [c]Radiation-Applied Biology Division, QuBS, JAEA, [d]Environment and Industrial Materials Research Division, QuBS, JAEA

A focusing type high-energy heavy ion microbeam system with a sub-micron level spatial resolution had been established in the vacuum system[1]. Now an end-station was developed to extract microbeams out to the atmosphere through a thin film, so as to evaluate response of specific part of intracellular structure such as a cell nucleus, a cytoplasm or cell wall with a high spatial resolution of 1 μm level.

Figure 1 shows the schematic draw of an end-station, which was connected with a lower plate of the Q-lens frame through a flange of the ICF-70 standard, was simply designed to evaluate the beam size at the beam exit window on the atmosphere, and to perform the preliminary microbeam applications. It has flexibility of the bellows-seal and positioning mechanism with a movable range of ±12.5mm in each direction by X/Y stage with stepping motor drive. The manifold connected to the bellows is 42mm in outer diameter, 32mm in inner diameter, and 49mm in length. It has two ports for a secondary electron detector; one is for a light-guide connected to a ring-type plastic scintillator set at a height of 14 mm from the under-surface of the manifold to detect scintillation by secondary electron from the sample, and the other is for high-voltage supply on a moralized surface of the scintillator. On the bottom of the manifold, there are three penetration holes with diameters of 1 mm, 2 mm and 3 mm, respectively. A copper-grid (1000 lines per inch) standard sample, which was utilized to measure the beam size by secondary electronic mapping, and a plastic scintillator film to monitor beam spot profile at the target were attached outside of the 1-mm and 3-mm holes, respectively. The 2-mm hole was a blank for use of irradiation experiments. All holes together with the grid and the film were covered with a polyimide thin film of 7.5 μm thickness to keep the vacuum inside of the chamber. The flat bottom of the manifold was designed, so that an air-gap between the film and sample should be as small as possible in the irradiation set-up for the experiments.

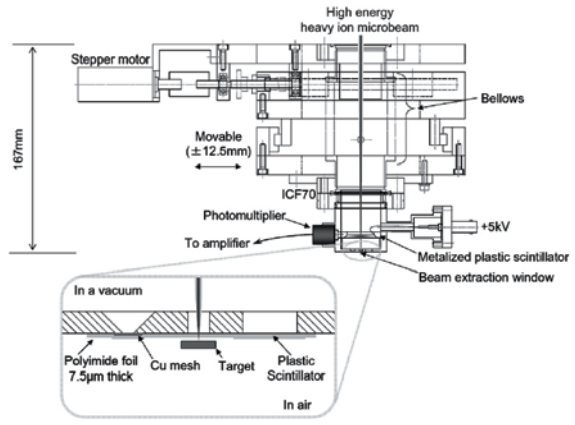

Fig.1 Schematic view of the end-station of the high-energy heavy-ion microbeam system.

Figure 2 shows a typical secondary electron image of the grid at the beam exit window obtained with this new setup using a microbeam of 260MeV Ne ion. The average beam size was obtained at about 2 μm from the peak fitting for the secondary electron yield curves along lines for X and Y directions, respectively, so far. The spatial resolution of the beam at the sample in the atmosphere can be deteriorated by scattering in the film and the air gas.

Further work will focus onto reliability in forming the higher spatial resolution microbeam, which depends on stabilization of a beam current from a cyclotron, as well as on establishment of automated single ion hit system.

Reference

1) M. Oikawa, , T. Kamiya, M. Fukuda, S. Okumura, H. Inoue, S. Masuno, S. Umemiya, Y.Oshiyama and Y. Taira, *Nucl. Instr. and Meth. B*, **20** 54 (2003).

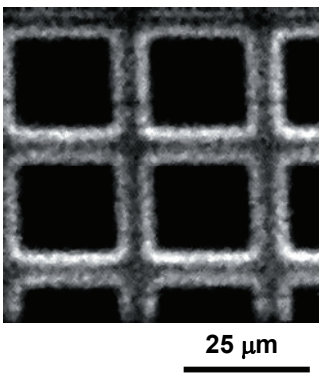

Fig.2 Typical secondary electron image of copper mesh in gray-scale obtained by a 260 MeV Ne microbeam scanning. The mesh has 6-μm width lines and 19 μm

4-49 Development of Irradiation Position Control Techniques for Ion Microsurgery Using an Ion Beam Induced Fluorescent Analysis

H. Shimada [a,b,d], M. Oikawa [a,b,d], T. Satoh [b], S. Okumura [b], M. Taguchi [c], T. Sato [d], Y. Horiuchi [d], H. Katoh [d], K. Yusa [e], T. Kamaiya [a,b], S. Kishi [d], T. Nakano [a,d,e] and K. Arakawa [a,b,d,e]

[a]21st Century COE Program, Graduate School of Medicine, Gunma University, [b]Department of Advanced Radiation Technology, TARRI, JAEA, [c]Environment and Industrial Materials Research Division, QuBS, JAEA, [d]Department of Medicine, Graduate School of Medicine, Gunma University, [e]Gunma University Heavy Ion Medical Center, Gunma University,

The heavy ions have unique characteristics of high energy transfer localized in the vicinity of almost straightforward tracks. The heavy ions are suitable for the treatment of small tumors with the size of several millimeters or less. This research aims at developing an innovative microsurgery treatment system, using the carbon-ion pencil beam, for AMD (age-related macular degeneration). The AMD treatment system has been studied using the carbon-ion pencil beam system.

我々は、群馬大学21世紀COEプログラム「加速器テクノロジーによる医学・生物学研究」の主要なテーマのひとつとして、原子力機構・高崎研と連携して、高精度炭素イオンマイクロサージェリー技術の開発を行っている。従来のX線やγ線照射などよりも生物への照射効果の大きな重粒子線を用い、エネルギー付与の大きなブラッグピークを利用して狭小領域の患部に集中的にエネルギー付与し、選択的かつ集中的に治療を行うことを目指している。

本研究では、難病にも指定されている眼底疾患のひとつである加齢黄斑変性症を治療想定症例として、高精度炭素イオンマイクロサージェリー技術の検討を進めている。黄斑部は網膜の中で最も視神経が集中する非常に重要な部位であり、この部位周辺に網膜下の狭小領域に新生血管が発生し網膜を歪めてしまうのが加齢黄斑変性症(以下AMD)である。症状として、非可逆的かつ高度な視力低下や視野の中心が歪む変視症の症状が見られ、最悪の場合、視野の中心が完全に失われてしまう。推定の患者数は約40万人で、その予備群も含めると約600万人にもなり、今後、超高齢化社会を迎える我が国において、無視できない患者数である。

これまで、ビーム径0.1～5 mmφのペンシルビームを形成するための光学計算、構成機器およびその最適配置に関する検討を行ってきた。[1] 今回、照射位置決め法として、眼底蛍光造影剤を用いた重イオンビーム誘起蛍光法を考案し、重イオンビーム誘起蛍光計測システムを用いて実験を行うとともに、照射照準位置制御技術の検討を行った。

現在、眼底の狭小・微細領域にある患部を正確に3次元精密照射するために必要な照射照準制御技術の開発が最大の課題となっている。その方法として、眼底患部に注入した眼底蛍光造影剤（インドシアニングリーン；ICG）に、重粒子線を照射し、飛程をレンジシフタで微調整しながら、ICGからの発光を専用特殊眼底カメラ等を用いて観測する。その発光画像を解析して照射位置の決定を行う。

眼底蛍光造影剤への照射実験は原子力機構・高崎研TIARA 施設の AVF サイクロトロン・HA コースを用いて行った。空気飽和した眼底蛍光造影剤水溶液（ICG およびフルオレセイン；Fl）に、炭素イオンビーム（C^{5+}-220 MeV, C^{6+}-320 MeV）を照射し、眼底蛍光造影剤水溶液からの発光スペクトルおよび発光画像を観察した。サンプルの濃度は標準的な人体に投与した際の最高血中濃度（1.0 x 10^{-2} mg/mL, 1.3 x 10^{-5} M）に調整した。

その結果、重粒子線照射による眼底蛍光造影剤からの発光画像および発光スペクトルが取得できた。Fig.1にイオンビーム照射直後に測定したFlの蛍光スペクトルを示す。光励起に比べ、発光波長はほぼ同じであるが、Flの蛍光量子収率（0.98）に対して発光強度が非常に微弱である。このため、発光色素や検出系の再検討が必要である。

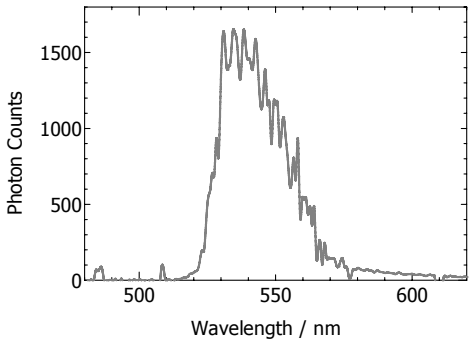

Fig.1 The fluorescence spectrum of fluorescein in water at 293 K obtained to C^{5+} beam irradiation.

Reference

1) H. Shimada, *et al*., JAEA Takasaki Ann. Rep. 2005, JAEA-Review 2006-042 (2007) 186.

4-50 Development of the Cyclotron System for Advanced Irradiation

N. Miyawaki, S. Okumura, S. Kurashima, Y. Yuri, T. Yuyama, T. Ishizaka, H. Kashiwagi, K. Yoshida, I. Ishibori, T. Agematsu, T. Nara and W. Yokota

Department of Advanced Radiation Technology, TARRI, JAEA

Microbeam Formation

For production of a focused heavy-ion microbeam[1] in the JAEA AVF cyclotron, the beam energy spread has been improved by optimizing the operating parameters including flat-top (FT) acceleration[2]. In the case of a 260 MeV-$^{20}Ne^{7+}$ beam, the energy spread of 0.05 % was achieved and both of the spatial resolution and the hitting accuracy were evaluated at less than 1 μm[3]. In the next place, the FT acceleration of a 220 MeV-$^{12}C^{5+}$ beam was tested. The beam phase in the FT acceleration was controlled by a pair of phase defining slits in the center region of the cyclotron. The beam current was as high as 0.6 μA when both of the sinusoidal and the saw-tooth waveform bunchers were turn on. As shown in Fig. 1, we observed the clear turn separation of the beam intensity distribution with the deflector probe. The extraction efficiency at the deflector was successfully increased up to 98 % with the single-turn extraction.

In order to reduce the sources that cause instability of ion beam current, we have exchanged the temperature control system of magnet power supplies. By the temperature control of the feedback control circuit with Peltier devices, a beam current fluctuation caused by power supplies was significantly reduced.

Uniform Irradiation Using Multipole Magnets

We are now developing the uniform-beam irradiation system using multipole magnets with the aim of the advance in uniform-irradiation technique. It enables us to obtain homogeneous irradiation effects on over a sample with a large area or on a large number of samples simultaneously without scanning the beam.

We have theoretically studied the beam dynamics under the nonlinear magnetic fields to produce a beam with a uniform transverse intensity profile in the beam transport at the AVF cyclotron facility[4]. Although all the odd-order multipole magnetic fields are, in theory, required for uniformization of a Gaussian beam, it is practically possible to produce a uniform beam only with an octupole focusing. Its integrated strength is $1/(\varepsilon\beta_0^2 \tan\theta)$, where ε is the rms emittance of the beam, β_0 is the beta function at the octupole magnet, and θ is the betatron phase advance from the magnet to a target. The full width of the resultant uniform is $\sqrt{2\pi}\sqrt{\varepsilon\beta_t}\,|\cos\theta|$, where β_t is the beta function at the target. Based on these formulae, we have optimized the optics of the beam line. It is possible to produce a beam with a uniform profile of 10 cm square at the target. The effect of beam emittance and energy spread on beam uniformization has also been explored through systematic simulations.

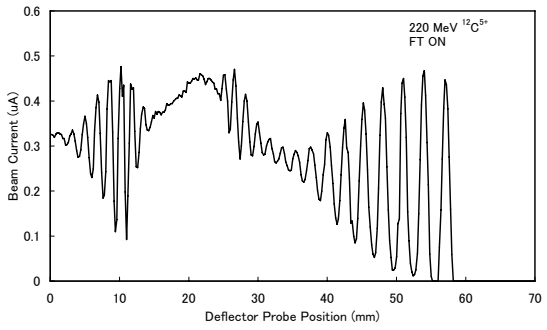

Fig.1 Beam intensity distribution measured with the deflector probe. The final peak, extracted through the deflector electrodes, was cleared by the FT acceleration.

Intensity Control with Beam Attenuators

Beam current control over a very wide range is required for experiments and beam tuning in the JAEA cyclotron. A beam attenuator (ATT) to attenuate the beam current without changing the beam profile is set in the injection line of the cyclotron. The beam current is controllable in the range of 10^{-1} to 10^{-12} by combining the ATT meshes of 10^{-3}, 10^{-2} and 10^{-1}. It was found that the ATT did not always keep the beam profile at a target point and did not control the beam current precisely according to the combination of the meshes. We estimated the beam size at the installation point of the ATTs with the design value of the emittance. Influence of combination of the meshes to the beam profile was also examined by the Gaf film which allows the beam profile measurement easily. As a result, we realized that the intervals of the meshes were too short at the beam diagnostic station of IS2, and the spacing of the holes in the mesh was too long at that of IS5, which is a waist point in the beam transport.

References

1) M. Fukuda, *et al.*, Nucl. Instrum. Methods Phys. Res. B 210, 33 (2003).
2) S. Kurashima, *et al.*, Nucl. Instrum. Methods Phys. Res. B 260, 65 (2007).
3) M. Oikawa, *et al.*, Nucl. Instrum. Methods Phys. Res. B 260, 85 (2007).
4) Y. Yuri *et al.*, in *Proceedings of the 3rd Annual Meeting of Particle Accelerator Society of Japan and the 31st Linear Accelerator Meeting in Japan*, 913 (2006)

4-51 Development of All-permanent-magnet ECR Ion Source for the JAEA Cyclotron （Ⅱ）

K. Yoshida , T. Nara , Y. Saitoh and W. Yokota

Department of Advanced Radiation Technology, TARRI, JAEA

We have been developing an all-permanent-magnet type ECR ion source (LECR) since 2003 to realize the high stability of beam intensity and reduction of the adjustment time of the JAEA AVF cyclotron[1]. The magnetic field distribution of LECR is changeable by an axially moving the mirror tuning magnets of the extraction and the gas injection side[2]. The beam current of LECR increased 10 times as much as that of the original design, and the continuous operation became possible by the previous modification[3]. In this paper, we report the new modification for further increase of beam intensity and the result.

In the original design, the entire magnets of LECR can be slide in the axial direction within 60 mm to adjust the relative position of the beam extraction hole against the magnetic field. The vacuum was deteriorated by outgas from the inner wall of long puller by hit of extracted beam. It appeared that the distance of 5 mm in the axial direction is enough by experiment. Therefore, we modified design of the high-voltage insulation and the joint parts of the plasma chamber, and changed the diameter of einzel lens.

There was a clearance of 2 mm between the plasma chamber and the magnet for the high-voltage insulation sheet. The inner diameter of the plasma chamber was extended to increase confinement efficiency by decrease in clearance of 2 mm. The material of a plasma chamber was changed into oxygen free copper from stainless steel to improve the cooling efficiency.

A schematic drawing that describes the modification is shown in Fig 1, and the modification is summarized in Table.1.

Table.1 the modification in FY2006

Diameter of plasma chamber(ID)	32 mm → 36 mm
Materials of plasma chamber	SUS316 → C1020
Puller length	190 mm → 107 mm
Diameter of einzel lens	25 mm → 48 mm

The improvement of LECR by the modifications is shown in table 2. The beam current of O^{7+} increased from 0.6 to 1.8 μA. A considerable amount of beam loss may takes place in the analyzing magnet because its chamber inner gap is 54 mm, not enough for beams from an ECR ion source with a large emittance.

Table.2 The performance of LECR

	O^{4+}	O^{5+}	O^{6+}	O^{7+}
LECR (original)	2	1	0.6	<0.01
LECR (2005)	16	15	10	0.6
LECR (2006)	44	33	18	1.8

We are, therefore, planning to install LECR in an injection line of the cyclotron with an analyzing magnet whose inner gap of the chamber is designed 92 mm.

References

1) S. Kurashima, et all, Nucl. Instr. and Meth B, 260(2007)65-70.
2) K.Yoshida, T.Nara, Y.Saitoh, W.Yokota, TIARA annual report2003 (2004) 316.
3) K.Yoshida, T.Nara, Y.Saitoh, W.Yokota, JAEA Review2005 (2006) 190.

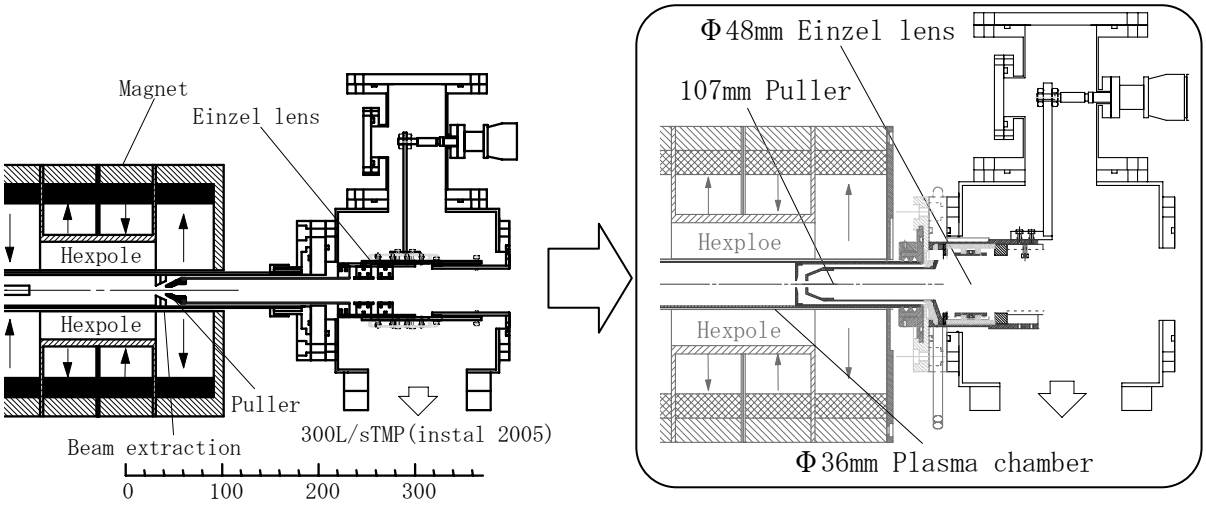

Fig.1 The modification of LECR ion source in 2006.

4-52 Development of Beam Generation and Irradiation Technology for Electrostatic Accelerator

K. Yamada, S. Uno, K. Ohkoshi, A. Chiba, Y. Saitoh, Y. Ishii, T. Satoh and K. Mizuhashi

Department of Advanced Radiation Technology, TARRI, JAEA

1. Measurement of beam-energy spread in a 3 MeV TANDEM accelerator

The monochromatism of the beam energy is the most important for the highly precise irradiation such as a micro-beam technique, and it great depends on the stability of the terminal voltage in the electrostatic accelerator. We aim at establishing the accurate measurement system of the beam-energy spread to evaluate the acceleration performance. In the TANDEM accelerator, the monochromatism of the beam energy would be affected from not only the terminal voltage stability but also from the energy loss by the collision with the N_2 stripper gas. Therefore we tried to measure the beam-energy spread dependent on the stripper gas pressure by using the nuclear reaction with narrow resonance width (150eV) in $^{24}Mg(p,\gamma)^{25}Al$. The result of the Fig.1 suggested that this measurement system could accurately evaluate the monochromatism of the beam in 10^{-5} order.

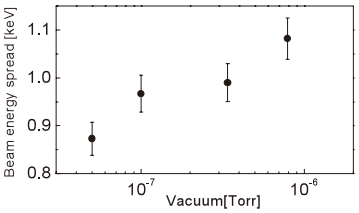

Fig.1. The relation between the beam-energy spread and the stripper gas flow. The horizontal axis is the vacuum in an acceleration tube relative to the stripper gas flow.

2. Voltage calibration for TIARA 3 MV single-ended accelerator using a resonance of RBS

The voltage calibration has been carried out using the resonance nuclear reactions of $^{27}Al(p,\gamma)^{28}Si$ and $^{24}Mg(p,\gamma)^{25}Al$ with narrow reaction energy spreads. The incident proton beam energies for the former and the latter are used at 992 keV, 1317 keV and 2010 keV, 2400 keV, respectively. The calibration at 3 MV was difficult because a resonance reaction with a narrow energy spread did not exist in the vicinity of the incident proton beam at 3 MeV. Therefore the resonance for the Rutherford Back Scattering (RBS) of (^{8}O, ^{4}He) at 3.04 MeV at a direction of 180 degrees[1] was used for the calibration of the accelerator voltage. The thin TiO_2 layer of 50 nm was evaporated on glassy carbon as a sample. The sample was placed on the 15 degree beam line (SC). The He^+ beams generated by the accelerator were injected into the sample. The back-scattered He+ particles were detected by a SSD detector at 170 degrees. The He+ yields were measured as a function of the He+ energy.

The difference between the indicated voltage of the accelerator controller and measured one, 3.04 MV, was estimated to be 1%.

3. Acceleration of Ge cluster ion to MeV energy region

We tried to accelerate Ge cluster (Ge_n : n=2-4) ions up to 6MeV with a tandem accelerator for applying them to the study of interaction between swift cluster ions and matter. Negative Ge cluster ions are generated by a Cs sputter ion source. The mass spectrum of negative ions extracted from the source is shown in the Fig. 2. We can recognize Ge clusters (Ge_n) up to Ge_4 in the beam current of nano ampere order. Clusters of Al are also obtained because Ge-Al alloy is used for the sputter cathode to stabilize the beam current. Ge cluster ions, which have the medium mass between that of a carbon cluster and that of a gold cluster, are required by users.

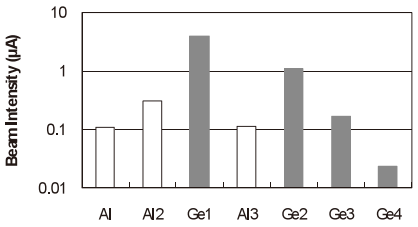

Fig.2. The mass spectrum of cluster ions extracted from the ion source

4. Study of Faraday cup (FC) for a fullerene ion beam current measurement

A current of fullerene beam was difficult to measured with a conventional FC, because a large number of secondary positive ions produced by fullerene collision escape through the electron-suppression field. Therefore we developed of the FC that applied the external magnetic field (430 Gauss) to a conventional FC for suppressing both secondary electrons and secondary positive ions. A fullerene beam current was measured with this FC and a high-aspect ratio FC, and measurement values were 3.3 nA and 4.5 nA, respectively. The difference of measurement values indicated that magnetic field was not enough to suppress secondary positive ions. Nevertheless, for install in beam transport line, it is notable that a fullerene beam current is able to measure without changing shape of a conventional FC. We will optimize magnetic field for a fullerene beam measurement in future.

Reference

1) L. C. Feldman and J. W. Mayer, *Fundamentals of Surface and Thin Film Analysis* (North-Holland, Amsterdam, 1986), pp.26

4-53 Design of a Compact High-energy Focusing Lens System Combined with an Acceleration Tube

Y. Ishii [a)], T. Ohokubo [a)], J. Haga [a)], A. Kobayashi [b)] and S. Adachi [b)]

[a)]Department of Advanced Radiation Technology, TARRI, JAEA, [b)]Kobe Steel Ltd

A fine fabrication using high-energy focused proton beams, proton beam writing (PBW), is a promising technique for development of 3D structures such as optical devices and high sensitive sensors. High energy focused gaseous ion micro-/nanobeams are formed by the combination of a MV electrostatic accelerator, a beam line with a high resolution analyzing magnet and a high-energy focusing ion beam (MeV focused ion beam) system. Since each component combined in the system is longer than 10 m, the total size of its system reaches to several tens of meters. The wide usage of the MeV focused ion beam in various researches and development fields is, thereby, difficult due to the large size of the combination system.

The acceleration lens system, a series of acceleration lenses each of which has the both effects of focusing and accelerating ion beams in an electric field, was developed to achieve the demagnification over 1000 in JAEA. The focusing potential of the acceleration lens system was so far demonstrated by using the keV gaseous ion nanobeam system and forming the 170 nm H_2^+ beam at 50 keV[1)].

On the other hand, a compact 1 MV focused ion beam system (compact 1 MV system) was developed using the combination of a 1 MV accelerator and a MeV focused ion beam system with magnetic quadruple lenses in Kobe Steel, LTD (KSL). Beam sizes with several micrometers in diameter are formed using the compact 1 MV system for the investigation of material element analysis in various materials using RBS techniques. JAEA in cooperation with KSL is developing a compact 2 MeV level gaseous ion nanobeam system aiming at 100 nm sized special resolution achieved by combining the acceleration lens system with the compact 1 MV system.

The MeV high demagnification lens system was designed using the acceleration lens system and an acceleration tube in the last year. The basic data of a multicusp ion source developed for another study were also measured to evaluate the conditions of beam current, energy and energy-spread required to its source.

The two kinds of performance of the acceleration lens and the acceleration tube needs to be investigated to design the compact MV high-energy focusing lens system. The performance data of the acceleration lens was a priori investigated from that of the keV gaseous ion nanobeam system.

The relation between focusing point and magnification was calculated employing Elkind's equation applying accelerator tube parameters used in the compact 1 MV accelerator as a function of N value (accelerated beam energy/injection beam energy). The relation shows that the focusing points are formed in the accelerator tube when the N value of 27 and 20 for object points of 300 mm and 500 mm, respectively. Thereby, the usage of large demagnification, that is large N value, provide impossible to irradiate samples.

A 1.7 MeV focused proton with one hundred nm in diameter could be formed using the schematic design of the compact MV high-energy lens system as shown in Fig.1 with the parameters as listed in Table 1. The beam current at a focusing point is, however, small due to using a small aperture to inject small beam divergence angle into the accelerator tube. The one order smaller divergence beam angle injected into the accelerator tube is required to reduce aberrations as compared with the outgoing beam angle of the second acceleration lens. The acceleration lenses with a controllable outgoing beam divergence angle are investigating to increase the beam current at the focusing point. Furthermore, a multicusp ion source has been developing to increase beam current at the focusing point.

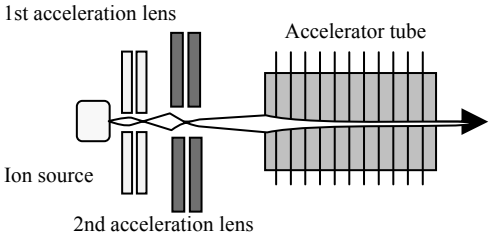

Fig.1 A schematic design of a compact high-energy focusing lens system

Table.1 Parameters of the design

	1st accel. lens	2nd accel. lens	Accel. tube
voltage (kV)	5	100	1700
Incident angle (rad)	1×10^{-3}	1×10^{-3}	1×10^{-4}
Outgoing angle (rad)	2.5×10^{-2}	5.7×10^{-3}	
Magnification	-0.0056	-0.039	1.03
Beam size	2.2μm	86nm(between electrodes)	92nm

Reference

1) Y.Ishii, et. al. Nucl. Instr. and Meth. B210(2003)70

4-54 Micro-machining of Resists on Silicon by Proton Beam Writing: Part 2 (Fabrication of 3-D Structures Using a Negative resist)

N. Uchiya [a)], Y. Furuta [a)], H. Nishikawa [a)], J. Haga [b)], T. Satoh [b)], M. Oikawa [b)], T. Ohkubo [b)], Y. Ishii [b)], T. Kamiya [b)] and S. Yamamoto [c)]

[a)]Department of Electrical Engineering, Shibaura Institute of Technology, [b)]Department of Advanced Radiation Technology, TARRI, JAEA, [c)]Environment and Industrial Materials Research Division, QuBS, JAEA

Proton beam writing (PBW) is a direct write technique for the purpose of micro- or nano-meter sized machining [1)]. This technique does not require an expensive mask for patterning as well as electron beam though the mask is required for the exposure with UV (EUV) and x-ray. The lateral straggling of proton beam with energy of MeV order is far smaller compared with electron beam. The depth of fabrication is reached to several tens of micro-meter in a resist and controlled by the beam energy. The PBW is a promising technique for the micro-machining of thick resist and three-dimensional (3-D) structures with high aspect ratios [2)].

In our previous report [3)], we confirmed the fabrication of micro-structures with smooth and vertical side wall by the PBW on PMMA and SU-8. In this paper we report the results of fabrication of 3-D structures using two ranges of proton beams in SU-8 layer controlled by the beam energies. The micro-meter-sized structures by the PBW were observed by a scanning electron microscope (SEM).

We used a layer of negative resist SU-8 (N-02 Wafer, MEMS CORE) with a thickness of 50 μm on Si wafer.

The resist layer on silicon was exposed by focused proton beam formed by the micro-beam system in TIARA, JAEA. The beam size was estimated at about 1 μm in diameter from secondary electron images of a commercially available Ni mesh. The PBW was carried out with a resolution of 8192 x 8192 pixels in an area of 700 x 700 μm^2 by an electrostatic scanner. The projected ranges of proton beam into the resist layer were controlled by using two different proton beam energies of 1.2- and 3.0-MeV. The fluence of protons was controlled ranging from 20 to 80 nC/mm^2. [4)]

In the first step, irradiation of the proton beam was carried out at the energy of 3.0 MeV to form posts on the substrate with a projected range of more than 50 μm. In the next step, the irradiation was carried out at the lower energy of 1.2 MeV to bridge across the posts at a depth of 28 μm.

After the development process for 3 minutes using a developer for SU-8 and rinse in isopropyl alcohol, the samples, which were coated with Pt by sputter to avoid charging, were observed by the SEM.

The fabricated 3-D structures were shown in Fig.1. The depth of the lines written by 1.2-MeV PBW were 22 μm from the resist surface that was close to 21 μm estimated by SRIM simulation [5)]. The vertical and smooth side wall of the posts was formed by 3.0-MeV PBW. Using this technique, we demonstrated fabrication of the structure like the Arch of Triumph showed at Fig. 2.

The controlled ranges of the proton beam by changing the beam energies enabled us to fabricate the multi-level structures in the single resist layer. This shows the capability of the PBW in the formation of 3-D high-aspect-ratio structures.

References

1) S. V. Springham et al., Proc. SPIE Int. Soc. Opt. Eng. 3183 (1997) 128.
2) A. A. Bettiol et al., Proc. SPIE Int. Soc. Opt. Eng. 5347 (2004) 255.
3) N. Uchiya et al., TIARA annual report 2005 (2006) 174.
4) N. Uchiya et al., Nucl. Instr. and Meth. B 260 (2007) 405
5) J.F. Ziegler et al, The Stopping and Range of Ions in Solids, Pergamon Press, New York, 1985.

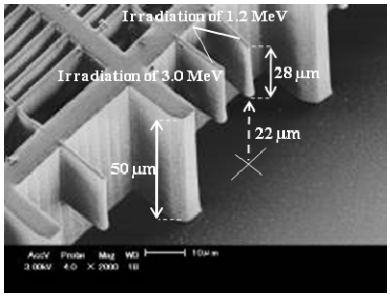

Fig. 1 SEM image of the grid structure of SU-8 fabricated by PBW of energies of 1.2 and 3.0 MeV.

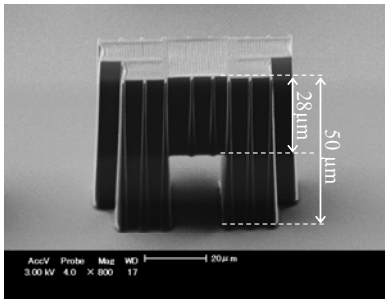

Fig. 2 SEM image of 3-D structure of SU-8 like the Arch of Triumph fabricated by PBW at energies of 1.2 and 3.0 MeV.

4-55 Measurement Technique of Two Dimensional Dose Distribution Using B3 Film Dosimeters and a PC-scanner

H. Hanaya, T. Agematsu and T. Kojima

Department of Advanced Radiation Technology, TARRI, JAEA

1. Introduction

Measurement of 2D dose distribution in large ion beam irradiation area is one of the indispensable techniques for R&D in material science and bio-technology using a cyclotron. Measurement technique for 2D distribution of relative ion beam fluence has been developed using Gaf-chromic films (HD-810) and an image scanner for a personal computer[1]. This combined system has advantages such as costless, easiness of handling and speedy measurement with high spatial resolution. The measurable dose using this system is, however, not applicable to doses above 1200 Gy. The use of B3 film dosimeters (GEX B3002) was tested instead of Gaf-chromic films to expand measurable dose range of the combined system to higher dose region. The B3 dosimeters are commercially available in the aluminum package but would be used for measurement of ion beams after removing it, since ion beams have generally short penetration range. The optical readout of B3 dosimeters associates with heat treatment after irradiation for stabilization of dose response before readout. In the preliminary study, dose response of B3 films irradiated in the package by 2 MeV electron beams was linear up to 100kGy when readout using Green color component without heat treatment after irradiation [2]. Dose responses of B3 film dosimeters irradiated with and without package were examined including their stability after irradiation.

2. Experimental and result

B3 film dosimeters with and without 200 μm-thick aluminum package were irradiated by 2 MeV electron beams to doses of 5 - 100 kGy. The irradiated dosimeters without heat treatment were readout using the image scanner (Canon LiDE50) with Green color components at different elapse times after irradiation.

The dose response curves for different elapse time after irradiation were shown in Fig.1: a) when dosimeters were kept in the package, and b) when dosimeters were not kept in the package. Any dose responses increase with dose and their curves are similarly linear up to at least 40 kGy. The dose responses increase with elapse time, but the slopes become gentle 24 h after irradiation, not depending on the use of the package.

3. Discussion

The B3 dosimeters show the linear dose response up to at least 40 kGy even used without package. It demonstrates that the dosimeters are usable also for ion beams having short penetration range. The dose response increases as a function of elapse time after irradiation. Such a variation can be minimized with heat treatment, but it becomes negligible order (< 3%) 24 h after irradiation without heat treatment.

The combined system with the B3 film dosimeters and an image scanner has a potential to be applied to measurement of 2D relative dose distribution of ion beams in the dose range of a few tens kGy, although further studies should be done using ion beams instead of electron beams.

References

1) T. Agematsu and H. Hanaya, JAEA Annual Report 2005, 183 (2006).
2) H. Hanaya and T. Agematsu, JAEA Annual Report 2005, 184 (2006).

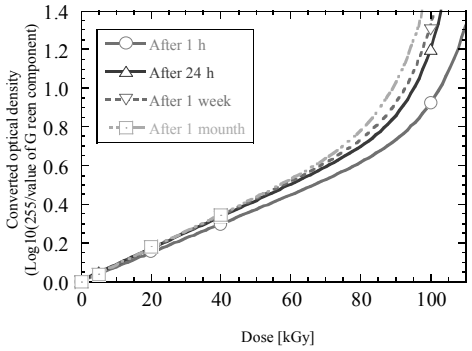

a) B3 film dosimeters kept in the aluminum package.

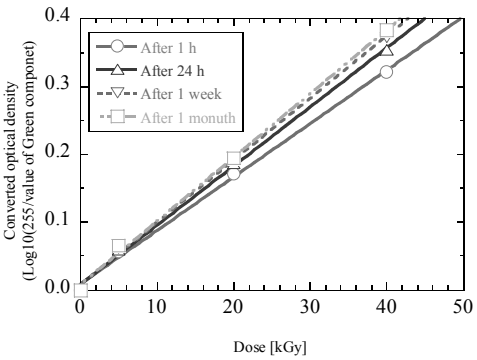

b) B3 film dosimeters not kept in the aluminum package.

Fig.1 The dose response of B3 film dosimeters for 2MV electron beams when readout using the image scanner with Green color component.

4-56 Properties of Radiochromic Film Dosimeters for Low Energy Electron Beam

H. Seito [a)], T. Kojima [a)], T. Takei [b)], T. Ide [b)] and I. Mori [b)]

[a)]Department of Advanced Radiation Technology, TARRI, JAEA, [b)]IWASAKI ELECTRIC Co., Ltd

Introduction

Application of low energy electron accelerators (50-300 keV) is expanding in the field of radiation processing. Radiochromic film dosimeters have been used widely both in the industrial processes and research employing gamma-rays and electron beams[1)]. These dosimeters have been calibrated commonly only for cobalt-60 gamma-rays, therefore the feasibility of this calibration should be studied also for their application to low energy electron beams.

Experimental

Two different radiochromic dosimeters were used in this study. One is nylon-based FWT60[2)] with thickness of 10 μm, containing hexahydroxyethyl pararosaniline cyanide as the radiation-sensitive component. Another is GEX B3 radiochromic film dosimeter[3)]. The B3 radiochromic dosimeter contains a radiochromic dye precursor of pararosaniline cyanide dissolved in polyvinyl butyral. Fundamental properties of these dosimeters were studied preliminalily for gamma-rays. The gamma-ray irradiation was carried out using a ^{60}Co plaque source (2.6 PBq) at a dose rate of 10 kGy/h, which was measured with the ionization chamber periodically calibrated at AIST. Optical density was measured using Hitachi spectrophotometer model U-3310. Wavelength of 600 nm and 554 nm is used for dose measurement of FWT60 and B3, respectively.

Results and discussion

Response curves of the two different dosimeters are shown in Fig.1. The dose response of FWT60 is larger than that of B3. The response curve of FWT60 is nearly linear with dose up to 30 kGy and become sublinear at higher doses, on the other hand, that of B3 is nearly linear with dose up to 60 kGy.

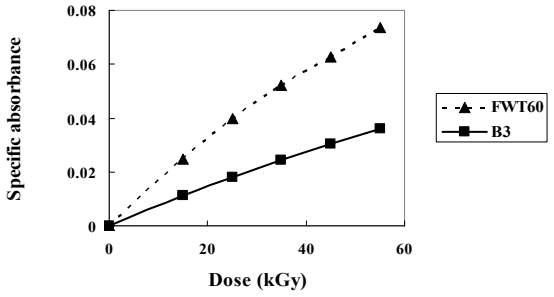

Fig.1 Dose response curves of FWT-60 and B3

The stability of absorbance is studied both for FWT60 and B3 after irradiation to doses of 15、25、35、45、and 55 kGy, for 1 month. The variation of absorption occurred after irradiation is less than 2% for both dosimeters showing long shelf-life stability.

These results should be a base for application of these radiochromic dosimeters to low energy electron beams.

References

1) ISO/ASTM 51275 (2004) Standard Practice for Use of a Radiochromic Film Dosimetry System
2) A. Miller , Riso-M-2401. (1983)
3) A. Miller et al., Radiat. Phys. Chem. 31 (1988) 491

4-57 Standard Dosimetry of a few MeV Electron and ^{60}Co Gamma-ray in Radiation Processing

H. Seito , T. Kojima , H. Kaneko and N. Haneda

Department of Advanced Radiation Technology, TARRI, JAEA

Introduction

The high-dose calibration technique using a parallel-plate ionization chamber system has been developed in the JAEA dose calibration facility[1]. The facility equips two ^{60}Co γ -ray plaque sources covering wide dose-rate range of 5-20000 Gy/h which have overlapping dose-rate region with that at the National Institute of Advanced Industrial Science and Technology (AIST), the national standard dosimetry laboratory in Japan. Consistency of dose calibration results at JAEA and those at AIST was verified without additional correction regarding to difference in characteristics of radiation fields involving current/exposure-rate conversion coefficients given in the dose rate level of 10-100 Gy/h at the AIST and high-dose rates of 5-20000 Gy/h at JAEA.

Results and discussion on dose intercomparison

The uncertainty associated with the established standard dose measurement procedure in JAEA has been reviewed. The total uncertainty in ^{60}Co gamma-ray absorbed dose delivered by the JAEA calibration system is evaluated to be 2.2%(2 σ). The uncertainty of dose measurement using JAEA alanine/ESR transfer dosimeters is also estimated to be 3.4%(2 σ) for ^{60}Co gamma-ray irradiation. A dose intercomparison study in the dose range of 1-50 kGy was carried out with National Physical Laboratory (NPL) to confirm our estimated uncertainty, employing transfer dosimeters: alanine dosimeters and dichromate dosimeters[2]. The results of dose intercomparison between JAEA and NPL show good agreement within about 2% in the dose range of 1-50 kGy. The results assure the uncertainties in gamma-ray

absorbed dose measurement at JAEA using parallel-plate ionization chamber as a working reference dosimeter and alanine dosimeters as reference transfer dosimeters.

Dose comparison was performed for 2-MeV electrons employing cellulose triacetate (CTA) and alanine film dosimeters which were independently calibrated for 2-MeV electrons and ^{60}Co gamma-rays using the calorimeter and the ionization chamber systems respectively[3]. Agreement of two different dose evaluations was better than 2.0% (1 σ) as shown in Fig 1. These results should enable us to achieve highly reliable dosimetry for the quality assurance in electron radiation processing on the basis of gamma-ray dose standards.

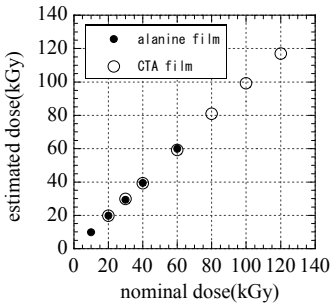

Fig.1 Correspondence of electron dose evaluation (nominal dose) with gamma-ray dose evaluation (estimated dose)

References

1) T. Kojima, H. Tachibana, N. Haneda, H. Kaneko, Y. Haruyama and R. Tanaka, RADIOISOTOPES 50 (2001) 291

2) T. Kojima, H. Tachibana, N. Haneda, I. Kawashima and P.H.G. Sharpe, Radiat.Phys.Chem 54 (1999) 619

3) T. Kojima, H. Sunaga, and R. Tanaka, IAEA-CSP-18/CD IAEA-SM-365/56, (2003) 216

This is a blank page.

5 Status of Irradiation Facilities 2006

This is a blank page.

5-01 Safety Measures, Utilization Status and Spread of Research Results at TIARA Facility

Y. Nakamura, K. Nishimura, H. Takizawa, M. Hosono, H. Kaneko, H. Watanabe, H. Tachibana, S. Kaneya, S, Mochizuki, M. Kawabata, M. Iijima and K. Daikubara

Department of Advanced Radiation Technology, TARRI, JAEA

Periodical inspections per every month and three months were performed surely and safety of the facility was also maintained certainly[1]. Several safety measures in the TIARA facility, such as the injection of sealing material to repair the cracked surface on the side wall of the building where leaking of rain sometimes occurred, the repair of cracked concrete surface on the higher ceiling and the exchange of ceiling fluorescent lamps in the second target room, the exchange of batteries in the emergency lamps, and so on, were carried out. Furthermore, a safety handrail on the roof and supplementary garden lights along a narrow walking trail as shown in Photo. 1 were also installed.

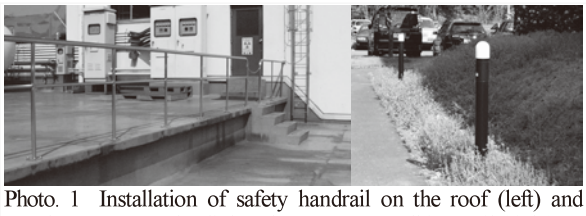

Photo. 1 Installation of safety handrail on the roof (left) and supplementary garden lights along narrow walking trail (right).

The shifts of utilization time of cyclotron and electrostatic accelerators assigned to the respective research fields are shown in Fig. 1 and Fig. 2. For recent 9 years, the total utilization time of cyclotron was constantly about 2500 h after it was about 2800 h for initial 5 years since 1993. However in fact, operation time of the cyclotron for above period was increased slightly to compensate time losses because the efficiency of the utilization gradually deteriorated by the frequent alteration of the operation condition. On the other hand, especially in 2006, utilization time of three electrostatic accelerators increased remarkably up to 491 days because of the increase of common use, although it was 440-460 days per year since 1995.

In regard to new utilization system introduced from last year, some issues were also improved. The application forms for research subjects and experimental planning was treated by an "electronic application system" which was newly

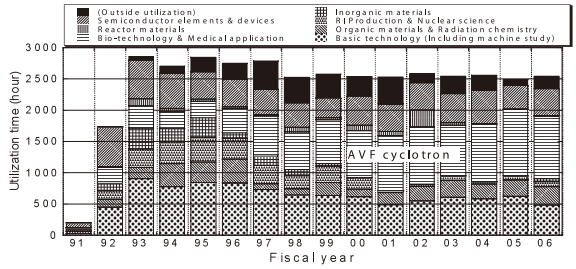

Fig. 1 Shift of utilization time of cyclotron assigned to the respective research fields since 1991.

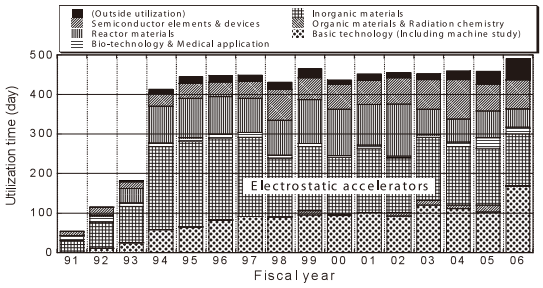

Fig. 2 Shift of utilization time of electrostatic accelerators assigned to the respective research fields since 1991.

constructed. The number of times for the application to research subjects per year was changed to once from twice. The designed percentage for internal, common and effective use in whole utilization frame was unified to 70:20:10 comprehensively for 4 accelerators.

The ratio of allotment time to application one for the first half period through 2007 was estimated to be 0.454 and 0.410 for cyclotron and electrostatic accelerators, respectively, which were the worst values so far because of the propose of reduction of appropriation. Actually, proposed budget was replenished rather enough after the allotment of utilization time. Therefore, utilization time for 2007 will be recovered to normal state.

The works for utilization and usher's window were smoothly performed similarly to past years. The average number of persons for one month was 49.3 (58.4 for last three years) for staying, 52.5 (41.7) for the loan of glass budge and ID card, 41.9 (38.3) for the reception of facility utilization, 179 (115) for the short term visitors in TIARA facility, and so on.

The first Takasaki Advanced Radiation Research Symposium instead of the former TIARA Research Review Meeting was held successfully on June 22-23 at Takasaki city gallery. The number of presentations for oral and poster sessions was 21 and 158, respectively. Participants to this symposium were 412, which increased 85 persons compared to last meeting.

In addition, the JAEA Takasaki annual report 2005 was also issued firstly instead of TIARA annual report. This annual report summarized research results and activities which were done during fiscal year 2005 at Takasaki Advanced Radiation Research Institute. This report consists of 240 pages including several coloured sheets, and was printed as 700 books.

Electric power saving in TIARA facility during the "golden week" in Japan was achieved by the complete stop of large devices and equipments similar to a few past years.

Reference

1) Y. Nakamura et al., JAEA Takasaki annual report 2005 (2006) 195

5-02 Operation of AVF Cyclotron

T. Nara [a)], T. Agematsu [a)], I. Ishibori [a)], S. Kurashima [a)], K. Yoshida [a)], T. Yuyama [a)], T.Ishizaka [a)], S. Okumura [a)], N. Miyawaki [a)], H. Kashiwagi [a)], Y. Yuri [a)], W. Yokota [a)], K. Akaiwa [b)], To. Yoshida [b)], S. Ishiro [b)], Y. Arakawa [b)], Tu. Yoshida [b)], S. Kanou [b)], A. Ihara [b)] and K. Takano [b)]

[a)] Department of Advanced Radiation Technology, TARRI, JAEA. [b)] Beam Operation Service, Co., Ltd.

Operation

The AVF cyclotron was smoothly operated in fiscal 2006 and all the planned experiments were carried out without cancellation due to troubles relating to the cyclotron. The operation condition of the cyclotron is frequently changed because many kinds of ion species are required for the research in materials science and biotechnology with short irradiation time around an hour. Therefore the number of annual experiments reached 840. Table 1 shows the statistics for the cyclotron operation. The total operation time amounts to 3459.2 hours which is the longest so far.

Table 1. Statistics for cyclotron operation in fiscal 2006.

Beam service time	2715.3 hr
Machine tuning	693.0 hr
Beam development	50.9 hr
Total operation time	3459.2 hr
Change of particle and/or energy	247 times
Change of beam course	370 times
Change of harmonic number	69 times
The number of experiments	840
Experiment canceled due to machine trouble	0

The percentages of operation time of the year used for experiments, joint-use, machine tuning, and beam development are 72.8%, 5.7%, 20.0%, and 1.5%, respectively.

A multi-cusp ion source used to produce hydrogen ions. In the case of production of ions heavier than He, two ECR ion sources are used alternatively. Table 2 shows the ratios of operation time of each ion source. Figure 1 shows popularity of major ions used for experiments. The tendency of those statistics is similar to that of the past years.

Table 2. Operation times of ion sources.

Ion source	Operation time	Ratio
Multi-cusp	1027.2 hr	26.7%
ECR (OCTOPUS)	1826.7 hr	47.5%
ECR (HYPERNANOGAN)	991.5 hr	25.8%

Maintenance

The number of the troubles of the year was 324, and they were quickly repaired without cancellation of experiments.

The regular yearly overhaul was carried out for five weeks in summer. About two hundreds of the rubber hoses which deteriorated in a high temperature and radiation environment for more than 15 years were renewed. The internal seals of about four hundreds Vebeo joints which were used for copper pipes of the trim-coils were replaced because cracks were found on a number of the seals.

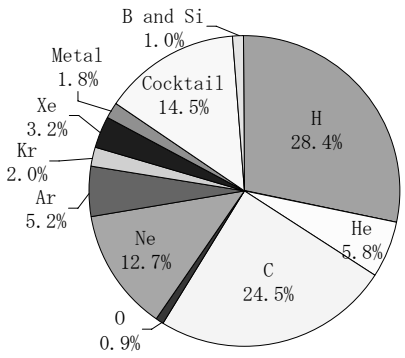

Fig. 1 Major ion species used in fiscal 2006.

The routine maintenance of power supplies for a week in autumn Most current power supplies were modified to maintain good performance for the next reason. A DAC amplifier of a current feedback control circuit in each power supply was enclosed in a constant-temperature box heated to 50℃ by a thermostat-controlled oven for high current stability. However, breakdown of some parts in the DAC amplifier was increasing, and it was found that this temperature hastened deterioration of the parts. Therefore, the temperature has been changed to 25℃ which is kept by a Peltier device. The stability of intensity and position of beam has been improved as a result, which helps to shorten the time of beam tuning for the microbeam formation.

Technical development

The beam acceleration tests were successfully carried out for 14 MeV H^+, 39 MeV $^{28}Si^{10+}$ and 60MeV $^{11}B^{3+}$, and they are ready to be used for experiments.

The development of a multipole magnets system for uniform-irradiation has been started. It allows exactly simultaneous beam irradiation over a wide area at high uniformity[1)], which is impossible by means of raster scanning of a spot beam.

The main beam-probe of the cyclotron has been modified to measure a beam phase width using a plastic scintillator and a test experiment was successfully done.

Reference

1) Y. Yuri et al., Proc. 3rd Annual Meeting of Particle Accelerator Society of Japan 31st Linear Accelerator Meeting in Japan, (2006) 913.

5-03 Operation of the Electrostatic Accelerators

K. Mizuhashi [a)], S. Uno [a)], K. Ohkoshi [a)], A. Chiba [a)], K. Yamada [a)], Y. Saitoh [a)], Y. Ishii [a)], T. Satoh [a)], W. Yokota [a)], T. Kitano [b)], T. Takayama [b)], T. Orimo [b)], S. Kanai [b)], A. Ohmae [b)], M. Kouka [b)] and Y. Aoki [b)]

[a)]Department of Advanced Radiation Technology, TARRI, JAEA, [b)]Beam Operation Service, Co., Ltd

1. Status of electrostatic accelerators

Three electrostatic accelerators of the TIARA facility operated smoothly in fiscal 2006 and all the planned experiments were carried out, except those canceled by users. The operating times of the tandem accelerator, the single-ended accelerator and the ion implanter were 1959.6, 2498.6 and 1898.9 hours respectively. These are almost same as the past years but the number of operating day increased. The total operating times since operation started are 24821, 29585 and 23226 hours, respectively. Figure 1 shows the total time of each accelerator from 1991 to 2006.

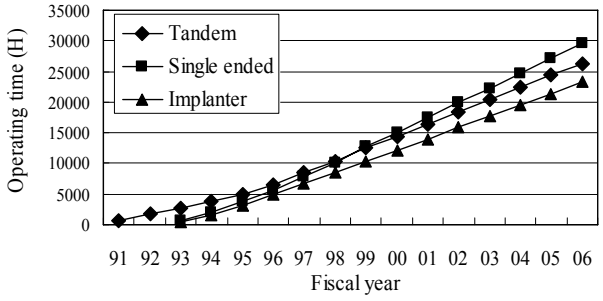

Fig.1 Total operating time of each accelerator since operation started

The number of the troubles was small compared with the past years. The troubles of the year are characterized by the failure of condensers. Many condensers are used in the power supplies and the computers of the accelerator system. A lifetime of a condenser is generally about 10 years, but most of power supplies of the TIARA facility are used over 15 years. Main troubles of condenser are as follows. The condensers used in the computers of the tandem accelerator control system for seven years failed and a number of the abnormal condensers were found in three of six control computers. The single-end accelerator was stopped for two days since the condenser of the RC oscillation circuit for the RF ion source was shorted. All the lost beam time due to the troubles was compensated in the year.

2. Improvement for the accelerators

The sliding mechanism for one of a couple of the chain motors of the tandem accelerator, which give constant tension to the pellet chain, was modified to move more lightly. This drastically reduced the dust production by the chain rotation at high speed [1)], and the ripple of the high voltage terminal attributed to the chain vibration lowered by about 20% due to better stability of the chain rotation. As to single-ended accelerator, the damage of the plastic electric insulation support for the RF-electrode frequently occurred because of the heating by the electric discharge occurred at the bubble parts in the support. In order to prevent the damage, the supports made of polypropylene were replaced with those of polycarbonate after checking that they had no bubbles by eyes through their transparency.

The cluster ions of C and Au are accelerated by the tandem accelerator, but most (more than 90%) of clusters are broken up by the collision with the charge exchange gas N_2. Therefore, the gas stripper system was modified so as to measure the charge exchange efficiency for various gas species. The results of the measurement indicate that a gas with a larger molecular weight gives the higher charge exchange efficiency [2)].

3. New beam development

As to the ion implanter, the Ge ion, which was requested by the users of the inorganic functional material research, was newly accelerated. It is difficult to stably generate ions of a low melting-point material, such as Ge, with a Freeman ion source because it easily runs from the material holder. Therefore, the holder has been modified so that the short of the arc circuit by the melted material and its loss should not take place. Stable Ge ion beam was successfully generated as a result and about 5μA was accelerated.

References

1) K.Mizuhashi,et al.,JAEA Takasaki Annual Report 2005(2006)197
2) K.Ohkoshi,et al.,JAEA Takasaki Annual Report 2005(2006)192

5-04 Radiation Control in TIARA

T. Seki, T. Tsujimoto and K. Ida

Department of Administrative Services, TARRI, JAEA

1 Individual monitoring

(1) Individual monitoring for the radiation workers

Table 1 shows a distribution of effective dose of the radiation workers in FY 2006. The effective dose values of almost all radiation workers were below the detection limit (0.1 mSv).

The maximum dose was 0.6 mSv/y due to the overhaul of the TIARA AVF cyclotron.

Table 1. Distributions of the effective dose of the radiation workers in FY 2006.

Items \ persons		Number of persons in each periods				Total
		1st quarter	2nd quarter	3rd quarter	4th quarter	
Distribution range of effective dose HE:Effective dose *1 (mSv)	HE < 0.1	512	553	542	567	631
	0.1 ≦ HE ≦ 1.0	0	8	2	0	9
	1.0 < HE ≦ 5.0	0	0	0	0	0
	5.0 < HE ≦ 15.0	0	0	0	0	0
	15.0 < HE	0	0	0	0	0
Number of persons under radiation control (A)		512	561	544	567	640
Exposure above 1mSv	Number of persons (B)	0	0	0	0	0
	(B)/(A)×100(%)	0	0	0	0	0
Mass effective dose (Person・mSv)		0.0	2.2	0.3	0.0	2.5
Mean dose (mSv)		0.00	0.00	0.00	0.00	0.00
Maximum dose (mSv)		0	0.6	0.2	0	0.6

*1 Not detected according to internal exposure.

(2) Individual monitoring for the visitors and others

Table 2 shows number of persons who temporally entered the radiation controlled areas. The effective dose of all persons was less than 0.1 mSv.

Table 2. Number of persons who temporary entered the radiation controlled areas in FY 2006.

Periods	1st quarter	2nd quarter	3rd quarter	4th quarter	Total
Number of persons	425	545	622	491	2083

2 Monitoring of radioactive gas and dust

Table 3 shows the maximum radioactive concentrations and total activities for radioactive gases released from the stack of TIARA, during each quarter of FY 2006.

Small amount of ^{41}Ar, ^{11}C, ^{13}N, ^{18}F, ^{77}Kr and ^{133}Xe were detected for some time during operation of the cyclotron or experiment, but the pulverized substances (^{65}Zn, etc.) were not detected.

Table 3. Monitoring results of released radioactive gases and dust in FY 2006.

Nuclide	Items \ Periods	1st quarter	2nd quarter	3rd quarter	4th quarter	Total
^{41}Ar	Maximum concentration (Bq/cm^3)	$<1.4\times10^{-4}$	1.4×10^{-4}	$<1.5\times10^{-4}$	1.8×10^{-4}	1.8×10^{-4}
	Activity (Bq)	1.2×10^{8}	3.8×10^{8}	1.7×10^{8}	8.6×10^{8}	1.5×10^{9}
^{11}C	Maximum concentration (Bq/cm^3)	$<1.4\times10^{-4}$	$<1.4\times10^{-4}$	$<1.5\times10^{-4}$	$<1.5\times10^{-4}$	$<1.5\times10^{-4}$
	Activity (Bq)	5.9×10^{8}	1.8×10^{8}	1.5×10^{8}	1.2×10^{8}	1.0×10^{9}
^{13}N	Maximum concentration (Bq/cm^3)	——	——	——	$<1.5\times10^{-4}$	$<1.5\times10^{-4}$
	Activity (Bq)	——	——	——	2.3×10^{7}	2.3×10^{7}
^{18}F	Maximum concentration (Bq/cm^3)	——	——	——	$<1.5\times10^{-4}$	$<1.5\times10^{-4}$
	Activity (Bq)	——	——	——	4.1×10^{7}	4.1×10^{7}
^{77}Kr	Maximum concentration (Bq/cm^3)	$<1.4\times10^{-4}$	——	$<1.5\times10^{-4}$	$<1.5\times10^{-4}$	$<1.5\times10^{-4}$
	Activity (Bq)	8.6×10^{6}	——	7.1×10^{7}	1.3×10^{7}	9.3×10^{7}
^{133}Xe	Maximum concentration (Bq/cm^3)	——	$<1.4\times10^{-4}$	——	$<1.5\times10^{-4}$	$<1.5\times10^{-4}$
	Activity (Bq)	——	1.3×10^{7}	——	2.8×10^{6}	1.6×10^{7}
^{65}Zn	Maximum concentration (Bq/cm^3)	$<5.1\times10^{-10}$	$<6.3\times10^{-10}$	$<6.7\times10^{-10}$	$<6.3\times10^{-10}$	$<6.7\times10^{-10}$
	Activity (Bq)	0	0	0	0	0

3 Monitoring for external radiation and surface contamination

External radiation monitoring was routinely carried out in/around the radiation controlled areas and surface contamination monitoring was also carried out. Neither unusual value of dose equivalent rate nor surface contamination were detected.

Figure 1 shows a typical example of distribution of the dose equivalent rate at the radiation controlled area in the cyclotron building.

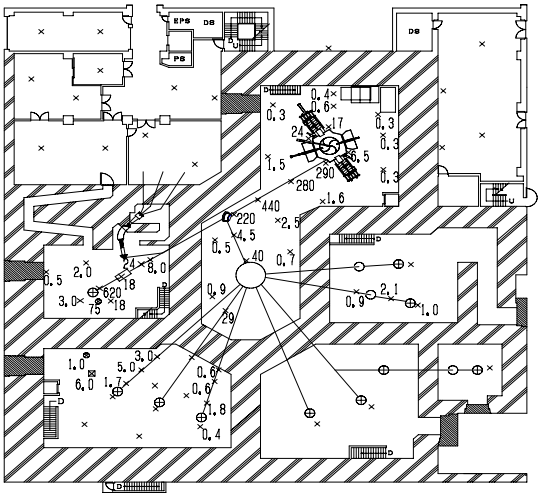

Fig.1. Dose equivalent rate distribution at the radiation controlled area in the cyclotron building.
Measurement date : 27th March 2007
Measuring position : Indicated with × 1m above floor
Unit : μ Sv/h (the dose equivalent rate less than 0.2 μ Sv/h is not indicated)

5-05 Radioactive Waste Management in TIARA

J. Yoshii and N. Higuchi

Department of Administrative Services, TARRI, JAEA

1. The radioactive wastes management

The radioactive wastes generated in TIARA are managed by Utilities and Maintenance Section. The main radioactive wastes are the solid wastes generated by the research experiment and the maintenance of the cyclotron. Other radioactive wastes are the liquid wastes such as inorganic waste fluids generated from the research experiment and the air-conditioning machines in controlled area. These wastes are managed according to properties.

2. Solid radioactive waste

Table 1 shows the amounts of solid wastes at various properties and kinds generated in each quarter of FY 2006. The main solid waste is generated by the research experiment and the maintenance of the cyclotron.

Combustible wastes are rubber gloves, paper, and clothes, etc. Incombustible wastes are metal pieces, the glasses, and contaminated parts.

3. Liquid radioactive waste

Table 2 shows the amounts of liquid wastes generated in each quarter of FY 2006. Liquid waste was almost inorganic waste water generated with chemical experiments and operation of air conditioning units installed in each room of the first class radiation controlled area. Larger quantity of waste water in summer season (2nd quarter) is mainly due to condensed water, which is treated by evaporation, and inorganic water is reused in the controlled area. Only small amounts of concentrated liquid are generated by the evaporation.

Table 1. Radioactive solid wastes generated in FY 2006.

Amounts / Items	Amounts of generation in each periods (m^3)					Number of package /drum
	1st quarter	2nd quarter	3rd quarter	4th quarter	Total	
Category A*	0.38	0.44	0.28	0.38	2.73	
1)Combustible	0.30	0.44	0.40	0.48	1.40	9**
2)Incombustible	0.08	0	0.14	1.11	1.33	0
Compressible	0.08	0	0.14	0.24	0.46	3**
Filters	0	0	0	0.87	0.87	0
Incompressible	0	0	0	0	0	0
Ion exchange resin	0	0	0	0	0	0
Category B*	0	0	0	0	0	0

* defined by dose at the outer surface of container : (A) ＜ 2 mSv/h ≦ (B)

** 200-liter drum

Table 2. Radioactive liquid waste generated in FY 2006.

Amounts / Items	Amounts of generation in each periods (m^3)					Number of package /drum
	1st quarter	2nd quarter	3rd quarter	4th quarter	Total	
Category A*	10.42	16.90	6.08	8.60	42.00	
1)Inorganic	10.42	16.90	6.08	8.40	41.80	treatment
2)Organic	0	0	0	0	0	0
Organic	0	0	0	0	0	0
Oil	0	0	0	0	0	0
3)Sludge	0	0	0	0.10	0.10	1
4)Evaporation residue	0	0	0	0.10	0.10	1
Category B*	0	0	0	0	0	0

* defined by concentrations in Bq/cm^3(β , γ) : (A) ＜ 3.7×10 ≦ (B) ＜ 3.7×10^4

5-06 Utilization of the Electron Accelerator and Gamma-ray Irradiation Facilities

T. Kojima [a)], H. Kaneko [a)], N. Haneda [a)], H. Hanaya [a)], R. Yamagata [a)], H. Seito [a)], T. Kanazawa [a)], S. Koyama [b)], T. Yamaguchi [b)], I. Kawashima [b)], N. Yagi [b)] and M. Takagi [b)]

[a)] Department of Advanced Radiation Technology, TARRI, JAEA ,
[b)] Radiation Application Development Association, RADA

1. Present status of the utilization of electron accelerator and gamma-ray irradiation facilities

An electron accelerator and three gamma ray irradiation facilities were operated for various research subjects as operation plan in FY 2006 without serious trouble. Distribution of research fields and number of experiment subjects are shown in Fig.1 and Fig.2, respectively. The number of research subjects for the electron accelerator, the cobalt first facility, the cobalt second facility, and the food irradiation facility, is 544, 159, 622, and 357, respectively. Those for gamma-ray irradiation facilities in FY 2006 are lower than those in FY 2005, while it shows the increase of longer-time irradiation for radiation-resistance tests of materials and apparatus used in nuclear power plants or space.

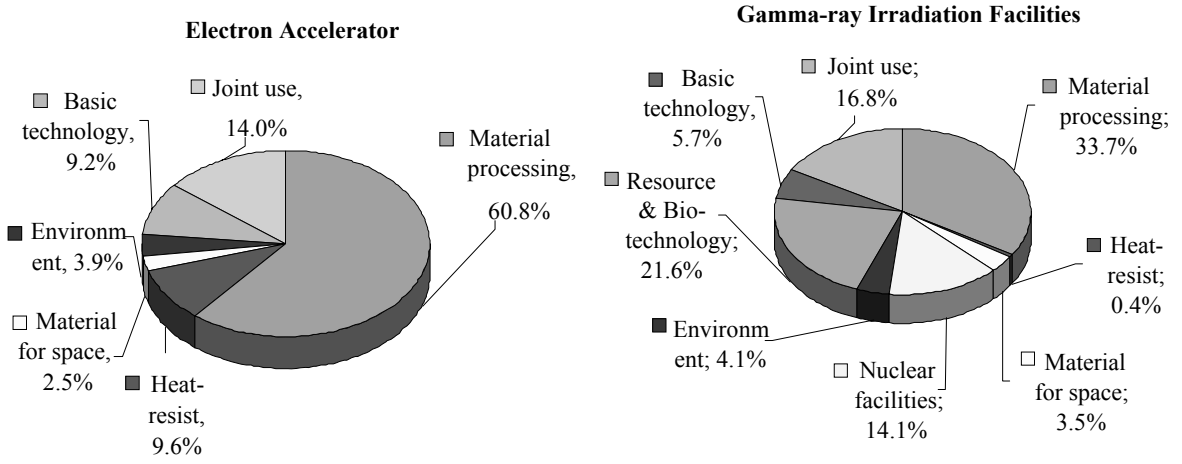

Fig.1 Distribution of research fields (FY 2006).

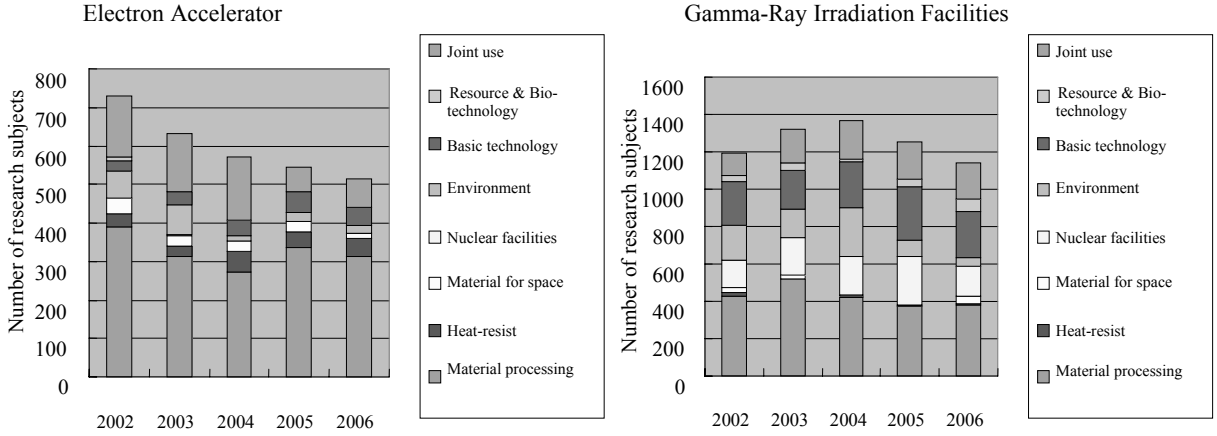

Fig.2 Number of research subjects (FY 2002-2006).

5-07 Operation of the Electron Accelerators and Gamma-ray Irradiation Facilities

H. Kaneko [a)], H. Hanaya [a)], N. Haneda [a)], R. Yamagata [a)], H. Seito [a)], T. Kanazawa [a)], T.Kojima [a)], S.Koyama [b)], T. Yamaguchi [b)], I. Kawashima [b)], N. Yagi [b)] and M. Takagi [b)]

[a)]Department of Advanced Radiation Technology, TARRI, JAEA ,[b)]Radiation Application Development Association , RADA

1. Operation

1.1 Electron accelerator

The electron accelerator was on service without serious trouble in 9:00～17:30 on Monday and Friday, and in 8:30～23:00on Tuesday to Thursday, to satisfy demand of operation time from users.

The annual operation time for the electron accelerator, as shown in Fig.1, is 597.4 h (517 h for vertical beams, 80.4 h for horizontal beams) . That for the accelerator No.2 operated until 2004 is also shown in Fig.1. Total operation time of the accelerator No.1 in FY2006 is about 30 % lower than that in FY2005, but the number of research subject in FY2006 is the same as that in FY2005 indicating the increase of short time irradiation experiments. The accelerator served mainly for graft-polymerization for new material development, radiation effect study on semiconductors, and various experiments of visiting users.

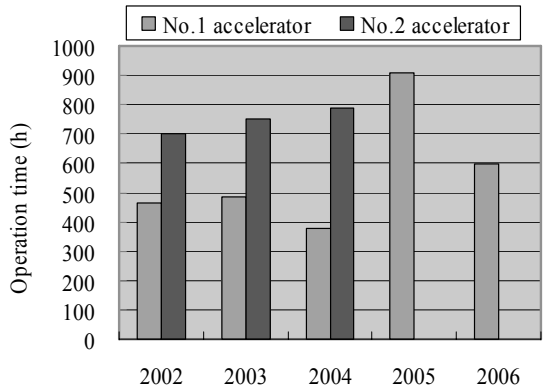

Fig.1 Sift of annual operation time of electron accelerators

1.2 Gamma-ray irradiation facilities

The Co-60 gamma-ray irradiation facilities consist of three buildings (8 rooms) and cover a wide dose-rate range from 0.04 Gy/h to 20 kGy/h with eight irradiation cells. The annual operation time for the cobalt first, second irradiation facilities and food irradiation facility is 20,844 h, 6,335 h and 3,150 h, respectively, as shown in Fig.2.

The first irradiation facility served mainly for radiation-resistance testing of cables used in nuclear power plants and various materials used in J-PARC facility with long irradiation period. The second irradiation facility served mainly

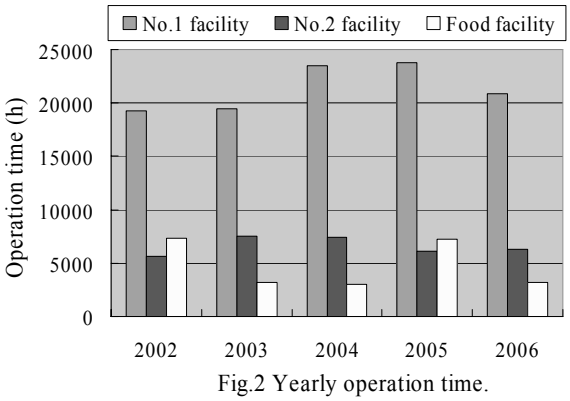

Fig.2 Yearly operation time.

Fig.2 Sift of annual operation of ^{60}Co gamma-ray irradiation facilitiestime

for development of new functional materials and other research subjects of visiting users, involving irradiation room No.6 operated as hourly scheduled. The food irradiation facility served mainly for development of detection method for irradiated foods and radiation resistance testing at lower dose rates.

2. Maintenance

2.1 Electron accelerator

The operation of the accelerator was interrupted for 10 days in October, 2006 and 5 days in March 2007 because of periodical maintenance check of accelerator body and incidental equipment, e.g. conveyor and doors of irradiation room and repair of current measurement system at the horizontal beam line.

2.2 Gamma-ray irradiation facilities

The periodical maintenance check mainly of mechanical system for radiation source transportation has been performed every three year among three gamma-ray irradiation facilities one by one. The periodical check mainly of interlock system has been performed two times a year for all the facilities.

The maintenance check of the cobalt first irradiation facility was done in July 2006, with 18 days interruption. The control system for the cobalt second irradiation facility was 18 years old and therefore waiting for replacement of the sequencer for operation.

Co-60 sources were purchased and loaded to the irradiation room No.6 in the second irradiation facility to maintain total activities of the room. The old waste sources of about 30 pieces were disposed through JRIA.

5-08 COMMON USE PROGRAM in Takasaki

M. Otsubo , M. Hoto and R. Suzuki

Department of Advanced Radiation Technology, TARRI, JAEA

1. Introduction

The facilities of JAEA is widely opened to users like from universities, public institutes, and the industries, etc. COMMON USE PROGRAM, the system of facility use for the user's purpose on fee-charging basis, started since 2006 taking over the former system. There are 3 OPEN USE facilities in Takasaki; Co-60 Gamma-ray Irradiation Facilities, Electron Accelerator and TIARA. In addition to these, some of the off-line devices can be used.

We round up the Research Proposals dividing one year into two terms, and the execution possibility and the validity of the experimental plan are checked by the special committee. The facility usage fee will be the total of the admission fee, irradiation fee and additional charge. In case of Non-proprietary research, the users must report the irradiation result to JAEA, and could be exempt from irradiation fee. JAEA will open the reports to the public. It is also possible for universities to apply from the facility use program of Tokyo University. Those applications are accepted as priority case. Table.1 shows the outline of the program.

Table.1 Classification of COMMON USE PROGRAM

purpose	research and development			except R&D
classify-cation	general		priority case	commercial
result	Non-proprietary	proprietary		
applica-tion	regular& irregular	regular	irregular	irregular
referee	yes	no		
charge*	A	B		C

*A= admission fee + additional charge
B= admission fee + irradiation fee + additional charge
C= admission fee + irradiation fee + depreciation

2. Public relations

The information like an outline of this system, guidelines for applicants, format download, etc can be seen on JAEA website(http://www3.tokai-sc.jaea.go.jp/sangaku/3-facility/index.html). In addition to this, we go out for publicity and to search current needs of the outside of JAEA. In 2006, we participated in 15th Polymer Material Forum(Osaka),Seminar for advancement of RI/radiation use(Nagoya), Opening Symposium of Center for Flexible Micro machining(Tokyo), and so on.

3. Use in 2006

There were 28 Research Proposals in 2006 at Takasaki, and 16 of all hoped to use with open result. Including the users from priority case, we accepted 325 applications from 54 users and half of the users were new. We can find that the percentage of users from universities exceeds the others except Co-60 Facility from Table.2. However we expect there should be latent needs in the industries. Therefore we are trying to find them by the public relations as above-mentioned and also going to start another new system.

Figure.1 shows classification of all 325 applications. On TIARA, Non-proprietary use represents more than 50%, while Co-60 Facility and Electron Accelerator have a few%. This tendency may come from the user's affiliation.

Table.2 User's affiliation of each facility

Facility \ User		University	Public Institute	Others	Total
TIARA	AVF Cyclotron	5	2	3	10
	3MV Tandem Accelerator	3	0	2	5
	3MV Single-ended Accelerator	1	0	0	1
	400kV Ion Implanter	6	0	1	7
Co-60 Gamma-ray Irradiation Facility		5	0	12	17
Electron Accelerator		8	0	6	14
Total		28	2	24	54

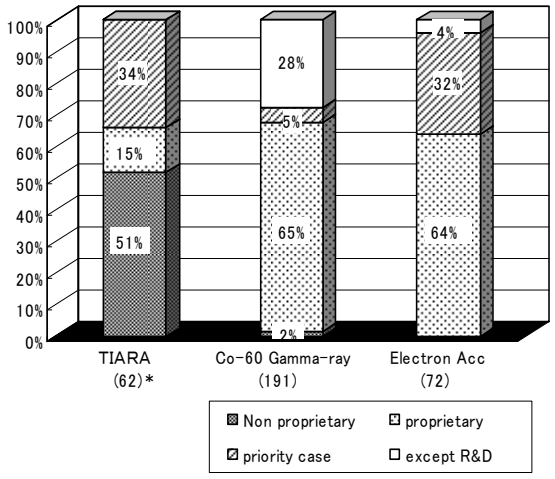

Fig.1 Percentage of each classification
* the number of application

Appendix

This is a blank page.

Appendix 1. List of Publication

A1.1 Publications in Journal

06J001 1-06 I

F. Takano, W. Wang, H. Akinaga, H Ofuchi,
S. Hishiki and T. Ohshima,
"Characterization of Mn-doped 3C-SiC prepared by ion implantation"
J. Appl. Phys., 101 (2007) 09N510.

06J002 1-06 E

G. Pensl, F. Schmid, S. A. Reshanov, H. B. Weber, M. Bockstedte, A. Mattausch, O. Pankratov, T. Ohshima and H. Itoh,
"(Nitrogen-Vacancy)-Complex Formation in SiC: Experiment and Theory"
Materi. Sci. Forum., 556-557 (2007) 307-310.

06J003 1-06 I , G

K. K. Lee, M. Laube, T. Ohshima, H. Itoh and G. Pensl,
"Hall Effect and Admittance Measurements of n-channel 6H-SiC MOSFETs"
Materi. Sci. Forum., 556-557 (2007) 791-794.

06J004 1-06 T, I

T. Ohshima, T. Satoh, M. Oikawa, S. Onoda,
S. Hishiki, T. Hirao, T. Kamiya, T. Yokoyama,
A. Sakamoto, R. Tanaka, I Nakano, G. Wagner, and H. Itoh,
"Degradation of Charge Collection Efficiency Obtained for 6H-SiC n+p Diodes Irradiated with Gold Ions"
Materi. Sci. Forum., 556-557 (2007) 913-916.

06J005 1-06 T , I

T. Ohshima, T. Satoh, M. Oikawa, S. Onoda, T. Hirao and H. Itoh,
"Charge Induced in 6H-SiC PN Diodes by Irradiation of Oxygen Ion Microbeams"
Materi. Sci. Forum., 527-529 (2006) 1347-1350.

06J006 1-06 E

F. Schmid, S. A. Reshanov, H. B. Weber, G. Pensl, M. Bockstedte, A. Mattausch, O. Pankratov, T. Ohshima and H. Itoh,
"Deactivation of nitrogen donors in silicon carbide"
Phys. Rev., B 74 (2006) 245212.

06J007 1-06 I, S

S. Kuroda, S. Marcet, E. Bellet-Amalric, J. Cibert, H. Mariette, S. Yamamoto, T. Sakai, T. Ohshima and H. Itoh,
"Structural Analysis of (Ga,Mn)N Epilayers and Self-Organized Dots using MeV Ion Channeling"
Phys. Stattus. solidi (a) 203 (2006) 1724.

06J008 1-07 E

T. Umeda, J. Isoya, T. Ohshima, N. Morishita,
H. Itoh and A. Gali,
"Identification of positively charged carbon antisite-vacancy pairs in 4H-SiC"
Phys. Rev., B 75 (2007) 245202.

06J009 1-07 E

T. Umeda, N. Morishita, T. Ohshima, H. Itoh and J. Isoya,
"Electron paramagnetic resonance study of carbon antisite-vacancy pair in p-type 4H-SiC"
Materi. Sci. Forum., 556-557 (2007) 453-456.

06J010 1-07 T

J. Isoya, M. Katagiri, T. Umeda, N. T. Son,
A. Henry, E. Janzén, T. Ohshima and H. Itoh,
"Shallow phosphorus donors in 3C-, 4H-, and 6H-SiC"
Materi. Sci. Forum., 527-529 (2006) 593-596.

06J011 1-07 E TGE

T. Umeda, N. T. Son, J. Isoya, N. Morishita,
T. Ohshima, H. Itoh and E. Janzén,
"Electron paramagnetic resonance of the HEI4/SI5 center in 4H-SiC"
Materi. Sci. Forum., 527-529 (2006) 543-546.

06J012 1-07 E

N. T. Son, T. Umeda, J. Isoya, A. Gali, M. Bockstedte, B. Magunsson, A. Ellison, N. Morishita, T. Ohshima, H. Itoh and E. Janzén,
"Divacancy model for P6/P7 centers in 4H- and 6H-SiC"
Materi. Sci. Forum., 527-529 (2006) 527-530.

06J013 1-08 E

H. Matsuura, S. Kagamihara, Y. Itoh, T. Ohshima and H. Itoh,
"Mechanisms of reduction in hole concentration in Al-doped 4H-SiC by electron irradiation"
Microelectron. Eng., 83 (2006) 17.

06J014 1-08 E

H. Matsuura, S. Kagamihara, Y. Itoh, T. Ohshima and H. Itoh,
"Relationship between defects induced by irradiation and reduction of hole concentration in Al-doped 4H-SiC"
Physica B 376-377 (2006) 342.

06J015 1-09 O

Miyashita, T.Ohnuma, M.Iwasawa, H.Tsuchida and M.Yoshikawa,
"Generation of amorphous SiO2/SiC interface structure by the first-principles
molecular dynamics simulation"
Materi. Sci. Forum., 556-557 (2007) 521.

06J016 1-09 O

T.Ohnuma, A.Miyashita, M.Iwasawa, M.Yoshikawa and H.Tsuchida,
"Dynamical simulation of SiO2/4H-SiC(0001) interface oxidation process: from first-principles"
Materi. Sci. Forum., 556-557 (2007) 615.

06J017 1-10 I

H. Ofuchi, T. Nishiwaki, K. Takaba, K. Ogawa,
M. Tabuchi, Y. Takeda, A. Wakahara, A. Yoshida,
T. Ohshima and H. Itoh,
"Fluorescence EXAFS study on local structures around Eu atoms implanted in AlxGa1-xN"
Physica B 376-377 (2006) 496-498.

06J018 1-10 I

A. Wakahara
"IMPACT OF AlGaN ON LUMINESCENCE CAPABILITY OF RARE?EARTH IONS IN AlGaN"
Opt. Mater., Vol. 28, Issues 6-7 (2006) 731-737.

06J019 1-27 C, E, G

T. Yamaki, Y. Kozone, A. Hiroki, M. Asano, H. Kubota and M. Yoshida,
"Nano-structure controlled polymer electrolyte membranes for fuel cell applications prepared by ion beam irradiation"
ESC Transaction, 3 (2006) 103-112.

06J020 1-27 C, E, G

T. Yamaki, Y. Kozone, A. Hiroki, K. Hosoi, M. Asano, H. Kubota and M. Yoshida,
"Proton exchange membranes for fuel cell applications prepared by ion track technology"
Electrochemistry, 75, No. 2 (2007) 175-178.

06J021 1-28 E, G

J. Chen, M. Asano, Y. Maekawa and M. Yoshida,
"Suitability of some fluoropolymers used as base films for preparation of polymer electrolyte fuel cell membranes"
J. Membr. Sci., 277 (2006) 249-257.

06J022 1-28 E, G

J. Chen, M. Asano, T. Yamaki and M. Yoshida,
"Preparation and characterization of chemically stable polymer electrolyte membranes by radiation-induced copolymerization of four monomers into ETFE films"
J. Membr. Sci. 269(1-2) (2006) 194-204.

06J023 1-28 E, G

J. Chen, M. Asano, T. Yamaki and M. Yoshida,
"Chemical and radiation crosslinked polymer electrolyte membranes prepared from radiation-grafted ETFE films for DMFC applications"
J. Power Sources, 158 (2006) 69-77.

06J024 1-28 E, G

J. Chen, M. Asano, Y. Maekawa, T. Sakamura, H. Kubota and M. Yoshida,
"Preparation of ETFE-based fuel cell membranes by UV-induced photografting and electron beam-induced crosslinking techniques"
J. Membr. Sci., 283 (1-2) (2006) 373-379.

06J025 2-03 E

N. Ito, A. Mase, N. Seko, M. Tamada, E. Sakata and Y. Kogi,
"Surface Treatment of Poly(tetrafluoroethylene) and Perfluoroethylene-propylene by Radiation Grafting"
Jpn. J. Appl. Phy., 45 (12), (2006) 9244.

06J026 2-04 E

A. Iwanade, T. Nomoto, D. Umeno, .K. Saito and T. Sugo,
"Protein Binding Characteristics of Amphoteric Polymer Brushes Grafted onto Porous Hollow-Fiber Membrane"
J. Ion Exch., accepted.

06J027 2-06 E

Y. Wada, M. Tamada N. Seko and H. Mitomo,
"Emulsion grafting of vinyl acetate onto pre-irradiated poly(3-hydroxybutyrate) film"
J. Appl. Polym. Sci., in press.

06J028 2-07 E, G

N. Seko, Y. Ueki, H. Hoshina and M. Tamada,
"Preparation of graft adsorbent having amine groups and its Au(III) adsorption performance"
J. Ion Exch., in press.

06J029 2-08 E

H. Hoshina, N. Seko, Y. Ueki and M. Tamada,
"Synthesis of graft adsorbent with N-methyl-D-glucamine for boron adsorption"
J. Ion. Exch., in press.

06J030 2-09 E

Md. R. Awual, A. Jyo, M. Tamada and A. Katakai,
"Zirconium(IV) loaded bufucntuonal fiber containing both phosphonate and sulfonate as

arsenate adsorbent“
J. Ion Exch., Vol. 18, No.4 (2007) in press.

06J031 2-13 E
Y. Ueki, N. Seko, H. Hoshina and M. Tamada,
“Preparation of Polylactic Acid Nonwoven Fabric-based Metal Adsorbent by Radiation-Induced Graft Polymerization”
J. Ion. Exch., in press.

06J032 2-17 E, G
T. M. Quynh, H. Mitomo, N. Nagasawa, Y. Wada, F. Yoshii and M. Tamada,
“Properties of crosslinked polylactides (PLLA & PDLA) by radiation and its biodegradability”
Eur. Polym. J., 43 (2007) 1779-1785.

06J033 2-18 E, G, O
M. Takigami, H. Amada, N. Nagasawa, T. Yagi, T. Kasahara, S. Takigami and M. Tamada
”Preparation and characterization of CMC gels”
Trans. Mater. Res. Soc. Jpn., in press.

06J034 2-23 E,G
A. Kimura, M. Taguchi, Y. Ohtani, Y. Shimada, H. Hiratsuka and T. Kojima,
“Treatment of wastewater having estrogen activity by ionizing radiation”
Radiat. Phys. Chem., 76 (2007) 699-706.

06J035 3-03 C, G
Y. Yokota, S. Yamada, Y. Hase, N. Shikazono, I. Narumi, A. Tanaka and M. Inoue,
“Initial yields of DNA double-strand breaks and DNA fragmentation patterns depend on linear energy transfer in tobacco BY-2 protoplasts irradiated with helium, carbon and neon ions”
Radiat. Res., 167 (2007) 94-101.

06J036 3-06 C
H. Yamaguchi, T. Morishita, K. Degi, A. Tanaka, N. Shikazono and Y. Hase,
“Effect of Carbon-ion Beams Irradiation on Mutation Induction in Rice”
Plant Mutation Reports 1(1) (2006) 25-27.

06J037 3-20 C
Y.Matuo, S. Nishijima, Y. Hase, A. Sakamoto, A. Tanaka and K. Shimizu,
“Specificity of mutations induced by carbon ions in budding yeast Saccharomyces cerevisiae”
Mutat. Res., 602 (2006) 7-13.

06J038 3-23 C
W. O. Reyes-Borja, I. Sotomayor, I. Garzón, D. Vera, M. Cedeño, A. Tanaka, Y. Hase, Y. Sekozawa, S. Sugaya and H. Gemma.
“Alteration of black Sigatoka (Mycosphaerella fijiensis Morelet) resistance in banana by in vitro irradiation using carbon ion-beams”
Plant Biotechnology 24 (2007) 349-353.

06J039 3-26 G
K. Satoh, H. Ohba, H. Sghaier and I. Narumi,
“Down-regulation of radioresistance by LexA2 in Deinococcus radiodurans”
Microbiology 152 (2006) 3217.

06J040 3-30 T
K. Akamatsu,
“A novel methodology for characterizing strand-break termini and damaged bases in plasmid DNA exposed to ionizing radiation”
Anal. Biochem. 362 (2007) 229.

06J041 3-31 C
A. Urushibara, N. Shikazono, R. Watanabe,

K. Fujii, P. O'Neill and A. Yokoya,
"DNA damage induced by the direct effect of He ion particles"
Radiat. Prot. Dosim., 122 (2006) 163-165.

06J042 3-33 C
H. Matsumoto, A. Takahashi andT. Ohnishi,
"Nitric oxide radicals choreograph a radioadaptive response"
Cancer Res., 67 (2007) in press.

06J043 3-33 C
H. Matsumoto, H. Hamada, A. Takahashi,
Y. Kobayashi and T. Ohnishi,
"Vanguards of paradigm shift in radiation biology: Radiation-induced adaptive and bystander responses"
J. Radiat. Res., 48 (2007) 97.

06J044 3-33 C
N. Hamada, H. Matsumoto, T. Hara and
Y. Kobayashi,
"Intercellular and intracellular signaling pathways mediating ionizing radiation-induced bystander effects"
J. Radiat. Res., 48 (2007) 86.

06J045 3-33 C
Z.-G. Cui, T. Kondo and H. Matsumoto,
"Enhancement of apoptosis by nitric oxide released from α-phenyl-tert-butyl nitrone under hyperthermic conditions"
J. Cell. Physiol., 206 (2006) 468.

06J046 3-34 C
N. Hamada, T. Hara, T. Funayama, T. Sakashita and Y. Kobayashi,
"Energetic heavy ions accelerate differentiation in the descendants of irradiated normal human diploid fibroblasts"
Mutat. Res., (2007) in press (DOI: 10.1016/j.mrfmmm.2007.07.002).

06J047 3-34 C
N. Hamada, H. Matsumoto, T. Hara and
T. Y. Kobayashi,
"Intercellular and intracellular signaling pathways mediating ionizing radiation-induced bystander effects"
J. Radiat. Res. 48 (2007) 87.

06J048 3-34 C
N. Hamada, T. Funayama, S. Wada, T. Sakashita, T. Kakizaki, M. Ni and Y. Kobayashi,
"LET-dependent survival of irradiated normal human fibroblasts and their descendents"
Radiat. Res., 166 (2006) 24.

06J049 3-34 C
N. Hamada, G. Schettino, G. Kashino, M. Vaid,
K. Suzuki, S. Kodama, B. Vojnovic, M. Folkard,
M. Watanabe, B.D. Michael and K.M. Prise,
"Histone H2AX phosphorylation in normal human cells irradiated with focused ultrasoft X-rays: Evidence for chromatin movement during repair"
Radiat. Res., 166 (2006) 31.

06J050 3-39 C, T
M. Hino, S. Wada, Y. Tajika, Y. Morimura,
N. Hamada, T. Funayama, T. Sakashita,
T. Kakizaki, Y. Kobayashi and H. Yorifuji,
"Heavy ion microbeam irradiation induces ultrastructural changes in isolated single fibers of skeletal muscle"
Cell Struct. Funct., 32 (2007) 51-56.

06J051 3-42 C

K. Akeo, T. Funayama, A. Ogawa, N. Hamada,
Y. Akeo and Y. Kobayashi,
"Effects of gamma irradiation on bcl-2 and p53 expression in the porcine ciliary body"
Exp. Anim., 55 (2006) 375-381.

06J052 3-43 C

T. Kakizaki, N. Hamada, S. Wada, T. Funayama,
T. Sakashita, T. Hohdatsu, T. Sano, M. Natsuhori,
Y. Kobayashi and N. Ito,
"Distinct modes of cell death by ionizing radiation observed in two lines of feline T-lymphocytes"
J. Radiat. Res., 47 (2006) 237-243.

06J053 3-43 C

T. Kakizaki, N. Hamada, T. Funayama,
T. Sakashita, S. Wada, T. Hohdatsu, M. Natsuhori,
T. Sano, Y. Kobayashi and T. Ito,
"Killing of feline T-lymphocytes by gamma-rays and energetic carbon ions"
J. Vet. Med. Sci ., 68 (2006) 1269-73.

06J054 3-43 C

T. Kakizaki, N. Hamada, T. Sakashita, S. Wada,
T. Hara, T. Funayama, T. Hohdatsu, M. Natsuhori,
T. Sano, Y. Kobayashi and N. Ito,
"Vulnerability of feline T-lymphocytes to charged particles"
J. Vet. Med. Sci., in press.

06J055 3-47 C

M. Watanabe, T. Sakashita, A. Fujita, T. Kikawada,
D.D. Horikawa, Y. Nakahara, S. Wada,
T. Funayama, N. Hamada, Y. Kobayashi and
T. Okuda,
"Biological effects of anhydrobiosis in an African chironomid, Polypedilum vanderplanki on radiation tolerance"
Int. J. Radiat. Biol., 82 (2006) 587-592.

06J056 3-47 C

M. Watanabe, T. Sakashita, A. Fujita, T. Kikawada,
Y. Nakahara, N. Hamada, D.D. Horikawa,
S. Wada, T. Funayama, Y. Kobayashi and
T. Okuda,
"Estimation of radiation tolerance against high LET heavy ions in an anhydrobiotic insect, Polypedilum vanderplanki"
Int. J. Radiat. Biol., 82 (2006) 835-842.

06J057 3-47 C

D.D. Horikawa, T. Sakashita, C. Katagiri,
M. Watanabe, T. Kikawada, Y. Nakahara,
N. Hamada, S. Wada, T. Funayama, S. Higashi,
Y. Kobayashi, T. Okuda and M. Kuwabara,
"Radiation tolerance in the tardigrade Milnesium tardigradum"
Int. J. Radiat. Biol., 82 (2006) 843-848.

06J058 3-47 C

M. Watanabe, Y. Nakahara, T. Sakashita,
T. Kikawada, A. Fujita, N. Hamada,
D.D. Horikawa, S. Wada, Y. Kobayashi and
T. Okuda,
"Physiological changes leading to anhydrobiosis improve radiation tolerance in Polypedilum vanderplanki larvae"
J. Insect Physiol., 51 (2007) 537-579.

06J059 3-48 C

E. Ling, K. Shirai, R. Kanekatsu, K. Kiguchi,
Y. Kobayashi, T. Funayama and H. Watanabe
"Contribution of circulating hemocytes to the regeneration of heavy ion beams ($^{12}C^{5+}$) irradiated hematopoietic organs in the silkworm, Bombyx

mori, through the way of phagocytosis of injured cells after invasion"
Dev. Comp. Immunol., 30 (2006) 531-541.

06J060 3-48 C

K. Fukamoto, K. Shirai, T. Sakata, T. Sakashita, T. Funayama, N. Hamada, S. Wada, T. Kakizaki, S. Shimura, Y. Kobayashi and K. Kiguchi.
"Development of the irradiation method for the first instar silkworm larvae using locally targeted heavy-ion microbeam"
J. Radiat. Res., 48 (2007) 247-253.

06J061 3-52 G

M. Ukai and Y. Shimoyama,
"Free radicals in irradiated wheat flour detected by electron spin resonance"
Appl. Magn. Reson. 29 (2005) 315.

06J062 3-53 O, G

T. Fujiwara, T. Yamaoka, Y. Kimura and K. J. Wynne,
"Poly(lactide) swelling and melting behavior in supercritical carbon dioxide and post-venting porous material"
Biomacromolecules 6 (2005) 2370.

06J063 3-53 O

T. Sakamoto, A. Mahara, R. Iwase, T. Yamaoka and A. Murakami,
"Analytical method for estimation of kinetics of oligonucleotide/RNA hybridization using fluorescence depolarization spectroscopy"
Anal. Biochem. 340 (2005) 369.

06J064 3-53 O

T. Kitagawa, R. Iwase, K.Ishihara, T. Yamaoka and A. Murakami,
"Facilitated disassembly of polyplexes composed of self-assembling amphiphilic polycations enhances the gene transfer efficacy"
Chem. Lett., 34 (2005) 1478.

06J065 3-53 O

A. EL-Salmawy, T. Kitagawa, I. K. Ko, A. Murakami, Y. Kimura, T.Yamaoka and H. Iwata,
"Preparation and properties of ProNectin F-coated biodegradable hollow fibers"
Journal of Artificial Organs 8 (2005) 245.

06J066 3-53 O

T. Sakamoto, A. Mahara, K. Yamagata, R. Iwase, T. Yamaoka and A. Murakami,
"Evaluation of dynamic feature of Escherichia coli 16S ribosomal RNA in homogeneous physiological solution"
Biophys. J. 89 (2005) 4122.

06J067 3-54 C

N. Kawachi, K. Sakamoto, S. Ishii, S. Fujimaki, N. Suzui, N. S. Ishioka and S. Matsuhashi,
"Kinetic analysis of carbon-11-labeled carbon dioxide for studying photosynthesis in a leaf using positron emitting tracer imaging system"
IEEE Trans. Nucl. Sci., 53 (2006) 2991.

06J068 3-59 C

T. Tsukamoto, H. Nakanishi, S. Kiyomiya, S. Watanabe, S. Matsuhashi, N. K. Nishizawa and S. Mori,
"52Mn translocation in barley monitored using a positron-emitting tracer imaging system"
Soil. Sci. Plant Nutr., 52 (2006) 717-725.

06J069 3-59 C

M Suzuki, M. Takahashi, T. Tsukamoto,
S. Watanabe, S. Matsuhashi, U. Yazaki,
N. Kishimoto, S. Kikuchi, H. Nakanishi, S. Mori and N. K. Nishizawa,
"Biosynthesis and secretion of mugineic acid family phytosiderophores in zinc-deficient barley"
Plant. J., 48 (2006) 85-97.

06J070 3-62 C

K. Endo, N. Oriuchi , T. Higuchi , Y. Iida ,
H. Hanaoka , M. Miyakubo, T. Ishikita and
K. Koyama .,
"PET and PET/CT using ^{18}F-FDG in the diagnosis and management of cancer patients"
Int. J. Clin. Oncol., 11 (2006) 286-296.

06J071 3-63 O

S. Watanabe, T. Katabuchi, N. S. Ishioka,
S. Matsuhashi and H. Muramatsu,
"Production of Endohedral 133Xe-Higher Fullerenes by Ion Implantation"
J. Radioanal. Nucl. Chem., 272 (2007) 467-469.

06J072 3-63 O

S. Watanabe, T. Katabuchi, N. S. Ishioka and
S. Matsuhashi,
"Synthesis of Endohedral 133Xe-Fullerenol by Using Higher Fullerene"
Journal of Nuclear and Radiochemical Science, in press.

06J073 3-68 S

S. Harada, K. Ishii and T. Kamiya.
"The detection of apoptosis by kinetic of Ca and Fe, using micro PIXE camera"
RADIOISOTOPES, 55 (2006) 419-428.

06J074 3-68 S

S. Harada, K. Ishii, H. Yamazaki, S. Matsuyama,
K. Mizuma, K. Hotta, T. Izukawa, S. Anbe,
M. Fukuda, T. Kamiya, S. Takuro, T. Satoh and
M. Oikawa.
"The Targetchemotherapy directed by the radiation"
Int. J. PIXE., Vol.15, Nos.3&4 (2005) 221-224.

06J075 3-68 S

S. Harada, K. Ishii, A. Tanaka, T. Satoh,
S. Matsuyama, H. Yamazaki, T. Kamiya, T. Sakai,
K. Arakawa, M. Saitoh, M.Oikawa and K. Sera,
"Method for Determing the localization of Trace Elements Observed by the Micro PIXE camera"
Int. J. PIXE., Vol.14, Nos.3&4 (2004) 83-87.

06J076 3-68 S

S. Harada, S. Ehara, K. Ishii, A. Tanaka, T. Satoh,
S. Matsuyama, H. Yamazaki, Y. Komori,
T. Kamiya, T. Arakawa, M. Saitoh and
M. Oikawa.
"Improvement of radiosensitive liquid-core microcapsules by Y polymerization"
Int. J. PIXE., IN PRESS.

06J077 3-68 S

S. Harada, S. Ehara, K. Ishii, A. Tanaka, T. Satoh,
S. Matsuyama, H. Yamazaki, Y. Komori,
T. Kamiya, T. Arakawa, M. Saitoh, M. Oikawa.
"Optimizing the radiosensitive liquid core microcapsules for the targeting of chemotherapeutic agents"
Nucl. Instum. Phys. Res., B 260 (2007) IN PRESS.

06J078 3-68 S

S. Harada, S. Ehara, K. Ishii, A. Tanaka, T. Satoh,

S. Matsuyama, H. Yamazaki, Y. Komori,
T. Kamiya, T. Arakawa, M. Saitoh, M. Oikawa, and K. sera.
“The kinetics of Fe and Ca for the development of apoptosis”
Nucl. Instum. Phys. Res., B 210 (2003) 388-394.

06J079 4-01 E, G, O

R.A. Wach, M. Sugimoto and M. Yoshikawa,
“Formation of Silicone Carbide Membrane by Radiation Curing of Polycarbosilane and Polyvinylsilane and Its Gas Separation up to 250^{o}C”
J. Am. Ceram. Soc. 90, (2007) 275-278.

06J080 4-01 E, G, O

R.A. Wach, M. Sugimoto and M. Yoshikawa,
“Development of Silicone Carbide Coating on Al2O3 Ceramics form Precursor Polymers by Radiation Curing”
Key Eng. Mater., 317-318 (2006) 573-76.

06J081 4-02 C, T, I

R.A.Wach, M.Sugimoto, A.Idesaki and M.Yoshikawa,
“Molecular sieve SiC-based membrane for hydrogen separation produced by radiation curing of preceramic polymers”
Mater. Sci. & Eng., B, in press, (2007).

06J082 4-06 T, I, S

T. Taguchi, N. Igawa, E. Wakai, S. Jitsukawa,
L. L. Snead and A. Hasegawa,
“Effect of Al and Be ions pre-implantation on formation and growth of helium bubbles in SiC/SiC composites”
Nucl. Instrum. Methods., B 256[2] (2007) 669-674.

06J083 4-06 T, I, S

T. Taguchi, N. Igawa, S. Miwa, E. Wakai,
S. Jitsukawa, L. L. Snead and A. Hasegawa,
“Effect of displacement damage up to 50 dpa on microstructural development in SiC/SiC composites”
J. Nucl. Mater., 367-370 [1] (2007) 698-702.

06J084 4-09 T, I, O

K. Takano, A. Inouye, S. Yamamoto, A. Miyashita and M. Yoshikawa,
“Effect of Tungsten Valence States on Gasochromic Properties in Tungsten Oxide Thin Films”
Trans. Mater. Res. Soc. Jpn., 32 (2007) 159.

06J085 4-10 S

S. Yamamoto, K. Takano, A. Inouye and
M. Yoshikawa,
“Effect of Annealing Temperature of Palladium Oxide Films on Gasochromic Performance”
Trans. Mater. Res. Soc. Jpn., 32[1] (2007) 171-174.

06J086 4-10 S

A. Inouye, S. Yamamoto, S. Nagata, K. Takano,
M. Yoshikawa and T. Shikama,
“Gasochromic Coloration of Non-stoichiometric WO3-x Films”
Trans. Mater. Res. Soc. Jpn., 32[1] (2007)107-110.

06J087 4-10 S, I

K. Takano, A. Inouye, S. Yamamoto, A. Miyashita and M. Yoshikawa,
“Effect of Tungsten Valence States on Gasochromic Properties in Tungsten Oxide Thin Films”
Trans. Mater. Res. Soc. Jpn., 32[1](2007) 159-162.

06J088 4-11 S

S. Yamamoto, K. Takano, A. Inouye and
M. Yoshikawa,
"Effects of Composition and Structure on Gasochromic Coloration of Tungsten Oxide Films Investigated with XRD and RBS"
Nucl. Instum. Phys. Res., B 262 (2007) 29-32.

06J089 4-14 G

K. Nagashima, R. Tada, A. Tani, S. Toyoda,
Y. Sun and Y. Isozaki.
"Orbital- and millennial-scale variations in Asian dust transport path to the Japan Sea. Palaeogeogr"
Palaeoclimatol. Palaeoecol. 247 (2007) 144-161.

06J090 4-14 G

K. Nagashima, R. Tada, A. Tani, S. Toyoda,
Y. Sun and Y. Isozaki.
"Contribuion of aeolian dust in Japan Sea sediments estimated from ESR signal intensity and crystallinity of quartz"
Geochemistry Geophysics Geosystems, 8, Q02Q04, doi:10.1029/2006GC001364 (2007).

06J091 4-14 G

Y. Sun, R. Tada, J. Chen, H. Chen, S. Toyoda,
A. Tani, Y. Isozaki, K. Nagashima, H. Hasegawa and J. Ji.
"Distinguishing the sources of Asian dust based on electron spin resonance signal intensity and crystallinity of quartz"
Atmos. Environ. in press.

06J092 4-15 C, I

H. Koshikawa and Y. Maekawa,
"Formation of Composite Films of Ion-Track Membranes Embedded with Oblique Cu Nanowires for Anisotropic Infrared Absorption"
Radist. Phys. Chem., in Press.

06J093 4-16 C

M. Taguchi and T. Kojima,
"Yield of OH radicals in water under heavy ion irradiation. Dependence on mass, specific energy and elapsed time"
Nuclear Science and Techniques, 18 (2007)25-38.

06J094 4-19 E, G

R. Nagaishi, Z. Yoshida, R. Yamada and
Y. Hatano,
"Radiation-induced catalytic reduction of chromium(VI) in aqueous solution containing TiO2, Al2O3 or SiO2 fine particles"
Radiat. Phys. Chem., 75 (2006) 1051-1054.

06J095 4-19 G

Y. Sugo, Y. Izumi, Y. Yoshida, S. Nishijima,
Y. Sasaki, T. Kimura, T. Sekine and H. Kudo,
"Influence of diluent on radiolysis of amides in organic solution"
Radiat. Phys. Chem., 76 (2007) 794-800.

06J096 4-19 E, G

N. Aoyagi, R. Nagaishi, F. Esaka and R. Yamada,
"Hydrogen production and morphological change of chrysotile asbestos in the radiolysis of aqueous solutions"
Chem. Lett., 36(7) (2007) 890-891.

06J097 4-20 C

K. Nakashima, N. Chikumoto, A. Ibi, S. Miyata,
Y. Yamada, T. Kubo, A. Suzuki and T. Terai,
"Effect of ion-irradiation and annealing on superconductive property of PLD prepared YBCO tapes"
Physica C 463-465 (2007) 665.

06J098 4-23 S

V, Lavrentiev, H, Naramoto, K, Narumi, S, Sakai and P, Avramov,
"Planar doping of crystalline fullerene with cobalt"
Chem. Phys. Lett., 423 (2006) 366-370.

06J099 4-23 S

S. Sakai, K. Yakushiji, S. Mitani, K. Takanashi,
H. Naramoto, Pavel V. Avramov, K. Narumi,
V. Lavrentiev and Y. Maeda,
"Tunnel magnetoresistance in Co nanoparticle/Co-C_{60} compound hybrid system"
Appl. Phys. Lett., 89 (2006) 113118-1-113118-3.

06J100 4-23 S

H. Tanimoto, K. Yamada, H. Mizubayashi,
S. Sakai, K. Narumi and H. Naramoto,
"Elasticity study of the irradiation-induced polymerization and decomposition of C60 solid"
Mater. Sci. & Eng., A442, (2006) 319-322.

06J101 4-23 S

J. Vacik, V. Havranek, J. Subrtz, S. Bakardjievaz,
H. Naramoto and K. Narumi,
"Synthesis and microstructure characterization of Ni/C_{60} composite material"
Acta Phys. Slovaca 56 (2006) 133-136.

06J102 4-23 S

P. Avramov, H. Naramoto, S. Sakai, K. Narumi,
V. Lavrentiev and Y. Maeda,
"Quantum chemical study of atomic structure evolution of Cox/C60 (x= 2.8) composites"
J. Phys. Chem., A 111 (2007) 2299-2306.

06J103 4-23 S

S. Sakai, H. Naramoto, P. V. Avramov, T. Yaita,
V. Lavrentiev, K. Narumi, Y. Baba and Y. Maeda,
"Comparative study of structures and electrical properties in cobalt-fullerene mixtures by systematic change of cobalt content"
Thin Solid Films 515 (2007) 7758-7764.

06J104 4-25 O

A. Saeki, S. Seki, and S. Tagawa,
"Electrodeless Measurement of Charge Carrier Mobility in Pentacene by Microwave and Optical Spectroscopy Techniques"
J. Appl. Phys., 100 (2006) 0237031-0237036.

06J105 4-25 O

Y. Koizumi, S. Seki, S. Tsukuda, S. Sakamoto and S. Tagawa,
"Self-Condensed Nanoparticles of Oligofluorenes with Water-soluble Side Chains"
J. Am. Chem Soc., 128 (2006) 9036-9037.

06J106 4-25 O

K. Enomoto, J. A. LaVerne, S. Seki, and
S. Tagawa,
"Formation and Decay of the Triplet Excited State of Pyridine"
J. Phys. Chem., A 110 (2006) 9874-9879.

06J107 4-25 O

H. Uno, Z. L. Zhang, M. Suzui, R. Tero,
Y. Nonogaki, S. Nakao, S. Seki, S. Tagawa,
S. Oiki and T. Urisu,
"Noise Analysis of Si-Based Planar-Type Ion-Channel Biosensors"
Jpn. J. Appl. Phys., 45 (2006) L1334-L1336.

06J108 4-25 O

S. Tsukuda, S. Seki, M. Sugimoto and S. Tagawa,
"Customized morphologies of Self-condensed multi-segment polymer nanowires"

J. Phys. Chem., B, 110 (2006) 19319-19322.

06J109 4-25 O

S. Seki, S. Tsukuda, S. Tagawa, and M. Sugimoto
"Correlation between Width Roughness of Nanowires and Backbone Conformation of Polymer Materials"
Macromolecules, 39 (2006) 7446-7450.

06J110 4-25 O

Y. Yamamoto, T. Fukushima, Y. Suna, N. Ishii,
A. Saeki, S. Seki, M. Taniguchi, S. Tagawa, T. Kawai and T. Aida,
"Photoconductive Coaxial Nanotubes of Molecularly Connected Electron Donor and Acceptor Layers"
Science, 314 (2006) 1761-1764.

06J111 4-25 O

A. Saeki, S. Seki, Y. Koizumi and S. Tagawa,
"Dynamics of Photogenerated Charge Carrier and Morphology Dependence in Polythiophene Films Studied by In-Situ Time-Resolved Microwave Conductivity and Transient Absorption Spectroscopy"
J. Photochem. Photobiol., A, 186 (2007) 158-165.

06J112 4-25 O

K. Maehashi, H. Ozaki, Y. Ohno, K. Inoue,
K. Matsumoto, S. Seki and S. Tagawa,
"Formation of Single Quantum Dot in Single-Walled Carbon Nanotube Channel Using Focused-Ion-Beam Technique"
Appl. Phys. Lett., 90 (2007) 023103.

06J113 4-25 O

S. Seki, S. Tsukuda, M. Sugimoto and S. Tagawa,
"Cross-Linked Silicon Based Polymer Nanowire Formation by High Energy Charged Particles"
Surf. Coat. Technol., 201 (2007) 8486-8489.

06J114 4-25 O

S. Seki and S. Tagawa,
"Optoelectronic Properties and Nanostructure Formation of σ-Conjugated Polymers"
Polymer J., 39 (2007) 277-293.

06J115 4-25 O

S. Tsukuda, S. Seki, M. Sugimoto, and S. Tagawa,
"Effect of Ion Beam Energy and Polymer Weight on the Thickness of Nanowires Produced by Ion Bombardment of Polystyrene Thin Films"
Surf. Coat. Technol., 201 (2007) 8526-8530.

06J116 4-25 O

S. Tagawa, S. Tsukuda, S. Seki, M. Sugimoto,
T. Sato, M. Oikawa, and T. Sakai
"Ion Beam Induced Nano-Space Reactions and Nanowire Formation in Polymers by High Energy Sub-μm Heavy Ion Beams"
Surf. Coat. Technol., 201 (2007) 8495-8498.

06J117 4-25 O

Y. Koizumi, S. Seki, A. Saeki, and S. Tagawa,
"Electronic Properties of the Charge Carriers on Oligofluorene Backbone"
Radiat. Phys. Chem., 76 (2007) 1337-1341.

06J118 4-25 O

S. Seki, S. Tsukuda, S. Tagawa, M. Sugimoto,
A. Watanabe, and T. Miyashita
"Formation of Isolated Ultrafine Optical Nanofibers by Single Particle Nanofabrication Technique"
J. Photopolym. Sci. Technol., 20 (2007) 125-128.

06J119 4-25 O

Y. Koizumi, S. Seki, K. Okamoto, A. Saeki, and S. Seki,
"Radiation Induced One-Step One-pod Polymerization of Functional Conjugated Molecules"
J. Photopolym. Sci. Technol., 20 (2007) 97-100.

06J120 4-25 O

Y. Yamamoto, T. Fukushima, A. Saeki, S. Seki, S. Tagawa, N. Ishii, and T. Aida,
"Molecular Engineering of Coaxial Donor-Acceptor Heterojunction by Coassembly of Two Different Hexabenzocoronenes: Graphitic Nanotubes with Enhanced Photoconducting Properties"
J. Am. Chem Soc., 129（2007）9276-9277.

06J121 4-25 O

K. Yamaguchi, T. Inoue, M. Fujii, M. Haraguchi, T. Okamoto, M. Fukui, S. Seki, and S. Tagawa,
"Electric Field Enhancement of Nano Gap of Silver Prisms"
Chin. Phys. Lett., 24 (2007) 2934-2937.

06J122 4-25 O

A. Sharma, M. Katiyar, Deepak, S. Seki, and S. Tagawa,
"Polysilane Based Organic Light Emitting Diodes: Simultaneous Ultraviolet and Visible Emission"
J. Appl. Phys., 102 (2007) 0845061-0845067.

06J123 4-25 O

H. Imahori, M. Ueda, S. Kang, H. Hayashi, S. Hayashi, H. Kaji, S. Seki, A. Saeki, S. Tagawa, T. Umeyama, Y. Matano, K. Yoshida, S. Isoda, M. Shiro, N. V. Tkachenko, and H. Lemmetyinen,
"Effects of Porphyrin Substituents on Film Structure and Photoelectrochemical Properties of Porphyrin-Fullerene Composite Clusters Electrophoretically Deposited on Nanostructured SnO_2 Electrodes"
Chem. Eur. J., in press.

06J124 4-26 T

Y. Horino, A. Chayahara, Y. Mokuno, H. Yamada and N. Fujimori,
"High-rate growth of large diamonds by microwave plasma chemical vapor deposition with newly designed substrate holders"
New Diamond and Frontier Carbon Technology 16 (2006) 63.

06J125 4-26 T

Y. Mokuno, A. Chayahara, Y. Soda, H. Yamada, Y. Horino and N. Fujimori,
"High rate homoepitaxial growth of diamond by microwave plasma CVD with nitrogen addition"
Diam. Relat. Mater., 15 (2006) 455.

06J126 4-30 T

Y. Chimi, N. Ishikawa, A. Iwase and F. Ono,
"Modification of magnetic properties in Fe-Ni alloy thin films induced by energetic ion irradiation"
Nucl. Instrum. Methods., B 257 (2007) 388.

06J127 4-27, 4-28 S

K. Takahiro, S. Oizumi, A. Terai, K. Kawatsura, B. Tsuchiya, S. Nagata, S. Yamamoto, H. Naramoto, K. Narumi and M. Sasase,
"Core-level and valence-band photoemission spectra of Au clusters embedded in carbon"
J. Appl. Phys., 100 (2006) 084325.

06J128 4-27, 4-28 S

K. Takahiro, K. Kawatsura, S. Nagata, B. Tsuchiya, S. Yamamoto, H. Naramoto

"Improvement in Crystal Quality of Epitaxial Ag and Cu Films Induced by Self-ion Irradiation"

Surf. Coat. Technol., 201 (2007) 8273.

06J129 4-32 O

M. Hashimoto, Y. Fukaya, A. Kawasuso and A. Ichimiya,

"Surface structure of In/Si(111) studied by reflection high-energy positron diffraction"

Surf. Sci., (2007) in press.

06J130 4-33 O

Y. Fukaya, A. Kawasuso and A. Ichimiya,

"Reflection high-energy positron diffraction study on Si(111)-$\sqrt{3}\times\sqrt{3}$-Ag surface"

Phys. Rev., B 75 (2007) 115424.

06J131 4-33 O

Y. Fukaya, A. Kawasuso and A. Ichimiya,

"Structural analysis of Si(111)-$\sqrt{21}\times\sqrt{21}$-Ag surface by reflection high-energy positron diffraction"

Surf. Sci., 600 (2006) 3141.

06J132 4-33 O

Y. Fukaya, A. Kawasuso and A. Ichimiya,

"Structural analysis of Ge(111)-3×3-Sn surface at low temperature by reflection high-energy positron diffraction"

Surf. Sci., 600 (2006) 4086.

06J133 4-33 O

Y. Fukaya, A. Kawasuso and A. Ichimiya,

"Order-disorder phase transition of Sn/Ge(111) surface studied by reflection high-energy positron diffraction"

e-J. Surf. Sci. Nanotech., 4 (2006) 435.

06J134 4-34 I

M. Maekawa, R. S. Yu, and A. Kawasuso,

"Characterization of ion beam-induced SiC-OI structures by positron annihilation spectroscopy"

Phys. Stattus. solidi. (c) 4, No. 10, (2007) 3680-3683.

06J135 4-35 S

H.Shibata, Y.Kohno, K.Shibata, T.Sato, M.Oikawa, J.Haga and T.Sakai,

"Nuclear Reaction Microanalysis of Boron Doped Steels"

Nucl. Instrum. Phys. Res., B 260 (2007) 321-324.

06J136 4-37 S

T. Kusakabe, K. Nakajima, K. Suzuki ,

K. Nakazato, H. Takada, T. Satoh, M. Oikawa,

K. Kobayashi, H. Koyama, K. Arakawa and T. Nagamine,

"The changes of heavy metal and metallothionein distribution in testis induced by cadmium exposure"

Biometals, 2007 Apr 19; [Epub ahead of print].

06J137 4-40 S

K.Ishii, H.Yamazaki, S.Matsuyama, W. Galster, T.Satoh and M.Budnar.

"Contribution of Atomic Bremsstrahlung in PIXE spectra and screening effect in atomic bremsstrahlung"

X-ray Spectrom., 34 (2005) 363-365.

06J138 4-40 S

K. Ishii, S. Matsuyama, H. Yamazaki,

Y. Watanabe, T. Yamaguchi, G. Momose,
T. Amartaivan, A. Suzuki, Y. Kikuchi and W.Galster.
“Micron-CT using PIXE with Micro-beams”
Int. J. PIXE., Vol.15, Nos. 3&4(2005) 111-124.

06J139 4-40 S

T. Yamaguchi, K. Ishii, H. Yamazaki, S.Matsuyama, Y. Watanabe, S. Abe, M. Inomata, A. Ishizaki, R.Oyama and Y.Kawamura.
“Development of an image reconstruction method for Micron-CT using PIXE”
Int. J. PIXE., Vol.15, Nos. 3&4 (2005) 195-202.

06J140 4-40 S

S.Matsuyama, K.Ishii, H.Yamazaki, Y.Kikuchi, Ts.Amartaivan, S.Abe, K.Inomata, Y.Watanabe, A.Ishizaki, R.Oyama, Y.Kawamura, A.Suzuki, G.Momose, T.Yamaguchi and H. Imaseki.
“Microbeam analysis of single aerosol particles at Tohoku University”
Int. J. PIXE., Vol.15, Nos.3&4 (2005) 257-262.

06J141 4-40 S

H.Yamazaki, K.Ishii, Y.Takahashi, S.Matsuyama, Y.Kikuchi, Ts. Amartaivan, T.Yamaguchi, G.Momose, S.Abe, K.Inomata, Y.Watanabe and A.Ishizaki.
“Identification of Qxidation States of Trace-Level Arsenic in Environmental Water Samples Using PIXE”
Int. J. PIXE., Vol.15, Nos.3&4 (2005) 241-248.

06J142 4-40 S

S. Matsuyama, K. Ishii, S. Abe, H. Ohtsu, H. Yamazaki, Y. Kikuchi, Ts. Amartaivan,
K. Inomata, Y. Watanabe, A. Ishizaki,
Y. Barbotteau, A. Suzuki, T. Yamaguchi,
G. Momose and H. Imaseki.
“MICROBEAM ANALYSIS AT TOHOKU UNIVERSITY FOR BIOLOGICAL STUDIES”
Int. J. PIXE., Vol.15, Nos 1&2 (2005) 41-46.

06J143 4-46 C

D. Satoh, T. Sato, A. Endo, Y. Yamaguchi,
M. Takada and K. Ishibashi.
“Measurement of response functions of liquid organic scintillator for neutrons up to 800 MeV”
J. Nucl. Sci. Technol., 43 (2006) 714-719.

06J144 4-46 C

T. Sato, D. Satoh, A. Endo and Y. Yamaguchi.
“DARWIN: Dose monitoring system applicable to various radiations with wide energy ranges”
Radiat. Prot. Dosim., in press.

06J145 4-46 C

D. Satoh, T. Sato, A. Endo, N. Matsufuji,
M. Takada and S. Sato.
“Extension of applicable neutron energy of DARWIN up to 1 GeV”
Radiat. Prot. Dosim., in press.

06J146 4-48 T, I, G

T. Ohshima, T. Satoh, M. Oikawa, T. Yamakawa,
S. Onoda, T. Wakasa, J. S. Laird, T. Hirao,
T. Kamiya, H. Itoh, A. Kinoshita, R. Tanaka,
I. Nakano, M. Iwami and Y. Fukushima,
“Characterization of charge generated in silicon carbide n+p diodes using transient ion beam-induced current”
Nucl. Instrum. Methods., A 541 (2005) 236.

06J147 4-49 S

M. Oikawa, T. Satoh, T. Sakai, N. Miyawaki,
H. Kashiwagi, S. Kurashima, S. Okumura,
M. Fukuda, W. Yokota and T. Kamiya,
"Focusing high-energy heavy ion microbeam system at the JAEA AVF cyclotron"
Nucl. Instrum. Methods., B 260 (2007) 85-90.

06J148 4-50 C

S. Kurashima, N. Miyawaki, S. Okumura,
M. Oikawa, K. Yoshida, T. Kamiya, M. Fukuda,
T. Satoh, T. Nara, T. Agematsu, I. Ishibori,
W. Yokota and Y. Nakamura,
"Improvement in beam quality of the JAEA AVF cyclotron for focusing heavy-ion beams with energies of hundreds of MeV"
Nucl. Instrum. Methods., B 260 (2007) 65.

06J149 4-54 S, T

N. Uchiya, T. Harada, M. Murai, H. Nishikawa,
J. Haga, T. Sato, Y. Ishii and T. Kamiya,
"Micro-machining of resists on silicon by proton beam writing"
Nucl. Instrum. Methods., B 260 (2007) 405.

06J150 4-57 G

T. Kojima, H. Sunaga, N. Haneda, I. Kawashima and P.H.G. Sharpe,
"Uncartainty estimation in ^{60}Co gamma-ray dosimetry at JAERI involving a two-way dose intercomparison study with NPL in the dose range 1-50 kGy"
Radiat. Phys. Chem., 54 (1999) 619-626.

06J151 3-16

M. Okamura, A. Tanaka, M. Momose.
N. Umemoto. J. Teixeira da Silva and T. Toguri.
"Advances of Mutagenesis in Flowers and their Industrialization. Floriculture"
Oranamental and Plant Biotechnology Vol.I, pp619-628, Global Science Books (2006).

06J152 3-23

W. O. Reyes-Borja, I. Sotomayor, I. Garzón,
D. Vera, M. Cedeño, A. Tanaka, Y. Hase,
K. Degi,S. Nagatomi,Y. Sekozawa, S. Sugaya and H. Gemma
"Mutation induction by gamma-rays and carbon ion beam irradiation in banana (*Musa spp.*): a study with an emphasis on the response to black"
Sigatoka disease. In M Miranda, A Lebeda (eds). Disease Resistance – Methods for mass screening of banana and other crops (book chapter 2007, in press).

A1.2 Publication in Proceedings

06C001 1-01 I, C, T, E

C. Morioka, M. Imaizumi, T. Ohshima, H. Itoh and K. Kibe

"Study on Optimum Structure of AlInGaP Top Cell for Triple-Junction Space Solar Cell"

Proc. of 4th World Conf. on Photovoltaic Energy Conversion, May 2006 (Waikoloa), pp.1846-1849.

06C002 1-02 C

A. Makihara, M. Midorikawa, T. Yamaguchi, Y. Iide, T. Yokose, Y. Tsuchiya, T. Arimitsu, H. Asai, H. Shindou, S. Kuboyama and S. Matsuda

"Hardness-by-Design Approach for 0.15 μ m FullyDepleted CMOS/SOI Digital Logic Devices with Enhanced SEU/SET Immunity"

The IEEE Nuclear and Space Radiation Effects Conference (NSREC 2005).

06C003 1-02 C

H. Shindou, S. Kuboyama, T. Hirao and S. Matsuda

"Local and pseudo SELs observed in digital LSIsand their implication to SEL test method"

The IEEE Nuclear and Space Radiation Effects Conference (NSREC 2005).

06C004 1-02 C

N. Ikeda, S. Kuboyama, S. Matsuda and T. Handa

"Analysis of Angular Dependence of Proton-Induced Multiple-Bit Upsets in a Synchronous SRAM"

The IEEE Nuclear and Space Radiation Effects Conference (NSREC 2005).

06C005 1-02 C

H. Shindou, S. Kuboyama, N. Ikeda, S. Matsuda. and T.Hirao

"Bulk Damage Caused by Single Protons in SDRAMs"

The IEEE Nuclear and Space Radiation Effects Conference (NSREC 2003).

06C006 1-02 C

S. Kuboyama, H.Shindo S. Matsuda. and T.Hirao.

"Consistency of Bulk Damage Factor and NIEL for Electrons, Protons, and Heavy Ions in Si CCDs"

The IEEE Nuclear and Space Radiation Effects Conference (NSREC 2002).

06C007 1-04 C, T

高橋芳浩、芝田利彦、大西一功、平尾敏雄、小野田忍、神谷富裕

"MOS 構造における重イオン照射誘起電流"

電子情報通信学会論文誌, J89-C, 3 (2006) 104.

06C008 1-09 O

Miyashita, T.Ohnuma, M.Iwasawa, T.Sakai, T.Kano, M.Yoshikawa and N.Soneda,

"Generation of Amorphous SiO2/SiC Interface and Dynamical Simulation of

Interface Oxidation Process of SiC Device"

Annual Report of the Earth Simulator Center Apr.2005-Mar.2006, (2006) 287.

06C009 1-10 I

A. Wakahara(Invited)

"Monolithic Optoelectronic Integrated Circuits"

4th International Workshop on Nanoscale Semiconductor Devices (April 5-6, 2007, Jeju, Korea) pp.221-234

06C010 1-10 I

A. Wakahara, K. Takemoto, F. Oikawa and H. Okada

“Energy transfer process in AlGaN:Tb by time-resolved photoluminescence analysis”

IUMRS-ICA-2006 (Sept. 10-14, 2006, Jeju, Korea) 3-O-6, Abstract book p.30

06C011 1-13 G

A. Idesaki, N. Koizumi, M. Sugimoto, N. Morishita, T. Ohshima, and K. Okuno

“Gas Evolution from Insulating Materials for Superconducting Coil of ITER by Gamma Ray Irradiation at Liquid Nitrogen Temperature”

Proceedings of Cryogenic Engineering Conference & International Cryogenic Materials Conference 2007, 16-20 July 2007, U.S.A. (To be published in Advances in Cryogenic Engineering in 2008

06C012 1-19 T

K. Kondo, Y. Miwa, N. Okubo, Y. Kaji, T. Tsukada.

“The effects of residual stress on corrosion behavior of ion irradiated type 316L stainless steel”

Proceedings of 13th International Conference on Environmental Degradation of Materials in Nuclear Power Systems - Water Reactors, 2007, to be published.

06C013 1-19 T

Y. Kaji, Y. Miwa, N. Okubo, K. Kondo, T. Igarashi and T. Tsukada.

“New concept of damage evaluation method for core internal materials considering radiation induced stress relaxation”

Proceedings of Second International Symposium on Nuclear Power Plant Life Management, 2007, to be published.

06C014 2-04 E

A. Iwanade, D. Umeno, K. Saito and T. Sugo

“Protein Binding to Amphoteric Polymer Brushes Grafted onto Porous Hollow-Fiber Membrane submitted to Biotechnol”

Prog. submitted to Biotechnol. Prog.

06C015 2-21 E

島田明彦、田久保剛、箱田照幸、岩崎達行、木下忍、小嶋拓治

“ホルムアルデヒド殺菌ガスの電子ビーム処理”

第 43 回　アイソトープ・放射線研究発表会要旨集　p.119

06C016 2-22 G

広田耕一、趙常礼、小嶋拓治、星正敏

“有機溶媒中ダイオキシン類の放射線分解　―ダイオキシン類分析廃液処理法の開発―”

環境と測定技術　Vol33　No8　23-28

06C017 3-05 C

飯塚正英、木村康夫、長谷純宏、田中淳

“イオンビーム照射によるオステオスペルマム突然変異体の誘発”

園芸学研究 6 別 1．470（2006）.

06C018 3-07 C

遠嶋太志、白尾吏、上野敬一郎、大江正和、安庭誠、長谷純宏、田中淳

“サトウキビの有用変異体作出に適するイオンビーム線量”

九州農業研究発表会　専門部会発表要旨集

2006 年　8 月　P41

06C019 3-10 C

Y.Kawashima,Y.Hase,Y.Yokota,A.Tanaka,
"Effect of Irradiation on spore germination,mycerial growth and fruit body formation of mushrooms"
Bulletin of the Gunma Prefectural Forestry Experiment Station,12,13-20(2007).

06C020 3-25 C

杉浦俊浩、柿薗俊英、西尾尚道
"単細胞緑藻 Haematococcus pluvialis の従属栄養培養におけるアスタキサンチン生成の検討"
第59回日本生物工学会大会要旨集 iD10-3, p60 (2006).

06C021 3-33 C

H. Matsumoto and T. Ohnishi.
"Radiation-induced advantageous bystander effect and adaptive response through NO radical generations"
Proc. of Int. Symposium on Low-dose radiation exposure and bio-defense system. Ed. S. Tanaka, K. Fujikawa, Y. Oghiso. (Sept. 28-30, 2005, Rokkasho, Japan) pp23-26 (2006).

06C022 3-34 C

N. Hamada, M. Ni, T. Funayama, T. Sakashita, T. Kakizaki, S. Wada, Y. Yokota and Y. Kobayashi.
"Bystander killing in normal human fibroblasts by heavy-ion microbeams"
Extended Abstracts of the 7th International Workshop: Microbeam Probes of Cellular Radiation Response (Mar 15-17, 2006, Columbia Univ., NY, USA)
Radiat. Res. 166, 684-685, 2006.

06C023 3-40 C

Y. Suzuki, K. Shirai, T. Mizui, N. Hamada, S. Noda, T. Funayama, Y. Yoshida, Y. Kobayashi, T. Shirao, T. Nakano
"Relative Biological Effectiveness Value of Carbon Ion Beam To X-ray on Immature Hippocampal Neurons in vitro"
Proceedings of the 48th Annual ASTRO Meeting, Vol. 66, p. 591 (2006)

06C024 3-40 C

Y. Yoshida, Y. Suzuki, A. Takeuchi, N. Hamada, K. Shirai, T. Funayama, T. Sakashita, Y. Kobayashi, S. Ozawa and T. Nakano
"Effects of X-ray and Carbon Ion Beam on the Postnatal Cerebellum in Organotypic Slice Cultures"
Proceedings of the 48th Annual ASTRO Meeting, Vol. 66, p. 250 (2006)

06C025 3-40 C

鈴木義行、白井克幸、水井利幸、浜田信行、野田真永、舟山知夫、吉田由香里、小林泰彦、白尾智明、中野隆史
"培養ラット未熟神経細胞における、アポトーシスを指標とした炭素線の生物学的効果比"
Proceedings of the 19th Annual Meeting of JASTRO, Vol. 18, p. 186 (2006).

06C026 3-46 C

森ちひろ、東谷篤志
"線虫の放射線応答：重イオンマイクロビームを用いた研究結果を中心に"
放射線生物研究 41(4), 399-408 (2006)"

06C027 3-46 C

東谷篤志
"放射線照射に対する生物応答：モデル生物 C

エレガンスを用いたイオンマイクロビームの照射研究”
放射線と産業　111,　(2006)　13-18

06C028 3-53　O

T. Hashimoto, A. Kobori, A. Murakami and T. Yamaoka.
“The destabilization of polyplexes facilitates intranuclear transcription dfficiency”
Nucleic Acids Symposium Series, 49, 365-366 (2005).

06C029 3-53　O

T. Sakamoto, A. Mahara, A. Kobori, T. Yamaoka, A. Murakami.
“Luminescence anisotropy-based detection of nucleic acids and proteins using long-lifetime Ru(II) complex as a luminescent label”
Nucleic Acids Symposium Series, 49, 203-204 (2005).

06C030 3-53　O

M. Higuchi, A. Yamayoshi, A. Kobori, T. Yamaoka, A. Murakami.
“Synthesis and properties of photo-reactive antisense oligonucleotides contining 2’-O-psoralen-conjugated adenosine”
Nucleic Acids Symposium Series, 49, 331-332 (2005).

06C031 3-53　O

R. Iwase, U. Fukui, A. Kobori, T. Yamaoka, A. Murakami.
“Synthesis of antisense oligonucleotides containing a photocleavable protecting group on a guanine base and theier photoinduced duplex formation”
Nucleic Acids Symposium Series, 49, 151-152 (2005).

06C032 3-54　C

N. Kawachi, S. Fujimaki, S. Ishii, N. Suzui, N. S. Ishioka, and S. Matsuhashi.
“A new method for parametric imaging of photosynthesis with C-11 carbon dioxide and positron emitting tracer imaging system (PETIS)”
Proceedings of International Conference on Nuclear Data for Science and Technology, 2006 IEEE Nuclear Science Symposium Conference Record, 3 (2006) 1519.

06C033 3-58　C

本田修三、関本均、加藤翔太、落合由記子、山口良恵、米山香織、米山弘一、竹内安智、河地有木、藤巻秀、鈴井伸郎、石井里美、石岡典子、松橋信平
“ホスト植物が同化した炭素・窒素の根寄生植物への分配様式のＰＥＴＩＳ法によるイメージング”
2006 年度日本土壌肥料学会関東支部大会講演要旨集、ｐ15．2006 年 11 月（宇都宮）

06C034 3-58　C

H.Sekimoto and S.Honda
“Ealuation of Effect of Root Parasite on Carbon and Nitrogen Translocation and Distribution in the Host Plant by Positron Emitting Tracer Imaging System (PETIS) ”
Proceedings of the Bi-national Japan-Israel Workshop on Aspects of Parasitic Weeds: biology and Control.Agricultural Research Organization the Volcani Center, March 2007 (Israel)

06C035 3-62　C

Y. Iida, H. Hanaoka, T. Katabuchi, S. Watanabe, S. N. Ishioka, S. Matsuhashi, N. Oriuchi,

T. Higuchi, M. Miyakubo and K. Endo
“Utility of 64Cu for immuno-PET; in vivo measurement of radiation dose for radioimmunotherapy”
Proc. of The Fifth Annual Meeting of the Society for Molecular Imaging, The Big Island of Hawaii, USA, 5, 361 (2006).

06C036 3-62 C
Y. Iida, H. Hanaoka, T. Katabuchi, S. Watanabe, S. N. Ishioka, S. Matsuhashi, N. Oriuchi, T. Higuchi, M. Miyakubo, K. Endo
“Application of PET imaging with [Cu-64] for quantitative evaluation of radioimmunotherapy”
Proc. of 9th Congress of the World Federation of Nuclear Medicine & Biology, Seoul, Korea, 5, supple1, S189 (2006).

06C037 3-66 S
櫻井英幸、岡本雅彦、新雅子、竹内あい子、長谷川正俊、佐藤隆博、及川将一、神谷富裕、荒川和夫、中野隆史
“大気マイクロ PIXE を用いたヒト肺癌細胞内シスプラチンの可視化，定量化の試み”
第 9 回癌治療増感研究シンポジウム p30（2007）

06C038 3-68 S
S. Harada, K. Ishii and T. Kamiya.
“Kinetics of cis-platinum after radiation, and targeting of cis-platinum, directed by radiation”
INNERVISION (2006) 61.

06C039 3-68 S
S. Harada, K. Ishii and S. Obara.
“Determination of radiation Induced apoptosis by the kinetics of the trace-elements, and predicting the antitumor effect and prognosis of radiation therapy”
INNERVISION 17/7 (2004) 27-28.

06C040 3-68 S
S. Harada, S. Ehara, K. Ishii, A. Tanaka, T. Satoh, S. Matsuyama, H. Yamazaki, Y. Komori, T. Kamiya, T. Arakawa, M. Saitoh, M. Oikawa, and K. sera.
“Innovation of the Target preparation of the micro PIXE Camera for the floating cells”
Proceeding of the 10th International Conference on Particle-Induced X-ray Emission and its Analytical Applications (CDR publication)

06C041 3-68 S
S. Harada, S. Ehara, K. Ishii, A. Tanaka, T. Satoh, S. Matsuyama, H. Yamazaki, Y. Komori, T. Kamiya, T. Arakawa, M. Saitoh, M. Oikawa and K. sera.
“The alteration of the cis-platinum (Platinum analogues for cancer therapy) by the low dose irradiation studied in human leukemia, A preliminary study”
Proceeding of the 1oth International Conference on Particle-Induced X-ray Emission and its Analytical Applications (CDR publication)

06C042 4-08 I
H.Iwata, Y.Tokuda, M.Takagi and T.Imura,
“Effect of Boron Co-implantation on Hydrogen induced Exfoliation”
Proceedings of 16th International Microscopy Congress, Vol.3, pp.1352 (2006.9)

06C043 4-17 C
S. Nakagawa, M. Taguchi and T. Kojima
“LET effect on radiation of hydroxymaleimide in 2-propanol”
Proceeding of 49th Annual Meeting of Japanese

Society of Radiation Chemistry, 61-62 (2006).

06C044 4-19 E, G

R. Nagaishi, N. Aoyagi, R. Yamada, Y. Hatano and Z. Yoshida,
"Radiation-induced reduction of metal ions in aqueous solution systems and its application"
Conference abstract book of the 1st asia-pacific symposium on radiation chemistry, 83 (2006).

06C045 4-19 E, G

Y. Sugo, Y. Sasaki, T. Kimura and T. Sekine,
"Radiolysis studies of amidic extractants for partitioning of HLW"
Proceedings of 15th International Conference on Nuclear Engineering (ICONE-15), 10573 (2007).

06C046 4-25 O

関修平
"量子ビームと高分子材料の創る世界"
Optronics, 25 (2006) 166-167.

06C047 4-25 T,I,S

杉本雅樹、吉川正人、関修平、田川精一
"イオンビームによるセラミックナノファイバーの合成"
Material Stage, 7 (2007) 63-67.

06C048 4-25 T,I,S

関修平、佃諭志、田川精一
"高分子材料の単一粒子ナノ加工と構造制御"
放射線化学, 83 (2007) 10-20.

06C049 4-41 T,I,S

斎藤勇一、千葉敦也、鳴海一雅、阿達正浩
"TIARA におけるクラスター加速の現状"
第１９回タンデム加速器とその周辺技術の研究会報告集 p.13 (2006)

06C050 4-41 T,I,S

阿達正浩、斎藤勇一、千葉敦也、鳴海一雅、金子敏明
"炭素薄膜中での高エネルギー炭素クラスターイオンの荷電変換断面積の評価"
第 54 回 応用物理学関係連合講演会 予稿集 第 I 分冊 p.150 (2007)

06C051 4-41 T,I,S

齋藤勇一、千葉敦也、 阿達正浩、鳴海一雅
"クラスターイオンのタンデム加速器透過率の測定"
春季第 54 回応用物理学関係連合講演会 予稿集 第 I 分冊 p.150 (2007)

06C052 4-41 T,I,S

斎藤勇一、千葉敦也、阿達正浩、鳴海一雅
"薄膜を通過させた MeV クラスターイオン構成原子の電荷のクラスター形状依存性"
第７回「イオンビームによる表面・界面解析」特別研究会１２月９日岡山理科大学

06C053 4-45 C

岩元洋介、松田規宏、坂本幸夫、落合謙太郎、中根佳弘、中島宏、柴田徳思
"10MeV 陽子入射によるベリリウムからの中性子成二重微分断面積"
原子力学会「2007 年春の年会」、E09（2007）

06C054 4-46 C

佐藤達彦、佐藤大樹、遠藤章
"高エネルギー中性子対応マルチ放射線モニタ DARWIN の開発"
放射線, 32, (2006) 233-238.

06C055 4-46 C

D. Satoh, T. Sato, N. Shigyo and K. Ishibashi.
"SCINFUL-QMD; Monte Carlo based computer

code to calculate response function and detection efficiency of a liquid organic scintillator for neutron energies up to 3 GeV”
JAEA-Data/Code 2006-023 (2006).

06C056 4-50 C
S. Okumura, S. Kurashima, N. Miyawaki, H. Kashiwagi, K. Yoshida, I. Ishibori, Y. Yuri, T. Nara and T. Agematsu,
“Measurement of the beam energy spread at the JAEA AVF cyclotron”
Proceedings of the 3rd Annual Meeting of Particle Accelerator Society of Japan and the 31th Linear Accelerator Meeting in Japan, Sendai, Japan (2006).p.919.

06C057 4-50 C
Y. Yuri, N. Miyawaki, T. Kamiya, W. Yokota, K. Arakawa, T. Agematsu, I. Ishibori, H. Kashiwagi, S. Kurashima, T. Nara, S. Okumura, K. Yoshida, M. Fukuda,
“Study on Large-area Uniform Ion Beam Formation Using Multipole Magnets”
Proceedings of the 3rd Annual Meeting of Particle Accelerator Society of Japan and the 31th Linear Accelerator Meeting in Japan, Sendai, Japan (2006) p.913.

06C058 4-50 C
N.Miyawaki, S.Okumura, S.Kurashima, H.Kashiwagi, K.Yoshida, I.Ishibori, Y.Yuri, T.Nara, T.Agematsu, M.Fukuda,
“DEVELOPMENT OF THE CENTRAL REGION FOR CONTROL OF A BEAM PHASE WIDTH AT THE JAEA AVF CYCLOTRON”
Proceedings of the 3rd Annual Meeting of Particle Accelerator Society of Japan and the 31th Linear Accelerator Meeting in Japan, Sendai, Japan (2006) p.907.

06C059 4-54 S, T
N. Uchiya, T. Harada, M. Murai, H. Nishikawa, J. Haga, T. Satoh, Y. Ishii and T. Kamiya,
“Micro-machining of resists on silicon by proton beam writing”
Proceedings of 10th International Conference on Nuclear Microprobe Technology and Applications, July 2006 (Singapore), p.189.

06C060 4-54 S, T
打矢直之、古田祐介、西川宏之、芳賀潤二、佐藤隆博、石井保行、神谷富裕
“集束プロトンビーム描画による厚膜レジストの微細加工”
秋季第 67 回応用物理学会、p.649、2006 年 8 月(滋賀)

06C061 4-54 S, T
古田祐介、打矢直之、西川宏之、芳賀潤二、佐藤隆博、及川将一、石井保行、神谷富裕
“集束プロトンビーム描画によるマイクロマシニングプロセス”
第 37 回電気電子絶縁材料システムシンポジウム、D-1、2006 年 10 月(千葉)

06C062 4-54 S, T
吉田栄治、西川宏之、打矢直之、古田祐介、芳賀潤二、及川将一、佐藤隆博、石井保行、神谷富裕
“集束プロトンビームによる高アスペクト比微細加工”
プラスチック成形加工学会 第 14 回秋季大会 成形加工シンポジア 06 特別セッション、A-08、2006 年 11 月(岐阜)

06C063 4-54 S, T

古田祐介、打矢直之、西川宏之、芳賀潤二、及川将一、佐藤隆博、石井保行、神谷富裕、“集束プロトンビーム描画による三次元構造体の作製”

春季第 54 回応用物理学会、p.780、2007 年 3 月(神奈川).

06C064 4-57 E

T. Kojima, H. Sunaga and R. Tanaka,

“Consistency in evaluation of a few MeV electron dose and 60Co gamma-ray dose in radiation processing”

Radiation Technology in Emerging Industrial Applications, Conference & Symposium , IAEA-SM-365/56, 216-219 (2003)

Appendix 2

List of Related Patents

06PAT001　　1-20
井岡郁夫（原子力機構）他神戸製鋼所、コベルコ科研との共同出願、
「耐粒界腐食性および耐応力腐食割れに優れたオーステナイト系ステンレス鋼およびその製造方法」
出願番号　特願 2007-117981 号

06PAT002　　1-27
高木、小林、斉藤（トヨタ自動車）、吉田、八巻、浅野（原子力機構）
「Functional membrane and electrolyte membrane for fuel cell and method for producing the same」, PCT/JP2006/303504

06PAT003　　1-27
廣木、八巻、浅野、吉田（原子力機構）
「プロトン伝導度測定方法と装置」
特願 2006-043562 号

06PAT004　　1-27
小林(トヨタ自動車)、八巻、浅野、吉田、前川（原子力機構）
「機能性膜の製造方法、及び燃料電池用電解質膜の製造方法」
特願 2006-317281 号

06PAT005　　2-3
瀬古、玉田（原子力機構）、伊藤、坂田（九州日立マクセル）
「高周波基盤およびその製造方法」
特願 2005-359923 号

06PAT006　　2-7
瀬古、玉田、吉井（原子力機構）
「金を吸着回収する吸着材の合成方法及び排水処理」
特開 2005-154973 号

06PAT007　　2-16
玉田、八木、長澤（原子力機構）金澤（住友電工ファインポリマー）
「ポリ乳酸製熱収縮材」
特願 2006-212502 号

06PAT008　　2-16
金澤、川野（住友電工ファインポリマー）、玉田、長澤、八木（原子力機構）
「ポリ乳酸製架橋材の製造方法およびポリ乳酸製架橋材」
特願 2006-213951 号

06PAT009　　2-16
玉田、八木、長澤（原子力機構）金澤（住友電工ファインポリマー）
「ポリ乳酸弾性体」
特願 2006-216068 号

06PAT010　　2-18
瀧上、天田（群馬県産業支援機構）、長澤、八木、玉田、笠井、吉井（原子力機構）
「カルボキシメチルセルロースゲルの製造方法」
特願 2006-250947 号

06PAT011　　2-18
瀧上（群馬県産業支援機構）、長澤、八木、玉田（原子力機構）
「カルボキシメチルセルロースを主成分とするゲルの製造方法とそのゲル」
特願 2007-70145 号

06PAT012　　2-19
八木、長澤、廣木、玉田（原子力機構）、Charito T. Aranilla（フィリピン原子力研究所）
「多糖類を原料とするゲルの製造方法」
特願 2006-331679 号

06PAT013　　2-20
笠井昇、吉井文男（原子力機構）、湯浅淳一（積水化学工業）
「ポリオレフィン系樹脂管の曲げ加工方法」
特願　2007-129566 号

06PAT014　　3-52
鵜飼光子、下山雄平（北海道教育大学）
「放射照射食品の検査方法」
特願 2005-61622 号

06PAT015　　3-53
藤里俊哉、山岡哲二、中谷武嗣、北村惣一郎（国立循環器病センター）
「生体組織マトリックスへの細胞播種方法」
特願 2005-180344 号

06PAT016　　3-54
河地有木、藤巻秀、松橋信平（原子力機構）
「光合成機能イメージングのための新規方法」
特開 2007-154225 号

06PAT017　　4-19
山田、永石（原子力機構）
「石英、アルミナなどの耐強酸性の酸化物を触媒とするアルコール添加硫酸水溶液を使用する放射線誘起水素製造法」
特願 2006-161019 号

06PAT018　　4-19
永石、山田、簇野、吉田（原子力機構）
「固体を共存した水溶液への放射線照射による水溶液中の強酸化性金属イオンの処理回収方法」
特開 2006-247485 号

06PAT019　　4-19
山田、永石、簇野、吉田（原子力機構）
「石英、アルミナなどの耐強酸性の酸化物固体を触媒とする放射線誘起水素製造法」
特開 2006-248822 号

06PAT020　　4-19
山田、永石、吉田（原子力機構）
「高レベル放射性廃棄物を線源とする放射線誘起触媒反応による水素製造法」
特開 2006-248821 号

06PAT021　　4-25
杉本雅樹、吉川正人（原子力機構）、関修平、佃諭志、田川精一(大阪大学)
「イオンビーム照射によるセラミックナノワイヤーの製造法」
特開 2007-76978 号

06PAT022　　4-25
関修平、佃諭志、田川精一（大阪大学）、杉本雅樹、吉川正人（原子力機構）
「高分子多段ナノワイヤー及びスターバースト型ナノ粒子とそれらの製造法」
特願　2007-64288 号

06PAT023　　4-49

島田、及川、加藤、佐藤、堀内、遊佐、岸、中野（群馬大学）、佐藤、酒井、上松、福田、荒川（原子力機構）

「荷電粒子線の照準位置決定装置，その使用方法，及び照準位置決定装置を用いた治療装置」

PCT/JP2007/050347

06PAT024　　4-51

吉田、田島（原子力機構）、横山（信越化学）

「ECR イオン源に用いられるプラズマ閉じ込め用のミラー磁場発生装置及び方法」

特開 2006-049020 号

Appendix 3

List of Related Press-Release and TV Programs

06NP001　2-01
平成１８年７月２８日、日経産業新聞に掲載、
「ホタテ内臓　捨てずに利用　無害化し肥料などに」

06NP002　2-16
平成１９年６月２１日、２５日、２６日読売新聞他７紙に掲載、
「塩ビに替わる柔らかいポリ乳酸の開発に成功－植物由来プラスチックの応用範囲を大幅に拡大－」

06NP003　2-18
平成１８年１２月８、１２、２１日、日本経済新聞他８紙に掲載、
「環境に優しい植物由来のゴムのような弾性ゲル体の開発に成功」、「吸水・弾力性のゲル開発」

06NP004　3-01
平成１８年４月２５日、毎日新聞他８紙に掲載、
「植物を紫外線に強くするメカニズム」

06NP005　4-33
平成１８年８月７日、上毛新聞他４紙に掲載、
「高輝度陽電子ビームを用いて表面ナノ物質の原子立体配列の観測に成功―陽電子で物質最表面の顕微技術が可能に―」

06NP006　4-54
平成１９年２月２０日、日刊工業新聞他７紙に掲載、
「原子力機構と芝浦工大　PBW で長深度加工　神鋼と先端素子装置開発へ」「陽子ビーム加工技術開発　原研機構など」「プロトンビームライティング　超精密金型作製に応用　原子力機構－芝浦工大－神戸製鋼」等

06TV001　3-33
平成１８年８月３日１９時３０分、NHK 総合、[クローズアップ現代]、
「残留放射線の脅威　～“第３の被爆”を追う～」

Appendix 4 Type of Research Collaboration

Section of this Report	Type of Research Collaboration[*1]					Irradiation Facilites[*2]						Section of this Report	Type of Research Collaboration[*1]					Irradiation Facilites[*2]					
	Joint Res,	Coop. Res, Univ.	Joint Res, Proj,	JAEA	Com. U. P.,	C	T	I	S	Co	E		Joint Res,	Coop. Res, Univ.	Joint Res, Proj,	JAEA	Com. U. P.,	C	T	I	S	Co	E
1-01	●					C	T	I			E	3-01				●		C					
1-02	●				●	C						3-02				●		C					
1-03				●		C	T	I				3-03	●					C				G	
1-04		●				C	T	I				3-04	●					C					
1-05	●					C	T					3-05	●					C					
1-06	●			●			T	I	S	G	E	3-06	●					C					
1-07		●					T			G	E	3-07	●					C					
1-08		●									E	3-08	●					C					
1-09				●O.L								3-09	●					C					
1-10		●						I				3-10	●					C					
1-11		●								G		3-11	●					C					
1-12		●									E	3-12	●					C					
1-13				●						G		3-13	●					C					
1-14				●						G		3-14	●					C					
1-15	●									G		3-15					●	C					
1-16				●						G		3-16	●					C					
1-17				●						G		3-17	●					C					
1-18				●						G		3-18	●					C					
1-19				●			T					3-19	●					C					
1-20				●			T	I	S			3-20		●				C					
1-21				●			T	I	S			3-21		●				C					
1-22				●			T		S			3-22		●				C					
1-23				●					S			3-23		●				C					
1-24				●			T					3-24		●				C					
1-25			●				T	I	S			3-25		●				C					
1-26				●						G		3-26				●						G	
1-27				●		C				G	E	3-27	●					C					
1-28				●						G	E	3-28	●					C					
												3-29	●					C					
2-01	●										E	3-30				●			T			G	
2-02	●										E	3-31				●		C					
2-03	●									G	E	3-32				●		C	T				
2-04		●									E	3-33		●				C					
2-05	●										E	3-34			●			C					
2-06				●						G	E	3-35			●			C					
2-07				●						G	E	3-36			●			C					
2-08	●									G	E	3-37			●			C					
2-09		●			●						E	3-38			●			C					
2-10	●									G	E	3-39			●			C	T				
2-11	●										E	3-40			●			C					
2-12	●									G	E	3-41	●					C					
2-13				●						G	E	3-42		●				C					
2-14	●									G	E	3-43		●				C					
2-15				●						G	E	3-44				●						G	
2-16	●									G	E	3-45				●		C					
2-17		●								G	E	3-46		●				C					
2-18	●									G	E	3-47	●					C					
2-19				●O.L						G	E	3-48		●				C					
2-20	●									G	E	3-49		●				C					
2-21				●						G	E	3-50		●				C					
2-22				●						G	E	3-51		●				C					
2-23				●						G	E	3-52		●								G	

Section of this Report	Type of Research Collaboration[*1]					Irradiation Facilites[*2]					
	Joint Res,	Coop. Res, Univ.	Joint Res, Proj,	JAEA	Com. U. P.,	C	T	I	S	Co	E
3-53	●									G	
3-54	●	●				C					
3-55				●		C					
3-56		●				C					
3-57		●				C					
3-58		●				C			S		
3-59		●				C					
3-60		●				C					
3-61				●	●	C					
3-62		●			●	C					
3-63				●O.L		C					
3-64			●						S		
3-65			●						S		
3-66			●						S		
3-67			●						S		
3-68			●						S		
3-69			●						S		
4-01				●O.L						G	E
4-02				●		C	T	I			
4-03					●			I			
4-04				●						G	E
4-05					●					G	E
4-06				●			T	I	S		
4-07	●							I			
4-08					●			I			
4-09				●O.L			T	I	S		
4-10				●			T	I	S		
4-11				●			T	I	S		
4-12		●						I			E
4-13					●					G	
4-14					●					G	
4-15				●		C		I			
4-16				●		C					
4-17	●					C					
4-18		●				C					
4-19				●						G	E
4-20					●	C				G	
4-21				●					S		
4-22					●				S		
4-23				●			T	I	S		
4-24			●				T	I	S		
4-25			●O.L		●		T	I	S		

Section of this Report	Type of Research Collaboration[*1]					Irradiation Facilites[*2]					
	Joint Res,	Coop. Res, Univ.	Joint Res, Proj,	JAEA	Com. U. P.,	C	T	I	S	Co	E
4-26	●						T				
4-27		●					T	I	S		
4-28		●						I	S		
4-29					●		T	I			
4-30				●			T				
4-31				●			T	I	S		
4-32				●O.L			T	I			
4-33				●O.L			T	I			
4-34				●			T	I			
4-35		●							S		
4-36			●						S		
4-37			●						S		
4-38			●						S		
4-39			●						S		
4-40			●				T		S		
4-41			●				T	I	S		
4-42			●				T	I	S		
4-43			●				T	I	S		
4-44			●				T	I	S		
4-45				●		C					
4-46				●		C					
4-47	●					C					
4-48				●		C	T	I		G	
4-49		●				C			S		
4-50				●		C					
4-51				●O.L		C					
4-52				●			T	I	S		
4-53				●O.L							
4-54		●					T		S		
4-55				●						G	E
4-56	●									G	
4-57				●						G	E
4-58	●									G	E
5-01						C	T	I	S		
5-02						C					
5-03							T	I	S		
5-04						C	T	I	S		
5-05						C					
5-06										G	E
5-07										G	E
5-08						C	T	I	S	G	E

Type of Research Collaboration[*1]

Joint Res.: Joint research with private company or governmental institution

Coop. Res. Univ.: Cooperative research with a university or universities

Joint Res. Proj. : The Joint Research Project #

#For administration of these programs, we appreciate the cooperation of Research Center for Nuclear Science and Technology, The University of Tokyo.

Com.U.P.: Common Use Program,

O.L, Off line

Irradiation Facilities[*2]

C; AVF Cyclotron System

T; Tandem Electrostatic Accelerator

I; Ion implanter

S; Single-ended Electrostatic Accelerator

G; Co-60 Gamma-Ray Irradiation Facilities

E; Electron Accelerator

Symbol used in the Appendix

Written example

06	**J**	**173**	**4-42**	**C**
①	②	③	④-⑤	⑥

① Abbreviation of A.D. year

② **J** : Publications in Journal
C : Publications as Proceeding
NP : Press-Release
TV : TV Programs
PA : Patent

③ Reference number

④ The number of research field
1 Space,nuclear and energy engineering
2 Environment conservation and resource security
3 Bioyechnology and medical application
4 Advanced materials, analysis and novel technology

⑤ The number of papers

⑥ Irradiation Facilities
C AVF Cyclotron System
T Tandem Electrostatic Accelerator
I Ion implanter
S Single-ended Electrostatic Accelerator
G Co-60 Gamma-Ray Irradiation Facilities
E Electron Accelerator
O Off-line

This is a blank page.

国際単位系（SI）

表１．SI 基本単位

基本量	SI 基本単位	
	名称	記号
長さ	メートル	m
質量	キログラム	kg
時間	秒	s
電流	アンペア	A
熱力学温度	ケルビン	K
物質量	モル	mol
光度	カンデラ	cd

表２．基本単位を用いて表されるSI組立単位の例

組立量	SI 基本単位	
	名称	記号
面積	平方メートル	m^2
体積	立法メートル	m^3
速さ，速度	メートル毎秒	m/s
加速度	メートル毎秒毎秒	m/s^2
波数	毎メートル	m-1
密度（質量密度）	キログラム毎立法メートル	kg/m^3
質量体積（比体積）	立法メートル毎キログラム	m^3/kg
電流密度	アンペア毎平方メートル	A/m^2
磁界の強さ	アンペア毎メートル	A/m
（物質量の）濃度	モル毎立方メートル	mol/m^3
輝度	カンデラ毎平方メートル	cd/m^2
屈折率	（数の） 1	1

表５．SI 接頭語

乗数	接頭語	記号	乗数	接頭語	記号
10^{24}	ヨタ	Y	10^{-1}	デシ	d
10^{21}	ゼタ	Z	10^{-2}	センチ	c
10^{18}	エクサ	E	10^{-3}	ミリ	m
10^{15}	ペタ	P	10^{-6}	マイクロ	μ
10^{12}	テラ	T	10^{-9}	ナノ	n
10^{9}	ギガ	G	10^{-12}	ピコ	p
10^{6}	メガ	M	10^{-15}	フェムト	f
10^{3}	キロ	k	10^{-18}	アト	a
10^{2}	ヘクト	h	10^{-21}	ゼプト	z
10^{1}	デカ	da	10^{-24}	ヨクト	y

表３．固有の名称とその独自の記号で表されるSI組立単位

組立量	SI 組立単位			
	名称	記号	他のSI単位による表し方	SI基本単位による表し方
平面角	ラジアン(a)	rad		$m \cdot m^{-1}=1$(b)
立体角	ステラジアン(a)	sr(c)		$m^2 \cdot m^{-2}=1$(b)
周波数	ヘルツ	Hz		s^{-1}
力	ニュートン	N		$m \cdot kg \cdot s^{-2}$
圧力，応力	パスカル	Pa	N/m^2	$m^{-1} \cdot kg \cdot s^{-2}$
エネルギー，仕事，熱量	ジュール	J	N・m	$m^2 \cdot kg \cdot s^{-2}$
工率，放射束	ワット	W	J/s	$m^2 \cdot kg \cdot s^{-3}$
電荷，電気量	クーロン	C		s・A
電位差（電圧），起電力	ボルト	V	W/A	$m^2 \cdot kg \cdot s^{-3} \cdot A^{-1}$
静電容量	ファラド	F	C/V	$m^{-2} \cdot kg^{-1} \cdot s^4 \cdot A^2$
電気抵抗	オーム	Ω	V/A	$m^2 \cdot kg \cdot s^{-3} \cdot A^{-2}$
コンダクタンス	ジーメンス	S	A/V	$m^{-2} \cdot kg^{-1} \cdot s^3 \cdot A^2$
磁束	ウエーバ	Wb	V・s	$m^2 \cdot kg \cdot s^{-2} \cdot A^{-1}$
磁束密度	テスラ	T	Wb/m^2	$kg \cdot s^{-2} \cdot A^{-1}$
インダクタンス	ヘンリー	H	Wb/A	$m^2 \cdot kg \cdot s^{-2} \cdot A^{-2}$
セルシウス温度	セルシウス度(d)	℃		K
光束	ルーメン	lm	cd・sr(c)	$m^2 \cdot m^{-2} \cdot cd=cd$
照度	ルクス	lx	lm/m^2	$m^2 \cdot m^{-4} \cdot cd=m^{-2} \cdot cd$
（放射性核種の）放射能	ベクレル	Bq		s^{-1}
吸収線量，質量エネルギー分与，カーマ	グレイ	Gy	J/kg	$m^2 \cdot s^{-2}$
線量当量，周辺線量当量，方向性線量当量，個人線量当量,組織線量当	シーベルト	Sv	J/kg	$m^2 \cdot s^{-2}$

(a)ラジアン及びステラジアンの使用は、同じ次元であっても異なった性質をもった量を区別するときの組立単位の表し方として利点がある。組立単位を形作るときのいくつかの用例は表４に示されている。
(b)実際には、使用する時には記号rad及びsrが用いられるが、習慣として組立単位としての記号“１”は明示されない。
(c)測光学では、ステラジアンの名称と記号srを単位の表し方の中にそのまま維持している。
(d)この単位は、例としてミリセルシウス度m℃のようにSI接頭語を伴って用いても良い。

表４．単位の中に固有の名称とその独自の記号を含むSI組立単位の例

組立量	SI 組立単位		
	名称	記号	SI 基本単位による表し方
粘度	パスカル秒	Pa・s	$m^{-1} \cdot kg \cdot s^{-1}$
力のモーメント	ニュートンメートル	N・m	$m^2 \cdot kg \cdot s^{-2}$
表面張力	ニュートン毎メートル	N/m	$kg \cdot s^{-2}$
角速度	ラジアン毎秒	rad/s	$m \cdot m^{-1} \cdot s^{-1}=s^{-1}$
角加速度	ラジアン毎平方秒	rad/s^2	$m \cdot m^{-1} \cdot s^{-2}=s^{-2}$
熱流密度，放射照度	ワット毎平方メートル	W/m^2	$kg \cdot s^{-3}$
熱容量，エントロピー	ジュール毎ケルビン	J/K	$m^2 \cdot kg \cdot s^{-2} \cdot K^{-1}$
質量熱容量（比熱容量），質量エントロピー	ジュール毎キログラム毎ケルビン	J/(kg・K)	$m^2 \cdot s^{-2} \cdot K^{-1}$
質量エネルギー（比エネルギー）	ジュール毎キログラム	J/kg	$m^2 \cdot s^{-2} \cdot K^{-1}$
熱伝導率	ワット毎メートル毎ケルビン	W/(m・K)	$m \cdot kg \cdot s^{-3} \cdot K^{-1}$
体積エネルギー	ジュール毎立方メートル	J/m^3	$m^{-1} \cdot kg \cdot s^{-2}$
電界の強さ	ボルト毎メートル	V/m	$m \cdot kg \cdot s^{-3} \cdot A^{-1}$
体積電荷	クーロン毎立方メートル	C/m^3	$m^{-3} \cdot s \cdot A$
電気変位	クーロン毎平方メートル	C/m^2	$m^{-2} \cdot s \cdot A$
誘電率	ファラド毎メートル	F/m	$m^{-3} \cdot kg^{-1} \cdot s^4 \cdot A^2$
透磁率	ヘンリー毎メートル	H/m	$m \cdot kg \cdot s^{-2} \cdot A^{-2}$
モルエネルギー	ジュール毎モル	J/mol	$m^2 \cdot kg \cdot s^{-2} \cdot mol^{-1}$
モルエントロピー，モル熱容量	ジュール毎モル毎ケルビン	J/(mol・K)	$m^2 \cdot kg \cdot s^{-2} \cdot K^{-1} \cdot mol^{-1}$
照射線量（X線及びγ線）	クーロン毎キログラム	C/kg	$kg^{-1} \cdot s \cdot A$
吸収線量率	グレイ毎秒	Gy/s	$m^2 \cdot s^{-3}$
放射強度	ワット毎ステラジアン	W/sr	$m^4 \cdot m^{-2} \cdot kg \cdot s^{-3}=m^2 \cdot kg \cdot s^{-3}$
放射輝度	ワット毎平方メートル毎ステラジアン	$W/(m^2 \cdot sr)$	$m^2 \cdot m^{-2} \cdot kg \cdot s^{-3}=kg \cdot s^{-3}$

表６．国際単位系と併用されるが国際単位系に属さない単位

名称	記号	SI 単位による値
分	min	1 min=60s
時	h	1h =60 min=3600 s
日	d	1 d=24 h=86400 s
度	°	1° =(π/180) rad
分	’	1’ =(1/60)° =(π/10800) rad
秒	”	1” =(1/60)’ =(π/648000) rad
リットル	l、L	1l=1 $dm^3=10^{-3}m^3$
トン	t	1t=10^3 kg
ネーパ	Np	1Np=1
ベル	B	1B=(1/2)ln10(Np)

表７．国際単位系と併用されこれに属さない単位で SI単位で表される数値が実験的に得られるもの

名称	記号	SI 単位であらわされる数値
電子ボルト	eV	1eV=1.60217733(49)×10^{-19}J
統一原子質量単位	u	1u=1.6605402(10)×10^{-27}kg
天文単位	ua	1ua=1.49597870691(30)×10^{11}m

表８．国際単位系に属さないが国際単位系と 併用されるその他の単位

名称	記号	SI 単位であらわされる数値
海里		1海里=1852m
ノット		1ノット=1海里毎時=(1852/3600)m/s
アール	a	1a=1 $dam^2=10^2m^2$
ヘクタール	ha	1ha=1 $hm^2=10^4m^2$
バール	bar	1bar=0.1MPa=100kPa=1000hPa=10^5Pa
オングストローム	Å	1 Å=0.1nm=10^{-10}m
バーン	b	1b=100$fm^2=10^{-28}m^2$

表９．固有の名称を含むCGS組立単位

名称	記号	SI 単位であらわされる数値
エルグ	erg	1 erg=10^{-7} J
ダイン	dyn	1 dyn=10^{-5}N
ポアズ	P	1 P=1 dyn・s/cm^2=0.1Pa・s
ストークス	St	1 St =1$cm^2/s=10^{-4}m^2/s$
ガウス	G	1 G ≙10^{-4}T
エルステッド	Oe	1 Oe ≙(1000/4π)A/m
マクスウェル	Mx	1 Mx ≙10^{-8}Wb
スチルブ	sb	1 sb =1$cd/cm^2=10^4cd/m^2$
ホト	ph	1 ph=$10^4$1x
ガル	Gal	1 Gal =1$cm/s^2=10^{-2}m/s^2$

表10．国際単位に属さないその他の単位の例

名称	記号	SI 単位であらわされる数値
キュリー	Ci	1 Ci=3.7×10^{10}Bq
レントゲン	R	1 R = 2.58×10^{-4}C/kg
ラド	rad	1 rad=1cGy=10^{-2}Gy
レム	rem	1 rem=1 cSv=10^{-2}Sv
X線単位		1X unit=1.002×10^{-4}nm
ガンマ	γ	1γ=1 nT=10^{-9}T
ジャンスキー	Jy	1 Jy=10^{-26}W・m^{-2}・Hz^{-1}
フェルミ		1 fermi=1 fm=10^{-15}m
メートル系カラット		1 metric carat = 200 mg = 2×10^{-4}kg
トル	Torr	1 Torr = (101 325/760) Pa
標準大気圧	atm	1 atm = 101 325 Pa
カロリー	cal	
ミクロン	μ	1 μ =1μm=10^{-6}m

（第７版，1998年改訂）

この印刷物は再生紙を使用しています